INVESTIGATING ISOCITRATE DEHYDROGENASE MUTATIONS IN CANCER USING NEW METABOLOMICS METHODS



JOHN WALSBY-TICKLE

DEPARTMENT OF CHEMISTRY

UNIVERSITY OF OXFORD

HILARY TERM 2020

A THESIS SUBMITTED TO THE BOARD OF THE MATHEMATICAL, PHYSICAL AND LIFE SCIENCES DIVISION AT THE UNIVERSITY OF OXFORD IN PARTIAL FULFILMENT OF THE REQUIREMENTS FOR THE DEGREE OF DOCTOR OF PHILOSOPHY

I. Abstract

Altered cellular metabolism, as a result of oncogenic mutations, has been observed in a range of cancer types. A detailed understanding of how cancers modify cellular metabolism, which includes changes to the genome, proteome and metabolome, is therefore integral for the development of effective and targeted therapeutic treatments.

Isocitrate dehydrogenase mutations lead to a change of enzyme function, which causes the production of high intracellular concentrations of 2-hydroxyglutarate, and are found in a range of cancer types including leukaemia, chondrosarcoma, T-cell lymphoma and glioma. Although a range of epigenetic and metabolic effects of isocitrate dehydrogenase 1 and 2 mutations have been identified, which suggest a pro-oncogenic role, the tumorigenic mechanism is not well understood. Over 70 % of low grade glioma (grade 2 and 3) in humans have isocitrate dehydrogenase 1 or 2 mutations, and have one of the lowest 5-year survival rates of all cancer types. Consequently, there is a need for better diagnostic and therapeutic approaches. Small-molecule inhibitors, which are specific to isocitrate dehydrogenase mutations and reduce the abundance of 2-hydroxyglutarate, have been developed; however, resistance to treatment has since been reported, including the manifestation of second-site mutations. Increased understanding of the metabolic changes associated with isocitrate dehydrogenase mutations has the potential to improve therapeutic efficacy, and elucidate new therapeutic pathways.

Metabolomics, the comprehensive analysis and identification of low molecular weight compounds in biological systems, allows the discovery of metabolic adaptations to disease and changes in environment, enabling hypothesis generation and directing

further investigations. Untargeted metabolomics is typically used for the identification of biomarkers, in a discovery-led approach using statistical analysis of experimental groups. A challenge for untargeted metabolomics is the comprehensive analysis of all metabolites present in a biological sample, due to the range of chemical functionalities and matrix complexity. Analysis of polar and ionic metabolites, especially those which represent central carbon metabolism, are not well characterised by the most common hyphenated analytical methods including reversed-phase chromatography, ion-pair chromatography and hydrophobic interaction liquid chromatography, coupled to mass spectrometry. Development of selective eluent suppression technology has enabled the hyphenation of conventional ion-chromatography to mass spectrometry, providing a potentially effective method for the analysis of polar metabolites. Anion-exchange chromatography has recently been applied to targeted analysis, demonstrating reproducible analysis of some polar and ionic metabolites. Comprehensive untargeted metabolomics using ion-chromatography mass spectrometry has not previously been explored to any significant extent.

In this thesis, an in-depth study of the metabolic effects associated an isocitrate dehydrogenase 1 mutation in cancer cells will be undertaken, which will include the development of new anion-exchange chromatography and ion-mobility spectrometry approaches coupled to existing state of the art mass spectrometry. The aims are to both develop and validate new methods, and use these to comprehensively explore how metabolism is altered in association with an isocitrate dehydrogenase 1 mutation. Human glioblastoma and embryonic kidney-derived cell lines with and without a transduced isocitrate dehydrogenase 1 mutation will be used as model systems.

It is demonstrated that anion-exchange chromatography-mass spectrometry provides increased sensitivity and comprehensive coverage of central carbon metabolites compared with an existing hydrophobic interaction liquid chromatography-mass spectrometry method. A new ion-mobility spectrometry-mass spectrometry method is also developed and used for the analysis of derivatised samples, offering improved sensitivity for metabolites with primary and secondary amine functionality, and increasing confidence in identification using collisional cross section measurements. These analyses revealed that lysine and tryptophan degradation products are altered in isocitrate dehydrogenase 1 mutant cells and the possibility for inhibition of 2-oxoglutate dependent pathways by 2-hydroxyglutarate is explored. Treatment of isocitrate dehydrogenase 1 mutant cells with 2-oxoglutarate and 2-hydroxyglutarate is investigated and the results suggest additional regulatory metabolic effects in isocitrate dehydrogenase 1 mutant cells, beyond the enrichment of 2-hydroxyglutarate and the depletion of 2-oxoglutarate. The relationship between an isocitrate dehydrogenase 1 mutation and the concentration of 2-hydroxyglutarate and 2-oxoglutarate, in transduced cell lines, demonstrated the potential for metabolic therapies, in combination with existing pharmacological treatment. The alteration of immunosuppressive metabolites such as kynurenine also provides a possible explanation for different median survival times of patients with isocitrate dehydrogenase mutation positive and wild-type tumours, and their distinct responses to treatment.

Anion-exchange chromatography-mass spectrometry and ion-mobility spectrometry-mass spectrometry were both shown to be robust and sensitive methods for untargeted analysis of cell extracts and provide benefits, beyond current methods, for hypothesis driven research. The sensitivity of isocitrate dehydrogenase 1 mutant cells to changes in

redox state and 2-oxoglutarate concentration elucidates new targets for combination therapies, to develop more selective and effective treatments. New potential biomarkers are also suggested for clinical classification of tumours with isocitrate dehydrogenase 1 mutations.

II. Declaration

The work in this thesis was carried out under the supervision of Professor James S. O. McCullagh. All work described herein is my own, unless stated otherwise, and material from other sources have been fully acknowledged. I confirm that no part of this thesis has been submitted, either partially or in full, for qualification at this University or any other institution.

John Walsby-Tickle
St Hugh's College, University of Oxford
Hilary Term 2020

III. Acknowledgements

Firstly I would like to thank James, my supervisor, for allowing me to join his group and providing me with a new and exciting project to work on. His hands-off approach gave me academic freedom to shape the project, and his guidance throughout my DPhil has been invaluable. I would also like to thank Joan for taking me under her wing at the start of my DPhil, introducing me to tissue culture and mentoring me during that formative time. Our initial work together produced some interesting findings for me to follow up on. The trips over the road to Biochemistry, to escape the basement lab, were particularly memorable. The staff and students of the McCullagh group have also made the process enjoyable and rewarding, especially Tom and Dave who tirelessly let me bounce ideas off them and provided salient advice, with their seemingly limitless biological and clinical knowledge. To all of you who dragged me away from my desk while I was writing up, to help solve a problem, I forgive you, but thank you for the moments of respite! I am also grateful for the assistance of my family and the opportunities for education that they have provided for me. Finally I would like to thank Katherine, for her endless patience and selfless support in good times and bad. She convinced me to apply in the first place and kept up my morale throughout. Without her, none of this work would have been possible.

IV. Abbreviations

2-HG	2-hydroxyglutarate
2-OG	2-oxoglutarate
ADP	Adenosine diphosphate
AGC	Automatic gain control
AMP	Adenosine monophosphate
AMQ	6-aminoquinoline
ANOVA	Analysis of variance
AQC	6-aminoquinolyl-N-hydroxysuccinimidyl carbamate
ATP	Adenosine triphosphate
au	Arbitrary units
CCS	Collisional cross section
CE	Capillary electrophoresis
CID	Collision-induced dissociation
CV	Coefficient of variation
DDA	Data-dependent acquisition
dGDP	Deoxyguanosine diphosphate
dGMP	Deoxyguanosine monophosphate
DIA	Data-independent acquisition
DMEM	Dulbecco's Modified Eagle Medium
DNA	Deoxyribonucleic acid
ESI	Electrospray ionisation
ESM	Electronic supplementary material
FC	Fold change
FDR	False discovery rate
FET	Fisher’s exact test
GC	Gas chromatography
HILIC	Hydrophilic interaction chromatography
HMDB	Human Metabolome Database
IC	Ion chromatography
ICH	International Conference on Harmonisation of Technical Requirements for Registration of Pharmaceuticals for Human Use
IDH	Isocitrate dehydrogenase
IDO	Indoleamine 2,3-dioxygenase
IMS	Ion-mobility spectrometry
IT	Injection time
KEGG	Kyoto Encyclopaedia of Genes and Genomes
LC	Liquid chromatography
LLoD	Lower limit of detection
LLoQ	Lower limit of quantification
m/z	Mass to charge ratio
min	Minutes
mM	Millimolar

MS	Mass spectrometry
MS/MS	Tandem mass spectrometry
Mut	IDH1 R132H mutant
MWCO	Molecular weight cut-off
NAA	N-acetylaspartate
NAAG	N-acetylaspartylglutamate
NAD	Nicotinamide adenine dinucleotide
NADP	Nicotinamide adenine dinucleotide phosphate
NHS	N-hydroxysuccinimide
NMR	Nuclear magnetic resonance spectroscopy
OPLS-DA	Orthogonal partial least squares-discriminant analysis
PCA	Principal component analysis
PLS-DA	Partial least squares-discriminant analysis
PTEN	Phosphatase and tensin homolog
Q^2	Predictive ability
QC	Quality control
R132H	Arginine 132 to histidine
R^2	Goodness of fit
RP	Reversed-phase chromatography
RT	Retention time
s	Seconds
TCA	Tricarboxylic acid cycle
TDO	Tryptophan 2, 3-dioxygenase
TOF	Time of flight
T-wave	Travelling wave
UDP	Uridine diphosphate
VBA	Visual Basic for Applications
VIP	Variable importance in projection
WT	Wild-type

V. Table of contents

I. Abstract ii

II. Declaration vi

III. Acknowledgements vi

IV. Abbreviations vii

V. Table of contents ix

VI. List of figures xv

VII. List of tables xxxii

Chapter 1. Introduction and aims 1

1.1. Metabolic impacts of cancer 1

1.2. Isocitrate dehydrogenase mutations in cancer 5

1.3. Metabolomics 8

1.4. Liquid chromatography for metabolomics 16

1.5. Ion chromatography for metabolomics 21

1.6. Derivatisation for metabolomics 24

1.7. Ion-mobility spectrometry for metabolomics 29

1.8. Research Summary 32

Chapter 2. Development and validation of IC-MS/MS for untargeted analysis of polar and ionic metabolites in cell extracts 35

2.1. Introduction 35

2.2. IC-MS/MS method development 36

2.2.1. Optimisation of chromatographic conditions 37

2.2.2. Chromatographic separation of polar and ionic metabolites 47

2.3. Optimisation of ESI source conditions for IC-MS/MS 51

2.4. IC-MS/MS scan parameter development 61

2.5. IC-MS/MS method validation and comparison with HILIC-MS/MS 62

2.5.1. RT and ion abundance reproducibility of IC-MS/MS 63
2.5.2. Comparison of IC-MS/MS and HILIC-MS/MS 67
2.6. IC-MS/MS linearity and sensitivity compared with HILIC-MS/MS 70
2.7. IC-MS/MS metabolome coverage 74
2.7.1. IC-MS/MS analysis of LN18 wild-type glioblastoma cells 76
2.7.2. HILIC-MS/MS analysis of LN18 wild-type glioblastoma cells 84
2.8. Chapter summary 89
Chapter 3. Exploring central carbon metabolism in IDH1 mutant and wild-type cells 91
3.1. Introduction 91
3.2. Polar and ionic metabolite database 92
3.3. Untargeted IC-MS/MS analysis of LN18 IDH1 mutant and wild-type glioblastoma cells 93
3.3.1. Univariate statistical analysis of LN18 IDH1 mutant and wild-type glioblastoma cells analysed by IC-MS/MS 96
3.3.2. Multivariate statistical analysis of LN18 IDH1 mutant and wild-type glioblastoma cells analysed by IC-MS/MS 109
3.4. Untargeted HILIC-MS/MS analysis of LN18 IDH1 mutant and wild-type glioblastoma cells 116
3.4.1. Univariate statistical analysis of LN18 IDH1 mutant and wild-type glioblastoma cells analysed by HILIC-MS/MS 117
3.4.2. Pathways analysis for LN18 IDH1 mutant and wild-type glioblastoma cells121
3.5. Untargeted IC-MS/MS analysis of U87-MG IDH1 mutant and wild-type glioblastoma cells 129
3.6. Untargeted IC-MS/MS analysis of 293T IDH1 mutant and wild-type embryonic kidney cells 143
3.7. Discussion of IC-MS/MS analysis of IDH1 mutant and wild-type cells 158
3.8. Chapter summary 164

Chapter 4. Exploring metabolism in IDH1 mutant and wild-type cells using derivatised RP-IMS-MS/MS 166

4.1. Introduction 166

4.2. Optimisation of ESI source conditions for the analysis of derivatised amines. 167

4.3. Reproducibility and linearity of analysis for RP-IMS-MS/MS 172

4.3.1. RP-IMS-MS/MS reproducibility 172

4.3.2. RP-IMS-MS/MS linearity 175

4.4. Identification of unknown amines in cell extracts 179

4.5. Derivatised metabolite identification using RP-IMS-MS/MS 182

4.6. IMS-MS/MS analysis of derivatised 1° and 2° amines in biological samples ... 188

4.7. Derivatised RP-IMS-MS/MS sensitivity compared with HILIC-IMS-MS/MS 191

4.8. Untargeted RP-IMS-MS/MS analysis of 293T wild-type embryonic kidney cells to investigate the metabolic effects of glucose concentration 195

4.8.1. Univariate statistical analysis of 293T wild-type embryonic kidney cells analysed by untargeted RP-IMS-MS/MS 196

4.8.2. Multivariate statistical analysis of 293T wild type embryonic kidney cells analysed by untargeted RP-IMS-MS/MS 201

4.9. Untargeted RP-IMS-MS/MS analysis of LN18 IDH1 mutant and wild-type cells209

4.10. Derivatised RP-MS analysis of lysine degradation products 214

4.11. Derivatised RP-MS analysis of tryptophan degradation products 218

4.12. Discussion of derivatised RP-MS analysis of LN18 IDH1 mutant and wild-type glioblastoma cells 222

4.13. Chapter summary 224

Chapter 5. Analysis of IDH1 mutant and wild-type cells using multiple LC-MS/MS methods…….. 226

5.1. Introduction 226

5.2. Non-derivatised RP-MS/MS analysis of LN18 IDH1 mutant and wild-type glioblastoma cells 227

5.2.1. Exploring the effect of the IDH1 mutation on central carbon metabolite abundances 231

5.2.2. Exploring the effect of the IDH1 mutation on pentose phosphate pathway intermediate abundances 233

5.2.3. Exploring the effect of the IDH1 mutation on the abundance of metabolites with amine functional groups 234

5.2.4. Pathway visualisation of metabolite abundances in LN18 IDH1 mutant and wild-type glioblastoma cells 236

5.3. Investigation of cell line specific effects of the IDH1 mutation 242

5.3.1. Exploring the effect of the IDH1 mutation on glycolysis and TCA cycle metabolite abundances in multiple cell lines 243

5.3.2. Exploring the effect of the IDH1 mutation on the abundance of metabolites with amine functional groups in multiple cell lines 245

5.4. Discussion of the effect of the IDH1 mutation on metabolite abundances in multiple cell lines 247

5.5. Chapter summary 249

Chapter 6. Exploring the metabolic effects of altering 2-HG and 2-OG abundance in LN18 IDH1 mutant and wild-type glioblastoma cells 251

6.1. Introduction 251

6.2. Treatment of LN18 wild-type glioblastoma cells with 2-HG 252

6.2.1. Exploring the effect of 2-HG treatment on TCA cycle, glycolysis and pentose phosphate pathway metabolite abundances 253

6.2.2. Exploring the effect of 2-HG treatment on tryptophan and lysine degradation product abundances 255

6.2.3. Exploring the effect of 2-HG treatment on glutamine and glutamate -derived metabolite abundances 257

6.3. Treatment of LN18 IDH1 mutant and wild-type glioblastoma cells with 2-OG 258

6.3.1. Exploring the effect of 2-OG treatment on TCA cycle, glycolysis and pentose phosphate pathway metabolite abundances 260

6.3.2. Exploring the effect of 2-OG treatment on tryptophan and lysine degradation product abundances 264

6.3.3. Exploring the effect of 2-OG treatment on glutamine and glutamate-derived metabolite abundances 269

6.4. Discussion of the effects associated with extracellular treatment of LN18 IDH1 mutant and wild-type glioblastoma cells with 2-HG and 2-OG 271

6.5. Chapter summary 274

Chapter 7. Conclusions and further work 276

7.1. Conclusions 276

7.2. Limitations 278

7.3. Future work 281

Chapter 8. Materials and methods 285

8.1. Mobile phases and solvents 285

8.2. Mobile phase additives 285

8.3. Authentic metabolite standards 285

8.4. IC-MS/MS method for Q Exactive 285

8.5. HILIC-MS/MS method for Q Exactive 286

8.6. HILIC-MS/MS method for Vion IMS QTof 287

8.7. Derivatised RP-MS method for Q Exactive 287

8.8. Derivatised RP-IMS-MS/MS method for Vion IMS QTof 288

8.9. Non-derivatised RP-MS/MS method for Q Exactive 289

8.10. Non-derivatised RP-MS/MS method for Xevo G2-XS QTof 290

8.11. Data processing for untargeted metabolomics using MetaboAnalyst 290

8.12. Data processing for metabolite identification 292

8.13. Lentiviral vector transduction of IDH1 mutant cells.....292

8.14. Metabolomics of LN18 IDH1 mutant and wild-type glioblastoma cells cultured at 2 glucose concentrations.....293

8.15. Metabolomics of U87-MG IDH1 mutant and wild-type glioblastoma cells 294

8.16. Metabolomics of 293T IDH1 mutant and wild-type embryonic kidney cells 295

8.17. Metabolomics of 293T wild-type embryonic kidney cells cultured at 2 glucose concentrations 295

8.18. Metabolomics of LN18 IDH1 mutant and wild-type glioblastoma cells treated with 2-OG or 2-HG.....296

Chapter 9. References 297

Chapter 10. Appendices.....315

10.1. List of 170 authentic metabolite standards.....315

10.2. List of metabolites characterised by IC-MS/MS 318

10.3. List of derivatised metabolites characterised by RP-MS and RP-IMS-MS/MS ..326

10.4. List of metabolites characterised by non-derivatised RP-MS/MS.....330

10.5. Data for LN18 IDH1 mutant and wild-type glioblastoma cells cultured at 2 glucose concentrations 333

10.6. Data for U87-MG IDH1 mutant and wild-type glioblastoma cells.....345

10.7. Data for 293T IDH1 mutant and wild-type embryonic kidney cells 350

10.8. Data for LN18 IDH1 mutant and wild-type glioblastoma cells treated with 2-HG or 2-OG.....354

VI. List of figures

Figure 1.1. Normal and neomorphic reactions of IDH without and with an R132H mutation. 5

Figure 1.2: Activity and localisation of IDH with and without an R132H mutation. 6

Figure 1.3: The frequency distribution of 4245 compound-features, within 0.1 Da of one another, in a metabolite extract from LN18 cells analysed by IC-MS (Section 8.4)..... 10

Figure 1.4: Schematic of an ion suppressor, used to remove counter ions from the eluent stream and allow the hyphenation of anion-exchange chromatography to MS. 23

Figure 1.5: AQC derivatisation reaction and fragmentation products of serine in both positive and negative ion modes. 27

Figure 1.6: Extracted ion chromatograms for AQC derivatised histidine (a), lysine (b), isoleucine / leucine (c), and phenylalanine (d). 28

Figure 1.7: Schematic showing the movement of ions with various CCS values though a drift gas, moved by an electric field. 29

Figure 1.8: Ion-mobiligram showing the relationship between drift time and *m/z* for the analysis of a derivatised metabolite extract from 293T cells (Section 8.8). 30

Figure 2.1: TIC of a mix of 170 authentic metabolite standards (listed in Table 10.1), analysed by IC-MS/MS using manufacturer recommended parameters. 37

Figure 2.2: EIC for *m/z* 259.02244, from a mix of 170 authentic metabolite standards (listed in Table 10.1), analysed by IC-MS/MS using manufacturer recommended parameters (a) and by the optimised method described in Section 8.4 (b). 39

Figure 2.3: EICs for the isomers citrate (i) and isocitrate (ii) analysed by IC-MS/MS using the 60 min method (a) and the 37 min optimised method described in Section 8.4. 40

Figure 2.4: EICs for the isomers AMP and dGMP analysed by IC-MS/MS using the 60 min method (a) and the 37 min optimised method described in Section 8.4. 41

Figure 2.5: EICs for the isomers glutarate and ethylmalonate analysed by IC-MS/MS using the 60 min method (a) and the 37 min optimised method described in Section 8.4. 42

Figure 2.6: EICs for the isomers citrate and isocitrate analysed by IC-MS/MS with column temperature maintained at 20 °C (a) or 40 °C (b) using the optimised method described in Section 8.4. 43

Figure 2.7: EICs for the isomers AMP and dGMP analysed by IC-MS/MS with column temperature maintained at 20 °C (a) or 40 °C (b) using the optimised method described in Section 8.4. 44

Figure 2.8: EICs for the isomers glutarate and ethylmalonate analysed by IC-MS/MS with column temperature maintained at 20 °C (a) or 40 °C (b) using the optimised method described in Section 8.4. 45

Figure 2.9: EIC for *m/z* 259.02244, from a mix of 170 authentic metabolite standards (listed in Table 10.1), analysed by IC-MS/MS with column temperature maintained at 20 °C (a) or 40 °C (b) using the optimised method described in Section 8.4. 46

Figure 2.10: EICs for 2 & 3-phosphoglycerate (a), phosphoenolpyruvate (b) and pyruvate (c) analysed by IC-MS/MS (Section 8.4). 47

Figure 2.11: EICs for oxaloacetate (a), citrate (b(i)), isocitrate (b(ii)), cis-aconitate (c), 2-OG (d), succinate (e), fumarate (f) and malate (g), analysed by IC-MS/MS (Section 8.4). 48

Figure 2.12: EICs for 2-HG (a) and glutamate (b) analysed by IC-MS/MS (Section 8.4). 49

Figure 2.13: EICs for ribulose 5-phosphate (a(i)), ribose 5-phosphate (a(ii)) and ribulose 1,5-disphosphate (b) analysed by IC-MS/MS (Section 8.4). 50

Figure 2.14: EICs for sedoheptulose 7-phosphate (a), erythrose 4-phosphate (b), glyceraldehyde 3-phosphate (c) and fructose 1,6-diphosphate (d) analysed by IC-MS/MS (Section 8.4). 51

Figure 2.15: Ion intensities for 5 μM authentic standards of glycerol-3-phosphate (a), 2-oxoadipate (b) and pyruvate (c), analysed in triplicate by IC-MS/MS (Section 8.4) with sheath gas flow rate between 50-70 au. 53

Figure 2.16: Ion intensities for 5 μM authentic standards of fumarate (a), O-phosphoserine (b) and lactate (c), analysed in triplicate by IC-MS/MS (Section 8.4) with auxiliary gas flow rate between 15-25 au. 54

Figure 2.17: Ion intensities for 5 μM authentic standards of 2-OG (a, $[C_5H_6O_5\text{-}H]^-$, b, $[C_5H_6O_5\text{-}H\text{-}CO_2]^-$) and erythrose-4-phosphate (c), analysed in triplicate by IC-MS/MS (Section 8.4) with heater temperature between 150-450 ^oC. 55

Figure 2.18: Relative ion intensities for the $[C_5H_6O_5\text{-}H]^-$ and $[C_5H_6O_5\text{-}H\text{-}CO_2]^-$ ions at heater temperatures between 50-450 ^oC from the analysis of a 5 μM authentic standard of 2-OG analysed in triplicate by IC-MS/MS (Section 8.4). 56

Figure 2.19: Relative ion intensities for the $[C_5H_8O_5\text{-}H]^-$, $[C_5H_8O_5\text{-}H_2O]^-$ and $[C_5H_8O_5\text{-}H\text{-}CO_2]^-$ ions at heater temperatures between 50-450 ^oC from the analysis of a 5 μM authentic standard of 2-HG analysed in triplicate by IC-MS/MS (Section 8.4). 57

Figure 2.20: Ion intensities for 5 μM authentic standards of cis-aconitate (a), citrate (b) and 2-HG (c), analysed in triplicate by IC-MS/MS (Section 8.4) with capillary temperature between 240-360 ^oC. 58

Figure 2.21 Ion intensities for 5 μM authentic standards of quinate (a), glucose 6-phosphate (b), protocatechuate (c) and 2-HG (d), analysed in triplicate by IC-MS/MS (Section 8.4) with spray voltage between 3.0-3.8 kV. 59

Figure 2.22: Relative ion intensities of precursor and in-source fragment ions for 5 μM authentic standards of 2-OG (a) and 2-HG (b) at spray voltages between 3.0-3.8 kV analysed in triplicate by IC-MS/MS (Section 8.4). 60

Figure 2.23: TIC of a mix of authentic metabolite standards (listed in Table 10.1), analysed by IC-MS/MS (Section 8.4) using optimised scan parameters. 62

Figure 2.24: Reproducibility in RT for a representative subsection of metabolites, from a mix of 170 authentic standards (listed in Table 8.1), analysed by IC-MS/MS (Section 8.4) over 3 months. 64

Figure 2.25: Reproducibility of ion abundance for a representative subsection of metabolites, from a mix of 170 authentic standards (listed in Table 8.1), analysed by IC-MS/MS (Section 8.4) over 3 months. 65

Figure 2.26: The effect of 10 kDa MWCO filtration on ion abundance for selected metabolites from a 293T QC sample (Section 8.16) analysed in triplicate by IC-MS/MS (Section 8.4). 66

Figure 2.27: Reproducibility in RT for a representative subsection of metabolites, from a mix of 170 authentic standards (listed in Table 8.1), analysed by IC-MS/MS (a) and HILIC-MS/MS (b), as described in Sections 8.4 and 8.5 respectively, over 2 weeks. 68

Figure 2.28: Extracted ion chromatograms for the metabolites AMP, ADP and ATP analysed by IC-MS/MS (a, Section 8.4) and HILIC-MS/MS (b, Section 8.5). 70

Figure 2.29: Extracted ion chromatograms for the metabolites succinate, 2-HG, 2-OG, fumarate, citrate, isocitrate and cis-aconitate by IC-MS/MS (Section 8.4). 73

Figure 2.30: Calibration curves for authentic standards of NAA (a) and malate (b) analysed in triplicate by IC-MS/MS (Section 8.4). 73

Figure 2.31: PCA scores plot of compound-feature abundances for LN18 WT cells cultured under 1.5 g / L or 4.5 g / L glucose conditions (Section 8.14), analysed by IC-MS/MS (Section 8.4). 77

Figure 2.32: Volcano plot showing the compound-features with a FC greater than 1.5 and FDR-adjusted t-test p-value less than 0.05, from univariate statistical analysis of LN18 WT cells cultured under 1.5 g / L or 4.5 g / L glucose conditions (Section 8.14), analysed by IC-MS/MS (Section 8.4). 78

Figure 2.33: Metabolic pathway heat map representing central carbon metabolism and related metabolic processes, showing FC and significance for LN18 WT cells cultured under 1.5 g / L or 4.5 g / L glucose conditions (Section 8.14), analysed by IC-MS/MS (Section 8.4)..... 82

Figure 2.34: PCA scores plot of compound-feature abundances for LN18 WT cells cultured under 1.5 g / L or 4.5 g / L glucose conditions (Section 8.14), analysed by HILIC-MS/MS (Section 8.5). 85

Figure 2.35: Volcano plot showing the compound-features with a FC greater than 1.5 and FDR-adjusted t-test p-value less than 0.05, from univariate statistical analysis of LN18 WT cells cultured under 1.5 g / L or 4.5 g / L glucose conditions (Section 8.14), analysed by HILIC-MS/MS (Section 8.5). 86

Figure 2.36: Box plots showing the abundances (normalised to all compounds) for the unidentified compound-feature 1.75_215.0144 (a), dihydrolipoate (b) and methyl fucose (c) in LN18 WT cells cultured under 1.5 g / L or 4.5 g / L glucose conditions (Section 8.14), analysed by HILIC-MS/MS (Section 8.5). 87

Figure 3.1: PCA scores plot of compound-feature abundances from the analysis of LN18 Mut and WT cells cultured under 4.5 g / L glucose conditions (experimental replicate 1, Section 8.14), by IC-MS/MS (Section 8.4). 95

Figure 3.2: Box plots showing the abundance of 2-HG (a), 2-OG (b), citrate (c), succinate (d) and malate (e) in LN18 Mut and WT cells cultured under 4.5 g / L glucose conditions (experimental replicate 1, Section 8.14), analysed by IC-MS/MS (Section 8.4). 97

Figure 3.3: Box plots showing the abundance of 2 & 3-phosphoglycerate (a), phosphoenolpyruvate (b), and lactate (c) in LN18 Mut and WT cells cultured under 4.5 g / L glucose conditions (experimental replicate 1, Section 8.14), analysed by IC-MS/MS (Section 8.4). 98

Figure 3.4: Box plots showing the abundance of pyruvate (a) and glutamate (b) in LN18 Mut and WT cells cultured under 4.5 g / L glucose conditions (experimental replicate 1, Section 8.14), analysed by IC-MS/MS (Section 8.4). 99

Figure 3.5: Volcano plot showing the compound-features with a FC greater than 1.5 and FDR-adjusted t-test p-value less than 0.05, from univariate statistical analysis of LN18 Mut and WT cells cultured under 4.5 g / L glucose conditions (experimental replicate 1, Section 8.14), by IC-MS/MS (Section 8.4). 100

Figure 3.6: Box plots showing the abundance of glucosamine 6-phosphate (a), glycineamide ribonucleotide (b) and fructose 6-phosphate (c) in LN18 Mut and WT cells cultured under 4.5 g / L glucose conditions (experimental replicate 1, Section 8.14), analysed by IC-MS/MS (Section 8.4). 104

Figure 3.7: Lactate / pyruvate ratio calculated from the analysis of LN18 Mut and WT cells cultured under 4.5 g / L glucose conditions (experimental replicate 1, Section 8.14), analysed by IC-MS/MS (Section 8.4). 106

Figure 3.8 Box plots showing the abundance of β-citryl glutamate (a), NAAG (b) and NAA (c) in LN18 Mut and WT cells cultured under 4.5 g / L glucose conditions (experimental replicate 1, Section 8.14), analysed by IC-MS/MS (Section 8.4). 107

Figure 3.9: Box plots showing the abundance of 2-oxoadipate (a) and glutarate (b) in LN18 Mut and WT cells cultured under 4.5 g / L glucose conditions (experimental replicate 1, Section 8.14), analysed by IC-MS/MS (Section 8.4). 108

Figure 3.10: Box plots showing the abundance of AMP (a), ADP (b), ATP (c) and dGDP (d) in LN18 Mut and WT cells cultured under 4.5 g / L glucose conditions (experimental replicate 1, Section 8.14), analysed by IC-MS/MS (Section 8.4). 111

Figure 3.11: Relative abundances of AMP, ADP and ATP compared with the total adenine nucleotide pool calculated from the analysis of LN18 Mut and WT cells cultured under 4.5 g / L glucose conditions (experimental replicate 1, Section 8.14), analysed by IC-MS/MS (Section 8.4). 112

Figure 3.12: Box plots showing the abundance of sedoheptulose 1,7-bisphosphate (a), sedoheptulose 7-phosphate (b), sedoheptulose 1-phosphate (c) and erythrose 4-phosphate (d) in LN18 Mut and WT cells cultured under 4.5 g / L glucose conditions (experimental replicate 1, Section 8.14), analysed by IC-MS/MS (Section 8.4). 114

Figure 3.13: PCA scores plot of compound-feature abundances from the analysis of LN18 Mut and WT cells cultured under 4.5 g / L glucose conditions (experimental replicate 1, Section 8.14), by HILIC-MS/MS (Section 8.5). 117

Figure 3.14: Volcano plot showing the compound-features with a FC greater than 1.5 and FDR-adjusted t-test p-value less than 0.05, from univariate statistical analysis of LN18 Mut and WT cells cultured under 4.5 g / L glucose conditions (experimental replicate 1, Section 8.14), by HILIC-MS/MS (Section 8.5). 118

Figure 3.15: Box plots showing the abundance of N-decoanoylglycine (a), formyl anthranilate (b) and 2-oxoadipate (c) in LN18 Mut and WT cells cultured under 4.5 g / L glucose conditions (experimental replicate 1, Section 8.14), analysed by HILIC-MS/MS (Section 8.5). 120

Figure 3.16: KEGG human metabolic pathway annotated using Mummichog analysis of LN18 Mut and WT cells cultured under 4.5 g / L glucose conditions (experimental replicate 1, Section 8.14), analysed by IC-MS/MS (a) and HILIC-MS/MS (b), as described in Sections 8.4 and 8.5 respectively. 123

Figure 3.17: Bar graph of the number of identified metabolites in enriched pathways from Mummichog analysis of LN18 Mut and WT cells cultured under 4.5 g / L glucose conditions (experimental replicate 1, Section 8.14), analysed by IC-MS/MS (Section 8.4) and HILIC-MS/MS (Section 8.5). 126

Figure 3.18: PCA scores plot of compound-feature abundances for U87-MG Mut and WT cells cultured under 4.5 g / L glucose conditions (Section 8.15), analysed by IC-MS/MS (Section 8.4). 130

Figure 3.19: Volcano plot showing the compound-features with a FC greater than 1.5 and FDR-adjusted t-test p-value less than 0.05, from univariate statistical analysis of U87-MG

Mut and WT cells cultured under 4.5 g / L glucose conditions (Section 8.15), by IC-MS/MS (Section 8.4). 131

Figure 3.20: Box plots showing the abundance of 2-HG (a), 2-OG (b), citrate (c) and malate (d) in U87-MG Mut and WT cells cultured under 4.5 g / L glucose conditions (Section 8.15), analysed by IC-MS/MS (Section 8.4). 133

Figure 3.21: Box plots showing the abundance of 2 & 3-phosphoglycerate (a), phosphoenolpyruvate (b) and lactate (c) in U87-MG Mut and WT cells cultured under 4.5 g / L glucose conditions (Section 8.15), analysed by IC-MS/MS (Section 8.4). 135

Figure 3.22: Box plots showing the abundance of pyruvate (a) and glutamate (b) in U87-MG Mut and WT cells cultured under 4.5 g / L glucose conditions (Section 8.15), analysed by IC-MS/MS (Section 8.4). 136

Figure 3.23: Lactate / pyruvate ratio calculated from the analysis of U87-MG Mut and WT cells cultured under 4.5 g / L glucose conditions (Section 8.15), analysed by IC-MS/MS (Section 8.4). 137

Figure 3.24: Box plots showing the abundance of AMP (a), ATP (b) and dGDP (c) in U87-MG Mut and WT cells cultured under 4.5 g / L glucose conditions (Section 8.15), analysed by IC-MS/MS (Section 8.4). 138

Figure 3.25: Relative abundances of AMP and ATP compared with the total adenine nucleotide pool calculated from the analysis of U87-MG Mut and WT cells cultured under 4.5 g / L glucose conditions (Section 8.15), analysed by IC-MS/MS (Section 8.4).. 139

Figure 3.26: Box plots showing the abundance of β-citryl glutamate (a), NAAG (b), NAA (c) and aspartate (d) in U87-MG Mut and WT cells cultured under 4.5 g / L glucose conditions (Section 8.15), analysed by IC-MS/MS (Section 8.4). 140

Figure 3.27: Box plots showing the abundance of 2-oxoadipate (a) and glutarate (b) in U87-MG Mut and WT cells cultured under 4.5 g / L glucose conditions (Section 8.15), analysed by IC-MS/MS (Section 8.4). 141

Figure 3.28: Box plots showing the abundance of sedoheptulose 1,7-bisphosphate (a), sedoheptulose 7-phosphate (b), sedoheptulose 1-phosphate (c), erythrose 4-phosphate (d) and fructose 6-phosphate (e) in U87-MG Mut and WT cells cultured under 4.5 g / L glucose conditions (Section 8.15), analysed by IC-MS/MS (Section 8.4). 142

Figure 3.29: PCA scores plot of compound-feature abundances for 293T Mut and WT cells cultured under 4.5 g / L glucose conditions (Section 8.16), analysed by IC-MS/MS (Section 8.4). 145

Figure 3.30: Box plots showing the abundance of 2-HG (a), 2-OG (b), citrate (c), succinate (d) and malate (e) in 293T Mut and WT cells cultured under 4.5 g / L glucose conditions (Section 8.16), analysed by IC-MS/MS (Section 8.4). 146

Figure 3.31: Box plots showing the abundance of 2 & 3-phosphoglycerate (a), fructose 1,6-bisphosphate (d) and lactate (c) in 293T Mut and WT cells cultured under 4.5 g / L glucose conditions (Section 8.16), analysed by IC-MS/MS (Section 8.4). 148

Figure 3.32: Box plots showing the abundance of AMP (a), ADP (b), ATP (c) in 293T Mut and WT cells cultured under 4.5 g / L glucose conditions (Section 8.16), analysed by IC-MS/MS (Section 8.4). 149

Figure 3.33: Relative abundances of AMP, ADP and ATP compared with the total adenine nucleotide pool calculated from the analysis of 293T Mut and WT cells cultured under 4.5 g / L glucose conditions (Section 8.16), analysed by IC-MS/MS (Section 8.4). 150

Figure 3.34: Volcano plot showing the compound-features with a FC greater than 1.5 and FDR-adjusted t-test p-value less than 0.05, from univariate statistical analysis of 293T Mut

and WT cells cultured under 4.5 g / L glucose conditions (Section 8.16), by IC-MS/MS (Section 8.4). 151

Figure 3.35: Box plots showing the abundance of pyruvate (a) and glutamate (b) in 293T Mut and WT cells cultured under 4.5 g / L glucose (Section 8.16), analysed by IC-MS/MS (Section 8.4). 153

Figure 3.36: Lactate / pyruvate ratio calculated from the analysis of in 293T Mut and WT cells cultured under 4.5 g / L glucose conditions (Section 8.16), by IC-MS/MS (Section 8.4). 154

Figure 3.37: Box plots showing the abundance of β-citryl glutamate (a), NAAG (b), NAA (c), aspartate (d), glutarate (e) and 2-oxoadipate (f) in 293T Mut and WT cells cultured under 4.5 g / L glucose conditions (Section 8.16), analysed by IC-MS/MS (Section 8.4). 155

Figure 3.38: Box plots showing the abundance of sedoheptulose 1,7-bisphosphate (a), sedoheptulose 7-phosphate (b), sedoheptulose 1-phosphate (c) and erythrose 4-phosphate (d) in 293T Mut and WT cells cultured under 4.5 g / L glucose conditions (Section 8.16), analysed by IC-MS/MS (Section 8.4). 157

Figure 4.1: AQC derivatisation reaction for a generic metabolite with a 1° amine group. 167

Figure 4.2: Mean ion intensities for the derivatised mix of 17 authentic metabolite standards (listed in Table 4.1), analysed in triplicate by the method described in Section 8.8. 169

Figure 4.3: Mean ion intensities for the derivatised mix of 17 authentic metabolite standards (listed in Table 4.1), analysed in triplicate by the method described in Section 8.8. 170

Figure 4.4: Mean ion intensities for the derivatised mix of 17 authentic metabolite standards (listed in Table 4.1), analysed in triplicate by the method described in Section 8.8. 171

Figure 4.5: Reproducibility in RT for a derivatised mix of authentic amine metabolite standards analysed over 3 months, by RP-IMS-MS/MS (Section 8.8, n=40). 173

Figure 4.6: PCA scores plot of compound-feature abundances for 293T WT cells cultured in 1.0 g / L or 4.5 g / L glucose DMEM (Section 8.16), derivatised and analysed by RP-MS (Section 8.7) and data processed in MetaboAnalyst with normalisation by sum and Pareto scaling (Section 8.11). Shaded areas represent the 95 % confidence interval for each group. 174

Figure 4.7: Linearity of analysis for the derivatised metabolites glutamate, alanine and isoleucine across 3 orders of magnitude for diluted 293T QC sample (Section 8.17), derivatised and analysed by RP-MS/MS (Section 8.8). 177

Figure 4.8: Linearity of analysis for 3 unidentified compound-feature across 3 orders of magnitude for diluted 293T QC sample (Section 8.17), derivatised and analysed by RP-MS/MS (Section 8.8). 178

Figure 4.9: MS/MS spectra for a derivatised authentic standard of glutamate analysed by RP-MS/MS (Section 8.8), in positive (a) and negative (b) ion modes. 180

Figure 4.10: EICs for a derivatised authentic standard of glutamate analysed by RP-MS/MS (Section 8.8), in positive (a) and negative (b) ion modes. 181

Figure 4.11: Schematic of a Vion IMS QTof. 183

Figure 4.12: Reproducibility in CCS for a derivatised mix of authentic amine metabolite standards analysed over 3 months, by RP-IMS-MS/MS (Section 8.8, n=40). 184

Figure 4.13: Comparison of the RP-MS/MS (Section 8.8) spectra acquired from IMS-MS/MS (a) and DIA MS/MS (b) for the fragmentation of tryptophan, from a derivatised QC sample of 293T cells (Section 8.16). 186

Figure 4.14: Graph showing the relationship between collisional cross section and m/z for the $1x10^4$ most intense ions from RP-IMS-MS/MS (Section 8.8) analysis of a derivatised QC sample from 293T cells (Section 8.17). 189

Figure 4.15: Extracted ion chromatogram for *m/z* 132.1024, corresponding to the metabolites isoleucine and leucine in a mixed amino acid authentic standard analysed by HILIC-IMS-MS/MS in positive ion mode (Section 8.6). 192

Figure 4.16: Ion mobiligrams corresponding to the metabolites isoleucine and leucine analysed in a mixed amino acid authentic standard in positive ion mode. 193

Figure 4.17: Ion mobiligrams for authentic standards of adenosine mono- (a), di- (b) and tri- (c) phosphates as well as cyclic AMP (d) analysed by HILIC-IMS-MS/MS (Section 8.6). 194

Figure 4.18: PCA scores plot of compound-feature abundances for the analysis of 293T WT cells cultured under 1.0 g / L or 4.5 g / L glucose conditions (Section 8.17), derivatised and analysed by RP-IMS-MS/MS (Section 8.8). 196

Figure 4.19: Volcano plot showing the compound-features with a FC greater than 1.5 and FDR-adjusted t-test p-value less than 0.05, from univariate statistical analysis of 293T WT cells cultured under 1.0 g / L or 4.5 g / L glucose conditions (Section 8.17), derivatised and analysed by RP-IMS-MS/MS (Section 8.8). 197

Figure 4.20: Plot showing the top 35 most important compound-features identified from PLS-DA analysis of 293T WT cells cultured under 1.0 g / L or 4.5 g / L glucose conditions (Section 8.17), derivatised and analysed by RP-IMS-MS/MS (Section 8.8)..... 203

Figure 4.21: Overview of the OPLS-DA model generated from the analysis of 293T WT cells cultured under 1.0 g / L or 4.5 g / L glucose conditions (Section 8.17), derivatised and analysed by RP-IMS-MS/MS (Section 8.8)..... 205

Figure 4.22: S-plot showing the variable importance in the OPLS-DA model generated from the analysis of 293T WT cells cultured under 1.0 g / L or 4.5 g / L glucose conditions (Section 8.17), derivatised and analysed by RP-IMS-MS/MS (Section 8.8). Ions were identified by OPLS-DA analysis, filtered by RT and *m/z.*..... 206

Figure 4.23: PCA scores plot of compound-feature abundances for LN18 Mut and WT cells cultured under 4.5 g / L glucose conditions (experimental replicate 1, Section 8.14), derivatised and analysed by RP-IMS-MS/MS (Section 8.8)..... 210

Figure 4.24: Volcano plot showing the important compound-features from univariate statistical analysis of LN18 Mut and WT cells cultured under 4.5 g / L glucose conditions (experimental replicate 1, Section 8.14), derivatised and analysed by RP-IMS-MS/MS (Section 8.8)..... 212

Figure 4.25: Lysine degradation pathway (reproduced from the KEGG human metabolic pathway database).[167]..... 215

Figure 4.26: Box plots showing the abundance of saccharopine (a) and 2-aminoadipate (b) in LN18 Mut and WT cells cultured under 4.5 g / L glucose conditions (experimental replicate 1, Section 8.14) derivatised and analysed by RP-MS (Section 8.7)..... 216

Figure 4.27: Box plots showing the abundance of saccharopine (a) and 2-aminoadpate (c) in experimental replicate 2 of LN18 Mut and WT cells cultured under 4.5 g / L glucose (Section 8.14), and saccharopine (b) and 2-aminoadpate (d) in experimental replicate 3. 217

Figure 4.28: Tryptophan degradation pathway (reproduced from the KEGG human metabolic pathway database).[167] 219

Figure 4.29: Box plots showing the abundance of tryptophan (a) and hydroxytryptophan (b) in LN18 Mut and WT cells cultured under 4.5 g / L glucose conditions (experimental replicate 1, Section 8.14), derivatised and analysed by RP-MS (Section 8.7). 220

Figure 4.30: Box plots showing the abundance of kynurenine in LN18 Mut and WT cells cultured under 4.5 g / L glucose conditions (Section 8.14) for experimental replicate 1 (a), 2 (b) and 3 (c). 221

Figure 5.1: PCA scores plot of compound-feature abundances for LN18 Mut and WT cells cultured under 4.5 g / L glucose conditions (experimental replicate 1, Section 8.14) analysed by RP-MS/MS (Section 8.9). 228

Figure 5.2: Box plots showing the abundance of β-citryl glutamate (a), NAAG (b), N-acetylglutamate (c) and 2-oxoadipate (d) in LN18 Mut and WT cells cultured under 4.5 g / L glucose conditions (experimental replicate 1, Section 8.14), analysed by RP-MS/MS (Section 8.9). 229

Figure 5.3 Box plot showing the abundance of N-formylkynurenine in LN18 Mut and WT cells cultured under 4.5 g / L glucose conditions (experimental replicate 1, Section 8.14), analysed by RP-MS/MS (Section 8.9). 230

Figure 5.4: Pathway heat map of tryptophan and lysine degradation pathways for the analysis of LN18 Mut and WT cells cultured under 4.5 g / L glucose conditions (experimental replicate 1, Section 8.14), analysed by IC-MS/MS (Section 8.4), derivatised RP-MS (Section 8.7) and non-derivatised RP-MS/MS (Section 8.9). 239

Figure 5.5: Pathway heat map of glutamine and glutamate metabolism for the analysis of LN18 Mut and WT cells cultured under 4.5 g / L glucose conditions (experimental replicate 1, Section 8.14), analysed by IC-MS/MS (Section 8.4), derivatised RP-MS (Section 8.7) and non-derivatised RP-MS/MS (Section 8.9)..... 240

Figure 6.1: Box plots showing the abundance of 2-HG in media (a) and cell extracts (b) for LN18 WT cells cultured under 4.5 g / L glucose conditions, treated with 10 mM 2-HG or vehicle control for 24 hours (Section 8.18), analysed by IC-MS/MS (Section 8.4). 253

Figure 6.2: Pathway heat map of the TCA cycle, glycolysis and pentose phosphate pathway for the analysis of LN18 WT cells cultured under 4.5 g / L glucose conditions, treated with 10 mM 2-HG or vehicle control for 24 hours (Section 8.18), analysed by IC-MS/MS (Section 8.4), derivatised RP-MS (Section 8.7) and non-derivatised RP-MS/MS (Section 8.9). 254

Figure 6.3: Pathway heat map of the tryptophan and lysine degradation pathways for the analysis of LN18 WT cells cultured under 4.5 g / L glucose conditions, treated with 10 mM 2-HG or vehicle control for 24 hours (Section 8.18), analysed by IC-MS/MS (Section 8.4), derivatised RP-MS (Section 8.7) and non-derivatised RP-MS/MS (Section 8.9). 256

Figure 6.4: Pathway heat map of glutamine and glutamate metabolism for the analysis of LN18 WT cells cultured under 4.5 g / L glucose conditions, treated with 10 mM 2-HG or vehicle control for 24 hours (Section 8.18), analysed by IC-MS/MS (Section 8.4), derivatised RP-MS (Section 8.7) and non-derivatised RP-MS/MS (Section 8.9)..... 257

Figure 6.5: Box plots showing the abundance of 2-OG in LN18 Mut and WT cells cultured under 4.5 g / L glucose conditions, treated with 10 mM 2-OG or vehicle control for 24 hours (Section 8.18), analysed by IC-MS/MS (Section 8.4). 259

Figure 6.6: Pathway heat map of the TCA cycle, glycolysis and pentose phosphate pathway for the analysis of LN18 Mut cells cultured under 4.5 g / L glucose conditions, treated with 10 mM 2-OG or vehicle control for 24 hours (Section 8.18), analysed by IC-MS/MS (Section 8.4), derivatised RP-MS (Section 8.7) and non-derivatised RP-MS/MS (Section 8.9). 261

Figure 6.7: Pathway heat map of the tryptophan and lysine degradation pathways for the analysis of LN18 Mut cells cultured under 4.5 g / L glucose conditions, treated with 10 mM 2-OG or vehicle control for 24 hours (Section 8.18), analysed by IC-MS/MS (Section 8.4), derivatised RP-MS (Section 8.7) and non-derivatised RP-MS/MS (Section 8.9). 265

Figure 6.8: Box plot showing the abundance of 2-oxoadipate in LN18 Mut and WT cells cultured under 4.5 g / L glucose conditions, treated with 10 mM 2-OG or vehicle control for 24 hours (Section 8.18), analysed by IC-MS/MS (Section 8.4). 266

Figure 6.9: Box plot showing the abundance of kynurenine in LN18 Mut and WT cells cultured under 4.5 g / L glucose conditions, treated with 10 mM 2-OG or vehicle control for 24 hours (Section 8.18), analysed by derivatised RP-MS (Section 8.7). 267

Figure 6.10: Pathway heat map of glutamine and glutamate metabolism for the analysis of LN18 Mut cells cultured under 4.5 g / L glucose conditions, treated with 10 mM 2-OG or vehicle control for 24 hours (Section 8.18), analysed by IC-MS/MS (Section 8.4), derivatised RP-MS (Section 8.7) and non-derivatised RP-MS/MS (Section 8.9). 269

Figure 6.11: Box plot showing the abundance of β-citryl glutamate in LN18 Mut and WT cells cultured under 4.5 g / L glucose conditions, treated with 10 mM 2-OG or vehicle control for 24 hours (Section 8.18), analysed by IC-MS/MS (Section 8.4). 270

VII. List of tables

Table 2.1: Comparison of LLoD, LLoQ and R^2 for the calibration curves of polar metabolites analysed by IC-MS/MS (Section 8.4) and HILIC-MS/MS (Section 8.5). 72

Table 2.2: Top 35 compound-features identified in the volcano plot (Fig. 2.32) from univariate statistical analysis of LN18 WT cells cultured under 1.5 g / L or 4.5 g / L glucose conditions (Section 8.14), analysed by IC-MS/MS (Section 8.4). 80

Table 2.3: Top 35 compound-features identified in the volcano plot (Fig. 2.35) from univariate statistical analysis of LN18 WT cells cultured under 1.5 g / L or 4.5 g / L glucose conditions (Section 8.14), analysed by HILIC-MS/MS (Section 8.5). 88

Table 3.1: Top 35 compound-features identified in the volcano plot (Fig. 3.5) from univariate statistical analysis of LN18 Mut and WT cells cultured under 4.5 g / L glucose conditions (experimental replicate 1, Section 8.14), by IC-MS/MS (Section 8.4)..... 101

Table 3.2: Top 35 compound-features identified from volcano plot analysis for filtered univariate statistical analysis of LN18 Mut and WT cells cultured under 4.5 g / L glucose conditions (experimental replicate 1, Section 8.14), by IC-MS/MS (Section 8.4)..... 103

Table 3.3: Table of the compound-features with a VIP score greater than 2, identified from PLS-DA analysis of LN18 cells cultured under 4.5 g / L glucose conditions (experimental replicate 1, Section 8.14), by IC-MS/MS (Section 8.4)..... 109

Table 3.4: Compound-features identified from the volcano plot (Fig. 3.14) from univariate statistical analysis of LN18 Mut and WT cells cultured under 4.5 g / L glucose conditions (experimental replicate 1, Section 8.14), by HILIC-MS/MS (Section 8.5). 119

Table 3.5: Enriched pathways from Mummichog analysis of LN18 Mut and WT cells cultured under 4.5 g / L glucose conditions (experimental replicate 1, Section 8.14), analysed by IC-MS/MS (Section 8.4), ranked by FET significance..... 124

Table 3.6: Enriched pathways from the Mummichog analysis of LN18 Mut and WT cells cultured under 4.5 g / L glucose conditions (experimental replicate 1, Section 8.14) by HILIC-MS/MS (Section 8.5), ranked by FET values. 127

Table 3.7: Enriched pathways from targeted pathways analysis of LN18 Mut and WT cells cultured under 4.5 g / L glucose conditions (experimental replicate 1, Section 8.14) by HILIC-MS/MS (Section 8.5), ranked by p-values. 128

Table 3.8: Top 35 compound-features identified in the volcano plot (Fig. 3.19) from univariate statistical analysis of U87-MG Mut and WT cells cultured under 4.5 g / L glucose conditions (Section 8.15), analysed by IC-MS/MS (Section 8.4). 132

Table 3.9: Top 35 compound-features identified in the volcano plot (Fig. 3.34) from univariate statistical analysis of 293T Mut and WT cells cultured under 4.5 g / L glucose conditions (Section 8.16), by IC-MS/MS (Section 8.4). 152

Table 3.10: Heat map showing the FC for selected metabolites from IC-MS/MS analysis (Section 8.4) of Mut and WT LN18 (experimental replicate 1, Section 8.14), U87-MG (Section 8.15) and 293T (Section 8.16) cells, cultured under 4.5 g / L glucose conditions. 159

Table 4.1: Mix of authentic amine metabolite standards used for method development and performance testing. 168

Table 4.2: Comparison of LLoD, LLoQ and R^2 values for the calibration curves of amines analysed by derivatised RP-MS (Section 8.7) and HILIC-MS (Section 8.5). 176

Table 4.3: R^2 values for derivatised metabolites across 3 orders of magnitude for a diluted 293T QC sample (Section 8.17), derivatised and analysed in triplicate by RP-MS/MS (Section 8.8). 178

Table 4.4: Chemical formulae predicted from *m/z* 317.1603 in a 293T cell sample, derivatised and analysed by RP-MS/MS (Section 8.8). 182

Table 4.5: Comparison of LLoD, LLoQ and R^2 for the calibration curves of derivatised amine metabolites, analysed by RP-MS/MS (Section 8.8) in IMS-MS/MS and DIA MS/MS modes. 187

Table 4.6: Compounds in HMDB with the chemical formula $C_5H_{11}NO_2$. 190

Table 4.7: Top 35 compound-features identified in the volcano plot (Fig. 4.19) from univariate statistical analysis of 293T WT cells cultured under 1.0 g / L or 4.5 g / L glucose conditions (Section 8.17), derivatised and analysed by RP-IMS-MS/MS (Section 8.8). ... 198

Table 4.8: Top 35 compound-features, filtered by RT and *m/z*, identified in the volcano plot (Fig. 4.19) from univariate statistical analysis of the filtered dataset for 293T WT cells cultured under 1.0 g / L or 4.5 g / L glucose conditions (Section 8.17), derivatised and analysed by RP-IMS-MS/MS (Section 8.8)..... 200

Table 4.9: Predicted chemical formulae and corresponding identified metabolites for the top 10 important compound-features from PLS-DA analysis of 293T WT cells cultured under 1.0 g / L or 4.5 g / L glucose conditions (Section 8.17), derivatised and analysed by RP-IMS-MS/MS (Section 8.8)..... 204

Table 4.10: Table of the top 10 important compound-features in 293T WT cells cultured under 1.0 g / L or 4.5 g / L glucose conditions (Section 8.17), derivatised and analysed by RP-IMS-MS/MS (Section 8.8). Ions were identified by OPLS-DA analysis, filtered by RT and *m/z*. 207

Table 4.11: Table of the top 10 important compound-features, ordered by their distance from the origin for the S-plot (Fig. 4.22) prepared from OPLS-DA of 293T WT cells cultured

under 1.0 g / L or 4.5 g / L glucose conditions (Section 8.17), derivatised and analysed by RP-IMS-MS/MS (Section 8.8). 208

Table 4.12: Top 35 compound-features ranked by their FDR-adjusted t-test p-value from the analysis of LN18 Mut and WT cells cultured under 4.5 g / L glucose conditions (experimental replicate 1, Section 8.14), derivatised and analysed by RP-IMS-MS/MS (Section 8.8). 211

Table 4.13: Top 35 important compound-features, filtered by RT and *m/z*, identified in the volcano plot (Fig. 4.24) from univariate statistical analysis of LN18 Mut and WT cells cultured under 4.5 g / L glucose conditions (experimental replicate 1, Section 8.14), derivatised and analysed by RP-IMS-MS/MS (Section 8.8). 213

Table 5.1: Heat map showing FC and significance for selected central carbon metabolites from experimental replicates of LN18 Mut and WT cells cultured under 4.5 g / L glucose conditions (Section 8.14), analysed by IC-MS/MS (Section 8.4), derivatised RP-MS (Section 8.7) and non-derivatised RP-MS/MS (Section 8.9). 232

Table 5.2: Heat map showing FC and significance for selected pentose phosphate intermediates from experimental replicates of LN18 Mut and WT cells cultured under 4.5 g / L glucose conditions (Section 8.14), analysed by IC-MS/MS (Section 8.4), derivatised RP-MS (Section 8.7) and non-derivatised RP-MS/MS (Section 8.9). 233

Table 5.3: Heat map showing FC and significance for selected metabolites with amine functional groups, from experimental replicates of LN18 Mut and WT cells cultured under 4.5 g / L glucose conditions (Section 8.14), analysed by IC-MS/MS (Section 8.4), derivatised RP-MS (Section 8.7) and non-derivatised RP-MS/MS (Section 8.9). 235

Table 5.4: Heat map showing FC and significance for selected central carbon metabolites from LN18 (experimental replicate 1, Section 8.14), U87-MG (Section 8.15) and 293T (Section 8.16), Mut and WT cells cultured under 4.5 g / L glucose conditions. 244

Table 5.5: Heat map showing FC and significance for selected metabolites with amine functional groups, from LN18 (experimental replicate 1, Section 8.14), U87-MG (Section 8.15) and 293T (Section 8.16), Mut and WT cells cultured under 4.5 g / L glucose conditions. 245

Table 6.1: Heat map showing FC and significance for selected central carbon metabolites from LN18 Mut and WT cells cultured under 4.5 g / L glucose conditions, treated with 10 mM 2-OG or vehicle control for 24 hours (Section 8.18), analysed by IC-MS/MS (Section 8.4), derivatised RP-MS (Section 8.7) and non-derivatised RP-MS/MS (Section 8.9). 263

Table 6.2: Heat map showing FC and significance for selected tryptophan and lysine degradation products from LN18 Mut and WT cells cultured under 4.5 g / L glucose conditions, treated with 10 mM 2-OG or vehicle control for 24 hours (Section 8.18), analysed by IC-MS/MS (Section 8.4), derivatised RP-MS (Section 8.7) and non-derivatised RP-MS/MS (Section 8.9). 268

Table 6.3: Heat map showing FC and significance for selected glutamine and glutamate metabolites from LN18 Mut and WT cells cultured under 4.5 g / L glucose conditions, treated with 10 mM 2-OG or vehicle control for 24 hours (Section 8.18), analysed by IC-MS/MS (Section 8.4), derivatised RP-MS (Section 8.7) and non-derivatised RP-MS/MS (Section 8.9). 271

Table 10.1: Table of 170 authentic metabolite standards in the mix used for IC-MS/MS evaluation. 315

Table 10.2: Table of metabolites characterised by IC-MS/MS (Section 8.4)..... 318

Table 10.3: Table of derivatised metabolites characterised by RP-MS (Section 8.7) and RP-IMS-MS/MS (Section 8.8)..... 326

Table 10.4: Table of metabolites characterised by non-derivatised RP-MS/MS (Sections 8.9 and 8.10)..... 330

Table 10.5: Metabolite identification information for the analysis of LN18 Mut and WT cells cultured under 1.0 g / L or 4.5 g / L glucose conditions (experimental replicate 1, Section 8.14), analysed by IC-MS/MS (Section 8.4), derivatised RP-MS (Section 8.7) and non-derivatised RP-MS/MS (Section 8.9)..... 333

Table 10.6: Metabolite identification information for the analysis of LN18 Mut and WT cells cultured under 4.5 g / L glucose conditions (experimental replicate 2, Section 8.14), analysed by IC-MS/MS (Section 8.4), derivatised RP-MS (Section 8.7) and non-derivatised RP-MS/MS (Section 8.9). 338

Table 10.7: Metabolite identification information for the analysis of LN18 Mut and WT cells cultured under 4.5 g / L glucose conditions (experimental replicate 3, Section 8.14), analysed by IC-MS/MS (Section 8.4), derivatised RP-MS (Section 8.7) and non-derivatised RP-MS/MS (Section 8.9). 342

Table 10.8: Metabolite identification information for the analysis of U87-MG Mut and WT cells cultured under 4.5 g / L glucose conditions (Section 8.15), analysed by IC-MS/MS (Section 8.4), derivatised RP-IMS-MS/MS (Section 8.8) and non-derivatised RP-MS/MS (Section 8.10). 346

Table 10.9: Metabolite identification information for the analysis of 293T Mut and WT cells cultured under 4.5 g / L glucose conditions (Section 8.16), analysed by

IC-MS/MS (Section 8.4), derivatised RP-MS (Section 8.7) and non-derivatised RP-MS/MS (Section 8.9). 351

Table 10.10: Metabolite identification information for the analysis of LN18 Mut and WT cells cultured under 4.5 g / L glucose conditions, treated with 10 mM 2-HG, 10 mM 2-OG or vehicle control for 24 hours (Section 8.18), analysed by IC-MS/MS (Section 8.4), derivatised RP-MS (Section 8.7) and non-derivatised RP-MS/MS (Section 8.9)..... 355

Chapter 1. Introduction and aims

1.1. Metabolic impacts of cancer

The development of effective therapeutic approaches for the treatment of a disease is enhanced by a detailed understanding of how the disease affects cellular function and treatment.[1] Precision medicine promises new approaches for the treatment of disease using a personalised treatment strategy, based on the genetic, phenotypic and psychosocial characteristics, which distinguish an individual patient's optimal therapeutic strategy.[2] Such strategies require the analysis and profiling of the effects of the disease, on biochemical processes, both generally and in a specific patient to allow individualised treatment. Changes to the patient's genome, proteome and metabolome are often complex in pathologies and investigation of a single domain can therefore be insufficient for diagnosis and treatment.[3] For example, a genetic mutation which is characteristic of certain types of cancer, may lead to changes in the expression of specific proteins that ultimately modify metabolic pathways.[4] Genetic treatment may not have a metabolic effect and therefore the analysis of how a disease affects metabolism can improve diagnosis, and provide treatments which recover normal metabolism. Changes in a patient's metabolome can provide useful biomarkers of a disease, but can also be potential targets for the design of therapeutic interventions.[5] The aetiology of disease may also not be revealed by genotypic analysis alone and therefore phenotypic analysis, which is influenced by environmental factors, can aid a more detailed understanding of disease-associated metabolic pathways and enable more targeted treatments.[6] Metabolomics is developing rapidly as a technique and provides a comprehensive approach to investigate metabolic changes; however, technical challenges remain.[7]

Reproducibility and confidence in metabolite identification continue to be limiting factors.[8]

Metabolic reprogramming is commonly associated with tumour development and affects gene expression, cell proliferation and modification of the tumour microenvironment, as direct and indirect consequences of genetic mutations.[9] Cancer cell metabolism is typically altered to maintain cell viability and growth with non-typical energy sources, or to upregulate energy pathways such as glycolysis, which results in increased lactate production, known as the Warburg effect.[10, 11] The Warburg effect has been observed in a range of cancer types and has been associated with alterations in acidification, acetylation and the intracellular concentrations of adenosine triphosphate (ATP) and reactive oxygen species however, its biological function remains unclear.[12] Tumours have been observed to evolve from benign to malignant by acquiring a number of mutations over time, caused by hereditary and environmental factors.[13] The majority of cancers are a result of point mutations which cause missense or loss-of-function, rather than deletion of multiple codons.[14] For example, the tumour suppressing enzyme p53 is often mutated in a range of cancers, inhibiting its ability to maintain genetic integrity and stimulate apoptosis if deoxyribonucleic acid (DNA) damage is detected.[15] The primary function of p53 is as a transcription factor which regulates the expression of a range of genes and micro ribonucleic acids.[16, 17] Regulation by p53 determines the cells response to stressors, such as DNA damage, hypoxia and nutrient fluctuation, all commonly observed as a result of mutations in cancer.[18] Mutations in p53 are therefore beneficial for cancer cells, to maintain their proliferation and avoid the various cellular mechanisms of regulated apoptosis or necrosis.[19] The complete functions of p53 are not known and therefore it is not currently a therapeutic target as treatment may have off-target effects.[18] Other

genetic modifications, such as change-of-function mutations, can result in active production of a metabolite rather than depletions which are normally observed. Change-of-function mutations are relatively rare but have also been observed in a number of cancer types including leukaemia, chondrosarcoma, T-cell lymphoma and glioma, causing the accumulation of fumarate and succinate, due to neomorphic activity of tricarboxylic acid cycle (TCA) enzymes.[20, 21]

The disruption of cellular energy pathways is typically observed as the predominant metabolic effect of mutations in cancer cells.[22] Astrocytes principally rely on glycolysis whereas neurons use oxidative phosphorylation however mutations, especially those where the Warburg effect is observed alter these energetic mechanisms to shuttle carbon to biosynthetic pathways to produce fatty acids and nucleic acids for proliferation.[23, 24] Activation of cellular signalling pathways, such as mammalian target of rapamycin and protein kinase B, are also commonly observed in cancers and have been shown to promote cell growth and survival through regulation of glycolytic and biosynthetic metabolism.[24, 25] These alterations in cellular energy pathways have also been observed to cause permanent mitochondrial dysfunction in glioma, including structural abnormalities, impaired apoptosis and mutations in mitochondrial DNA.[26] Mitochondrial mutations may be responsible for the shift to glycolytic metabolism by disrupting the electron transport chain.[27] Selective treatment of these mutations can be a challenge due to the reliance of non-cancer cells on glycolysis and oxidative phosphorylation. Pharmacological intervention, such as the inhibition of glucose uptake with 2-deoxy glucose reduces glycolytic flux, and decreases tumour progression; however, is not cancer specific and therefore has the same effects in normal cells.[28] Mitochondria-targeted treatments include inhibition of mitochondrial activity, increasing sensitivity to reactive

oxygen species and mitochondrial priming to increase the efficacy of chemotherapy.[26] These treatments are also typically not cancer specific although some success has been observed for the use of metformin and phenformin, to inhibit complex 1 and therefore reduce proliferation and prolong tumour remission.[29]

Another typical mutation observed in cancer is of the phosphatase and tensin homolog (PTEN) gene, which is a negative regulator of the phosphoinositide 3-kinase signalling pathway and therefore closely related to the regulation of cell cycle and longevity by preventing activation of downstream kinases.[30] PTEN therefore acts as a tumour suppressor by halting cell cycle progression and inducing cell senescence in response to tumorigenic mutations.[31] PTEN, through its regulation of kinase activity, is associated with a range of metabolic processes including insulin sensitivity, *de novo* lipogenesis and phosphorylation of glucose in the mitochondria.[32] Mutations in PTEN (typically leading to loss-of-function) in cancers can therefore regulate tumour metabolism and have been associated with tumorigenesis by the activation of the protein kinase B and mammalian target of rapamycin signalling pathways.[33] Defects in homologous recombination in PTEN-deficient tumour cells has been observed to sensitise the cells to polyadenosine diphosphate ribose polymerase inhibitors.[34] PTEN-deficient cells tumour cells, with a higher incidence of DNA damage, may therefore be selectively targeted, as repair mechanisms using polyadenosine diphosphate ribose polymerase will be inhibited.[35] Resistance to targeted treatment of PTEN-deficient glioblastoma multiforme tumours has also been observed, caused by post-translational modifications, highlighting the challenge of therapeutic treatment of genetic mutations.[36] An increased understanding of cancer-associated metabolic modifications and the various genetic

alterations associated with them is therefore of clinical interest, to design therapeutic strategies which are selective for cancer cells and therefore improve patient prognosis.[5, 6]

1.2. Isocitrate dehydrogenase mutations in cancer

Gliomas currently have one of the lowest 5-year survival rates of all cancer types making them a prime clinical target.[37, 38] Isocitrate dehydrogenase (IDH) mutations are observed in the majority of grade 2 and 3 gliomas in humans, especially impacting individuals between the ages of 20 and 40.[20] IDH mutations are change-of-function mutations which catalyse the production of 2-hydroxyglutarate (2-HG), as shown in Fig. 1.1, and can disrupt the normal IDH reaction of isocitrate to 2-oxoglutarate (2-OG); the mutation of arginine 132 to histidine (R132H) is typically associated with glioma, although other mutations have been observed.[39, 40]

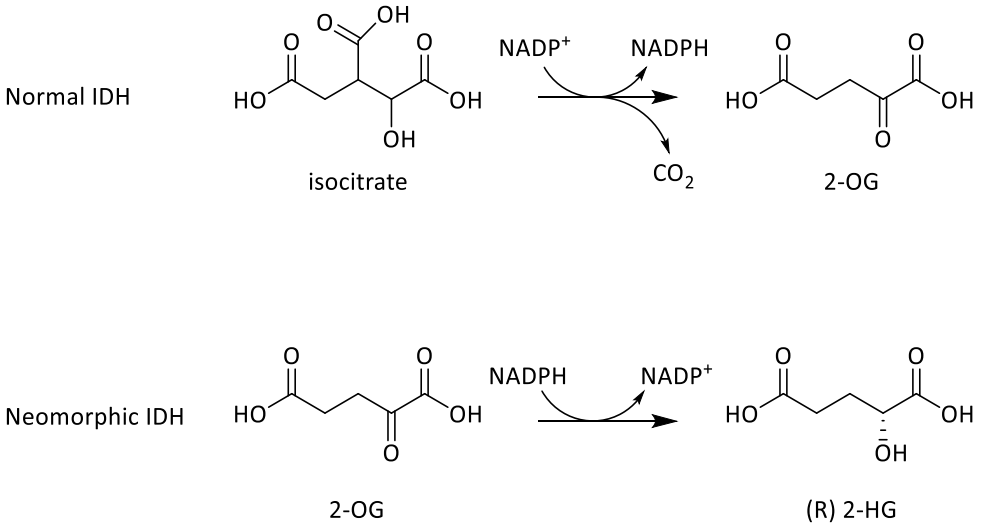

Figure 1.1. Normal and neomorphic reactions of IDH without and with an R132H mutation.

IDH has 3 isozymes (IDH1, IDH2 and IDH3) which perform the oxidative decarboxylation of isocitrate (Fig. 1.1), and have different cellular localisation as shown in Fig. 1.2. Wild-type (WT) IDH1 is located in the cytosol and peroxisome, whereas IDH2 and IDH3 are only present in mitochondria. IDH1 and IDH2 catalyse reversible reactions which use

$NADP^+$ as a cofactor.[41] IDH3 is irreversible and uses NAD^+ and is therefore an essential source of NADH as part of the TCA cycle.[42] IDH mutations have been observed in a range of cancer subtypes including acute myeloid leukaemia, myelodysplastic syndromes, myeloproliferative neoplasms and cholangiocarcinoma.[43-46] An understanding of the metabolic effects of the mutations and identification of therapeutic treatments is therefore of clinical interest.

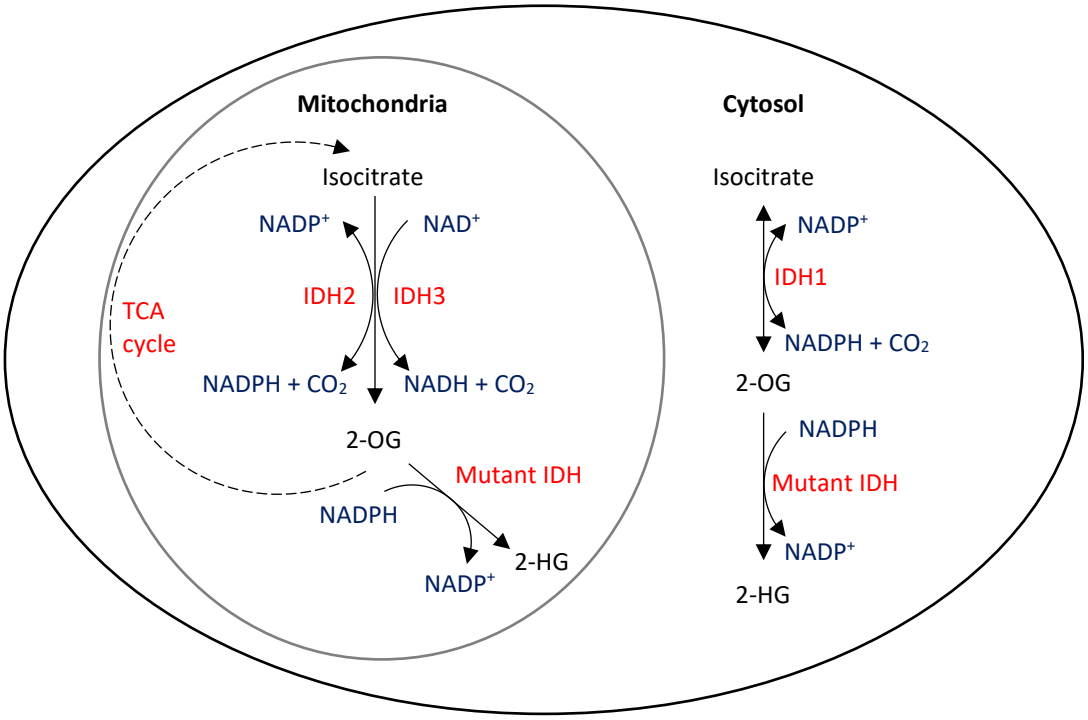

Figure 1.2: Activity and localisation of IDH with and without an R132H mutation.

The reaction products of IDH mutations are enantiospecific and (R)2-HG has been observed to accumulate over hundred-fold in IDH1 R132H mutant (Mut) cells compared with WT cells, to millimolar (mM) concentrations, making it an important biomarker for the presence of an IDH mutation.[40, 47]

The physiological purpose for the enrichment of 2-HG is not currently known and requires further investigation, as several competing mechanisms of action for the mutation have been postulated, including chromatin modification, DNA methylation alteration and

accumulation of hypoxia induced factors, which have all been associated with tumour progression.[48-51] The inhibition of 2-OG dependent oxygenases by 2-HG has also been suggested, but not comprehensively demonstrated.[52] Oxygenases for example, are associated with the expression of the genes involved in cell differentiation and post-translational modification of proteins and therefore competitive inhibition by 2-HG may alter regulatory pathways in IDH mutant cells.[53] Another effect of the IDH mutation is the depletion of NADPH in the cytosol (for IDH1) and mitochondria (for IDH2), as IDH has been demonstrated to contribute to the majority of $NADP^+$ production in glioblastoma.[54] NADPH is depleted in Mut cells, as WT activity is lost and NADPH is consumed as a cofactor in the neomorphic reaction, resulting in glutathione depletion and an increase in reactive oxygen species.[55] The mutation has also been observed in early glioma development suggesting a pro-oncogenic role.[56] *In vivo* evidence in a mouse model suggests that an IDH mutation is not tumourigenic unless combined with upregulation of platelet-derived growth factor subunit A and the knock-out of multiple tumour suppression genes.[57]

Current treatment of glioblastoma ranges from surgical resection to radiotherapy and chemotherapy, as the IDH inhibitors developed to date are not approved for the treatment of glioblastoma, and further mutations leading to resistance, have been observed for the treatment of IDH mutations in acute myeloid leukaemia.[58, 59] Surgical treatment for IDH WT glioma, where maximal subtotal resection can be achieved, leads to increased median survival times.[60] Variable prognosis with treatment is observed in IDH mutant glioma, such as the more diffuse astrocytoma and oligodendroglioma which are less amenable to surgical intervention.[61] Radiotherapy is used both in the management of glioma and as part of postoperative treatment, and maximal survival time is observed for

combination treatment with chemotherapeutic agents, such as temozolomide.[62] IDH mutant tumours have been shown to have increased sensitivity to chemotherapeutic approaches; however, like radiotherapy, chemotherapy is not a selective treatment technique.[63] Increased understanding of the effects of IDH mutations and their tumourigenic processes may consequently aid in drug discovery and the development of targeted treatment approaches.

The prevalence of IDH mutations in glioma, variable survival rate and absence of specific treatments necessitates an increased understanding of their mechanisms of action.[20, 42, 56] The majority of research into IDH mutations in cancer has focussed on genetic and epigenetic consequences and therefore the metabolic effects of an IDH mutation is an area which requires further study.[39, 40, 43-46] Increased understanding of metabolic changes including accumulation of 2-HG, intracellular acidification, change in redox balance, glucose and energy cofactor utilisation in Mut cells using metabolomics may elucidate the role of the IDH mutation in tumourigenesis, cell proliferation and survival. Comprehensive evaluation of the metabolome associated with Mut cells may therefore assist in the design of therapeutic approaches, or identify metabolic strategies for the recovery of normal metabolism.

1.3. Metabolomics

Metabolomics is the quantitative study of the small molecules in a biological system, typically with a molecular weight less than 1500 Da, in order to determine the metabolic component of a particular disease or physiological state.[7, 64, 65] Metabolomics is typically used as a bottom-up approach which analyses the molecules produced by networks of enzymes, to discover how biological function has altered in response to disease or

changes in environment, and identify targets for further study.[66] Metabolites are normally classified into two groups based on their origin, endogenous metabolites, which are produced by the host organism and exogenous, which are absorbed into the system, usually from dietary sources. The abundance of metabolites in a system therefore varies and so are typically studied at a specific point in time.[67] Certain metabolite concentrations, including glucocorticoids, are constantly altered during cell cycle and have been shown to be coupled with circadian rhythm.[68] Metabolomics is therefore either performed with cells which are synchronised to measure metabolic effects associated with cell cycle, or unsynchronised which results in a metabolic average.[69] As *in vivo* metabolite concentrations are influenced by multiple sources, and are highly sensitive to stimuli such as genetic and environmental changes, experiments require careful design to ensure consistent and reliable comparisons can be made.[8] Metabolite concentrations can also be modified during sample harvesting and processing, sample preparation and storage conditions therefore need to be controlled to minimise metabolite degradation and minimise intra-group variation.[70-72] A range of analytical techniques, each with advantages for specific metabolite classes, can be used for metabolomics including mass spectrometry (MS), nuclear magnetic resonance spectroscopy (NMR) and vibrational spectroscopy techniques such as Raman.[73-76] Metabolomics provides unique and valuable information about the phenotype of environmental modification or disease state and can be essential for the understanding of how a disease affects cellular function, especially when genetic or enzymatic effects are not known. Understanding of how metabolites interact with pathways and enzymes provides important therapeutic information including novel targets for intervention.[77]

MS remains the primary analytical tool for metabolic profiling due to its high sensitivity and selectivity which allows the detection of thousands of individual metabolite ions, in complex mixtures, down to femtomolar concentrations.[78] MS also provides structural information which can facilitate the identification of metabolites in addition to accurate mass to charge ratio (*m/z*) values and isotope patterns. The wide dynamic range (typically 4 orders of magnitude) of MS allows quantitation of ions based on abundance, even when ion intensities (within and between samples) are different by orders of magnitude. The concentration of a specific analyte in a sample can be calculated by comparing its ion abundance with a calibration curve, or relative quantification can also be utilised when authentic standards are not available. The mass range below ca. 1500 Da, used for metabolomics by MS, results in a large number of mass spectral peaks when analysing biological samples. As shown in Fig. 1.3, the frequency distribution of *m/z* values within 0.1 Da of one another are plotted for the 4245 compound-features detected in a metabolite extract from LN18 cells, illustrating the complexity of metabolomics samples analysed by MS.

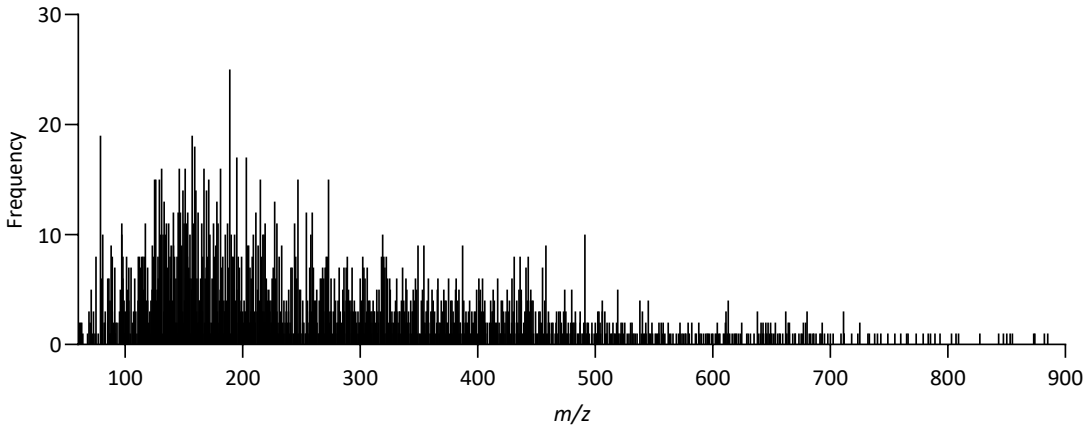

Figure 1.3: The frequency distribution of 4245 compound-features, within 0.1 Da of one another, in a metabolite extract from LN18 cells analysed by IC-MS (Section 8.4).

The low mass range provides a challenge for identification, as it is also where most impurities and contaminants are also found using electrospray ionisation (ESI) hyphenated to MS.[79] Metabolites with the same chemical formulae, such as structural isomers and enantiomers, are prevalent in biological systems and cannot be separated by *m/z* alone. MS analysis of complex mixtures therefore requires additional techniques such as liquid chromatography (LC) or gas chromatography (GC) to assist in separation and identification.

A range of mass analysers can be used for MS, depending on the mass precision and resolution required for a specific experiment. The simplest and oldest of which are sector mass analysers, which use the deflection of an ion beam to filter ions based on their *m/z*, using an electromagnetic field.[80] Quadrupole mass analysers are widely used in MS for mass filtering, and are typically hyphenated to higher resolution analysers such as time of flight (TOF) or Orbitrap analysers.[81] Quadrupoles uses opposing oscillating electric fields produced along four parallel electrodes to separate ions based on their *m/z*, as variation of the electrode potentials allows specific destabilisation of the ions travelling through the field. TOF mass analysers accelerate ions with an electric field towards a detector, causing the ions to separate according to their *m/z* as they travel through a drift tube, based on their different velocities.[82] Increased mass resolution can be achieved by using a reflectron to increase the path length that the ions travel and hence increase the separation between ions with similar *m/z*.[83] Increased mass resolution can be achieved using Orbitrap mass analysers, which use a central electrode to trap ions in an elliptical trajectory, based on their electrostatic attraction and velocity, which subsequently causes the ions to emit distinct axial frequencies. When specific ions are destabilised by applying an RF voltage to the outer electrode, their harmonic frequencies induce additional

current in the outer detection electrode according to their m/z. The ions are detected using image current detection and are transformed into mass spectra using fast Fourier transform.[84]

NMR also provides quantitative and structural information and can be used for metabolomics; however, it requires larger volumes of sample than MS and is less sensitive by a factor of 10-100.[75] The structural information obtained from NMR experiments, such as chemical shifts, coupling constants and through space nuclear Overhauser effect couplings, are all highly characteristic of specific metabolites and therefore high confidence in identification is possible.[85] NMR is not readily hyphenated to chromatographic techniques and therefore the complexity of biological samples means that high field strength instruments, or long acquisition times, are usually required to increase resolution and minimise background interference from the matrix. In addition, proton chemical shifts are highly pH dependent and are affected by the close coordination of metal cations.[86] The sensitivity of chemical shifts to environmental factors is a weakness for the analysis of biological materials, especially as metal cations are highly abundant and are required as a cofactor in a range of enzyme reactions. For example, in the presence of an IDH mutation, 2-HG and lactic acid are both produced at high intracellular concentrations leading to acidification of Mut compared with WT samples and therefore samples may need buffering prior to analysis to ensure chemical shifts are comparable between samples. A key advantage of NMR is that it is a non-destructive technique and therefore the same sample can be used for further analyses. Recent studies have also collated NMR and MS analyses to increase coverage of the metabolome, especially for metabolites which don't readily ionise.[87] NMR is also inherently quantitative, as signal intensity correlates directly with sample concentration and

therefore sample and matrix specific calibration curves are not required.[75] Multi-dimensional techniques in NMR allow highly selective experiments, such as correlation spectroscopy, to be performed and have been used for the analysis and classification of tumours with IDH1 and IDH2 mutations as well as the enantioselective detection of 2-HG.[47, 88] The specificity of NMR is highly diagnostic and magnetic resonance imaging has been used *in vivo* for the quantification of 2-HG in glioma with IDH1 and IDH2 mutations.[89]

Targeted metabolomics is an inherently sensitive technique, as analytical conditions are optimised for a predefined set of metabolites.[90] Analytical quality is also maintained by adherence with guidelines from various regulatory bodies, including instrument precision, lower limit of detection (LLoD), lower limit of quantification (LLoQ), and linearity.[91] In MS, authentic standards are analysed at a range of concentrations on the same instrument and calibration curves prepared, to allow absolute quantification of metabolites. Data can therefore be collected from the authentic standards to allow the matching of accurate *m/z*, isotopic pattern and fragment ions, if tandem mass spectrometry (MS/MS) data is collected. Hyphenation to LC also allows retention time (RT) to be used as an additional identification parameter. A confidence scale for metabolite identification has been recommended from 1-5, where the lowest certainty identification (level 5) only includes accurate mass measurement, which allows database searching.[92] Increased certainty is provided by orthogonal information, for example, level 2 (putative) identification involves identification based on comparison of physiochemical properties including RT and fragmentation pattern matching with spectral libraries.[93] The highest certainty in identification (level 1) is provided by comparison with data acquired for an authentic metabolite standard on the same instrument.[92]

A targeted approach is by definition, focussed on specific metabolites of interest and therefore important changes in other pathways and metabolites, which may be useful targets or biomarkers, can be missed. In a targeted workflow, an inclusion list can be used to ensure fragmentation data is collected for analytes with specific *m/z*, which can then be used to confirm identification. Fragmentation patterns can be compared with previously acquired spectra from an authentic standard analysed on the same system, or with predicted spectra obtained from *in silico* fragmentation. Untargeted workflows can also utilise an *m/z* inclusion list to collect MS/MS spectra however, this expends duty cycles collecting fragmentation data for analytes which may not be present and therefore doesn't make efficient use of scan time. A more common approach is data-dependent acquisition (DDA), where a number of ions in full scan spectra are isolated and fragmented.[94, 95] This approach requires a balance of full scan acquisition time and the number of MS/MS spectra which can be acquired, while still maintaining the required number of full scan spectra across a chromatographic peak to ensure reliable quantitation. This approach is biased towards the most abundant ions which may be highly abundant species, easily ionised metabolites or even solvent impurities. DDA is therefore less useful for untargeted metabolomics, as the majority of analytes will not have MS/MS spectra associated with them and consequently this additional information will not be available for metabolite identification. If fragmentation spectra are required (to ensure positive identification) then samples may have to be analysed again with an inclusion list, to guarantee that MS/MS spectra are obtained for low abundance species.

Data-independent acquisition (DIA) of MS/MS spectra is becoming more widely adopted; this approach fragments all ions across the MS scan range and therefore fragment ions

for all analytes are present in the acquired MS/MS spectra. The disadvantage of DIA is that the fragment ions are not unique to a specific precursor and therefore, the collected MS/MS spectra are not as reliable for spectral matching. There are however, various approaches to increase this specificity for example, MS^E SONAR™ (Waters, Milford, MA, USA) moves a fixed isolation window across the quadrupole and then records the data as two channels, at high and low collision energy. The arrival time of the precursor and fragment ions, to the TOF stage of the MS, can therefore be used to computationally assign fragment ions to their precursor.[96] The width of the quadrupole isolation window is directly related to the specificity of the assignment of fragment to precursor ions. A smaller isolation window increases confidence in precursor matching, but requires longer acquisition times which negate the previously discussed speed advantages of DIA. The MS/MS spectra produced by MS^E SONAR™ have reduced spectral noise than conventional DIA approaches and consequently increase confidence when comparing an acquired fragmentation pattern with library spectra.

Untargeted metabolomics aims to measure as much of the metabolome as possible and hence provide information about relative changes in the abundance of individual metabolites.[97] This holistic approach is a powerful discovery tool with potential for investigating the effects of gene mutations on cellular small molecule chemistry, both *in vitro* and *in vivo*.[4, 98] Typically untargeted metabolomics is used to find biomarkers of a particular disease in a discovery-led approach; identifying pathways which can then be further investigated using complementary techniques such as proteomics, to provide mechanistic insights into metabolic change.[5, 7, 78] The complexity and size of data acquired from untargeted approaches requires data processing techniques such as univariate and multivariate statistical analysis, to elucidate trends in the data.[99] Univariate statistics, as

the name suggests, evaluates each variable in isolation. For metabolomics this is usually ion abundance or peak area and therefore univariate statistical analysis provides useful tools, such as analysis of variance (ANOVA), for the comparison of the same ion across multiple samples. Multivariate statistics analyses multiple variables simultaneously and can therefore be used to perform regression or correlation analysis. Visualisation of data using principal component analysis (PCA), demonstrates reproducibility of analysis and whether variables contribute to statistical differences between experimental groups.[100] Statistical models can also be generated from a dataset, to identify variables which are prognostic of an experimental group, and are an effective technique for hypothesis-generating approaches and biomarker discovery. Multivariate statistical analysis is particularly beneficial for high throughput analysis, as it does not require metabolite identification and can therefore be used for biomarker discovery in large datasets, obtained from untargeted analysis.[101] Potential biomarkers can subsequently be confirmed with targeted analysis and the biological significance investigated. Although care must be taken when using statistical methods to analyse data, as it is possible to over-fit data, or use an unsuitable technique, if the wrong assumptions are made for the generation of a model from a data set.[102]

1.4. Liquid chromatography for metabolomics

In metabolomics applications, untargeted LC-MS methods are increasingly being used for biomarker discovery and to investigate the metabolic effects of pharmacological interventions, as LC provides selectivity by RT and sensitivity of analysis by MS detection.[103-105] The most common separation methods currently used for LC-MS metabolomics are reversed-phase chromatography (RP) and hydrophilic interaction

chromatography (HILIC).[106] RP is ubiquitous in LC-MS analysis due to its reproducibility, wide range of stationary phase chemistries and ease of use.[107] RP-MS is typically used for the analysis of lipids and other low and medium polarity metabolites. Most mobile phase gradients for RP-MS start with high aqueous component and therefore polar and ionic metabolites are not well characterised, as they elute with, or close to, the solvent front. Polar and ionic metabolites are consequently not separated from one another by RP and will simultaneously compete for ionisation, resulting in lower sensitivity, if MS detection is used.[108]

Improved retention of polar analytes using RP can be achieved with the use of ion-pairing reagents. Ion-pairing reagents allow the retention of polar analytes on an RP column, using an additive with a polar head group and a non-polar tail. The ion-pairing reagent therefore binds strongly to the stationary phase of the column and provides a surface which can interact with polar metabolites and increase retention.[109] Selectivity of analysis can be controlled, using ion-pairing reagents with functional end-groups and have previously been used for the analysis of metabolites such as TCA cycle intermediates and amino acids.[110, 111] Improvements in stationary phase chemistry and the use of mixed-mode columns has reduced the use of ion-pairing reagents, as they have a number of disadvantages. Typically ion-pairing methods have slow equilibration times and therefore mobile phase gradients are not commonly used, which increases chromatographic run time. The dual functionality of ion-pairing reagents means that they readily bind to LC and MS components and require extensive washing to remove.[112] Ion suppression in ESI can also be caused the high concentration of ion-pair adducts with background small molecular weight species, such as metal ions.

HILIC is commonly used for the analysis of polar compounds, due to its solvent compatibility with MS and relatively fast speed of analysis. The technique requires extensive column equilibration, so that an aqueous layer is constantly maintained on the stationary phase, as well as pH balancing of mobile phases. HILIC utilises a hydrophilic stationary phase such as amide or diol modified silica to retain polar and ionic metabolites. A buffered hydrophobic mobile phase, with an increasing gradient of an aqueous phase is used to overcome the interactions of polar analytes with the stationary phase. The mechanism of retention is complex and a number of different mechanisms have been postulated; however, the most widely accepted mechanism is the formation of a semi static water layer on the surface of the stationary phase.[113-115] The adhered water layer allows stronger interactions of the analytes with the stationary phase than would normally be possible, at high organic mobile phase conditions. The increased interest in HILIC for LC-MS metabolomics has resulting in increased number of stationary phases being developed, bare silica as well as amide and zwitterionic end-capped stationary phases show the most promise for metabolomics.[116] This is due to their chemical selectivity for a range of metabolite classes and stability across a range of pH values. The mobile phases are similar across these stationary phases, normally only varying in pH and buffer concentration, to ensure optimal interactions of the analytes with the stationary phase. HILIC is therefore complementary to RP, as it retains polar and ionic analytes, however, stationary phases are selective for specific metabolite classes and therefore multiple analyses may be required to ensure sufficient pathway coverage for comprehensive analysis. The inter- and intra-analysis reproducibility of HILIC, for both RT and peak area, has been shown to be worse than RP, but conditions can be optimised in targeted approaches.[117] Poor column conditioning or insufficient re-equilibration time

after each injection can lead to depletion of the water layer, which drastically reduces RT reproducibility, and is therefore detrimental to efficient data processing and metabolite identification. The injection solvent used for HILIC must be compatible with the composition of the mobile phase and gradient, to achieve acceptable chromatographic peak shape. For example, an injection solvent which is entirely non-polar can deplete the adsorbed water layer and an aqueous solvent can reduce the movement of analytes into the water layer, causing early elution. Hydrophobic solvents are also not ideal for the extraction of polar and ionic metabolites from biological material. If a predominantly aqueous solvent is used, to ensure efficient extraction of polar metabolites, the samples must be dried down and resuspended in a compatible injection solvent. This dry down step can cause the degradation, or even loss, of labile metabolites and increase analysis variability. HILIC is often used for the analysis of amino acids and their related metabolites as it has good mobile phase compatibility with MS however, the zwitterionic properties of amino acids can result in lower sensitivity compared with metabolites with fixed charge. Specific amino acid methods have been reported with chromatographic run time between 15-25 minutes (min) and peak widths of around 30 seconds (s); however, these methods suffer the disadvantages of other HILIC methods, including RT variability and chemical specificity for certain analyte functionalities.[118, 119] HILIC methods are suitable for routine targeted analysis, such as the quantification of essential amino acids; however, have limited application to untargeted analysis, due to lower sensitivity and RT variability. Despite these issues, HILIC is the most widely used LC method for the analysis of polar metabolites and the range of stationary phase materials allows highly specific methods for targeted metabolic analysis. Biological material and fluids have the added complexity of a wide range of analyte concentrations, as well as challenging matrices, and

therefore a more robust and sensitive method than HILIC would be of benefit to the field of metabolomics.

Capillary electrophoresis (CE) can also be used for the separation and identification of ionic metabolites.[120, 121] The technique separates ions based on their electrophoretic mobility in solution by applying a voltage to a silica tube, containing the solvated sample, and therefore does not resolve neutral species. The viscosity of the buffered solution within the capillary, and the applied voltage, can be varied to vary the movement of the ions through the capillary, separating metabolites based on their charge and size, providing fast separations (typically < 10 min). The Van Deemter equation describes the factors which influence the theoretical plate number of a column, based on column length, particle size, packing quality, flow rate, instrument quality and retention factor and can be used to compare column quality and separation power.[122] Theoretical plate number, an index which indicates column efficiency (according to plate theory), is based on the diffusion coefficient of the analyte, compared to the mobility of the solution, CE has very narrow peak widths and therefore high chromatographic resolution.[123] Small sample volumes can also be used for CE (typically nanolitre), as the capillaries are very narrow, and therefore CE-MS is the predominant technique for single cell metabolomics.[124] For MS detection, a specific interface is required as the flow rates used for CE are lower than those typically used for ESI. The simplest solution is to use a make-up flow of volatile solvent to aid ionisation, however as this method dilutes the analyte, sensitivity can be reduced. Advances in nanospray ionisation have also been incorporated in more recent source designs.[125] ESI also requires a voltage at the emitter end of the capillary to facilitate ionisation and therefore either a lined stainless tube capillary or a sheath which surrounds at the tip of the capillary is required. As CE only

separates ionic metabolites, its coverage of metabolic pathways is hindered and is therefore not further investigated for untargeted metabolomics.

1.5. Ion chromatography for metabolomics

Recent advances in eluent suppression technologies for ion chromatography (IC) and hyphenation to MS has enabled polar and physiologically ionic metabolites to be measured in biological matrices.[126] Polar molecules such as the TCA cycle metabolites, including the oncometabolite 2-HG, have been challenging to analyse using traditional chromatographic techniques, such as HILIC, due to their similar chemical functionality and close molecular weights. RT instability and reduced sensitivity for analysis by HILIC-MS has also been observed, as discussed in Section 1.4.[117-119] Consequently IC-MS presents an opportunity for the development of new methods for targeted and untargeted analysis of polar and ionic metabolites, especially in central carbon metabolism and related pathways.

Conductivity detection is traditionally used for IC analysis, as the analytes are already in their ionised form.[127, 128] Conductivity detection is a bulk physical property measurement of the eluent and any ions, in the detector cell. The total conductivity is measured capacitively by measuring the electrical impedance between two electrodes placed within the eluent flow path. As ions pass between the two electrodes, the resistance of the circuit is altered based on the concentration of ions, which can consequently be used as a detection method. As conductivity detection is not a selective detection technique, it was not pursued for untargeted metabolomics.

To date, the application of IC analysis to metabolomics is relatively rare and requires eluent suppression for hyphenation to MS. The pH range required for the separation of

analytes in IC is not compatible with ESI, as high ion concentration can supress ionisation and high concentrations of salts can cause source degradation of source conditions. A method of neutralising pH of the eluent and removing counter ions before MS detection is therefore required. For IC-MS a suppressor containing ion-exchange membranes is used, as shown in Fig. 1.4. Ion-exchange membranes are used to separate the eluent path from two electrodes with constant water flow. The electrodes allow the production of hydroxide and hydronium ions, dependent on the polarity of the electrode, evolving hydrogen or oxygen gas as by-product of the process. Only small ions can cross the membrane, in this case for anion-exchange, the hydronium ions can associate with the analyte anions and any counter ions are attracted by the hydroxide ions and therefore removed from the eluent stream. The use of a suppressor to remove counter ions, as well as allowing hyphenation to MS, also decreases background noise and increases analyte conductivity by association with the highly conductive hydronium ion. The specificity of conductivity detection is also increased by ion suppression as the conductivity of the eluent is consequently only dependent on the analyte ions.

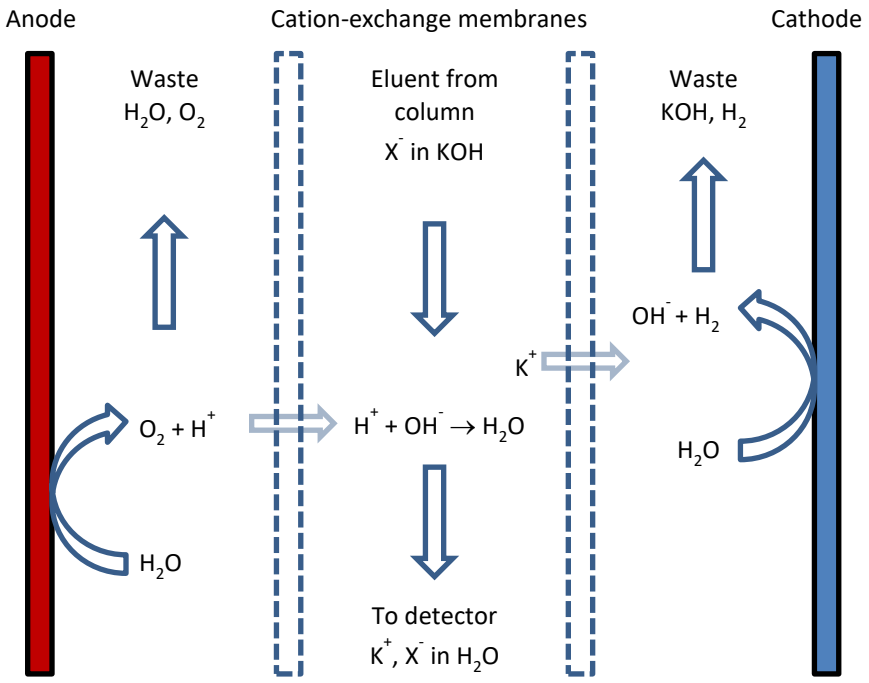

Figure 1.4: Schematic of an ion suppressor, used to remove counter ions from the eluent stream and allow the hyphenation of anion-exchange chromatography to MS.

IC also has highly reproducible chromatographic conditions due to on-line mobile phase preparation by an eluent generator. A concentrated stock solution is contained in the eluent generation cartridge and (as for the suppressor technology mentioned previously), is separated from the eluent path by an ion-exchange membrane. An electrode is present either side of a membrane which electrolyses water into hydroxide and hydronium ions based on the electrode polarity. The selective membrane prevents the two species from reverting to water and therefore a counter ion from the stock solution is drawn across the membrane to form the eluent. The concentration of the eluent is therefore dependent on the voltage applied to the electrodes and is therefore precise and reproducible. Common eluents used for IC are potassium hydroxide, as a source of hydroxide ions for anion-exchange chromatography, and methanesulphonate, to produce methanesulphonic acid eluent for cation-exchange. Stationary phases have to be chemically resistant to pH change, due to the extreme pH values required for analyte separation. Polymeric resin

particles or end-capped silica particles with permanently ionised functionality are typically used.[129, 130] As the stationary phase is ionic, IC has high matrix tolerance as separation is only based on ionic strength and therefore other separation modes such as partitioning are minimised. Robust column chemistries and an aqueous mobile phase means that injection solvent does not cause any detrimental effects to chromatographic performance and therefore range of solvents (or even mixed solvents) at high or low pH can be used as metabolite extraction solvents.

To date, IC-MS has only been demonstrated for targeted metabolomics, initially by Wang *et al.,* using capillary IC-MS for the analysis of 41 anionic metabolites in stem-like cancer cells.[131] This was followed by the quantification of 45 metabolites in yeast cells, using internal standards and an isotope dilution method.[126] These studies demonstrate the potential for analysis of the polar metabolome, using IC-MS, and the discovery of new biomarkers of disease, due to highly reproducible chromatographic conditions and wide matrix and solvent compatibility.

1.6. Derivatisation for metabolomics

Analysis of metabolites with amine functionality remains a challenge for both targeted and untargeted analysis by LC-MS, as many of these metabolites share similar chemical functionality. Analytes with amine functional groups are often zwitterionic and consequently aren't easily separated using routine chromatographic techniques such as RP.[132] Zwitterions can accommodate positive and negative charges based on the pKa of their functional groups. The behaviour of the analytes can therefore change when removed from their physiological environment, attenuating ionisation by ESI. Chromatographic performance can also be severely reduced, particularly in the analysis of

complex mixtures, if the mobile phase and extraction solvents are not buffered to be compatible with the pKa values of the analytes.[118]

Derivatisation of specific functional groups is widely used in GC-MS for targeted and untargeted analyses, where it is used to change the physical properties of the analytes of interest, to make them more amenable to retention and MS analysis.[133-135] Derivatisation is not used as frequently for LC analysis, especially in metabolomics, despite the potential for increased selectivity and sensitivity of analysis.[136, 137] Esterification of metabolites with carboxylic acid functionality, such as fatty acids, is typically performed prior to analysis by GC-MS and has also been demonstrated for LC-MS analysis.[138] Esterification is used to introduce a permanently charged amide group and has been shown to increase sensitivity of MS detection by up to $6x10^4$-fold.[138] Esterification of hydroxyl groups has also been demonstrated for LC-MS analysis of adenine bases, ribosides and nucleotides, to enhance ionisation efficiency and improve analyte retention.[139] Increased sample preparation is required for derivatisation, which can introduce errors and variability between samples.[140] Stability of the derivatisation must also be considered as the derivatised species can degrade over time for example, by hydrolysis.[141] An additional problem is that the extent of derivatisation in complex mixtures is not usually known; however, the enhancement of selective metabolite classes is beneficial for targeted analysis.

Phenylisothiocyanate is typically used for the sequencing of amino acids in a peptide but can also be used for the derivatisation of free amino acids, with an uncharged amine group and subsequent targeted analysis using RP chromatography hyphenated to ultraviolet absorption detection or MS.[142] Phenylisothiocyanate derivatisation suffers from a relatively long derivatisation reaction time (up to 10 min) and poor separation of

certain amino acids, such as valine and methionine as well as isoleucine and leucine.[142, 143] Salt tolerance is another limitation of pre-column derivatisation with phenylisothiocyanate, resulting in reduced detection of aspartic acid and other acidic amino acids and is therefore not an ideal method for untargeted analysis of amine metabolites in complex biological samples.[144]

6-aminoquinolyl-N-hydroxysuccinimidyl carbamate (AQC) is a commercially available derivatising reagent that protects 1° or 2° amine groups, subsequently increasing chromatographic retention under RP conditions (as described in Section 8.7), and to date has not been applied to untargeted metabolomics. The derivatisation reaction is a nucleophilic attack of the carbamate ester group on AQC by an amine, producing a stable urea and a side product of N-hydroxysuccinimide (NHS), as the leaving group. This results in increased sensitivity as the derivatised urea species is not zwitterionic and therefore more volatile and readily protonated in positive ESI. As shown in Fig. 1.5, the derivatisation reagent reacts with the amine group, undergoing a substitution reaction with a reaction time of < 1 s. This derivatisation relies on the removal of a proton from the nitrogen centre so any 1° or 2° amine can act as a nucleophile and therefore any metabolite which has an 1° or 2° amine functional group can be analysed.[141] These 1° or 2° amines are ubiquitous in biological systems due their use in DNA, RNA and protein synthesis as well as their use as signalling molecules and neurotransmitters.[145]

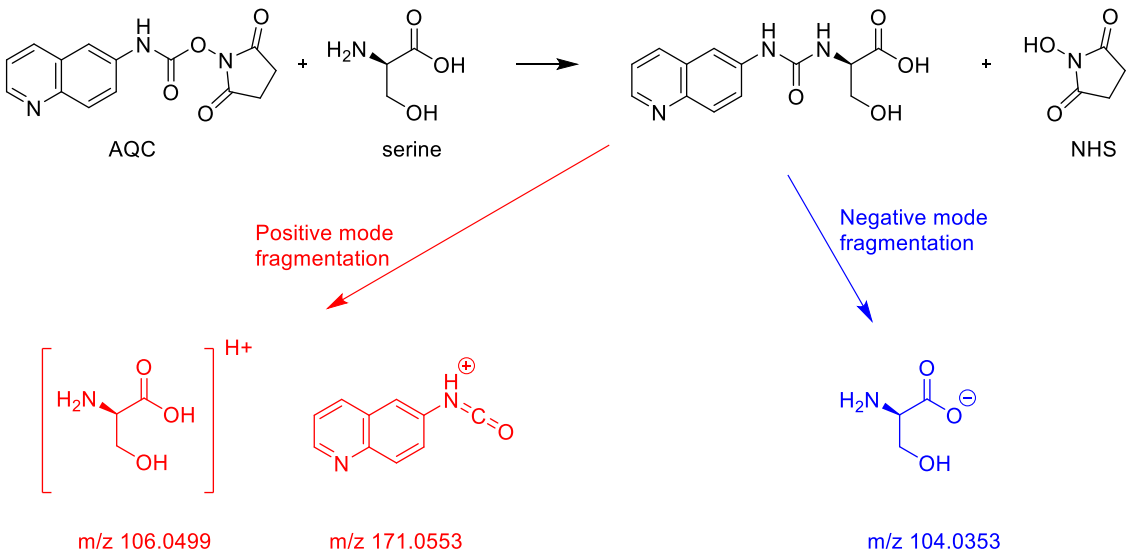

Figure 1.5: AQC derivatisation reaction and fragmentation products of serine in both positive and negative ion modes.

The derivatisation reaction can be monitored, as the reagents and products are all amenable to identification and quantification by LC-MS. Excess AQC reagent is slowly (15-30 s) hydrolysed into 6-aminoquinoline (AMQ), NHS and CO_2. The concentration of reagent can be adjusted to ensure that AMQ is present and therefore a complete reaction has occurred, with all 1° or 2° amines present in the sample. The use of a borate buffer as part of the sample preparation maintains an optimum pH for derivatisation, between 8.2-10.0.[141] Borate can form metal ligand complexes with metabolites, particularly those with diol functional groups such as carbohydrates and nucleotides; however, this will not disrupt the detection of the derivatised amine species as complexes are readily ionised by ESI.[146, 147] It has also been demonstrated that the presence of the borate buffer reduces the oxidative degradation of the derviatised products and therefore increases the reproducibility of analysis for the AQC derivatisation method.[145] The ring system in AQC is UV absorbent and fluorescent and therefore the derivatised analytes can also be detected using non-mass spectrometric techniques if the

derivatised product does not ionise readily.[141, 148] In addition to increased sensitivity, derivatisation with AQC allows fast chromatography using a high flow rate (0.70 mL / min).[149] The method utilises a C18 RP column and therefore has the benefits of using aqueous solvents and a robust hydrophobic stationary phase, as described in Section 8.7. The combination results in peak widths of less than 20 s for a range of amino acids, as shown in Fig. 1.6, and a total run time of 12.5 min including column wash and equilibration steps. The narrow peak width also results in a high chromatographic resolution, consequently reducing competitive ionisation and matrix effects. Of particular note is the chromatographic separation of isobaric species, such as the structural isomers leucine and isoleucine (Fig. 1.6(c)), which are baseline separated by the method.

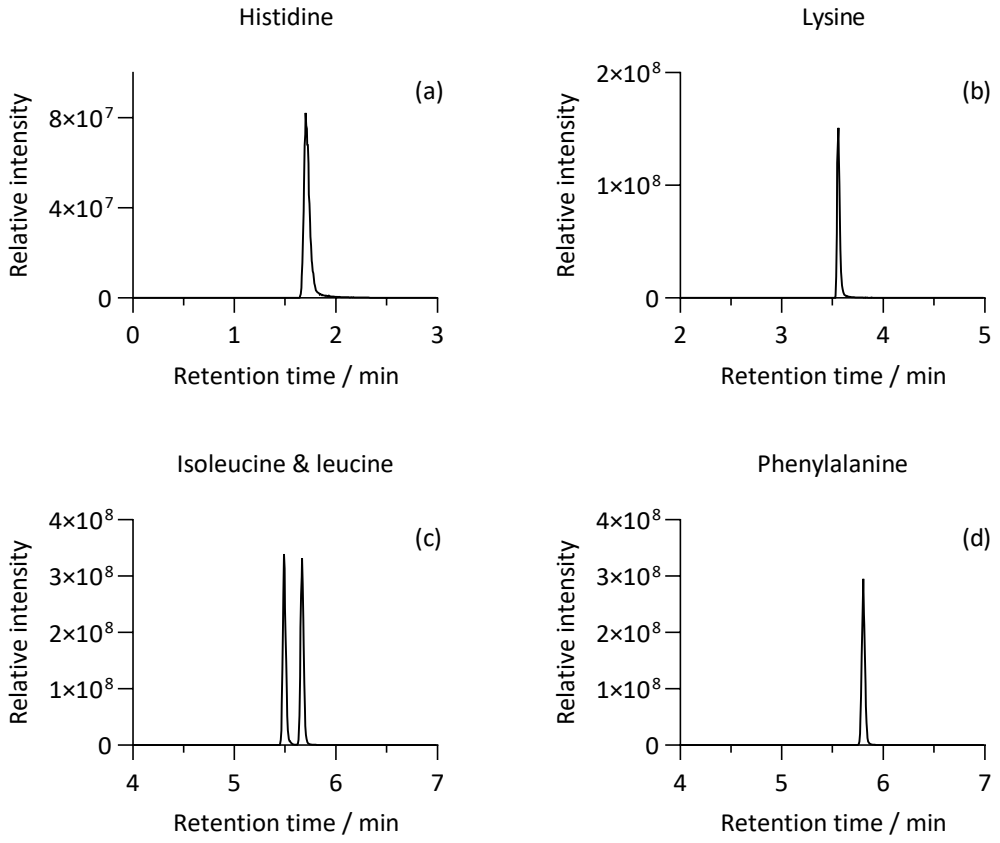

Figure 1.6: Extracted ion chromatograms for AQC derivatised histidine (a), lysine (b), isoleucine / leucine (c), and phenylalanine (d).

1.7. Ion-mobility spectrometry for metabolomics

Ion-mobility spectrometry (IMS) is an analytical technique which separates ions in the gas phase, based on their collisional cross section (CCS). This CCS value is a rotational average of the ion, corresponding to its size and structure. An ion with a larger CCS will take longer to pass thorough a gas, as shown in Fig. 1.7. For example, two structural isomers with the same *m/z* can be separated by structural differences, resulting in distinct CCS values.[150]

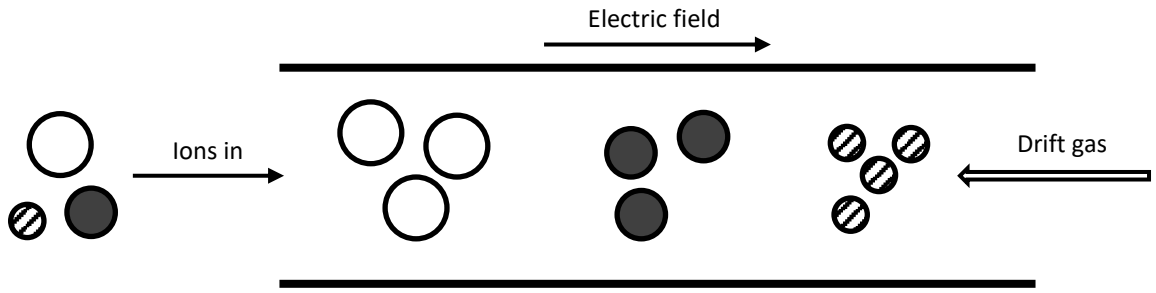

Figure 1.7: Schematic showing the movement of ions with various CCS values though a drift gas, moved by an electric field.

The drift time (the time taken for an ion to pass through the ion-mobility cell) is correlated to the ion's *m/z* value, as shown in Fig. 1.8. Branching in backbone structure, elemental composition and functional groups can also influence the CCS of an analyte. Polar or ionic functionality will result in a smaller CCS, due to increased charge density on those functional groups and therefore smaller volume occupied by those atoms. The CCS of an ion is characteristic of a specific analyte and orthogonal to its *m/z*, and can therefore be used as an additional identification parameter.

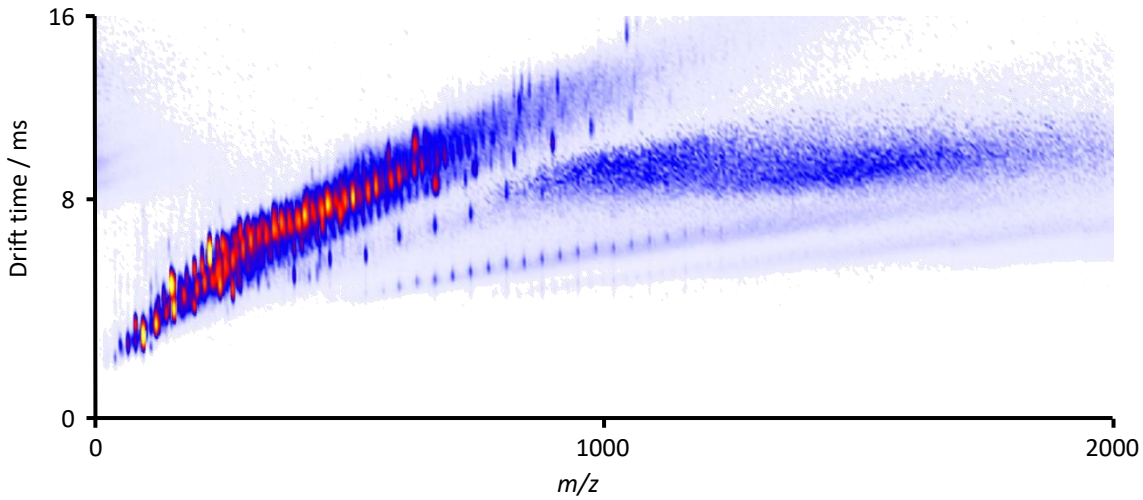

Figure 1.8: Ion-mobiligram showing the relationship between drift time and *m/z* for the analysis of a derivatised metabolite extract from 293T cells (Section 8.8).

The CCS of an analyte can be obtained in 2 ways, experimentally by measurement using an appropriate ion-mobility instrument or computationally, using molecular modelling. Although the drift time of an ion is specific to variables such as drift gas composition and pressure, the CCS value calculated using the Mason-Schamp equation is instrument independent.[150] Typically, instruments use a fixed length drift tube, constant gas pressure and electric field, and therefore the CCS can be calculated directly from the drift time. The precision of this approach is predominantly influenced by the length of the drift tube and therefore physically large instruments are required. An alternative approach for IMS is the travelling wave (T-wave) method, where the applied electric field is varied, to separate ions using a shorter drift tube. The T-wave method uses an RF signal along a stacked ring ion guide; by applying a voltage to each electrode in turn, a travelling electric field is produced which propels the ions through the drift tube. This electric field can be optimised for specific analytes by altering the shape of the RF signal, as well as the number of electrodes which have a voltage applied to them in each cycle.[151] The electric field used for the IMS cell in the Vion IMS QTof (Waters, Milford, MA, USA), used for the experiments described in this thesis, has been tuned to achieve effective mobility

separation, within the duty cycle of a TOF-MS system and therefore can be coupled to LC without any loss of MS performance. CCS calibration using authentic standards can also be performed across the *m/z* and CCS range to allow accurate CCS values to be experimentally determined using a T-wave approach.

Metabolite libraries that include CCS values, provide additional information that can increase confidence in the identification of unknown metabolites. For example, the Online Collision Cross Section Compendium, produced by the McLean Research Group, has experimentally-derived CCS values for over 3800 biochemical molecules, with various adducts and a range of charge states.[152] As CCS values are independent of instrumentation, the values in the McLean compendium can complement current databases, which already contain RT and formulae, or can be used to confirm CCS calibration. If the CCS value of a metabolite of interest is not already in a database, or is not available as an authentic standard, then a number of theoretical approaches can be used to predict a CCS value. The McLean group has divided their compendium into 157 subclasses across a range of *m/z* values and then used regression fitting to predict correlations between CCS and *m/z* based on analyte functionality. This can consequently be used to predict a CCS value, within a confidence band, or to help identify an unknown ion from its CCS and *m/z*. Molecular modelling can also be used to predict CCS values, but is a computationally intensive approach, requiring significant time or extensive computational resources to calculate accurate values. Molecular modelling utilises a range of calculation types to predict the positions of atoms within a structure and therefore a corresponding CCS value. These calculations are optimised for specific applications and are also highly dependent on the energy minimised structure (which is used as the starting point), as well as the localisation of charge within a structure.[153]

The process of generating theoretical CCS values is computationally intensive and time-prohibitive for the identification of unknown analytes, in most contexts, as multiple species (based on each predicted chemical formulae), would need to be modelled. Another limitation of molecular modelling is that currently there is no approach which can be used to predict a structure from *m/z* and CCS values. More recently, machine learning has been applied to the calculation of CCS values, using a support vector regression algorithm to build a model using data from databases.[154] CCS values can therefore be predicted from chemical structure more quickly than from molecular modelling and with adequate precision (ca. 3 %) when compared with experimental values.

1.8. Research Summary

The metabolic impact of an IDH1 mutation, to date, has not been extensively studied and insight into the phenotype associated with Mut cells is of clinical interest for the development of targeted therapeutic strategies. The analysis of central carbon metabolism and related pathways is beneficial for all cancer types. The polar and ionic metabolites present in these pathways are not well characterised by current methods, such as RP-MS and HILIC-MS. The analysis of polar and ionic metabolites has only been demonstrated using IC-MS in a targeted approach. To date, IC-MS has not been used as for comprehensive untargeted, discovery-led metabolomics. Derivatisation can also provide selectivity for metabolite classes, such as amines, and increases sensitivity when used with LC-MS analysis. The development of new strategies to reduce sample complexity, in addition to LC, is also required for metabolomics, due to the high incidence of structural isomers in biological samples, which are not easily separated by standard

chromatographic approaches. It is therefore advantageous to have an orthogonal separation, such as drift time from IMS, to assist with isomer differentiation and to provide an additional identification parameter.

The research objective of this thesis, is the investigation of the metabolic effects of an IDH1 mutation, with a particular focus on glioma-derived cell lines. Mut and WT metabolism will be characterised across different cell lines using multiple chromatographic techniques coupled to MS, to ensure comprehensive metabolic coverage. The ultimate aim of this research is to identify new areas of metabolism which are modified by an IDH1 mutation, and investigate whether these changes are driving tumourigenesis through metabolic effects such as the enrichment of 2-HG. If metabolite abundances are altered as a result of an IDH1 mutation, can the metabolite abundances in Mut cells be recovered to the concentrations observed in WT cells by therapeutic treatment. The analysis of polar metabolites is of specific interest and therefore IC-MS/MS will be developed as a technique for untargeted analysis of biological samples and this will be validated alongside conventional methods.

The following research questions will be investigated:

1. What LC-MS methods can be used or improved for the analysis of physiologically ionic and polar metabolites?
2. How can metabolite identification confidence be improved?
3. What is the metabolic impact of an IDH1 mutation and could this be influencing the process of tumourigenesis?
4. Can changes in metabolite abundance as a result of an IDH1 mutation be recovered in in Mut cells?

The research questions will be answered by investigation of the following aims:

- Establish and validate an IC-MS/MS method for untargeted metabolic profiling of cell samples.
- Compare performance of IC-MS/MS against an established HILIC-MS/MS method.
- Investigate the depth of metabolite coverage, by IC-MS, for the analysis of cell extracts, focussed on central carbon metabolism including anaplerotic and cataplerotic processes.
- Investigate changes in metabolism associated with an IDH1 mutation by comparison of Mut and WT cells.
- Identify specific enzymes and/or metabolic pathways in IDH1 mutant cells which could be potential therapeutic targets.
- Establish and validate a method for the analysis of metabolites with 1° or 2° amine groups.
- Investigate some of the advantages IMS-MS/MS can provide for metabolomics.
- Investigate changes in metabolism associated with IDH1 mutant cells.
- Identify pathway-level changes linked to an IDH1 mutation in multiple cell lines.
- Investigate the reproducibility of the observed metabolic effects across experimental replicates and multiple cell lines.

Chapter 2. Development and validation of IC-MS/MS for untargeted analysis of polar and ionic metabolites in cell extracts

2.1. Introduction

In this chapter, the development, validation and application of IC-MS/MS for untargeted metabolic analysis of cell extracts will be investigated. Some of the data analysed in this chapter, relating to optimisation of conditions, reproducibility and reliability has been published by the author.[155] Polar and ionic metabolites are insufficiently characterised using current LC-MS/MS techniques such as HILIC-MS/MS, and the application of IC-MS/MS to metabolomics is recent and has only been demonstrated in targeted analysis, of a relatively small number of metabolites.[126, 131] Organic acids and nucleotides have similar chemical functionality within their classes, and are essential for comprehensive metabolic analysis, as they are both intrinsically linked with cell cycle and cell division. The degradation and in-source fragmentation products of organic acids and nucleotides are isobaric with lower molecular weight species and therefore require chromatographic separation for accurate quantification using LC-MS/MS. Sugar phosphates are used for energy transfer in various biological processes and share a common chemical formula and therefore cannot be identified by MS alone. For example, hexose amines have been characterised by a range of HILIC-MS methods, but the analysis of hexose sugars and homologues remain particularly challenging.[156] An IC-MS/MS method for untargeted and targeted metabolomics was therefore developed, increasing coverage of these challenging metabolite classes, as well as delivering broad selectivity for other polar and ionic metabolites.

The research aims of this chapter were to:

- Establish and validate an IC-MS/MS method for untargeted metabolic profiling of cell samples.
- Compare performance of IC-MS/MS against an established HILIC-MS/MS method.
- Investigate the depth of metabolite coverage, by IC-MS, for the analysis of cell extracts, focussed on central carbon metabolism including anaplerotic and cataplerotic processes.

2.2. IC-MS/MS method development

A Dionex ICS-5000+ Capillary HPIC system (Thermo Scientific, San Jose, CA, USA) consisting of a dual pump, eluent generator, detector compartment and autosampler, coupled to a Q Exactive hybrid quadrupole-Orbitrap MS (Thermo Scientific, San Jose, CA, USA). The on-line eluent generation of the IC system enabled consistent and precise formation of aqueous potassium hydroxide eluent for anion exchange. The column selected was a Dionex IonPac AS11-HC (2 × 250 mm, 4 μm; Thermo Scientific, San Jose, CA, USA), for its high capacity and resolution for anions and organic acids, previously demonstrated for targeted analysis of TCA cycle metabolites using conductivity detection.[157] The column packing material comprised 4 μm particles of supermacroporous polyvinylbenzyl polymer, cross-linked with divinylbenzene and alcohol quaternary ammonium ion end-capping, providing a stable and pH resistant stationary phase, with hydrophobicity suitable for the adsorption of biological anions. For completeness, the experimental methods developed and applied in this thesis, are listed in Chapter 8, but for brevity throughout, Sections containing individual methods or

experimental conditions are referenced without further annotation, for example, IC-MS/MS (Section 8.4).

2.2.1. Optimisation of chromatographic conditions

In order to investigate the capability of IC-MS/MS for untargeted metabolomics, initial experiments were performed using a manufacturer recommended method for the separation of organic anions with an AS11-HC column; a hydroxide gradient between 1.0-60.0 mM and a total chromatographic run time of 60.0 min (for aqueous eluent or 50.6 min, with methanol supplemented eluent). Methanol was used as an additive to modify elution order and increase separation of specific inorganic anions; however, it was found to reduce the ionisation of organic acids and consequently the sensitivity of the method. The 60 min method was evaluated using mix of 170 authentic metabolite standards (listed in Table 10.1) and, as shown in Fig. 2.1, the total ion chromatogram (TIC) demonstrated resolved chromatographic peaks across the full length of the chromatographic run.

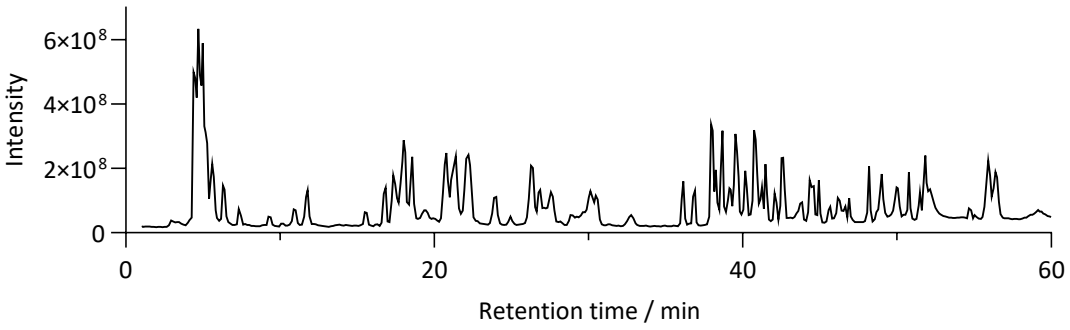

Figure 2.1: TIC of a mix of 170 authentic metabolite standards (listed in Table 10.1), analysed by IC-MS/MS using manufacturer recommended parameters.

The high intensity chromatographic peaks around 3 min, correspond to metabolites which were not retained by the column and eluted simultaneously after the void volume,

consequently a higher total ion count was observed. The 60 min method provided chromatographic resolution and separation for a wide range of metabolites, including sugar phosphates (which are challenging to resolve in biological samples by HILIC-MS) with the exception of galactose 6-phosphate (27.67 min), fructose 6-phosphate (28.83 min) and glucose 6-phosphate (29.64 min), which were not resolved. Fig. 2.2 shows the extracted ion chromatogram (EIC) for *m/z* 259.02244, which corresponded to the deprotonated ion of sugar phosphates, with common chemical formula $C_6H_{13}O_9P$. A range of gradients and run times were extensively explored and tested in order to increase analytical efficiency and chromatographic resolution. This led to a 37 min chromatographic method which maintained resolution for isobaric species and resolved glucose 1-phosphate (11.89 min, Fig. 2.2(b)(iii)) from the subsequent co-eluting sugar phosphates (Fig. 2.2(b)(iv,v)).

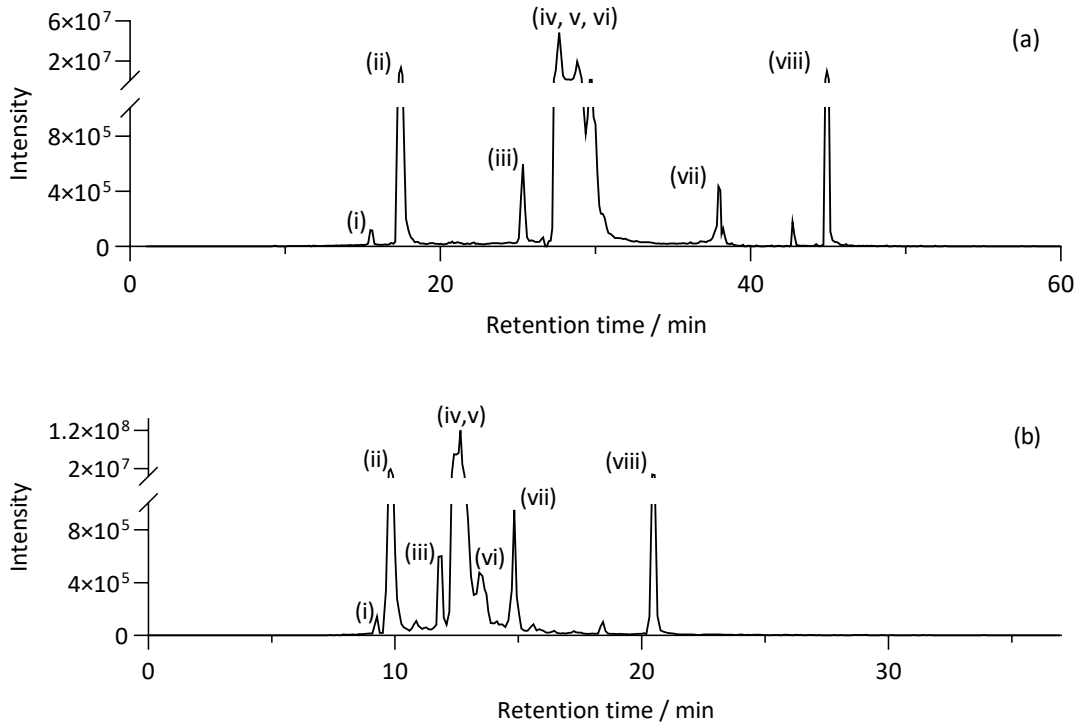

Figure 2.2: EIC for *m/z* 259.02244, from a mix of 170 authentic metabolite standards (listed in Table 10.1), analysed by IC-MS/MS using manufacturer recommended parameters (a) and by the optimised method described in Section 8.4 (b). The labels correspond to galactose 1-phosphate (i), fructose 1-phosphate (ii), glucose 1-phosphate (iii), galactose 6-phosphate (iv), fructose 6-phosphate (v) glucose 6-phosphate (vi), sorbose 6-phosphate (vii) and mannose 6-phosphate (viii).

Authentic metabolite standards containing the structural isomer pairs: citrate and isocitrate (Fig. 2.3, $C_6H_8O_7$, *m/z* 191.01973); adenosine monophosphate (AMP) and deoxyguanosine monophosphate (dGMP, Fig. 2.4, $C_{10}H_{14}N_5O_7P$, *m/z* 346.05581); glutarate and ethylmalonate (Fig. 2.5, $C_5H_8O_4$, *m/z* 131.03498), at a concentration of 5 μg / mL were analysed by IC-MS/MS using the 60 min and 37 min methods, and the EICs compared.

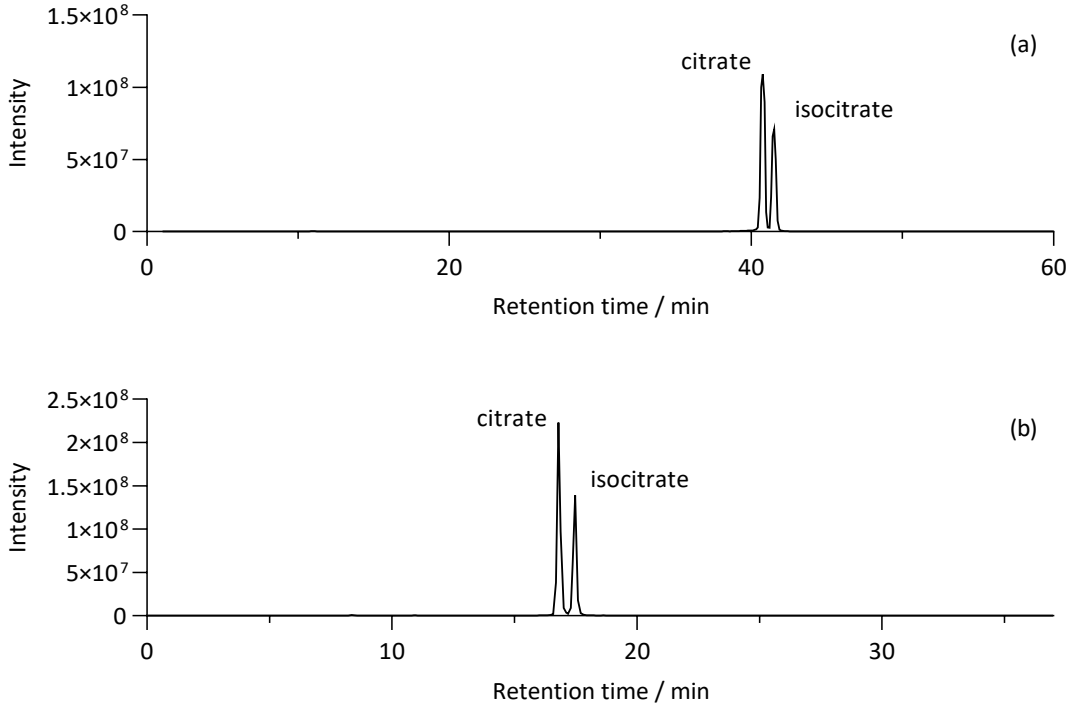

Figure 2.3: EICs for the isomers citrate (i) and isocitrate (ii) analysed by IC-MS/MS using the 60 min method (a) and the 37 min optimised method described in Section 8.4.

The TCA cycle structural isomers citrate and isocitrate (Fig. 2.3), were baseline separated using both methods and ion intensity was increased for the 37 min method. The lower intensity for the 60 min method was caused by peak broadening due to increased RT and a shallower hydroxide gradient. The resolution of the isomers was likely due to the hydroxyl group on citrate sharing the same carbon as one of the carboxylate groups, lowering the pKa and therefore reducing interactions with the stationary phase compared to isocitrate.

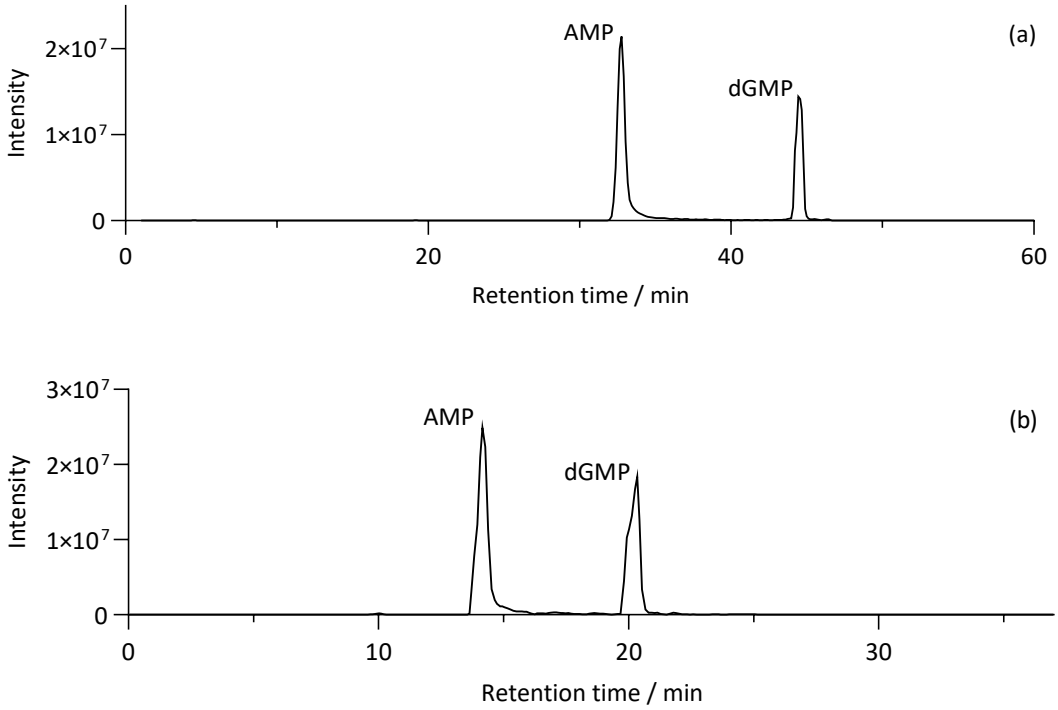

Figure 2.4: EICs for the isomers AMP and dGMP analysed by IC-MS/MS using the 60 min method (a) and the 37 min optimised method described in Section 8.4.

The nucleotide isomers AMP and dGMP (Fig. 2.4), were completely resolved using both methods. AMP is a critical energy pathway metabolite and has a regulatory role in various biological processes and therefore precise and accurate quantification is desirable. The baseline separation from dGMP therefore adds confidence for both identification and quantification. As observed for the isomers citrate and isocitrate (Fig. 2.3), the 37 min method also increased ion intensity and therefore sensitivity.

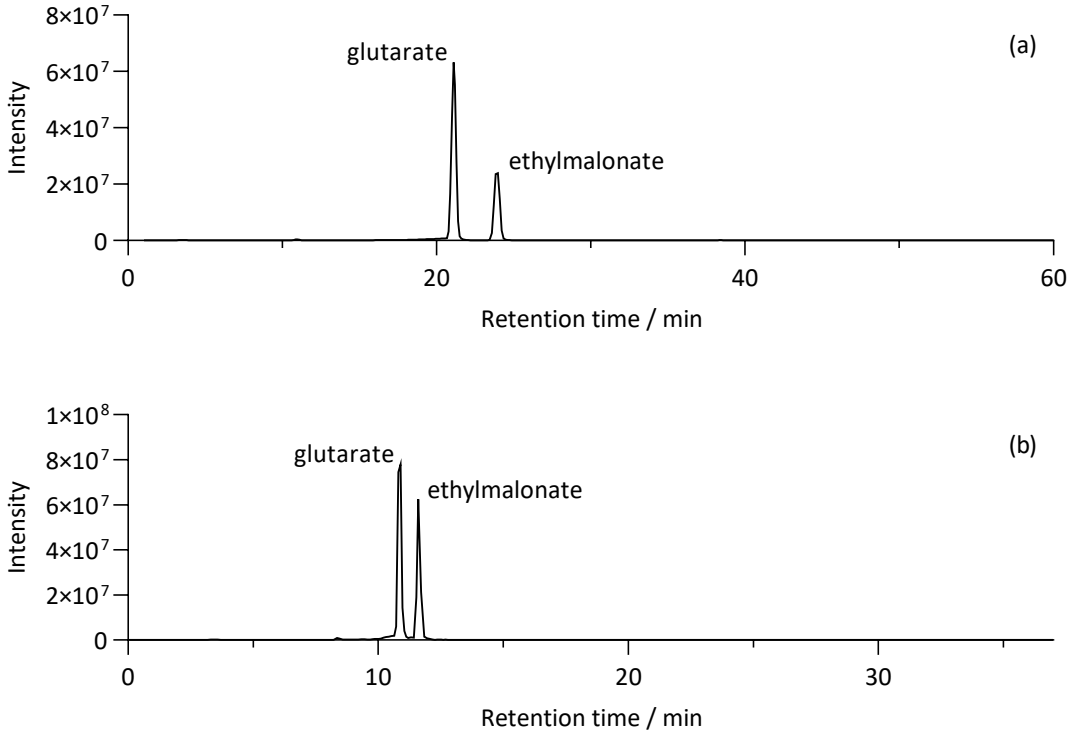

Figure 2.5: EICs for the isomers glutarate and ethylmalonate analysed by IC-MS/MS using the 60 min method (a) and the 37 min optimised method described in Section 8.4.

The greatest resolution for glutarate and ethylmalonate (Fig. 2.5) was observed using the 60 min method; however, baseline resolution achieved by both methods. The 37 min optimised method, described in Section 8.4, was therefore used for all subsequent IC-MS/MS analyses.

Column temperature was also optimised for chromatographic performance. Increased column temperature led to longer RT, likely caused by stronger interactions of the analytes with the stationary phase. Authentic metabolite standards containing the isomers citrate and isocitrate (Fig. 2.6); AMP and dGMP (Fig. 2.7); glutarate and ethylmalonate (Fig. 2.8) at a concentration of 5 μg / mL were analysed by IC-MS/MS (Section 8.4), with column temperature maintained at 20 °C or 40 °C.

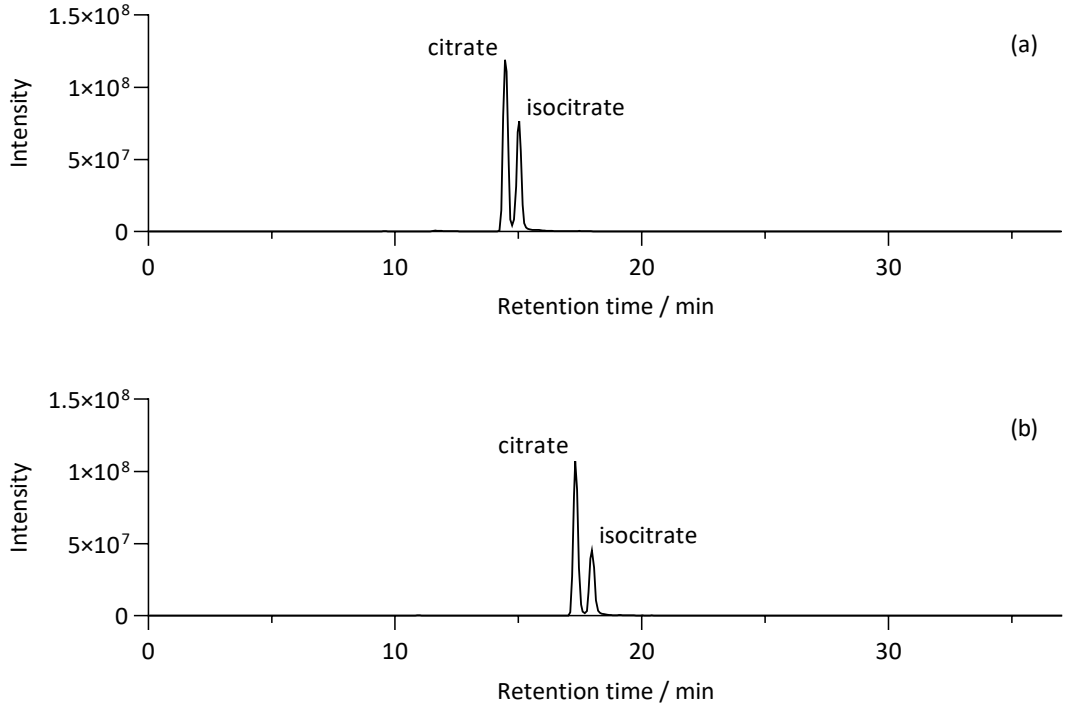

Figure 2.6: EICs for the isomers citrate and isocitrate analysed by IC-MS/MS with column temperature maintained at 20 °C (a) or 40 °C (b) using the optimised method described in Section 8.4.

At a column temperature of 20 °C, overlap was observed at the base of the chromatographic peaks for citrate and isocitrate (Fig. 2.6(a)). The resolution achieved at a column temperature of 40 °C was comparable to the resolution observed at 30 °C and therefore no benefit was observed from increased column temperature in this case.

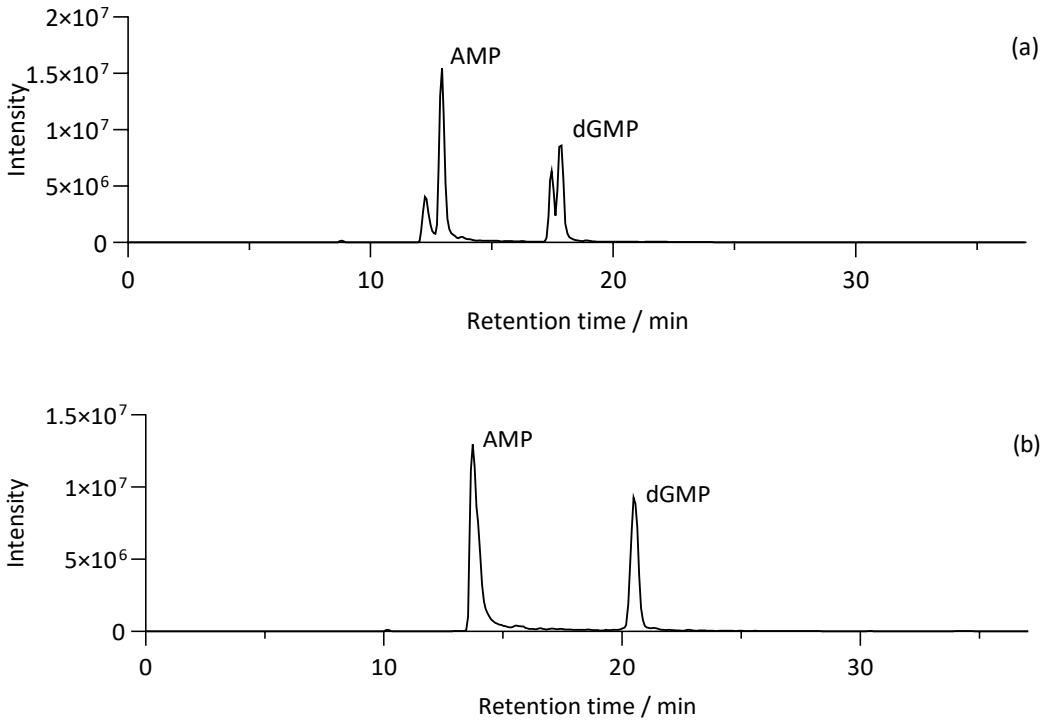

Figure 2.7: EICs for the isomers AMP and dGMP analysed by IC-MS/MS with column temperature maintained at 20 °C (a) or 40 °C (b) using the optimised method described in Section 8.4.

Peak splitting was observed for both AMP and dGMP (Fig. 2.7(b)), at a column temperature of 20 °C, possibly due to deprotonation of different functional groups or the resolution of different conformers. This observation could not be confirmed without structural analysis such as hyphenation of IC to NMR, using fraction collection. The peak splitting was observed to be temperature dependent and an optimal peak shape was achieved at a column temperature of 40 °C (Fig. 2.7(b)). As analyte retention increased with column temperature, improved resolution at higher column temperatures was at the expense of longer chromatographic run times.

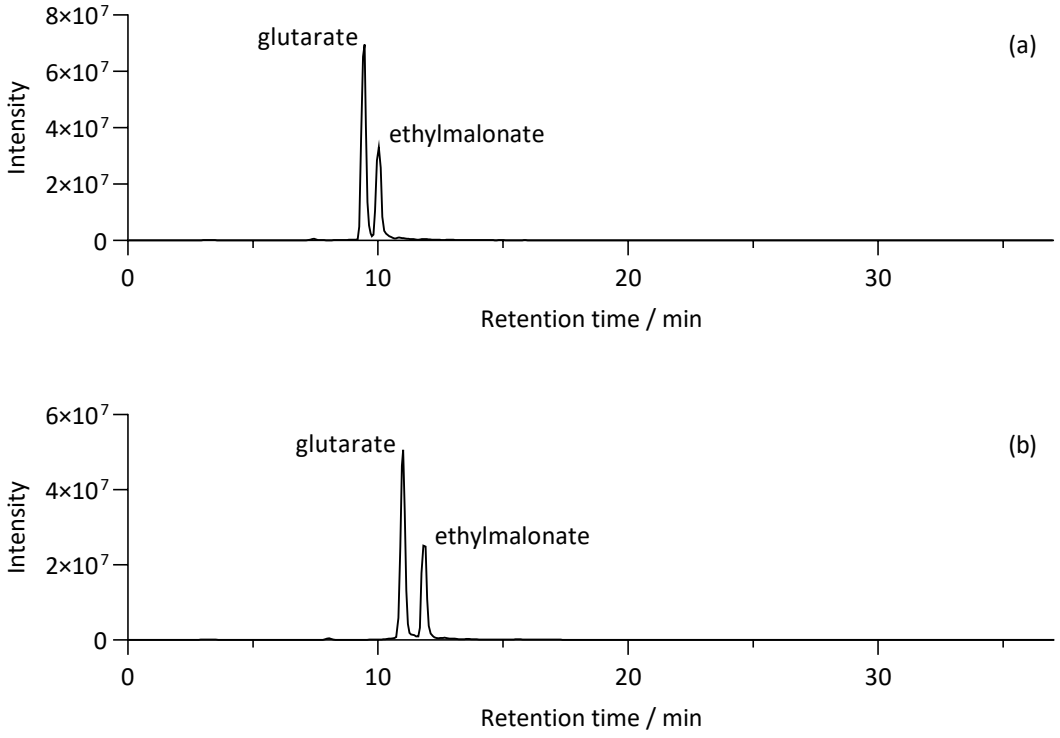

Figure 2.8: EICs for the isomers glutarate and ethylmalonate analysed by IC-MS/MS with column temperature maintained at 20 °C (a) or 40 °C (b) using the optimised method described in Section 8.4.

As observed for citrate and isocitrate (Fig. 2.6(a)), a column temperature of 20 °C caused minor chromatographic overlap of the isomers glutarate and ethylmalonate (Fig. 2.8(a)). Resolution at a column temperature of 40 °C (Fig. 2.8(b)) was comparable to that achieved at 30 °C (Fig. 2.5(b)). For sugar phosphates (Fig. 2.9), decreased column temperature increased chromatographic resolution but also caused overlap of previously separated isomers. Temperatures above 30 °C resulted in peak broadening and tailing for mannose 6-phosphate (21.35 min, Fig. 2.9(b)). A column temperature of 30 °C was therefore selected to provide an optimum balance between peak shape, resolution and speed of analysis.

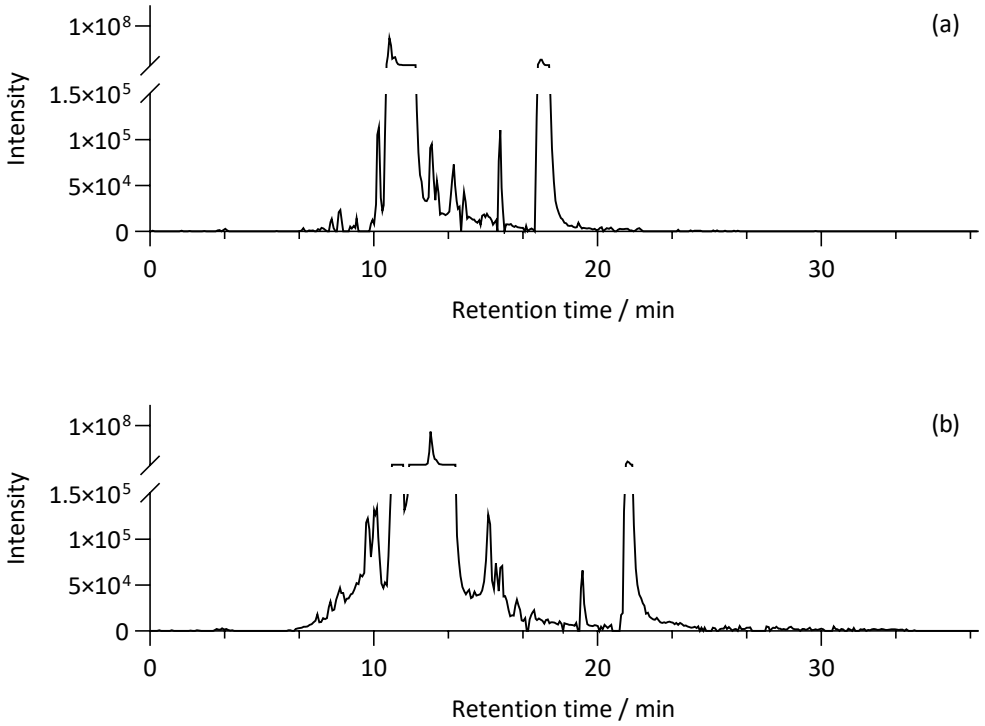

Figure 2.9: EIC for *m/z* 259.02244, from a mix of 170 authentic metabolite standards (listed in Table 10.1), analysed by IC-MS/MS with column temperature maintained at 20 °C (a) or 40 °C (b) using the optimised method described in Section 8.4.

The 37 min IC-MS/MS method with a column temperature of 30 °C also chromatographically resolved metabolites at the end of the glycolytic pathway (Fig. 2.10): phosphoenolpyruvate (18.12 min) and pyruvate (6.84 min) had peak widths of ca. 30 s; however, 2- and 3-phosphoglycerate (15.85 min) were not resolved by any of the chromatographic conditions investigated.

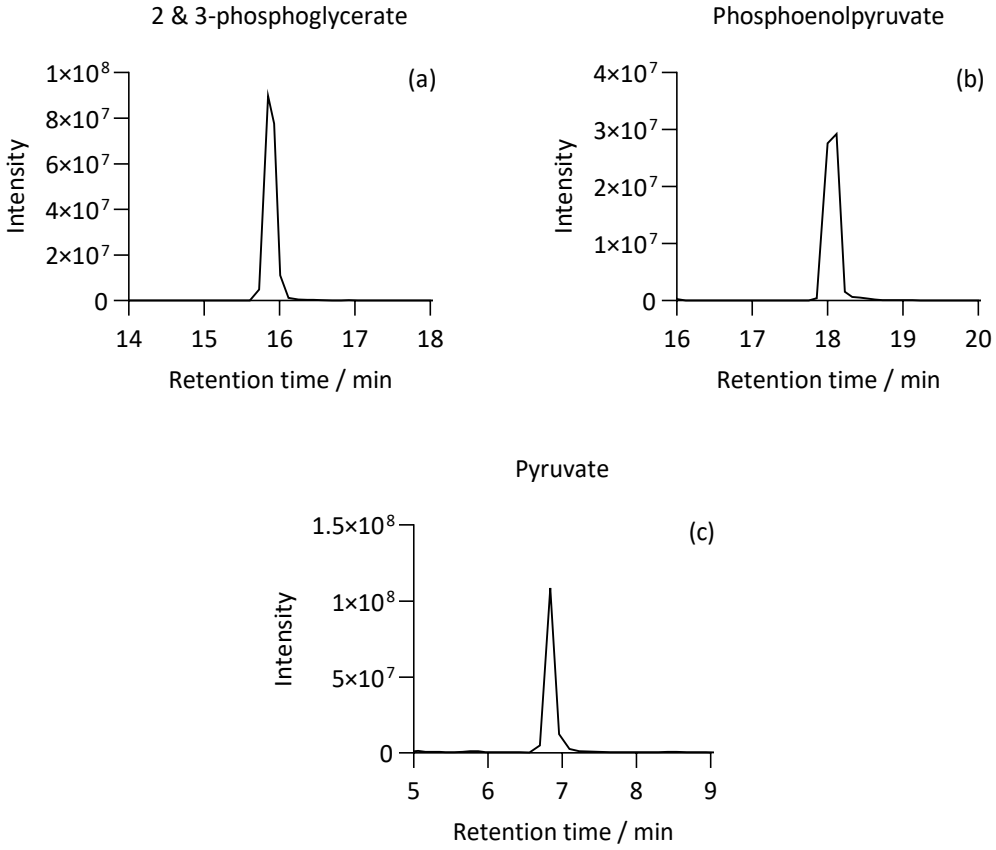

Figure 2.10: EICs for 2 & 3-phosphoglycerate (a), phosphoenolpyruvate (b) and pyruvate (c) analysed by IC-MS/MS (Section 8.4).

2.2.2. Chromatographic separation of polar and ionic metabolites

TCA cycle metabolites were resolved with the following RTs: oxaloacetate (11.22 min), citrate (16.98 min), cis-aconitate (18.10 min), isocitrate (17.58 min), 2-OG (12.91 min), succinate (11.15 min), fumarate (13.67 min) and malate (11.28 min), as shown in Fig. 2.11. Oxaloacetate was observed to have a lower ion abundance at the same concentration (5.0 μM) as the other TCA cycle metabolites. The lower ion abundance may be attributed to reduced ionisation capacity, however could also be caused by spontaneous degradation in solution, forming pyruvate.[158]

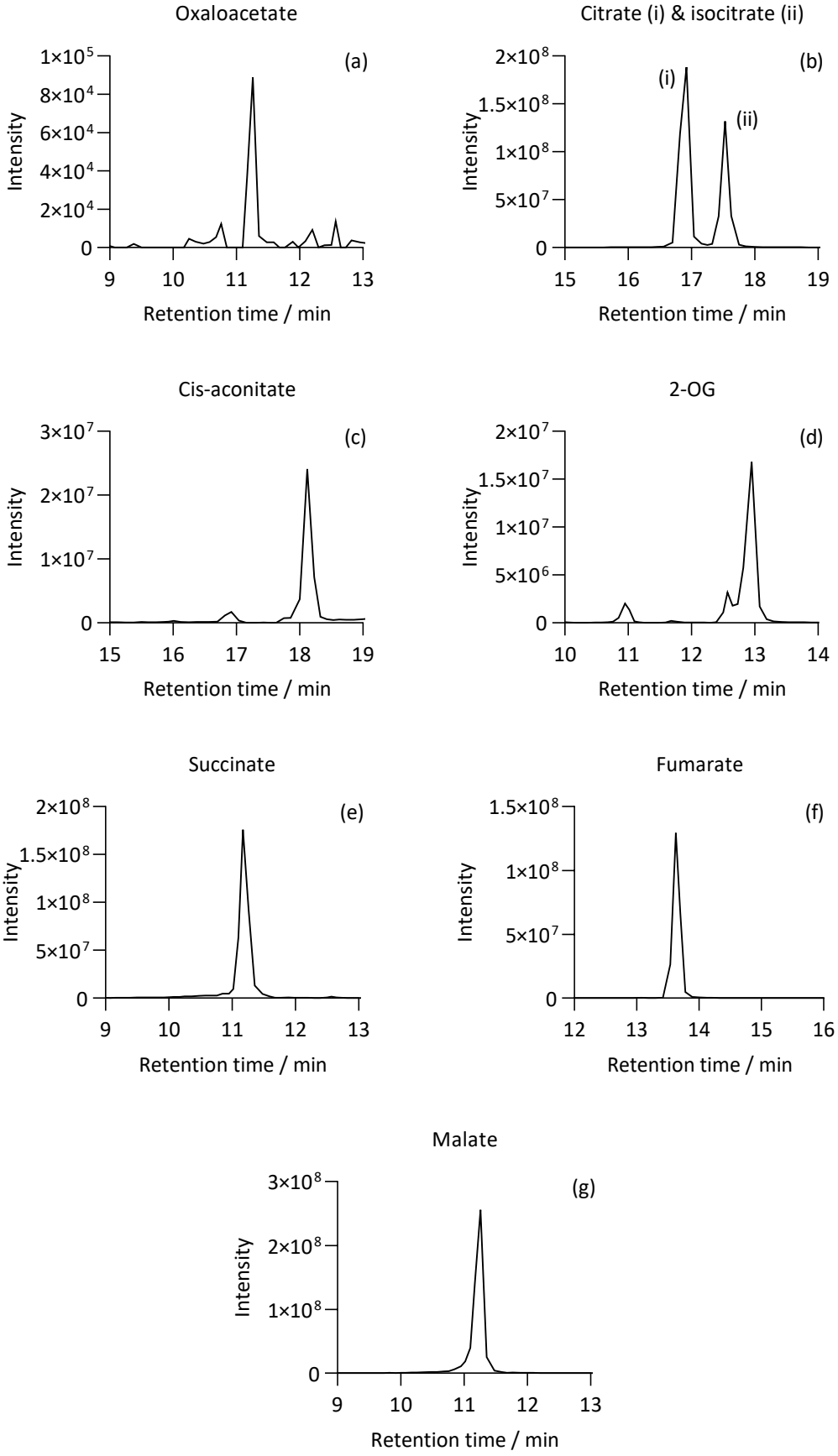

Figure 2.11: EICs for oxaloacetate (a), citrate (b(i)), isocitrate (b(ii)), cis-aconitate (c), 2-OG (d), succinate (e), fumarate (f) and malate (g), analysed by IC-MS/MS (Section 8.4).

The oncometabolite 2-HG was included in the metabolite standard mix (listed in Table 10.1) and had a RT 2 min shorter (10.95 min) than its oxidised analogue (2-OG), as shown in Fig. 2.12, which was also in the metabolite standard mix. The chromatic separation ensured accurate quantitation of both metabolites in the same sample, as the EIC for 2-OG also displayed a peak at 10.95 min (Fig. 2.11(d)) corresponding to an in-source fragment of 2-HG, which was isobaric with 2-OG. Glutamate was also analysed by IC-MS/MS and was of interest due to its interconversion with 2-OG, by glutamine oxoglutarate transaminase, as well as hypotheses from stable isotope labelling studies which suggest that glutamine is source for 2-HG production, especially under hypoxic conditions.[40, 159] The chromatographic peak shape for glutamate by IC-MS/MS (Fig. 2.12(b)) was poor across a range of concentrations, displaying tailing and satellite peaks, likely caused by the zwitterionic properties of the coupled amine-carboxylic functionality.

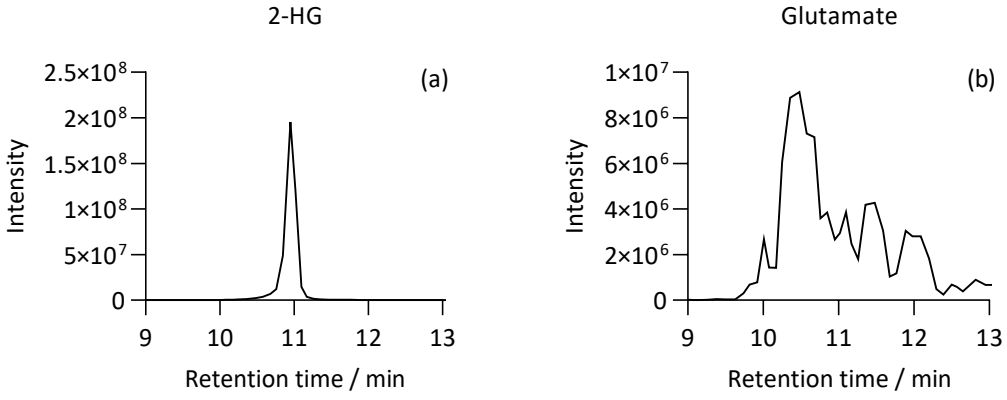

Figure 2.12: EICs for 2-HG (a) and glutamate (b) analysed by IC-MS/MS (Section 8.4).

The isomers ribulose 5-phosphate and ribose 5-phosphate are present at the boundary between the oxidative and non-oxidative pentose phosphate pathway, and are of metabolic interest as they can be characteristic of enzyme activity within the pathways. Ribulose 5-phosphate and ribose 5-phosphate were baseline resolved using IC-MS/MS, as

shown in Fig. 2.13(a). The mitochondrial metabolite ribulose-1,5-disphosphate, which has degradation products which are isobaric with ribulose 5-phosphate and ribose 5-phosphate, also had a distinct RT (20.96 min).

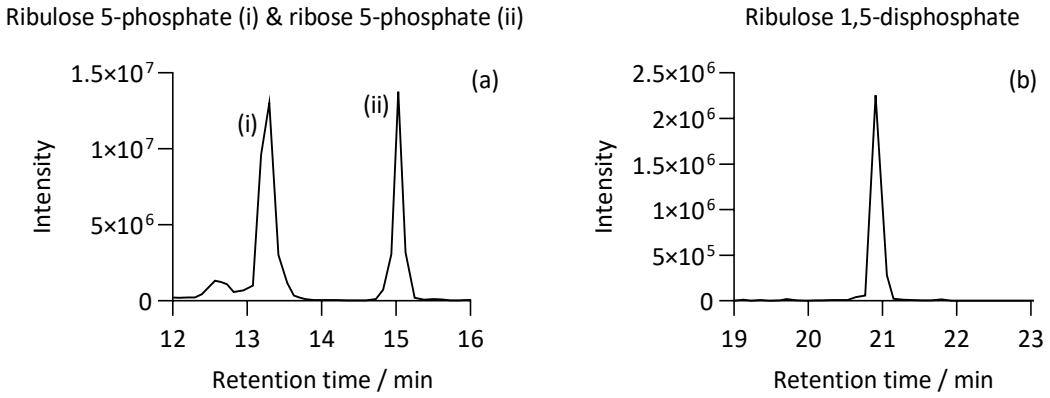

Figure 2.13: EICs for ribulose 5-phosphate (a(i)), ribose 5-phosphate (a(ii)) and ribulose 1,5-disphosphate (b) analysed by IC-MS/MS (Section 8.4).

The non-oxidative pentose phosphate metabolites, which connect to glycolysis via glyceraldehyde 3-phosphate, were also all chromatographically separated, as shown in Fig. 2.14. Fructose 1,6-diphosphate (Fig. 2.14(d)) was also well characterised by the method and therefore metabolites either side of the rate limiting step in glycolysis could be identified and individually quantified.

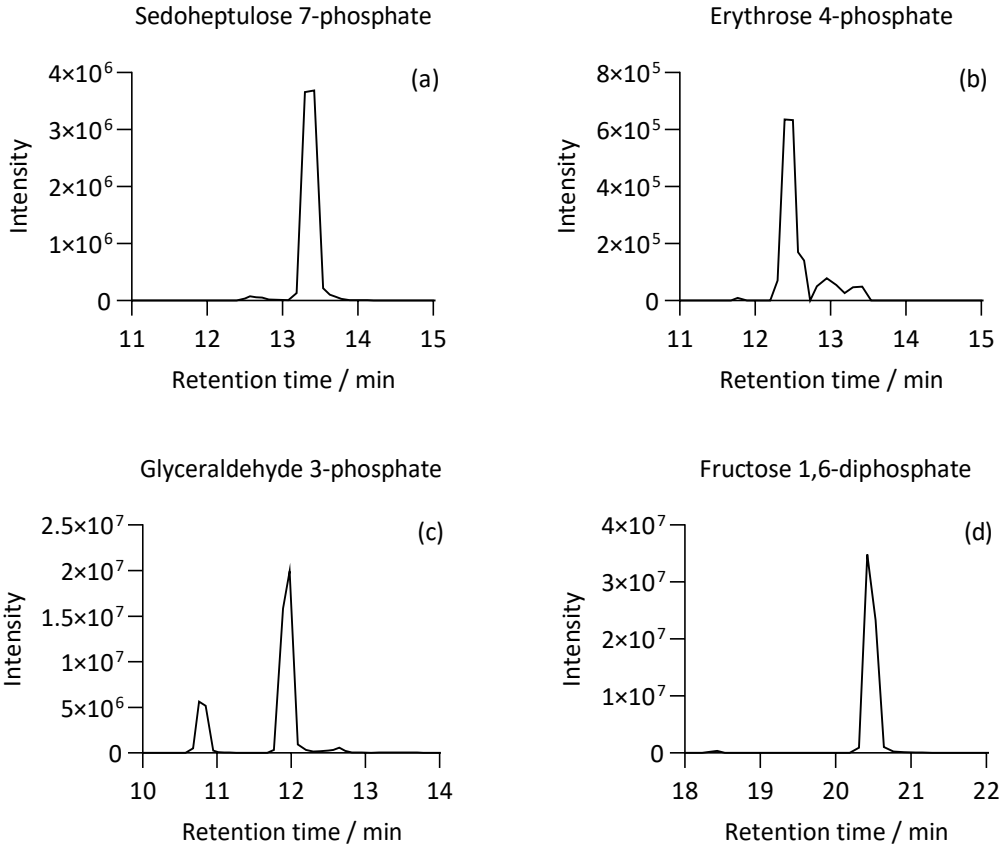

Figure 2.14: EICs for sedoheptulose 7-phosphate (a), erythrose 4-phosphate (b), glyceraldehyde 3-phosphate (c) and fructose 1,6-diphosphate (d) analysed by IC-MS/MS (Section 8.4).

In summary, IC enabled the separation of glycolysis, TCA cycle and pentose phosphate pathway metabolites, including key isobaric species such as citrate and isocitrate. As anion-exchange separates analytes based on their ionic strength, carboxylated and phosphorylated metabolites (common functionalities present in central carbon metabolism) were chromatographically resolved and could therefore be efficiently quantified.

2.3. Optimisation of ESI source conditions for IC-MS/MS

Degradation of metabolites, before and during analysis, is an inherent problem associated with metabolomics as many functional groups involved in metabolic processes, such as phosphates, are labile and therefore degradation can lead to changes in abundance.[160]

For example, carboxylic acids readily decarboxylate, via an enol, to a ketone form which is an irreversible reaction, as CO_2 is a product. Prior to analysis, metabolite degradation in solution was minimised by processing metabolite extracts on ice, storage at low temperature (typically -80 ^oC) and minimising freeze-thaw cycles. Degradation at the interface between chromatography and MS is also known to occur, particularly at the ESI source where analytes experience a phase transition and a significant change in pressure as they enter the MS.

In order to maximise sensitivity and minimise in-source fragmentation, ESI parameters including capillary voltage, gas flows and source temperatures were optimised.[160] A mix of 170 authentic metabolite standards (listed in Table 10.1) was analysed in triplicate using IC-MS/MS, as described in Section 8.4, whilst iteratively altering source parameters and the abundance of labile metabolites was monitored. The data associated with this experiment has been deposited in the Oxford University Research Archive (title: IC-MS ESI Development) and is freely accessible (https://doi.org/10.5287/bodleian:JVopr0ZyM).

Desolvation gas flows were first optimised to match the mobile phase flow rate, starting with the sheath gas flow rate (Fig. 2.15), between 50-70 arbitrary units (au) and then the auxiliary gas flow rate (Fig. 2.16), between 15-25 au.

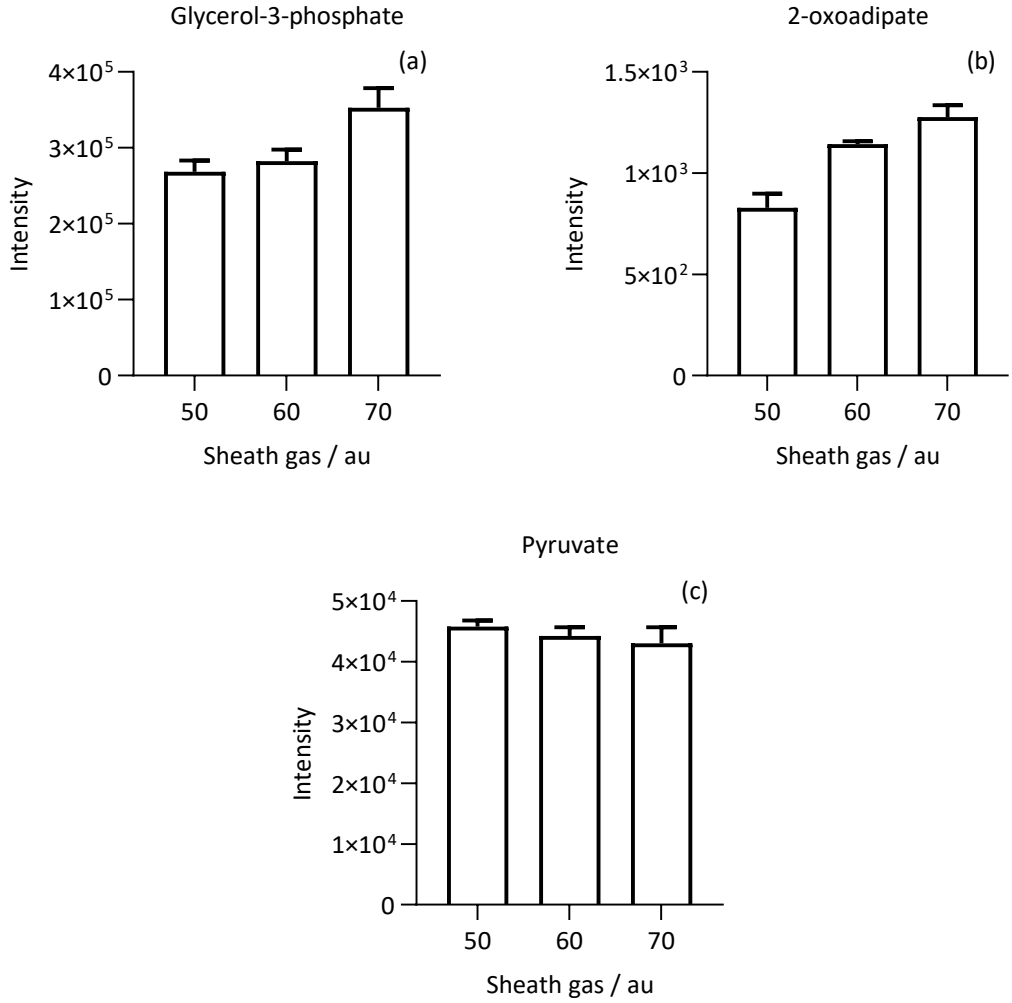

Figure 2.15: Ion intensities for 5 μM authentic standards of glycerol-3-phosphate (a), 2-oxoadipate (b) and pyruvate (c), analysed in triplicate by IC-MS/MS (Section 8.4) with sheath gas flow rate between 50-70 au. Error bars represent standard deviation of the mean.

Ion intensities, for most metabolites, increased with sheath gas flow rate, resulting in more efficient ionisation, with the exception of pyruvate which did not significantly alter in abundance with flow rate. A sheath gas rate of 70 au was therefore chosen for all subsequent analyses as it was optimal for 78 % of all metabolites identified in the standard mix. Auxiliary gas flow was outside the sheath gas and helped shape the ion spray, from the ESI needle, and did not have a dramatic effect on ion intensity at higher sheath gas flow rates, as shown in Fig. 2.16.

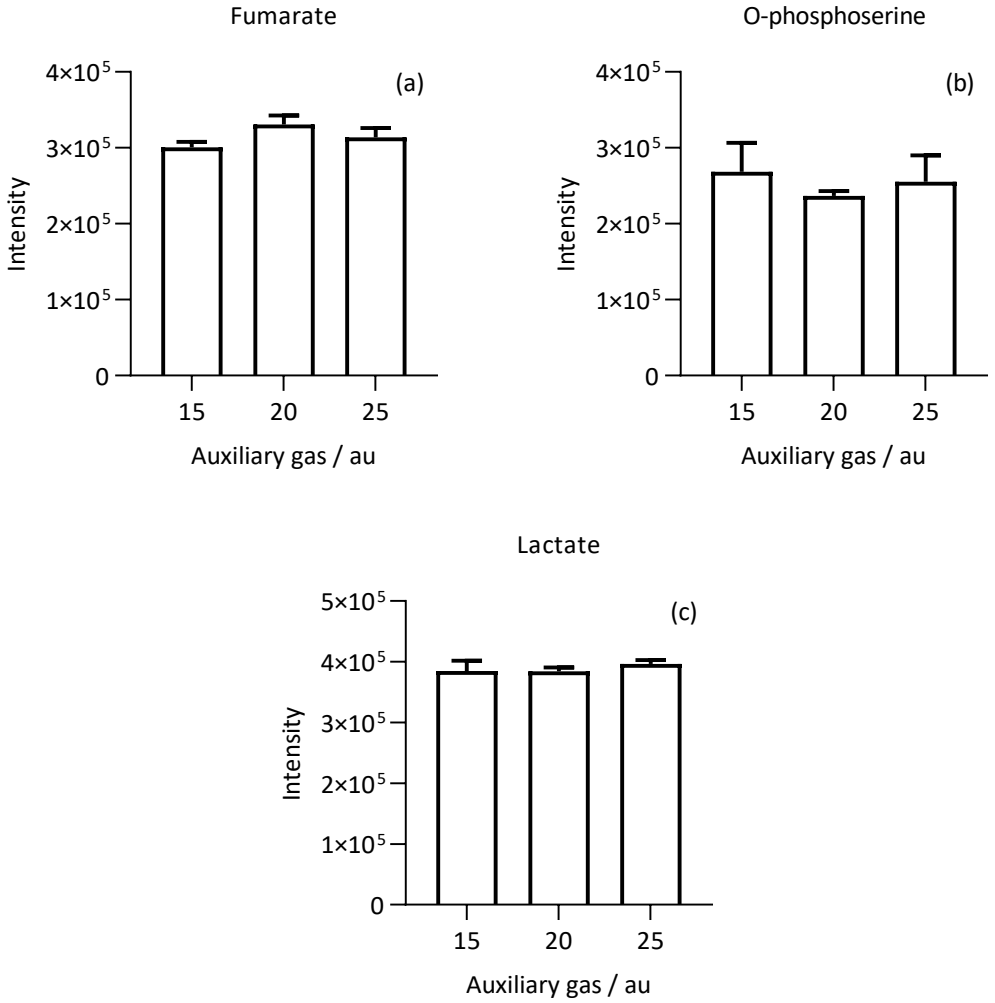

Figure 2.16: Ion intensities for 5 μM authentic standards of fumarate (a), O-phosphoserine (b) and lactate (c), analysed in triplicate by IC-MS/MS (Section 8.4) with auxiliary gas flow rate between 15-25 au. Error bars represent standard deviation of the mean.

The abundance of fumarate (Fig. 2.16(a)) was increased at an auxiliary gas flow of 20 au; however, both O-phosphoserine (Fig. 2.16(b)) and lactate (Fig. 2.16 (c)) had lower abundances, as was observed for 35 % of identified metabolites in the standard mix, compared to 15 or 20 au. The variability in intensity between samples was lower for O-phosphoserine and lactate, as well as 61 % of the identified metabolites, and therefore 20 au was selected as the auxiliary gas flow rate despite the marginally lower abundances observed.

Desolvation and therefore ionisation of metabolites was further improved by the optimisation of the gas heater temperature (auxiliary temperature) between 150-450 °C, as shown in Fig. 2.17.

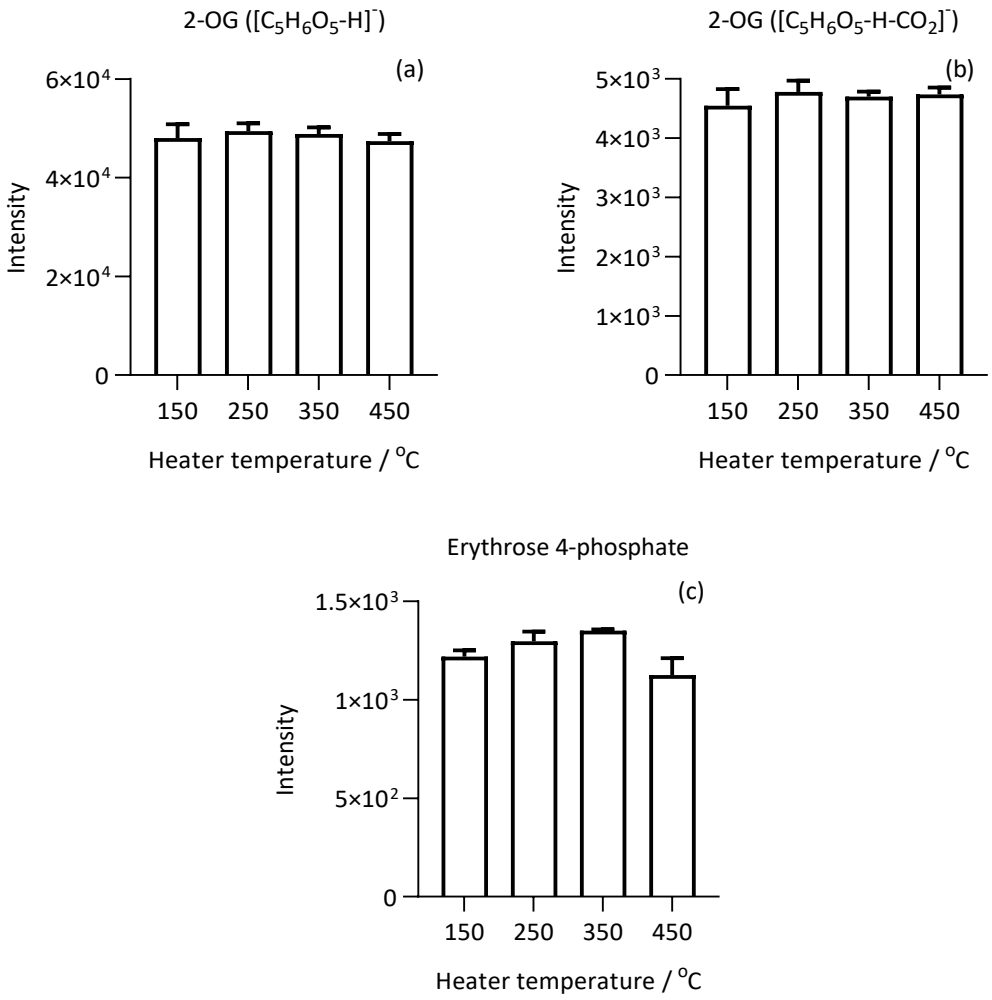

Figure 2.17: Ion intensities for 5 μM authentic standards of 2-OG (a, $[C_5H_6O_5\text{-}H]^-$, b, $[C_5H_6O_5\text{-}H\text{-}CO_2]^-$) and erythrose-4-phosphate (c), analysed in triplicate by IC-MS/MS (Section 8.4) with heater temperature between 150-450 °C. Error bars represent standard deviation of the mean.

Increased heater temperature assisted with analyte ionisation; however, for metabolites with labile functional groups, such as phosphates (Fig. 2.17(b)), intensity was diminished as there was enough thermal energy to cause in-source fragmentation. Higher sensitivity was observed for 78 % of the metabolites identified in the standard mix, at a heater temperature of 350 °C, compared to 450 °C. Lower heater temperatures introduced

increased variability, likely due to incomplete desolvation therefore reducing ionisation efficiency. In-source fragmentation was also observed for carboxyl groups, demonstrated by the decrease in intensity with temperature for 2-OG (Fig. 2.17(a)), in contrast with its decarboxylated ion which increased in intensity, due to the thermal lability of the 2-OG carboxyl groups, as shown in Fig. 2.18.

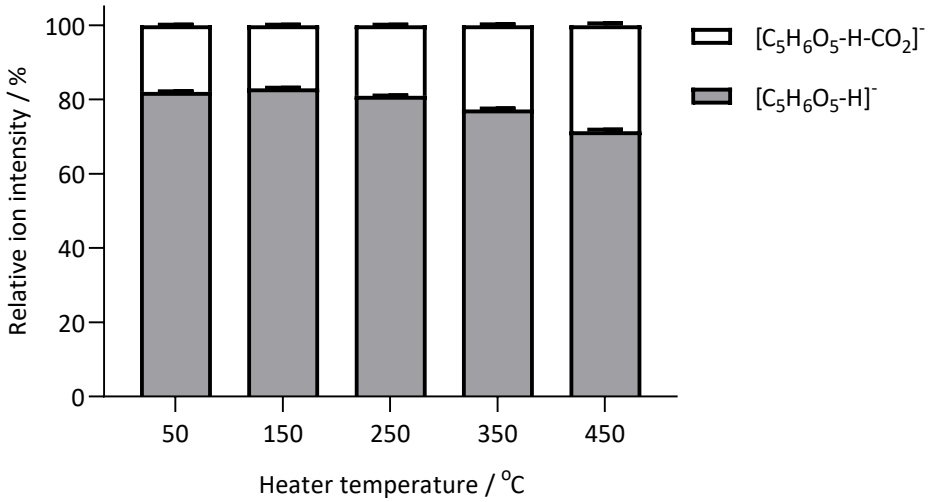

Figure 2.18: Relative ion intensities for the $[C_5H_6O_5\text{-}H]^-$ and $[C_5H_6O_5\text{-}H\text{-}CO_2]^-$ ions at heater temperatures between 50-450 °C from the analysis of a 5 μM authentic standard of 2-OG analysed in triplicate by IC-MS/MS (Section 8.4). Error bars represent standard deviation of the mean.

At higher heater temperatures, more energy was transferred to the deprotonated 2-OG anion ($[C_5H_6O_5\text{-}H]^-$) causing in-source fragmentation and producing the decarboxylated ion $[C_5H_6O_5\text{-}H\text{-}CO_2]^-$, which was isobaric with the deprotonated ion of the metabolite methyl pyruvate. Decarboxylation and dehydration were also observed for the metabolite 2-HG (Fig. 2.19) which formed ions that were isobaric with the deprotonated ions of citraconate and methyl pyruvate.

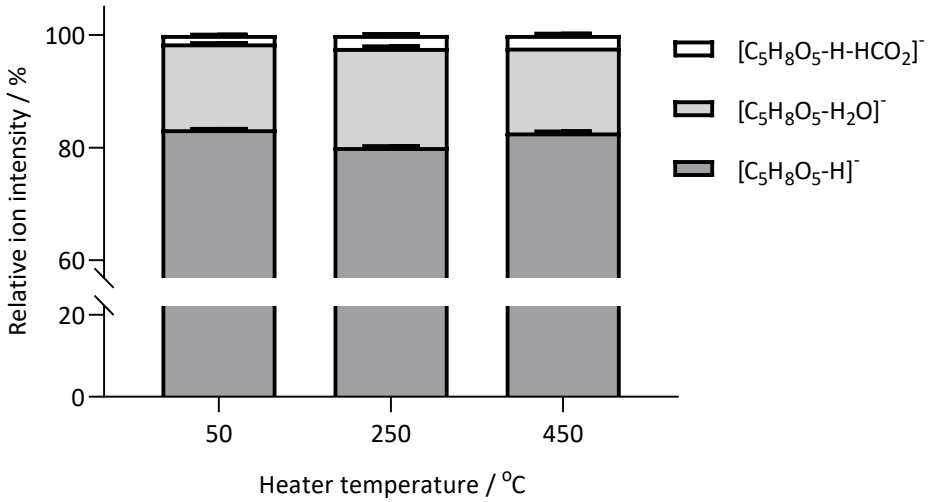

Figure 2.19: Relative ion intensities for the $[C_5H_8O_5\text{-}H]^-$, $[C_5H_8O_5\text{-}H_2O]^-$ and $[C_5H_8O_5\text{-}H\text{-}CO_2]^-$ ions at heater temperatures between 50-450 °C from the analysis of a 5 μM authentic standard of 2-HG analysed in triplicate by IC-MS/MS (Section 8.4). Error bars represent standard deviation of the mean.

A heater temperature of 350 °C was selected as a compromise between minimising in-source fragmentation and ensuring efficient and reproducible ionisation. The capillary temperature was also optimised between 240-360 °C, as shown in Fig. 2.20, to improve desolvation of deprotonated molecules and reduce solvated molecules entering the source vacuum region.

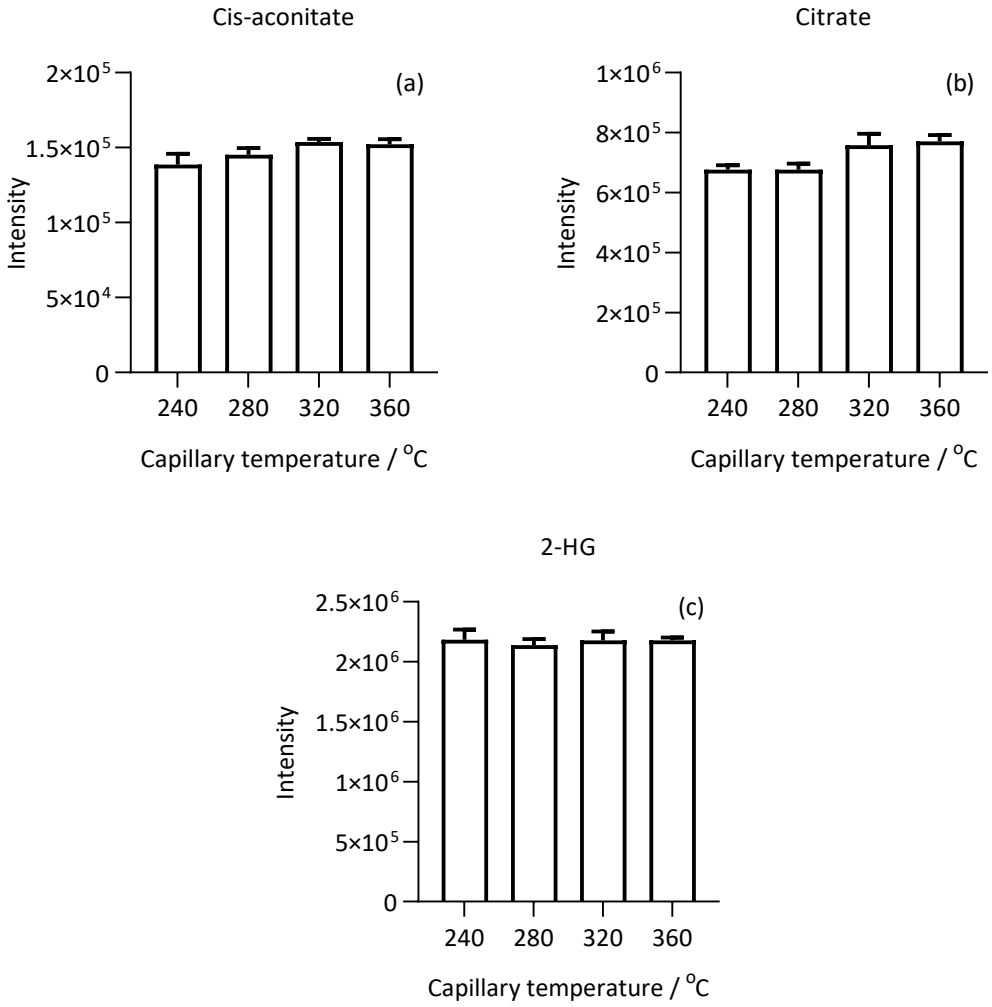

Figure 2.20: Ion intensities for 5 μM authentic standards of cis-aconitate (a), citrate (b) and 2-HG (c), analysed in triplicate by IC-MS/MS (Section 8.4) with capillary temperature between 240-360 °C. Error bars represent standard deviation of the mean.

As observed for most metabolites, ion intensities for cis-aconitate (Fig. 2.20(a)) and citrate (Fig. 2.20(b)) were both increased at higher capillary temperatures. The exception to this was 2-HG (Fig. 2.20(c)), which did not vary significantly with temperature. A temperature of 320 °C was selected to ensure efficient desolvation and minimise in-source fragmentation for labile metabolites as 48% of identified metabolites in the standard mix had a higher intensity at a capillary temperature of 320 °C, compared to 360 °C and 78 % had a higher intensity at a capillary temperature of 320 °C, compared to 280 °C. Spray voltage was the final source parameter to be optimised, using the mix of

authentic metabolite standards (listed in Section 10.1), and had the largest impact on ion intensity, as shown in Fig. 2.21.

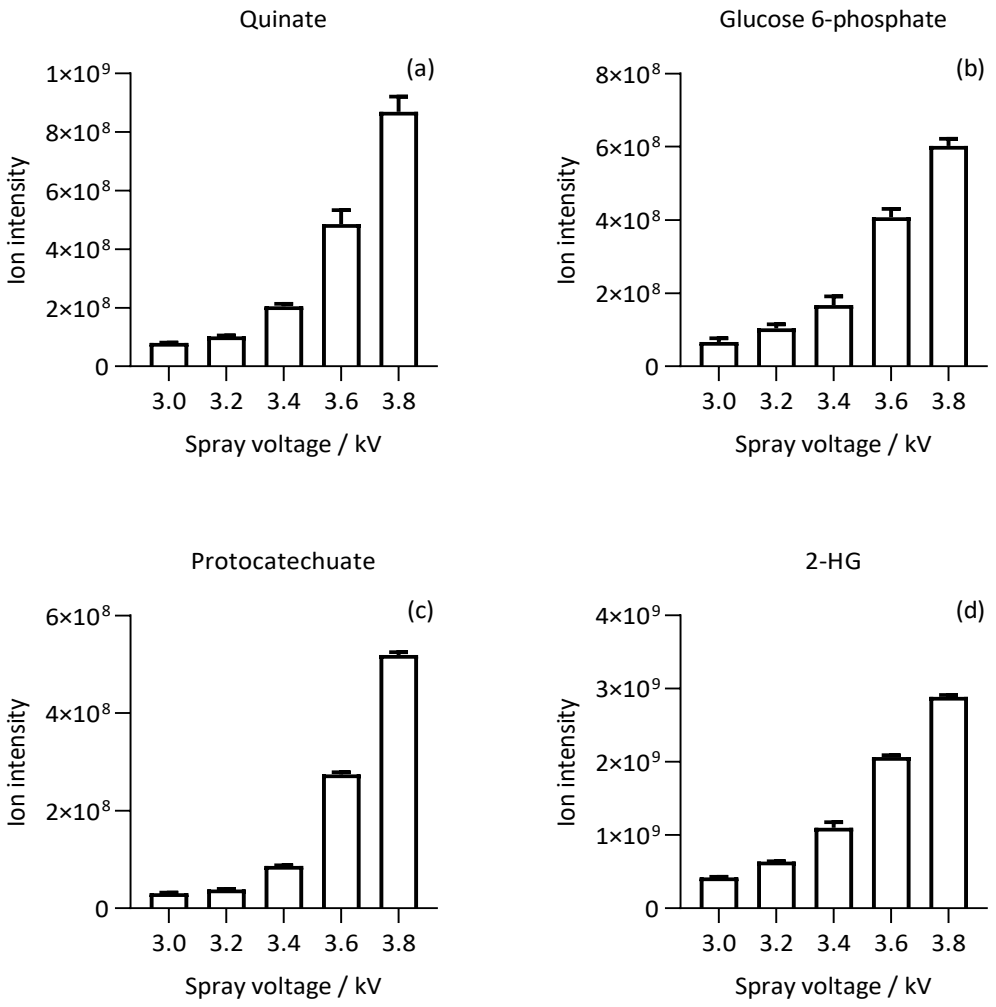

Figure 2.21 Ion intensities for 5 μM authentic standards of quinate (a), glucose 6-phosphate (b), protocatechuate (c) and 2-HG (d), analysed in triplicate by IC-MS/MS (Section 8.4) with spray voltage between 3.0-3.8 kV. Error bars represent standard deviation of the mean.

Increased spray voltage resulted in higher sensitivity for 100 % of the metabolites identified in the standard mix and did not significantly decrease reproducibility. A spray voltage of 3.8 kV was observed to be optimal for all metabolites and sensitivity was increased 2-fold for protocatechuate (Fig. 2.21(c)), compared to a spray voltage of 3.6 kV. The increase in sensitivity would therefore lead to reduced LLoD and LLoQ for most metabolites. To minimise premature degradation to the tip of the ESI needle, the spray

voltage was not increased above 3.8 kV. Compared with heater temperature, the energy transfer from increased spray voltage did not cause additional in-source fragmentation, of the analysed metabolites. The metabolites 2-OG and 2-HG, which produced isobaric in-source fragment ions and were progressively more labile at higher temperatures (Figs. 2.18 and 2.19), had relative abundances of precursor and fragment ions which were consistent across the voltage range, as shown in Fig. 2.22.

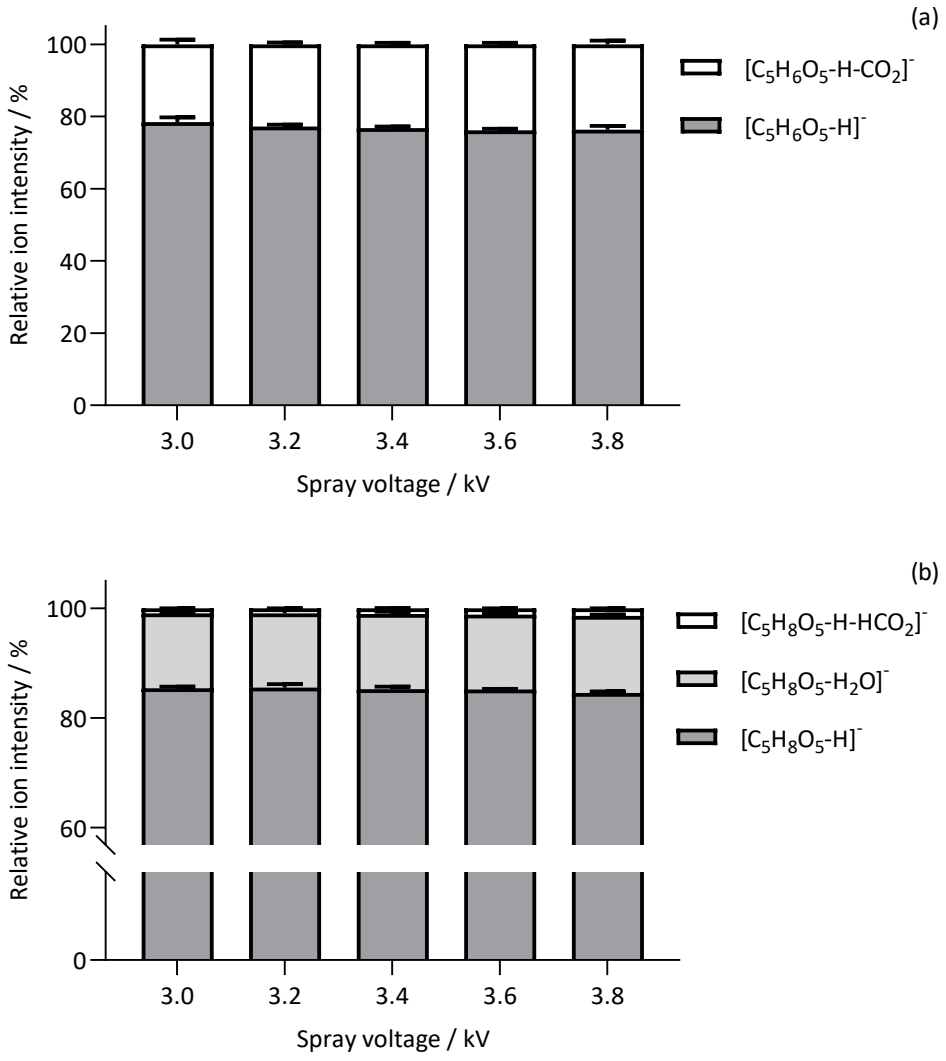

Figure 2.22: Relative ion intensities of precursor and in-source fragment ions for 5 μM authentic standards of 2-OG (a) and 2-HG (b) at spray voltages between 3.0-3.8 kV analysed in triplicate by IC-MS/MS (Section 8.4). Error bars represent standard deviation of the mean.

The relative intensity of each ion, compared to the total abundance of the precursor and fragment ions, was constant despite the alteration in sensitivity with spray voltage. The metabolites analysed here were therefore more susceptible to thermal degradation and consequently a spray voltage of 3.8 kV was selected for further analyses.

Response to variation of source conditions was not equal across all metabolites; however the optimal overall conditions were selected, taking multiple functional groups and metabolite classes into consideration. In-source fragmentation was minimised to reduce the complexity of analysis and decrease the likelihood of misidentification (with isobaric fragment ions) which would cause inaccuracies in quantification.

2.4. IC-MS/MS scan parameter development

Parameters for MS and MS/MS scans were optimised to ensure a suitable number of scans per peak (for relative quantification), balanced with the acquisition of MS/MS spectra (to provide an additional identification parameter). The Q Exactive MS scan parameters were originally set as follows: in-source collision-induced dissociation (CID), 0.0 eV; microscans, 10; resolution, 70,000; automatic gain control (AGC) target, $1x10^6$ ions; maximum injection time (IT), 120 ms; and scan range, 60-900 *m/z*. Data dependent MS/MS parameters: microscans, 2; resolution, 17500; AGC target, $1x10^5$ ions; minimum AGC target, $5x10^3$ ions; maximum IT, 250 ms; loop count, 10; multiplex count, 1; topN, 10; isolation window, 2.0 *m/z*; collision energy, 35; and dynamic exclusion, 10.0 s.

MS/MS coverage of metabolites was improved, without losing MS scan performance in the LC peak timescale, as shown in Fig. 2.23, by optimising data dependent MS/MS parameters to the following: Microscans, 1; minimum AGC target, $1x10^3$ ions; maximum

IT, 50 ms; loop count, 5; topN, 10; apex trigger 1-15 s; charge exclusion, 3-8, > 8 and dynamic exclusion, 20.0 s.

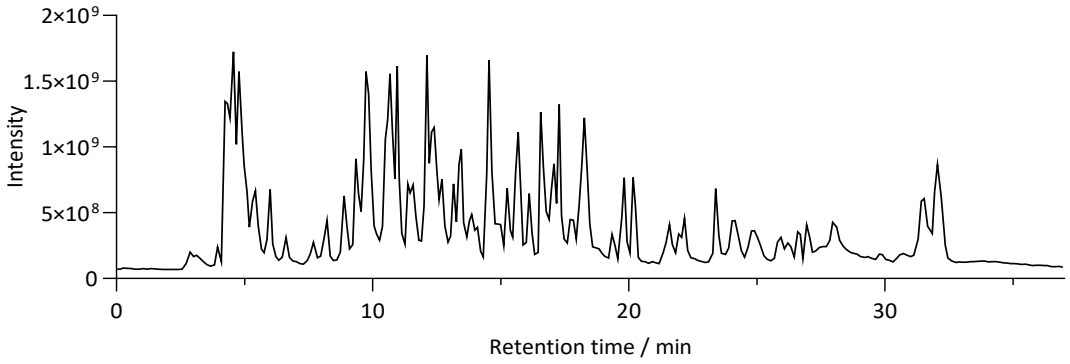

Figure 2.23: TIC of a mix of authentic metabolite standards (listed in Table 10.1), analysed by IC-MS/MS (Section 8.4) using optimised scan parameters.

The reduction of AGC target and max IT values ensured that 6 MS scans were collected over a 30 s peak, while still collecting MS/MS spectra, for the top 10 most intense ions in the MS scan. Targeted quantification could also be improved by using MS only acquisition, increasing the number of MS scans to 14 over a 30 s peak. Although fragmentation spectra were not collected in MS only mode, identification could still be made from accurate mass, isotope pattern and RT compared with the authentic metabolite standards. If fragmentation pattern was required, as an additional identification parameter in a targeted method, then a QC sample could be analysed in both MS and MS/MS modes.

2.5. IC-MS/MS method validation and comparison with HILIC-MS/MS

Method validation was performed, including investigation of reproducibility of RT and ion abundances for IC-MS/MS (Section 8.4). IC-MS/MS was also compared with a complementary HILIC-MS/MS method (Section 8.5), commonly used for the analysis of polar and ionic metabolites, to evaluate IC-MS/MS for metabolomics. An amide column

was used in the HILIC-MS/MS method, chosen for its robust stationary phase and broad chemical selectivity, which has been shown to be selective for polar metabolites.[116, 161]

2.5.1. RT and ion abundance reproducibility of IC-MS/MS

To demonstrate the reproducibility of the IC-MS/MS method and ensure reliability for untargeted analysis, RT and ion abundance for a mix of authentic metabolite standards (listed in Table 10.1), were observed over a period of 3 months, analysed using the method described in Section 8.4 before and after metabolomics projects. The data associated with this experiment has been deposited in the Oxford University Research Archive (title: IC-MS and HILIC-MS Retention Time and Intensity Reproducibility) and is freely accessible (https://doi.org/10.5287/bodleian:xQOdY1e05). From the 170 metabolites in the mix of authentic standards, 16 were selected to ensure coverage of the whole chromatographic range and RT variability was observed to be less than 2 %, as shown in Fig. 2.24.

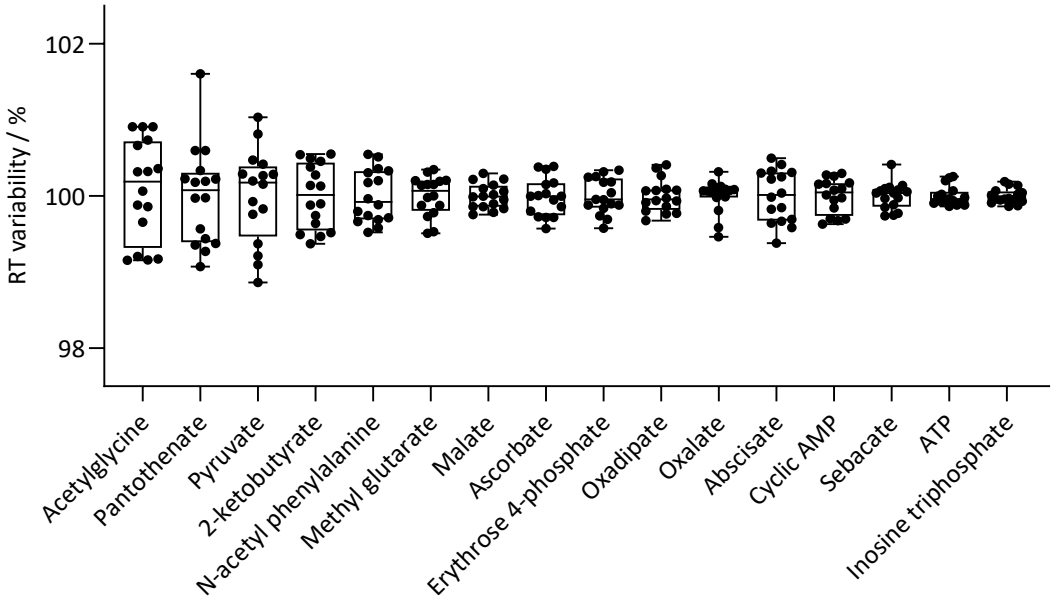

Figure 2.24: Reproducibility in RT for a representative subsection of metabolites, from a mix of 170 authentic standards (listed in Table 8.1), analysed by IC-MS/MS (Section 8.4) over 3 months. The box plot shows the mean, 25-75th percentiles and whiskers extend from the minimum to maximum values. The number of samples are denoted with dots.

RT variability was expressed as a percentage error for each metabolite, from the originally observed RT. The selected metabolites were ordered by their RT (Fig. 2.24), to assess variability throughout the chromatographic gradient, from lowest (acetylglycine, 4.53 min) to highest (inosine triphosphate, 30.53 min). RT variability generally decreased as RT increased. For example, a change in RT by 5 s for a metabolite which eluted at 5 min had a larger percentage error, compared with a metabolite which eluted at 20 min. The metabolites which eluted early on also had fewer interactions with the stationary phase and were therefore more susceptible to variations in the mobile phase and injection solvent. The stability of RT was due to precisely controlled on-line eluent generation (as discussed in Section 1.5), which produced highly reproducible chromatographic conditions and resulted in coefficient of variation (CV) values of less than 1 % for all identified metabolites over 3 months.

Variability in ion abundance, for the mix of authentic metabolite standards analysed before and after metabolomics projects (Fig. 2.25) by IC-MS/MS (Section 8.4), was much larger than the RT variability across the 3 months (Fig. 2.24).

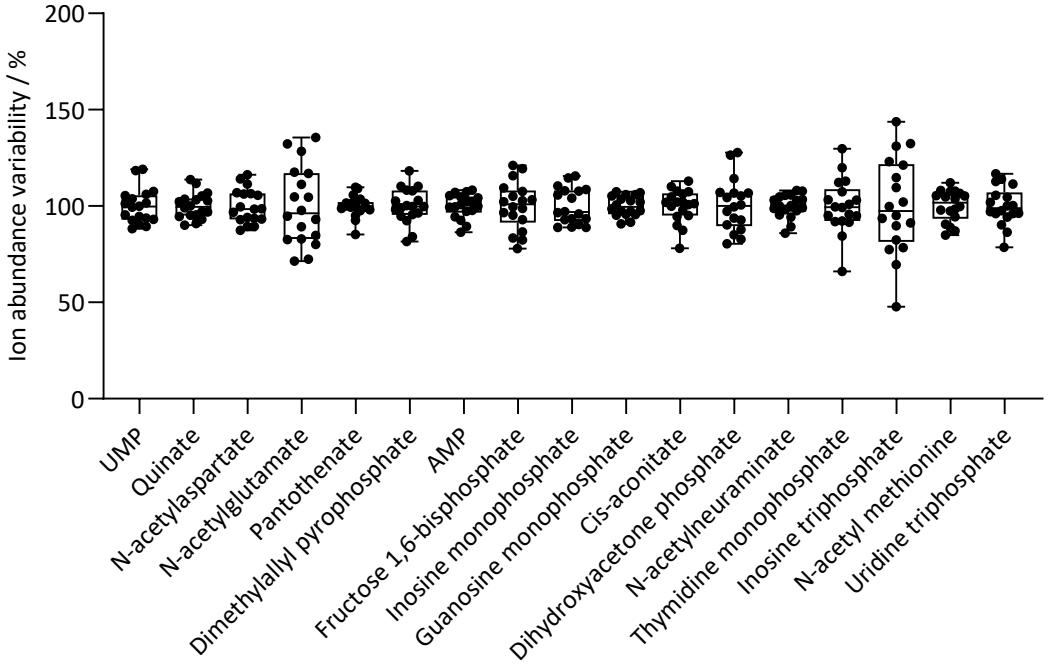

Figure 2.25: Reproducibility of ion abundance for a representative subsection of metabolites, from a mix of 170 authentic standards (listed in Table 8.1), analysed by IC-MS/MS (Section 8.4) over 3 months. The box plot shows the mean, 25-75th percentiles and whiskers extend from the minimum to maximum values. The number of samples are denoted with dots.

Ion abundances generally varied across the 3 month period, due to a number of factors with all identified metabolites below a CV of 35 % and 88 % with a CV below 20 %. Source cleanliness had the largest effect on ion abundance and the abundances for an authentic metabolite standard mix analysed after a project, was generally lower than mix analysed before, as throughout the sequence the source was increasingly contaminated by non-volatile salts which were present in the biological matrices. Ion abundances were generally recovered after source cleaning between analyses. Variability in ion abundance was also caused by the degradation of metabolites in the mix of authentic standards over time, including oxidation, hydrolysis and dephosphorylation.

The effect of molecular weight cut-off (MWCO) filtration was investigated, to reduce matrix interference from soluble protein and therefore increase sensitivity. A QC sample from 293T cells (Section 8.16) was analysed by IC-MS/MS (Section 8.4), with and without filtration using a 10 kDa MWCO filter (Merck Millipore, Darmstadt, Germany), and the log scaled ion abundance for a range of metabolites was plotted (Fig. 2.26).

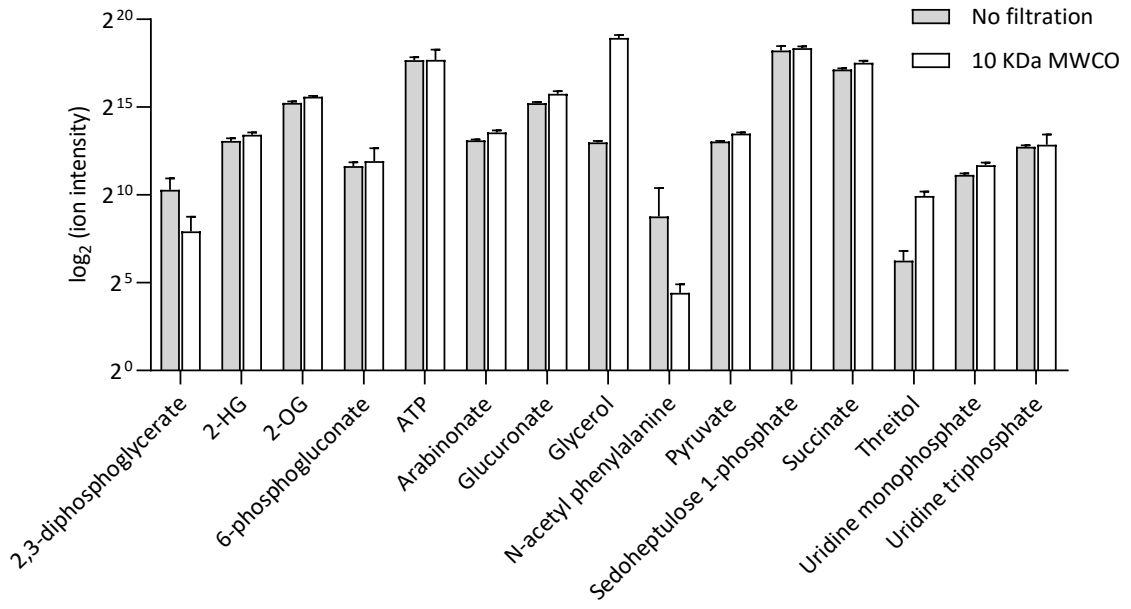

Figure 2.26: The effect of 10 kDa MWCO filtration on ion abundance for selected metabolites from a 293T QC sample (Section 8.16) analysed in triplicate by IC-MS/MS (Section 8.4). Error bars represent standard deviation of the mean.

Metabolites with various chemical functionalities, across the chromatographic range, were selected to show the general trends of MWCO filtration. Filtration increased sensitivity with the exception of the metabolites 2,3-diphosphoglycerate and N-acetyl phenylalanine and the variation in ion abundance was not significantly altered by filtration. Sensitivity was increased for 80 % of the metabolites identified in the QC sample. One metabolite of note was glycerol which was enriched greater than 50-fold by filtration. This increase in ion abundance was caused by the presence of glycerol in the MWCO filter membranes, which was reduced by washing with MilliQ water prior to use.

Suppressor lifetime was also observed to increase when using MWCO filtration, likely due to reduced accumulation of protein on the suppressor membranes. MWCO filtration was chosen as it minimised the number of interactions with the sample prior to analysis, and therefore reduced the likelihood of increased variability associated with sample preparation. Alternative clean up techniques such as solid-phase extraction require multiple sample preparation steps, including sample loading, washing and eluting where analytes can be lost or modified.[162]

2.5.2. Comparison of IC-MS/MS and HILIC-MS/MS

To evaluate IC-MS/MS against an existing method for metabolomics, the mix of 170 authentic metabolite standards (listed in Table 8.1) dissolved in acetonitrile was analysed by IC-MS/MS (Section 8.4) and HILIC-MS/MS (Section 8.5) multiple times over 2 weeks, before and after analyses of various sample types. The authentic metabolite standard mix was analysed 16 times and the difference in RT for each metabolite from the mean value plotted, as shown in Fig. 2.27. The data associated with this experiment has been deposited in the Oxford University Research Archive (title: IC-MS and HILIC-MS Retention Time and Intensity Reproducibility) and is freely accessible (https://doi.org/10.5287/bodleian:xQOdY1e05).

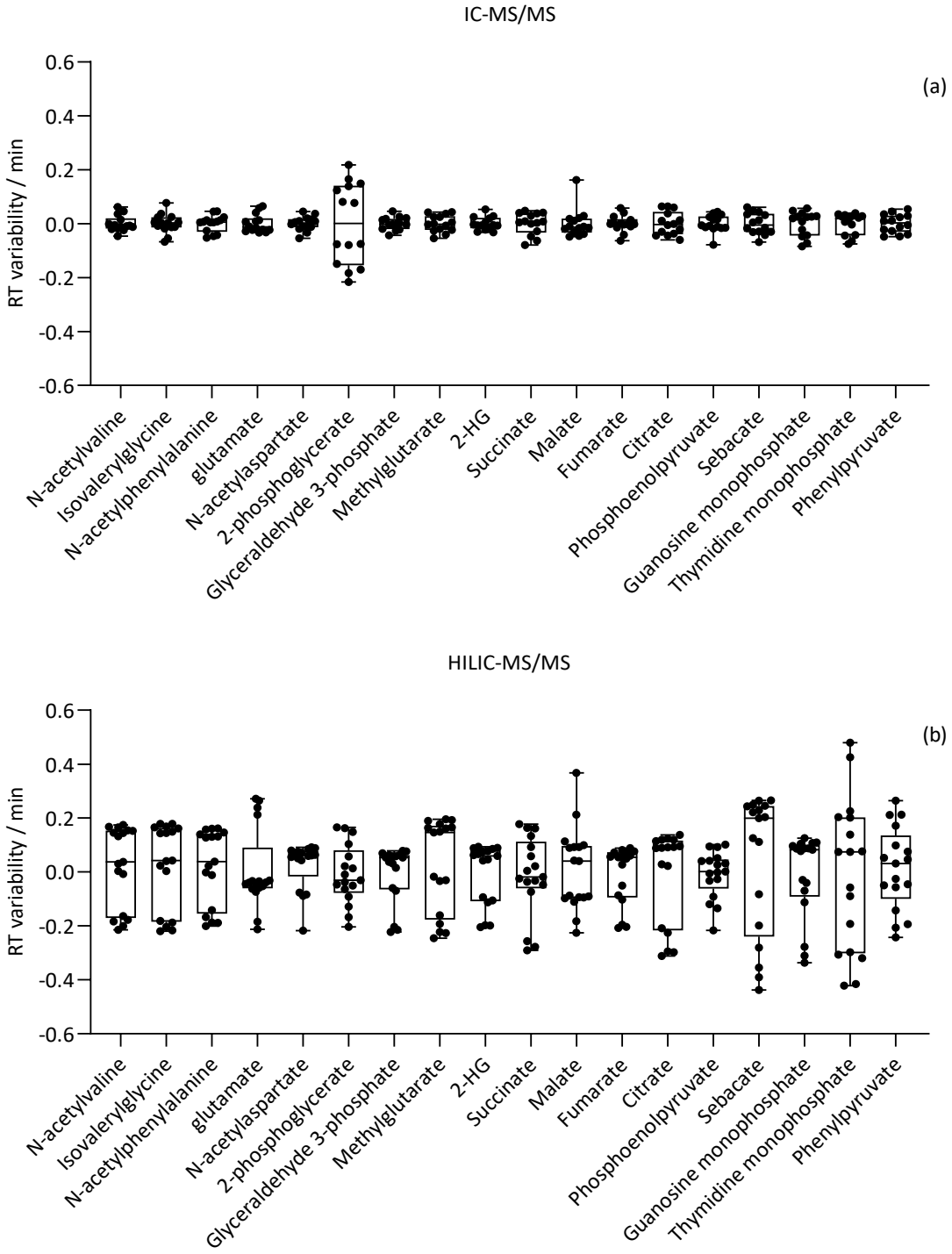

Figure 2.27: Reproducibility in RT for a representative subsection of metabolites, from a mix of 170 authentic standards (listed in Table 8.1), analysed by IC-MS/MS (a) and HILIC-MS/MS (b), as described in Sections 8.4 and 8.5 respectively, over 2 weeks. The box plots show the mean, 25-75th percentiles and whiskers extend from the minimum to maximum values. The number of samples are denoted with dots.

RT for the metabolites analysed by IC-MS/MS (Fig. 2.27(a)) were extremely reproducible. The variation in RT observed for IC-MS/MS was less than ± 6 s for all metabolites, with the exception of 2-phosphoglycerate and malate. Malate had one outlier which when

removed reduced the variation to ± 6 s and the variation for 2-phosphoglycerate was likely caused by a reduced abundance of the ion across all analyses, compared with the other authentic metabolite standards in the mix. Overall, 95 % of the metabolites identified in the standard mix, over 2 weeks, had a RT CV less than 1.5 % and all metabolites had a CV less than 5 %. HILIC-MS/MS (Fig. 2.27(b)) had a 2-fold larger RT variability than IC-MS/MS despite the shorter chromatographic run time of 15.0 min, compared with IC-MS/MS (37.0 min). The RT variation for HILIC-MS/MS was likely due to inconsistency in the composition of the mobile phase, which was prepared before each analysis. The variability for HILIC-MS/MS analysis of authentic metabolite standards before and after projects was typically ± 12 s, this inconsistency reduced confidence in the use of RT as an identification parameter for targeted analysis. Only 28 % of the identified metabolites identified in the standard had a RT CV less than 1.5 % and 94 % of metabolites had a CV less than 5 %.

Nucleotides consist of a base (adenine, thymine, guanine, or cytosine), a sugar linkage and 1 or more phosphate groups. The nucleotides are important biologically as they are used as structural components for DNA and RNA and therefore fluctuate during the cell cycle. Nucleotides are therefore essential metabolites to quantify as part of phased studies or for any experiments which may affect cell division. The loss of phosphate group, by a gas phase ion, is a common phenomenon.[163] For example, the dephosphorylated ions of a triphosphate nucleotide are isobaric with the molecular ion for the mono- and diphosphate nucleotide. Quantification is therefore susceptible to overestimation for nucleotides with a lower number of phosphate groups. Baseline separation was observed for AMP, adenosine diphosphate (ADP) and ATP analysed by IC-MS/MS (Fig. 2.28(a)) however, ADP and ATP were not resolved by

HILIC-MS/MS (Fig. 2.28(b)). Chromatographic resolution by IC-MS/MS was observed for the mono-, di- and triphosphorylated forms of all the nucleotides. As the isobaric fragment ions were chromatographically resolved, quantification of nucleotides by IC-MS/MS would not result in overestimation.

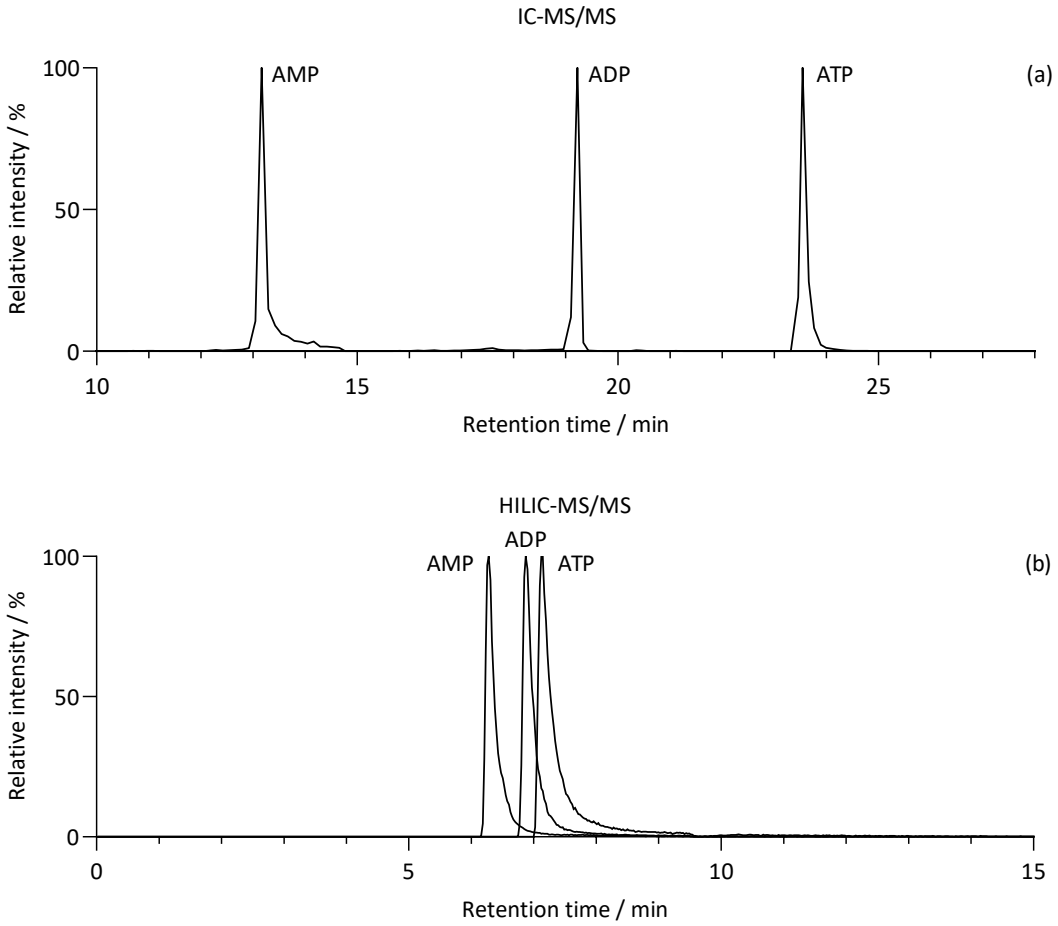

Figure 2.28: Extracted ion chromatograms for the metabolites AMP, ADP and ATP analysed by IC-MS/MS (a, Section 8.4) and HILIC-MS/MS (b, Section 8.5).

2.6. IC-MS/MS linearity and sensitivity compared with HILIC-MS/MS

To further validate the IC-MS/MS method for metabolomics, standard curves of authentic metabolite standards were prepared across 5 orders of magnitude from concentrations ca. 30 μM to 3 nM. The standards were then analysed by IC-MS/MS (Section 8.4) and HILIC-MS/MS (Section 8.5), in triplicate, and calibration curves prepared. LLoQ and LLoD

were calculated using eq. 2.1 and eq. 2.2 respectively, according to International Conference on Harmonisation of Technical Requirements for Registration of Pharmaceuticals for Human Use (ICH) guidelines and ISO 11843-2 where σ_c was the standard deviation of the y-intercept and m was the gradient of the line of best fit for each calibration curve.[164, 165]

$$LLoQ = (10 \sigma_c) / m \quad (2.1)$$

$$LLoD = (3.3 \sigma_c) / m \quad (2.2)$$

Metabolites with RTs across the chromatographic time range with distinct chemical functionalities were selected to show general trends of the whole data set. LLoD, LLoQ and linearity for each method was therefore calculated for the metabolites as shown in Table 2.1. Values for LLoD, LLoQ and R^2 were used here to allow the comparison of IC-MS/MS and HILIC-MS/MS for the analysis of the same metabolites, and should not be used as absolute limits for either method. If metabolite quantification is required then standards should be analysed above and below the expected concentration, at the same time as the analysis of samples, and a calibration curve prepared.

Table 2.1: Comparison of LLoD, LLoQ and R^2 for the calibration curves of polar metabolites analysed by IC-MS/MS (Section 8.4) and HILIC-MS/MS (Section 8.5).

	IC-MS/MS			HILIC-MS/MS		
Compound	**LLoD / μM**	**LLoQ / μM**	**R^2**	**LLoD / μM**	**LLoQ / μM**	**R^2**
2-HG	0.55	1.67	0.9991	1.29	3.91	0.9951
2-OG	1.85	5.61	0.9900	2.26	6.86	0.9852
Citrate	0.39	1.19	0.9992	3.80	11.51	0.9881
Isovalerylglycine	0.51	1.54	0.9991	0.43	1.30	0.9994
Malate	0.61	1.86	0.9991	1.30	3.94	0.9958
N-acetylaspartate	1.10	3.32	0.9952	1.61	4.87	0.9897
N-acetylphenylalanine	0.44	1.33	0.9989	0.12	0.38	0.9999
Phenylpyruvate	0.64	1.93	0.9985	1.54	4.68	0.9911
Phosphoenolpyruvate	0.90	2.72	0.9991	18.59	56.32	0.9242
Phosphoserine	1.59	4.81	0.9993	ND	ND	ND
Sebacetate	0.33	1.01	0.9994	0.53	1.62	0.9985

Sensitivity was higher for metabolites analysed by IC-MS/MS, compared with HILIC-MS/MS (Table 2.1), despite the aqueous mobile phase, and the linearity of response was also higher, with R^2 values larger than 0.9950 for all metabolites compared to HILIC-MS/MS, which had values ranging from 0.9242 (phosphoenolpyruvate) to 0.9999 (N-acetylphenylalanine). The higher sensitivity of IC-MS/MS resulted in reduced LLoD and LLoQ with the exception of N-acetylphenylalanine and isovalerylglycine, likely due to their zwitterionic functionality and consequent degradation in the suppressor. IC-MS/MS was particularly suited to the analysis of phosphorylated metabolites, such as phosphoenolpyruvate which had a 20-fold reduced LLoD, compared to HILIC-MS/MS and phosphoserine, which was only detected by IC-MS/MS method. TCA cycle metabolites such as citrate and malate were also well characterised by IC-MS/MS with 2-fold reduced LLoD and LLoQ compared to HILIC-MS/MS. The TCA cycle metabolites, as well as the oncometabolite 2-HG, were all baseline separated by the IC-MS/MS method as shown in Fig. 2.29.

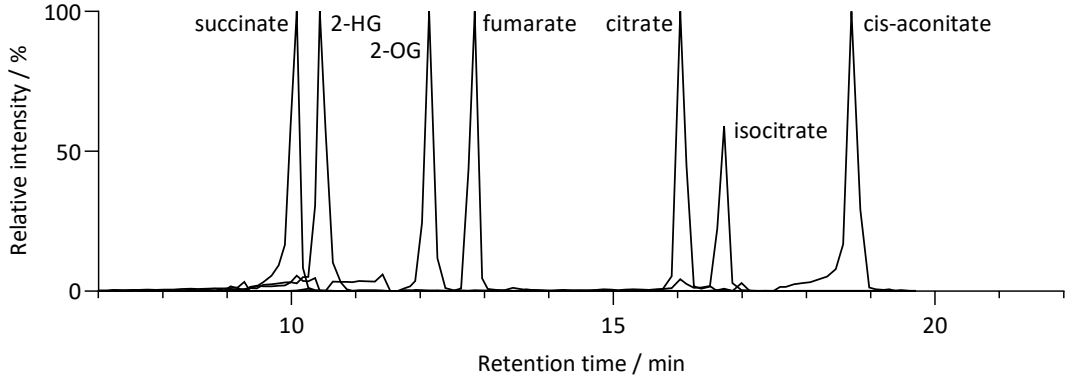

Figure 2.29: Extracted ion chromatograms for the metabolites succinate, 2-HG, 2-OG, fumarate, citrate, isocitrate and cis-aconitate by IC-MS/MS (Section 8.4).

Preparation of external standard calibration curves, for example, the metabolites N-acetylaspartate (NAA) and malate, as shown in Fig. 2.30, enabled absolute quantification in extracts from cells.

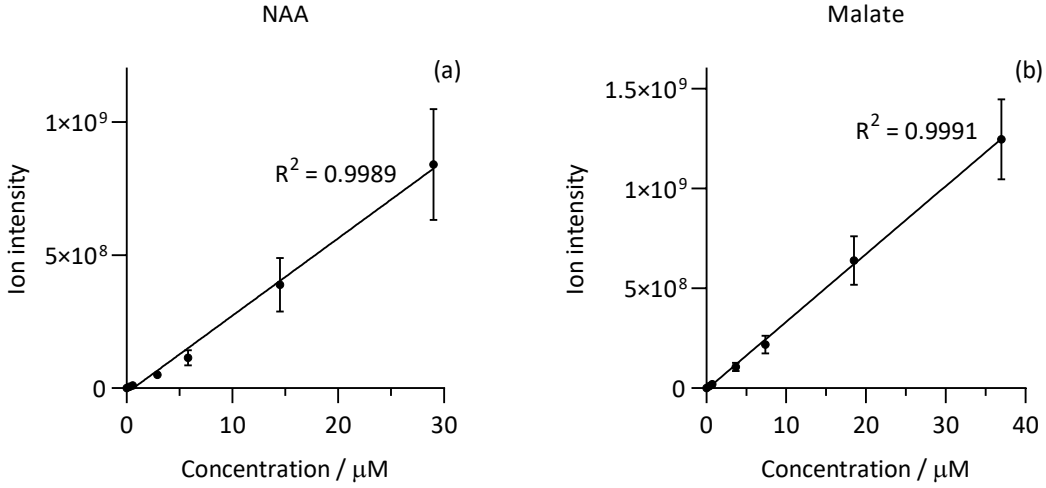

Figure 2.30: Calibration curves for authentic standards of NAA (a) and malate (b) analysed in triplicate by IC-MS/MS (Section 8.4). Error bars represent standard deviation of the mean.

The total concentration of NAA and malate in an extraction from LN18 WT cells cultured under 4.5 g / L glucose conditions (Section 8.14), analysed by IC-MS/MS (Section 8.4) were calculated from the gradient and y-intercept of their calibration curves (Fig. 2.30) to be 4.2 μM and 20.7 μM respectively. Internal standards were not used for analyses as it was deemed unsuitable for untargeted metabolomics, due to the range of metabolite

classes and *m/z* which could be detected and therefore a disproportionate number of standards would be required to achieve absolute accurate quantitation. The demonstrated linearity of the IC-MS/MS method is suitable for relative quantitation of metabolites over at least 4 orders of magnitude.

IC-MS/MS had reduced LLoD and LLoQ compared with HILIC-MS/MS for the analysis of authentic metabolite standards, with a range of chemical functionalities. A wide dynamic range for the IC-MS/MS method would allow analysis of metabolites which were enriched or depleted by orders of magnitude in biological samples, such as 2-HG in Mut cells. Especially where metabolite concentrations were unknown and therefore reduced the likelihood of repeat analysis with consequent sample dilution or concentration step, which may also introduce additional variability. Some metabolites which had zwitterionic functionality, such as amino acids and carnitines, were not reliably detected by IC-MS/MS and therefore HILIC-MS/MS remains a complementary analysis method when coverage of a specific area of metabolism is required.

2.7. IC-MS/MS metabolome coverage

To investigate the coverage of polar metabolome achieved using IC MS/MS, LN18 WT cells were cultured under 1.5 g / L or 4.5 g / L glucose DMEM (without HEPES or sodium pyruvate) supplemented with 10 % FBS and 1 % GlutaMAX. Experimental groups with 9 biological replicates were cultured in 6 cm diameter plates with a seeding density of 20 % and a total media volume of 5 mL. At 80 % cell confluency (after ca. 48 hours), media was removed and the adherent monolayer of cells were washed with ca. 10 mL phosphate buffered saline. Cells were snap frozen with ca. 3 mL liquid N_2 to arrest metabolic processes and cells mechanically lysed, with the addition of

300 μL ice-cold 80 % methanol$_{(aq)}$, to extract metabolites into solution. Metabolite extracts were centrifuged at 2.2x10^4 x g for 20 min to remove cell debris, normalised to DNA concentration by addition of 80 % methanol$_{(aq)}$ and filtered using 10 kDa MWCO filters (Merck Millipore, Darmstadt, Germany), following the manufacturers protocol, prior to analysis. A QC sample was prepared by the pooling of equal volumes of all individual samples and analysed before, during and at the end of each LC-MS method to assess analytical reproducibility. Metabolite extracts were analysed by IC-MS/MS (Section 8.4) and HILIC-MS/MS (Section 8.5). Raw MS data were processed in Progenesis QI (Nonlinear Dynamics, Newcastle upon Tyne, UK) to perform spectral alignment as well as peak detection, to calculate compound-feature abundances, consisting of the sum of isotope ion intensities. All runs were assessed for suitability as the alignment reference and chromatograms were automatically aligned to correct for RT drift. Peak picking utilised run aggregation, chromatographic peak detection, isotope and adduct deconvolution was performed using automatic sensitivity adjustment, no minimum chromatographic peak width or retention time limits and normalisation to all compounds was used. Normalisation to all compounds was used to avoid closure constraints caused by large changes in the abundance of a small number of compound-features, which would cause bias in the dataset by techniques such as normalisation by sum. Normalisation to all compounds determined a standard deviation estimate for each sample compared to every other sample in the dataset using a $\log_{10}$ ratio calculation for scalar estimation (to avoid abundance bias) and outliers were rejected using median and mean absolute deviation. Univariate statistical analysis was performed on compound-feature abundance tables (exported without normalisation from Progenesis QI) using MetaboAnalyst as described in Section 8.11.[166] The data

associated with this experiment has been deposited in the Oxford University Research Archive (title: Metabolomics of LN18 wild-type cells cultured under different glucose conditions) and is freely accessible (https://doi.org/10.5287/bodleian:0zJjXpoEK).

2.7.1. IC-MS/MS analysis of LN18 wild-type glioblastoma cells

Over $2.9x10^5$ chromatographic peaks were integrated from the analysis of LN18 WT cells by IC-MS/MS method which resulted in the assignment of $4.2x10^3$ compound-features in Progenesis QI and $2.8x10^3$ MS/MS spectra. The PCA scores plot of compound-feature abundances for LN18 WT cells cultured under different glucose conditions analysed by IC-MS/MS (Section 8.4), are shown in Fig. 2.31.

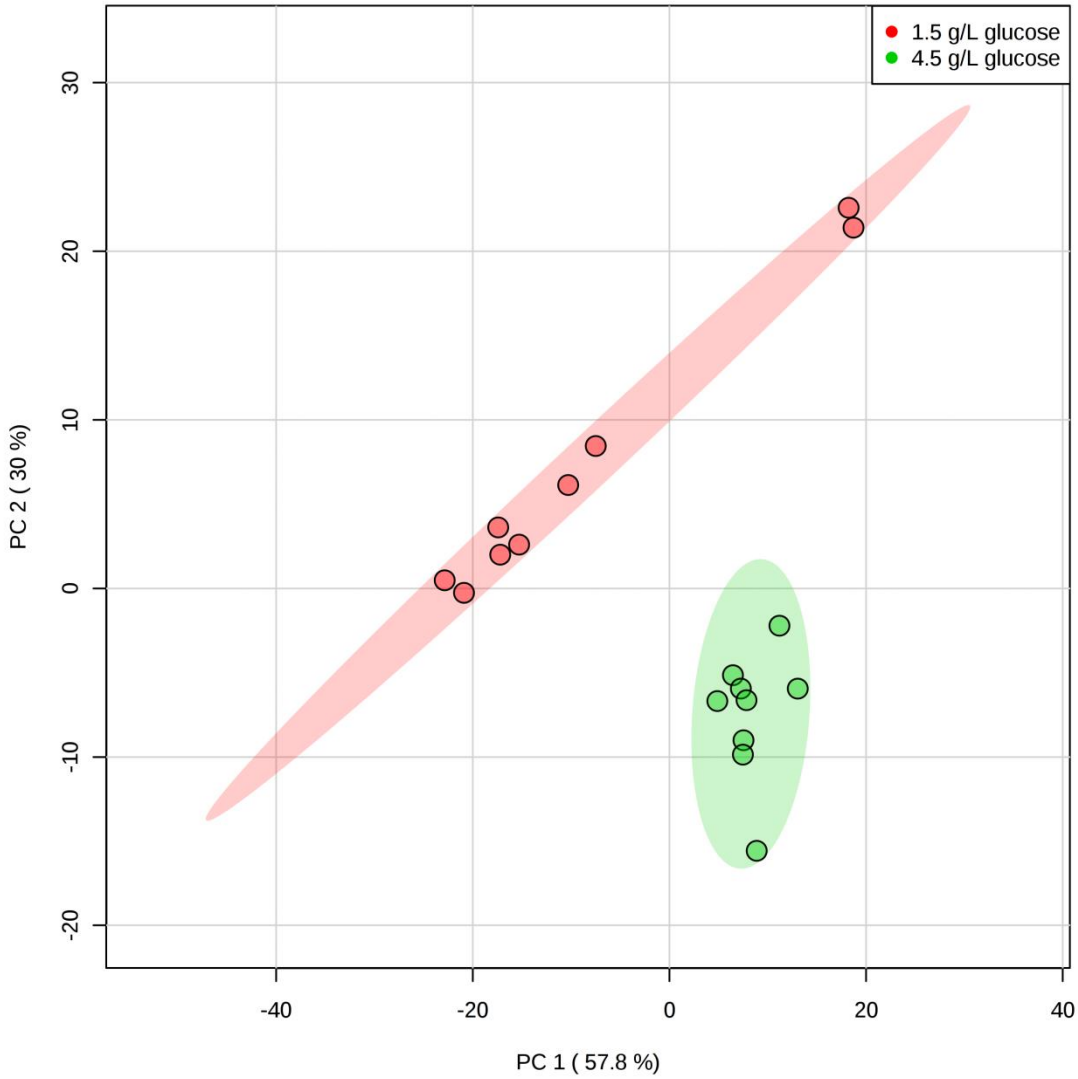

Figure 2.31: PCA scores plot of compound-feature abundances for LN18 WT cells cultured under 1.5 g / L or 4.5 g / L glucose conditions (Section 8.14), analysed by IC-MS/MS (Section 8.4). Statistical analysis was performed using MetaboAnalyst with normalisation by sum and Pareto scaling (Section 8.11). Shaded areas represent the 95 % confidence interval for each experimental group.

The PCA scores plot of compound-feature abundances for the LN18 WT cells, analysed by IC-MS/MS, showed significant separation between the glucose conditions and all samples were within 95 % confidence intervals, as shown in Fig. 2.31. There were clear outliers (samples 8 and 9 cultured in 1.5 g / L glucose) which did not reduce PCA separation of the experimental groups, but were excluded from further data analysis.

The metabolomics data were analysed using a volcano plot, which combines fold change (FC) and the false discovery rate (FDR)-adjusted t-test p-value of detected

compound-features. Volcano plots are a useful tool for biomarker discovery as significant altered compound-features, with large FC values, are positioned at the extremes of the plot. Volcano plots visually reduce the complexity of the data and the number of compound-features for further investigation can be reduced with FC and FDR-adjusted t-test p-value cut-off limits. A volcano plot (Fig. 2.32) was prepared for IC-MS/MS analysis of LN18 WT cells cultured under different glucose conditions. The number of compound-features with a FC greater than 1.5 and an FDR-adjusted t-test p-value less than 0.05 was 2155, demonstrating the extent of metabolic changes which are associated with a change in media glucose concentration.

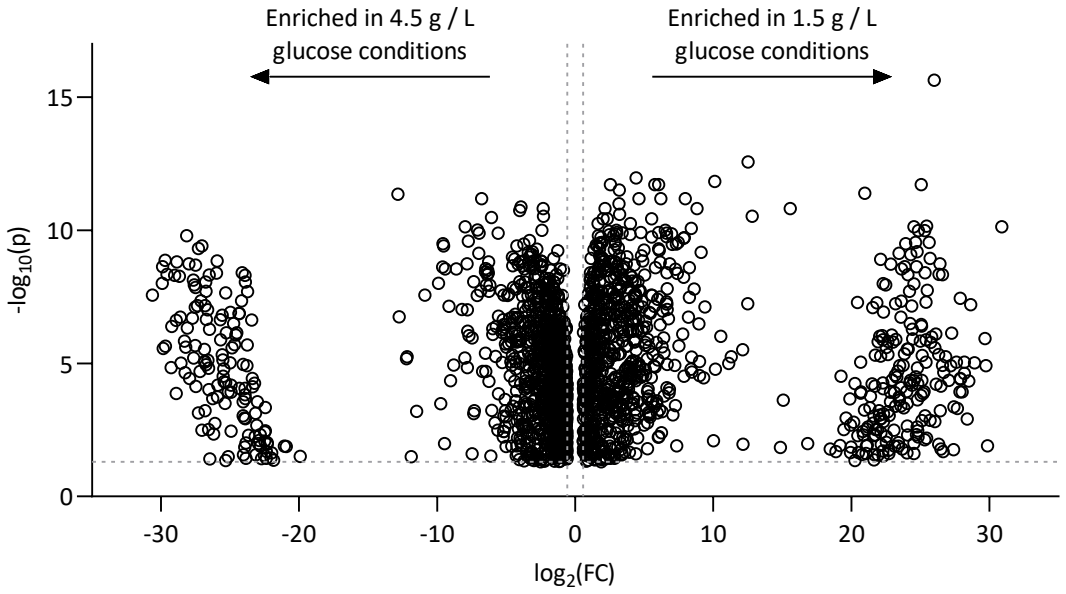

Figure 2.32: Volcano plot showing the compound-features with a FC greater than 1.5 and FDR-adjusted t-test p-value less than 0.05, from univariate statistical analysis of LN18 WT cells cultured under 1.5 g / L or 4.5 g / L glucose conditions (Section 8.14), analysed by IC-MS/MS (Section 8.4).

Ions with positive log_2(FC) values were enriched in 1.5 g / L glucose conditions (932 compound-features) and negative log_2(FC) values were enriched in 4.5 g / L glucose conditions (1223 compound-features). The compound-feature observed at the top right of the volcano plot (20.51_320.0627), was the most important feature but

was not identified; however, and the compound-features ranked 9th, 14th and 25th, were subsequently identified as methyl isocitrate, 6-phosphogluconate and orotate respectively. The values to the extreme right and left of the volcano plot were as a result of compound-features (782 of 2155) which were predominantly observed in either 1.5 g / L or 4.5 g / L glucose conditions, as the data was filtered to ensure that the compound-features were detected in at least 50 % of the samples.

Table 2.2: Top 35 compound-features identified in the volcano plot (Fig. 2.32) from univariate statistical analysis of LN18 WT cells cultured under 1.5 g / L or 4.5 g / L glucose conditions (Section 8.14), analysed by IC-MS/MS (Section 8.4).

Compound-feature	FC	FDR-adjusted p-value	Enriched Group
20.51_320.0627	6.75E+07	2.27E-16	1.5 g / L glucose
7.56_413.1152	5.86E+03	2.69E-13	1.5 g / L glucose
20.51_159.5267	21.35	1.06E-12	1.5 g / L glucose
7.56_413.6170	1.10E+03	1.44E-12	1.5 g / L glucose
26.08_238.6603	3.51E+07	1.93E-12	1.5 g / L glucose
23.44_216.9881	65.98	1.93E-12	1.5 g / L glucose
3.65_322.1146	54.43	1.93E-12	1.5 g / L glucose
25.53_296.4986	5.81	1.93E-12	1.5 g / L glucose
15.78_205.0346	9.20	3.10E-12	1.5 g / L glucose
23.04_244.9976	2.06E+06	4.04E-12	1.5 g / L glucose
11.41_447.0236	7.37E+03	4.35E-12	4.5 g / L glucose
5.59_274.1057	24.64	6.44E-12	1.5 g / L glucose
18.63_201.5431	2.53E+02	6.46E-12	1.5 g / L glucose
14.47_275.0169	1.10E+02	6.46E-12	4.5 g / L glucose
20.51_258.0375	73.86	6.46E-12	1.5 g / L glucose
25.12_311.5040	9.01	1.01E-11	1.5 g / L glucose
17.07_189.5033	15.32	1.33E-11	4.5 g / L glucose
5.46_490.1409	4.85E+04	1.52E-11	1.5 g / L glucose
23.31_405.0008	4.53E+02	1.52E-11	1.5 g / L glucose
16.25_111.0196	5.01	1.52E-11	4.5 g / L glucose
5.59_168.0425	4.49	1.52E-11	1.5 g / L glucose
15.05_245.0061	16.12	1.82E-11	4.5 g / L glucose
6.37_195.0326	9.24	2.48E-11	1.5 g / L glucose
7.56_827.2330	7.20E+03	2.94E-11	1.5 g / L glucose
16.25_155.0093	4.89	2.94E-11	4.5 g / L glucose
11.41_349.0547	67.46	3.30E-11	4.5 g / L glucose
7.70_494.6429	46.64	3.67E-11	1.5 g / L glucose
14.47_289.0676	5.00	3.67E-11	1.5 g / L glucose
5.46_182.0581	4.06	3.67E-11	1.5 g / L glucose
11.53_209.0941	3.14	5.54E-11	1.5 g / L glucose
20.91_256.5148	16.07	5.59E-11	1.5 g / L glucose
4.74_158.0815	4.62E+07	6.90E-11	1.5 g / L glucose
23.31_200.9929	2.01E+09	7.34E-11	1.5 g / L glucose
11.81_131.8243	2.43E+07	7.34E-11	1.5 g / L glucose
14.47_137.5062	2.51E+02	7.34E-11	4.5 g / L glucose

IC-MS/MS analysis of LN18 WT cells measured over 1000 significantly altered compound-features and demonstrated the profound effect that extracellular glucose concentration has on cell metabolism.

To explore the coverage of central carbon metabolites for untargeted IC-MS/MS analysis of LN18 WT cells (Section 8.14), and the metabolic effect of glucose concentration, a

"pathway heat map" was prepared (Fig. 2.33), demonstrating FC for identified metabolites, and their pathways based on the Kyoto Encyclopaedia of Genes and Genomes (KEGG) human metabolic network.[167] Metabolite identifications were confirmed by comparison of accurate mass (within 5 ppm), RT (within 3 min), isotopic distribution (greater than 85 % similarity), fragmentation pattern matching (greater than 25 % similarity where available) and CV (less than 35 % for QC samples), with values obtained from analysis of authentic polar and ionic metabolite standards, listed in Table 10.2. The complete list of confirmed metabolite identifications for the dataset is found in Table 10.5.

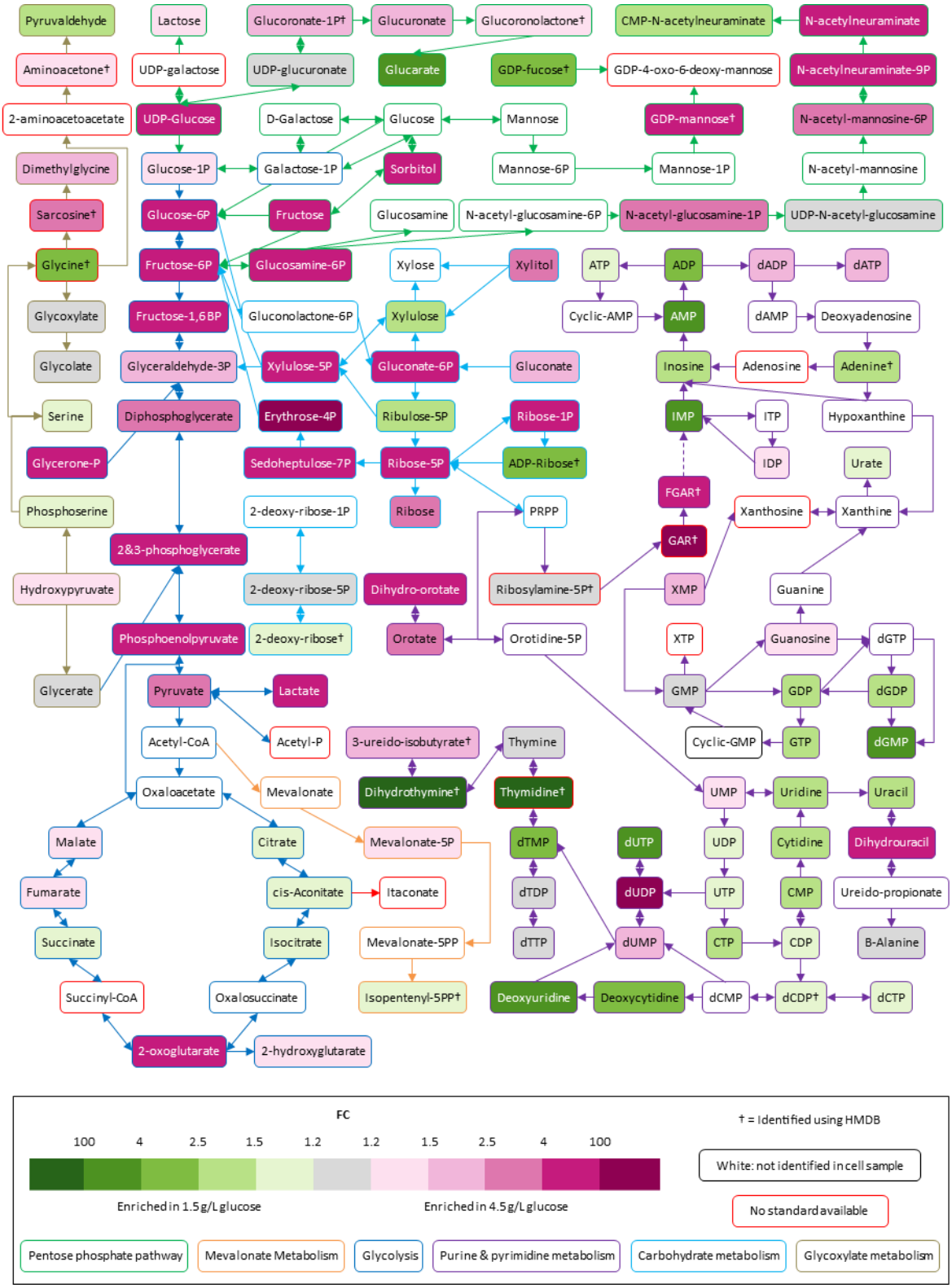

Figure 2.33: Metabolic pathway heat map representing central carbon metabolism and related metabolic processes, showing FC and significance for LN18 WT cells cultured under 1.5 g / L or 4.5 g / L glucose conditions (Section 8.14), analysed by IC-MS/MS (Section 8.4).

The pathway heat map demonstrated the comprehensive coverage of central carbon metabolites and illustrated pathways which were significantly altered as a result of the change in media glucose concentration. Metabolites with a FC greater than 1.2 were coloured in shades of green or purple, for enrichment in 1.5 and 4.5 g / L glucose conditions respectively, and grey represented an enrichment below 1.2-fold. Metabolites which were not identified in the cell extracts were not shaded and a red outline denoted that no authentic standard was available. The identification of all shaded metabolites was performed as described in Section 8.12 and putative identifications (level 2, denoted by †) were made using accurate mass, isotopic distribution and *in silico* fragmentation pattern, obtained from the Human Metabolome Database (HMDB).[168] As observed from univariate statistical analysis of IC-MS/MS data, where more compound-features were observed to be enriched in LN18 WT cells cultured under 4.5 g / L glucose conditions, 88 identified metabolites (of 226) were enriched in 1.5 g / L glucose conditions.

The enrichment in 4.5 g / L glucose conditions, for glycolysis and pentose phosphate pathway intermediates, was indicative of increased utilisation of glucose. Increased energy storage, by means of the glycogen pathway, was inferred by the enrichment of glucose 1-phosphate and uridine diphosphate-glucose. The enrichment of lactate also provided further evidence for increased glycolytic activity in LN18 WT cells cultured under 4.5 g / L glucose conditions. Compared with other metabolic pathways, the TCA cycle was not radically altered, with the exception of 2-OG which was enriched 10.0-fold (t-test p-value 2.69×10^{-6}), under 4.5 g / L glucose conditions. This was likely due to high glycolytic capacity and anaplerotic flux from glutamate to 2-OG, generally observed in cancer cell metabolism.[169] Nucleotide metabolites were observed to be enriched in cells cultured under 1.5 g / L glucose conditions including the adenine, cytidine, guanosine, uridine and

thymidine phosphates, possibly caused by increased utilisation in DNA and RNA synthesis for cell division in cells cultured under 4.5 g / L glucose conditions.

2.7.2. HILIC-MS/MS analysis of LN18 wild-type glioblastoma cells

To further evaluate IC-MS/MS for untargeted metabolomics compared with an existing metabolomics method, the LN18 WT cells cultured under different glucose conditions (Section 8.14), were also analysed by HILIC-MS/MS (Section 8.5). MS data were processed using Progenesis QI and MetaboAnalyst, as described in Section 8.11. Analysis by HILIC-MS/MS resulted in a larger number of integrated chromatographic peaks ($7.4x10^5$); however, of these, only $3.4x10^3$ compound-features were assigned and $3.5x10^3$ MS/MS spectra were acquired. The PCA scores plot of compound-feature abundances for LN18 WT cells cultured under 1.5 g / L or 4.5 g / L glucose conditions, analysed by HILIC-MS/MS, is shown in Fig. 2.34.

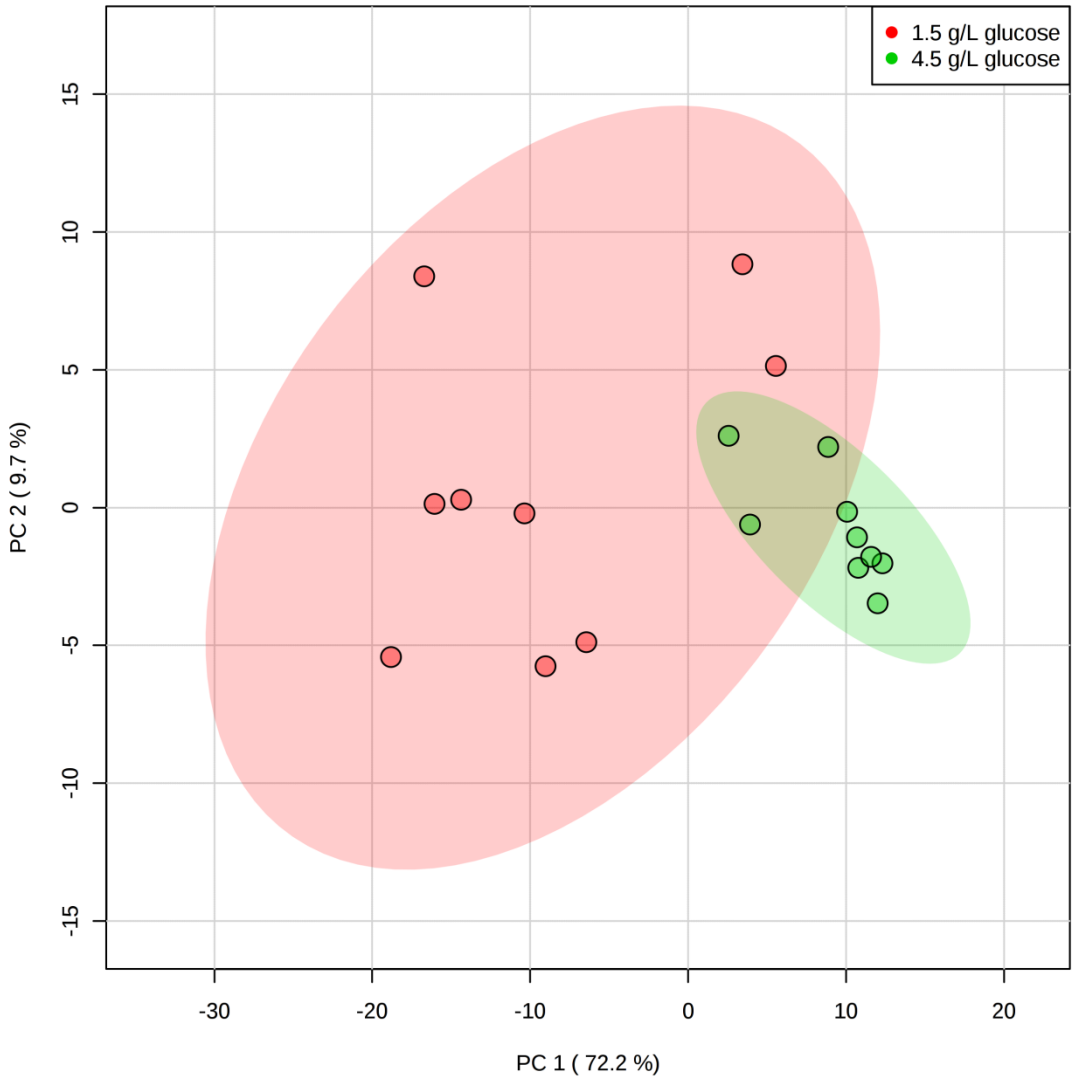

Figure 2.34: PCA scores plot of compound-feature abundances for LN18 WT cells cultured under 1.5 g / L or 4.5 g / L glucose conditions (Section 8.14), analysed by HILIC-MS/MS (Section 8.5). Statistical analysis was performed using MetaboAnalyst with normalisation by sum and Pareto scaling (Section 8.11). Shaded areas represent the 95 % confidence interval for each experimental group.

The PCA scores plot of compound-feature abundances for HILIC-MS/MS analysis (Fig. 2.34), showed reduced separation of the experimental groups compared with IC-MS/MS (Fig. 2.31) and overlap of the 95 % confidence intervals was observed. IC-MS/MS was therefore better at resolving compound-features which contributed to metabolic differences between LN18 WT cells, cultured at difference glucose conditions.

The volcano plot for HILIC-MS/MS (Fig. 2.35) analysis of LN18 WT cells, showed a larger number of compound-features which were enriched in 1.5 g / L glucose conditions (699 of 1110 compound-features). The FDR-adjusted p-values obtained from t-tests, were generally higher compared to IC-MS/MS analysis. The reduced statistical significance was likely due to the reduced reproducibility of HILIC-MS/MS compared with IC-MS/MS analysis, as discussed in Section 2.5.

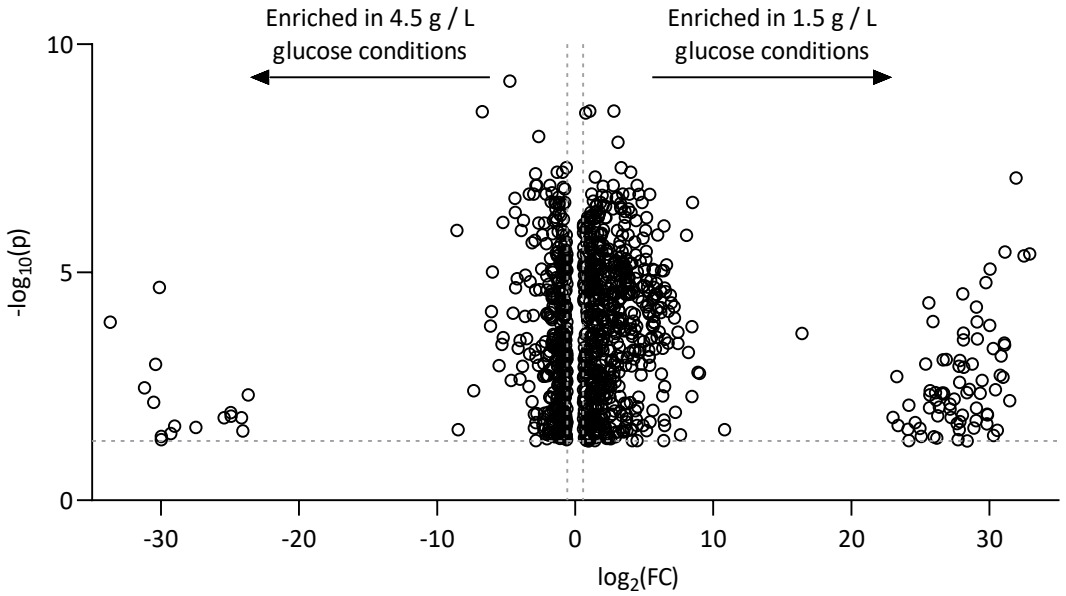

Figure 2.35: Volcano plot showing the compound-features with a FC greater than 1.5 and FDR-adjusted t-test p-value less than 0.05, from univariate statistical analysis of LN18 WT cells cultured under 1.5 g / L or 4.5 g / L glucose conditions (Section 8.14), analysed by HILIC-MS/MS (Section 8.5).

A greater number of compound-features with large FC values were observed on the far right hand side of the volcano plot, which corresponded to compound-features which were enriched over $1x10^6$-fold in LN18 WT cells cultured under 1.5 g / L glucose conditions. The values to the extreme left and right of the plot corresponded to compound-features which were predominantly observed in only one of the experimental groups, leading to large FC values. The most important compound-feature (1.75_215.0144), in the volcano plot was enriched

26.78-fold (p-value 6.46×10^{-10}) in LN18 WT cells cultured under 4.5 g / L glucose conditions (Fig. 2.36(a)), but was not identified.

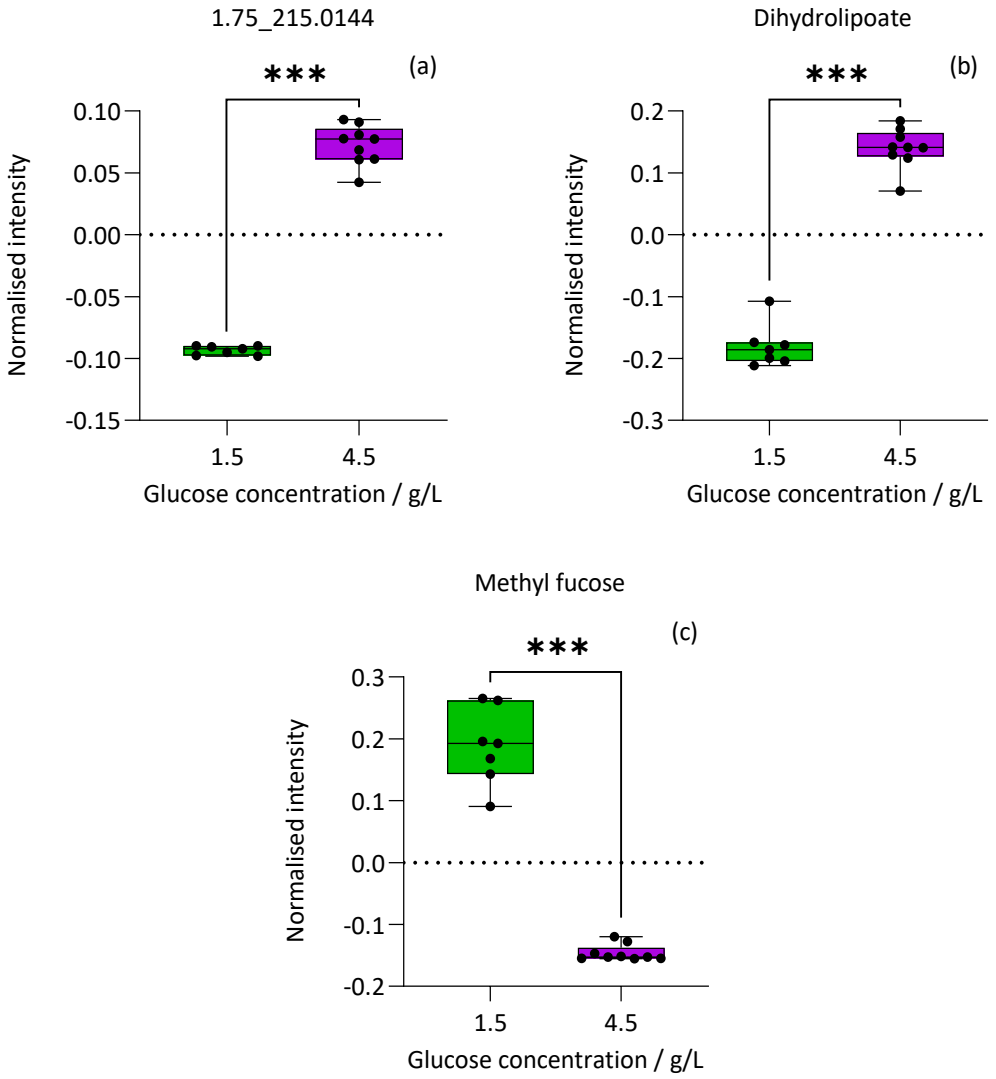

Figure 2.36: Box plots showing the abundances (normalised to all compounds) for the unidentified compound-feature 1.75_215.0144 (a), dihydrolipoate (b) and methyl fucose (c) in LN18 WT cells cultured under 1.5 g / L or 4.5 g / L glucose conditions (Section 8.14), analysed by HILIC-MS/MS (Section 8.5). The box plots show the mean, 25-75th percentiles and whiskers extend from the minimum to maximum values. The number of samples are denoted with dots and significance from t-tests are annotated (ns, p-value greater than 0.05; *, p-value less than 0.05; **, p-value less than 0.01; and ***, p-value less than 0.001).

The top 35 compound-features (Table 2.3), ranked by the magnitude of their distance from the origin, were relatively equally distributed between the two experimental groups with 18 compound-features enriched in 1.5 g / L glucose and 16 compound-features enriched in 4.5 g / L glucose.

Table 2.3: Top 35 compound-features identified in the volcano plot (Fig. 2.35) from univariate statistical analysis of LN18 WT cells cultured under 1.5 g / L or 4.5 g / L glucose conditions (Section 8.14), analysed by HILIC-MS/MS (Section 8.5).

Compound-feature	FC	FDR-adjusted p-value	Enriched Group
1.75_215.0144	26.78	6.46E-10	4.5 g / L glucose
2.32_198.0618	6.97	2.92E-09	1.5 g / L glucose
4.79_132.9000	2.07	2.92E-09	1.5 g / L glucose
1.74_240.0365	1.07E+02	3.03E-09	4.5 g / L glucose
4.85_134.8944	1.70	3.19E-09	1.5 g / L glucose
1.60_207.0510	6.24	1.06E-08	4.5 g / L glucose
9.07_141.0122	8.61	1.41E-08	1.5 g / L glucose
1.94_247.9996	10.05	5.05E-08	1.5 g / L glucose
4.82_209.9491	1.57	5.05E-08	4.5 g / L glucose
1.24_177.0768	16.34	6.39E-08	1.5 g / L glucose
4.59_179.9554	2.47	6.39E-08	4.5 g / L glucose
7.34_179.9185	1.88	6.39E-08	4.5 g / L glucose
2.72_424.1783	7.31	6.89E-08	4.5 g / L glucose
1.94_257.0160	2.74	8.16E-08	1.5 g / L glucose
2.06_263.0442	4.13E+09	8.57E-08	1.5 g / L glucose
1.60_183.0066	7.21	1.24E-07	4.5 g / L glucose
3.01_144.0122	6.78	1.24E-07	1.5 g / L glucose
1.94_210.9736	22.36	1.25E-07	1.5 g / L glucose
1.58_147.0298	6.92	1.25E-07	4.5 g / L glucose
5.25_220.8731	3.58	1.25E-07	4.5 g / L glucose
1.94_314.9287	4.08	1.31E-07	1.5 g / L glucose
4.42_176.9809	1.83	1.38E-07	4.5 g / L glucose
1.75_71.0129	1.69	1.48E-07	4.5 g / L glucose
4.75_180.9567	3.20	1.79E-07	4.5 g / L glucose
1.29_179.0924	15.29	1.92E-07	1.5 g / L glucose
1.22_181.0618	10.84	1.92E-07	1.5 g / L glucose
1.68_149.0244	10.07	1.92E-07	4.5 g / L glucose
7.68_315.8361	8.11	1.92E-07	4.5 g / L glucose
8.10_360.9773	4.30	1.92E-07	4.5 g / L glucose
1.94_172.9577	2.30	1.92E-07	1.5 g / L glucose
2.32_235.0997	42.47	1.96E-07	1.5 g / L glucose
1.94_211.0278	24.52	1.96E-07	1.5 g / L glucose
1.67_217.0307	3.88	2.06E-07	1.5 g / L glucose
1.63_169.0272	4.81	2.22E-07	1.5 g / L glucose
1.51_192.0877	8.19	2.28E-07	1.5 g / L glucose

The compound-features 1.60_207.0510 and 1.24_177.0768 were putatively identified (level 2) using accurate mass, isotope pattern and *in silico* fragmentation pattern (from HMDB), as dihydrolipoate and methyl fucose respectively.[168]

Dihydrolipoate (Fig. 2.36(b)) was 6.24-fold (p-value $1.06x10^{-8}$) enriched in LN18 WT cells cultured under 4.5 g / L glucose conditions and methyl fucose (Fig. 2.36(c)) was depleted 16.34-fold (p-value $6.39x10^{-8}$).

The coverage provided by IC-MS/MS for metabolites in central carbon metabolism and surrounding metabolic networks was demonstrated by untargeted analysis of LN18 WT cells cultured under 1.5 g / L or 4.5 g / L glucose conditions. IC-MS/MS was also compared with HILIC-MS/MS, and was shown to have a larger number of detected compound-features.

2.8. Chapter summary

An untargeted IC-MS/MS method was developed for the separation and identification of polar and ionic metabolites in biological samples, and validated for linearity, LLoD and LLoQ using authentic metabolite standards and cell extracts. Eluent gradient conditions were optimised for chromatographic separation of a range of polar and ionic metabolites including sugar phosphates, pentose phosphate pathway and glycolytic intermediates, as well as TCA cycle metabolites. Degradation and in-source fragmentation of metabolites was investigated and source conditions established, to maximise sensitivity and reproducibility. MS and MS/MS scan parameters were also optimised to ensure an adequate number of spectra were acquired across a chromatographic peak for relative quantitation, in addition to the acquisition of fragmentation spectra for metabolite identification. Reproducibility of RT and ion abundances for IC-MS/MS, over a 3 month period, were compared with HILIC-MS/MS. IC-MS/MS was demonstrated to have increased sensitivity and linearity than HILIC-MS/MS and consequently had reduced LLoD and LLoQ for the majority of the authentic metabolite standards analysed. Untargeted

analysis of LN18 WT cells cultured under 1.5 g / L or 4.5 g / L glucose conditions was also performed, demonstrating the application of IC-MS/MS to the analysis of biological samples. Statistical analysis of IC-MS/MS data revealed a greater number of significantly altered compound-features than HILIC-MS/MS and provided increased separation between experimental groups in PCA scores plots of compound-feature abundances. IC-MS/MS displayed comprehensive coverage of central carbon metabolism and identified significant differences in glycolysis, pentose phosphate pathway and nucleotide metabolism, for LN18 WT cells cultured at different media glucose concentrations. The enrichment of the majority of identified metabolites in LN18 WT cells, cultured under 4.5 g / L glucose conditions, was indicative of increased utilisation of glycolysis as well as storage of glucose as glycogen. A depletion of nucleotide metabolites was also observed, likely caused by increased proliferation of cells cultured under 4.5 g / L glucose conditions and associated requirement for DNA and RNA synthesis. The large FC observed between experimental groups, demonstrated the importance of culturing cells in appropriate media. The wide range of chemical selectivity, increased sensitivity compared with HILIC-MS/MS and coverage of pathways comprising polar and ionic metabolites therefore demonstrated the use of IC-MS/MS for untargeted metabolomics.

Chapter 3. Exploring central carbon metabolism in IDH1 mutant and wild-type cells

3.1. Introduction

IDH mutations have been shown to alter a number of metabolic pathways associated with central carbon metabolism, including specific metabolites in the TCA cycle, pentose phosphate pathways and cytoplasmic reactions, leading to the intracellular production of 2-HG.[40] A number of metabolites associated with central carbon metabolism and surrounding metabolic pathways are not well characterised by HILIC-MS/MS (as discussed in Sections 1.4 and 2.5).[116, 117] In order to more effectively investigate the metabolic effects association with an IDH1 mutation, the IC-MS/MS method developed in Chapter 2, will be applied to the analysis of Mut and WT cells. Exploration of the metabolic effects of an IDH1 mutation may lead to increased understanding of its tumourigenic role and aid the development of selective treatment strategies.[1, 6]

LN18, U87-MG and 293T Mut and WT cell lines were used to investigate the metabolic impact of an IDH1 mutation and differentiate cell-specific effects. LN18 cells are a human malignant glioma cell line, with epithelial morphology, established in 1976 from cells taken from a 65 year old male patient with a right temporal lobe glioma. The cell line is known to have a p53 mutation (cysteine to serine at codon 238) and is PTEN WT.[170] LN18 cells have a doubling time of 72 hours and injection of LN18 cells induced tumour formation in nude mice.[171] U87-MG cells are a glioblastoma cell line of unknown origin with epithelial morphology and a doubling time of 72 hours.[172, 173] Unlike the LN18 cell line, U87-MG cells are p53 WT but do have a PTEN mutation and therefore may have different basal metabolism and glucose uptake rate.[174, 175] 293T cells are a human embryonic kidney derived cell line expressing the simian virus 40 large T antigen with

epithelial morphology and a doubling time of 24 hours.[176] The cell line is PTEN WT and although the cells express WT p53, the simian virus 40 large T antigen can form a complex with p53 causing inhibition.[177-179] The cell lines were genetically modified to express R132H mutant IDH1 using lentiviral vector transduction (by Dr. Chiara Bardella, as described in Section 8.13). All cell lines in this chapter were cultured by the author with the exception of the LN18 cells harvested at passage 21 which were cultured by Dr. Joan Gannon. All samples were processed, analysed using the IC-MS/MS method (Section 8.4), and the results interpreted by the author. The data presented in this chapter relating to the LN18 cell line with and without an IDH1 mutation, analysed by IC-MS has previously been published by the author.[155]

The research aims of this chapter were to:

- Investigate changes in metabolism associated with an IDH1 mutation by comparison of Mut and WT cells.
- Compare performance of IC-MS/MS against an established HILIC-MS/MS method.
- Identify specific enzymes and/or metabolic pathways in IDH1 mutant cells which could be potential therapeutic targets.

3.2. Polar and ionic metabolite database

To extend the depth of coverage for IDH1 mutant pathways of interest, including metabolites in central carbon metabolism, anaplerotic and cataplerotic processes, authentic standards were obtained, as described in Section 8.3. Table 10.2 in the appendix contains the data used for the identification of metabolites characterised by the

IC-MS/MS method described in Section 8.4, including monoisotopic mass, chemical formula, RT and fragmentation pattern.

3.3. Untargeted IC-MS/MS analysis of LN18 IDH1 mutant and wild-type glioblastoma cells

LN18 Mut and WT cells were cultured in American Type Culture Collection recommended media (4.5 g / L glucose Dulbecco's Modified Eagle Medium (DMEM) supplemented with 10 % FBS and 1 % GlutaMAX), as described in Section 8.14. Experimental groups with 9 biological replicates were cultured in 6 cm diameter plates with a seeding density of 20 % and a total media volume of 5 mL. At 80 % cell confluency (after ca. 48 hours), media was removed and the adherent monolayer of cells were washed with ca. 10 mL phosphate buffered saline. Cells were snap frozen with ca. 3 mL liquid N_2 to arrest metabolic processes and cells mechanically lysed, with the addition of 300 μL ice-cold 80 % methanol$_{(aq)}$, to extract metabolites into solution. Prior to analysis, the DNA concentration of the samples were measured using a NanoDrop One microvolume UV-Vis Spectrophotometer (Thermo Scientific, San Jose, CA, USA) and normalised to a concentration of ca. 100 ng / μL, ensuring that experimental groups had the same DNA concentration and therefore number of cells. Metabolite extracts were centrifuged at 2.2×10^4 x g for 20 min to remove cell debris and filtered using 10 kDa MWCO filters (Merck Millipore, Darmstadt, Germany), following the manufacturers protocol, prior to analysis. A QC sample was prepared by the pooling of equal volumes of all individual samples and analysed before, during and at the end of each LC-MS method to assess analytical reproducibility. Spectral alignment and peak peaking was performed using Progenesis QI and where possible metabolites were identified by comparison of

accurate mass, RT, isotopic distribution and fragmentation pattern matching with the IC-MS/MS database (Section 10.2). All runs were assessed for suitability as the alignment reference and chromatograms were automatically aligned to correct for RT drift. Peak picking utilised run aggregation, chromatographic peak detection, isotope and adduct deconvolution was performed using automatic sensitivity adjustment and no minimum chromatographic peak width or retention time limits. The full non-normalised dataset (identified and unidentified compound-features) from Progenesis QI was exported as a .csv file and further data processing and statistical analysis was performed using MetaboAnalyst, as described in Section 8.11.[166] The PCA scores plot of compound-feature abundances demonstrated significant separation between Mut and WT cells and all samples within 95 % confidence intervals, as shown in Fig. 3.1. The data associated with this experiment has been deposited in the Oxford University Research Archive (title: Metabolomics of the first culture of LN18 IDH wild-type and mutant cells) and is freely accessible (https://doi.org/10.5287/bodleian:2abVOAvrg).

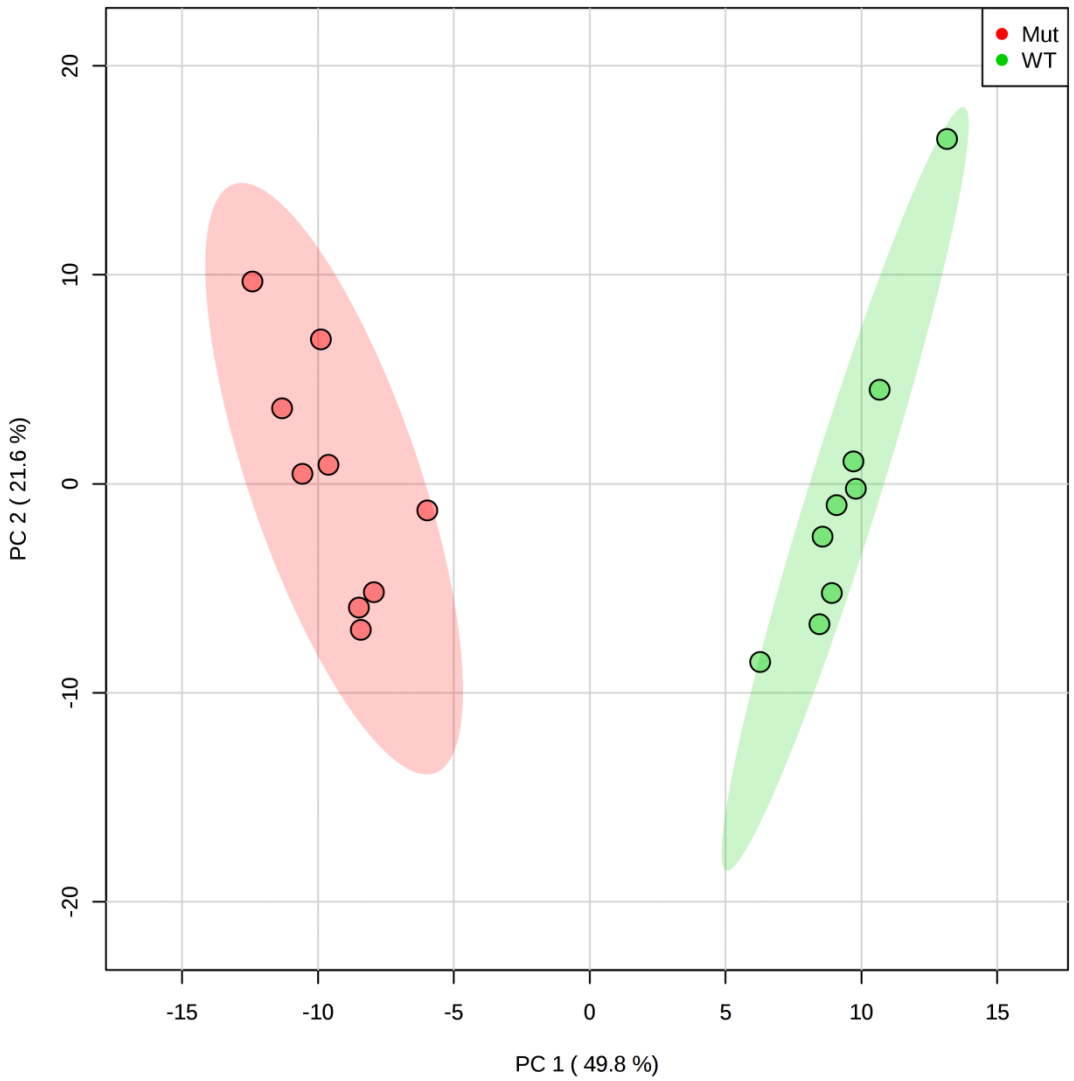

Figure 3.1: PCA scores plot of compound-feature abundances from the analysis of LN18 Mut and WT cells cultured under 4.5 g / L glucose conditions (experimental replicate 1, Section 8.14), by IC-MS/MS (Section 8.4). Statistical analysis was performed using MetaboAnalyst with normalisation by sum and Pareto scaling (Section 8.11). Shaded areas represent the 95 % confidence interval for each experimental group.

The PCA loadings plot (not shown) had significant contributions from 2-HG, lactate and glutathione, which led to separation between the experimental groups. Of the 4245 compound-features which were peak-picked from IC-MS/MS data, in Progenesis QI, 226 had their identifications confirmed (listed in Section 10.5) using authentic metabolite standards, as described in Section 8.12. The complete list of confirmed metabolite identifications for the dataset is found in Table 10.5.

3.3.1. Univariate statistical analysis of LN18 IDH1 mutant and wild-type glioblastoma cells analysed by IC-MS/MS

As expected from the literature, 2-HG (Fig. 3.2(a)) had the largest FC of the identified metabolites, from IC-MS/MS analysis of LN18 cells, with a 548-fold (p-value < 1.0×10^{-16}) enrichment in Mut cells and 2-OG (Fig. 3.2(b)) was significantly depleted (FC 6.29, p-value 7.7×10^{-11}).[40, 42, 133] Despite the depletion of 2-OG, other TCA cycle metabolites such as citrate, succinate and malate (Fig. 3.2(c,d,e) were not significantly altered.

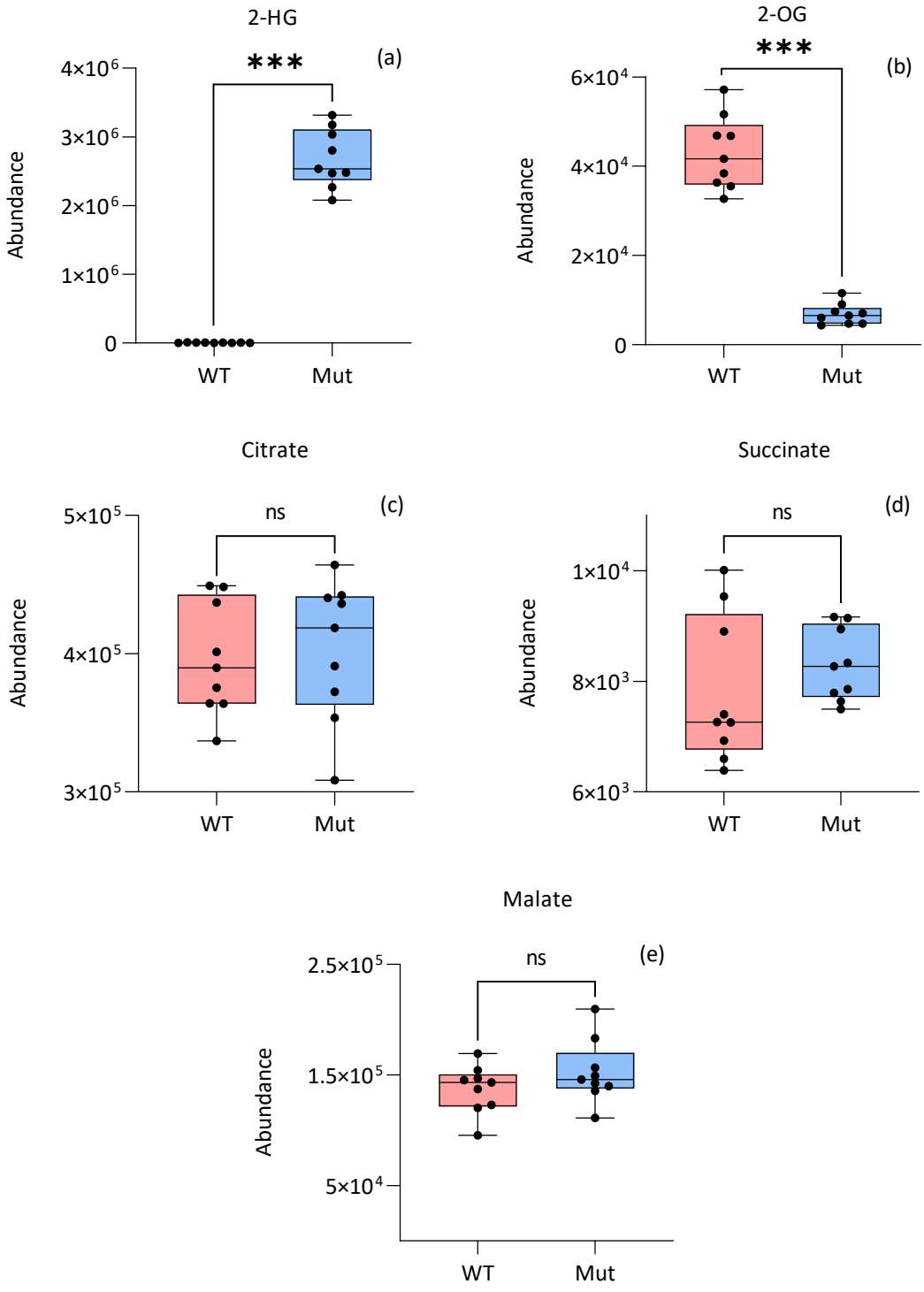

Figure 3.2: Box plots showing the abundance of 2-HG (a), 2-OG (b), citrate (c), succinate (d) and malate (e) in LN18 Mut and WT cells cultured under 4.5 g / L glucose conditions (experimental replicate 1, Section 8.14), analysed by IC-MS/MS (Section 8.4). The box plots show the mean, 25-75th percentiles and whiskers extend from the minimum to maximum values. The number of samples are denoted with dots and significance from t-tests are annotated (ns, p-value greater than 0.05; *, p-value less than 0.05; **, p-value less than 0.01; and ***, p-value less than 0.001).

As 2-OG was the only TCA cycle metabolite which was significantly depleted in Mut cells, it could be that the metabolic pathways which supply the TCA cycle were upregulated to sustain TCA cycle flux. 2 & 3-phosphoglycerate and phosphoenolpyruvate were both significantly depleted in Mut cells, as shown in Fig. 3.3, by 1.44-fold (p-value 6.5×10^{-4}) and 2.86-fold (p-value 4.2×10^{-5}) respectively.

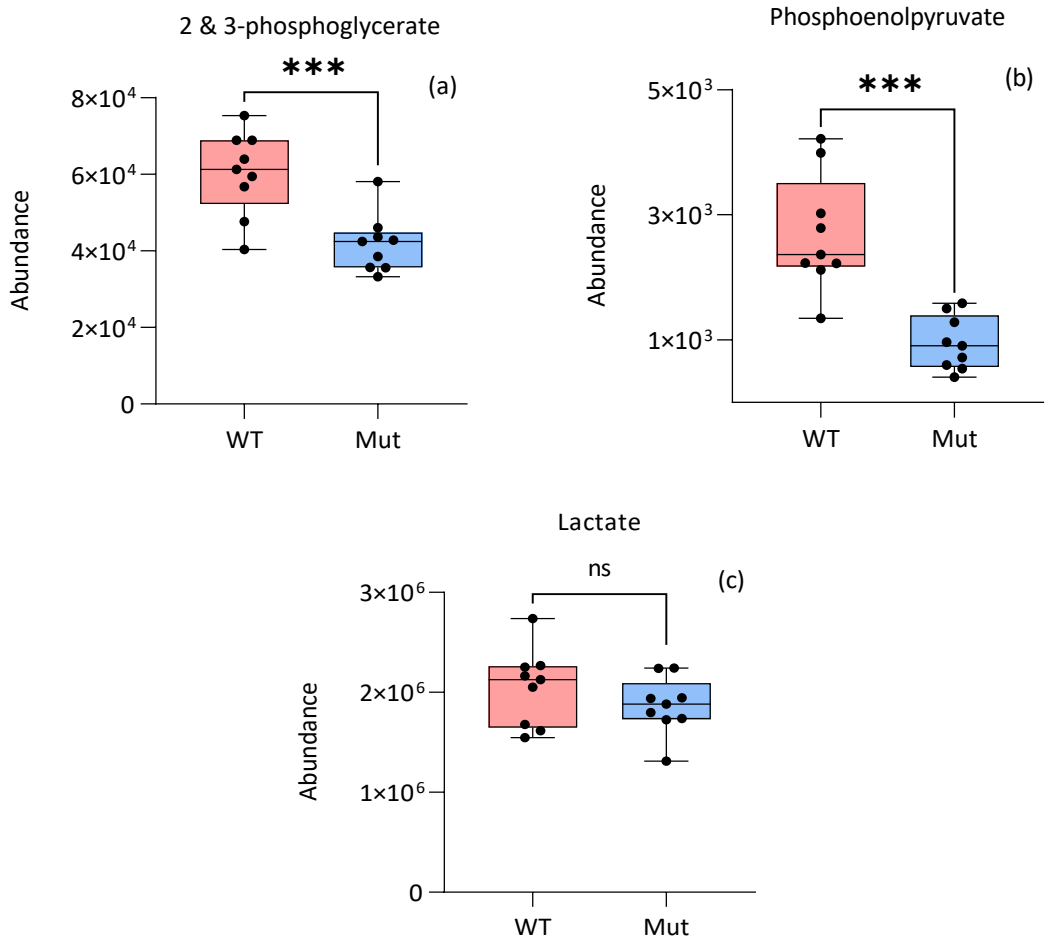

Figure 3.3: Box plots showing the abundance of 2 & 3-phosphoglycerate (a), phosphoenolpyruvate (b), and lactate (c) in LN18 Mut and WT cells cultured under 4.5 g / L glucose conditions (experimental replicate 1, Section 8.14), analysed by IC-MS/MS (Section 8.4). The box plots show the mean, 25-75th percentiles and whiskers extend from the minimum to maximum values. The number of samples are denoted with dots and significance from t-tests are annotated (ns, p-value greater than 0.05; *, p-value less than 0.05; **, p-value less than 0.01; and ***, p-value less than 0.001).

Lactate was not significantly enriched, as might have been expected as a result of the Warburg effect.[10] Metabolites at the end of the glycolytic pathway were still significantly depleted, possibly to sustain the TCA cycle. Pyruvate, a source of acetyl CoA for the TCA

cycle, from either glycolysis or alanine and cysteine metabolism, was also significantly depleted (Fig. 3.4(a), FC 1.08, p-value $9.6x10^{-3}$). Glutamate, an intermediate in the conversion of glutamine to 2-OG under low energy conditions was also significantly depleted in Mut cells (Fig. 3.4(b)), FC 1.61, p-value $1.3x10^{-3}$).[180] Glutamine abundance was not significantly altered, which suggests that intracellular concentration was maintained from alternative sources, despite the depletion of 2-OG in Mut cells.

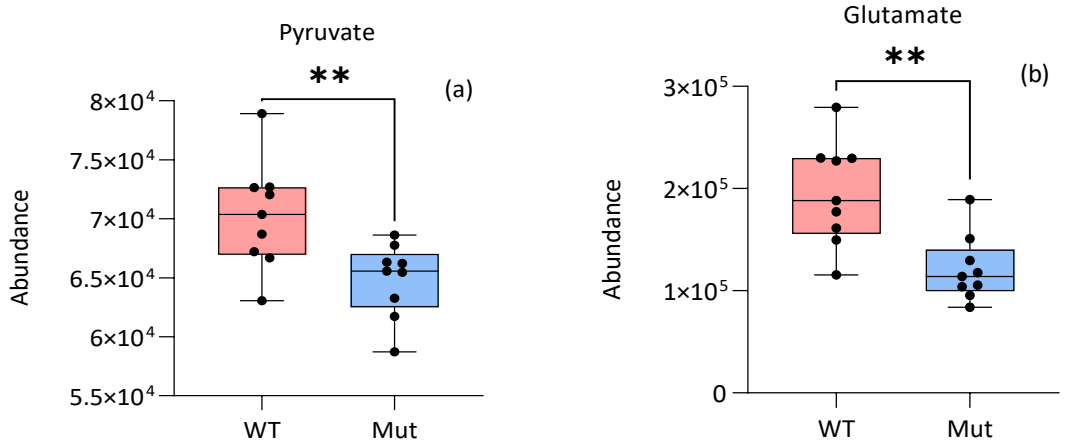

Figure 3.4: Box plots showing the abundance of pyruvate (a) and glutamate (b) in LN18 Mut and WT cells cultured under 4.5 g / L glucose conditions (experimental replicate 1, Section 8.14), analysed by IC-MS/MS (Section 8.4). The box plots show the mean, 25-75th percentiles and whiskers extend from the minimum to maximum values. The number of samples are denoted with dots and significance from t-tests are annotated (ns, p-value greater than 0.05; *, p-value less than 0.05; **, p-value less than 0.01; and ***, p-value less than 0.001).

A volcano plot was prepared for the data from IC-MS/MS analysis of LN18 Mut and WT cells, excluding compound-features below 1.5 FC and t-test p-value 0.05, which reduced the number of compound-features from 3325 to 473. As shown in Fig. 3.5, the FC values were generally less than 5 and most compound-features had negative log_2(FC) values, which signified that they were depleted in Mut samples.

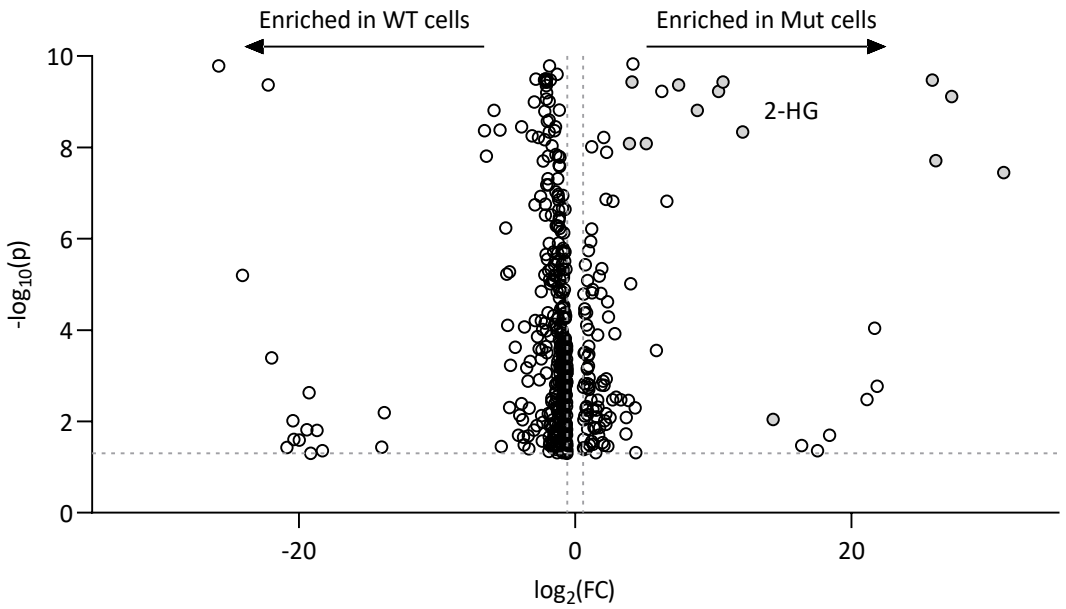

Figure 3.5: Volcano plot showing the compound-features with a FC greater than 1.5 and FDR-adjusted t-test p-value less than 0.05, from univariate statistical analysis of LN18 Mut and WT cells cultured under 4.5 g / L glucose conditions (experimental replicate 1, Section 8.14), by IC-MS/MS (Section 8.4).

The oncometabolite 2-HG (labelled in Fig. 3.5) was ranked 30th based on distance from the origin and the top 35 compound-features are listed in Table 3.1. The compound-features with large FC values at the top right of the volcano plot (circles with grey fill) were enriched in Mut samples and found to have the same RT as 2-HG (10.71 min).

Table 3.1: Top 35 compound-features identified in the volcano plot (Fig. 3.5) from univariate statistical analysis of LN18 Mut and WT cells cultured under 4.5 g / L glucose conditions (experimental replicate 1, Section 8.14), by IC-MS/MS (Section 8.4).

Compound-feature	FC	p-value	Enriched group	Identification
14.80_276.0721	18.16	1.48E-10	Mut	
10.71_316.0348	5.89E+07	1.64E-10	WT	
21.57_385.6969	3.65	1.64E-10	WT	
21.57_418.0308	2.47	2.50E-10	WT	
19.02_160.0610	7.21	3.21E-10	WT	
21.57_198.0401	4.53	3.21E-10	WT	
21.57_302.0518	4.45	3.21E-10	WT	
21.57_172.0610	4.21	3.21E-10	WT	
10.71_128.8696	6.09E+07	3.36E-10	Mut	
21.57_213.0636	4.70	3.36E-10	WT	
21.57_240.0508	4.47	3.36E-10	WT	
21.57_320.0625	4.43	3.36E-10	WT	β-citryl glutamate
21.57_128.5269	4.25	3.36E-10	WT	
21.69_196.0609	3.47	3.36E-10	WT	L-DOPA
10.71_147.2092	1.67E+03	3.68E-10	Mut	
10.71_101.0240	17.24	3.68E-10	Mut	Acetoacetate
21.57_137.5321	4.29	3.68E-10	WT	
21.57_216.0506	4.27	3.68E-10	WT	
10.71_174.0765	4.97E+06	4.32E-10	WT	
10.71_103.0397	1.79E+02	4.32E-10	Mut	
21.57_160.0286	4.29	4.39E-10	WT	
10.71_129.0189	77.43	5.89E-10	Mut	
10.71_146.8477	1.34E+03	5.91E-10	Mut	
21.69_154.0505	4.16	6.36E-10	WT	
10.71_150.0363	1.61E+08	7.69E-10	Mut	
21.57_159.5269	4.23	8.70E-10	WT	
23.17_233.0369	3.70	9.81E-10	WT	
19.02_142.0504	7.75	1.01E-09	WT	
9.52_231.0270	2.22	1.52E-09	WT	
10.71_147.0293	4.58E+02	1.56E-09	Mut	2-HG
25.53_216.0507	58.72	1.56E-09	WT	
21.57_107.5217	4.64	1.61E-09	WT	
2.87_187.0370	3.68	2.53E-09	WT	
21.57_150.5217	4.07	2.68E-09	WT	
12.52_159.0292	14.76	3.55E-09	WT	2-oxoadipate

The magnitude of FC values, for the depleted compound-features in Table 3.1, were generally smaller than the FC for enriched compound-features. The 9 compound-features which co-eluted with 2-HG at RT 10.71 min were enriched in Mut cells, with the exception of the compound-features 10.71_316.0348 and 10.71_174.0765, which were depleted in Mut cells. The compound-feature 21.57_320.0625 was putatively identified (level 2) as

β-citryl glutamate (with a mass error of 0.62 ppm, isotope similarity of 98.07 % and *in silico* fragmentation pattern matching), which was significantly depleted in Mut cells by 4.43-fold (p-value 3.36×10^{-10}). β-citryl glutamate and 2-HG were both highly abundant in the LN18 cells (abundances greater than 1.5×10^{4}) and 25 of the top 35 compound-features identified in the volcano plot (Fig. 3.5), were potential ion clusters or in-source fragments of these two metabolites. The dataset was therefore filtered to remove 46 co-eluting compound-features, which had similar fold change values, and reanalysed using MetaboAnalyst to reveal additional compound-features which had significantly altered abundance. The PCA scores plot of compound-feature abundances (not shown) for the filtered dataset, did not show any reduction in separation of Mut and WT cells and all samples were within 95 % confidence intervals. A volcano plot was prepared for the filtered dataset and 438 compound-features had a FC greater than 1.5 and a FDR-adjusted t-test p-value less than 0.05, the top 35 compound-features are shown in Table 3.2.

Table 3.2: Top 35 compound-features identified from volcano plot analysis for filtered univariate statistical analysis of LN18 Mut and WT cells cultured under 4.5 g / L glucose conditions (experimental replicate 1, Section 8.14), by IC-MS/MS (Section 8.4).

Compound-feature	FC	p-value	Enriched group	Identification
14.80_276.0721	18.14	1.53E-10	Mut	
10.71_316.0348	5.90E+07	2.58E-10	WT	
21.57_418.0308	2.47	3.53E-10	WT	
19.02_160.0610	7.22	4.72E-10	WT	
21.57_172.0610	4.21	4.72E-10	WT	N-acetyl-L-glutamate 5-semialdehyde
21.57_320.0625	4.43	7.13E-10	WT	β-citryl glutamate
21.69_196.0609	3.47	7.13E-10	WT	L-Dopa
10.71_101.0240	17.22	8.24E-10	Mut	Acetoacetate
10.71_174.0765	4.97E+06	9.89E-10	WT	
10.71_129.0189	77.34	1.34E-09	Mut	
21.69_154.0505	4.17	1.46E-09	WT	
23.17_233.0369	3.70	2.15E-09	WT	
19.02_142.0504	7.76	2.21E-09	WT	
9.52_231.0270	2.22	3.02E-09	WT	
10.71_147.0293	4.58E+02	3.10E-09	Mut	2-HG
25.53_216.0507	58.80	3.10E-09	WT	
2.87_187.0370	3.68	4.99E-09	WT	
12.52_159.0292	14.78	7.07E-09	WT	2-oxoadipate
21.57_111.0084	2.67	7.09E-09	WT	
24.11_223.0513	94.90	7.55E-09	WT	
13.29_258.0374	43.58	7.55E-09	WT	Glucosamine 6-phosphate
9.92_285.0493	2.82	7.55E-09	WT	Glycineamide ribonucleotide
21.57_126.0556	3.67	8.13E-09	WT	
14.93_304.0790	6.37	1.09E-08	WT	
11.41_162.0224	4.21	1.09E-08	Mut	Acetylcysteine
10.71_85.0291	15.27	1.52E-08	Mut	
4.26_217.0822	3.21	1.63E-08	WT	
11.66_132.0297	2.30	1.74E-08	Mut	Aspartate
3.76_471.1522	4.85	2.28E-08	Mut	
12.88_326.9795	2.66	2.38E-08	WT	
10.71_165.0397	86.18	2.60E-08	WT	
10.05_162.0403	2.34	2.60E-08	WT	
13.29_319.0438	2.17	2.71E-08	WT	
19.44_82.0658	2.27	4.11E-08	WT	
24.22_286.5216	2.17	4.31E-08	WT	

Of the 438 compound-features identified from volcano plot analysis, which were within the FC and FDR-adjusted t-test p-value cut-off values, the majority were depleted in Mut cells with only 97 compound-features enriched in Mut cells, suggesting that an IDH1 mutation generally causes depletion of polar and ionic metabolites. In addition to the depletion of 2-oxoadipate and β-citryl glutamate, observed in the top 35

compound-features from the unfiltered dataset, acetylcysteine and aspartate were enriched in Mut cells, suggesting that multiple aspects of amino acid metabolism were altered in the presence of an IDH1 mutation. Glucosamine 6-phosphate (Fig. 3.6(a)) and glycineamide ribonucleotide (Fig. 3.6(b)) in the amino sugar and nucleotide sugar pathways, were depleted in Mut cells which suggested an alteration of glycolysis or gluconeogenesis.

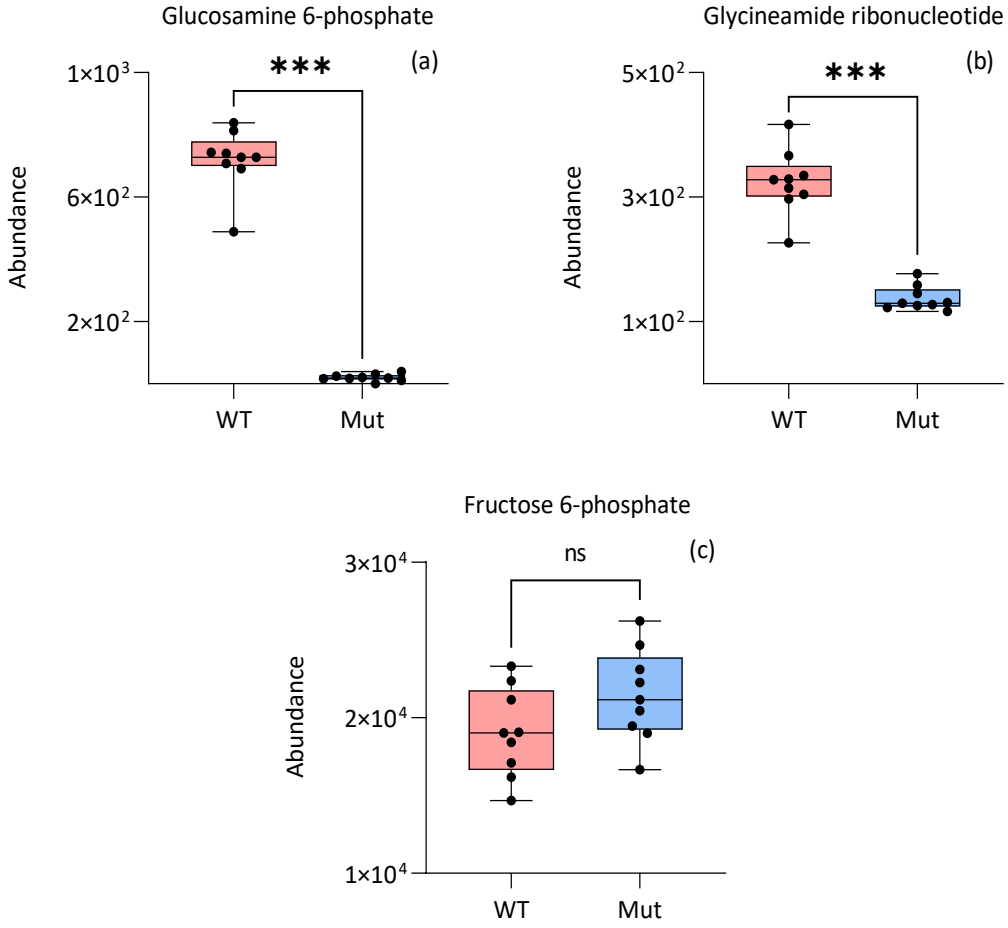

Figure 3.6: Box plots showing the abundance of glucosamine 6-phosphate (a), glycineamide ribonucleotide (b) and fructose 6-phosphate (c) in LN18 Mut and WT cells cultured under 4.5 g / L glucose conditions (experimental replicate 1, Section 8.14), analysed by IC-MS/MS (Section 8.4). The box plots show the mean, 25-75th percentiles and whiskers extend from the minimum to maximum values. The number of samples are denoted with dots and significance from t-tests are annotated (ns, p-value greater than 0.05; *, p-value less than 0.05; **, p-value less than 0.01; and ***, p-value less than 0.001).

Glucosamine 6-phosphate and glycineamide ribonucleotide are upstream of fructose 6-phosphate; their depletion in Mut cells (Fig. 3.6) by 36.22-fold (p-value 3.81×10^{-6}) and

2.37-fold (p-value $1.95x10^{-9}$) respectively, suggested an upregulation of amide sugar metabolism to supply glycolysis. Fructose 6-phosphate (Fig. 3.6(c)) was not significantly altered and therefore was produced by alternative metabolic pathways, or upstream enzymes were inhibited. Although glycolytic flux can be estimated from the NAD^+ / NADH ratio, neither cofactor can be detected directly by IC-MS/MS, as they rapidly degrade in biological matrices and NAD^+ is removed in the eluent suppressor. The concentrations of NAD^+ and NADH cannot therefore be calculated directly in the LN18 cells and the cellular redox state was estimated by measurement of the lactate / pyruvate ratio, which is maintained at equilibrium with the NAD^+ / NADH ratio.[181, 182] The cofactors NAD^+ and NADH are essential for electron transfer reactions in all biological systems and the intracellular concentration of both species is regulated, to ensure cellular reactions have either reducing or oxidising power.[183] A higher lactate / pyruvate ratio would suggest a higher NAD^+ / NADH ratio and consequently, an upregulation of glycolysis. The abundance of lactate and pyruvate were measured by IC-MS/MS and the ratio calculated, to evaluate relative changes in redox state between Mut and WT cells, as shown in Fig. 3.7.

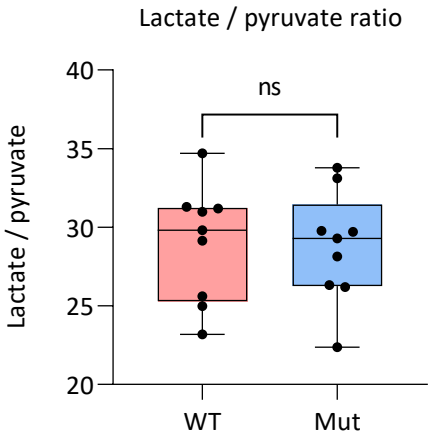

Figure 3.7: Lactate / pyruvate ratio calculated from the analysis of LN18 Mut and WT cells cultured under 4.5 g / L glucose conditions (experimental replicate 1, Section 8.14), analysed by IC-MS/MS (Section 8.4). The box plot shows the mean, 25-75th percentiles and whiskers extend from the minimum to maximum values. The number of samples are denoted with dots and significance from t-tests are annotated (ns, p-value greater than 0.05; *, p-value less than 0.05; **, p-value less than 0.01; and ***, p-value less than 0.001).

No significant change in the lactate / pyruvate ratio between Mut and WT cells suggests that there was no additional glycolytic activity in Mut cells and that cellular redox balance was maintained, despite additional acidification from the excess production of 2-HG and $NADP^+$ in Mut cells. Redox metabolism in IDH1 mutant cells, has previously been shown to be sensitive to NAD^+ depletion and the cells may therefore be utilising other metabolic energy pathways to maintain redox balance.[184] The LN18 cells may therefore be able to cope with the effects of an IDH1 mutation when cultured under 4.5 g / L glucose conditions; however, their capacity for further redox stress was unknown, especially when energy limited.

As observed from univariate statistical analysis (Table 3.9), β-citryl glutamate (Fig. 3.8(a)) was enriched in Mut cells by 3.70-fold (p-value 7.7×10^{-14}). β-citryl glutamate is a structural analogue of N-acetylaspartylglutamate (NAAG) and has previously been demonstrated to be enriched during early brain development in rodents.[185] NAAG is one of the most abundant neurotransmitters in the human brain and shares the same biosynthetic

pathways (which are known to be sensitive to glutamate and ATP concentration), as β-citryl glutamate.[186, 187] β-citryl glutamate has been proposed as an Fe(II) chelator and activator of aconitase, a critical TCA cycle enzyme which converts citrate to isocitrate.[188] The proposed role of β-citryl glutamate is as an 'address tag' for the transfer of Fe(II) to mitochondrial aconitase which can enhance mitochondrial activity and therefore promote neuronal proliferation and survival.[189]

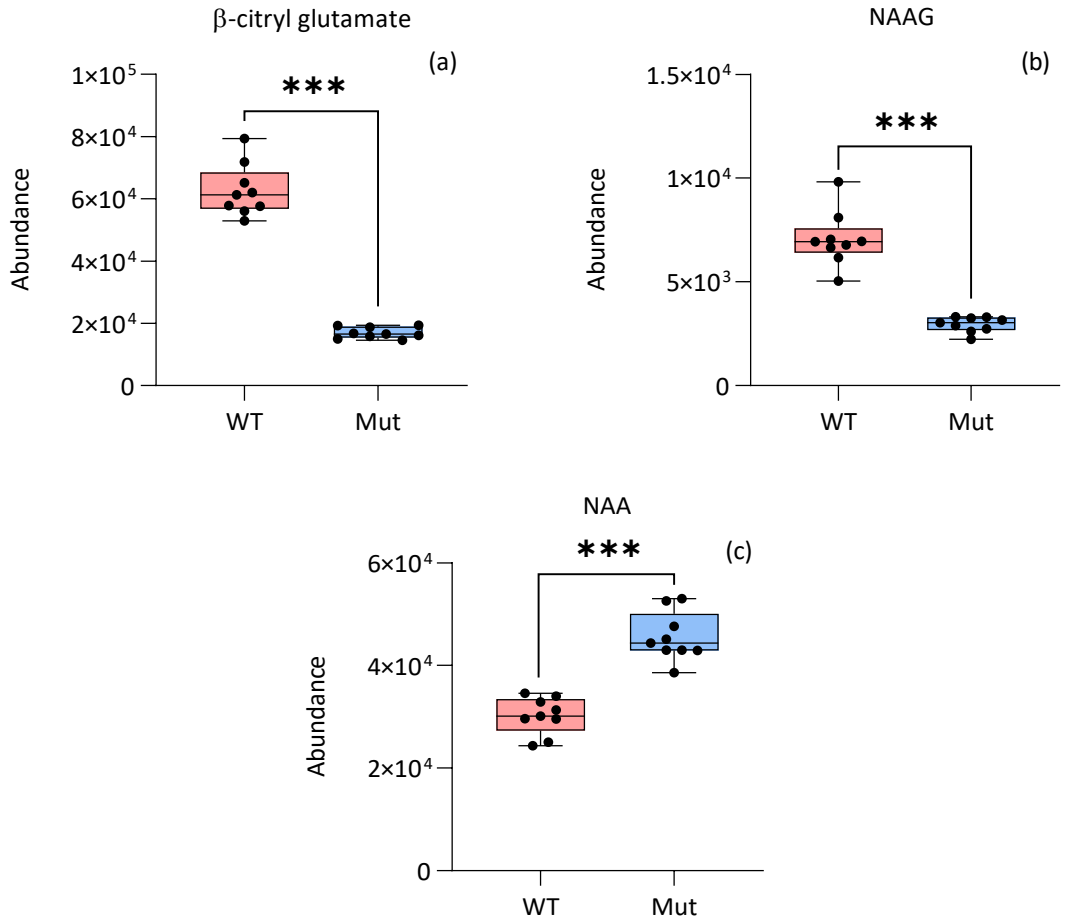

Figure 3.8 Box plots showing the abundance of β-citryl glutamate (a), NAAG (b) and NAA (c) in LN18 Mut and WT cells cultured under 4.5 g / L glucose conditions (experimental replicate 1, Section 8.14), analysed by IC-MS/MS (Section 8.4). The box plots show the mean, 25-75th percentiles and whiskers extend from the minimum to maximum values. The number of samples are denoted with dots and significance from t-tests are annotated (ns, p-value greater than 0.05; *, p-value less than 0.05; **, p-value less than 0.01; and ***, p-value less than 0.001).

NAAG was also depleted in Mut cells (Fig. 3.8(b), FC 2.39, p-value 3.40×10^{-9}) and NAA was enriched in Mut cells by 1.51-fold (p-value 8.62×10^{-7}), as shown in Fig. 3.8. NAA is the

primary source of acetate for neuronal cells and both NAA and NAAG have been shown to promote proliferation and inhibit differentiation in glioma stem cells.[190] It is possible that the intracellular concentration of NAA and NAAG may be regulated in Mut cells to maintain the mutation as the cells divide.

2-oxoadipate, a lysine degradation product, was observed in the analysis of LN18 cells by both HILIC-MS/MS and IC-MS/MS, and was depleted 12.3-fold in Mut cells, as shown in Fig. 3.9. The other metabolites in the lysine degradation pathway were not well characterised by IC-MS/MS due to their zwitterionic properties, although glutarate (Fig. 3.9(b), was significantly enriched 1.75-fold (p-value 3.5×10^{-11}), in Mut cells. Glutarate can be converted to 2-HG by glutarate dioxygenase and could have accumulated in Mut cells, if the enrichment of 2-HG caused product inhibition.

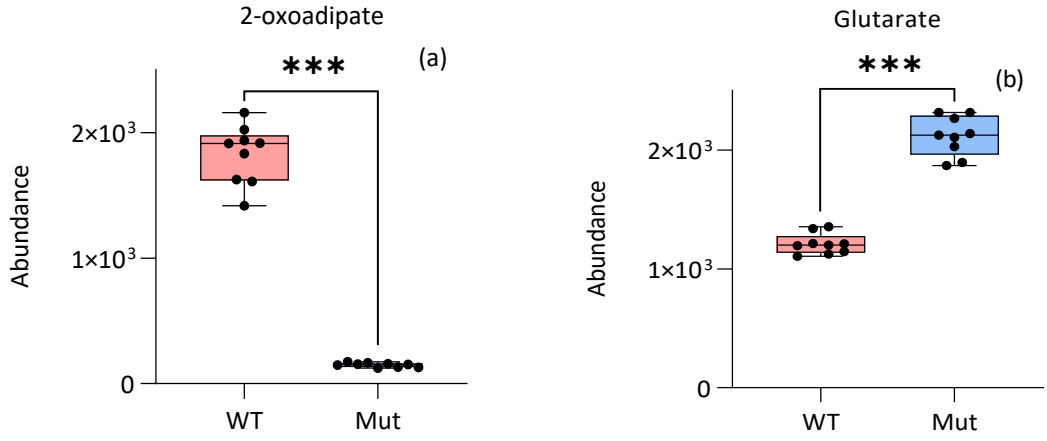

Figure 3.9: Box plots showing the abundance of 2-oxoadipate (a) and glutarate (b) in LN18 Mut and WT cells cultured under 4.5 g / L glucose conditions (experimental replicate 1, Section 8.14), analysed by IC-MS/MS (Section 8.4). The box plots show the mean, 25-75th percentiles and whiskers extend from the minimum to maximum values. The number of samples are denoted with dots and significance from t-tests are annotated (ns, p-value greater than 0.05; *, p-value less than 0.05; **, p-value less than 0.01; and ***, p-value less than 0.001).

3.3.2. Multivariate statistical analysis of LN18 IDH1 mutant and wild-type glioblastoma cells analysed by IC-MS/MS

Partial least squares-discriminant analysis (PLS-DA) is a supervised multivariate technique, which allows classification and modelling of high-dimensional data and is therefore useful for multivariate statistical analysis of metabolomics data.[191] PLS-DA consists of a series of calculations which are used to reduce the complexity of the data by forming a combined PLS component, followed by classification and the construction of a predictive model. The classification ability of the PLS-DA model was cross validated and the 1 component accuracy, goodness of fit (R^2) and predictive ability (Q^2) values were found to be 1.00, 0.97 and 0.95 respectively. The value for Q^2 should be greater than or equal to 0.4 for biological model.[192] The value of R^2 should be greater than 0.5 and $|R^2-Q^2|$ must be less than 0.3, otherwise the model may be over-fitted.[100, 193] PLS-DA was performed to allow the identification of compound-features which contributed to metabolic differences between Mut and WT LN18 cells, using variable importance in projection (VIP). The compound-features with a VIP score greater than 2 are shown in Table 3.3.

Table 3.3: Table of the compound-features with a VIP score greater than 2, identified from PLS-DA analysis of LN18 cells cultured under 4.5 g / L glucose conditions (experimental replicate 1, Section 8.14), by IC-MS/MS (Section 8.4).

Compound-feature	VIP score	Enriched group	Identification
10.71_147.0293	40.77	Mut	2-HG
4.74_89.0240	15.39	WT	Lactate
10.71_129.0189	15.20	Mut	
14.33_146.0453	10.99	WT	N-methyl-aspartate
24.22_426.0236	10.66	Mut	dGDP
15.05_306.0764	10.38	WT	Glutathione
16.38_146.0454	7.69	WT	Glutamate
21.57_320.0625	6.01	WT	β-citryl glutamate
24.22_505.9874	5.99	Mut	ATP
15.67_404.0548	5.40	WT	
17.70_331.5555	5.29	Mut	

Compound-feature	VIP score	Enriched group	Identification
12.66_145.0137	5.19	WT	2-OG
15.78_307.0801	4.99	WT	
16.60_191.0190	4.95	Mut	Citrate
4.39_128.0348	4.24	WT	1-pyrroline-4-hydroxy-2-carboxylate
15.58_184.9850	4.07	WT	2-phosphoglycerate
10.71_101.0240	3.91	Mut	Acetoacetate
19.02_160.0610	3.71	WT	
11.66_132.0297	3.62	Mut	Aspartate
4.87_218.1026	3.51	WT	Pantothenate
17.70_664.1162	3.47	Mut	
15.28_96.9692	3.43	Mut	
8.49_210.0279	3.38	WT	Phosphocreatine
4.97_124.0069	3.37	Mut	Taurine
3.89_273.0376	3.24	WT	
6.50_87.0084	3.21	WT	Pyruvate
14.33_147.0486	3.00	WT	
14.33_102.0557	2.93	WT	Dimethylglycine
24.22_252.4899	2.85	Mut	
15.28_176.9352	2.79	Mut	
12.88_229.0111	2.73	WT	Ribose 5-phosphate
17.70_332.0571	2.63	Mut	
15.91_613.1586	2.46	WT	
4.66_135.0294	2.45	WT	
18.24_323.0287	2.43	Mut	Uridine 5'-monophosphate
18.24_558.0626	2.37	WT	ADP ribose
8.49_421.0660	2.30	WT	
4.74_179.0554	2.27	WT	Fructose
26.89_402.9961	2.24	Mut	Uridine 5'-diphosphate
16.25_102.0557	2.14	WT	α-aminobutyrate
16.38_147.0487	2.14	WT	
15.58_492.0705	2.05	WT	
9.92_174.0401	2.03	Mut	NAA
15.67_244.0220	2.01	WT	
16.02_152.5340	2.00	WT	

Despite 2-HG not having the largest FC or lowest t-test p-value, from univariate statistical analysis, it was identified as the highest contributing compound-feature to the PLS-DA model, differentiating between Mut and WT cells. Lactate and citrate also contributed to the model, despite no significant alteration in abundance being observed for either metabolite. β-citryl glutamate and NAA also contributed to the model providing further

evidence for β-citryl glutamate as a biomarker of an IDH1 mutation. With the exception of some amide metabolites, the remaining identified metabolites were all nucleotide-derived and the enrichment of deoxyguanosine diphosphate (dGDP) and ATP suggested that nucleotide metabolism was modified in LN18 Mut cells. AMP and ADP were both significantly depleted in Mut cells by 1.4-fold (p-value 2.5×10^{-3}) and 3.2-fold (p-value 1.2×10^{-2}) respectively, ATP and dGDP were enriched in Mut cells, but not significantly, as shown in Fig. 3.10.

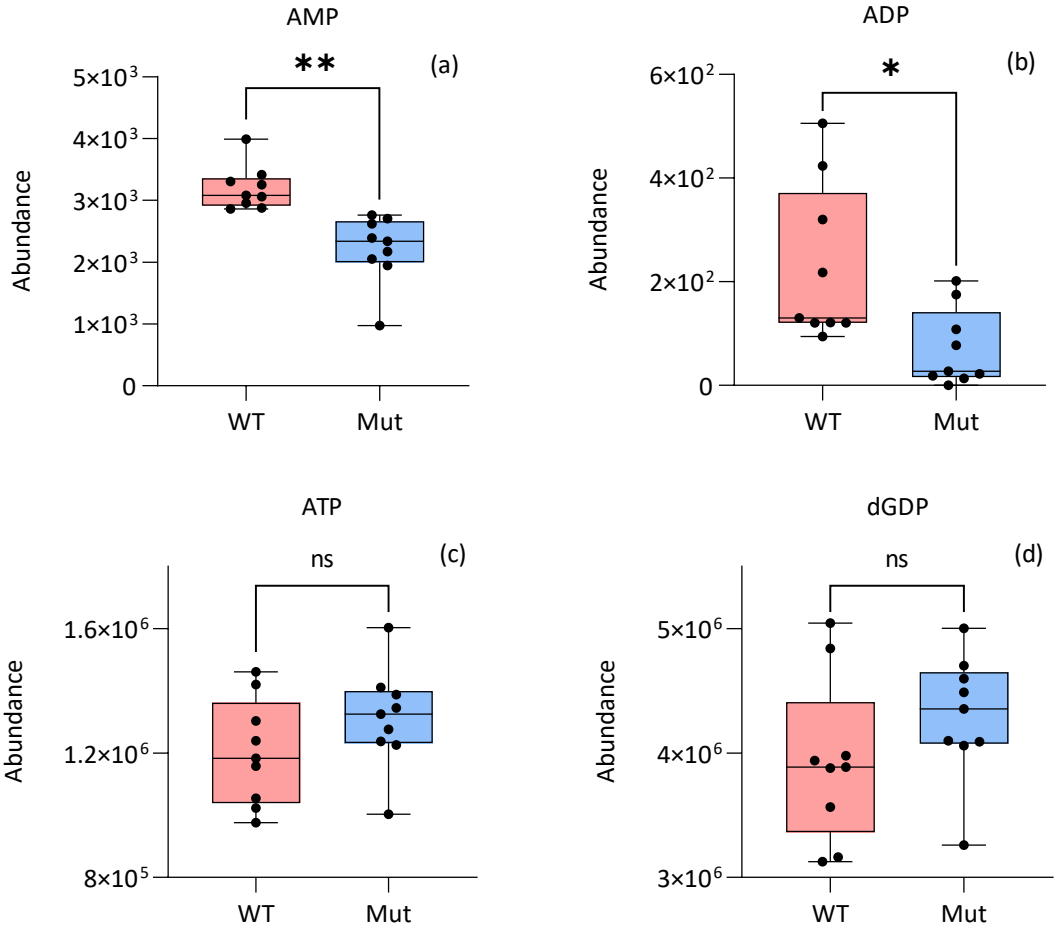

Figure 3.10: Box plots showing the abundance of AMP (a), ADP (b), ATP (c) and dGDP (d) in LN18 Mut and WT cells cultured under 4.5 g / L glucose conditions (experimental replicate 1, Section 8.14), analysed by IC-MS/MS (Section 8.4). The box plots show the mean, 25-75th percentiles and whiskers extend from the minimum to maximum values. The number of samples are denoted with dots and significance from t-tests are annotated (ns, p-value greater than 0.05; *, p-value less than 0.05; **, p-value less than 0.01; and ***, p-value less than 0.001).

To investigate whether energy production was modified in the presence of an IDH1 mutation, in response to redox stress or to intracellular acidification caused by 2-HG, the relative contributions of AMP, ADP and ATP to the total adenine nucleotide pool were calculated. Despite ATP not being significantly increased in Mut cells, the calculated contribution to the total adenine nucleotide pool was significantly enriched, as shown in Fig. 3.11.

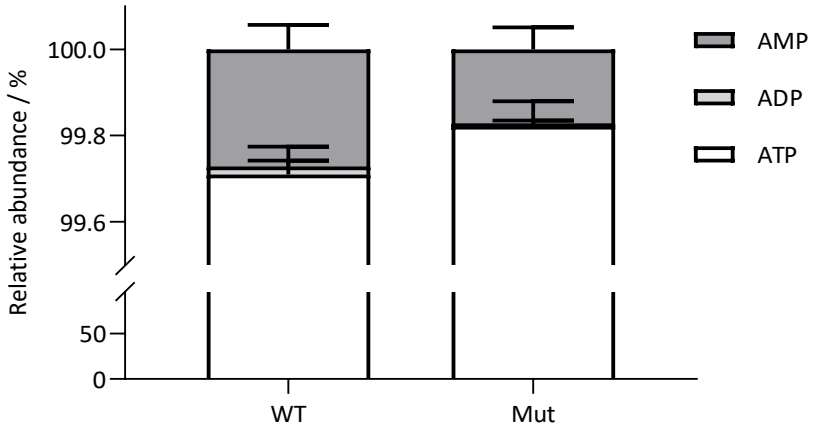

Figure 3.11: Relative abundances of AMP, ADP and ATP compared with the total adenine nucleotide pool calculated from the analysis of LN18 Mut and WT cells cultured under 4.5 g / L glucose conditions (experimental replicate 1, Section 8.14), analysed by IC-MS/MS (Section 8.4). Error bars represent standard deviation of the mean for 9 samples.

As the ion abundances for AMP, ADP and ATP were orders of magnitude different from one another, an additional calculation step (to calculate absolute concentration) would have introduced further uncertainty. Absolute concentrations were also not required as only two experimental groups were compared and therefore the relative changes in the metabolites could be used to assess their contribution to the total pool. As shown in Fig. 3.11, the contribution of ATP was significantly higher in Mut cells, when compared using 2-way ANOVA (p-value < $1x10^{-4}$), and AMP was significantly lower (p-value < $1x10^{-4}$). The change in ADP contribution was not significant, likely due to its low absolute abundance, which was near to the LLoD of the instrument. The increased contribution of

ATP in Mut cells suggested that energy production was augmented, in the presence of an IDH1 mutation, possibly to maintain NAD^+ / NADH and $NADP^+$ / NADPH balance, in response the increased intracellular acidification.

Pentose phosphate pathway metabolites were also analysed, as the pathway produces NADPH from $NADP^+$ and therefore may be utilised to remove excess $NADP^+$, produced by the IDH1 mutation, or to produce NADPH, to prevent oxidative stress. The rate determining step in the pentose phosphate pathway is controlled by the abundance of NADPH and $NADP^+$ and is therefore likely to be modified by the mutation.[194, 195] The 7-carbon metabolites in the pentose phosphate pathway were all characterised by IC-MS/MS, in the LN18 samples. Sedoheptulose 1,7-bisphosphate and sedoheptulose 7-phosphate were both significantly depleted in the Mut cells, as shown in Fig. 3.12, with FC values of 1.46 (p-value 3.3×10^{-3}) and 1.59 (p-value 1.7×10^{-3}) respectively.

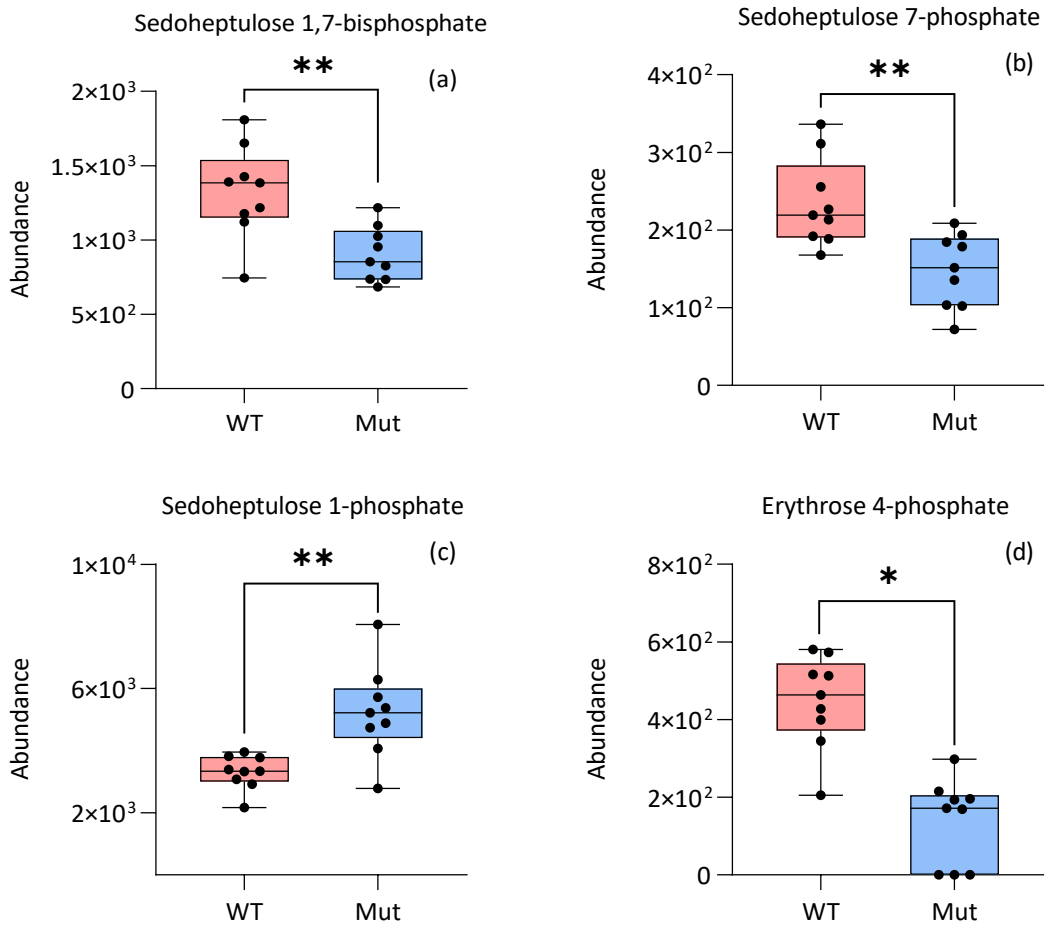

Figure 3.12: Box plots showing the abundance of sedoheptulose 1,7-bisphosphate (a), sedoheptulose 7-phosphate (b), sedoheptulose 1-phosphate (c) and erythrose 4-phosphate (d) in LN18 Mut and WT cells cultured under 4.5 g / L glucose conditions (experimental replicate 1, Section 8.14), analysed by IC-MS/MS (Section 8.4). The box plots show the mean, 25-75th percentiles and whiskers extend from the minimum to maximum values. The number of samples are denoted with dots and significance from t-tests are annotated (ns, p-value greater than 0.05; *, p-value less than 0.05; **, p-value less than 0.01; and ***, p-value less than 0.001).

Sedoheptulose 1-phosphate, an isomer of sedoheptulose 7-phosphate, found in the monosaccharide phosphate pathway, was enriched in Mut cells by 1.60-fold (p-value 3.3x10^{-3}). Erythrose 4-phosphate, which connects the pentose phosphate pathways to glycolysis via fructose 6-phoshate and glyceraldehyde 3-phosphate, was depleted 3.24-fold (p-value 1.4x10^{-2}). Ribose 5-phosphate, which connects the pentose phosphate pathway to glycolysis via glyceraldehyde 3-phosphate was not detected in LN18 Mut and WT cells, likely to be below the LLoD for IC-MS/MS

analysis. The pentose phosphate pathway intermediates were therefore generally depleted in Mut cells, providing further evidence an alteration of redox state.

In summary, untargeted analysis of LN18 Mut and WT cells by IC-MS/MS enabled investigation of metabolites which had significantly altered abundances, as a result of an IDH1 mutation. As expected, 2-HG was enriched in Mut cells and had the largest FC of all the metabolites identified. As a result of the enrichment of 2-HG, 2-OG was significantly depleted, however, other TCA cycle metabolites were not significantly altered. The glycolytic intermediates 2 & 3-phosphoglycerate as well as phosphoenolpyruvate, which supply the TCA cycle, were significantly depleted in Mut cells, likely due to increased requirement of oxaloacetate to maintain TCA cycle flux. Pyruvate was also significantly depleted in the Mut cells, but did not significantly change the lactate / pyruvate ratio, suggesting that Mut cells were able to manage the increased redox stress from the intracellular acidification caused by 2-HG as well as the production of $NADP^+$.

The neurotransmitter NAAG, as well as its structural analogue β-citryl glutamate share the same biosynthetic pathways and were both significantly depleted in Mut cells. β-citryl glutamate has been identified as an Fe(II) chelator and contributes to increased mitochondrial activity and neuronal proliferation in early brain development and therefore may contribute to glioblastoma development.[185, 188]

Cellular energy pathways including pentose phosphate pathways and adenine nucleotide pools were also significantly modified in response to the IDH1 mutation. The lysine degradation products 2-oxoadipate and glutarate were significantly depleted and enriched respectively, in LN18 Mut cells. The other metabolites in the amino acid degradation pathways were not well characterised by IC-MS/MS and will be investigated

further, using a LC-MS/MS method which is selective for amines. The metabolites identified in the LN18 cells will also be investigated in the U87-MG and 293T cells, to see if changes are common to the IDH1 mutation.

3.4. Untargeted HILIC-MS/MS analysis of LN18 IDH1 mutant and wild-type glioblastoma cells

To further compare IC-MS/MS and HILIC-MS/MS for untargeted metabolomics and explore the complementary chemical specificity of the methods, HILIC-MS/MS (Section 8.5) was also used for the analysis of LN18 Mut and WT cells cultured under 4.5 g / L glucose conditions (experimental replicate 1, Section 8.14). Due to solvent incompatibility with HILIC, the LN18 cell samples used for IC-MS/MS (Section 3.3) were dried down using $N_{2(g)}$ and resuspended in 95 % acetonitrile$_{(aq)}$ prior to analysis. The data were processed as described for LN18 cells (Section 3.3) and resulted in a lower number of detected compound-features in Progenesis QI (3409, compared to 4245 for IC-MS/MS). Separation between the experimental groups was not observed in the PCA scores plot of compound-feature abundances (Fig. 3.13), for the metabolite extracts analysed by HILIC-MS/MS. This suggests that there were an insufficient number of significantly altered compound-features detected by HILIC-MS/MS to distinguish between Mut and WT cells.

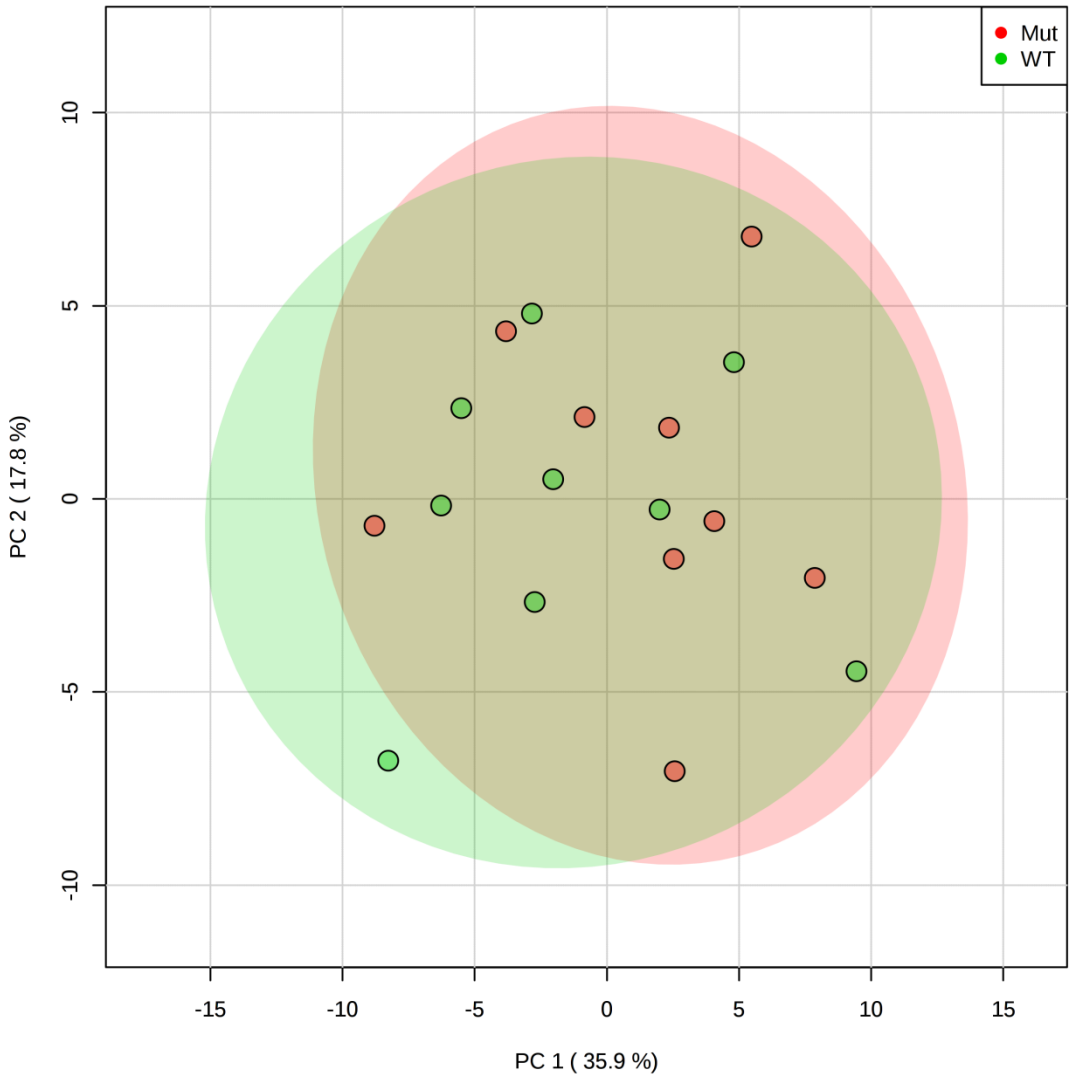

Figure 3.13: PCA scores plot of compound-feature abundances from the analysis of LN18 Mut and WT cells cultured under 4.5 g / L glucose conditions (experimental replicate 1, Section 8.14), by HILIC-MS/MS (Section 8.5). Statistical analysis was performed using MetaboAnalyst with normalisation by sum and Pareto scaling (Section 8.11). Shaded areas represent the 95 % confidence interval for each experimental group.

3.4.1. Univariate statistical analysis of LN18 IDH1 mutant and wild-type glioblastoma cells analysed by HILIC-MS/MS

The volcano plot for LN18 Mut and WT cell samples analysed by HILIC-MS/MS (Fig. 3.14) had only 23 compound-features with a FC greater than 1.5 and FDR-adjusted t-test p-value less than 0.05. The number of significantly altered compound-features was therefore reduced compared with IC-MS/MS analysis (473) and 2-HG was not observed, likely due to poor solubility in acetonitrile, despite the high intracellular concentration.

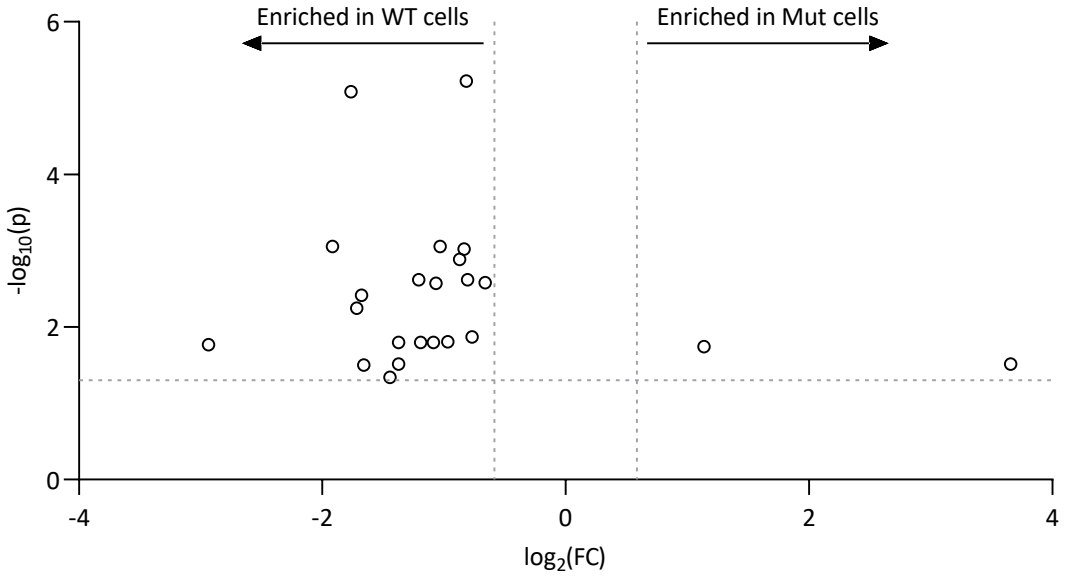

Figure 3.14: Volcano plot showing the compound-features with a FC greater than 1.5 and FDR-adjusted t-test p-value less than 0.05, from univariate statistical analysis of LN18 Mut and WT cells cultured under 4.5 g / L glucose conditions (experimental replicate 1, Section 8.14), by HILIC-MS/MS (Section 8.5).

Only 23 metabolites were significantly altered (listed in Table 3.4), which explained the overlap of experimental groups observed in PCA scores plot (Fig. 3.13). The low number of significantly modified compound-features (despite the 9 biological replicates in each experimental group), provided further evidence that HILIC-MS/MS provided different chemical selectivity to IC-MS/MS. The compound-features 1.76_159.0297, 1.29_129.0555 and 5.44_129.0192, were putatively identified (level 2) from accurate mass, isotope distribution and *in silico* fragmentation patterns, as 2-oxoadipate, adipate semialdehyde and mesaconate respectively, and had CV values of 14.6 %, 14.5 % and 22.5 %. The same metabolites were subsequently observed in analysis of the same samples by IC-MS/MS with lower CV values of 11.3 %, 13.4 % and 13.3 %, demonstrating reduced reproducibility of ion abundance for HILIC-MS/MS.

Table 3.4: Compound-features identified from the volcano plot (Fig. 3.14) from univariate statistical analysis of LN18 Mut and WT cells cultured under 4.5 g / L glucose conditions (experimental replicate 1, Section 8.14), by HILIC-MS/MS (Section 8.5).

Compound-feature	FC	p-value	Enriched group	Putative identification
1.36_164.0352	1.76	6.01E-06	WT	Formyl anthranilate
1.76_159.0297	3.40	8.24E-06	WT	2-oxoadipate
1.29_131.0620	3.77	8.81E-04	WT	
1.30_214.0334	2.05	8.81E-04	WT	
1.29_129.0953	1.79	9.50E-04	WT	
1.29_211.0588	1.83	1.30E-03	WT	
1.30_225.0437	2.31	2.41E-03	WT	
12.83_151.1108	1.75	2.41E-03	WT	
1.29_129.0555	1.58	2.62E-03	WT	Adipate semialdehyde
1.31_562.8829	2.09	2.68E-03	WT	
1.30_128.9068	3.20	3.83E-03	WT	
1.30_129.2032	3.29	5.67E-03	WT	
9.57_237.8713	1.70	1.35E-02	WT	
0.95_187.0611	1.96	1.57E-02	WT	
1.53_117.0442	2.59	1.60E-02	WT	
2.75_166.0508	2.28	1.60E-02	WT	Methoxyanthranilate
1.33_129.0160	2.13	1.60E-02	WT	
1.30_85.0652	7.65	1.70E-02	WT	
5.44_129.0192	2.20	1.81E-02	Mut	Mesaconate
1.09_228.1607	12.62	3.05E-02	Mut	N-decoanoylglycine
7.96_156.9852	2.59	3.05E-02	WT	
8.17_114.0558	3.16	3.14E-02	WT	Proline
1.94_112.9549	2.72	4.57E-02	WT	

All of the compound-features, in the volcano plot (Fig. 3.14) with the exception of the unidentified compound-features 12.83_151.1108, 9.57_237.8713, 7.96_156.9852 and proline had a RT less than 3 min. FC values were generally low for HILIC-MS/MS analysis with the largest significant enrichment by 12.62-fold (p-value $3.05x10^{2}$), in Mut cells of the compound-feature 1.09_228.1607 which was putatively identified (level 3) as N-decoanoylglycine (Fig. 3.15(a)), with a mass error of 0.64 ppm and an isotope similarity of 86.7 %. Ion abundance was low for N-decoanoylglycine which caused low isotope similarity due to background interference with the isotope peaks. An MS/MS spectrum was not acquired for N-decoanoylglycine, as it was not one of the top 10 most abundant compound-features in the full scan spectrum, and therefore could not be used for metabolite identification. The top 2 compound-features from volcano plot analysis were

putatively identified (level 2) as formyl anthranilate and 2-oxoadipate, both with a mass error less than 1 ppm, isotope similarity greater than 90 % and *in silico* fragment pattern matching. Formyl anthranilate (Fig. 3.15(b)) and 2-oxoadipate (Fig. 3.15(c)) were both significantly depleted in Mut cells by 1.76-fold (p-value 1.39×10^{-6}) and 3.39-fold (p-value 3.35×10^{-8}) respectively.

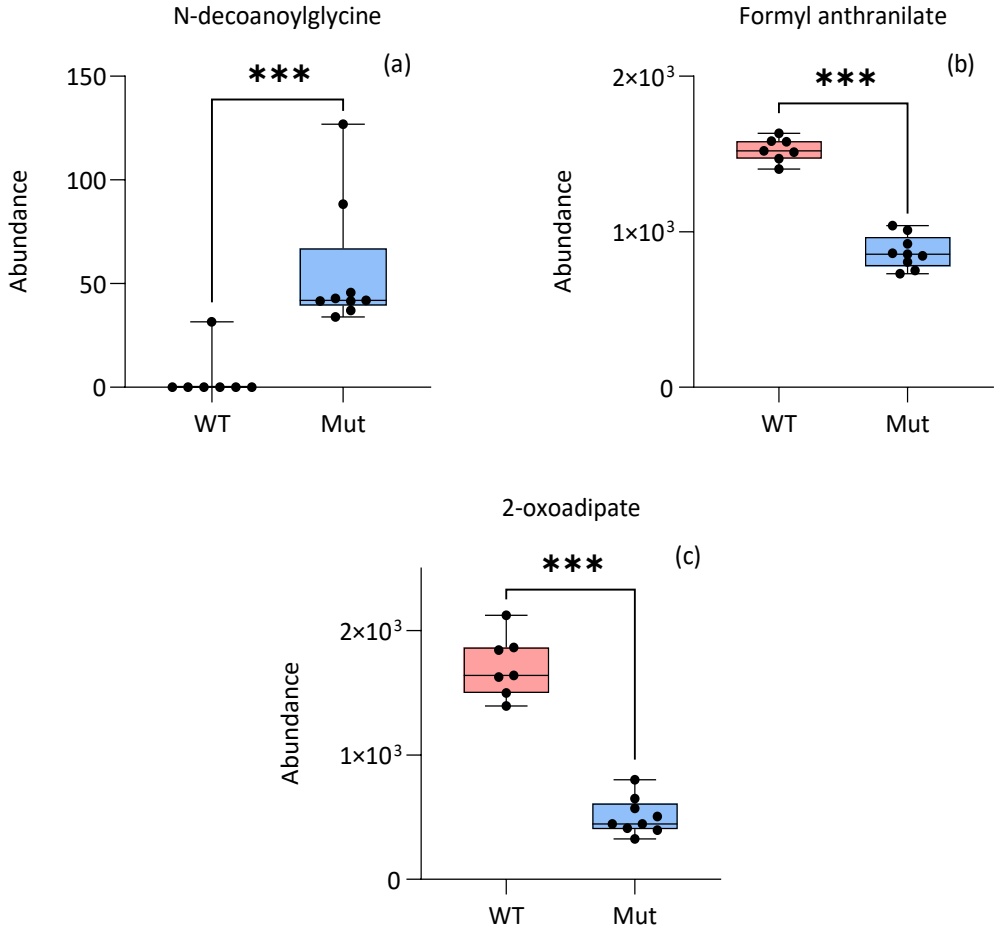

Figure 3.15: Box plots showing the abundance of N-decoanoylglycine (a), formyl anthranilate (b) and 2-oxoadipate (c) in LN18 Mut and WT cells cultured under 4.5 g / L glucose conditions (experimental replicate 1, Section 8.14), analysed by HILIC-MS/MS (Section 8.5). The box plots show the mean, 25-75th percentiles and whiskers extend from the minimum to maximum values. The number of samples are denoted with dots and significance from t-tests are annotated (ns, p-value greater than 0.05; *, p-value less than 0.05; **, p-value less than 0.01; and ***, p-value less than 0.001).

Of the 23 significant compound-features, with an FDR-adjusted t-test p-value less than 0.05, for LN18 cells analysed by HILIC-MS/MS (Table 3.4), only 2-oxoadipate, adipate semialdehyde and mesaconate were observed in analysis of the same samples by

IC-MS/MS. This further demonstrates the chemical selectivity the methods, and the benefits of using multiple complementary chromatographic techniques for analysis of biological samples. Of the remaining compound-features in Table 3.4, the compound-feature 2.75_166.0508 was putatively identified (level 2) as methoxyanthranilate and 1.94_112.9549 as proline, both significantly depleted in Mut cells. Significant depletion of proline and other metabolites with amine functional groups suggested a modification of amino acid metabolism in Mut cells. The low number of significantly altered compound-features observed from HILIC-MS/MS analysis of LN18 cells further confirmed that, in this case, IC-MS/MS was a more appropriate technique for the analysis of polar and ionic metabolism. Results from PLS-DA were not investigated for HILIC-MS/MS analysis of LN18 Mut and WT cells, as the separation distance permutation test had a p-value of 0.29. The PLS-DA model not significant, likely due to the increased CV compared with IC-MS/MS, caused by the increased number of co-eluting features across a shorter chromatographic run time.

3.4.2. Pathways analysis for LN18 IDH1 mutant and wild-type glioblastoma cells

To further identify pathways which were altered in the presence of an IDH1 mutation, Mummichog analysis was performed on compound-features from the analysis of LN18 Mut and WT cells by IC-MS/MS and HILIC-MS/MS.[196] Typical pathways analysis requires prior identification of metabolites before statistical analysis of metabolic networks and therefore has low pathway coverage, compared with untargeted approaches. Mummichog analysis combines unique feature identification of metabolites (level 5) in parallel with statistical variability at the pathways level, to bypass prior identification of metabolites. Metabolites are identified by the Mummichog algorithm based on *m/*z and

the magnitude of enrichments of other identified metabolites, in surrounding pathways. This approach provides increased confidence in identification, compared with accurate mass identification alone, as incorrectly identified metabolites would be distributed randomly and therefore not represent significantly altered metabolic pathways. As metabolites are only identified by *m/z*, identifications are not as reliable as those made with spectra matched to *in silico* fragmentation patterns and isotope distributions. Metabolites in LN18 Mut and WT cells cultured under 4.5 g / L glucose conditions (experimental replicate 1, Section 8.14), were identified (level 5) from datasets collected by IC-MS/MS (Section 8.4) and HILIC-MS/MS (Section 8.5) using Mummichog analysis, and mapped onto metabolic pathways using the KEGG human database, as shown in Fig. 3.16.[167]

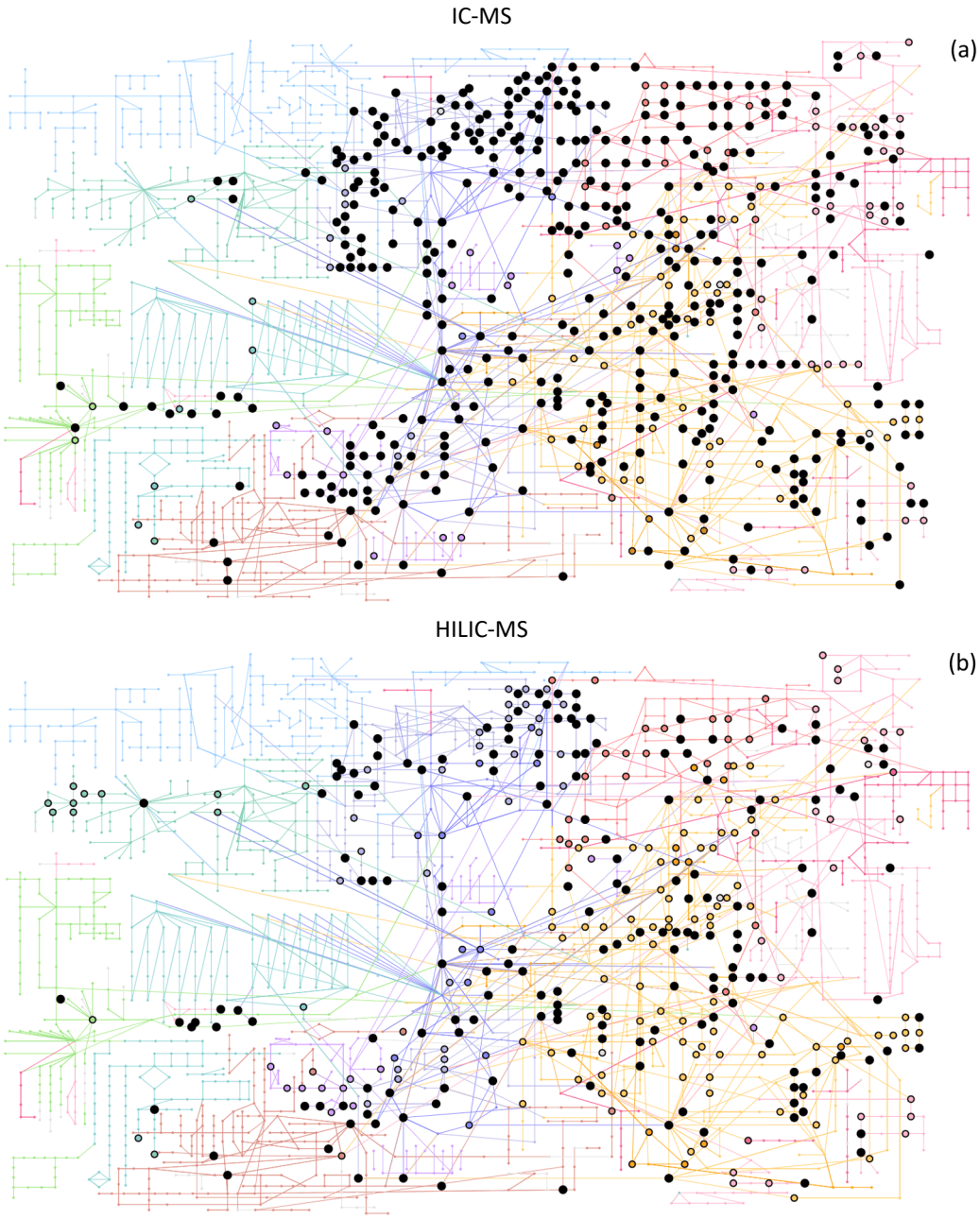

Figure 3.16: KEGG human metabolic pathway annotated using Mummichog analysis of LN18 Mut and WT cells cultured under 4.5 g / L glucose conditions (experimental replicate 1, Section 8.14), analysed by IC-MS/MS (a) and HILIC-MS/MS (b), as described in Sections 8.4 and 8.5 respectively. Filled circles denote significantly altered metabolites, unfilled circles were identified but were not significantly altered.

Untargeted pathways analysis of the LN18 cells, using unique feature identifications (level 5), from Mummichog analysis showed increased metabolite coverage, for IC-MS compared to HILIC-MS, particularly in the TCA cycle, glycolysis, pentose phosphate, nucleotide and hexose sugar metabolism pathways. IC-MS also had a greater number of significantly enriched pathways, compared to HILIC-MS, and the

pathways with a Fisher's exact test (FET) value greater than 0.05 are listed in Table 3.5. FET was used to carry out statistical analysis of complete pathways based on t-test permutation testing, for each identified metabolite (level 5) in the pathway. The reduced number of significantly altered metabolites was likely caused by higher LLoD and lower ion abundances observed for most metabolites analysed by HILIC-MS/MS, as well as the different chemical selectivity of the methods (discussed in Section 2.7). The increased variability may also have been caused by additional sample preparation steps required for HILIC-MS/MS analysis, as discussed in Sections 1.4 and 2.5.

Table 3.5: Enriched pathways from Mummichog analysis of LN18 Mut and WT cells cultured under 4.5 g / L glucose conditions (experimental replicate 1, Section 8.14), analysed by IC-MS/MS (Section 8.4), ranked by FET significance.

Pathway	Metabolites in pathway	Metabolites identified	Significantly altered metabolites	FET
Pentose and glucuronate interconversions	53	41	41	7.6E-07
Fructose and mannose metabolism	48	36	34	5.4E-04
Ascorbate and aldarate metabolism	45	34	32	9.6E-04
Pentose phosphate pathway	32	28	27	8.6E-04
Galactose metabolism	41	31	29	2.3E-03
Pyruvate metabolism	32	24	23	3.0E-03
Starch and sucrose metabolism	50	29	27	4.0E-03
Valine, leucine and isoleucine biosynthesis	27	18	18	2.2E-03
Glycolysis/gluconeogenesis	31	20	19	1.0E-02
Amino sugar and nucleotide sugar metabolism	88	58	48	3.0E-02
Pyrimidine metabolism	60	47	39	4.6E-02
TCA cycle	20	12	12	1.7E-02
Glycerolipid metabolism	32	12	12	1.7E-02
Butanoate metabolism	40	25	22	4.3E-02

Comprehensive coverage of the pathways shown in Table 3.5 was achieved using IC-MS, with over half of the metabolites identified within each pathway, with the exception of glycerolipid metabolism. Most of the pathways which were significantly altered were related to sugar metabolism or glycolysis, providing further evidence for the modification of cellular energy pathways in LN18 Mut cells. The observed enrichment of pentose and

glucuronate interconversions, as well as the pentose phosphate pathway, is in agreement with the enrichment of sedoheptulose 1-phosphate, and the depletion of sedoheptulose 7-phosphate, sedoheptulose 1,7-biphosphate and erythrose 4-phosphate observed from univariate analysis of LN18 Mut cells. Glycolysis/gluconeogenesis was identified by Mummichog analysis due to the significant depletion of 2 & 3-phosphoglycerate and phosphoenolpyruvate, in LN18 Mut cells. Changes in both glycolysis and the pentose phosphate pathway suggest different utilisation of cellular energy pathways in Mut cells, or an inhibitory effect of reduced NADPH, as discussed in Section 3.3. The significantly enriched contribution of ATP to the adenine nucleotide pool, as well as depletion of glucosamine 6-phosphate and glycineamide ribonucleotide, contributed to amino sugar and nucleotide sugar metabolism. Pyruvate, glutamate and 2-oxoadipate were significantly depleted in LN18 Mut cells and the identification (level 5) of an additional 15 metabolites in the valine, leucine and isoleucine biosynthesis pathways, suggests that further investigation of metabolites with amine functional groups would be of benefit. The TCA cycle was identified to be enriched, despite no significant alterations in metabolite abundance, apart from the significant depletion of 2-OG in LN18 Mut cells, highlighting that Mummichog analysis may define a pathway to be significantly altered based on a single metabolite in that pathway. Ions from background noise or in-source fragments which were isobaric with TCA cycle metabolites, were likely identified by the Mummichog algorithm to correlate with the significant 6.29-fold depletion of 2-OG, in LN18 Mut cells.

Mummichog analysis of the HILIC-MS dataset had fewer significantly enriched pathways than IC-MS/MS analysis of the same samples (Fig. 3.17), listed in Table 3.6. The coverage

of the pathways was also reduced as fewer metabolites were identified (level 5) by HILIC-MS (7435) compared with IC-MS (11727).

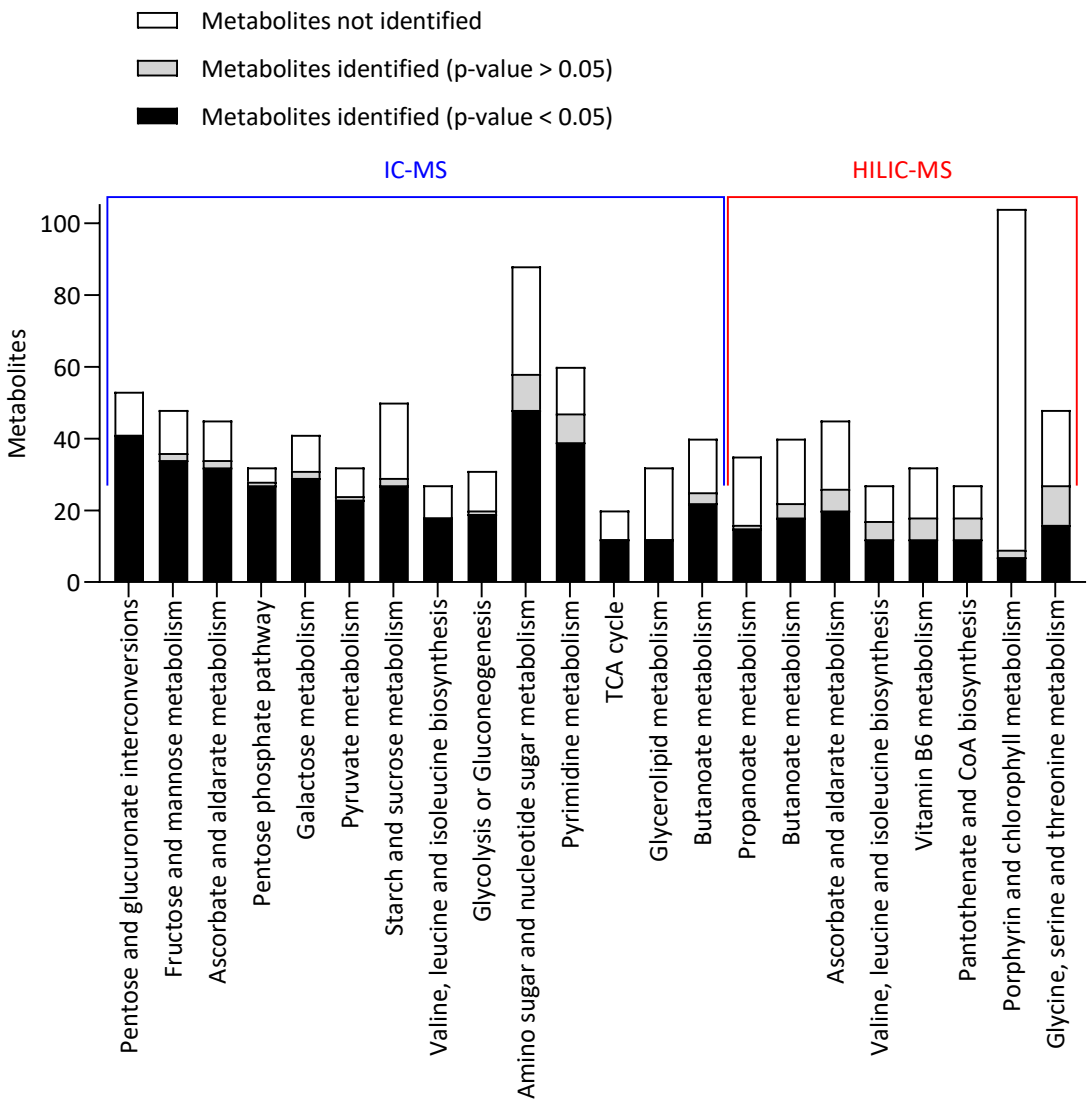

Figure 3.17: Bar graph of the number of identified metabolites in enriched pathways from Mummichog analysis of LN18 Mut and WT cells cultured under 4.5 g / L glucose conditions (experimental replicate 1, Section 8.14), analysed by IC-MS/MS (Section 8.4) and HILIC-MS/MS (Section 8.5).

For the enriched pathways, identified from Mummichog analysis of datasets from IC-MS/MS and HILIC-MS/MS analysis of LN18 Mut and WT cells (Tables 3.5 and 3.6 respectively), only butanoate, ascorbate and aldarate metabolism were identified to be significantly altered in both analysis methods. This observation further demonstrates the

differential chemical selectivity of IC-MS/MS and HILIC-MS/MS and the value of the chemical space accessed by IC-MS for untargeted metabolomics.

Table 3.6: Enriched pathways from the Mummichog analysis of LN18 Mut and WT cells cultured under 4.5 g / L glucose conditions (experimental replicate 1, Section 8.14) by HILIC-MS/MS (Section 8.5), ranked by FET values.

Pathway	Metabolites in pathway	Metabolites identified	Significantly altered metabolites	FET
Propanoate metabolism	35	16	15	4.0E-05
Butanoate metabolism	40	22	18	3.1E-04
Ascorbate and aldarate metabolism	45	26	20	6.2E-04
Valine, leucine and isoleucine biosynthesis	27	17	12	2.5E-02
Vitamin B6 metabolism	32	18	12	4.5E-02
Pantothenate and CoA biosynthesis	27	18	12	4.5E-02
Porphyrin and chlorophyll metabolism	104	9	7	4.4E-02
Glycine, serine and threonine metabolism	48	27	16	8.0E-02

In addition to untargeted pathways analysis, targeted pathways analysis was performed using MetaboAnalyst, for the 217 identified metabolites (Section 10.5) from IC-MS/MS analysis of LN18 cells (experimental replicate 1, Section 8.14). Targeted pathways analysis revealed a greater number of significantly altered pathways (p-value less than 0.05) than analysis using Mummichog, as shown in Table 3.7.

Table 3.7: Enriched pathways from targeted pathways analysis of LN18 Mut and WT cells cultured under 4.5 g / L glucose conditions (experimental replicate 1, Section 8.14) by HILIC-MS/MS (Section 8.5), ranked by p-values.

Pathway	Metabolites in pathway	Metabolites identified	p-value
Synthesis and degradation of ketone bodies	5	1	3.65E-14
Valine, leucine and isoleucine degradation	40	1	3.65E-14
Lysine degradation	25	1	9.50E-12
beta-Alanine metabolism	21	4	5.70E-11
Tyrosine metabolism	42	6	5.76E-11
Nicotinate and nicotinamide metabolism	15	1	5.94E-11
Tryptophan metabolism	41	4	7.08E-09
Alanine, aspartate and glutamate metabolism	28	13	1.48E-08
Terpenoid backbone biosynthesis	18	2	1.76E-08
Arginine biosynthesis	14	6	3.66E-08
Butanoate metabolism	15	6	3.75E-08
Ubiquinone and other terpenoid-quinone biosynthesis	9	1	1.08E-07
Phenylalanine, tyrosine and tryptophan biosynthesis	4	1	1.08E-07
Glycine, serine and threonine metabolism	33	11	1.87E-07
D-Glutamine and D-glutamate metabolism	6	3	3.02E-07
Arginine and proline metabolism	38	6	4.46E-07
Glyoxylate and dicarboxylate metabolism	32	12	8.64E-07
Aminoacyl-tRNA biosynthesis	48	5	8.68E-07
Histidine metabolism	16	2	8.70E-07
Cysteine and methionine metabolism	33	5	9.82E-07
TCA cycle	20	7	3.54E-06
Sphingolipid metabolism	21	1	7.72E-06
Nitrogen metabolism	6	2	8.37E-06
Porphyrin and chlorophyll metabolism	30	2	8.37E-06
Glutathione metabolism	28	3	1.17E-05
Primary bile acid biosynthesis	46	2	2.20E-05
Taurine and hypotaurine metabolism	8	2	2.20E-05
Pentose phosphate pathway	22	11	2.61E-05
Pantothenate and CoA biosynthesis	19	6	3.52E-05
Amino sugar and nucleotide sugar metabolism	37	13	5.85E-04
Pyruvate metabolism	22	5	7.59E-04
Glycolysis/gluconeogenesis	26	6	7.64E-04
Valine, leucine and isoleucine biosynthesis	8	1	2.01E-03
Ascorbate and aldarate metabolism	8	6	2.86E-03
Fatty acid biosynthesis	47	2	5.71E-03
Purine metabolism	65	23	6.85E-03
Inositol phosphate metabolism	30	3	8.63E-03
Propanoate metabolism	23	3	8.66E-03
Phosphatidylinositol signaling system	28	1	1.12E-02
Pyrimidine metabolism	39	24	2.57E-02
Glycerolipid metabolism	16	4	3.10E-02
Galactose metabolism	27	7	3.72E-02
N-Glycan biosynthesis	41	1	4.28E-02
Phenylalanine metabolism	10	1	4.87E-02

Targeted pathways analysis provided a greater number of pathways compared to Mummichog analysis, however, coverage of metabolites within each pathway was lower. The analysis provided a summary of pathways modified in LN18 Mut cells which could be used for further analysis of the data, or to select an appropriate LC-MS method to improve coverage of selected pathways. Untargeted and targeted pathways analysis also confirmed previous observations that cellular energy pathways and amino acid metabolism were perturbed.

3.5. Untargeted IC-MS/MS analysis of U87-MG IDH1 mutant and wild-type glioblastoma cells

To further investigate the changes in metabolism associated with an IDH1 mutation, and to validate the biomarkers observed for the LN18 Mut and WT cells, a different glioblastoma-derived cell line was transduced (Section 8.13) and analysed. U87-MG Mut and WT cells with 9 biological replicates in each experimental group were cultured under the same conditions (4.5 g / L glucose supplemented DMEM as described in Section 8.15) as the LN18 cell line (experimental replicate 1, Section 8.14). The cell extracts were analysed by IC-MS/MS (Section 8.4) and raw data processed, as described for LN18 cell line (Section 3.3). Of the 3337 compound-features which were peak-picked using Progenesis QI, 137 metabolites were identified (listed in Section 10.6) using the IC-MS/MS database (Section 10.2). The data associated with this experiment has been deposited in the Oxford University Research Archive (title: Metabolomics of U87-MG IDH wild-type and mutant cells) and is freely accessible (https://doi.org/10.5287/bodleian:nZZ0abQzr). The PCA scores plot of compound-feature abundances, for IC-MS/MS analysis of the U87-MG cells (Fig. 3.18), showed significant separation between Mut and WT cells. One

sample outlier was observed outside the 95 % confidence interval which was excluded from all subsequent analyses.

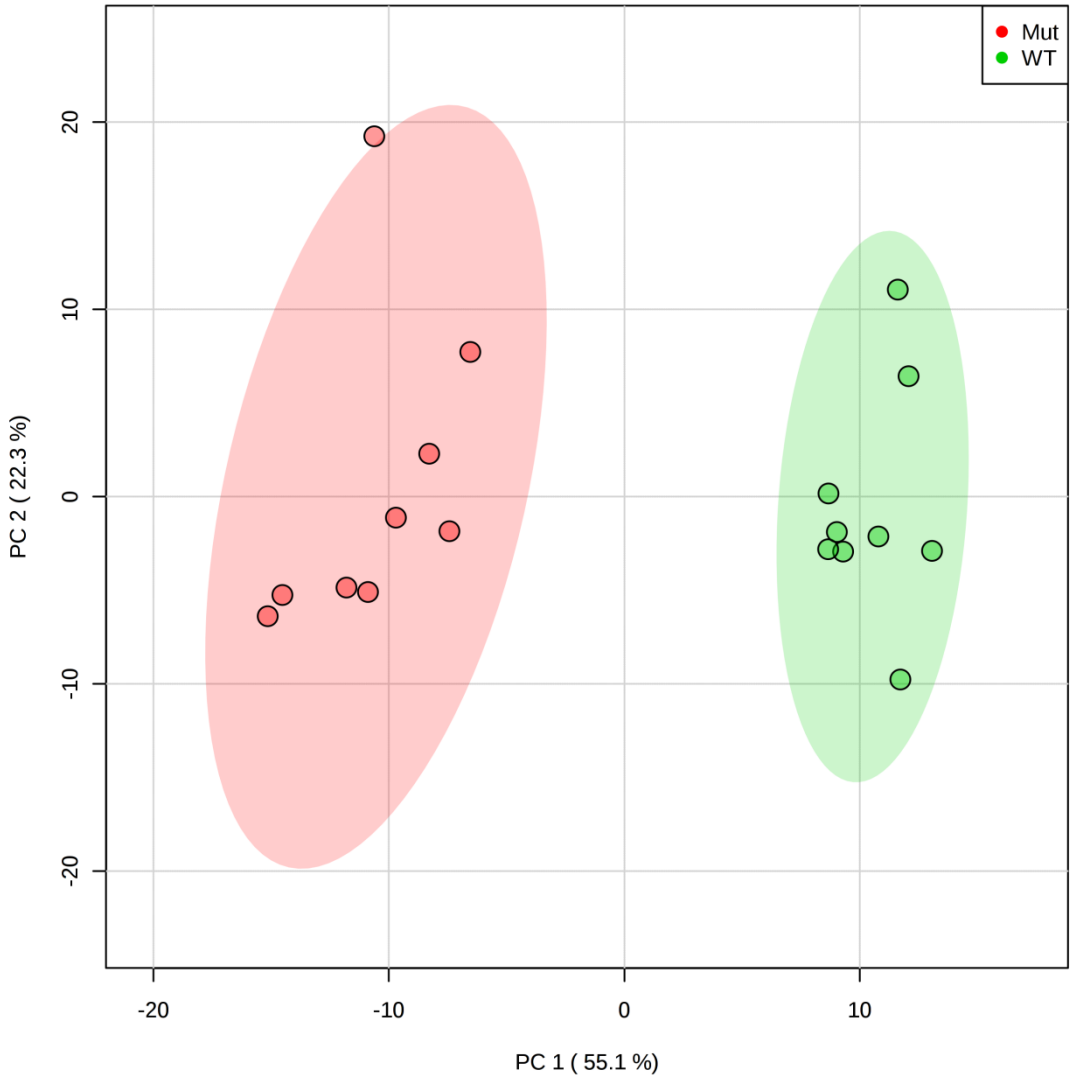

Figure 3.18: PCA scores plot of compound-feature abundances for U87-MG Mut and WT cells cultured under 4.5 g / L glucose conditions (Section 8.15), analysed by IC-MS/MS (Section 8.4). Statistical analysis was performed using MetaboAnalyst with normalisation by sum and Pareto scaling (Section 8.11). Shaded areas represent the 95 % confidence interval for each experimental group.

Analysis of the PCA loadings plot (not shown) revealed contributions from 2-HG, the nucleotides dGDP and ATP and an unidentified compound-feature (16.46_302.5325), which discriminated between Mut and WT cells.

Prior to further statistical analysis, the dataset was filtered to remove in-source fragments and ion clusters of 2-HG which co-eluted (at 10.38 min), and had similar FC values. A

volcano plot (Fig. 3.19) was then prepared which demonstrated 881 significantly altered compound-features, using FC and FDR-adjusted t-test p-value cut-off values of 1.5 and 0.05 respectively.

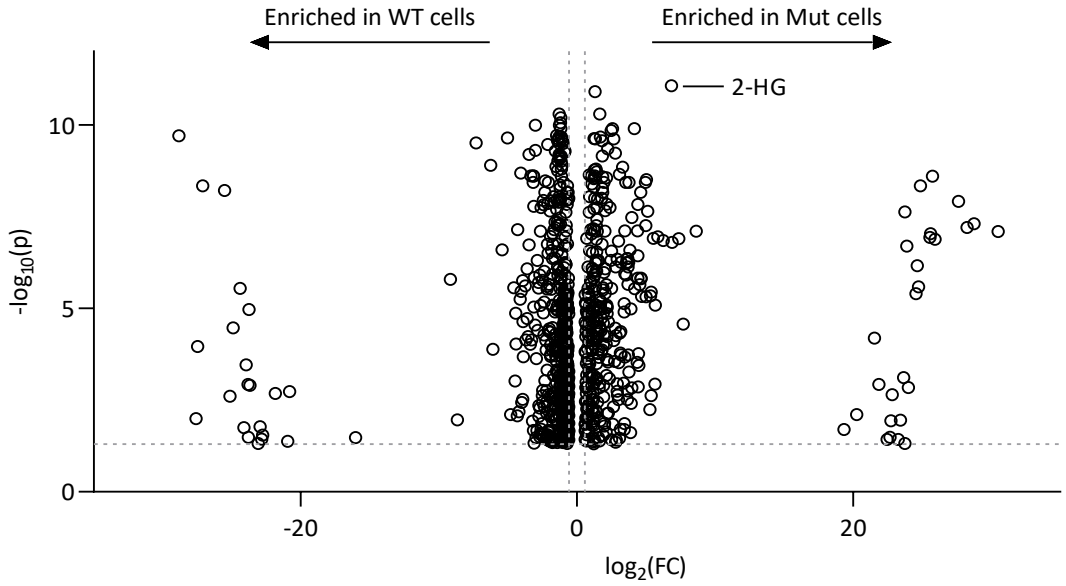

Figure 3.19: Volcano plot showing the compound-features with a FC greater than 1.5 and FDR-adjusted t-test p-value less than 0.05, from univariate statistical analysis of U87-MG Mut and WT cells cultured under 4.5 g / L glucose conditions (Section 8.15), by IC-MS/MS (Section 8.4).

There were a larger number of significant compound-features compared with the analysis of the LN18 cell line and 2-HG was the most important feature identified from the volcano plot, despite only a 116-fold enrichment in U87-MG Mut cells (compared with the 458-fold enrichment for LN18 Mut cells). The top 35 compound-features identified from analysis of the volcano plot (Fig. 3.19) are shown in Table 3.8.

Table 3.8: Top 35 compound-features identified in the volcano plot (Fig. 3.19) from univariate statistical analysis of U87-MG Mut and WT cells cultured under 4.5 g / L glucose conditions (Section 8.15), analysed by IC-MS/MS (Section 8.4).

Compound-feature	FC	p-value	Enriched group	Identification
10.38_147.0295	1.16E+02	8.72E-12	Mut	2-HG
9.49_176.0558	2.48	1.24E-11	Mut	
5.78_192.0331	3.13	5.05E-11	Mut	
12.20_278.0357	2.42	5.05E-11	WT	
32.69_339.5515	2.26	6.42E-11	WT	
12.20_278.5277	2.30	8.85E-11	WT	
17.82_217.0553	8.02	1.02E-10	WT	
12.20_557.0799	2.40	1.02E-10	WT	
9.89_293.0814	17.74	1.28E-10	Mut	
26.66_342.5107	5.99	1.28E-10	Mut	
17.57_558.0641	2.24	1.28E-10	WT	
11.35_162.0403	5.57	1.43E-10	Mut	
12.20_498.0429	2.76	1.94E-10	WT	
3.61_470.1504	4.75E+08	2.00E-10	WT	
12.20_558.0640	2.46	2.11E-10	WT	
26.41_259.7457	3.26	2.15E-10	Mut	
24.47_140.0350	2.18	2.15E-10	WT	
5.02_381.1092	32.67	2.29E-10	WT	
4.45_272.0899	2.37	2.36E-10	Mut	
3.98_329.1109	6.36	2.40E-10	Mut	
17.57_362.9879	2.56	2.40E-10	WT	
3.84_116.0347	2.52	2.40E-10	Mut	Acetylglycine
17.57_279.0296	2.14	2.40E-10	WT	
26.41_390.1227	3.53	2.72E-10	Mut	
11.21_132.0299	2.04	2.72E-10	WT	Aspartate
32.69_340.0529	2.63	2.73E-10	WT	
5.54_302.1000	1.58E+02	3.10E-10	WT	
17.57_278.5278	2.39	3.23E-10	WT	
19.20_346.0548	2.01	3.27E-10	WT	dGMP
23.72_224.0484	4.30	3.42E-10	WT	
8.97_140.0114	4.67	4.49E-10	Mut	
4.45_346.1261	8.02	4.99E-10	WT	
32.69_680.1124	2.94	5.16E-10	WT	
11.21_114.0190	1.83	5.16E-10	WT	
13.19_346.0548	1.87	5.56E-10	WT	AMP

As observed for IC-MS/MS analysis of LN18 Mut and WT cells, the majority of significantly altered compound-features were depleted in U87-MG Mut cells (553 of 881 compound-features). FC magnitudes were also similar, but lower than observed for the same metabolites in LN18 cells, possibly related to the different genetic mutations observed in the cell lines, leading to different basal metabolic rates. The high importance

of aspartate, dGMP and AMP (which were depleted in Mut cells), from univariate statistical analysis, further suggested that the IDH1 mutation affected central carbon, amine and nucleotide pathways therefore, further analysis of metabolites in those pathways was performed. As observed in LN18 cells (Section 3.3), 2-HG was enriched (FC 116, p-value < 1.0×10^{-16}) and 2-OG was depleted (FC 2.10, p-value 8.9×10^{-7}) in Mut cells, as shown in Fig. 3.20.

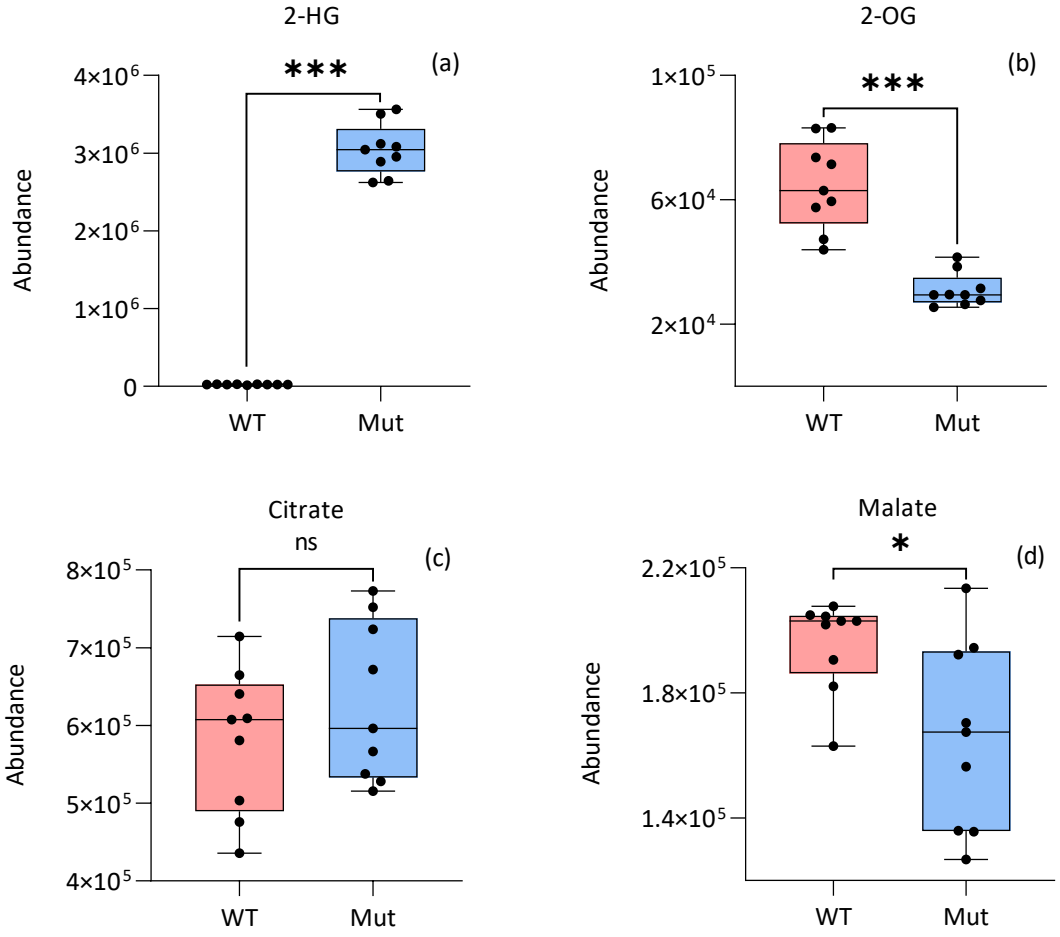

Figure 3.20: Box plots showing the abundance of 2-HG (a), 2-OG (b), citrate (c) and malate (d) in U87-MG Mut and WT cells cultured under 4.5 g / L glucose conditions (Section 8.15), analysed by IC-MS/MS (Section 8.4). The box plots show the mean, 25-75th percentiles and whiskers extend from the minimum to maximum values. The number of samples are denoted with dots and significance from t-tests are annotated (ns, p-value greater than 0.05; *, p-value less than 0.05; **, p-value less than 0.01; and ***, p-value less than 0.001).

The magnitude of the alteration in 2-HG and 2-OG abundances were smaller than those observed in the LN18 cells. Citrate (Fig. 3.20(c)) was not significantly enriched and

malate (Fig. 3.20(d)) was significantly depleted (FC 1.18, p-value $1.67x10^{-2}$) in Mut cells. This suggests that the TCA cycle may be perturbed in the presence of IDH1 mutation in U87-MG cells, contrary to the observation made for the LN18 cell line.

Glycolytic intermediates were also affected in the presence of an IDH1 mutation, as observed in the LN18 Mut and WT cells, although the depletion of 2 & 3-phosphoglycerate (Fig. 3.21(a)) was not significant. Phosphoenolpyruvate was also significantly depleted in U87-MG Mut cells, by 2.68-fold (p-value $7.2x10^{-5}$), which may explain the perturbation of the TCA cycle and depletion of malate.

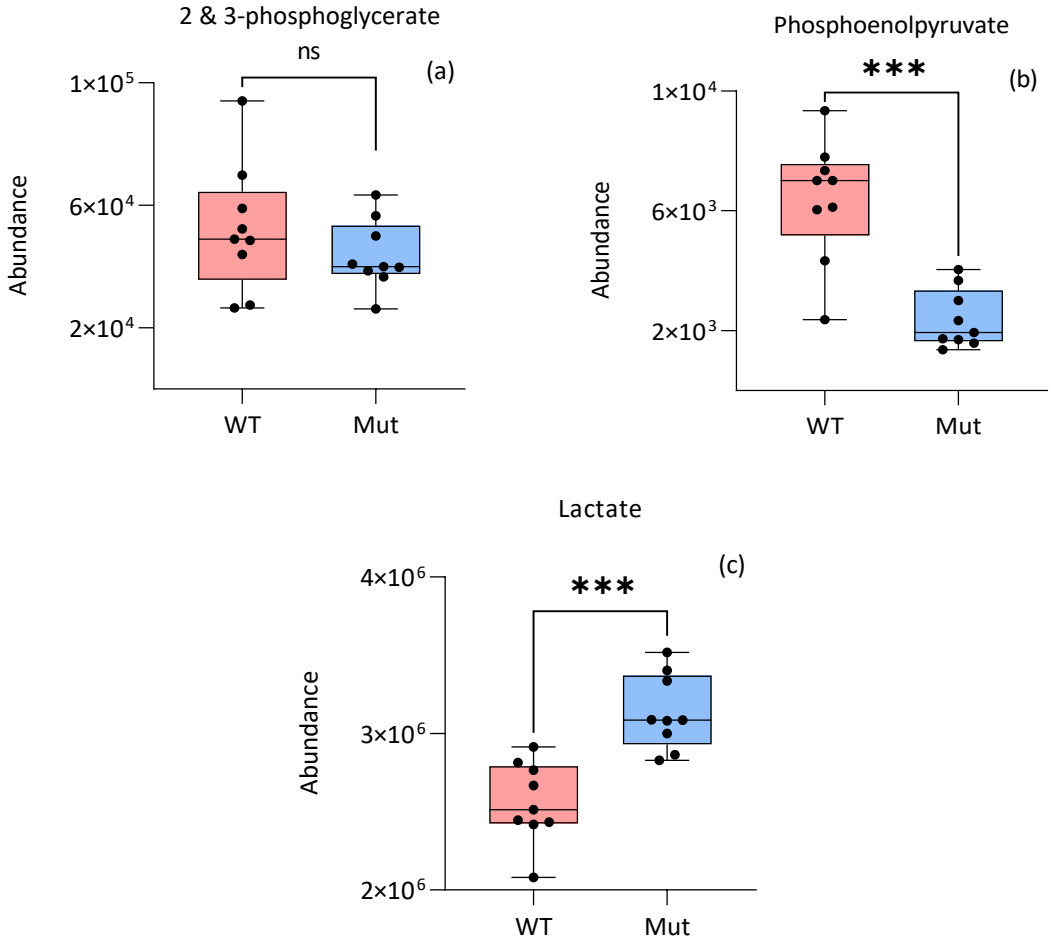

Figure 3.21: Box plots showing the abundance of 2 & 3-phosphoglycerate (a), phosphoenolpyruvate (b) and lactate (c) in U87-MG Mut and WT cells cultured under 4.5 g / L glucose conditions (Section 8.15), analysed by IC-MS/MS (Section 8.4). The box plots show the mean, 25-75th percentiles and whiskers extend from the minimum to maximum values. The number of samples are denoted with dots and significance from t-tests are annotated (ns, p-value greater than 0.05; *, p-value less than 0.05; **, p-value less than 0.01; and ***, p-value less than 0.001).

Unlike the LN18 cells, the Warburg effect was observed in U87-MG Mut cells with a significant enrichment of lactate (FC 1.22, p-value 2.0x10^{-4}), potentially indicating an upregulation of glycolysis as a result of the PTEN mutation.[10, 175] The depletion of pyruvate in LN18 Mut cells was not observed in U87-MG Mut cells, which showed a marginal enrichment (FC 1.14, p-value 2.2x10^{-2}), as shown in Fig. 3.22.

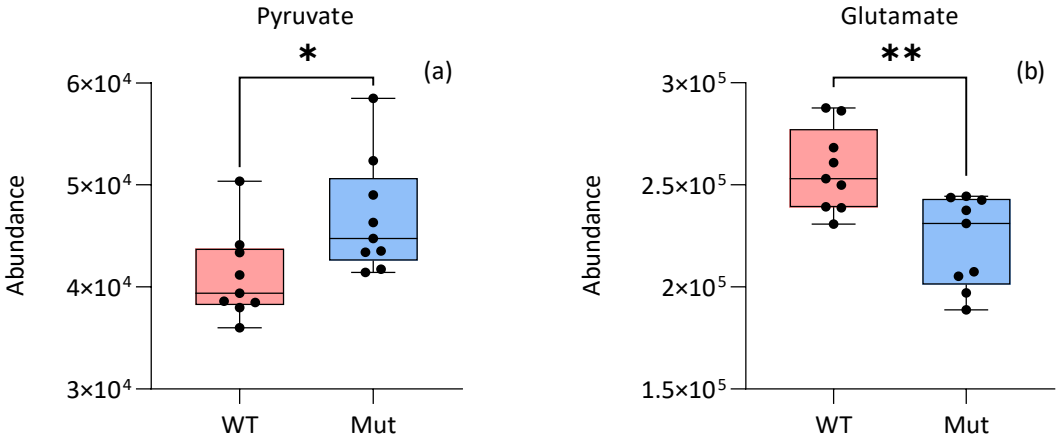

Figure 3.22: Box plots showing the abundance of pyruvate (a) and glutamate (b) in U87-MG Mut and WT cells cultured under 4.5 g / L glucose conditions (Section 8.15), analysed by IC-MS/MS (Section 8.4). The box plots show the mean, 25-75th percentiles and whiskers extend from the minimum to maximum values. The number of samples are denoted with dots and significance from t-tests are annotated (ns, p-value greater than 0.05; *, p-value less than 0.05; **, p-value less than 0.01; and ***, p-value less than 0.001).

Glutamate was significantly depleted (FC 1.16, p-value 3.1x10^{-3}), as was observed in LN18 Mut cells. This could suggest glutamine as an alternative energy source, for maintenance of the TCA cycle, or as a precursor for 2-HG production in Mut cells. U87-MG Mut cells may therefore be susceptible to redox stress, or the depletion of glutamine. The cellular redox state was estimated by measurement of the lactate / pyruvate ratio, as described for LN18 cells (Section 3.3). The significant enrichment of both lactate and pyruvate also resulted in a higher lactate / pyruvate ratio, as shown in Fig. 3.23. This inferred an increase in glycolysis, in agreement with what could be expected from the Warburg effect; however the change was not significant.

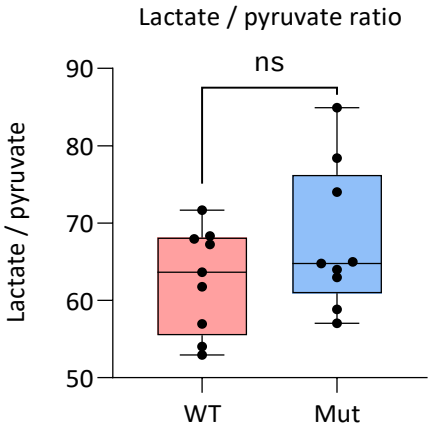

Figure 3.23: Lactate / pyruvate ratio calculated from the analysis of U87-MG Mut and WT cells cultured under 4.5 g / L glucose conditions (Section 8.15), analysed by IC-MS/MS (Section 8.4). The box plot shows the mean, 25-75th percentiles and whiskers extend from the minimum to maximum values. The number of samples are denoted with dots and significance from t-tests are annotated (ns, p-value greater than 0.05; *, p-value less than 0.05; **, p-value less than 0.01; and ***, p-value less than 0.001).

The nucleotides dGMP and AMP were ranked 29th and 35th respectively, from univariate analysis of U87-MG cells (Fig. 3.19). As shown in Fig. 3.24, AMP was significantly depleted 1.66-fold (p-value 5.0x10^{-13}) and ATP was significantly enriched 1.14-fold (p-value 1.6x10^{-2}) in U87-MG Mut cells, unfortunately ADP was apparently below the LLoD. dGDP (Fig. 3.24(c)), which contributed to PCA separation of the Mut and WT cells, was significantly enriched in U87-MG Mut cells by 1.16-fold (p-value 1.3x10^{-2}).

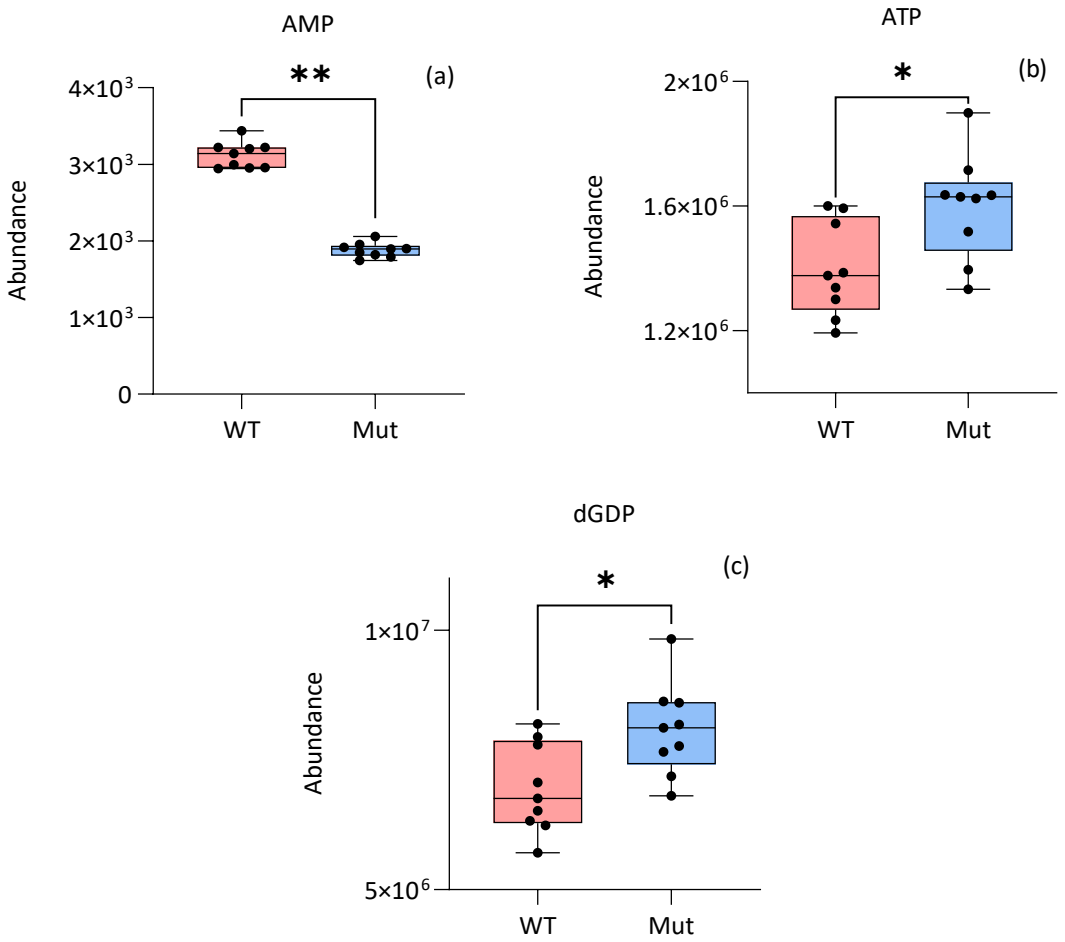

Figure 3.24: Box plots showing the abundance of AMP (a), ATP (b) and dGDP (c) in U87-MG Mut and WT cells cultured under 4.5 g / L glucose conditions (Section 8.15), analysed by IC-MS/MS (Section 8.4). The box plots show the mean, 25-75th percentiles and whiskers extend from the minimum to maximum values. The number of samples are denoted with dots and significance from t-tests are annotated (ns, p-value greater than 0.05; *, p-value less than 0.05; **, p-value less than 0.01; and ***, p-value less than 0.001).

The relative contributions of AMP and ATP to the nucleotide pool were calculated and the enrichment of ATP and depletion of AMP, as shown in Fig. 3.25, was consistent with changes observed in LN18 Mut cells. The larger contribution of ATP to the adenine nucleotide pool, seen in both LN18 and U87-MG Mut cells, may be due to reduced utilisation of ATP or the activation of ATP synthase, as a result of the IDH1 mutation. High concentrations of ATP have been observed to allosterically inhibit phosphofructokinase-1, the rate limiting enzyme in glycolysis which converts fructose 6-phosphate to fructose

1,6-bisphosphate.[197] The enrichment of ATP in U87-MG Mut cells may therefore explain the significant enrichment of fructose 6-phosphate.

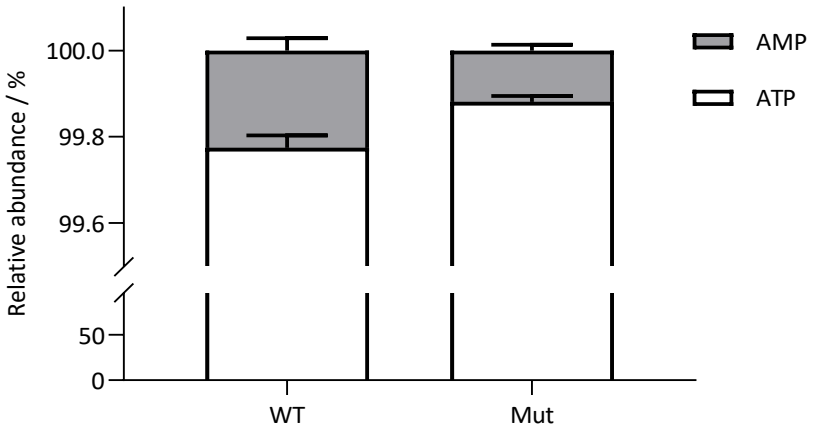

Figure 3.25: Relative abundances of AMP and ATP compared with the total adenine nucleotide pool calculated from the analysis of U87-MG Mut and WT cells cultured under 4.5 g / L glucose conditions (Section 8.15), analysed by IC-MS/MS (Section 8.4). Error bars represent standard deviation of the mean for 9 samples.

β-citryl glutamate was also observed to be significantly depleted (FC 1.66, p-value 9.3×10^{-6}) in U87-MG Mut cells, as shown in Fig. 3.26. NAAG and NAA were both significantly enriched in Mut cells by 23.0-fold (p-value $< 1.0 \times 10^{-16}$) and 80-fold (p-value 2.9×10^{-8}) respectively. The enrichment of NAAG was contrary to the effect observed in LN18 cells and potentially suggested a different utilisation of amino acid metabolism, as aspartate was also significantly depleted in U87-MG Mut cells by 1.84-fold (p-value 2.1×10^{-12}), as shown in Fig. 3.26.

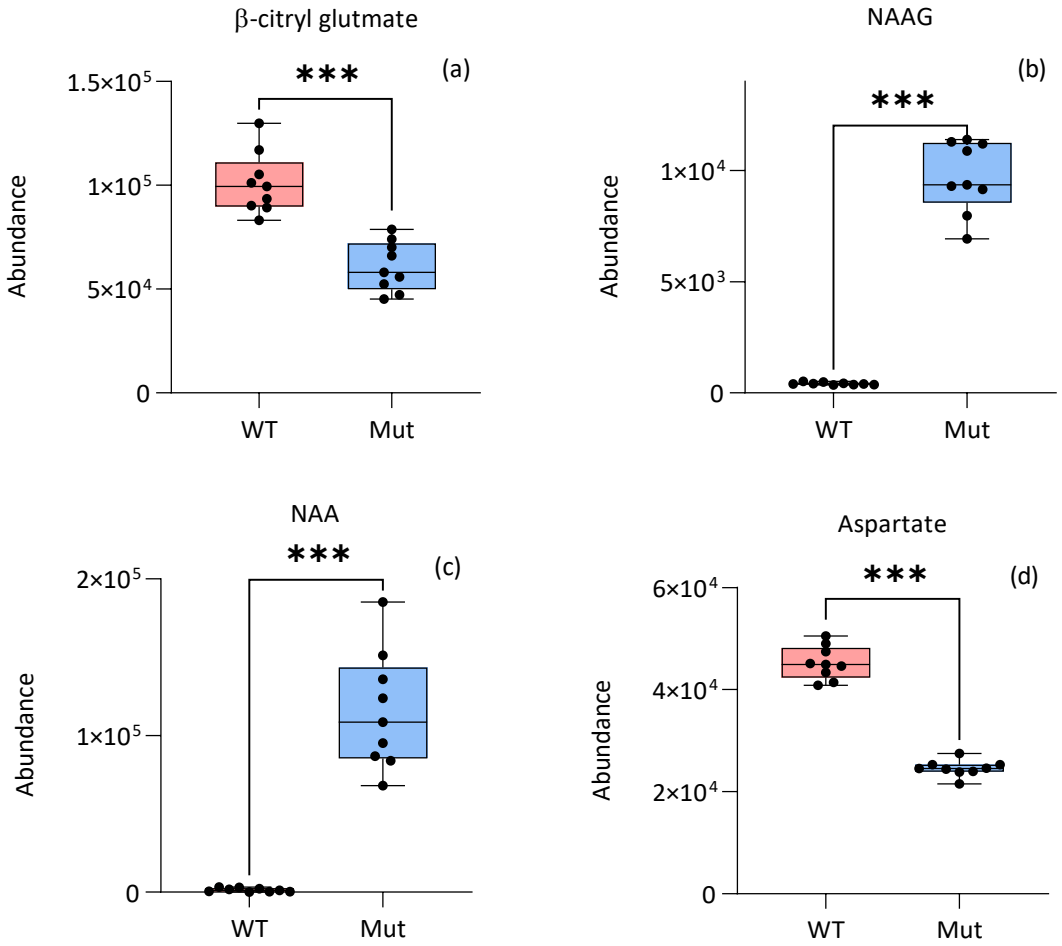

Figure 3.26: Box plots showing the abundance of β-citryl glutamate (a), NAAG (b), NAA (c) and aspartate (d) in U87-MG Mut and WT cells cultured under 4.5 g / L glucose conditions (Section 8.15), analysed by IC-MS/MS (Section 8.4). The box plots show the mean, 25-75th percentiles and whiskers extend from the minimum to maximum values. The number of samples are denoted with dots and significance from t-tests are annotated (ns, p-value greater than 0.05; *, p-value less than 0.05; **, p-value less than 0.01; and ***, p-value less than 0.001).

As well as the modification of aspartate metabolism, the depletion of 2-oxoadipate (observed in the LN18 Mut cells) was corroborated in U87-MG Mut cells. 2-oxoadipate was depleted 3.46-fold (p-value 5.8×10^{-11}) in Mut cells, as shown in Fig. 3.27, and further suggested that lysine degradation product abundances were modified in the presence of an IDH1 mutation; however, the abundance of glutarate (Fig. 3.27(b)) was not significantly altered.

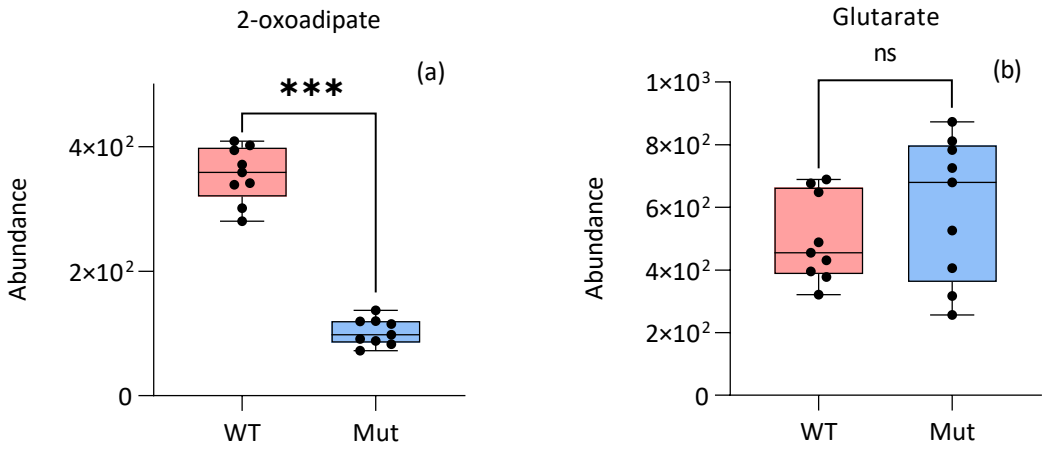

Figure 3.27: Box plots showing the abundance of 2-oxoadipate (a) and glutarate (b) in U87-MG Mut and WT cells cultured under 4.5 g / L glucose conditions (Section 8.15), analysed by IC-MS/MS (Section 8.4). The box plots show the mean, 25-75th percentiles and whiskers extend from the minimum to maximum values. The number of samples are denoted with dots and significance from t-tests are annotated (ns, p-value greater than 0.05; *, p-value less than 0.05; **, p-value less than 0.01; and ***, p-value less than 0.001).

A number of pentose phosphate pathway intermediates were also significantly altered in U87-MG Mut cells, including the significant depletion of sedoheptulose 1,7-bisphosphate (FC 1.53, p-value 7.1x10^{-4}) and significant enrichment of both sedoheptulose 7-phosphate by 2.94-fold (p-value 1.1x10^{-4}) and sedoheptulose 1-phosphate by 3.77-fold (p-value 2.3x10^{-10}), as shown in Fig. 3.28. Erythrose 4-phosphate (Fig. 3.28(d)) which connects the pentose phosphate pathways to glycolysis was also depleted 2.30-fold (p-value 1.3x10^{-3}), as observed in LN18 Mut cells and fructose 6-phosphate was enriched 3.28-fold (p-value 4.0x10^{-3}). These observations could suggest that the pentose phosphate pathway activity was upregulated and that metabolic flux through glycolysis was already maximal, and consequently caused fructose 6-phosphate to accumulate in the U87-MG Mut cells.

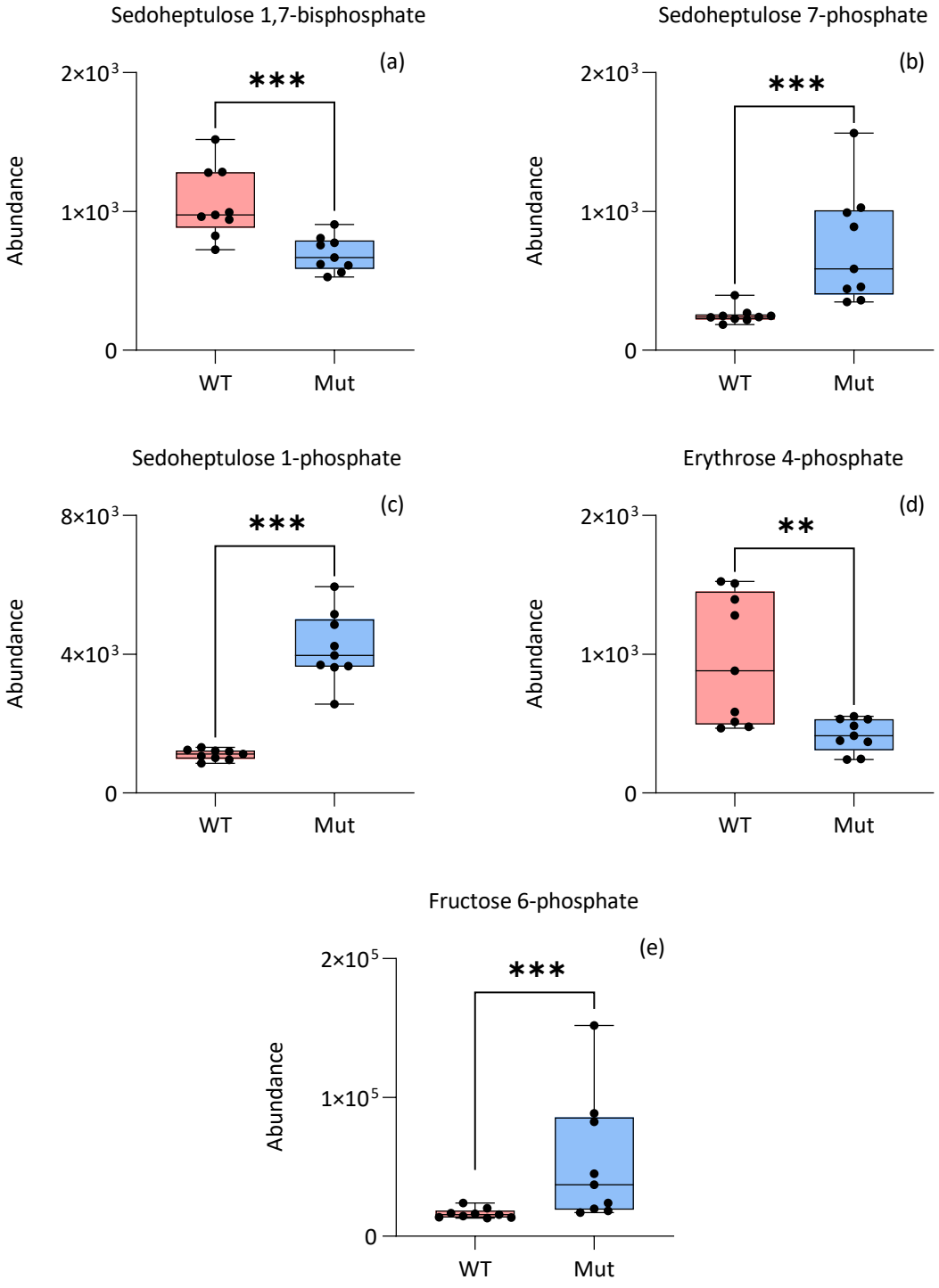

Figure 3.28: Box plots showing the abundance of sedoheptulose 1,7-bisphosphate (a), sedoheptulose 7-phosphate (b), sedoheptulose 1-phosphate (c), erythrose 4-phosphate (d) and fructose 6-phosphate (e) in U87-MG Mut and WT cells cultured under 4.5 g / L glucose conditions (Section 8.15), analysed by IC-MS/MS (Section 8.4). The box plots show the mean, 25-75th percentiles and whiskers extend from the minimum to maximum values. The number of samples are denoted with dots and significance from t-tests are annotated (ns, p-value greater than 0.05; *, p-value less than 0.05; **, p-value less than 0.01; and ***, p-value less than 0.001).

PLS-DA of the dataset obtained from IC-MS/MS analysis of U87-MG cells, provided a model with 1 component accuracy, R^2 and Q^2 values of 1.00, 0.95 and 0.92 respectively; however, the p-value obtained from a separation distance permutation test was 0.63 and therefore not significant, so no further multivariate statistical analysis was performed.

In summary, the significant enrichment of 2-HG and depletion of 2-OG were observed in the U87-MG cells but the FC magnitude was reduced compared with the analysis of LN18 cells. TCA cycle metabolites were not significantly altered with the exception of malate which was depleted. The Warburg effect of enriched lactate production was observed in Mut cells, as well as the depletion of phosphoenolpyruvate, suggesting that glycolysis may be upregulated to maintain the TCA cycle. Modifications to the nucleotide pool and glycolysis may mean that Mut cells are susceptible to further redox stress which may allow preferential targeting of Mut cells.

3.6. Untargeted IC-MS/MS analysis of 293T IDH1 mutant and wild-type embryonic kidney cells

Analysis of LN18 and U87 cell lines showed common changes in a range of metabolites for the glioblastoma-derived cell lines. In order to control for cell type and being brain tumour-derived, an immortalised human embryonic kidney cell line (293T) was transduced (as described for the glioblastoma-derived cell lines in Section 8.13) and analysed. 293T cells with 5 biological replicates in each experimental group were cultured under the same conditions (4.5 g / L glucose supplemented DMEM, as described in Section 8.16) as the glioblastoma-derived cell lines. The cell extracts were analysed by IC-MS/MS (Section 8.4), and the raw data processed as described for LN18 cells (Section 3.3). The data associated with this experiment has been deposited in the

Oxford University Research Archive (title: Metabolomics of 293T IDH wild-type and mutant cells) and is freely accessible (https://doi.org/10.5287/bodleian:BRY9rwZRR). The 293T cells were analysed as part of a larger study (not included in this thesis) on the metabolic effect of glucose concentration and therefore only 5 biological replicates of each condition were cultured. The 293T cells had the largest number of compound-features (6330), although only 132 metabolites were identified (listed in Section 10.7). The most prominent difference between the cell lines was the reduced enrichment of 2-HG, in 293T Mut cells, to 11.1-fold (p-value 2.4×10^{-10}). 2-HG was therefore no longer the greatest discriminating compound-feature between 293T Mut and WT cells; however, the two groups were still separated in principal component space, as shown in Fig. 3.29.

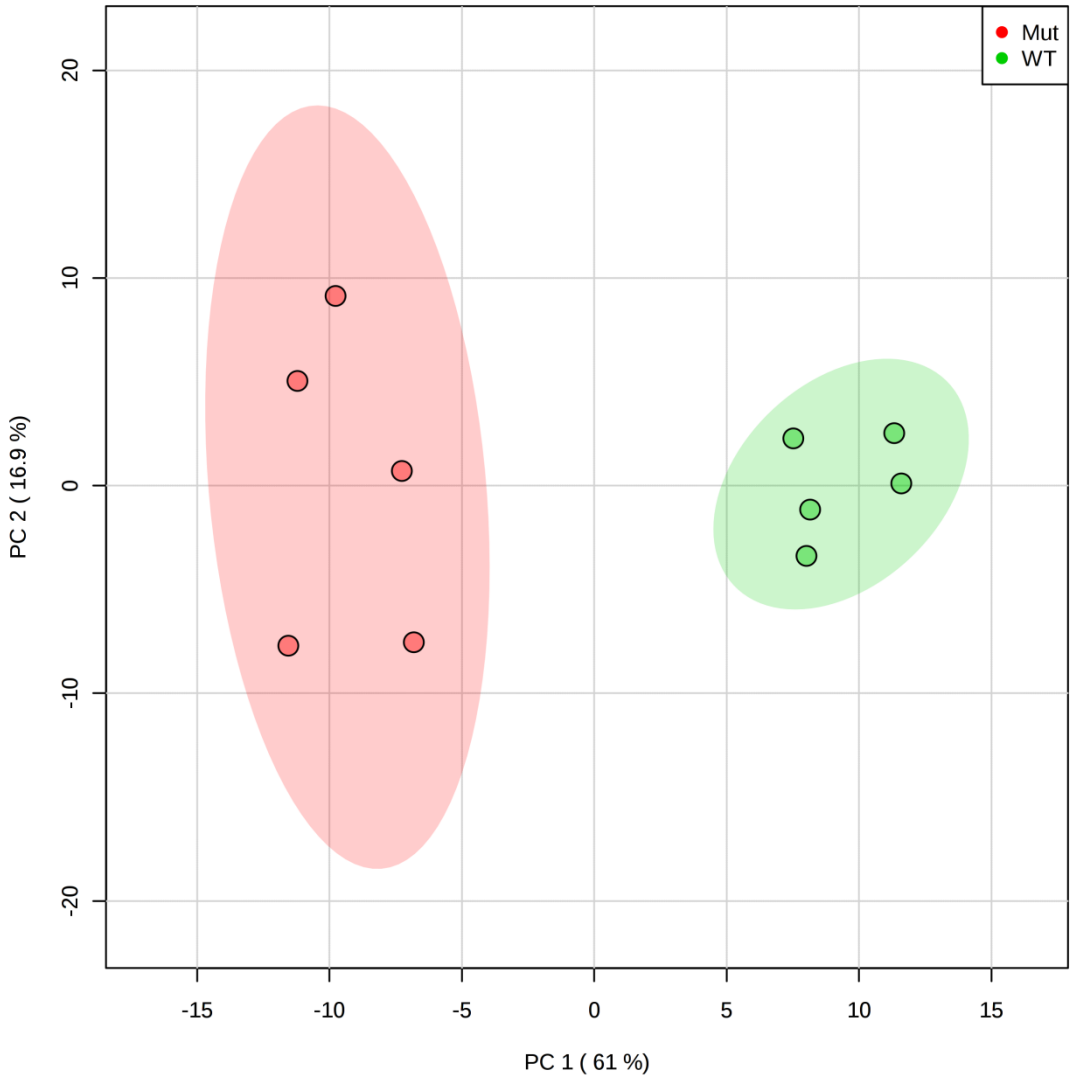

Figure 3.29: PCA scores plot of compound-feature abundances for 293T Mut and WT cells cultured under 4.5 g / L glucose conditions (Section 8.16), analysed by IC-MS/MS (Section 8.4). Statistical analysis was performed using MetaboAnalyst with normalisation by sum and Pareto scaling (Section 8.11). Shaded areas represent the 95 % confidence interval for each experimental group.

The loadings plot (not shown) indicated contributions from uridine diphosphate (UDP), dGDP, lactate, ATP and the unidentified compound-feature 15.84_302.5341, demonstrating that metabolism was altered in 293T Mut cells, even when 2-HG was only 11.1-fold enriched (Fig. 3.30(a)).

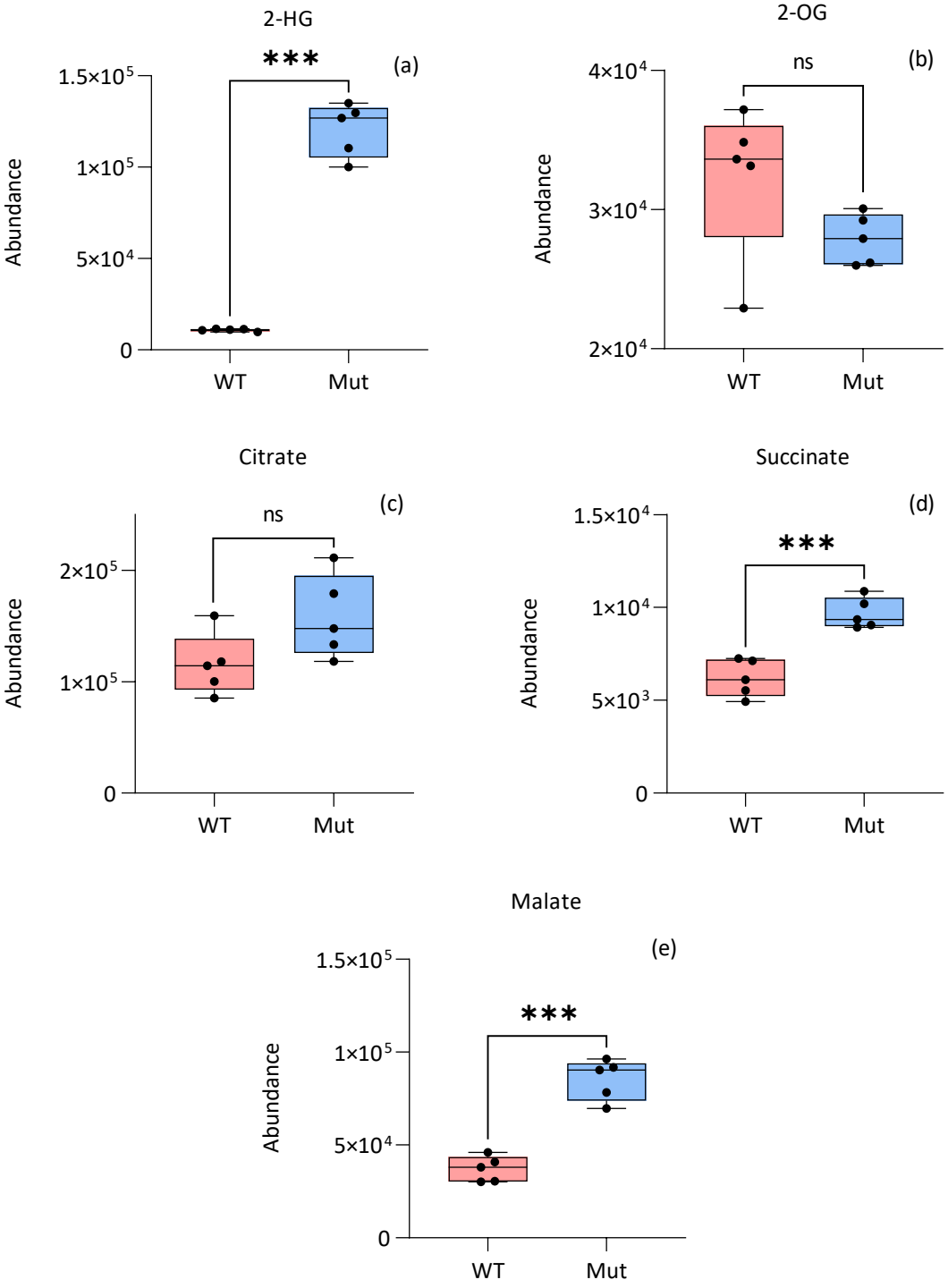

Figure 3.30: Box plots showing the abundance of 2-HG (a), 2-OG (b), citrate (c), succinate (d) and malate (e) in 293T Mut and WT cells cultured under 4.5 g / L glucose conditions (Section 8.16), analysed by IC-MS/MS (Section 8.4). The box plots show the mean, 25-75th percentiles and whiskers extend from the minimum to maximum values. The number of samples are denoted with dots and significance from t-tests are annotated (ns, p-value greater than 0.05; *, p-value less than 0.05; **, p-value less than 0.01; and ***, p-value less than 0.001).

The depletion of 2-OG (Fig. 3.30(b)) was not significant (due to one outlying measurement); however, the sample was not excluded from analysis as the abundance of

other TCA metabolites were comparable, across the 5 WT samples. The abundance of citrate (Fig. 3.30(c)) was also not significantly altered however, succinate (Fig. 3.30(d)) and malate (Fig. 3.30(e)) were both significantly enriched in Mut cells by 1.56-fold (p-value 5.8×10^{-4}) and 2.30-fold (p-value 3.6×10^{-5}) respectively. The enrichment of succinate and malate may suggest that the TCA cycle in the 293T cell line was more sensitive to 2-HG enrichment than the glioblastoma cells lines, and that 2-HG may have a regulatory effect on TCA cycle enzymes. The disruption of the TCA cycle in 293T Mut cells may also have been caused by the inhibition of an enzyme downstream of malate, or that oxaloacetate (not detected) was supplied to the TCA cycle from another source (for example, cytoplasmic pyruvate). Glycolysis pathway metabolites in the 293T cell line showed the opposite changes to those observed in the glioblastoma-derived cell lines, as shown in Fig. 3.31.

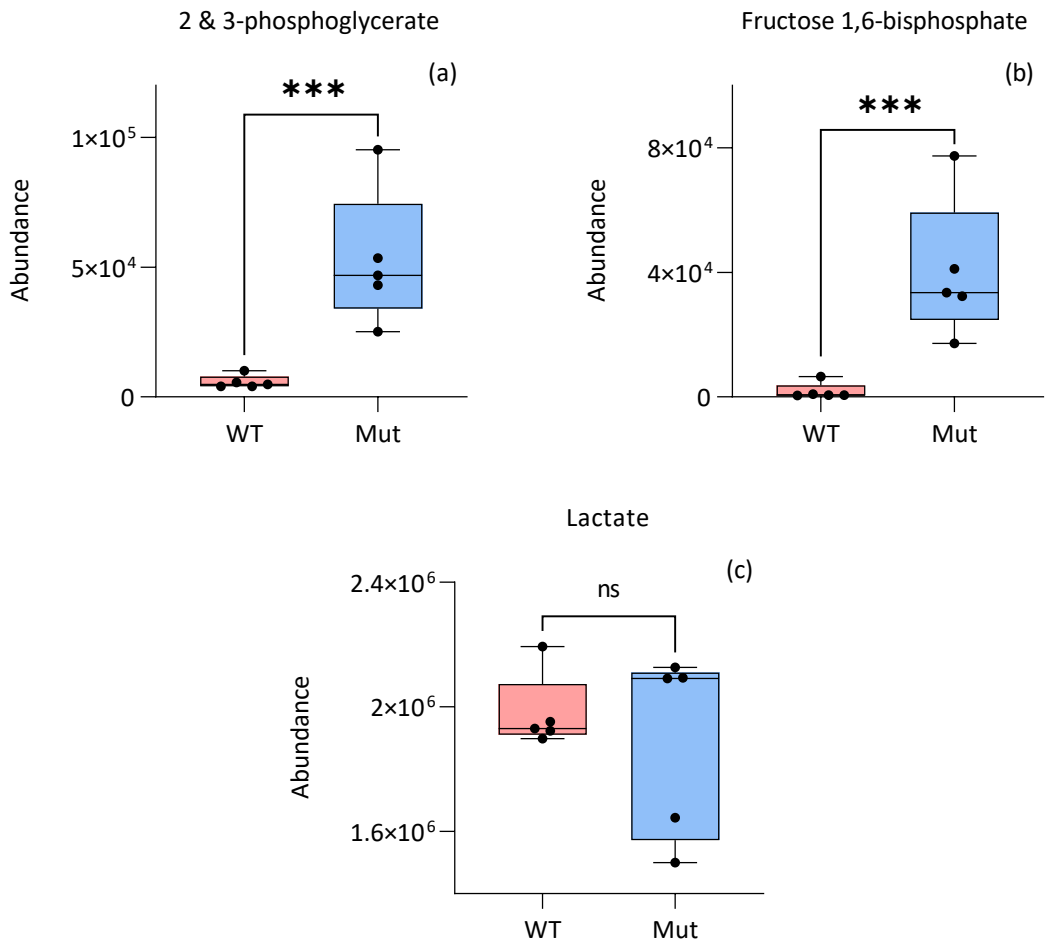

Figure 3.31: Box plots showing the abundance of 2 & 3-phosphoglycerate (a), fructose 1,6-bisphosphate (d) and lactate (c) in 293T Mut and WT cells cultured under 4.5 g / L glucose conditions (Section 8.16), analysed by IC-MS/MS (Section 8.4). The box plots show the mean, 25-75th percentiles and whiskers extend from the minimum to maximum values. The number of samples are denoted with dots and significance from t-tests are annotated (ns, p-value greater than 0.05; *, p-value less than 0.05; **, p-value less than 0.01; and ***, p-value less than 0.001).

The glycolytic intermediates 2 & 3-phosphoglycerate and fructose 1,6-bisphosphate were both significantly enriched 9.20-fold (p-value 4.0x10^{-5}) and 22.4-fold (p-value 2.2x10^{-3}) respectively; however, lactate (Fig. 3.31(c)) was not significantly altered. The different alteration of TCA cycle and glycolytic intermediates in 293T cells, compared with the glioblastoma-derived cell lines, may be associated with different utilisation of energy transduction pathways, as the 293T cell line did not originate from brain or cancer tissue. Glycolytic intermediates may have been enriched in the 293T cells as a result of the accumulation of malate in the TCA cycle and consequent regulation of glycolytic enzymes.

ATP (Fig. 3.32(a)) was significantly depleted (FC 1.28, p-value 7.9×10^{-4}) in 293T Mut cells, consistent with the anaplerotic conversion of pyruvate (which was also depleted in Mut cells) to oxaloacetate, by pyruvate decarboxylase.

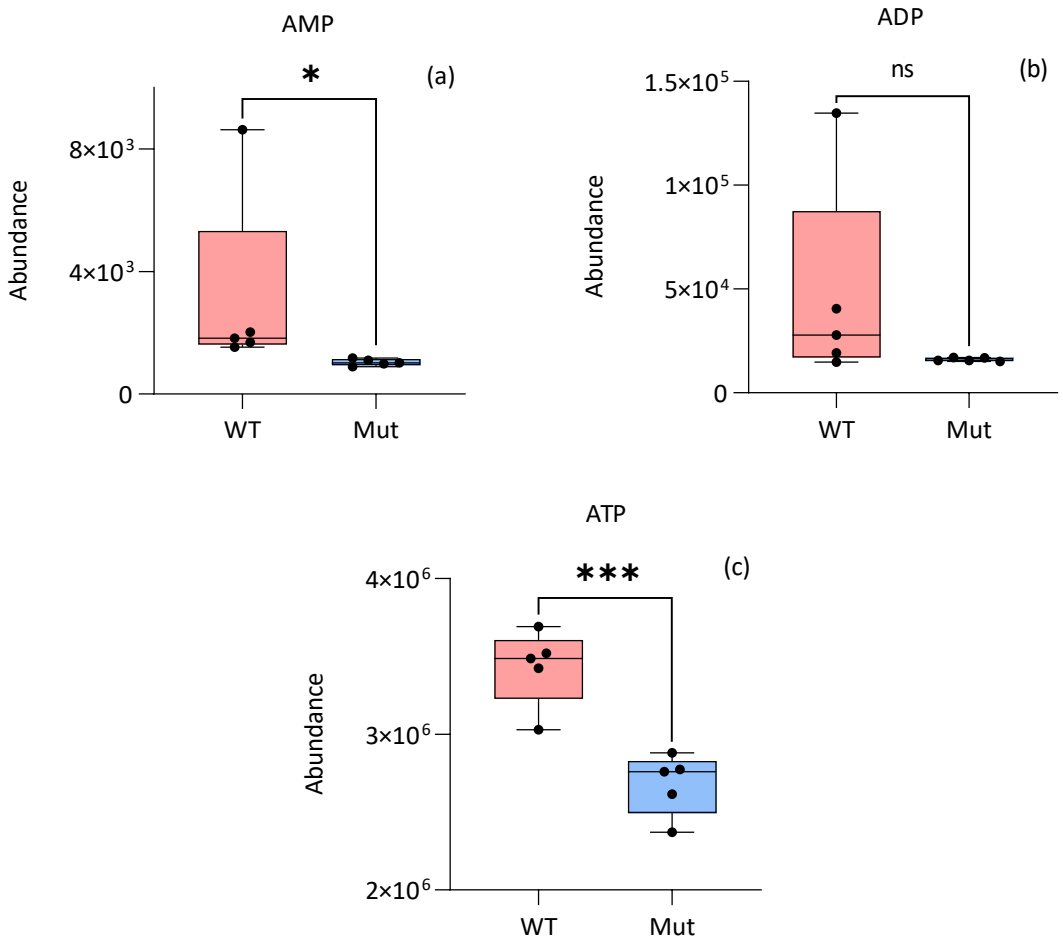

Figure 3.32: Box plots showing the abundance of AMP (a), ADP (b), ATP (c) in 293T Mut and WT cells cultured under 4.5 g / L glucose conditions (Section 8.16), analysed by IC-MS/MS (Section 8.4). The box plots show the mean, 25-75th percentiles and whiskers extend from the minimum to maximum values. The number of samples are denoted with dots and significance from t-tests are annotated (ns, p-value greater than 0.05; *, p-value less than 0.05; **, p-value less than 0.01; and ***, p-value less than 0.001).

AMP (Fig. 3.32(a)) was also significantly depleted 3.03-fold (p-value 3.1×10^{-2}) and ADP (Fig. 3.32(b)), although depleted, was not significant due to the large variance in the WT samples. The relative abundances of AMP, ADP and ATP and their contribution to the total pool were calculated; however, the differences between Mut and WT cells were also not significant, as shown in Fig. 3.33. Depletion of the total adenine nucleotide pool has

previously been shown in liver cells to diminish mitochondrial respiration and therefore the depletion of ATP may also be linked to increased anaplerosis in the 293T Mut cells.[198]

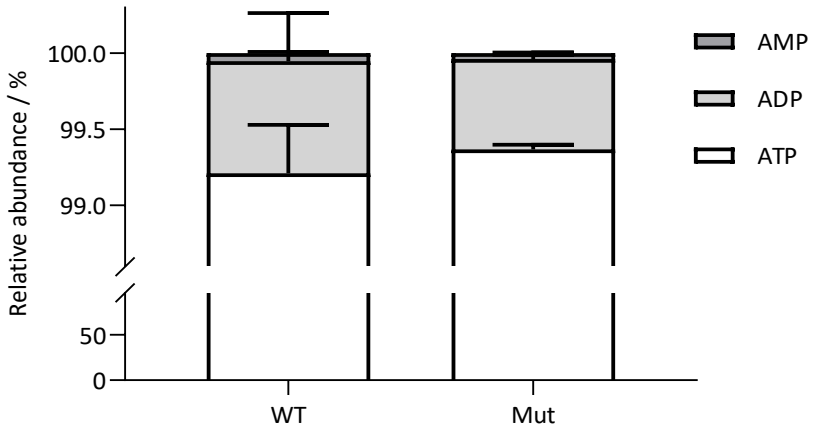

Figure 3.33: Relative abundances of AMP, ADP and ATP compared with the total adenine nucleotide pool calculated from the analysis of 293T Mut and WT cells cultured under 4.5 g / L glucose conditions (Section 8.16), analysed by IC-MS/MS (Section 8.4). Error bars represent standard deviation of the mean for 5 samples.

Univariate statistical analysis using a volcano plot (Fig. 3.34), reduced the number of significant compound-features down to 1099 from 6330. The volcano plot was similar in shape to the analysis of LN18 (Fig. 3.5) and U87-MG (Fig. 3.19) cells; however, FDR-adjusted t-test p-values were generally lower, as there were only 5 samples within each experimental group.

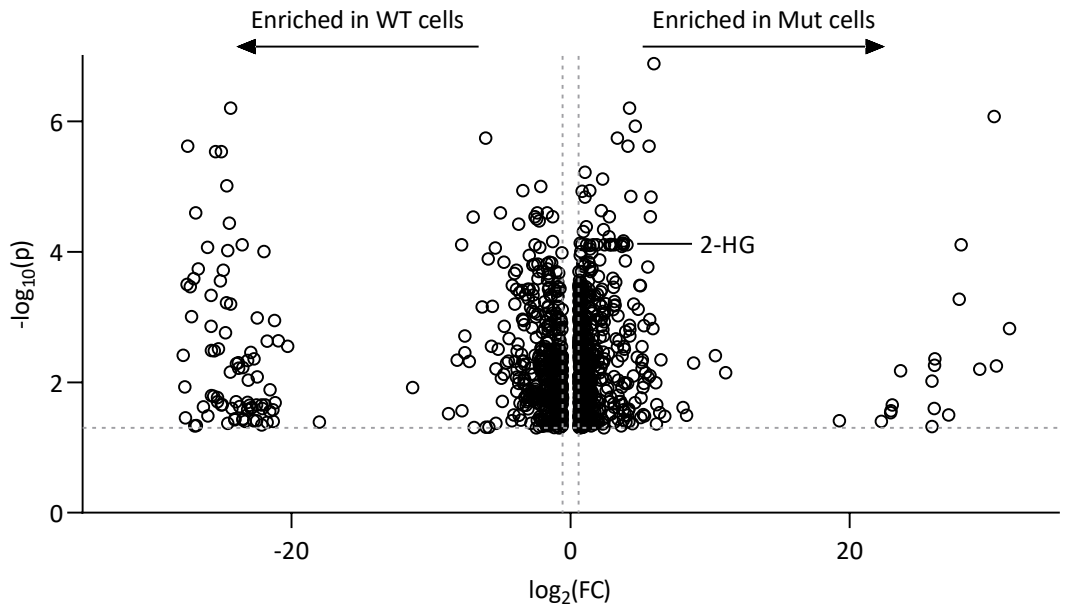

Figure 3.34: Volcano plot showing the compound-features with a FC greater than 1.5 and FDR-adjusted t-test p-value less than 0.05, from univariate statistical analysis of 293T Mut and WT cells cultured under 4.5 g / L glucose conditions (Section 8.16), by IC-MS/MS (Section 8.4).

Univariate statistical analysis confirmed that 2-HG was not the most discriminating feature of 293T Mut and WT cells, but large FC values were still observed between Mut and WT cells, as shown in Table 3.9. The low importance of 2-HG, compared to the other cell lines, was the result of a 13.0-fold enrichment in 293T Mut cells, compared with 458-fold for LN18 Mut cells and 113-fold for U87-MG Mut cells. The lower enrichment may have been caused by decreased expression of IDH1 in the Mut cells; however, a lower enrichment was not observed by western blot when the cells were originally transduced (Section 8.13). The 293T cells may have a mechanism which can reduce the intracellular concentration of 2-HG, however, it was not being actively exported from the Mut cells, as 2-HG was found to be 12.7-fold enriched in the cell culture media. Lactate was also only 1.22-fold enriched (p-value 1.99×10^{-4}) in Mut cells and therefore, the 293T cells did not strongly display evidence of the Warburg effect, which further suggested that the 239T cells were not as glycolytic as the LN18 and U87-MG cell lines.[10]

Table 3.9: Top 35 compound-features identified in the volcano plot (Fig. 3.34) from univariate statistical analysis of 293T Mut and WT cells cultured under 4.5 g / L glucose conditions (Section 8.16), by IC-MS/MS (Section 8.4).

Compound-feature	FC	p-value	Enriched group	Identification
11.70_406.0769	63.05	1.31E-07	Mut	
13.15_110.0082	2.18E+07	6.30E-07	WT	
11.26_259.0230	18.59	6.30E-07	Mut	Fructose 6-phosphate
11.26_199.0021	1.39E+09	8.43E-07	Mut	Erythrose 4-phosphate
11.26_257.0079	25.13	1.18E-06	Mut	
6.55_344.0775	67.85	1.81E-06	WT	
9.92_147.2102	10.21	1.81E-06	Mut	
11.57_335.0660	1.84E+08	2.39E-06	WT	
20.97_307.5557	49.83	2.39E-06	Mut	
11.26_519.0546	17.16	2.39E-06	Mut	
23.59_217.0673	4.57E+07	2.90E-06	WT	
15.04_250.0399	3.47E+07	2.90E-06	WT	
11.12_157.0145	2.03	6.04E-06	Mut	
3.27_314.1367	4.88	7.64E-06	Mut	
20.97_261.5829	2.63E+07	9.75E-06	WT	
4.25_177.0408	4.37	9.98E-06	WT	
8.44_360.0725	10.72	1.15E-05	WT	
26.14_225.0048	2.58	1.15E-05	Mut	
13.29_116.9830	1.77	1.18E-05	Mut	
11.26_356.9908	20.05	1.42E-05	Mut	
11.26_779.0863	54.52	1.46E-05	Mut	
20.30_158.9939	2.05	1.46E-05	Mut	
10.14_179.0201	4.63	2.35E-05	Mut	
2.85_78.9861	1.24E+08	2.52E-05	WT	
8.44_362.0776	32.73	2.52E-05	WT	
21.11_175.9990	5.24	2.52E-05	WT	
9.37_418.0771	3.21	2.52E-05	WT	
9.92_128.8708	52.61	2.89E-05	Mut	
9.92_145.0147	6.85	2.89E-05	Mut	
21.11_432.9723	5.88	2.89E-05	WT	
9.37_243.0281	2.44	2.89E-05	WT	
20.97_261.0810	1.26E+02	2.94E-05	WT	
21.11_216.4840	5.41	3.13E-05	WT	
21.11_353.0054	4.75	3.37E-05	WT	
9.63_216.0517	2.33E+07	3.65E-05	WT	

Contrary to analysis of the LN18 and U87-MG cell lines, enrichment of the top 35 compound-features in the volcano plot (Fig. 3.34) were relatively evenly divided between Mut and WT cells. Only one compound-feature (9.92_147.2102) co-eluted with 2-HG and had a different FC and therefore the full dataset was used for further analysis. Fructose 6-phosphate and erythrose 4-phosphate were the only identified metabolites in

the top 35 compound-features, further confirming modifications to glycolysis and the pentose phosphate pathway in 293T Mut cells. As observed for LN18 Mut cells, pyruvate (Fig. 3.35(a)) was significantly depleted (FC 1.36, p-value 4.6×10^{-3}) suggesting that anaplerotic processes were upregulated in 293T Mut cells. The enrichment of 2 & 3-phosphoglycerate, fructose 1,6-bisphosphate and erythrose 4-phosphate may therefore be caused by gluconeogenesis, rather than glycolysis.

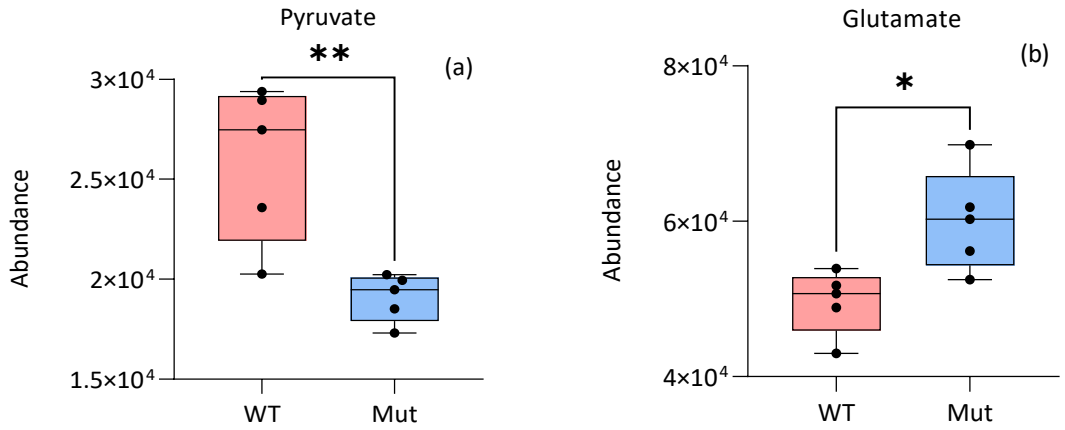

Figure 3.35: Box plots showing the abundance of pyruvate (a) and glutamate (b) in 293T Mut and WT cells cultured under 4.5 g / L glucose (Section 8.16), analysed by IC-MS/MS (Section 8.4). The box plots show the mean, 25-75th percentiles and whiskers extend from the minimum to maximum values. The number of samples are denoted with dots and significance from t-tests are annotated (ns, p-value greater than 0.05; *, p-value less than 0.05; **, p-value less than 0.01; and ***, p-value less than 0.001).

Glutamate (Fig. 3.35(b)) was significantly enriched in the 293T Mut cells by 1.21-fold (p-value 1.5×10^{-2}), in contrast to the glioblastoma-derived cell lines, and provides further evidence that anaplerotic processes may be activated as a consequence of an IDH1 mutation. The cellular redox state was estimated by measurement of the lactate / pyruvate ratio as described for LN18 cells (Section 3.3). The lactate / pyruvate was not significantly altered in the 293T Mut cells, as shown in Fig. 3.36; however, the slight increase in Mut cells suggest that the NAD^+ / NADH balance may still have been perturbed.

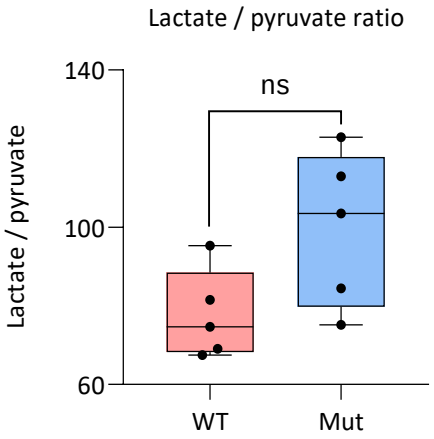

Figure 3.36: Lactate / pyruvate ratio calculated from the analysis of in 293T Mut and WT cells cultured under 4.5 g / L glucose conditions (Section 8.16), by IC-MS/MS (Section 8.4). The box plot shows the mean, 25-75th percentiles and whiskers extend from the minimum to maximum values. The number of samples are denoted with dots and significance from t-tests are annotated (ns, p-value greater than 0.05; *, p-value less than 0.05; **, p-value less than 0.01; and ***, p-value less than 0.001).

As observed in the LN18 cell line, β-citryl glutamate (Fig. 3.37(a)) and NAAG (Fig. 3.37 (b)) were both significantly depleted in the 293T Mut cells by 1.44-fold (p-value $5.6x10^{-3}$) and 1.39-fold (p-value $1.8x10^{-3}$), however, the abundance of NAA (Fig. 3.37 (c)) was not significantly altered.

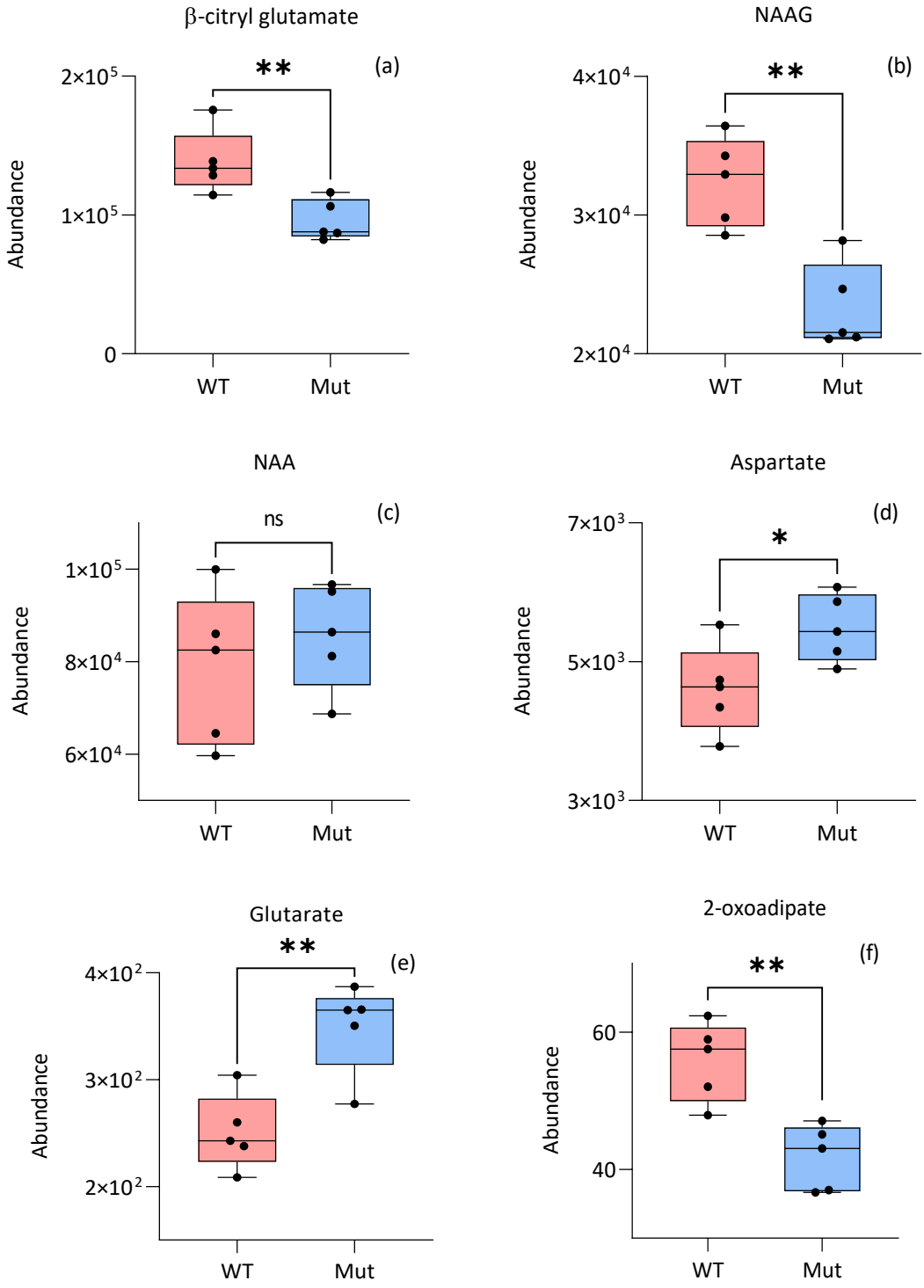

Figure 3.37: Box plots showing the abundance of β-citryl glutamate (a), NAAG (b), NAA (c), aspartate (d), glutarate (e) and 2-oxoadipate (f) in 293T Mut and WT cells cultured under 4.5 g / L glucose conditions (Section 8.16), analysed by IC-MS/MS (Section 8.4). The box plots show the mean, 25-75th percentiles and whiskers extend from the minimum to maximum values. The number of samples are denoted with dots and significance from t-tests are annotated (ns, p-value greater than 0.05; *, p-value less than 0.05; **, p-value less than 0.01; and ***, p-value less than 0.001).

Aspartate (Fig. 3.37(d)) was 1.19-fold enriched (p-value 4.1×10^{-2}) despite the depletion of the neurotransmitters (NAAG and NAA), and glutarate (Fig. 3.37(e)) was also significantly enriched (FC 1.39, p-value 4.4×10^{-4}), providing further evidence that amino acid metabolism was affected by the presence of an IDH1 mutation. The abundance of 2-oxoadipate (Fig. 3.37(f)) was lower than observed for the glioma-derived cell lines but it was significantly depleted in 293T Mut cells (FC 1.33, p-value 3.2×10^{-3}). Consistent with the changes to glycolytic intermediates in the 293T cell line, the abundance of metabolites in the pentose phosphate pathway were altered, as shown in Fig. 3.38.

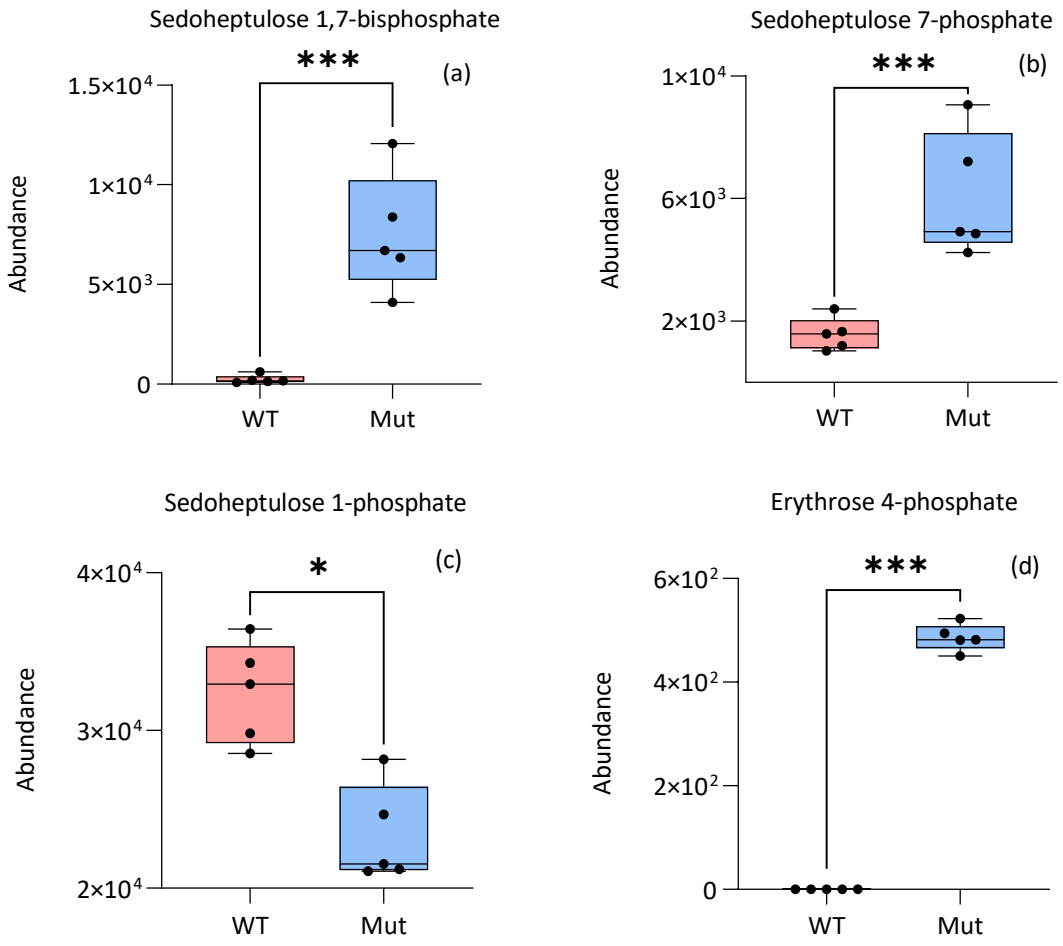

Figure 3.38: Box plots showing the abundance of sedoheptulose 1,7-bisphosphate (a), sedoheptulose 7-phosphate (b), sedoheptulose 1-phosphate (c) and erythrose 4-phosphate (d) in 293T Mut and WT cells cultured under 4.5 g / L glucose conditions (Section 8.16), analysed by IC-MS/MS (Section 8.4). The box plots show the mean, 25-75th percentiles and whiskers extend from the minimum to maximum values. The number of samples are denoted with dots and significance from t-tests are annotated (ns, p-value greater than 0.05; *, p-value less than 0.05; **, p-value less than 0.01; and ***, p-value less than 0.001).

The enrichment of sedoheptulose 1,7-bisphosphate (FC 31.6, p-value $1.0x10^{-5}$), sedoheptulose 7-phosphate (FC 3.84, p-value $1.7x10^{-4}$) and erythrose 4-phosphate (FC 3.03, p-value < $1.0x10^{-16}$), in 293T Mut cells suggests that either the pentose phosphate pathway was upregulated, or an activation of anaplerosis caused by the accumulation of pentose phosphate pathway intermediates.

PLS-DA of the 293 cells resulted in a model with 1 component accuracy, R^2 and Q^2 values of 1.00, 0.97 and 0.94 respectively; however, the p-value obtained from a separation

distance permutation test was 1.00 and therefore not significant, likely due to the low number of samples in each experimental group, and therefore further multivariate statistical analysis was not performed.

IC-MS/MS analysis of 293T Mut and WT cells demonstrated that the presence of an IDH1 mutation had a different effect (compared with the LN18 and U87-MG cell lines) on the embryonic kidney-derived cell line, despite its neuronal properties.[199] The depletion of 2-OG normally seen with the IDH1 mutation was also not observed in the 293T Mut cells, likely due to the lower enrichment of 2-HG. The presence of an IDH1 mutation did have a significant effect on some metabolic processes including central carbon metabolism, amino acid metabolism and the adenine nucleotide pool. Glycolysis was affected inversely to the glioblastoma cell lines, suggesting that the 293T Mut cells were more anaplerotic than WT cells.

3.7. Discussion of IC-MS/MS analysis of IDH1 mutant and wild-type cells

The different tissue origins of the cell lines led to distinct metabolic effects as a result of the IDH1 mutation, notably demonstrated by the difference in enrichment of 2-HG. Previous literature has shown 2-HG to be significantly elevated in the presence of an IDH1 mutation and analysis here, by IC-MS/MS (8.4), showed over hundred-fold enrichment in LN18 and U87-MG Mut cells (Sections 3.3 and 3.5).[40, 133] The 293T cell line (Section 3.6) did not have the same magnitude of enrichment of 2-HG in Mut cells. This was possibly due to reduced intracellular expression of the IDH1 mutation, or reduced activity due to different utilisation of the various cellular energy pathways, compared to the glioblastoma-derived cell lines which had p53 (LN18) or PTEN (U87-MG) mutations. The enrichment of 2-HG correlated with the significant alteration in abundance of a number

of metabolites, across the 3 cell lines, including glutarate, β-citryl glutamate, 2-OG and 2-oxoadipate, as shown in Table 3.10. Alteration of the abundance of β-citryl glutamate and 2-oxoadipate have not previously been associated with IDH mutations.

Table 3.10: Heat map showing the FC for selected metabolites from IC-MS/MS analysis (Section 8.4) of Mut and WT LN18 (experimental replicate 1, Section 8.14), U87-MG (Section 8.15) and 293T (Section 8.16) cells, cultured under 4.5 g / L glucose conditions.

Identified metabolite	LN18	U87-MG	293T
2-HG			
Glutarate			
Lactate			
Erythrose 4-phosphate			
Fructose 6-phosphate			
Sedoheptulose 1,7-diphosphate			
2-Phosphoglycerate			
Sedoheptulose 7-phosphate			
Glutamate			
Phosphoenolpyruvate			
β-citryl glutamate			
2-OG			
2-oxoadipate			

Key	FC								
	Enriched in WT					Enriched in Mut			
-100.0	-4.0	-2.5	-1.5	-1.2	1.2	1.5	2.5	4.0	100.0

The abundance of 2-OG was significantly depleted in LN18 and U87-MG Mut cells, but was not significantly altered between 293T Mut and WT cells. The lower FC magnitude for 2-OG was concomitant with the abundance of 2-HG, which may have been caused by lower activity of the IDH1 mutation in 293T Mut cells. The correlation may also be due to inhibition by 2-HG, which was diminished at lower intracellular concentration, and/or related to 2-OG concentration (which was inversely related to 2-HG).

TCA cycle metabolite abundance, in 293T cells, was also dissimilar to the glioblastoma-derived cell lines, possibly due to increased reliance on anaerobic glycolysis for glioblastoma-derived cell lines.[200] Contrary to observations made by Reitman *et al*., for

an oligodendroglioma-derived cell line with and without an IDH1 R132H mutation, TCA cycle metabolite abundances were not significantly modified, in the Mut cell lines analysed here.[133] Metabolic analysis by Reitman *et al*. identified 195 metabolites using 3 methods (GC-MS using electron impact ionisation and HILIC-MS in both negative and positive ESI modes).[133] Of the 195 metabolites investigated by Reitman *et al*., 48 were identified in negative ion mode compared with up to 266 (demonstrated here for LN18 cells in Section 3.3), by IC-MS/MS.[133] The coverage of metabolites in the pentose phosphate pathway and nucleotide metabolism in Mut cells was greater, compared with the data acquired by Reitman *et al*.[133] The depletion of 2-OG was not observed by Reitman *et al*. and suggests that the glioblastoma-derived cell lines may have different TCA cycle activities to oligodendroglioma cells.[133]

A negative correlation with 2-HG abundance was also observed (Table 3.10), for fructose 6-phosphate. No significant alteration of abundance was observed for fructose 6-phosphate in LN18 cells, which had the highest abundance 2-HG in Mut cells. Increased depletion of fructose 6-phosphate was observed in U87-MG and 293T Mut cells, as 2-HG concentration diminished, revealing a possible secondary metabolic effect caused by 2-HG, which may regulate specific enzymes in the pentose phosphate pathway. Differential effects on energy metabolism in Mut and WT cells were also observed, especially for comparison of the non-cancer and glioblastoma-derived cell lines. 2-phosphoglycerate, sedoheptulose 1,7-diphosphate and phosphoenolpyruvate were depleted in LN18 and U87-MG Mut cells; however, were enriched in 293T Mut cells, concomitant with a general enrichment of pentose phosphate pathway intermediates. Sedoheptulose 1,7-diphosphate was enriched in U87-MG and 293T Mut cells but depleted

in LN18 Mut cells, further demonstrating differential effects of the IDH1 mutation, related to cell line origin or mutation status.

Previous investigations have also suffered from poor coverage of glycolytic intermediates, as those metabolites are poorly characterised by HILIC-MS/MS, as discussed in Sections 1.4 and 2.5.[116, 133] The significant depletions of 2 & 3-phosphoglycerate, and phosphoenolpyruvate have not been reported previously and may suggest increased utilisation of glycolysis in Mut cells, to sustain the TCA cycle. An increase in lactate abundance as a result of the exploitation of anaerobic glycolysis, in accordance with the Warburg effect, was not observed for the LN18 Mut cells. This may be because glycolytic flux was already maximal in LN18 WT cells, validated by the depletion of glycolytic intermediates in LN18 Mut cells. Lactate was enriched in the U87-MG cells, suggesting further glycolytic capacity, compared with LN18 cells, under the same growth conditions. Glycolysis was observed to be at or near capacity, from the increased contribution of ATP to the total adenine nucleotide pool and high abundance of pentose phosphate intermediates, in the glioblastoma-derived Mut cell lines. The utilisation of alternative energy sources for the TCA cycle, such as pyruvate and glutamate, were differential of Mut and WT cells. Pyruvate is transported into the mitochondria from the cytosol and oxidised to form acetyl CoA for the TCA cycle.[201] As pyruvate dehydrogenase is known to be regulated by product inhibition, the depletion of acetyl CoA would result in the depletion of pyruvate, if supply from glycolysis or amino acid oxidation was limited.[202] The depletion of glutamate was also explained by the depletion of 2-OG and was probably used as an additional energy source, to maintain the TCA cycle. The lactate / pyruvate ratio was not altered in the glioblastoma cell lines, suggesting that the additional redox stress caused by the IDH1 mutation does not destabilise the NAD redox couple. The

increased contribution of ATP to the total adenine nucleotide pool in Mut cells also provided evidence for the modification of energy production, as a result of the IDH1 mutation. The intracellular acidification and the depletion in glycolytic intermediates, in Mut cells, may therefore make them vulnerable to additional redox stress. The cells may therefore be sensitive to external concentrations of glucose and glutamine and could be preferentially targeted by exploiting conditions to favour WT or Mut cells, in combination with therapeutic intervention.

Pentose phosphate pathway intermediates are usually not well characterised by HILIC-MS or GC-MS analyses and therefore were not reported by Reitman *et al*., but were measured by IC-MS/MS.[133] Significant changes in pentose phosphate pathway intermediate abundances were observed across all 3 cell lines, and correlated with the utilisation of glycolysis, inferred by alteration in metabolite abundances. Depletion of sedoheptulose 1,7-bisphosphate, sedoheptulose 7-phosphate and erythrose 4-phosphate in the glioblastoma-derived cell lines, as well as the depletion of glycolysis intermediates, suggested upregulated glycolytic activity in Mut cells, to support the production of 2-HG. The dependence of Mut cells on pentose phosphate pathway intermediates may allow selective therapeutic targeting of Mut cells using NADPH inhibitors. For example, the inhibitor 6-aminonicotinamide has been shown to be selective for pentose phosphate pathway enzymes, and has been used as part of combination treatment with traditional chemotherapeutics for the treatment of leukaemia lymphocytes.[203, 204] The 293T cell line showed evidence of increased anaplerosis in Mut cells and a consequent enrichment of both glycolysis and pentose phosphate pathway intermediates, contrary to the changes observed in the glioma-derived cell lines.

The depletion of β-citryl glutamate was consistently associated with an IDH1 mutation in all 3 cell lines studied in this thesis, as shown in Table 3.10. This depletion has not previously been reported in relation to IDH, and has not been extensively studied in the literature, despite observations of significant enrichment during early brain development.[185, 188] A proposed role of β-citryl glutamate is as an activator of mitochondrial aconitase, promoting neuronal proliferation and survival.[188] The depletion of β-citryl glutamate in Mut cells may therefore reduce the tumour progression and metastasis providing an explanation of the increased survival rate of patients with IDH1 mutant glioblastoma.[205] The depletion of NAAG and/or NAA was observed concurrently with the enrichment of β-citryl glutamate and the changes appeared to be linked to the enrichment of 2-HG (or the presence of the IDH1 mutation), rather than the depletion of 2-OG, as the effect was observed in all 3 cell lines. The proposed regulatory effect of β-citryl glutamate to control of cellular differentiation during brain development may therefore have a role in tumourigenesis and requires further investigation.

Amino acid metabolism may also have been altered in IDH1 Mut cells as the lysine degradation pathway metabolites 2-oxoadipate and glutarate were significantly depleted and enriched respectively. The interconversion of 2-oxoadipate and 2-aminoadipate, by aminoadipate transferase, is regulated by glutamate and 2-OG and therefore the depletion of 2-oxoadipate was consistent with the depletion of 2-OG in Mut cells.[206] The structural similarity of 2-OG and 2-HG could allow competitive inhibition of 2-OG dependent pathways, and the regulatory effect of increased 2-HG requires further investigation, especially for amino acid related metabolites, which are not well characterised by IC-MS.

3.8. Chapter summary

The IC-MS/MS method was used for untargeted analysis of 3 Mut and WT cell lines (LN18, U87-MG and 293T) to investigate the metabolic impact of an IDH1 mutation. A database of polar and ionic metabolites was established with monoisotopic mass, chemical formula, RT and fragmentation pattern data for authentic metabolite standards, which enabled IC-MS/MS to be used for the identification of metabolites. The IC-MS/MS method was also compared with HILIC-MS/MS to demonstrate sensitivity and metabolite coverage for the analysis of cell samples, as well as the different chemical selectivity of the methods. Univariate and multivariate statistical analysis of the IC-MS/MS data revealed metabolites which had significantly altered abundance in Mut cells, including intermediates in the pentose phosphate pathway, pyruvate metabolism and glycolysis, as well as nucleotides. Increased coverage of metabolic pathways for IC-MS/MS compared with HILIC-MS/MS was demonstrated using pathways analysis.

As well as the enrichment of 2-HG, which was observed in all Mut cells, 2-OG was depleted in the glioblastoma-derived Mut cell lines. In 293T Mut cells, 2-OG was not significantly depleted, but alteration of TCA cycle metabolite abundance, including the enrichment of succinate and malate were observed. Anaplerotic metabolism was potentially activated in the 293T cell line, suggested by the depletion of pyruvate and the enrichment of pentose phosphate pathway intermediates in 293T Mut cells. In the glioblastoma-derived Mut cell lines, glycolytic and pentose phosphate pathway intermediates were observed to be depleted, possibly as a result of their p53 or PTEN gene mutations. Glutamate was also significantly depleted in the glioma-derived Mut cells suggesting that it was a key source of carbon for the TCA cycle, to maintain flux, despite

the depletion of 2-OG and the enrichment of 2-HG. The adenine nucleotide pool was also significantly modified in the presence of an IDH1 mutation, and an increased contribution of ATP in Mut cells further confirmed that energy production was augmented by the IDH1 mutation. Adenylate energy charge was possibly modified to maintain the NAD^+ / NADH balance, despite the depletion of NADPH as a result of the production of 2-HG and the additional redox stress of intracellular acidification.

The changes in metabolism observed for the analysis of the 3 cell lines was compared with previous results in the literature and the potential role of the IDH1 mutation in tumourigenesis was discussed. Amino acid metabolism, cellular energy pathways and pentose phosphate pathway were all identified as potential targets for therapeutic intervention in cells. Further to the depletion of neurotransmitters and β-citryl glutamate, glutarate and 2-oxoadipate were significantly modified in IDH1 mutant cells. Coverage of adjacent metabolites in the amino acid-related metabolic pathways was poor, due to the zwitterionic nature of their amine groups, which were not well characterised by IC-MS/MS. A method for the analysis of metabolites containing amine groups will therefore be used to extend the depth of coverage of metabolites in amino acid metabolism and further identify pathways which may be affected by the IDH1 mutation.

Chapter 4. Exploring metabolism in IDH1 mutant and wild-type cells using derivatised RP-IMS-MS/MS

4.1. Introduction

As discussed in Chapters 2 and 3, many metabolites associated with primary metabolism are highly polar or physiologically ionic and may be structurally isomeric with other metabolites present in a biological sample. These polar metabolites are not well-resolved, or resolved at all, using conventional RP approaches. IC-MS provides a useful solution for separation and analysis of many anionic metabolites, as demonstrated in Chapters 2 and 3, however, cationic metabolites (containing amine groups for example) remain a challenge for untargeted metabolomics.

In this chapter a derivatised approach, aimed at amine cations, for untargeted metabolomics is developed and used to investigate metabolic changes associated with an IDH1 mutation. An inherent challenge for the derivatisation of complex biological samples is the requirement for ensuring extensive and complete derivatisation, and how to demonstrate that this has been achieved. Derivatisation can also increase sample complexity and lead to increased analytical variability.[207] For these, and a variety of additional reasons, derivatisation has not been widely adopted for metabolomics, despite often providing increased specificity and sensitivity. This is in contrast to GC-MS applications where derivatisation is used extensively.[133, 134, 136, 137] A new approach for derivatised LC-MS metabolomics is explored here with IMS-MS/MS, which will be used to evaluate the extent of derivatisation for biological samples. This will be a novel application of IMS-MS within the context of metabolomics so some time will also be spent exploring its performance and capabilities. Here AQC is used (as discussed in Section 1.6)

to derivatise any 1° and 2° amine groups present, as shown in Figure 4.1, including amino acids and other zwitterionic metabolites, in complex biological samples. This will make zwitterionic and cationic amine metabolites more amenable to analysis by RP-MS and increase sensitivity.

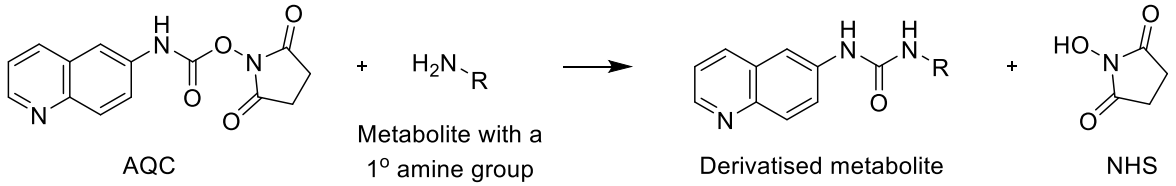

Figure 4.1: AQC derivatisation reaction for a generic metabolite with a 1° amine group.

The research aims of this chapter were to:

- Establish and validate a method for the analysis of metabolites with 1° or 2° amine groups.
- Investigate some of the advantages IMS-MS/MS can provide for metabolomics.
- Investigate changes in metabolism associated with an IDH1 mutation by comparison of Mut and WT cells.

4.2. Optimisation of ESI source conditions for the analysis of derivatised amines

ESI source conditions are closely interrelated with the sensitivity of a method for individual metabolites, and as discussed in Section 2.3, require optimisation for the mobile phase, flow rate and analyte lability of any LC method, to achieve optimal sensitivity.[160] ESI source conditions including cone voltage, source temperature, desolvation temperature and gas flow rate as well as capillary voltage were optimised to increase sensitivity for the amines listed in Table 4.1.

Table 4.1: Mix of authentic amine metabolite standards used for method development and performance testing.

HMDB code	Compound	Concentration / μM	Formula
HMDB0000161	L-Alanine	25.0	$C_3H_7NO_2$
HMDB0000517	L-Arginine	25.0	$C_6H_{14}N_4O_2$
HMDB0000191	L-Aspartate	25.0	$C_4H_7NO_4$
HMDB0000192	L-Cystine	12.5	$C_6H_{12}N_2O_4S_2$
HMDB0000148	L-Glutamate	25.0	$C_5H_9NO_4$
HMDB0000123	Glycine	25.0	$C_2H_5NO_2$
HMDB0000177	L-Histidine	25.0	$C_6H_9N_3O_2$
HMDB0000172	L-Isoleucine	25.0	$C_6H_{13}NO_2$
HMDB0000687	L-Leucine	25.0	$C_6H_{13}NO_2$
HMDB0000182	L-Lysine	25.0	$C_6H_{14}N_2O_2$
HMDB0000696	L-Methionine	25.0	$C_5H_{11}NO_2S$
HMDB0000159	L-Phenylalanine	25.0	$C_9H_{11}NO_2$
HMDB0000162	L-Proline	25.0	$C_5H_9NO_2$
HMDB0000187	L-Serine	25.0	$C_3H_7NO_3$
HMDB0000167	L-Threonine	25.0	$C_4H_9NO_3$
HMDB0000158	L-Tyrosine	25.0	$C_9H_{11}NO_3$
HMDB0000883	L-Valine	25.0	$C_5H_{11}NO_2$

The authentic metabolite standards were derivatised and analysed by RP-IMS-MS/MS (Section 8.8) whilst varying ESI source parameters, to maximise the signal to noise ratio for those metabolites and consequently reduce their LLoD. The amines were selected as they were commercially available as a standard mix and reproducible over multiple months. It was assumed that the similarity of the amines used would not detriment the validity of the experiments as the AQC derivative is the likely protonation site for positive ESI (as discussed in Section 1.6). The mean ion intensity for the derivatised metabolites was calculated and plotted to allow the comparison of each variable across a range of molecular weights and functionalities. The first parameters to be optimised were cone voltage and source temperature as shown in Fig. 4.2.

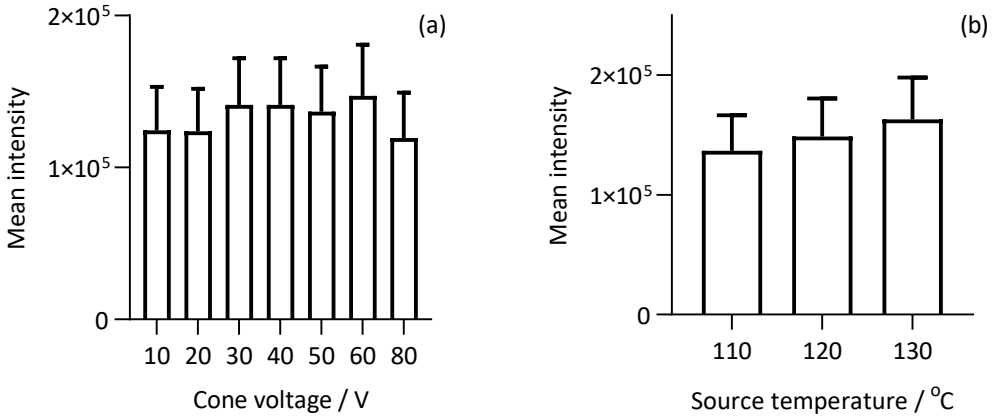

Figure 4.2: Mean ion intensities for the derivatised mix of 17 authentic metabolite standards (listed in Table 4.1), analysed in triplicate by the method described in Section 8.8. Source conditions were varied in positive ion mode with cone voltage between 10-80 V (a) and source temperature between 110-130 ^{o}C (b). Error bars represent standard deviation of the mean.

Cone voltage did not have a significant effect on ion intensity, for the metabolites investigated in positive ion mode, possibly because the analytes had similar ionisation properties once derivatised, as the AQC derivative has multiple likely protonation sites (structure shown in Fig. 1.5). Ion intensity did not decrease at higher cone voltage suggesting that in-source fragmentation of the ions was not taking place extensively. A cone voltage of 40 V was adopted to ensure efficient transfer of ions into the high vacuum region, with minimal energy transfer prior to reaching the ion optics of the instrument. Source temperature was investigated next and this had a significant effect on ion intensity, as sensitivity increased with temperature, presumably due to increased evaporation of electrospray solvent droplets and consequent improvement in charge transfer to the analytes. The standard deviation of the measurements did not increase with source temperature and 130 ^{o}C was selected for further optimisation of ESI parameters. Next it was shown that desolvation gas flow and temperature had the largest impact on sensitivity (Fig. 4.3).

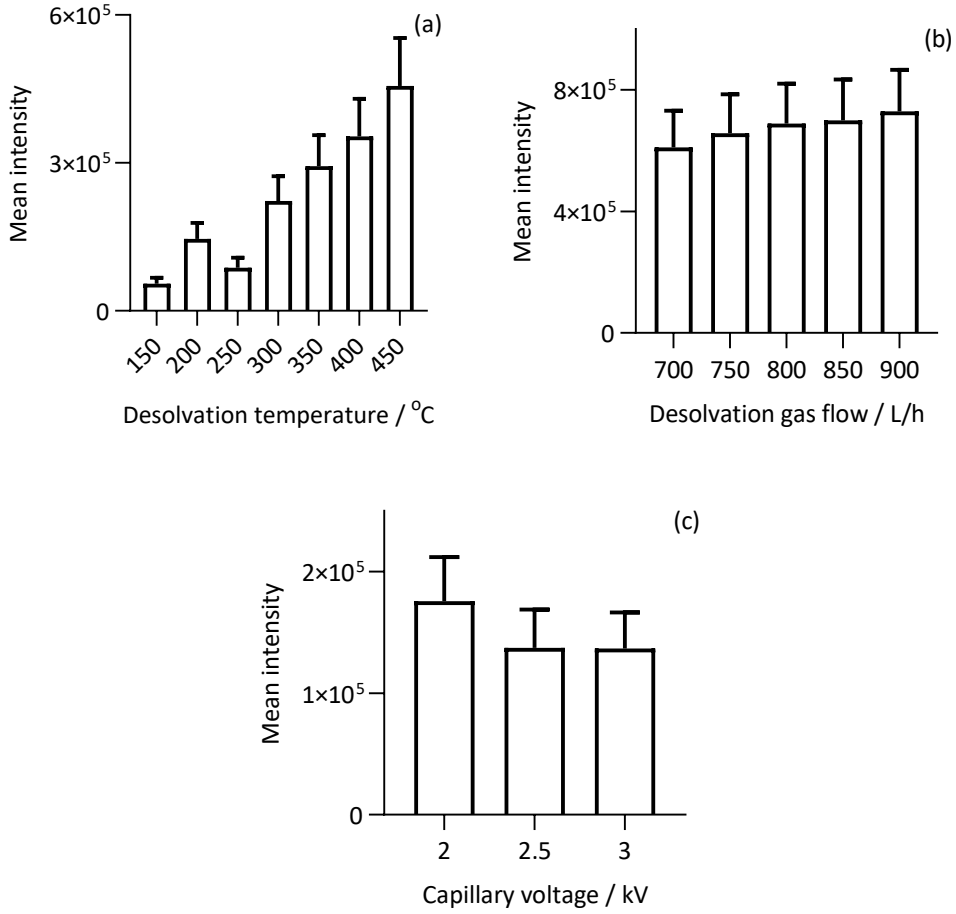

Figure 4.3: Mean ion intensities for the derivatised mix of 17 authentic metabolite standards (listed in Table 4.1), analysed in triplicate by the method described in Section 8.8. Source conditions were varied in positive ion mode with desolvation temperature between 150-450 °C (a), desolvation gas between 700-900 L / h (b) and capillary voltage between 2.0-3.0 kV (c). Error bars represent standard deviation of the mean.

Increased desolvation temperature also improved evaporation of the solvent droplets, increasing ionisation efficiency; however, the increased temperature also led to higher standard deviations for analytical replicates, as shown in Fig. 4.3(a). The gain in sensitivity with increased desolvation temperature compensated for the increased variance. No significant in-source fragmentation was observed and therefore a desolvation temperature of 450 °C was selected. Desolvation gas flow was subsequently optimised with the desolvation temperature maintained at 450 °C. The gain in sensitivity with increased desolvation gas flow was not as significant as observed for desolvation temperature but still increased ion intensity, as shown in Fig. 4.3(b). Capillary voltage was

also optimised, and in contrast to the other source parameters, ion intensity decreased with increased voltage, likely due to in-source fragmentation. A lower capillary voltage of 2.0 kV was therefore selected to minimise any in-source fragmentation. It was assumed that as the same LC flow rate and gradient were used in positive and negative ion modes, identical temperatures and flow rates could also be applied. The voltages would be different as the energies required for protonating and deprotonating ions would likely be different. The same authentic metabolite standard mix was analysed in negative ion mode, as described in Section 8.8, and the cone and capillary voltages were varied, as shown in Fig. 4.4, to maximise sensitivity.

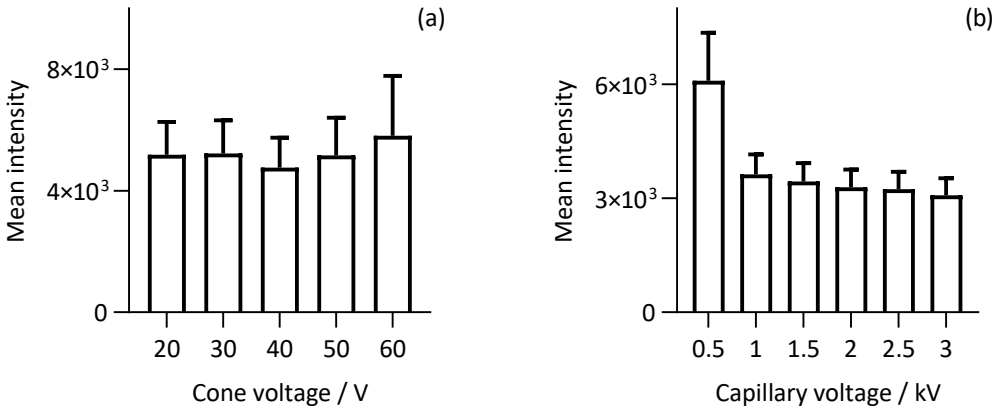

Figure 4.4: Mean ion intensities for the derivatised mix of 17 authentic metabolite standards (listed in Table 4.1), analysed in triplicate by the method described in Section 8.8. Source conditions were varied in negative ion mode with cone voltage between 20-60 V (a) and capillary voltage between 0.5-3.0 kV (b). Error bars represent standard deviation of the mean.

Cone voltage in negative ion mode did not have a significant effect on ion intensity, however, increased variability was observed above 50 V. The most reproducible intensity was observed at 40 V, which was therefore selected for further analyses. The trend for capillary voltage in negative ion mode (Fig. 4.4(b)) was comparable with positive ion mode (Fig. 4.3(c)). Sensitivity was increased by 1.68-fold at a voltage of 0.5 kV compared with 1.0 kV and any further increase of voltage reduced sensitivity.

The source conditions were optimised for both positive and negative ion modes in order to increase the sensitivity of the method and therefore provide optimal signal to noise ratios for a broad range of metabolites. A mix of amines with a range of *m/z* values were used to assess optimal ionisation conditions for derivatised analytes. The optimised source conditions used for the RP-IMS-MS/MS method are listed in Section 8.8 and were used for all subsequently described analyses.

4.3. Reproducibility and linearity of analysis for RP-IMS-MS/MS

In a targeted workflow, authentic metabolite standards can be analysed alongside samples to produce a calibration curve for absolute quantification. For untargeted approaches, relative quantification is used, which requires linearity over a wide concentration range. It is therefore important that a method is validated to ensure that quantification and linearity of response is demonstrated within normal concentration ranges for metabolites.

4.3.1. RP-IMS-MS/MS reproducibility

The RT associated with chromatographic separation of analytes was shown to be highly reproducible (Fig. 4.5). This RT stability provided the opportunity for the use of RT to aid in metabolite identification (RT for all analysed authentic metabolite standards are listed in Section 10.3). RT of derivatised amine metabolites (listed in Table 4.1) were plotted from the analysis of a mix of standards by RP-IMS-MS/MS (Section 8.8). This mix of authentic metabolite standards was analysed regularly over a 3 month period and the RT variability plotted in Fig. 4.5.

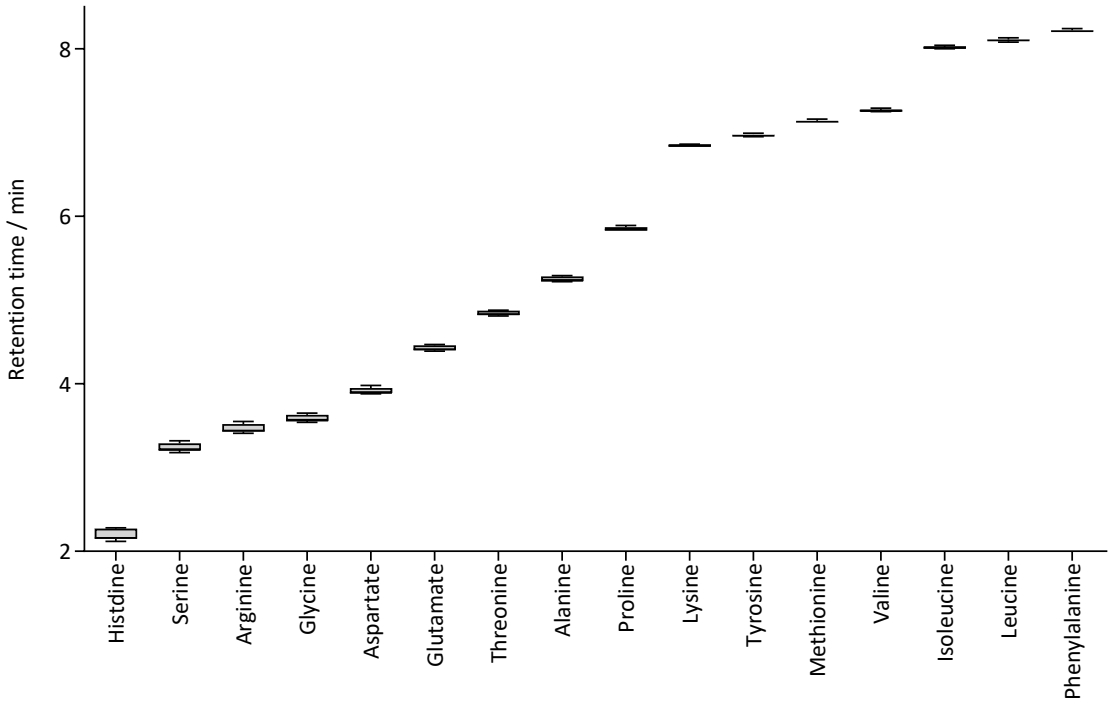

Figure 4.5: Reproducibility in RT for a derivatised mix of authentic amine metabolite standards analysed over 3 months, by RP-IMS-MS/MS (Section 8.8, n=40).

The RT of these analytes varied by less than 4.0 %, the largest variability was observed for histidine with a mean RT of 2.19 s and minimum and maximum values of 2.12 s and 2.27 s respectively). The overall mean RT error for the metabolites analysed was 0.95 %. RT variability was therefore superior than HILIC-MS/MS (Section 8.5), which had an overall mean RT error of 3.19 % for 24 analyses of the same amine standard mix, providing increased confidence in RT as a metabolite identification parameter. HILIC-MS/MS analysis of glutamate showed a RT variability of ± 14.5 s which corresponded to a 5.4 % variation across 3 months, compared with a variability of ± 2.4 s (1.8 % variation) for RP-IMS-MS/MS. Higher variation was observed for the earlier eluting analytes such as histidine and serine. This was likely caused by these analytes having a reduced number of interactions with the stationary phase, compared with later eluting analytes. These early

eluting analytes are therefore more susceptible to variabilities in mobile phase and injection solvent composition.

Evaluation of the derivatised method for reproducibility at an untargeted level was also investigated using PCA scores plot of compound-feature intensities, for the analysis of 293T WT cells cultured at different glucose concentrations (Section 8.16), derivatised and analysed by RP-MS (Section 8.7). All-ions data were processed in MetaboAnalyst, as described in Section 8.11, and a PCA scores plot of compound-feature abundances (Fig. 4.6), showed that there were differences in analyte abundance, between 293T cells cultured in 1.0 g / L or 4.5 g / L glucose DMEM.[166]

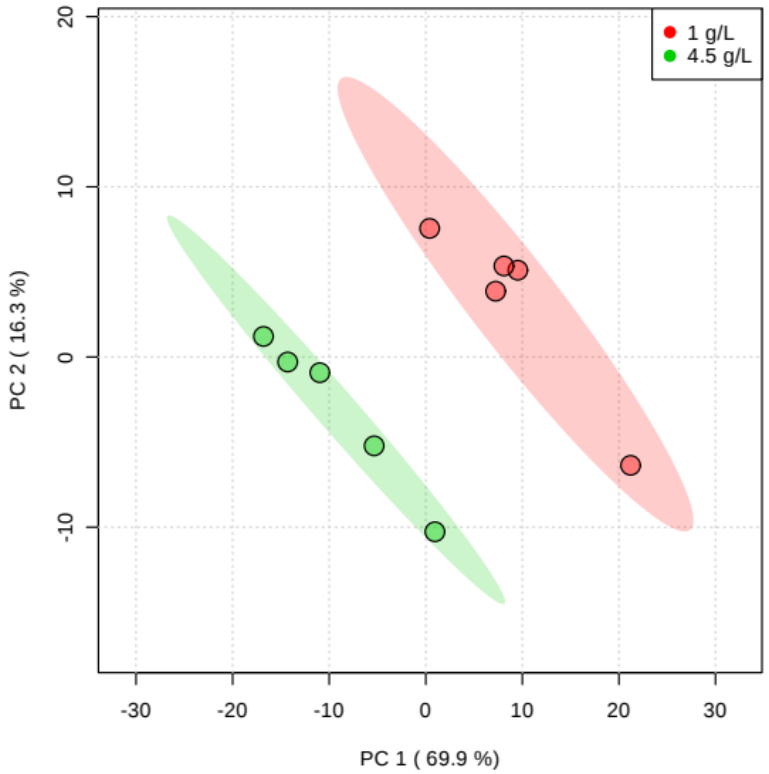

Figure 4.6: PCA scores plot of compound-feature abundances for 293T WT cells cultured in 1.0 g / L or 4.5 g / L glucose DMEM (Section 8.16), derivatised and analysed by RP-MS (Section 8.7) and data processed in MetaboAnalyst with normalisation by sum and Pareto scaling (Section 8.11). Shaded areas represent the 95 % confidence interval for each group.

The PCA scores plot showed clustering of individual samples by experimental group within 95 % confidence intervals. The separation between sample groups cultured

under 1.0 g / L and 4.5 g / L glucose conditions demonstrated that metabolite abundances vary with media glucose concentration and that derivatised RP-IMS-MS/MS was able to reproducibly distinguish these metabolic differences.

4.3.2. RP-IMS-MS/MS linearity

In order to evaluate the LLoD and LLoQ for the analysis of derivatised metabolites, authentic standards of the metabolites listed in Table 4.1, at concentrations from 25.0 μM down to 1.25 nM, were derivatised and analysed, as described in Section 8.7. To compare the method with an established technique for the analysis of metabolites with amine groups, the same samples were analysed before derivatisation by HILIC-MS (Section 8.5), and the LLoD, LLoQ and R^2 values for each method, as shown in Table 4.2, were calculated according to the ICH guidelines used in Section 2.6.[164, 165]

Table 4.2: Comparison of LLoD, LLoQ and R^2 values for the calibration curves of amines analysed by derivatised RP-MS (Section 8.7) and HILIC-MS (Section 8.5).

	Derivatised RP-MS			**HILIC-MS**		
Compound	**LLoD / μM**	**LLoQ / μM**	**R^2**	**LLoD / μM**	**LLoQ / μM**	**R^2**
Alanine	0.67	2.03	0.9976	0.30	0.92	0.9996
Arginine	0.21	0.64	0.9992	2.66	8.06	0.9882
Aspartate	1.42	4.29	0.9892	7.06	21.41	0.9220
Cystine	0.65	1.97	0.9996	ND	ND	ND
Glutamate	0.03	0.09	1.0000	0.61	1.85	0.9985
Glycine	0.50	1.53	0.9986	5.76	17.46	0.9709
Histidine	1.16	3.51	0.9775	2.06	6.23	0.9836
Isoleucine	0.32	0.98	0.9994	0.63	1.91	0.9989
Leucine	0.35	1.07	0.9993	0.49	1.50	0.9993
Lysine	0.25	0.76	0.9997	2.24	6.78	0.9955
Methionine	0.16	0.50	0.9999	1.12	3.38	0.9966
Phenylalanine	0.33	0.99	0.9994	1.39	4.21	0.9948
Proline	0.77	2.33	0.9968	0.21	0.64	0.9998
Serine	1.45	4.39	0.9981	5.48	16.60	0.8601
Threonine	0.17	0.51	0.9998	0.80	2.43	0.9975
Tyrosine	0.19	0.58	0.9999	3.17	9.61	0.9832
Valine	0.32	0.98	0.9994	1.03	3.12	0.9971

In almost all cases RP-MS had reduced LLoD and LLoQ compared to HILIC-MS as well as a higher R^2 value. Alanine and proline had reduced LLoD and LLoQ when analysed by HILIC-MS, likely due to their high R^2 values of 0.996 and 0.998 respectively. The R^2 values were generally lower for analysis by derivatised RP-MS and cystine was below the LLoD for HILIC-MS, at 12.5 μM and therefore no calibration curve could be plotted. The data shows that derivatised RP-MS was linear across 4 orders of magnitude, for a range of amine metabolites. The assumption was made that the same linearity and limits of detection will be observed in derivatised biological samples, as dilution with buffer is used (which reduces matrix effects). Support for this assumption was provided by the analysis (Section 8.8), of a 293T QC sample (Section 8.17) derivatised and diluted with buffer post derivatisation, over 3 orders of magnitude. The linearity of glutamate, alanine and isoleucine, is shown in Fig. 4.7, with R^2 values of 0.9981, 0.9992 0.9966 respectively,

which demonstrate the general trends of the other compounds analysed by derivatised RP-MS/MS.

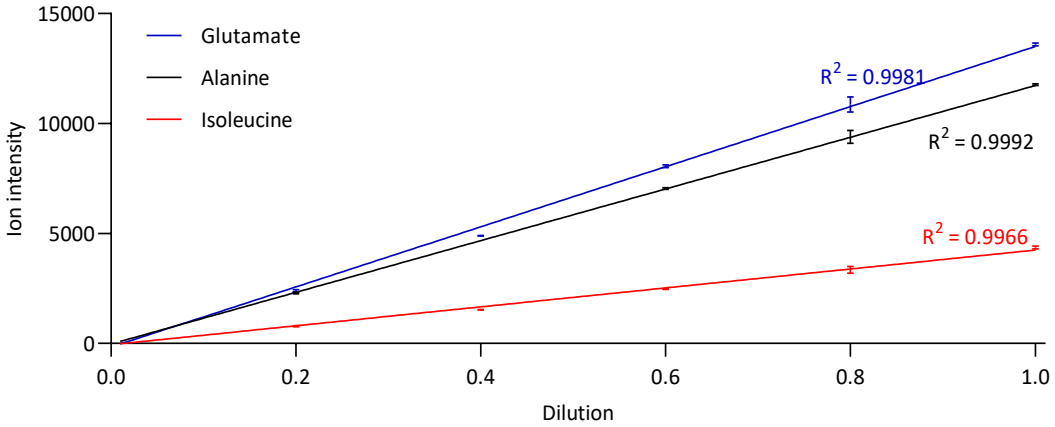

Figure 4.7: Linearity of analysis for the derivatised metabolites glutamate, alanine and isoleucine across 3 orders of magnitude for diluted 293T QC sample (Section 8.17), derivatised and analysed by RP-MS/MS (Section 8.8). Error bars represent standard deviation of ion intensity for triplicate measurements of each metabolite.

Derivatisation and analysis remained reproducible in the presence of biological matrix and displayed linearity of ion abundance across a dilution range of at least 3 orders of magnitude. As shown in Fig. 4.7, the plot of ion abundance against dilution factor, from undiluted to 100 times dilution of the sample, showed a trend toward reduced ion intensity with dilution for all analytes and no significant matrix effects. Matrix effects were reduced by the dilution of the samples by 10-fold in buffer as part of the derivatisation process and further dilution with buffer reduced the complexity of the samples by decreasing the concentration of salts and other species, which may have the potential to interfere with efficient ESI. A maximum variation below 2.5 % in ion abundance and R^2 greater than 0.995 (Table 4.3), was observed for all analytes. This demonstrated that the method was therefore appropriate for relative quantification over the expected concentration range for typical biological samples.[208]

Table 4.3: R^2 values for derivatised metabolites across 3 orders of magnitude for a diluted 293T QC sample (Section 8.17), derivatised and analysed in triplicate by RP-MS/MS (Section 8.8).

Compound	R^2
Alanine	0.9983
Arginine	0.9903
Aspartate	0.9952
Glutamate	0.9977
Glycine	0.9974
Histidine	0.9985
Isoleucine	0.9973
Leucine	0.9978
Methionine	0.9955
Phenylalanine	0.9980
Proline	0.9951
Serine	0.9960
Threonine	0.9988
Tyrosine	0.9980
Valine	0.9976

The unidentified compound-features 6.15_477.1314, 6.67_244.1085 and 2.71_296.0700 from a derivatised 293T QC sample (Section 8.17) also displayed linearity, as shown in Fig. 4.8, with R^2 values of 0.9953, 0.9975 and 0.9958 respectively, in line with the majority of other unidentified compound-features.

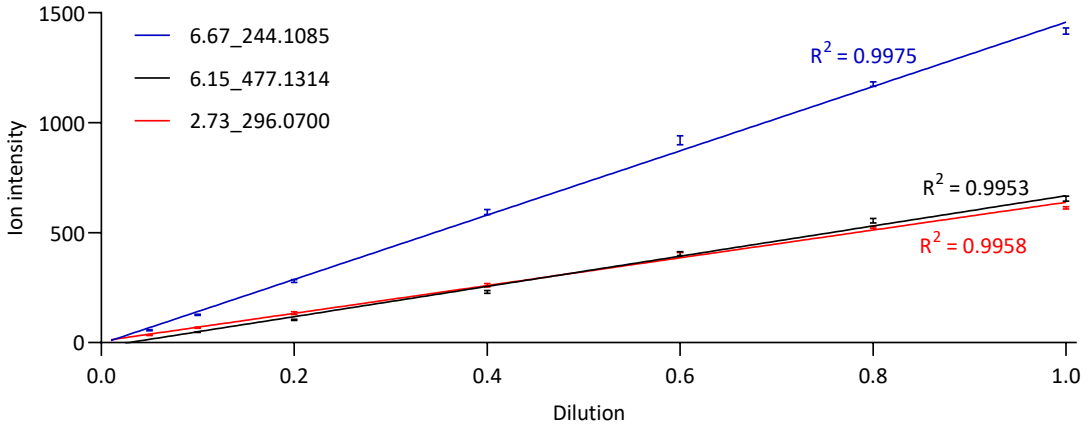

Figure 4.8: Linearity of analysis for 3 unidentified compound-feature across 3 orders of magnitude for diluted 293T QC sample (Section 8.17), derivatised and analysed by RP-MS/MS (Section 8.8). Error bars represent standard deviation of ion intensity for triplicate measurements of each compound-feature.

Linearity was only demonstrated over 3 orders of magnitude, as the absolute concentration of metabolites in the cell sample was reduced, compared with authentic

metabolite standards. Absolute concentration of the amino acids, in the undiluted sample, were measured to be in the low μM range. The majority of metabolites with amine functional groups in the cell samples were therefore below the LLoD when diluted by $1x10^4$-fold. The compound-feature 6.15_477.1314, in Fig. 4.8, was later identified with an authentic standard as glutathione.

In summary, RP-MS with sample derivatisation was validated for untargeted analysis by ensuring accurate quantification and linearity of response for authentic metabolite standards and biological samples. Linearity was demonstrated across 3 orders of magnitude in cell samples as well as increased sensitivity from more efficient ionisation compared with the underivatised species. Derivatisation also reduced LLoD and LLoQ as well as increased R^2, for the analysis of 1° and 2° amines, compared with HILIC-MS. RT was also shown to be extremely reproducible and demonstrated the suitability of the derivatised RP-IMS-MS/MS method for metabolic analysis of biological systems.

4.4. Identification of unknown amines in cell extracts

To allow investigation of unknown compound-features, and increase confidence in metabolite identification, additional information about analytes can be provided from their MS/MS fragment ions. As discussed in Section 1.6, higher-energy collisional dissociation fragmentation of a derivatised metabolite with amine functionality produced a fragment ion corresponding to the AQC reagent (Fig. 4.9(a), *m/z* 171.0553) and the neutral loss of the original amine containing metabolite (in positive ion mode). Fragmentation patterns can therefore be used to distinguish whether a specific ion was derivatised and therefore aid metabolite identification.

MS/MS fragment ions are also observed in negative ion mode, from cleavage of the amide bond, where the ion with amine functionality retains the charge. In the case of glutamate (Fig. 4.9(b)) in negative ion mode, the derivatising reagent was the neutral loss and *m/z* 146.0452 was observed, corresponding to the deprotonated form of the underivatised chemical formula, as shown in Fig. 1.5.

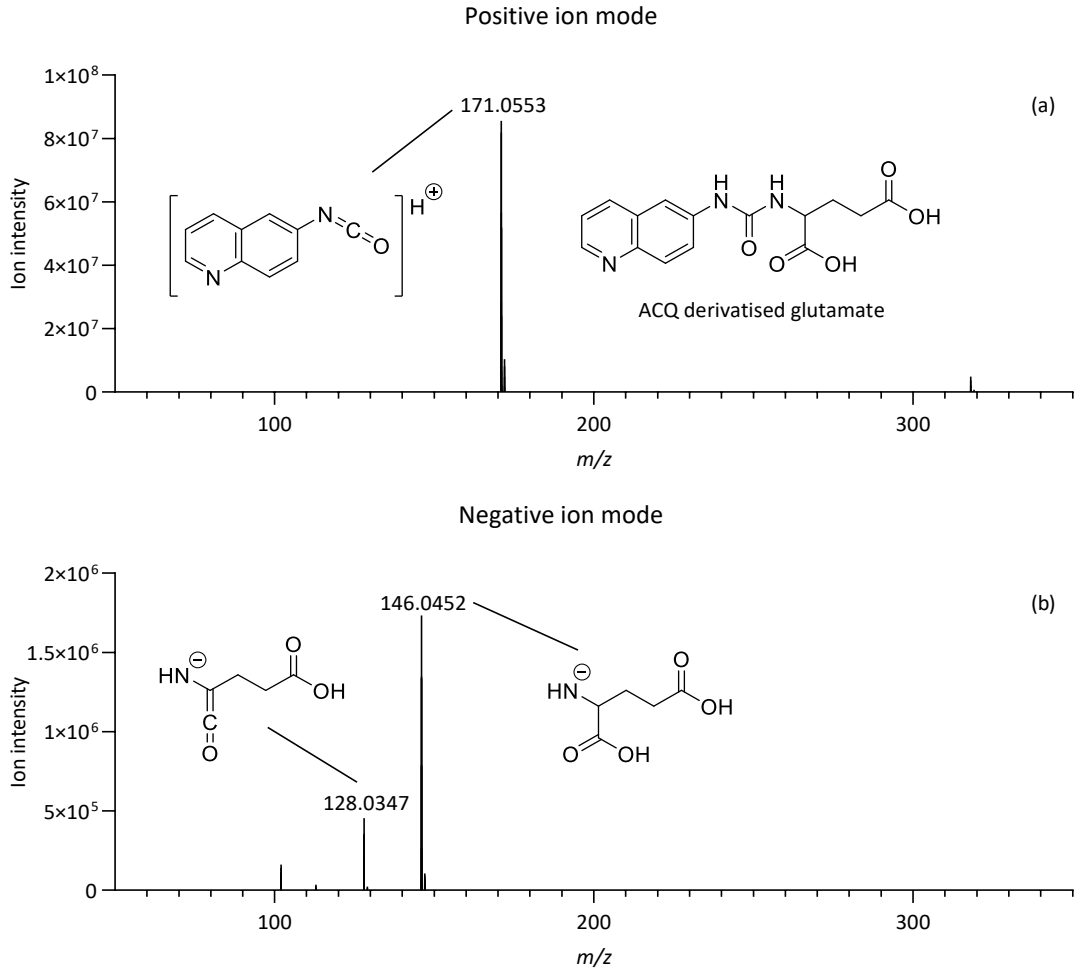

Figure 4.9: MS/MS spectra for a derivatised authentic standard of glutamate analysed by RP-MS/MS (Section 8.8), in positive (a) and negative (b) ion modes.

Negative ion mode had reduced MS/MS spectral coverage as the ion intensity, for all analytes, was lower than for positive ion mode. For example, peak area for the analysis of glutamate in negative ion mode is reduced by 68-fold, as shown in Fig. 4.10, likely caused by the reduced capacity of the derivatised analytes to hold a negative charge.

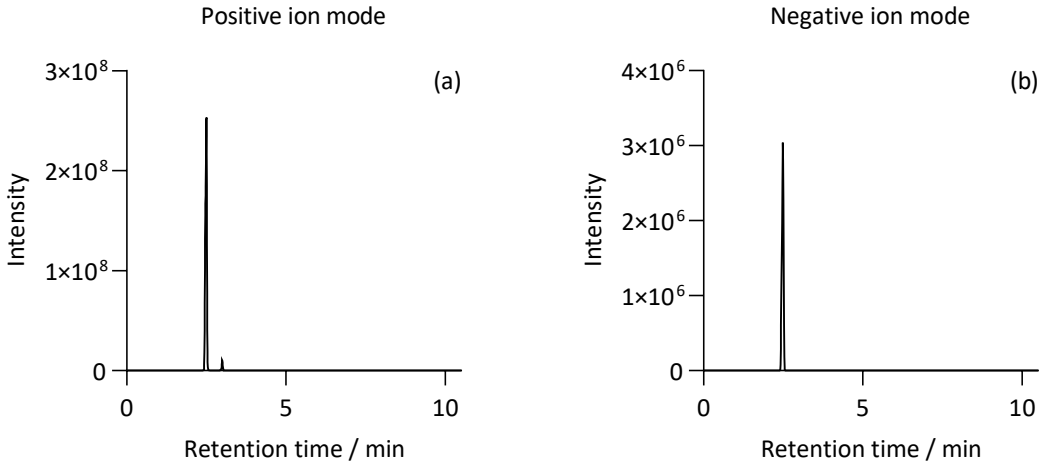

Figure 4.10: EICs for a derivatised authentic standard of glutamate analysed by RP-MS/MS (Section 8.8), in positive (a) and negative (b) ion modes.

Although the fragment ions for glutamate (Fig. 4.9) were not structurally revealing, the presence of the derivatisation reagent fragment ion was indicative of successful derivatisation and therefore by extension, the presence of 1 or more 1° and 2° amine functional group. Acquisition of fragmentation spectra for derivatised metabolites can therefore narrow down the possible identified for unknown compound-features and aid identification, in addition to accurate mass and isotope distribution data obtained from full scan acquisitions. The mass of the derivative (170.0480 Da) can be subtracted from the observed *m/z* for any analyte which had the common derivative fragment ion, to calculate the underivatised protonated *m/z* of that analyte. The corrected *m/z* in full scan mode can then be used to predict chemical formulae. For example, the ion at *m/z* 487.2083, from the analysis of a metabolite extract from 293T cells (Section 4.8), had the common derivative fragment ion in its MS/MS spectra. The original analyte therefore had original *m/z* 317.1603, with 10 possible chemical formulae (within the 5 ppm mass accuracy of the instrument), as shown in Table 4.4.

Table 4.4: Chemical formulae predicted from *m/z* 317.1603 in a 293T cell sample, derivatised and analysed by RP-MS/MS (Section 8.8).

Calculated *m/z*	*m/z* error / ppm	Double bond equivalents	Formula
317.1605	-0.6	4.5	$C_{11}H_{22}N_8OCl$
317.1600	0.9	3.5	$C_{15}H_{25}O_7$
317.1600	0.9	-1.5	$C_{11}H_{30}N_4S_2Cl$
317.1607	-1.3	-0.5	$C_8H_{25}N_6O_5S$
317.1609	-1.9	2.5	$C_{16}H_{29}O_2S_2$
317.1592	3.5	-0.5	$C_{10}H_{26}N_4O_5Cl$
317.1614	-3.5	8.5	$C_{16}H_{21}N_4O_3$
317.1592	3.5	1.5	$C_{15}H_{30}N_2Br$
317.1616	-4.1	-1.5	$C_9H_{29}N_6S_3$
317.1619	-5.0	1.5	$CH_{17}N_{16}O_4$

Accurate mass analysis was performed and the generated formulae were further narrowed using two parameters: the ion must contain the elements present in the derivative and the underivatised structure must have 1° or 2° amine functionality. Some of the predicted formulae were immediately discounted such as $CH_{17}N_{16}O_4$ which was not chemically possible and both $C_{15}H_{25}O_7$ and $C_{16}H_{29}O_2S_2$ do not have a nitrogen atom and therefore could not have been derivatised. Although all the other chemical formulae were possible, only the deprotonated forms of $C_{16}H_{21}N_4O_3$ and $C_{15}H_{30}N_2Br$ had structures listed on ChemSpider. Despite the challenges inherent in absolute identification of metabolite without an authentic standard, the ability to be able to predict that certain elements must be present and that it must contain an amine group is powerful differentiating information, for discovery-led metabolomics.

4.5. Derivatised metabolite identification using RP-IMS-MS/MS

Fragmentation spectra provide an additional benefit, beyond fingerprint similarity with an authentic standard, for the analysis of derivatised metabolomics samples. The inefficiency of precursor selection followed by fragmentation, using DDA, suffers from relatively long instrument duty cycle times and many potential precursors are inevitably missed (and

consequently no MS/MS spectra are recorded for these). IMS, as discussed in Section 1.7, separates ions based on their collisional cross section and, as an orthogonal parameter to *m/z*, can provide additional information to aid metabolite identification, as well as separate structural isomers. IMS provides an additional level of molecular specificity, as each precursor ion has a drift time associated with it, prior to MS/MS. IMS-MS/MS was used to investigate the extent of derivatisation in cell extracts and provide greater depth of MS/MS coverage in complex samples. Advances in IMS-MS/MS techniques and instrumentation have enabled the collection of both IMS and MS/MS data whilst hyphenated to LC.[151, 209] The drift time of product ions are the same as their precursor ion, when the ion-mobility cell is placed before the quadrupole, as is the case for the Vion IMS QTof used in these studies (schematic shown in Fig. 4.11). IMS-MS/MS therefore allows MS/MS spectra to be collected for all ions, dramatically increasing MS/MS coverage, with improved specificity compared to DDA fragmentation. The unique drift time for each precursor can be linked directly to its product ions, and alternating between MS and MS/MS scans in DIA mode significantly improves MS/MS coverage of precursors, compared to DDA.

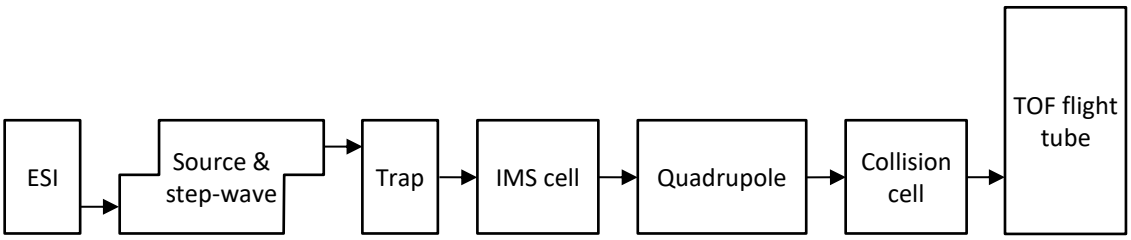

Figure 4.11: Schematic of a Vion IMS QTof.

An identification parameter is only beneficial if it provides precise and reproducible values. In order to assess the reproducibility of drift times and hence calculate CCS for individual compound-features, a mix containing 16 authentic metabolite standards (with

1° and 2° amine functional groups, listed in Table 4.1), was derivatised and analysed by RP-IMS-MS/MS, as described in Section 8.8, over a 3 month period. The CCS values obtained for 40 injections of these amino acids are shown in Fig. 4.12.

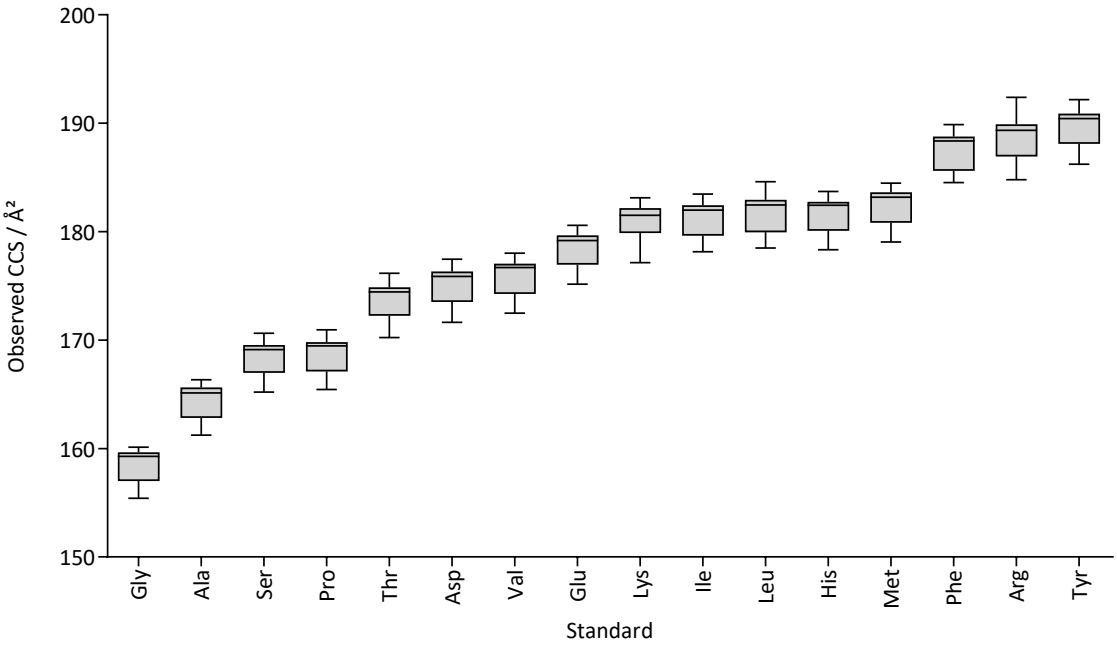

Figure 4.12: Reproducibility in CCS for a derivatised mix of authentic amine metabolite standards analysed over 3 months, by RP-IMS-MS/MS (Section 8.8, n=40).

Most authentic metabolite standards had a maximum error within 3 % and a standard error less than 0.3 Å²; this variation was principally due to differences in CCS calibration over the 3 months, as the intra-sequence error was less than 1 % for the authentic metabolite standards analysed in-between instrument calibrations. The maximum variation for these samples was observed for arginine, with a standard deviation of 1.7 Å², equivalent to an error less than 5 %. Despite variation in observed CCS, the relationship between CCS and *m/z* remained the same across the ion-mobility range and therefore variation in CCS had the same effect on all measurements, consequently CCS values remained the same relative with one another. For example, the structural isomers leucine and isoleucine which differed in the position of a methyl group, despite not being

baseline mobility separated, leucine consistently had a higher observed drift time and corresponding CCS.

As well as the additional identification parameter of CCS provided by IMS, the geometry of the instrument (Fig. 4.11) enabled MS/MS spectra to be filtered corresponding to their drift time. It was therefore possible to use a DIA MS/MS approach, where all co-eluting ions were fragmented and therefore fragmentation spectra were collected for every precursor ion, without the specificity disadvantage of MS/MS spectral overlap. In IMS-MS/MS the drift times of precursor ions are used post-data acquisition to select fragment ions which have identical drift times and therefore the specificity of DDA is combined with the coverage of DIA. Fragmentation pattern is therefore available as an additional identification parameter, even for low intensity ions which would normally be below the cut-off for DDA and would be concealed by the fragment ions of more abundant ions in DIA. The confidence in spectral matching is increased compared with DDA, as only the fragment ions from a specific precursor ion were observed in their MS/MS spectra. For example, the MS/MS spectra for tryptophan in IMS-MS/MS and DIA MS/MS modes, as shown in Fig. 4.13, for the derivatised quality control (QC) sample from 293T cells (Section 8.16), analysed by RP-IMS-MS/MS (Section 8.8).

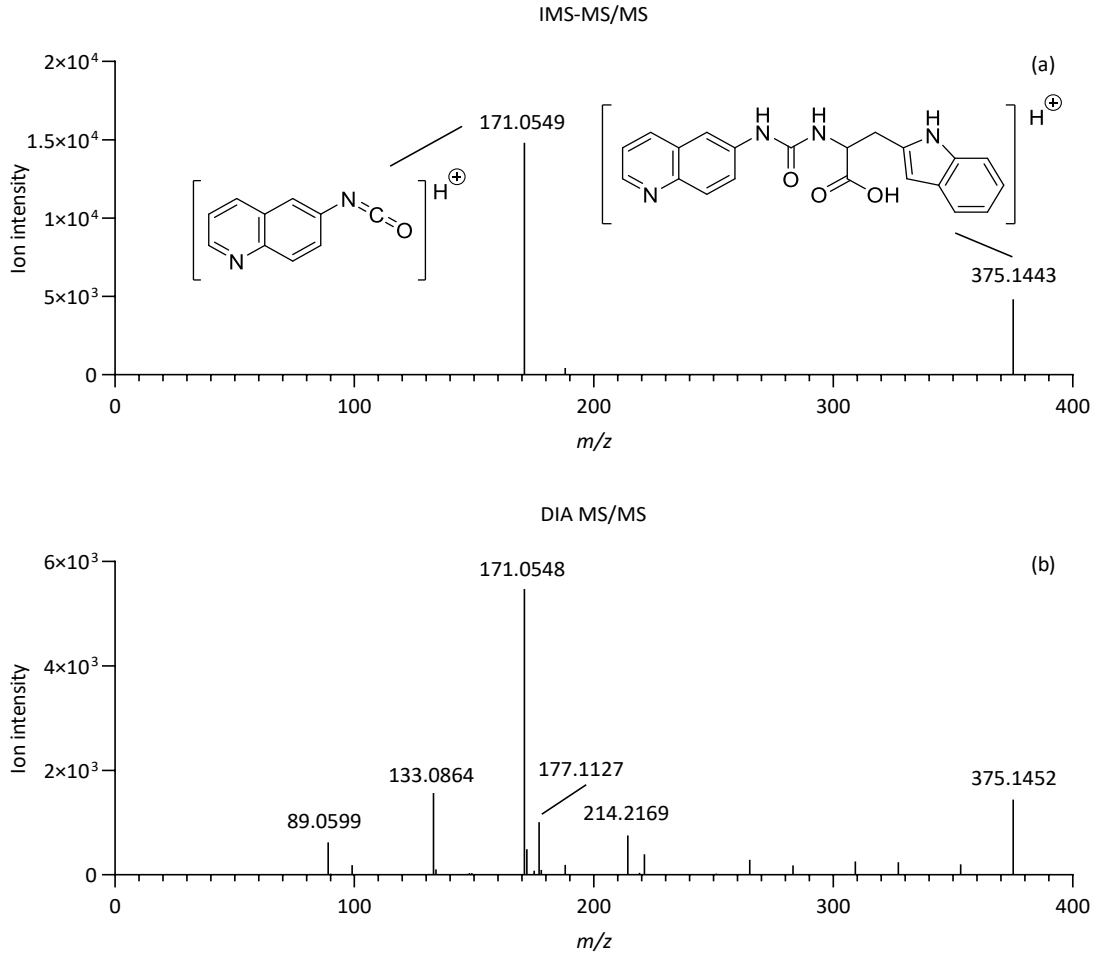

Figure 4.13: Comparison of the RP-MS/MS (Section 8.8) spectra acquired from IMS-MS/MS (a) and DIA MS/MS (b) for the fragmentation of tryptophan, from a derivatised QC sample of 293T cells (Section 8.16).

IMS-MS/MS and DIA MS/MS spectra for tryptophan both displayed the precursor ion (*m/z* 375.1143) in the same ratio with the derivative fragment ion (*m/z* 171.0549), as the collision energy was identical. The DIA MS/MS spectra (Fig. 4.13(b)) contained fragment ions from co-eluting analytes (*m/z* 89.0599, *m/z* 133.0864, *m/z* 177.1127 and *m/z* 214.2169), which would reduce the closeness-of-fit score if the acquired spectra were compared with a fragment library. Furthermore, misidentification could occur as fragment ions from more abundant species would dominate the MS/MS spectra. Filtering spectra using drift time in IMS-MS/MS also reduced interference from the matrix and

mobile phase, resulting in an increased signal to noise ratio and therefore a lower limit of detection for specific analytes.

A potential disadvantage of IMS-MS is a ca. 2-fold reduced sensitivity, compared to standard MS methods, as some ions are lost in the ion-mobility cell by collision with the drift gas. This compromise is, to some extent, offset by the increased signal to noise ratio of ion signals, as a result of drift time filtering. Consequently LLoD and LLoQ are reduced, compared with the use of MS/MS without IMS, on the same instrument, for the majority of the derivatised metabolites listed in Table 4.5.

Table 4.5: Comparison of LLoD, LLoQ and R^2 for the calibration curves of derivatised amine metabolites, analysed by RP-MS/MS (Section 8.8) in IMS-MS/MS and DIA MS/MS modes.

	IMS-MS/MS			**DIA MS/MS**		
Compound	**LLoD / μM**	**LLoQ / μM**	**R^2**	**LLoD / μM**	**LLoQ / μM**	**R^2**
Alanine	1.18	3.58	0.9956	2.01	6.08	0.9873
Arginine	1.00	3.03	0.9968	1.32	4.00	0.9945
Aspartate	0.82	2.48	0.9979	2.16	6.54	0.9854
Glutamate	0.70	2.13	0.9984	0.63	1.91	0.9987
Glycine	1.24	3.76	0.9951	4.27	12.94	0.9450
Histidine	0.63	1.92	0.9987	1.27	3.86	0.9949
Isoleucine	1.49	4.53	0.9959	3.39	10.28	0.9646
Leucine	0.67	2.03	0.9986	3.46	10.48	0.9633
Methionine	1.02	3.10	0.9967	2.91	8.82	0.9737
Phenylalanine	1.27	3.86	0.9959	3.80	11.51	0.9560
Proline	1.12	3.39	0.9960	2.36	7.15	0.9826
Serine	0.76	2.31	0.9982	0.86	2.60	0.9977
Threonine	0.95	2.88	0.9971	1.19	3.61	0.9955
Tyrosine	0.66	2.01	0.9986	2.33	7.05	0.9831
Valine	1.15	3.50	0.9502	2.83	8.57	0.9751

The R^2 values were higher in IMS-MS/MS mode with the exception of glutamate which also had a higher LLoD and LLoQ. If a lower LLoQ was required, samples could be analysed by MS only mode, as described in Section 4.3. The increased coverage and reduced signal to noise ratio consequently resulted in lower R^2 values compared with MS only

mode (Table 4.2), likely due to the reduced number of MS scans across the chromatographic peak.

In summary, the benefits of IMS for metabolomics, including drift time filtering of ions and the acquisition of CCS data were explored using authentic metabolite standards and cell extracts. Highly reproducible analysis of authentic metabolite standards was demonstrated, which increased confidence in metabolite identification and quantification, using fragmentation pattern matching and CCS as an orthogonal identification parameter. Drift time separation of ions reduced background noise in the acquired spectra and led to reduced LLoD and LLoQ for IMS-MS/MS compared with MS/MS mode. As MS/MS spectra were acquired for all-ions, and the fragment ions were assigned to their precursor using drift time separation, the coverage of derivatisation could be confirmed by spectral searching for the common derivative fragment in each sample. In untargeted analysis, the confirmation of derivatisation and chemical specificity provided by RP-IMS-MS/MS enabled accurate prediction of chemical formulae.

4.6. IMS-MS/MS analysis of derivatised 1° and 2° amines in biological samples

To explore metabolite coverage of RP-IMS-MS/MS, a 293T cell extract (a QC sample from the experiment described in Section 8.17) was derivatised and analysed by RP-IMS-MS/MS, as described in Section 8.8. The CCS values for the most abundant $1x10^4$ ions were plotted against their *m/z* value (Fig. 4.14, red dots). The IMS-MS/MS spectra were searched for the presence of the common derivative fragment ion (*m/z* 171.0553) and these ions were overlaid on the graph (denoted with orange dots).

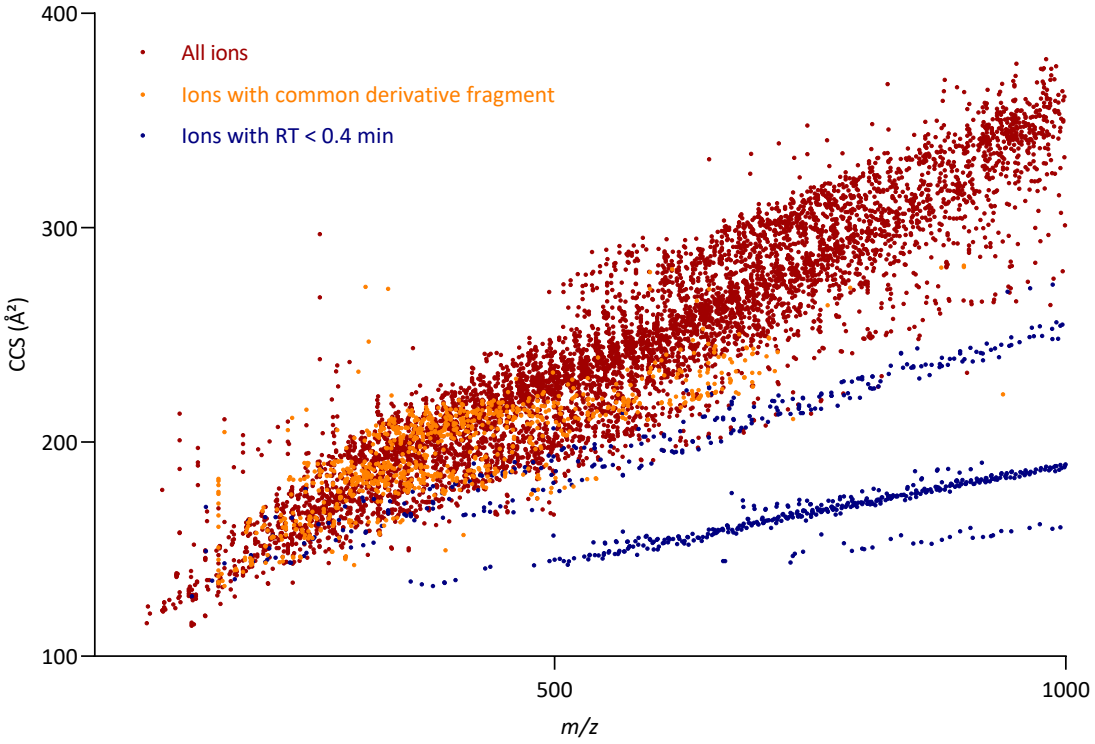

Figure 4.14: Graph showing the relationship between collisional cross section and m/z for the $1x10^4$ most intense ions from RP-IMS-MS/MS (Section 8.8) analysis of a derivatised QC sample from 293T cells (Section 8.17).

Evidence of derivatisation was provided for metabolites up to *m/z* 938.7571 and distinct clustering of analytes with similar CCS and *m/z* values was observed. The low mass analytes largely corresponded to metabolites with amine functionality associated with primary metabolism, including amino acids and their degradation products. The high mass derivatised species were consistent with secondary metabolism products formed by synthases, and may even have been short peptides used in protein synthesis. In this example, 1260 ions showed evidence of derivatisation, from the presence of the common derivative fragment ion, in their MS/MS spectra. The number of possible chemical formula predicted from each *m/z* value, as discussed in Section 4.4 was therefore reduced. For example, the compound-feature 7.25_288.1342, identified from PLS-DA analysis of a derivatised metabolite extract from 293T cells (Section 8.16) analysed by RP-IMS-MS/MS (Section 8.8), had the common derivative fragment ion in its MS/MS

spectrum. Its underivatised *m/z* was therefore 118.0862 which could only correspond to a protonated amine with the formula $C_5H_{12}NO_2$, within a 5 ppm mass window (based on the instrument mass accuracy). HMDB was searched with formula $C_5H_{11}NO_2$ and possible metabolites are listed in Table 4.6.

Table 4.6: Compounds in HMDB with the chemical formula $C_5H_{11}NO_2$.

HMDB code	**Compound name**
HMDB0000043	Betaine
HMDB0000883	L-valine
HMDB0001382	Vaporole
HMDB0002141	N-methyl-α-aminoisobutyrate
HMDB0003355	5-aminopentanoate
HMDB0013716	Norvaline
HMDB0015550	Amyl nitrite

From these possible metabolites, it was therefore possible to exclude any structures which did not contain 1° and 2° amines leaving only norvaline, N-methyl-α-aminoisobutyrate, 5-aminopentanoate and valine, as the ion had common derivative fragment in MS/MS spectrum.

A second trend was also observed in Fig. 4.14 (denoted with blue dots), a shallow relationship between CCS and *m/z*, corresponding to species with smaller CCS values than other metabolites in the sample, with the same *m/z* value. These compound-features had a RT of less than 0.4 min and were therefore likely to be polar or ionic metabolites which did not interact strongly with the C18 stationary phase, without an amine group that could be derivatised. The polar or ionic metabolites therefore eluted with or close to the solvent front and accounted for less than 10 % of the total compound-features (792). This information could be used to direct further investigation of those specific compound-features, using a more polar stationary phase or an alternative approach such as IC-MS.

Spectral searching for the common derivative fragment ion was performed and over 10 % of analytes in the sample showed evidence of derivatisation. The common derivative fragment was characteristic and identified from IMS-MS/MS data using a post-acquisition processing method. As the mass of the derivative was known and constant, any analytes with the common derivative fragment in their MS/MS spectrum had their *m/z* corrected by subtraction of the mass of the derivative. This corrected mass ion list could be processed using the untargeted workflow (Section 8.11) and was subsequently used in Section 4.8.

4.7. Derivatised RP-IMS-MS/MS sensitivity compared with HILIC-IMS-MS/MS

Most applications of untargeted metabolomics use HILIC-MS/MS for the analysis of polar metabolites.[106, 116, 117] HILIC-MS/MS has relatively poor RT stability, as demonstrated in Section 2.5, and therefore confidence in metabolite identification is reduced, compared to RP-IMS-MS/MS and IC-MS/MS. The high percentage of organic solvent required in the injection solvent for HILIC is also not optimal for the extraction of polar and ionic metabolites from biological materials and either requires further sample preparation, by either partial evaporation of the aqueous extraction solvent or dilution with organic solvent. These steps can introduce additional variability to the analysis and reduce precision, as well as increase sample preparation time.

In order to investigate relative performance, HILIC was hyphenated to the sample mass spectrometer used for derivatised RP-IMS-MS/MS analyses. The lack of sensitivity compared with derivatised RP-IMS-MS/MS (as discussed in Section 4.2) is exemplified here by the analysis of the isobaric metabolites leucine and isoleucine. The mix of authentic amine metabolite standards (Table 4.1), at a concentration of 25 μM, was

analysed by HILIC-IMS-MS/MS (Section 8.6) and derivatised RP-IMS-MS/MS (Section 8.8). Leucine and isoleucine were not chromatographically separated by HILIC-IMS-MS/MS, as shown in Fig. 4.15, and had a combined abundance of 343. Derivatised RP-IMS-MS/MS analysis of the sample provided an abundance of 4.66×10^4 for isoleucine, which was baseline separated from leucine. As the samples were analysed using the same volume of sample loaded onto the column and identical ESI conditions and MS/MS parameters, derivatisation increased sensitivity by over 250-fold.

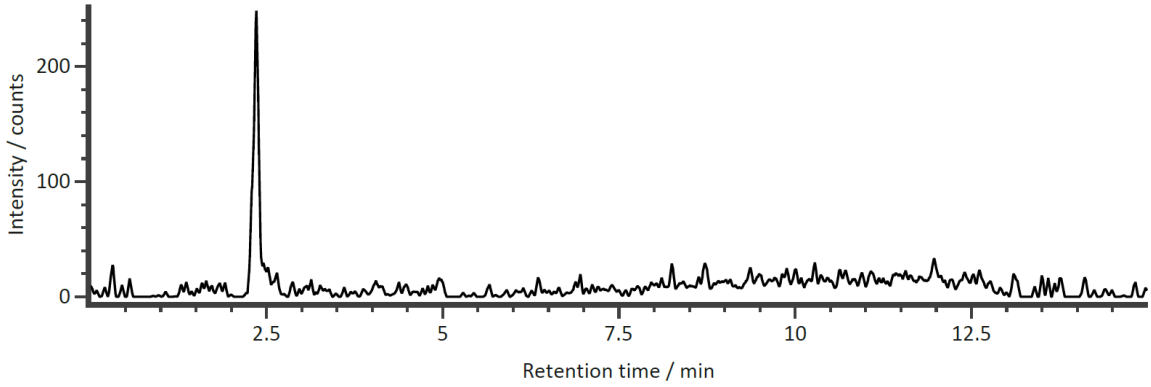

Figure 4.15: Extracted ion chromatogram for *m/z* 132.1024, corresponding to the metabolites isoleucine and leucine in a mixed amino acid authentic standard analysed by HILIC-IMS-MS/MS in positive ion mode (Section 8.6).

In addition to chromatographic separation of the isomers by derivatised RP-IMS-MS/MS, drift times for each isomer were obtained, as shown in Fig. 4.16. A consistently higher drift time and therefore larger CCS value was observed for leucine, due to the position of the methyl branch on $C_{(4)}$, one position further to the end of the carbon chain compared to isoleucine ($C_{(3)}$). The difference in CCS values observed for the two isomers was only 0.6 Å² and therefore within experimental error for the method; however, the CCS values could still be used to provide additional confidence in identification when the isomers are compared. The latent benefits of reduced spectral noise and the assignment of fragment ions to their precursor using drift time, further reduce the likelihood of false identification. As leucine and isoleucine were not chromatographically separated by HILIC,

the drift time was not as beneficial for identification, as the two co-eluting isomers were not separated in 3 dimensional space (RT, *m/z* and CCS). Leucine and isoleucine were therefore observed as a broadened peak in the ion mobiligram (Fig. 4.16(b)), compared with the analysis of either species in isolation. The peak shape as shown in Fig. 4.16(b) was not optimal, as a consequence of the low ion intensity for the species when analysed by HILIC-IMS-MS/MS. Despite poor peak shape, the observed CCS value of 126.6 Å² was within the experimental error compared with the CCS compendium value of 127.6 Å².[152] The observed drift times for leucine and isoleucine were different between the two methods, as the CCS was increased by derivatisation of the analytes. This increase in drift time was beneficial for analysis using the derivatised method as the larger drift time resulted in increased separation between the isomers. As percentage error in measurements were consistent across the CCS range, confidence in identification at lower CCS values, commonly observed for metabolites, was increased compared to HILIC-IMS-MS/MS.

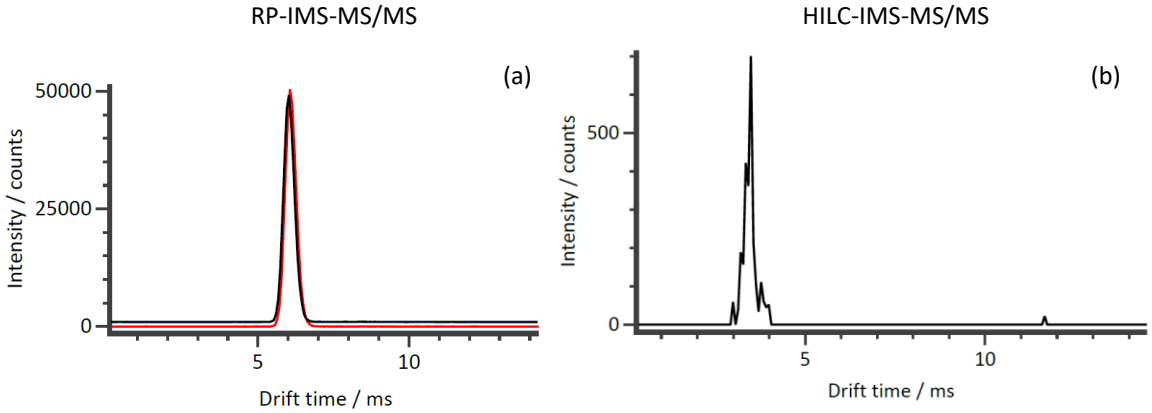

Figure 4.16: Ion mobiligrams corresponding to the metabolites isoleucine and leucine analysed in a mixed amino acid authentic standard in positive ion mode. Samples were analysed by derivatised RP-IMS-MS/MS (a, Section 8.8) and HILIC-IMS-MS/MS (b, Section 8.6).

Hyphenation of HILIC to IMS-MS/MS was beneficial for the analysis of underivatised isobaric species for example, nucleotides as discussed in Section 2.5. The adenine nucleotides (AMP, ADP and ATP) co-eluted with the exception of cyclic AMP using HILIC;

however, their ions could be separated by IMS drift time. Individual authentic metabolite standards, at a concentration of 10 μM, were analysed by HILIC-IMS-MS/MS (Section 8.6) and their ion mobiligrams shown in Fig. 4.17.

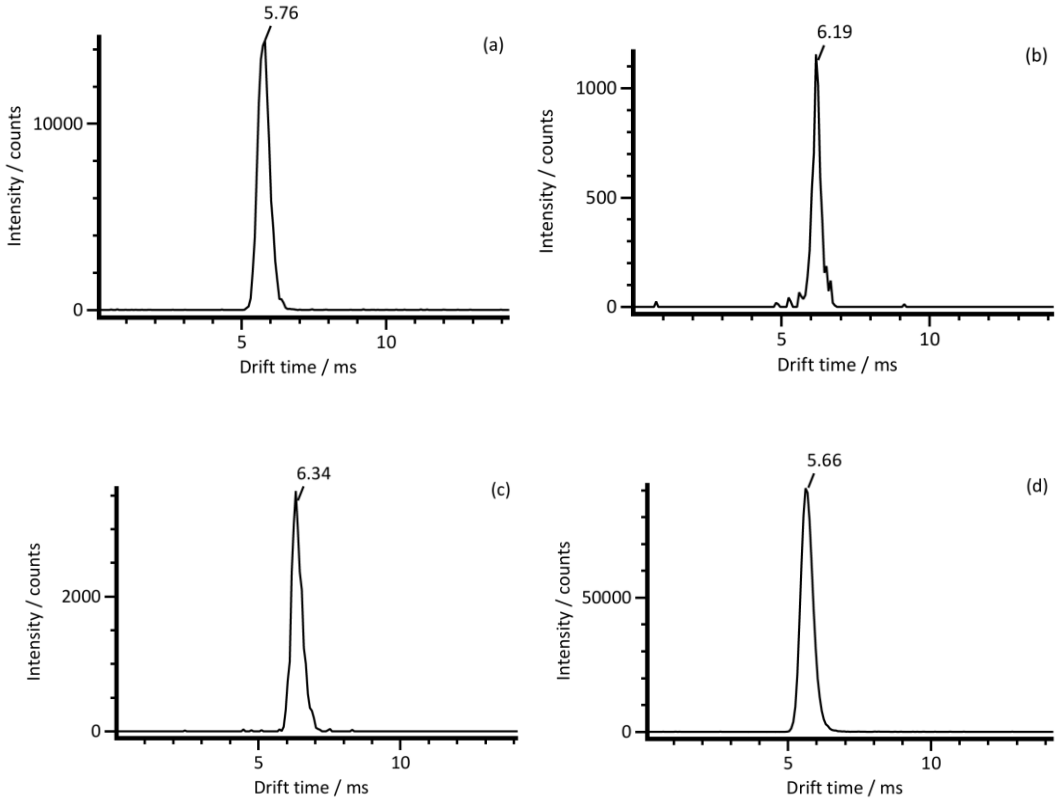

Figure 4.17: Ion mobiligrams for authentic standards of adenosine mono- (a), di- (b) and tri- (c) phosphates as well as cyclic AMP (d) analysed by HILIC-IMS-MS/MS (Section 8.6).

The mono-, di- and triphosphorylated nucleotides had observed CCS values of 175.60 Å², 182.50 Å² and 189.51 Å² respectively which matched, within experimental error, with values from the CCS compendium (174.1 Å², 184.3 Å² and 188.3 Å²).[152] The nucleotides could therefore be more accurately quantified, as any dephosphorylation after the ion-mobility cell would have resulted in a drift time higher than expected for the observed *m/z* value and could therefore be excluded from peak integration and quantification.

As discussed in Section 4.3, IMS-MS/MS analysis of authentic metabolite standards reduced spectral noise and improved quantification, independent of the LC method used. Analysis of metabolites with amine functional groups by derivatised RP-IMS-MS/MS (Section 8.8) was further demonstrated to be more sensitive than HILIC-IMS-MS/MS in IMS-MS/MS mode and drift time separation provided increased quantification accuracy. Co-eluting species such as the adenosine phosphates and their degradation products were separated using drift time and therefore any isobaric in-source fragmentation products could be excluded. Drift time separation increased confidence in relative quantification for untargeted analysis as well as providing an orthogonal parameter for metabolite identification.

4.8. Untargeted RP-IMS-MS/MS analysis of 293T wild-type embryonic kidney cells to investigate the metabolic effects of glucose concentration

To demonstrate the use of derivatised RP-IMS-MS/MS in the context of a discovery-led metabolomics workflow, 293T WT cells were analysed to investigate the metabolic effects of glucose concentration on cell metabolism. 293T WT cells were cultured in 1.0 g / L or 4.5 g / L glucose DMEM, with 9 biological replicates in each experimental group (Section 8.17). Metabolites were extracted from the cell lysate, derivatised and analysed by RP-IMS-MS/MS, as described in Section 8.8. The raw data were aligned and peak-picked using Progenesis QI and a peak abundance table comparing the abundances of 4392 compound-features, for the two glucose conditions, were processed using MetaboAnalyst as described in Section 8.11.[166] The data associated with this experiment has been deposited in the Oxford University Research Archive (title: Metabolomics of 293T wild-type cells cultured under different glucose conditions) and is freely

accessible (https://doi.org/10.5287/bodleian:aqEPAVew8). The PCA scores plot of compound-feature abundances, for the derivatised RP-IMS-MS/MS data (Fig. 4.18), showed no outliers and distinct separation between the experimental groups. Samples clustered within their experimental groups and both groups were significantly separated in principal component space.

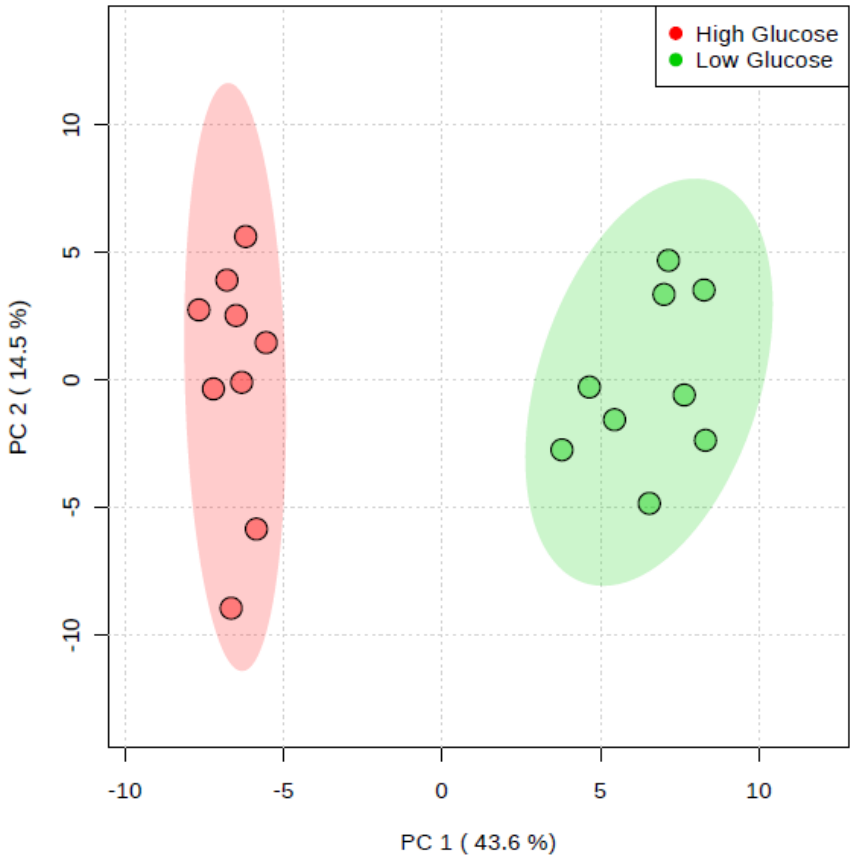

Figure 4.18: PCA scores plot of compound-feature abundances for the analysis of 293T WT cells cultured under 1.0 g / L or 4.5 g / L glucose conditions (Section 8.17), derivatised and analysed by RP-IMS-MS/MS (Section 8.8). Statistical analysis was performed using MetaboAnalyst with normalisation by sum and Pareto scaling (Section 8.11). Shaded areas represent the 95 % confidence interval for each experimental group.

4.8.1. Univariate statistical analysis of 293T wild-type embryonic kidney cells analysed by untargeted RP-IMS-MS/MS

Univariate statistical analysis was performed to identify compound-features which were significantly altered in abundance for cells cultured under 1.0 g / L or 4.5 g / L glucose

conditions, t-tests were performed for each compound-feature and a FC calculated. The compound-features which influenced the separation between experimental groups, with a FC greater than 1.5 and FDR-adjusted t-test p-value less than 0.05 are shown in Fig. 4.19, using log-transformed values.

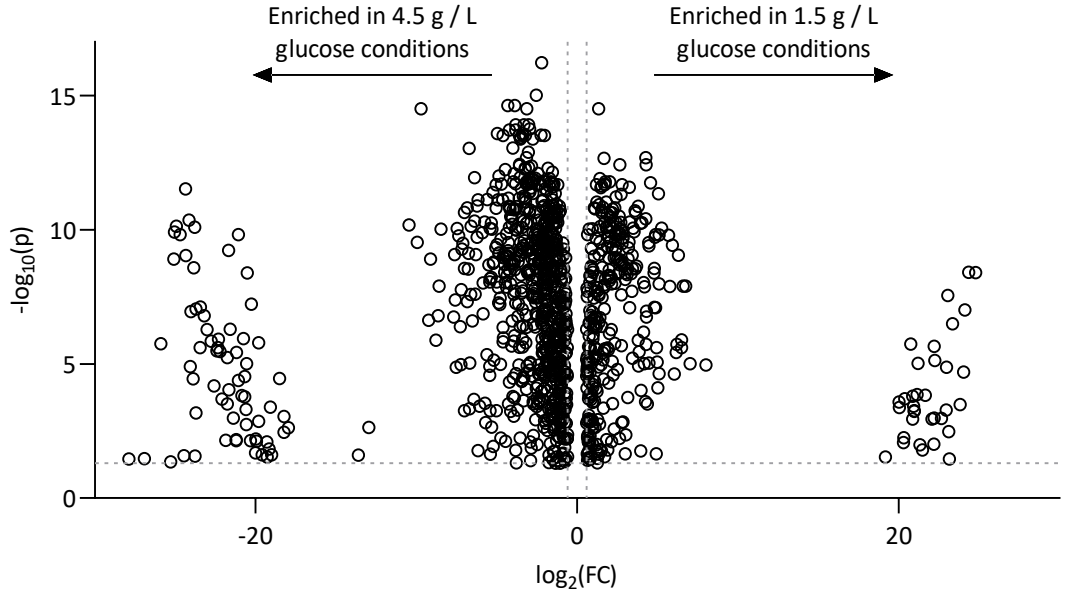

Figure 4.19: Volcano plot showing the compound-features with a FC greater than 1.5 and FDR-adjusted t-test p-value less than 0.05, from univariate statistical analysis of 293T WT cells cultured under 1.0 g / L or 4.5 g / L glucose conditions (Section 8.17), derivatised and analysed by RP-IMS-MS/MS (Section 8.8).

There were 1127 compound-features (of 4392) which had both a FC greater than 1.5 and an FDR-adjusted t-test p-value less than 0.05 and therefore the data required filtering to reduce the number of compound-features for investigation. The outermost points on the left and right of the graph (± 20 log_2(FC)) corresponded to compound-features with a FC greater than $1x10^6$-fold. Positive log_2(FC) values were enriched in 1.5 g / L glucose conditions and negative values were enriched in 4.5 g / L glucose conditions. Table 4.7 shows the top 35 compound-features which contributed to the separation between experimental groups, ranked by their position from the origin in the volcano plot (Fig. 4.19).

Table 4.7: Top 35 compound-features identified in the volcano plot (Fig. 4.19) from univariate statistical analysis of 293T WT cells cultured under 1.0 g / L or 4.5 g / L glucose conditions (Section 8.17), derivatised and analysed by RP-IMS-MS/MS (Section 8.8).

Compound-feature	FC	log_2(FC)	p-value	-log_{10}(p)	Enriched group
1.74_171.0549	4.63	-2.21	5.89E-17	16.23	1.0 g / L glucose
1.76_171.1746	5.78	-2.53	9.75E-16	15.01	1.0 g / L glucose
1.76_171.3014	14.82	-3.89	2.32E-15	14.63	1.0 g / L glucose
0.37_789.8009	19.93	-4.32	2.32E-15	14.63	1.0 g / L glucose
0.38_742.9444	2.53	1.34	3.07E-15	14.51	4.5 g / L glucose
1.75_171.2524	8.80	-3.14	3.07E-15	14.51	1.0 g / L glucose
0.38_557.9319	841.31	-9.72	3.07E-15	14.51	1.0 g / L glucose
4.39_320.1131	8.04	-3.01	1.23E-14	13.91	1.0 g / L glucose
0.37_590.8544	9.96	-3.32	1.23E-14	13.91	1.0 g / L glucose
0.38_724.8835	14.19	-3.83	1.23E-14	13.91	1.0 g / L glucose
0.38_790.8736	7.71	-2.95	1.78E-14	13.75	1.0 g / L glucose
0.38_586.9113	14.16	-3.82	1.89E-14	13.72	1.0 g / L glucose
0.37_722.8129	18.61	-4.22	1.89E-14	13.72	1.0 g / L glucose
6.46_237.0999	10.49	-3.39	2.57E-14	13.59	1.0 g / L glucose
7.25_289.3366	31.01	-4.95	2.57E-14	13.59	1.0 g / L glucose
1.77_188.2070	4.75	-2.25	2.95E-14	13.53	1.0 g / L glucose
3.44_345.1670	9.26	-3.21	2.95E-14	13.53	1.0 g / L glucose
0.38_548.8268	12.10	-3.60	2.95E-14	13.53	1.0 g / L glucose
1.79_188.0815	4.07	-2.02	3.07E-14	13.51	1.0 g / L glucose
0.38_792.8711	10.32	-3.37	3.07E-14	13.51	1.0 g / L glucose
0.38_480.8397	24.25	-4.60	3.07E-14	13.51	1.0 g / L glucose
0.38_640.8716	11.36	-3.51	3.66E-14	13.44	1.0 g / L glucose
0.37_750.7922	6.80	-2.77	4.12E-14	13.39	1.0 g / L glucose
6.46_473.1925	11.55	-3.53	4.12E-14	13.39	1.0 g / L glucose
0.38_775.8473	15.94	-3.99	9.10E-14	13.04	1.0 g / L glucose
3.44_173.0875	105.48	-6.72	9.23E-14	13.04	1.0 g / L glucose
7.13_320.1062	8.21	-3.04	1.29E-13	12.89	1.0 g / L glucose
6.24_389.1804	19.29	4.27	2.06E-13	12.69	4.5 g / L glucose
0.37_614.8172	8.84	-3.14	2.08E-13	12.68	1.0 g / L glucose
0.37_736.8567	3.17	1.66	2.17E-13	12.66	4.5 g / L glucose
0.38_654.8986	11.95	-3.58	3.70E-13	12.43	1.0 g / L glucose
0.38_675.4577	6.28	2.65	3.76E-13	12.43	4.5 g / L glucose
7.29_443.2180	19.59	4.29	3.76E-13	12.43	4.5 g / L glucose
4.39_318.3776	12.02	-3.59	4.05E-13	12.39	1.0 g / L glucose
0.37_888.7646	7.09	-2.83	4.25E-13	12.37	1.0 g / L glucose

Of the top 35 compound-features, 19 were within the void time of the column (< 0.4 min) and 5 were close to the *m/z* of the derivative fragment ion (171.0553) and were therefore not metabolites of interest. Of the top 35 compound-features only 11 were potential

metabolites when searched against HMDB and of these, the compound-features 1.77_188.2070, 1.79_188.0815, 4.39_318.3776 and 6.24_389.1804 had the common derivative fragment ion in their MS/MS spectra. The smallest *m/z* value which may be of biological interest and could be derivatised is theoretically an ammonium ion and therefore compound-features could be filtered out using an *m/*z cut-off at 188.0815. Chromatographic information could also be used to reduce the number of compound-features of interest, by only analysing compound-features which were retained by the column and therefore had a RT between 0.40-9.04 min. Using both criteria, the number of compound-features was reduced from 1127 to 460. The top 35 compound-features in the filtered dataset from the volcano plot (Fig. 4.19), are shown in Table 4.8.

Table 4.8: Top 35 compound-features, filtered by RT and *m/z*, identified in the volcano plot (Fig. 4.19) from univariate statistical analysis of the filtered dataset for 293T WT cells cultured under 1.0 g / L or 4.5 g / L glucose conditions (Section 8.17), derivatised and analysed by RP-IMS-MS/MS (Section 8.8).

Compound-feature	FC	$\log_2$(FC)	p-value	-$\log_{10}$(p)	Enriched group	Common derivative fragment
4.39_320.1131	7.90	-2.98	7.36E-14	13.13	1.0 g / L glucose	Not observed
7.25_289.3366	30.45	-4.93	8.19E-14	13.09	1.0 g / L glucose	Not observed
6.46_237.0999	10.32	-3.37	8.19E-14	13.09	1.0 g / L glucose	Not observed
3.44_345.1670	9.11	-3.19	8.19E-14	13.09	1.0 g / L glucose	Observed
1.77_188.2070	4.67	-2.22	8.19E-14	13.09	1.0 g / L glucose	Not observed
1.79_188.0815	4.00	-2.00	8.19E-14	13.09	1.0 g / L glucose	Observed
6.46_473.1925	11.35	-3.51	1.19E-13	12.93	1.0 g / L glucose	Not observed
7.13_320.1062	8.07	-3.01	2.01E-13	12.70	1.0 g / L glucose	Observed
6.24_389.1804	19.63	4.30	4.99E-13	12.30	4.5 g / L glucose	Observed
4.39_318.3776	11.81	-3.56	6.35E-13	12.20	1.0 g / L glucose	Observed
4.92_300.0972	9.20	-3.20	9.86E-13	12.01	1.0 g / L glucose	Observed
7.29_443.2180	19.95	4.32	1.32E-12	11.88	4.5 g / L glucose	Not observed
8.09_302.1499	2.85	-1.51	1.32E-12	11.88	1.0 g / L glucose	Observed
7.12_320.2687	28.75	-4.85	1.50E-12	11.82	1.0 g / L glucose	Observed
4.39_318.4438	11.52	-3.53	1.50E-12	11.82	1.0 g / L glucose	Not observed
3.17_292.1279	5.35	-2.42	1.50E-12	11.82	1.0 g / L glucose	Not observed
4.39_318.1081	7.58	-2.92	2.07E-12	11.68	1.0 g / L glucose	Observed
6.39_274.1178	3.92	-1.97	2.42E-12	11.62	1.0 g / L glucose	Observed
1.77_188.2887	5.92	-2.57	2.74E-12	11.56	1.0 g / L glucose	Observed
8.08_302.4771	4.25	-2.09	2.82E-12	11.55	1.0 g / L glucose	Observed
8.29_375.1446	2.83	-1.50	2.84E-12	11.55	1.0 g / L glucose	Observed
7.99_346.1130	5.29	-2.40	4.10E-12	11.39	1.0 g / L glucose	Not observed
6.96_352.1291	2.68	-1.42	4.20E-12	11.38	1.0 g / L glucose	Observed
8.00_302.1499	2.76	-1.47	4.76E-12	11.32	1.0 g / L glucose	Observed
5.16_216.1125	3.28	-1.72	5.52E-12	11.26	1.0 g / L glucose	Not observed
4.39_340.0894	7.50	-2.91	6.59E-12	11.18	1.0 g / L glucose	Not observed
7.11_320.4434	2.1E+07	-24.34	6.68E-12	11.18	1.0 g / L glucose	Not observed
8.00_302.4771	3.65	-1.87	7.71E-12	11.11	1.0 g / L glucose	Not observed
4.39_318.2697	9.36	-3.23	1.25E-11	10.90	1.0 g / L glucose	Observed
6.02_333.1307	9.15	-3.19	1.29E-11	10.89	1.0 g / L glucose	Not observed
0.49_198.0361	71.18	-6.15	1.33E-11	10.88	1.0 g / L glucose	Not observed
8.08_302.2510	19.16	-4.26	1.33E-11	10.88	1.0 g / L glucose	Observed
7.26_288.2873	4.21	-2.07	1.43E-11	10.84	1.0 g / L glucose	Observed
4.38_245.0913	2.51	-1.33	1.47E-11	10.83	1.0 g / L glucose	Not observed
8.08_302.6409	9.11	-3.19	2.36E-11	10.63	1.0 g / L glucose	Observed

The filtered dataset was examined and potentially relevant compound-features putatively identified (level 2) using HMDB. Of the top 35 compound-features, the common derivative fragment was observed in the MS/MS spectra of 19 compound-features as shown in Table 4.8. Putative identifications were made, based on corrected *m/z* and isotope pattern, as described in Section 4.4. The most important compound-feature which had the common derivative fragment (3.44_345.1670) was putatively identified (level 3) as arginine. The compound-features 1.79_188.0815 and 4.39_318.1081 were putatively identified (level 2) as ammonium and glutamate respectively.

4.8.2. Multivariate statistical analysis of 293T wild type embryonic kidney cells analysed by untargeted RP-IMS-MS/MS

Multivariate statistical analysis of the data was performed to identify compound-features which contributed to the metabolic differences between the two glucose conditions. Data were also filtered before processing using MetaboAnalyst to improve regression models and to speed up the identification of potential biomarkers. Of the 4392 compound-features characterised by data processing using Progenesis QI, from derivatised RP-IMS-MS/MS analysis of 293T WT cells. The number of compound-features eluting before 0.4 min was 757 (primarily with RT between 0.36-0.39 min) and the first compound-feature with the common derivatisation fragment eluted at 0.43 min. Ions which eluted in the column wash were also excluded, as they would not be well characterised by the method. The wash started at 8.64 min and column dwell time was 0.40 min, therefore any analyte eluting after 9.04 min was excluded from the dataset (507 compound-features). The common derivative fragment ion was present in

the MS/MS spectra of 139 of the excluded compound-features and therefore a longer gradient could be investigated if characterisation of less polar amines was of specific interest. The remaining compound-features were filtered using an *m/z* cut-off of 188.0815, therefore leaving 2945 compound-features which were processed using MetaboAnalyst, as described in Section 8.11. PLS-DA was used, as described in Section 3.3, to model the data and calculate VIP scores. The top 35 (of 2692) compound-features from PLS-DA analysis of 293T WT cells cultured under 1.0 g / L or 4.5 g / L glucose conditions are shown in Fig. 4.20.

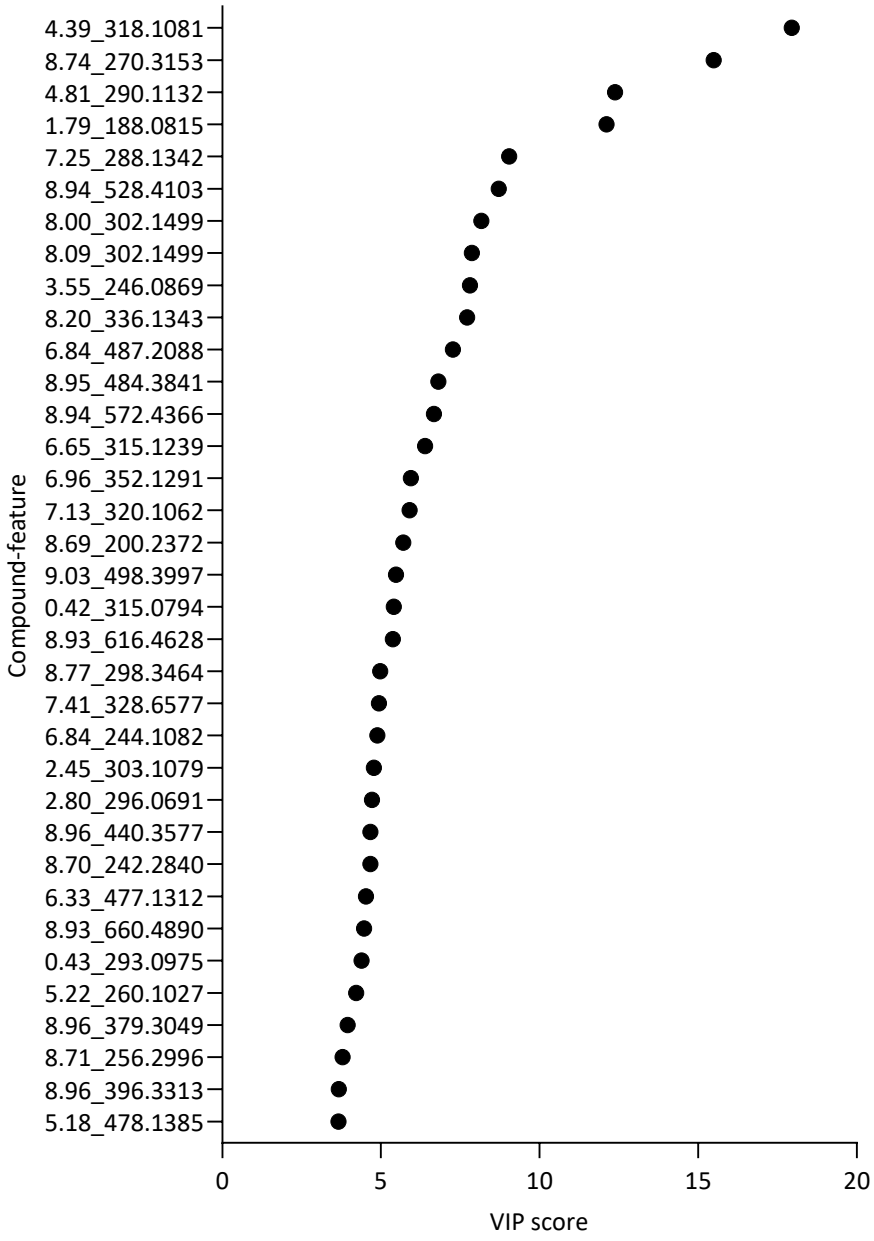

Figure 4.20: Plot showing the top 35 most important compound-features identified from PLS-DA analysis of 293T WT cells cultured under 1.0 g / L or 4.5 g / L glucose conditions (Section 8.17), derivatised and analysed by RP-IMS-MS/MS (Section 8.8).

Of the top 35 most important compound-features ranked by PLS-DA VIP score, 17 compound-features were enriched for cells cultured in 4.5 g / L glucose conditions. The top 10 compound-features were more abundant in 1.0 g / L glucose conditions with the exception of 8.74_270.3153 and 8.94_528.4103. Analysis the fragmentation spectra of these top 10 compound-features, showed the common derivative fragment in their

MS/MS spectra with the exception of compound-features 8.74_270.3153 and 8.94_528.4103, which were therefore not derivatised. The compound-features 8.74_270.3153 and 8.94_528.4103 were well retained by the C18 column and therefore likely had significant aliphatic character. The low mass species 1.79_188.0815, corresponded to a derivatised ammonium ion and was higher in abundance in the low glucose samples, likely due to the lower abundance of metabolites with amine functional groups in the sample, as observed from univariate FC analysis. The chemical formulae for the other important compound-features with the common derivative fragment ion were predicted from calculated *m/z* values, as described in Section 4.6. The identity of most of the metabolites (Table 4.9) were subsequently confirmed using RT matching with authentic metabolite standards.

Table 4.9: Predicted chemical formulae and corresponding identified metabolites for the top 10 important compound-features from PLS-DA analysis of 293T WT cells cultured under 1.0 g / L or 4.5 g / L glucose conditions (Section 8.17), derivatised and analysed by RP-IMS-MS/MS (Section 8.8).

Compound-feature	Formula	Compound name	Expected RT / min	FC	p-value
4.39_318.1081	C5H9NO4	Glutamate	4.05	8.36	< 1.0E-16
8.74_270.3153	N/A	Not derivatised	N/A	1.02	0.13
4.81_290.1132	C4H9NO3	Threonine	4.46	2.66	1.10E-15
1.79_188.0815	NH4	Ammonium ion	N/A	4.39	< 1.0E-16
7.25_288.1342	C5H11NO2	Valine	6.93	3.6	< 1.0E-16
8.94_528.4103	N/A	Not derivatised	N/A	1	0.76
8.00_302.1499	C6H13NO2	Isoleucine	7.68	3.01	< 1.0E-16
8.09_302.1499	C6H13NO2	Leucine	7.78	3.1	< 1.0E-16
3.55_246.0869	C2H5NO2	Glycine	3.19	1.6	9.0E-10
8.20_336.1343	C9H11NO2	Phenylalanine	7.88	3.12	1.1E-16

The top 10 metabolites, in Table 4.9, revealed that PLS-DA analysis was biased towards high abundance ions (unlike univariate ranking), as the underivatised compound-features (8.74_270.3153 and 8.94_528.4103) were not significantly altered, but were both in the top 10 most abundant compound-features. With the exception of leucine, the amino acids identified were all glucogenic and therefore scored highly in

PLS-DA as they were naturally highly abundant in the cell samples. Permutation testing for the PLS-DA model failed even though the compound-features showed significant and large changes between experimental groups. It is likely that the model was over-fitted because of the large number of compound-features, compared to the number of samples in each experimental group. Using orthogonal partial least squares-discriminant analysis (OPLS-DA), however, the permutation test passed with a Q^2 coefficient of 0.921 and R^2Y coefficient of 0.997 (model overview shown in Fig. 4.21).

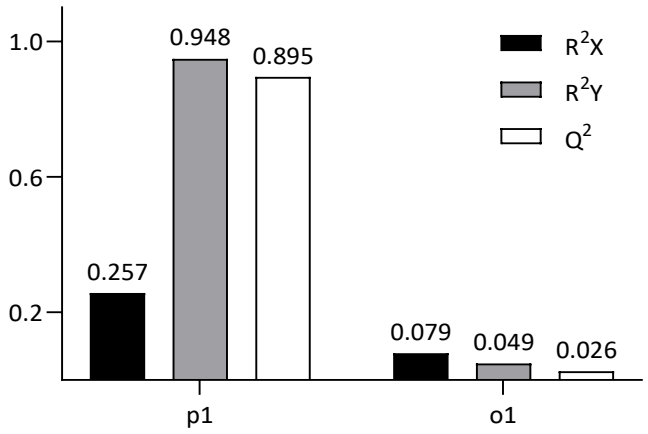

Figure 4.21: Overview of the OPLS-DA model generated from the analysis of 293T WT cells cultured under 1.0 g / L or 4.5 g / L glucose conditions (Section 8.17), derivatised and analysed by RP-IMS-MS/MS (Section 8.8).

OPLS-DA is a supervised multivariate statistical approach, similar to PLS-DA, which can be used to model data when the number of variables is much larger than the number of data points. OPLS-DA is therefore useful for metabolomics experiments when the number of replicates within each group is relatively small compared with the thousands of compound-features acquired.[210] OPLS-DA creates a model of how well the data matches a prediction by removing orthogonal variables which are uncorrelated to the trends in the rest of the data. The compound-features which are discriminative of experimental groups can therefore be identified from the model using an S-plot, combining the covariance

between samples (p[1]) and the reliability of the correlation (p(corr)[1]) to give a loading profile, as shown in Fig. 4.22.

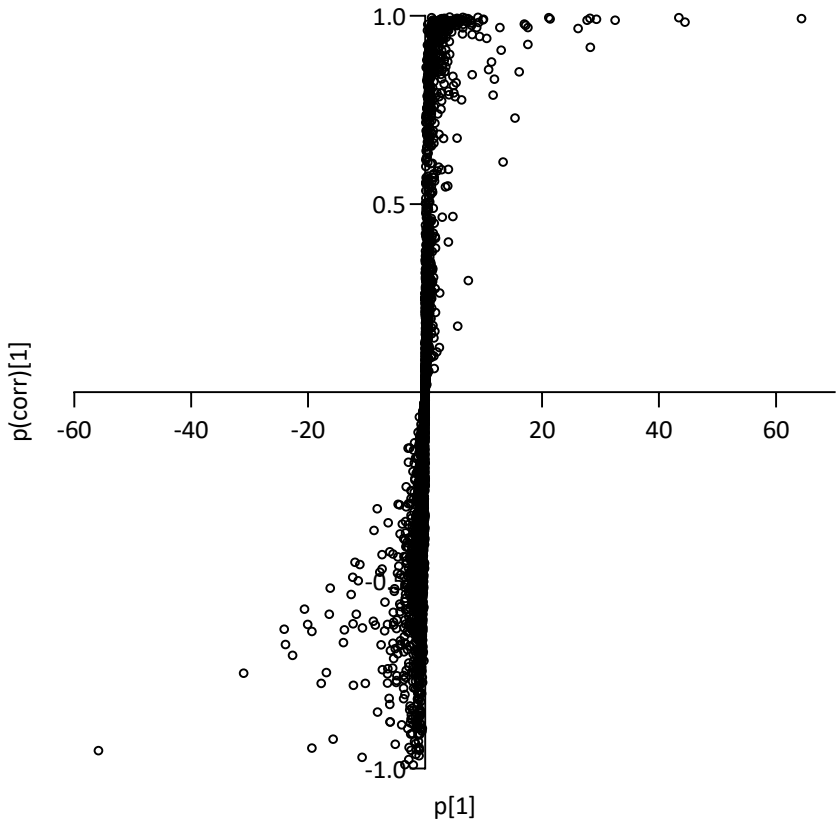

Figure 4.22: S-plot showing the variable importance in the OPLS-DA model generated from the analysis of 293T WT cells cultured under 1.0 g / L or 4.5 g / L glucose conditions (Section 8.17), derivatised and analysed by RP-IMS-MS/MS (Section 8.8). Ions were identified by OPLS-DA analysis, filtered by RT and *m/z.*

The important compound-features in an S-plot have the largest distance from the origin and are therefore found at the extremities of the loadings plot. The 5 most important compound-features with either negative or positive p[1] values from the OPLS-DA S-plot (Fig. 4.22) are listed in Table 4.10. Negative p[1] values corresponded to compound-features which had higher abundance in 293T WT cells cultured under 4.5 g / L glucose and positive p[1] values corresponded to compound-features which had higher abundance in 1.0 g / L glucose.

Table 4.10: Table of the top 10 important compound-features in 293T WT cells cultured under 1.0 g / L or 4.5 g / L glucose conditions (Section 8.17), derivatised and analysed by RP-IMS-MS/MS (Section 8.8). Ions were identified by OPLS-DA analysis, filtered by RT and *m/z*.

Compound-feature	p[1]	p(corr)[1]	Common derivative fragment
8.74_270.3153	-55.83	-0.95	Not observed
8.94_528.4103	-31.04	-0.75	Not observed
8.95_484.3841	-24.10	-0.63	Not observed
8.94_572.4366	-23.89	-0.67	Not observed
6.65_315.1239	-22.64	-0.70	Not observed
8.00_302.1499	29.29	0.99	Observed
7.25_288.1342	32.47	0.99	Observed
1.79_188.0815	43.38	1.00	Observed
4.81_290.113	44.46	0.98	Not observed
4.39_318.1081	64.36	0.99	Observed

Of the top 5 compound-features with negative p[1] values, the most important 2 (8.74_270.3152 and 8.94_528.4103) were identified previously from the PLS-DA model and the other 3 compound-features had higher covariance between samples than positive p[1] compound-features and none had the common derivative fragment in their MS/MS spectra. For the positive p[1] compound-features, 4 were identified previously from PLS-DA analysis (glutamate, 4.39_318.1081; ammonium, 1.79_188.0815; valine, 7.25_288.1342 and isoleucine, 8.00_302.1499). The remaining compound-feature (4.81_290.1132) did not have the common derivative fragment in its MS/MS spectrum. The analysis of the most important compound-features for each group was not optimal as the absolute correlation values for all of the negative values were smaller than all of the positive correlation. The distance from the origin was therefore calculated for each point in the S-plot and the top 10 important compound-features, irrespective of experimental group are shown in Table 4.11.

Table 4.11: Table of the top 10 important compound-features, ordered by their distance from the origin for the S-plot (Fig. 4.22) prepared from OPLS-DA of 293T WT cells cultured under 1.0 g / L or 4.5 g / L glucose conditions (Section 8.17), derivatised and analysed by RP-IMS-MS/MS (Section 8.8).

Compound-feature	p[1]	p(corr)[1]
4.39_318.1081	64.363	0.99239
8.74_270.3153	-55.833	-0.95234
4.81_290.1132	44.455	0.98324
1.79_188.0815	43.38	0.99568
7.25_288.1342	32.473	0.98852
8.94_528.4103	-31.035	-0.74652
8.00_302.1499	29.293	0.99122
3.55_246.0869	28.254	0.91679
8.09_302.1499	28.216	0.99386
8.20_336.1343	27.706	0.98842

The filtered and ordered top 10 important compound-features were much more similar to those identified from VIP analysis of the PLS-DA model (Fig. 4.20). The top 7 compound-features 4.39_318.1081, 8.74_270.3153, 4.81_290.1132, 1.79_188.0815, 7.25_288.1342 and 8.94_528.4103 were identically ranked compared with PLS-DA analysis. The underivatised compound-feature 8.74_270.3153 had the predicted formula $C_{18}H_{39}N$ and 8.94_528.4103 had 15 possible chemical formulae within 5 ppm. The compound-features 3.55_246.0869 (glycine) and 8.09_302.1499 (leucine) alternated order between PLS-DA and OPLS-DA. As the compound-features were observed in both multivariate analyses and had high abundance, these amino acids can therefore be further investigated as potential biomarkers for cell metabolism at different glucose conditions.

In summary, IMS-MS/MS provided additional information for the identification of biomarkers from drift time and increased confidence in analysis. The untargeted derivatised RP-IMS-MS/MS analysis of 293T WT cells cultured under different glucose conditions was used to optimise data univariate and multivariate processing strategies in MetaboAnalyst. The enrichment of glucogenic amino acids in cells cultured under

1.0 g / L glucose conditions, was contrary to the expected change, which was the depletion of amino acids caused by increased gluconeogenesis to maintain intracellular glucose. It is likely that under these conditions, gluconeogenesis was rate limiting and therefore the enrichment in 1.0 g / L glucose conditions was caused by increased transport of amino acids into the cell triggered by energy-sensing pathways.

4.9. Untargeted RP-IMS-MS/MS analysis of LN18 IDH1 mutant and wild-type cells

To further investigate changes in metabolism associated with an IDH1 mutation, LN18 Mut and WT cells were cultured under 4.5 g / L glucose conditions (experimental replicate 1, Section 8.14), metabolites extracted, derivatised and analysed by RP-IMS-MS/MS (Section 8.8). The derivatised method was used to investigate additional amine biomarkers in Mut cells, which were not well characterised by IC-MS/MS (Chapter 3) and to identify important compound-features for further investigation. The optimised processing parameters, including RT and *m/z* filtering of compound-features, described in Section 4.8, were used to remove 460 compound-features. The remaining 1732 compound-features were processed in MetaboAnalyst, as described in Section 8.11. The data associated with this experiment has been deposited in the Oxford University Research Archive (title: Metabolomics of the first culture of LN18 IDH wild-type and mutant cells) and is freely accessible (https://doi.org/10.5287/bodleian:2abVOAvrg). The PCA scores plot of compound-feature abundances demonstrated separation between experimental groups and all samples were within 95 % confidence intervals, as shown in Fig. 4.23.

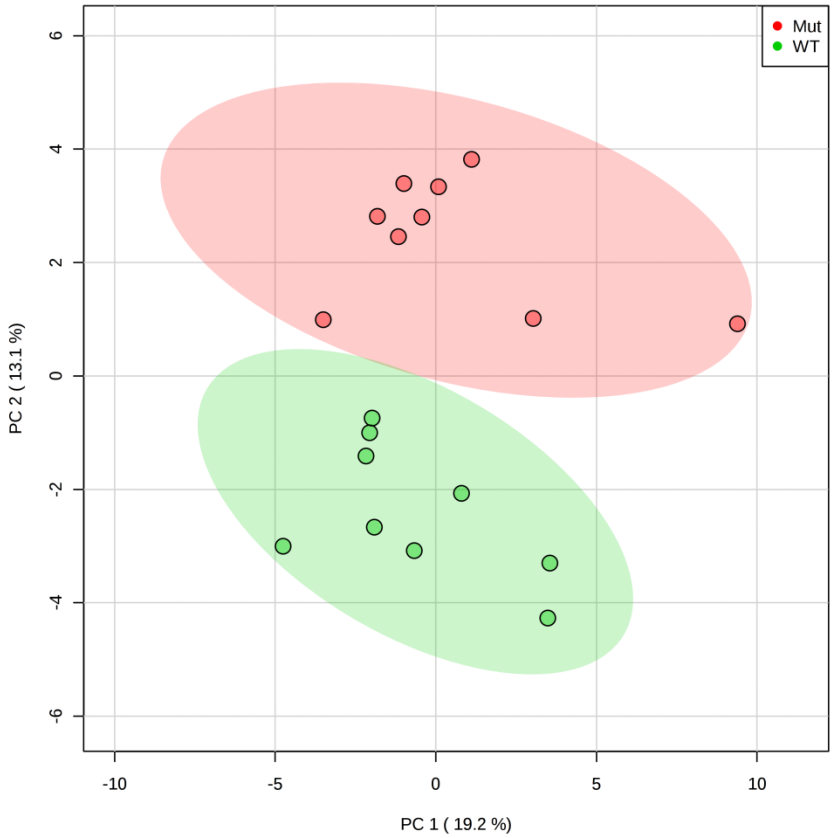

Figure 4.23: PCA scores plot of compound-feature abundances for LN18 Mut and WT cells cultured under 4.5 g / L glucose conditions (experimental replicate 1, Section 8.14), derivatised and analysed by RP-IMS-MS/MS (Section 8.8). Data were pre-processed and filtered with RT within 0.4-9.04 min and *m/z* greater than 188.1045 prior to analysis using MetaboAnalyst with normalisation by sum and Pareto scaling (Section 8.11). Shaded areas represent the 95 % confidence interval for each experimental group.

Overlap of the 95 % confidence intervals, from PCA analysis of the unfiltered dataset (not shown) was observed, further confirming the validity of the exclusion of compound-features from the dataset, as these must have been similar between experimental groups. The permutation test failed for both PLS-DA and OPLS-DA analysis likely due to this high number of compound-features compared with the number of samples and therefore only univariate statistical analysis was performed on the dataset. T-tests found 109 significant compound-features and the most important compound-feature ranked by FDR-adjusted t-test p-value was 5.31_332.1233 which had the common derivative fragment in its MS/MS spectrum, as shown in Table 4.12. The compound-feature 5.31_332.1233 was putatively identified (level 3), by accurate mass

and isotope distribution (as described in Section 4.4), as the lysine degradation product 2-aminoadipate.

Table 4.12: Top 35 compound-features ranked by their FDR-adjusted t-test p-value from the analysis of LN18 Mut and WT cells cultured under 4.5 g / L glucose conditions (experimental replicate 1, Section 8.14), derivatised and analysed by RP-IMS-MS/MS (Section 8.8). Data were pre-processed and filtered with RT within 0.4-9.04 min and *m/z* greater than 188.1045.

Compound-feature	p-value	Common derivative fragment
5.31_332.1233	1.8E-14	Observed
7.30_282.1223	3.8E-14	Not observed
7.16_300.6156	1.2E-12	Not observed
7.16_599.2235	1.6E-12	Not observed
3.60_447.1866	2.2E-12	Not observed
7.16_300.1140	8.5E-12	Not observed
7.23_599.2204	2.5E-11	Not observed
3.17_386.1102	4.8E-11	Observed
3.14_317.2867	2.7E-10	Observed
6.19_282.0881	4.4E-10	Not observed
3.14_317.1237	5.1E-10	Observed
3.16_412.1069	9.8E-10	Observed
7.73_379.1387	1.3E-09	Observed
3.16_214.0958	1.4E-09	Not observed
3.14_339.1052	1.5E-09	Not observed
3.66_304.0920	1.7E-09	Not observed
6.19_282.5891	3.3E-09	Not observed
4.72_545.0984	3.3E-09	Not observed
6.19_563.1698	4.1E-09	Not observed
4.73_547.0969	6.4E-09	Not observed
4.97_541.1792	7.1E-09	Not observed
3.16_317.4597	8.6E-09	Observed
4.73_242.0916	8.8E-09	Not observed
3.14_361.0870	1.1E-08	Observed
3.17_408.0914	1.9E-08	Observed
5.57_286.3745	2.0E-08	Observed
5.57_286.1179	3.8E-08	Observed
3.67_326.0729	6.9E-08	Not observed
4.15_245.0911	9.0E-08	Not observed
5.57_286.2728	1.5E-07	Observed
4.96_260.1967	1.8E-07	Observed
3.94_290.1120	2.0E-07	Not observed
3.14_317.3939	2.2E-07	Observed
6.15_274.1175	2.9E-07	Observed
5.57_330.0807	3.1E-07	Not observed

The MS/MS spectra of the top 35 ions were analysed for the presence of the common derivative fragment and underivatised chemical formulae were predicted. The compound-features 7.73_379.1387, 5.57_286.1179, 4.96_260.1967 and 6.15_274.1175

were putatively identified (level 2) as kynurenine, proline, alanine and aminobutyrate respectively. A volcano plot was also used to investigate the compound-features with a FC greater than 1.5 and an FDR-adjusted t-test p-value less than 0.05, as shown in Fig. 4.24.

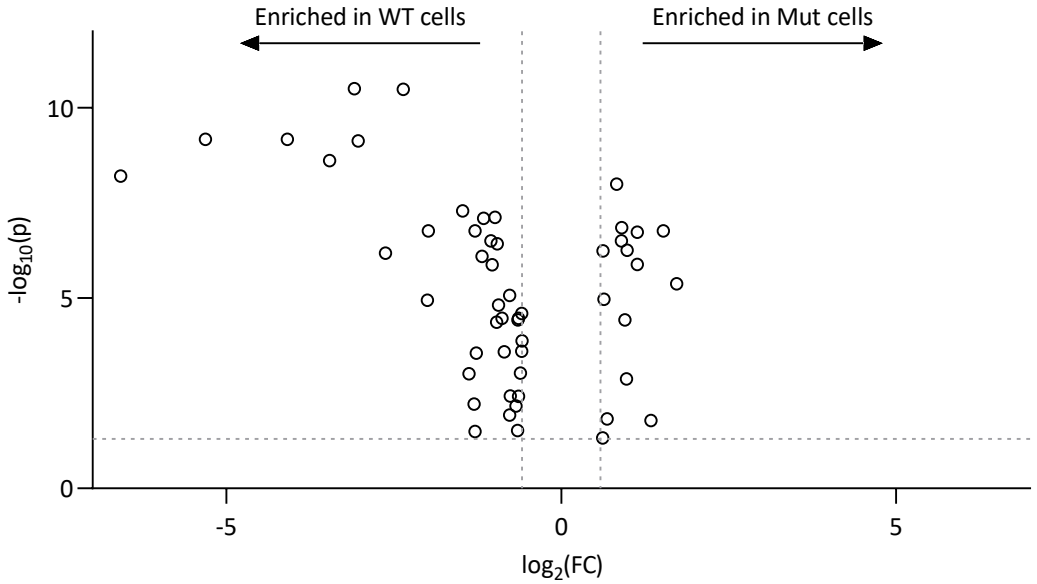

Figure 4.24: Volcano plot showing the important compound-features from univariate statistical analysis of LN18 Mut and WT cells cultured under 4.5 g / L glucose conditions (experimental replicate 1, Section 8.14), derivatised and analysed by RP-IMS-MS/MS (Section 8.8). Data were pre-processed and filtered with RT within 0.4-9.04 min and *m/z* greater than 188.1045.

Of the 53 significant compound-features in the volcano plot, the majority had negative FC values which corresponded to compound-features which had a lower abundance in Mut cells. The compound-features which were depleted in Mut cells had larger FC magnitudes, compared to the compound-features which were enriched, as shown in Table 4.13. The lysine degradation product 2-aminoadipate was the most important compound-feature from analysis of the volcano plot (Fig. 4.24).

Table 4.13: Top 35 important compound-features, filtered by RT and *m/z*, identified in the volcano plot (Fig. 4.24) from univariate statistical analysis of LN18 Mut and WT cells cultured under 4.5 g / L glucose conditions (experimental replicate 1, Section 8.14), derivatised and analysed by RP-IMS-MS/MS (Section 8.8). Data were pre-processed and filtered with RT within 0.4-9.04 min and *m/z* greater than 188.1045.

Compound-feature	FC	log2(FC)	p-value	-LOG10(p)	Enriched group
5.31_332.1233	8.53	-3.09	3.2E-11	10.50	WT
7.30_282.1223	5.13	-2.36	3.3E-11	10.48	WT
7.16_300.6156	39.74	-5.31	6.8E-10	9.17	WT
7.16_599.2235	17.01	-4.09	6.8E-10	9.17	WT
3.60_447.1866	8.17	-3.03	7.5E-10	9.12	WT
7.16_300.1140	11.00	-3.46	2.5E-09	8.61	WT
7.23_599.2204	95.57	-6.58	6.3E-09	8.20	WT
3.17_386.1102	1.77	0.83	1.0E-08	7.99	Mut
3.14_317.2867	2.77	-1.47	5.2E-08	7.29	WT
6.19_282.0881	1.98	-0.99	7.6E-08	7.12	WT
3.14_317.1237	2.23	-1.16	8.0E-08	7.10	WT
3.16_412.1069	1.87	0.90	1.4E-07	6.85	Mut
7.73_379.1387	3.96	-1.98	1.7E-07	6.76	WT
3.16_214.0958	2.88	1.52	1.7E-07	6.76	Mut
3.14_339.1052	2.44	-1.29	1.7E-07	6.76	WT
3.66_304.0920	2.20	1.14	1.9E-07	6.73	Mut
6.19_282.5891	2.07	-1.05	3.2E-07	6.50	WT
4.72_545.0984	1.86	0.90	3.2E-07	6.50	Mut
6.19_563.1698	1.94	-0.95	3.8E-07	6.42	WT
4.73_547.0969	1.98	0.99	5.6E-07	6.25	Mut
4.97_541.1792	1.54	0.62	5.8E-07	6.23	Mut
3.16_317.4597	6.18	-2.63	6.6E-07	6.18	WT
3.14_361.0870	2.27	-1.18	8.1E-07	6.09	WT
3.17_408.0914	2.20	1.14	1.3E-06	5.89	Mut
5.57_286.3745	2.04	-1.03	1.3E-06	5.87	WT
3.67_326.0729	3.30	1.72	4.3E-06	5.37	Mut
5.57_286.2728	1.71	-0.77	8.5E-06	5.07	WT
3.94_290.1120	1.56	0.64	1.1E-05	4.97	Mut
3.14_317.3939	4.00	-2.00	1.1E-05	4.95	WT
5.57_330.0807	1.91	-0.94	1.5E-05	4.82	WT
4.15_318.1080	1.51	-0.59	2.6E-05	4.59	WT
4.15_318.6129	1.84	-0.88	3.4E-05	4.47	WT
4.16_320.1133	1.55	-0.64	3.4E-05	4.47	WT
3.29_419.1166	1.93	0.95	3.8E-05	4.42	Mut
4.16_318.2704	1.56	-0.65	3.8E-05	4.42	WT

The top 20 compound-features in the volcano plot (Fig. 4.24) were identical to those observed from t-tests but the compound-features 4.73_242.0916, 4.96_260.1967 and 6.15_274.1175 were not observed in the volcano plot, as they had FC values below 1.5. These significantly altered compound-features were therefore prime targets for further

investigation and potential biomarkers associated with the IDH1 mutation. To increase metabolite identification for IDH1 mutant pathways of interest, authentic standards were obtained with 1° or 2° amine functionality. These metabolites were selected based on known human metabolic pathways (based on KEGG pathways) and from untargeted LC-MS/MS analysis of the samples described in Chapters 2 and 3.[167] Table 10.3 in the appendix contains the data used for the identification of derivatised metabolites, characterised by RP-MS (Section 8.7) and RP-IMS-MS/MS (Section 8.8), including monoisotopic mass, chemical formula and RT.

4.10. Derivatised RP-MS analysis of lysine degradation products

To further investigate changes in metabolism associated with an IDH1 mutation and increase coverage of the metabolites in amino acid metabolism and related pathways, extracts from LN18 Mut and WT samples were derivatised and analysed by RP-MS (Section 8.7). This analysis was carried out to investigate changes to metabolite abundances in the lysine degradation pathway (shown in Fig. 4.25), as 2-oxoadipate was identified by IC-MS/MS to be significantly depleted in LN18 Mut cells. The same LN18 cell extracts (experimental replicate 1, Section 8.14), as analysed by IC-MS/MS and HILIC-MS/MS were analysed by RP-MS. The data associated with this experiment has been deposited in the Oxford University Research Archive (title: Metabolomics of the first culture of LN18 IDH wild-type and mutant cells) and is freely accessible (https://doi.org/10.5287/bodleian:2abVOAvrg). It was assumed that as the cell extracts were frozen at -80°C between analyses that no significant degradation had occurred and therefore metabolite abundances were unaltered from previous analyses.

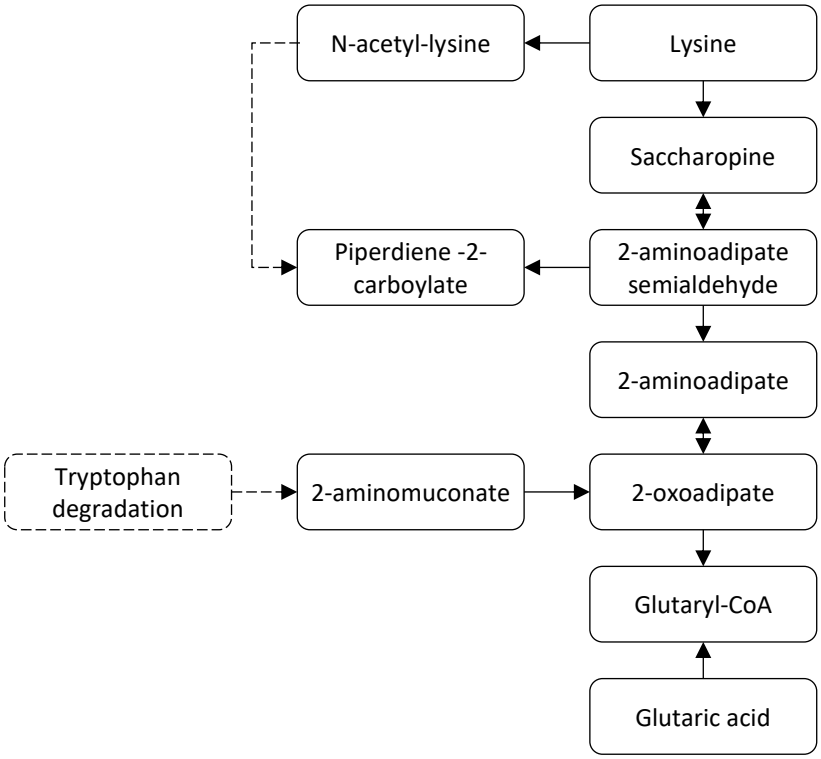

Figure 4.25: Lysine degradation pathway (reproduced from the KEGG human metabolic pathway database).[167]

Metabolites were identified, as described in Section 8.7, with authentic amine standards (listed in Table 10.3). The first metabolite of interest was lysine, which did not significantly alter in abundance between Mut and WT cells; likely due to the high concentration of essential amino acids which were present in the media, providing a large extracellular pool which could be utilised by the cells. The intracellular concentration of essential amino acids is highly regulated and are therefore not likely to deplete or accumulate, as their transport across cell membranes is controlled.[208] Two metabolites between lysine and 2-oxoadipate in the degradation pathway, saccharopine and 2-aminoadipate, were depleted significantly, as shown in Fig. 4.26, by 7.98-fold (p-value 1.5×10^{-6}) and 8.07-fold (5.6×10^{-16}) respectively.

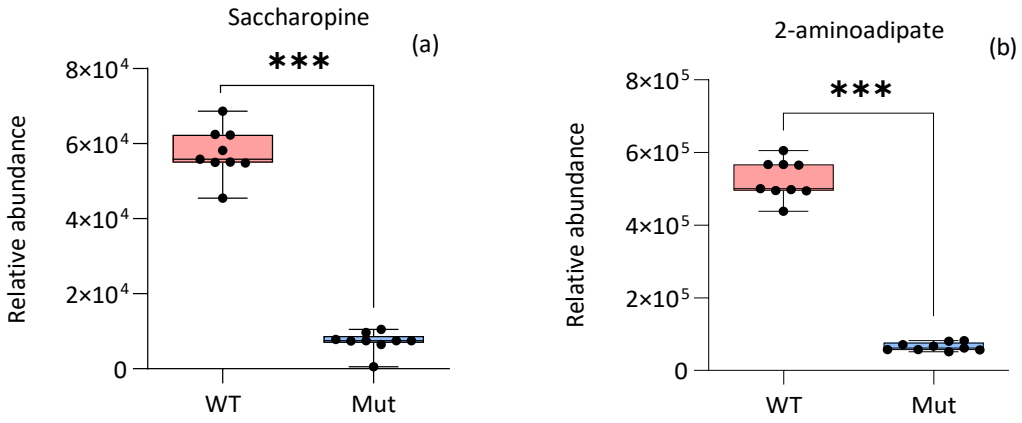

Figure 4.26: Box plots showing the abundance of saccharopine (a) and 2-aminoadipate (b) in LN18 Mut and WT cells cultured under 4.5 g / L glucose conditions (experimental replicate 1, Section 8.14) derivatised and analysed by RP-MS (Section 8.7). The box plots show the mean, 25-75th percentiles and whiskers extend from the minimum to maximum values. The number of samples are denoted with dots and significance from t-tests are annotated (ns, p-value greater than 0.05; *, p-value less than 0.05; **, p-value less than 0.01; and ***, p-value less than 0.001).

The depletion of saccharopine and 2-aminoadipate correlated negatively with the accumulation of 2-HG in the Mut cells. Further investigation is required to determine if this correlation was due to the inhibition of lysine degradation pathway enzymes (by 2-HG) or the depletion of 2-OG, as 2-OG is a known substrate in the conversion of lysine to saccharopine by α-aminoadipate semialdehyde synthase.[211]

To confirm the reliability of the observations, the experiment described in Section 8.14 was repeated with the same culture of LN18 cells at a later passage number (passage 24, experimental replicate 2) and from a separate culture of cells (passage 22, experimental replicate 3). All the LN18 cells were cultured under 4.5 g / L glucose conditions, metabolites extracted, derivatised and analysed by RP-MS (Section 8.7). The data associated with these experiments has been deposited in the Oxford University Research Archive and is freely accessible (Metabolomics of the second culture of LN18 IDH wild-type and mutant cells, https://doi.org/10.5287/bodleian:eyq4Qj8AR and Metabolomics of the third culture of LN18 IDH wild-type and mutant

cells, https://doi.org/10.5287/bodleian:1ReJ0yA8z). Both saccharopine and 2-aminoadipate were again observed to be significantly depleted in Mut cells, as shown in Fig. 4.27.

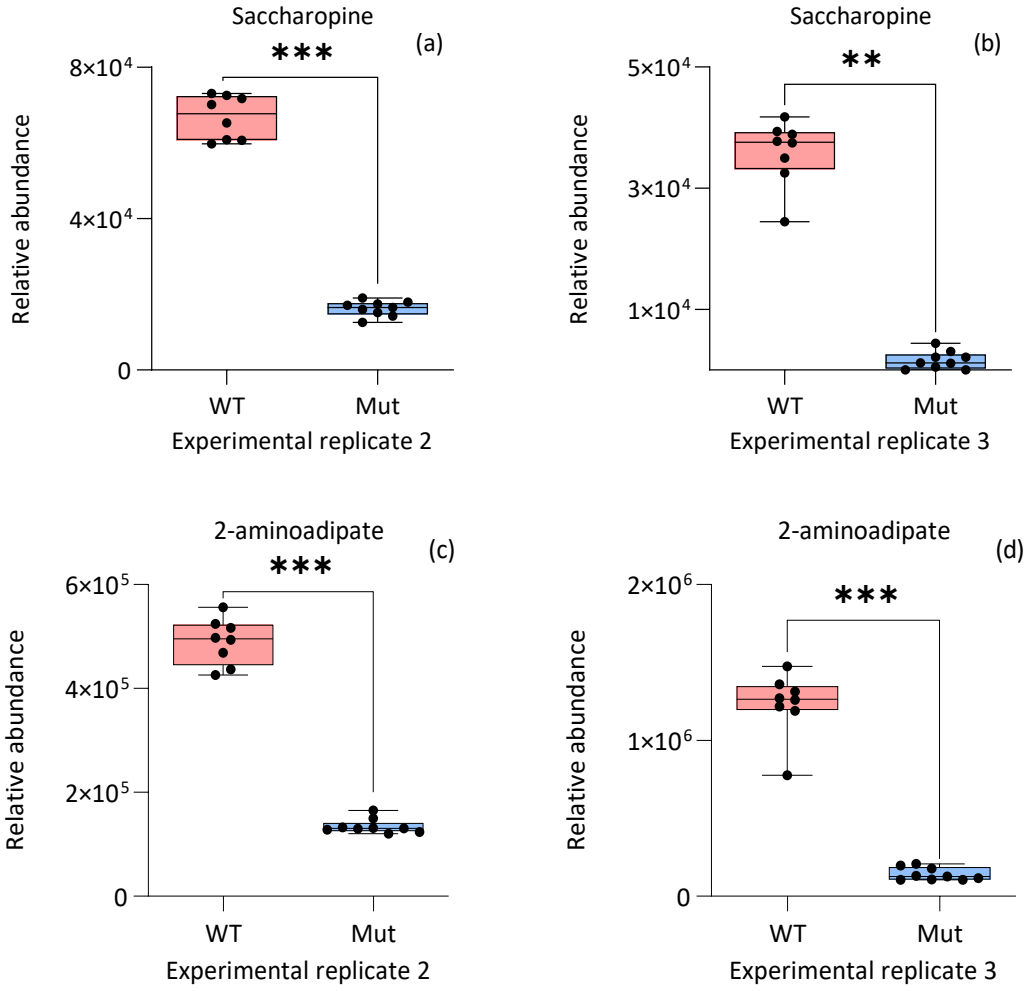

Figure 4.27: Box plots showing the abundance of saccharopine (a) and 2-aminoadpate (c) in experimental replicate 2 of LN18 Mut and WT cells cultured under 4.5 g / L glucose (Section 8.14), and saccharopine (b) and 2-aminoadpate (d) in experimental replicate 3. All metabolite extracts were derivatised and analysed by RP-MS (Section 8.7) and metabolites identified using the approach described in Section 8.12. The box plots show the mean, 25-75th percentiles and whiskers extend from the minimum to maximum values. The number of samples are denoted with dots and significance from t-tests are annotated (ns, p-value greater than 0.05; *, p-value less than 0.05; **, p-value less than 0.01; and ***, p-value less than 0.001).

Saccharopine (Fig. 4.27(a, b)) was depleted 2.12-fold (p-value $4.5x10^{-14}$) and in experimental replicate 3, the depletion was increased to 22.1-fold (p-value $2.0x10^{-3}$). The

significant depletion of 2-aminoadipate (Fig. 4.27(c, d)) was also observed in both repeat experiments by 3.65-fold (p-value $1.6x10^{-14}$) and 8.71-fold (p-value $7.9x10^{-12}$).

4.11. Derivatised RP-MS analysis of tryptophan degradation products

Metabolites in the tryptophan degradation pathway (shown in Fig. 4.28) were also investigated in LN18 Mut and WT samples (experimental replicate 1, Section 8.14), derivatised and analysed using RP-MS (Section 8.7). Kynurenine, a tryptophan degradation product was found to be significantly depleted in untargeted analysis of Mut cells (Section 4.9) and therefore other tryptophan metabolites were identified to further investigate the metabolic effects of an IDH1 mutation. The data associated with this experiment has been deposited in the Oxford University Research Archive (title: Metabolomics of the first culture of LN18 IDH wild-type and mutant cells) and is freely accessible (https://doi.org/10.5287/bodleian:2abVOAvrg).

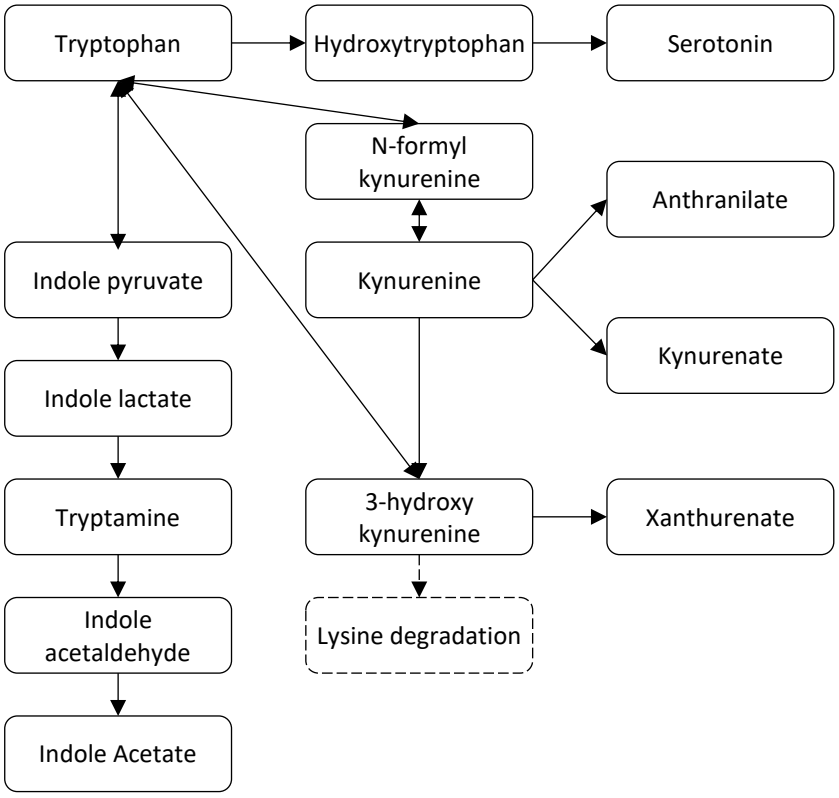

Figure 4.28: Tryptophan degradation pathway (reproduced from the KEGG human metabolic pathway database).[167]

Tryptophan degradation product abundances were also significantly altered, with an enrichment of tryptophan in Mut cells (FC 1.19, p-value 2.0×10^{-4}), as shown in Fig. 4.29. Conversely, hydroxytryptophan was depleted in Mut cells (FC 9.61, p-value $< 1.0 \times 10^{-16}$); however, serotonin, the next metabolite in the pathway was not significantly altered. Kynurenine (Fig. 4.30(a)) was also significantly depleted in Mut cells (FC 3.74, p-value $< 1.0 \times 10^{-16}$), despite the accumulation of tryptophan. The accumulation of tryptophan and depletion of the degradation pathways again suggests inhibition or regulation of the degradation pathway enzymes, as a consequence of the IDH1 mutation.

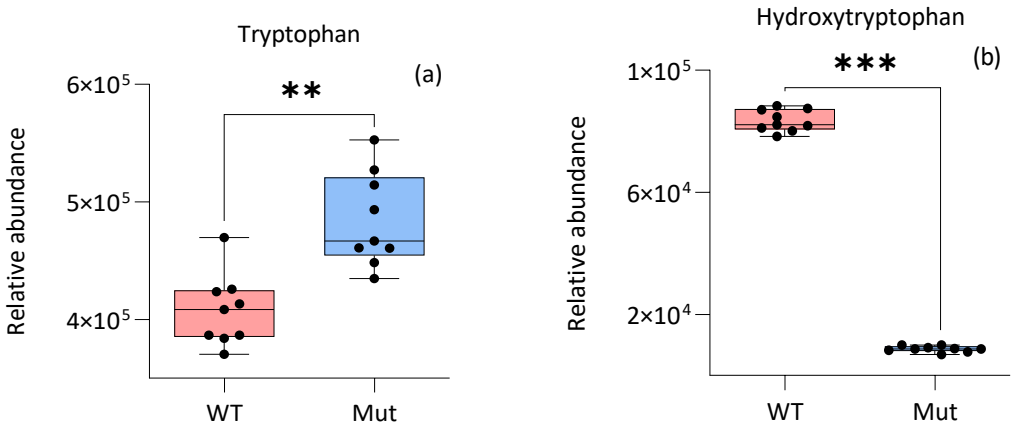

Figure 4.29: Box plots showing the abundance of tryptophan (a) and hydroxytryptophan (b) in LN18 Mut and WT cells cultured under 4.5 g / L glucose conditions (experimental replicate 1, Section 8.14), derivatised and analysed by RP-MS (Section 8.7). The box plots show the mean, 25-75th percentiles and whiskers extend from the minimum to maximum values. The number of samples are denoted with dots and significance from t-tests are annotated (ns, p-value greater than 0.05; *, p-value less than 0.05; **, p-value less than 0.01; and ***, p-value less than 0.001).

Tryptophan degradation products, via tryptamine, did not exhibit a consistent change in abundance along the whole pathway. Concomitant with the increase in abundance for tryptophan in Mut cells, indole pyruvate (FC 1.12, p-value 6.9×10^{-3}), tryptamine (FC 1.28, p-value < 1.0×10^{-16}), indole acetate (FC 1.15, p-value 7.6×10^{-5}) were all marginally but significantly enriched. Indole acetaldehyde, between tryptamine and indole acetate, was significantly depleted FC 2.16 (p-value < 1.0×10^{-16}). The cause of this depletion and possible inhibition of tryptamine deaminase, which is oxygen sensitive, is not clear and requires further investigation.

The depletion of tryptophan degradation pathway metabolites was confirmed in experimental replicates of LN18 cells, cultured under 4.5 g / L glucose conditions (Section 8.14), analysed by RP-MS, as described in Section 8.7. The data associated with these experiments has been deposited in the Oxford University Research Archive and is freely accessible (Metabolomics of the second culture of LN18 IDH wild-type and mutant cells, https://doi.org/10.5287/bodleian:eyq4Qj8AR and

Metabolomics of the third culture of LN18 IDH wild-type and mutant cells, https://doi.org/10.5287/bodleian:1ReJ0yA8z). The depletion of hydroxytryptophan was observed, but was not significant in the experimental replicates. Kynurenine was significantly depleted in all LN18 Mut experiments, as shown in Fig. 4.30.

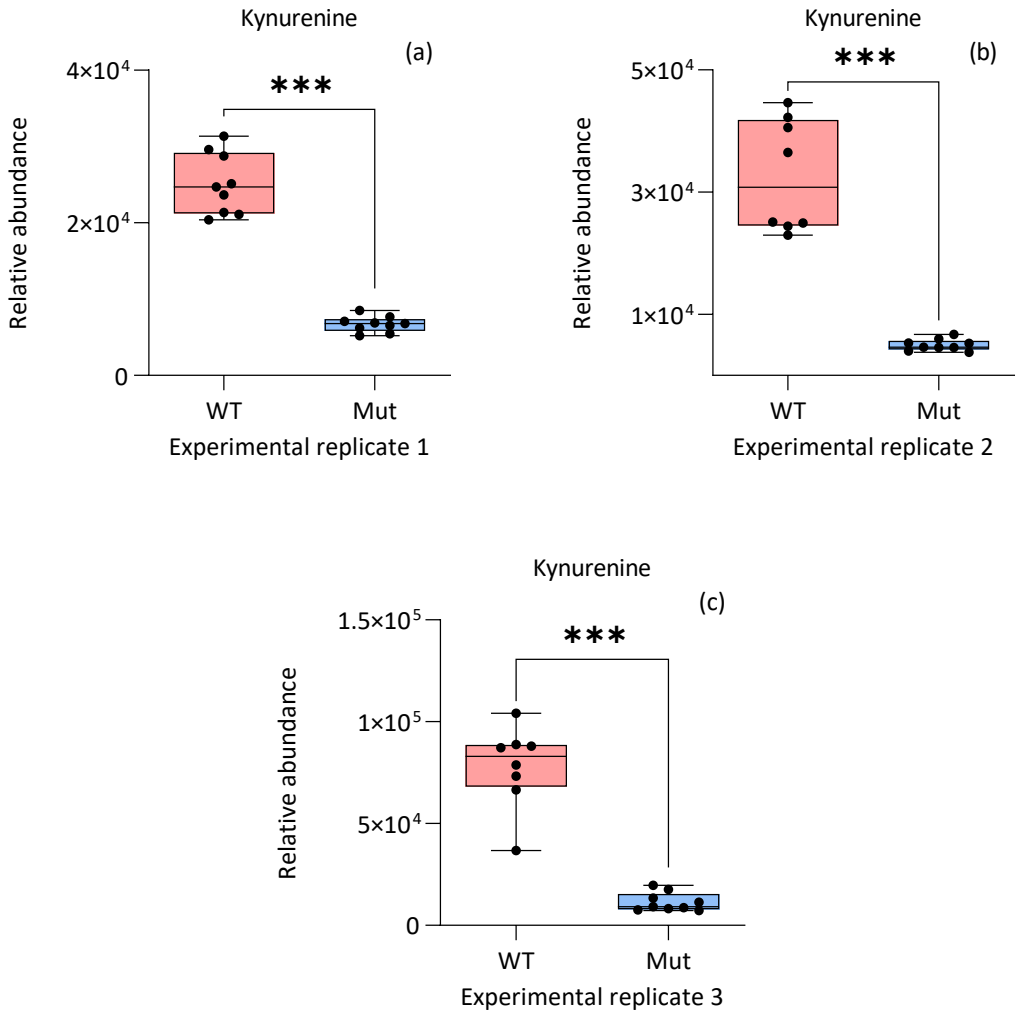

Figure 4.30: Box plots showing the abundance of kynurenine in LN18 Mut and WT cells cultured under 4.5 g / L glucose conditions (Section 8.14) for experimental replicate 1 (a), 2 (b) and 3 (c). All samples were derivatised and analysed by RP-MS (Section 8.7) and metabolites identified using the approach described in Section 8.12. The box plots show the mean, 25-75th percentiles and whiskers extend from the minimum to maximum values. The number of samples are denoted with dots and significance from t-tests are annotated (ns, p-value greater than 0.05; *, p-value less than 0.05; **, p-value less than 0.01; and ***, p-value less than 0.001).

Kynurenine was consistently significantly depleted in LN18 Mut cells across all analyses (Fig. 4.30), by 6.58-fold (p-value 5.6×10^{-11}) and 6.81-fold (p-value 7.0×10^{-9}), in

experimental replicates 2 and 3. This observation further suggests that tryptophan degradation pathway enzymes were being regulated as a consequence of the IDH1 mutation, possibly by inhibition of upstream enzymes or depletion of other metabolites downstream.

4.12. Discussion of derivatised RP-MS analysis of LN18 IDH1 mutant and wild-type glioblastoma cells

As metabolites in the tryptophan and lysine degradation pathways were observed to be significantly altered in LN18 Mut cells, from untargeted analysis by both IC-MS/MS and derivatised RP-MS, these pathways were therefore directly or indirectly modified by the IDH1 mutation, and may be involved in tumourigenesis or proliferation. The tryptophan and lysine degradation pathways may be potential therapeutic targets for WT or Mut cells and were therefore investigated further, including confirmation of metabolite identifications using derivatised authentic standards.

Lysine was not significantly altered between LN18 Mut and WT cells; however, this might be due to the large extracellular pool of lysine which is supplemented in DMEM. The intracellular concentration of lysine could therefore be maintained by the cell by both passive and active transport through the cell membrane, which is highly regulated.[208] Saccharopine is the first degradation product of lysine and is formed by α-aminoadipic semialdehyde synthase, which is a 2-OG dependent enzyme.[211] Saccharopine was observed to be significantly depleted in all analyses of LN18 Mut cells (Section 4.10), either caused by the depletion of 2-OG, or the hundred-fold upregulation of 2-HG (and potential competitive inhibition of α-aminoadipic semialdehyde synthase). The inhibition

of 2-OG dependent pathways by 2-HG has previously been observed and is attributed to the structural similarity and functionality shared between the metabolites.[49, 212]

The lysine degradation product 2-oxoadipate was observed to be significantly depleted in Mut cells by IC-MS/MS analysis of the LN18 cells (Section 3.3). A concomitant significant depletion was observed, by derivatised RP-MS, for 2-aminoadipate. 2-aminoadipate is upstream of 2-oxoadipate and downstream of saccharopine, in the lysine degradation pathway, and is inter-converted with 2-oxoadipate by the enzyme kynurenine / 2-aminoadipate transaminase. The depletion of all the lysine degradation products, observed over multiple analyses, suggests an association between the IDH1 mutation and the lysine degradation pathway, however the biological cause of this is not revealed by analysis of Mut and WT cells.

The tryptophan degradation product kynurenine was identified to be depleted, from untargeted RP-IMS-MS/MS analysis of LN18 cells (Section 4.9). Further analysis of the tryptophan degradation pathway showed that kynurenine was consistently depleted across all derivatised analyses of LN18 cells, despite a significant enrichment of tryptophan. The depletion of tryptophan degradation products provides further evidence for inhibition of amino acid degradation pathways, caused by the IDH1 mutation. The depletion of 2-OG may also account for the changes observed, as the tryptophan degradation pathway is regulated by several transaminase reactions which are 2-OG dependent. The enrichment of kynurenine and other tryptophan metabolites have been shown to cause T-cell immunosuppression and may be linked to the increased survival times for patients with identified IDH1 mutations.[205, 213] The enzymes indoleamine 2,3-dioxygenase (IDO) and tryptophan 2, 3-dioxygenase (TDO) are the rate limiting step in

the tryptophan degradation pathway (and the formation of kynurenine).[214] Both enzymes have been associated with immunosuppression and may therefore support tumourigenesis by either overexpression of the enzyme or regulation of associated metabolites.[214, 215] The effect of the IDH1 mutation on tryptophan degradation product abundances could therefore be caused by regulation of IDO in IDH1 Mut cells, as well as the potential inhibition of 2-OG dependent pathways, by 2-HG.

4.13. Chapter summary

The derivatised method for the analysis of amine metabolites developed and evaluated in this Chapter, was applied to the analysis of cell extracts. Derivatised RP-IMS-MS/MS was demonstrated to be reproducible and applicable to untargeted metabolomics for the investigation of metabolites with amine functional groups. The increased sensitivity, compared with other methods such as HILIC-IMS-MS/MS, enabled the detection of amines down to nanomolar concentrations, and therefore provided comprehensive coverage of metabolic pathways. Using the approach described in Section 8.12, a database containing chemical formulae, RT and fragmentation spectra for a range of biological compounds with 1° or 2° amine functionality was established, allowing the identification of metabolites in biological samples based on measurements from authentic metabolite standards.

IMS provided orthogonal separation based on CCS within the LC time scale and was not subject to carryover effects. Drift time measurement enabled fragment ions measured using a DIA approach to be assigned to their precursor ions, reducing spectral noise and improving specificity.

Significant and considerable changes to tryptophan and lysine degradation pathways were identified in LN18 Mut and WT cells, consistent with observations from IC-MS/MS analysis (Section 3.3). The depletion of tryptophan and lysine degradation products, with the exception of hydroxytryptophan, were observed consistently across multiple analyses of LN18 Mut cells, at different passage numbers. It is likely that the depletion of 2-OG in Mut cells caused the depletion of saccharopine but the possibility of competitive inhibition of 2-HG could not be excluded. The significant depletion of kynurenine was not accounted for by changes in 2-OG and therefore could be affected by the enrichment 2-HG or a regulatory effect on IDO or TDO. These changes have not previously been reported in association with an IDH1 mutation and require further investigation to determine whether the IDH1 mutation was directly or indirectly responsible for the alterations of metabolite abundance. The effect of increased concentrations of 2-OG and 2-HG on LN18 cells will be investigated to elucidate these observations.

Chapter 5. Analysis of IDH1 mutant and wild-type cells using multiple LC-MS/MS methods

5.1. Introduction

Analysis of the LN18 cell line with and without an IDH1 mutation (Sections 3.3, 4.10 and 4.11), identified the depletion of multiple tryptophan and lysine degradation products in LN18 Mut cells including saccharopine, kynurenine and 2-oxoadipate. Less polar metabolites in these (and other) pathways were not well characterised by IC-MS/MS and derivatised RP-IMS-MS/MS. To ensure that these types of metabolites were measured, an untargeted RP-MS/MS method was subsequently utilised without sample derivatisation. RP-MS is the most commonly used LC-MS method used for metabolic profiling of low and medium polarity polar metabolites and is therefore complementary to the methods already utilised.[106, 107]

The non-derivatised RP-MS/MS method used for analyses in this thesis, was based on the method published by Want *et al.* for the analysis of animal and human tissues.[98] Eluent flow rate and gradient conditions were optimised for the LC system and MS scan parameters were modified to ensure sufficient scans were collected, across a typical chromatographic peak, as well as fragmentation of the top 10 ions in each full scan spectrum (methods described in Sections 8.9 and 8.10).[216] Having applied non-derivatised RP-MS/MS to the analysis of multiple cell lines (LN18, U87-MG and 293T) with and without the IDH1 mutation, these data will be compiled with the datasets of identified metabolites from IC-MS/MS and derivatised RP-MS. Reproducibility of analysis, and the changes associated with the IDH1 mutation across the different cell lines will be reported.

The research aims of this chapter were to:

- Identify pathway-level changes linked to an IDH1 mutation in multiple cell lines.
- Investigate the reproducibility of the observed metabolic effects across experimental replicates and multiple cell lines.

5.2. Non-derivatised RP-MS/MS analysis of LN18 IDH1 mutant and wild-type glioblastoma cells

LN18 Mut and WT cells were cultured under 4.5 g / L glucose conditions (experimental replicate 1, Section 8.14) and analysed, without sample derivatisation, by RP-MS/MS (Section 8.9), with data processing and metabolite identification as described in Section 8.12. The data associated with this experiment has been deposited in the Oxford University Research Archive (title: Metabolomics of the first culture of LN18 IDH wild-type and mutant cells) and is freely accessible (https://doi.org/10.5287/bodleian:2abVOAvrg). Of 4.21×10^5 chromatographic peaks integrated in Progenesis QI, 5204 compound-features were picked and 79 metabolites were identified based on data obtained from authentic metabolite standards. A PCA scores plot of compound-feature abundances (Fig. 5.1) showed all samples within 95 % confidence intervals and separation of both experimental groups in principal component space.

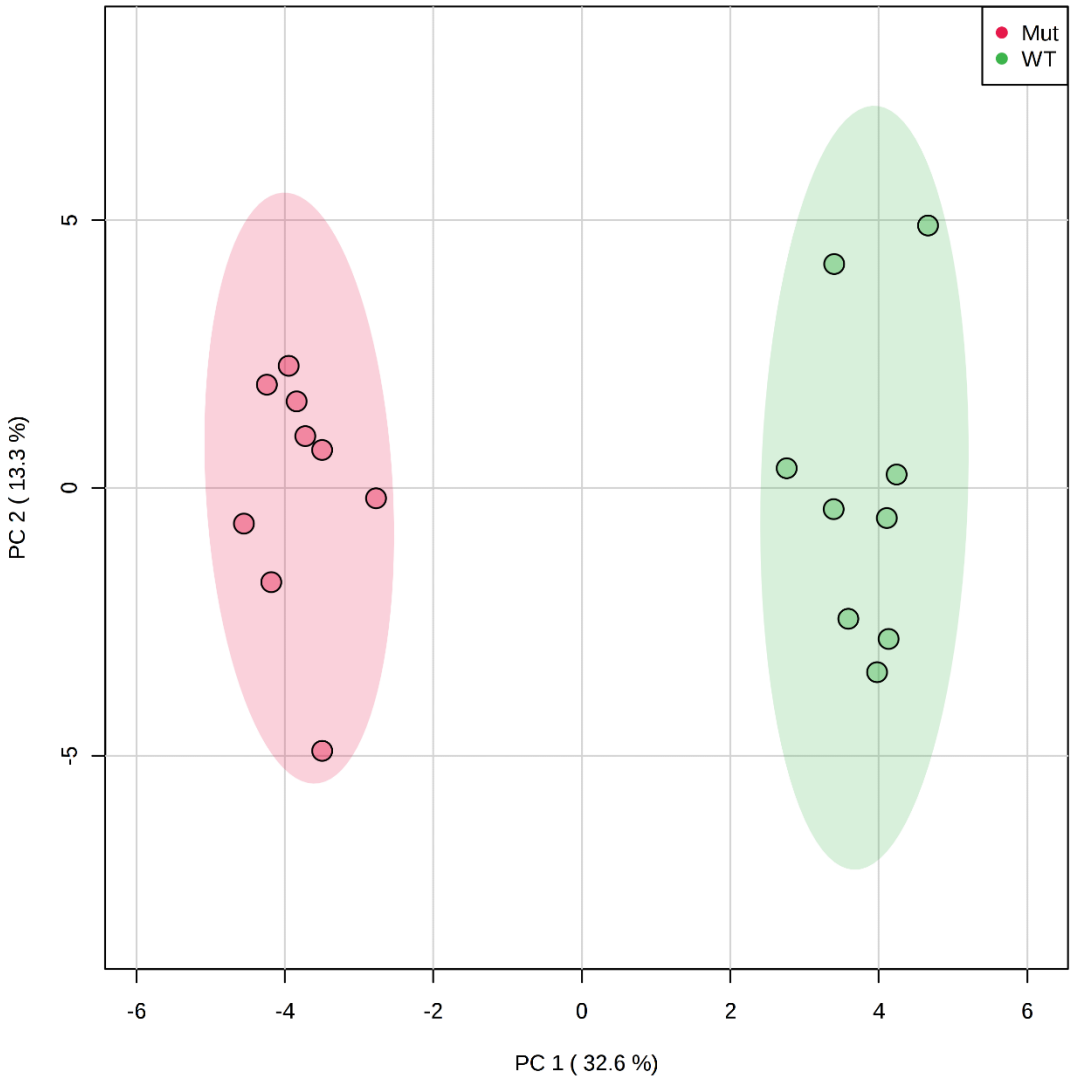

Figure 5.1: PCA scores plot of compound-feature abundances for LN18 Mut and WT cells cultured under 4.5 g / L glucose conditions (experimental replicate 1, Section 8.14) analysed by RP-MS/MS (Section 8.9). Statistical analysis was performed using MetaboAnalyst with normalisation by sum and Pareto scaling (Section 8.11). Shaded areas represent the 95 % confidence interval for each experimental group.

Initial observations from univariate statistical analysis, using FC and p-values obtained from t-tests, showed that many polar and ionic metabolites, including in-source fragments of 2-HG which eluted before 1.2 min, had large FC values and were statistically significant. For example, the highest ranked identified compound-feature from the volcano plot was β-citryl glutamate, which was enriched 4.21-fold (p-value 1.24×10^{-12}) in WT cells, as shown in Fig. 5.2.

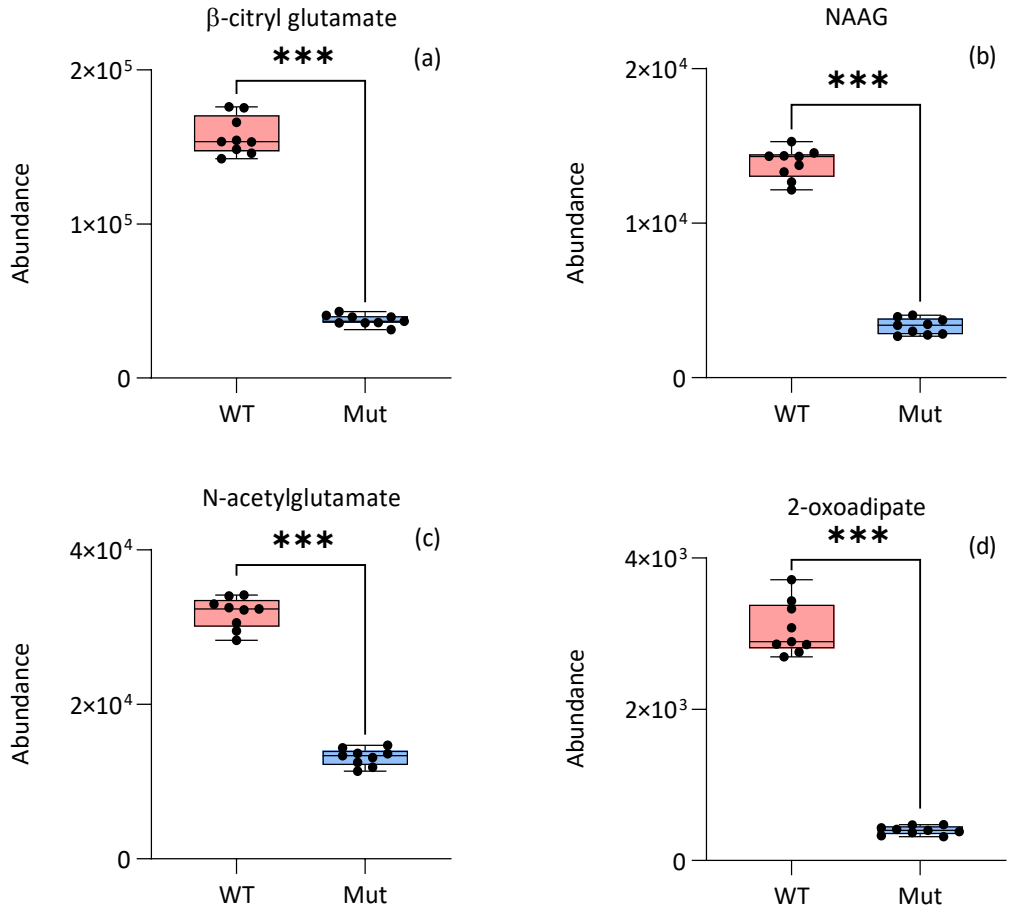

Figure 5.2: Box plots showing the abundance of β-citryl glutamate (a), NAAG (b), N-acetylglutamate (c) and 2-oxoadipate (d) in LN18 Mut and WT cells cultured under 4.5 g / L glucose conditions (experimental replicate 1, Section 8.14), analysed by RP-MS/MS (Section 8.9). The box plots show the mean, 25-75th percentiles and whiskers extend from the minimum to maximum values. The number of samples are denoted with dots and significance from t-tests are annotated (ns, p-value greater than 0.05; *, p-value less than 0.05; **, p-value less than 0.01; and ***, p-value less than 0.001).

NAAG (FC 4.21, p-value 3.37x10^{-12}), N-acetylglutamate (FC 2.44, p-value 2.81x10^{-11}) and 2-oxoadipate (FC 7.78, p-value 8.53x10^{-11}) were all significantly depleted in Mut cells by RP-MS/MS, in agreement with observations from IC-MS/MS analysis of LN18 cells (Section 3.3). The FC values for NAAG, N-acetylglutamate and 2-oxoadipate were different to those obtained from IC-MS/MS (3.70, 1.20 and 12.28-fold respectively), likely caused by ion suppression effects, as all 3 metabolites eluted close to the void, in RP-MS/MS analysis. The low and medium polarity metabolites which were retained by the column, and were not altered by as large a magnitude, were therefore obscured

during statistical analysis, by the large changes abundance for polar metabolites. A filter to exclude compound-features with a RT outside 1.2-16.0 min was used for subsequent analyses, which reduced the number of compound-features to 4146.

RP-MS/MS analysis also putatively identified (level 3) N-formylkynurenine (Fig. 5.3), an intermediate in the tryptophan degradation pathway, which was depleted in Mut cells by 25.37-fold (p-value 2.86×10^{-9}). The depletion of kynurenine, observed from derivatised RP-MS analysis of LN18 cells (Section 4.11), together with the depletion of N-formylkynurenine, provided further evidence for reduced tryptophan degradation in LN18 Mut cells. This could be due to inhibition, by 2-HG, of dioxygenase enzymes (specifically IDO or TDO as discussed in Section 4.12), or reduced dioxygenase activity caused by the depletion of 2-OG.

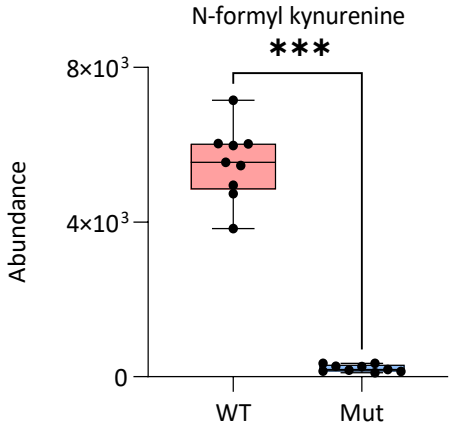

Figure 5.3 Box plot showing the abundance of N-formylkynurenine in LN18 Mut and WT cells cultured under 4.5 g / L glucose conditions (experimental replicate 1, Section 8.14), analysed by RP-MS/MS (Section 8.9). The box plot shows the mean, 25-75th percentiles and whiskers extend from the minimum to maximum values. The number of samples are denoted with dots and significance from t-tests are annotated (ns, p-value greater than 0.05; *, p-value less than 0.05; **, p-value less than 0.01; and ***, p-value less than 0.001).

The identification of some of the same metabolites in LN18 cells (using RP-MS/MS), as from IC-MS/MS and derivatised RP-MS analyses provided increased confidence that the changes in metabolite abundance discussed in Sections 3.7 and 4.12 were valid. Reduced

quantification accuracy was observed, likely due to poor chromatographic retention of polar metabolites. The metabolite identifications provided by RP-MS/MS, without sample derivatisation, still provided further evidence for metabolic change at the pathway level.

5.2.1. Exploring the effect of the IDH1 mutation on central carbon metabolite abundances

To investigate analytical reproducibility and confirm the alterations in central carbon metabolite abundance with an IDH1 mutation, experimental replicates of LN18 Mut and WT cells were cultured under 4.5 g / L glucose conditions (Section 8.14). Metabolite extracts were analysed by IC-MS/MS (Section 8.4), derivatised RP-MS (Section 8.7) and non-derivatised RP-MS/MS (Section 8.9), with data processing and metabolite identification as described in Section 8.12. Datasets containing identified metabolites, from each of the 3 LC-MS/MS methods, were compiled and duplicate identifications removed. For example, the nucleotides were observed in both IC-MS/MS and non-derivatised RP-MS/MS analysis, only the data from IC-MS/MS analysis were used, due to the increased chromatographic resolution, minimising any ion suppression effects. The abundance of TCA cycle metabolites and glycolytic intermediates were generally not significantly altered, as shown in Table 5.1, with the exception of the enrichment of 2-HG and the depletion of 2-OG, as discussed in Section 3.7.

Table 5.1: Heat map showing FC and significance for selected central carbon metabolites from experimental replicates of LN18 Mut and WT cells cultured under 4.5 g / L glucose conditions (Section 8.14), analysed by IC-MS/MS (Section 8.4), derivatised RP-MS (Section 8.7) and non-derivatised RP-MS/MS (Section 8.9).

	Experimental replicate		
Identified metabolite	**1**	**2**	**3**
2-HG			
2-OG			
Cis-aconitate			
Citrate			
Fumarate			
Lactate			
Malate			
Phosphoenolpyruvate			
Pyruvate			
Succinate			

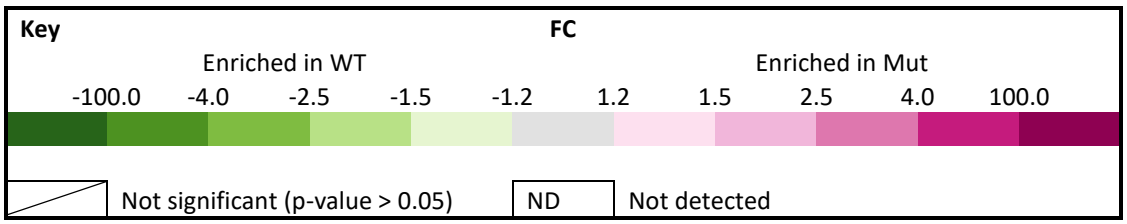

Despite the hundred-fold enrichment of 2-HG and depletion of 2-OG, TCA cycle metabolites were not significantly altered, across the experimental replicates. This may suggest that the alteration of certain central carbon metabolite abundances, observed in the first experiment replicate, may have been due to temporal changes in metabolite abundance during the cell cycle.[217] For example, phosphoenolpyruvate was significantly depleted in the first experimental replicate of LN18 cells, was not significantly altered in subsequent analyses and therefore was unlikely to be caused by the IDH1 mutation. The enrichment of 2-HG across multiple experiments demonstrates the stability of transduction (of the IDH1 mutation) in LN18 cells through multiple passages, and the freeze-thaw process of seeding a new culture from a frozen aliquot of cells (for experimental replicate 3). Analysis of multiple experimental replicates was beneficial to explore whether the significant changes which were observed in the first replicate were reproducible.

5.2.2. Exploring the effect of the IDH1 mutation on pentose phosphate pathway intermediate abundances

As the enrichment of sedoheptulose 7-phosphate and the depletion of sedoheptulose 1,7-diphosphate were associated with the IDH1 mutation (as discussed in Section 3.7), pentose phosphate pathway intermediates were also investigated, to identify if their abundances were consistently altered across multiple experimental replicates. As shown in Table 5.2, sedoheptulose 1,7-diphosphate was not detected in either subsequent experimental replicate. This could be due to sample degradation, or the lower total ion counts observed for the subsequent experiments, resulting in a lower number of total metabolite identifications.

Table 5.2: Heat map showing FC and significance for selected pentose phosphate intermediates from experimental replicates of LN18 Mut and WT cells cultured under 4.5 g / L glucose conditions (Section 8.14), analysed by IC-MS/MS (Section 8.4), derivatised RP-MS (Section 8.7) and non-derivatised RP-MS/MS (Section 8.9).

	Experimental replicate		
Identified metabolite	**1**	**2**	**3**
Erythrose 4-phosphate			
Fructose 1,6-bisphosphate			
Fructose 6-phosphate		ND	ND
Glucose 1-phosphate			
Sedoheptulose 1,7-diphosphate		ND	ND
Sedoheptulose 7-phosphate		ND	
UDP-glucose			

Key **FC**

Enriched in WT | Enriched in Mut

-100.0 -4.0 -2.5 -1.5 -1.2 1.2 1.5 2.5 4.0 100.0

Not significant (p-value > 0.05) ND Not detected

Sedoheptulose 7-phosphate was also not detected in the second experimental replicate and although depleted in the third experimental replicates, was not statistically significant. Erythrose 4-phosphate and glucose 1-phosphate were significantly depleted

and enriched respectively, in the second and third experimental replicate of LN18 Mut cells, despite no significant alteration of abundance in the first experiment. This could suggest increased storage of glucose as glycogen or increased glycolytic activity as a consequence of the IDH1 mutation, at a later passage number, but would require further experimental replicates and measurement of metabolic flux to confirm this hypothesis.

Despite the redox stress caused by enrichment of 2-HG, and probable enrichment of $NADP^+$ as a consequence of the IDH1 mutation, pentose phosphate pathway intermediate abundances were not consistently altered by the IDH1 mutation and therefore do not require further investigation.

5.2.3. Exploring the effect of the IDH1 mutation on the abundance of metabolites with amine functional groups

As discussed in Sections 4.10 and 4.11, and shown in Table 5.3, lysine and tryptophan degradation products were consistently depleted in LN18 Mut cells across multiple experimental replicates. The identification of N-formyl kynurenine by non-derivatised RP-MS/MS analysis, in the first and third experimental replicate, provided increased confidence that tryptophan degradation was consistently altered in the presence of the IDH1 mutation, as discussed in Section 4.12. The lysine degradation product 2-oxoadipate was also consistently depleted in experimental replicates of LN18 Mut cells, consistent with the depletion of 2-aminoadipate and saccharopine (discussed in Section 4.12). Glutamine and glutamate metabolism was also perturbed as a result of the IDH1 mutation, as shown in Table 5.3.

Table 5.3: Heat map showing FC and significance for selected metabolites with amine functional groups, from experimental replicates of LN18 Mut and WT cells cultured under 4.5 g / L glucose conditions (Section 8.14), analysed by IC-MS/MS (Section 8.4), derivatised RP-MS (Section 8.7) and non-derivatised RP-MS/MS (Section 8.9).

	Experimental replicate		
Identified metabolite	**1**	**2**	**3**
2-aminoadipate			
2-oxoadipate			
β-citryl glutamate			
Glucosamine 6-phosphate			ND
Glutamate			
Glutamine			
Glutathione			
Kynurenine			
Lysine			
N-formyl kynurenine		ND	
Saccharopine			
Tryptophan			

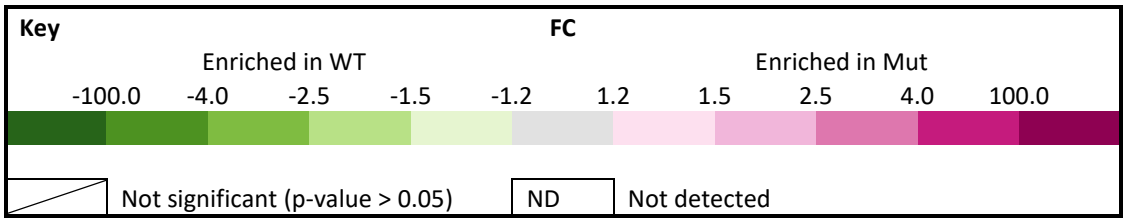

β-citryl glutamate was consistently depleted in all experimental replicates of LN18 Mut cells, despite variation in glutamine and glutamate abundance, which suggests that β-citryl glutamate abundance was correlated with the depletion of 2-OG, enrichment of 2-HG, or a combination of both. The different abundances of glutamate and glutamine across the experimental replicates could be caused by variation in the concentration of glutamine, supplemented in the media, or depletion of the extracellular pool over time. The increase in glutathione enrichment in LN18 Mut cells at later passage numbers may have been in response to increased redox stress caused by the IDH1 mutation over time, or the increased contribution of ATP to the nucleotide pool in Mut cells, as discussed in Section 3.3.

5.2.4. Pathway visualisation of metabolite abundances in LN18 IDH1 mutant and wild-type glioblastoma cells

Visualisation of metabolomics data is a challenge due to the large number of compound-features detected, and metabolite identifications made, using untargeted approaches. Tabulated heat maps can be used to show changes in compound-features between experimental groups, but do not show the biochemical relationship between metabolites. Pathways analysis allows mapping of alterations of metabolite abundance, revealed by comparison of experimental groups, onto known metabolic relationships but does not normally display changes to individual metabolites. Typically, topological and over-enrichment analyses are used to demonstrate the overall effect of metabolic differences between experimental groups.[166, 218] Further analysis of the datasets containing identified metabolites is therefore normally required, to find the specific points within metabolic pathways, which have been perturbed.

An approach to combine and visualise the data from multiple LC-MS methods was developed to aid the interpretation of the metabolic effects of the IDH1 mutation. Pictorial representations of metabolic pathways were prepared in Excel (Microsoft, Redmond, WA, USA), based on the KEGG human metabolic pathway database.[167] These pathway heat maps show FC using a colour scheme, to visualise the metabolic pathways which were altered between experimental groups, and individual metabolites are annotated with p-values, obtained from t-tests. A Visual Basic for Applications (VBA) program was written to automate some of the heat mapping process. To allow tabulated data entry, the pathway heat maps were prepared in Excel and the first tab of the spreadsheet was used to input the data, for each identified metabolite, obtained from

statistical analysis in Progenesis QI (Section 8.12). A blank Excel template is found in electronic supplementary material (ESM) A, to allow pathway heat maps to be generated. VLOOKUP functions were used to obtain the FC and significance values for each metabolite in a dataset and two VBA macros were used to identify significant metabolites, and then colour boxes based on a user adjustable FC scale. The first VBA macro (Sub Significance(), commentary listed alongside code denoted with ‘) coloured the metabolite boxes and text based on p-value and coefficient of variation (CV) to allow the user to annotate the metabolites based on their significance (*, p-value less than 0.05; **, p-value less than 0.01; ***, p-value less than 0.001 and ^, CV less than 35 %).

```
Sub Significance()
    Dim i As Integer
'Started at row 2 to ignore header row
    i = 2
'Continued loop until HMDB code field was empty
    Do While Sheet1.Cells(i, 6).Value <> ""
'Copied HMDB code from active line to cell labelled "ID"
    Range("ID").Value = Range("Sheet1!F" & i).Value
'Selects a shape with the HMDB code in "ID" and ignored error if a shape with the
HMDB code was not found
    On Error Resume Next
    ActiveSheet.Shapes(Range("ID").Value).Select
    On Error Resume Next
'Set shape background colour from a VLOOKUP function to allow user to label
metabolites which were significantly modified
    Selection.ShapeRange.Fill.ForeColor.RGB =
    Range(Range("PValueColour").Value).Interior.Color
'Set shape text colour from a VLOOKUP function to allow user to label metabolites
which had CV < 35 %
    Selection.ShapeRange.TextFrame.Characters.Font.Color =
    Range(Range("CValueColour").Value).Font.Color
'Selected cell A1 to avoid changing previous shape if HMDB code was not found
    Range("A1").Select
'Added 1 to count to select the next row in the subsequent loop
    i = i + 1
    Loop
    Range("A1").Select
'Displayed a popup which advised the user of the colour scheme used for
significance
```

```
        MsgBox "Black shading = *" & vbNewLine & "Dark blue shading = **" &
        vbNewLine & "Light blue shading = ***" & vbNewLine & "Orange text = ^"
        End Sub
```

The second VBA macro (Sub Shading(), commentary listed alongside code denoted with ‘) coloured the metabolite boxes and text based on their FC value, overwriting any previous colouring from Sub Significance().

```
        Sub Shading()
        Dim i As Integer
‘Started at row 2 to ignore header row
        i = 2
‘Continued loop until HMDB code field was empty
        Do While Sheet1.Cells(i, 6).Value <> ""
‘Copied HMDB code from active line to cell labelled “ID”
        Range("ID").Value = Range("Sheet1!F" & i).Value
‘Selected a shape with the HMDB code in “ID” and ignored error if a shape with the
HMDB code was not found
        On Error Resume Next
        ActiveSheet.Shapes(Range("ID").Value).Select
        On Error Resume Next
‘Set shape background colour from a VLOOKUP function which compared
metabolite FC with a user adjustable FC scale
        Selection.ShapeRange.Fill.ForeColor.RGB =
        Range(Range("Colour").Value).Interior.Color
‘Set shape text colour to improve contrast with dark background colours
        Selection.ShapeRange.TextFrame.Characters.Font.Color =
        Range(Range("Colour").Value).Font.Color
‘Selected cell A1 to avoid changing the previous shape if HMDB code was not
found
        Range("A1").Select
‘Added 1 to count to select the next row in the subsequent loop
        i = i + 1
        Loop
        Range("A1").Select
‘Displayed a popup which advised the user that shading of the heat map was
complete
        MsgBox "Done"
        End Sub
```

The VBA macros allowed semi-automated preparation of pathway heat maps which provided useful visualisation of annotated data in a biological context, as a starting point for functional interpretation at the pathway level.

For LN18 Mut and WT cells cultured under 4.5 g / L glucose conditions (experimental replicate 1, Section 8.14) a total of 355 metabolites were identified across the 3 LC-MS methods (IC-MS/MS, 226; derivatised RP-MS, 79; and non-derivatised RP-MS/MS, 50). The pathway heat map for lysine metabolism (Fig. 5.4), showed depletion of a number of consecutive degradation products (saccharopine, 2-aminoadipate and 2-oxoadipate) in LN18 Mut cells, as discussed in Sections 3.3 and 4.10. Depletion of lysine degradation pathway products suggested reduced activity of the 2-OG dependent enzyme α-aminoadipic semialdehyde synthase, as discussed in Section 4.12.

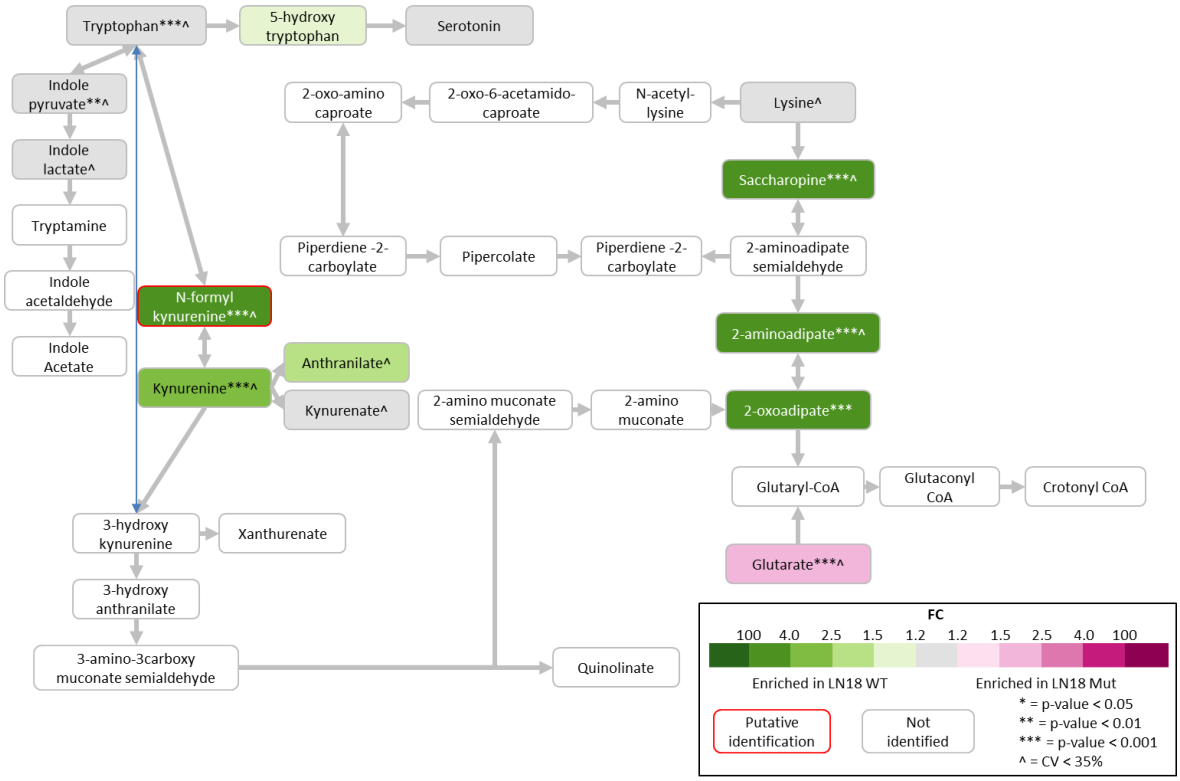

Figure 5.4: Pathway heat map of tryptophan and lysine degradation pathways for the analysis of LN18 Mut and WT cells cultured under 4.5 g / L glucose conditions (experimental replicate 1, Section 8.14), analysed by IC-MS/MS (Section 8.4), derivatised RP-MS (Section 8.7) and non-derivatised RP-MS/MS (Section 8.9).

Although glutarate was enriched in LN18 Mut cells, in the first experimental replicate (Fig. 5.4), no significant alteration of abundance was observed in subsequent experimental replicates. The depletion of lysine degradation metabolites may therefore

cause downstream depletion of glutaryl CoA and other CoA metabolites. The pathway heat map (Fig. 5.4), did not reveal any additional significantly altered metabolites in tryptophan metabolism beyond those already discussed. The absence of significantly altered tryptophan degradation products implied that only the kynurenine pathway was altered in the presence of the IDH1 mutation.

Glutamine, glutamate and related metabolites were also significantly depleted in LN18 Mut cells, with the exception of 4-amino butyrate which was enriched, as shown in Fig. 5.5.

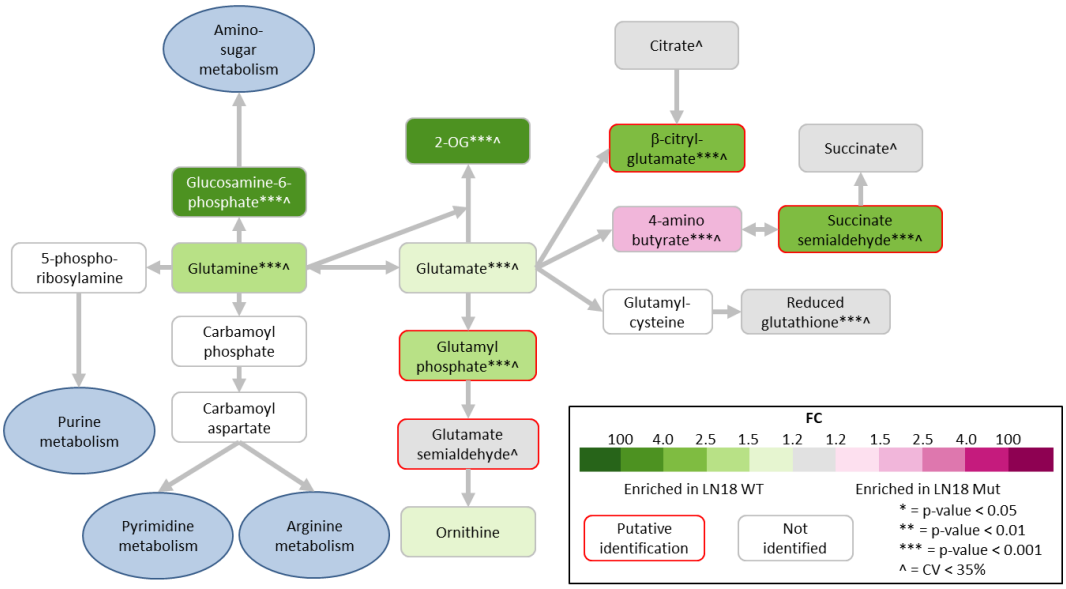

Figure 5.5: Pathway heat map of glutamine and glutamate metabolism for the analysis of LN18 Mut and WT cells cultured under 4.5 g / L glucose conditions (experimental replicate 1, Section 8.14), analysed by IC-MS/MS (Section 8.4), derivatised RP-MS (Section 8.7) and non-derivatised RP-MS/MS (Section 8.9).

Pathways analysis revealed that glucosamine 6-phosphate and glutamyl phosphate were depleted in LN18 Mut cells, in addition to the depletion of 2-OG and β-citryl glutamate, which were discussed in Section 3.3. Glucosamine 6-phosphate was also significantly depleted in the second experimental replicate of LN18 cells, but was not detected in the third experimental replicate, as shown in Table 5.3. Glucosamine 6-phosphate is

produced by glucosamine 6-phosphate synthase (an aminotransferase), from glutamine, and is a key metabolite in the production of glycoproteins, utilising amino sugar metabolism.[219] The dependence on nucleotides for multiple amino sugar metabolic pathways, may therefore explain the modification of nucleotide metabolism, discussed in Section 3.7, caused by a deficit of biosynthetic precursors in LN18 Mut cells. This hypothesis could be confirmed using saccharide specific chromatographic methods and metabolic flux analysis. The depletion of glucosamine 6-phosphate provides further evidence for the modification of transaminase enzymes, in the presence of an IDH1 mutation, which are regulated by both glutamate and 2-OG. 2-HG may also inhibit 2-OG dependent transaminases, which has previously been observed for branched-chain amino acid aminotransferases.[220, 221]

The consistent depletion of β-citryl glutamate, irrespective of the variation in abundance of citrate and glutamate, across multiple experimental replicates, suggested that the IDH1 mutation is linked to β-citryl glutamate abundance, likely as a result of alterations in 2-HG concentration, as discussed in Section 3.7. As β-citryl glutamate abundance has previously only been observed to alter during early brain development, the IDH1 mutation may cause regulation of dormant biosynthetic pathways, as a method of tumourigenesis, or could be a selective modification of cellular environment to favour Mut cells.[185] The role and source of β-citryl glutamate therefore requires additional biochemical investigation.

These observations indicate the that primary metabolic impact of the IDH1 mutation in LN18 cells, identified from the LC-MS analysis methods used here, was the depletion of metabolites with amine functional groups. The cause of this depletion however is not

revealed by the analysis of Mut and WT cells and requires investigation of the effect that 2-OG and 2-HG concentration has on metabolites with amine functional groups.

5.3. Investigation of cell line specific effects of the IDH1 mutation

To evaluate whether the alterations in metabolite abundance, observed for the analysis of LN18 cells (Section 5.2), were due to the IDH1 mutation or cell line specific effects, additional Mut and WT cell lines were analysed. U87-MG and 293T cells were cultured under the same conditions as the LN18 cells (Section 8.14) and analysed by multiple LC-MS methods. The identified metabolites from derivatised RP-MS and non-derivatised RP-MS/MS analyses were compiled with the data acquired using IC-MS/MS (Sections 3.3, 3.5 and 3.6). The data associated with these experiments has been deposited in the Oxford University Research Archive and is freely accessible (Metabolomics of U87-MG IDH wild-type and mutant cells, https://doi.org/10.5287/bodleian:nZZ0abQzr and Metabolomics of 293T IDH wild-type and mutant cells, https://doi.org/10.5287/bodleian:BRY9rwZRR). The compiled datasets were used to confirm whether metabolite abundances were consistently altered by the IDH1 mutation and to identify whether the depletion of metabolites with amine functional groups, observed in LN18 Mut cells, was cell line independent.

U87-MG Mut and WT cells, with 9 biological replicates in each experimental group (Section 8.15), were analysed by IC-MS/MS (Section 8.4), derivatised RP-IMS-MS/MS (Section 8.8), and non-derivatised RP-MS/MS (Section 8.10). A total of 210 metabolites (listed in Section 10.6) were identified in the U87-MG cells, across the LC-MS methods. Data were processed and metabolites identified as described in Section 8.12. 293T Mut and WT cells, with 5 biological replicates in each experimental

group (Section 8.16), were analysed by IC-MS/MS (Section 8.4), derivatised RP-MS (Section 8.7), and non-derivatised RP-MS/MS (Section 8.9). Fewer metabolites were identified overall for analysis of the 293T cell line (200, listed in Section 10.7), compared with the glioblastoma-derived cell lines. The smaller number of metabolite identifications, for the 293T cell line, was possibly due to a lower number of cells, correlated with a lower mean DNA concentration (76.9 ng / μL), compared with the LN18 (90.9 ng / μL) and U87-MG (201.0 ng / μL) cell extracts. The lower number of cells could have been caused by the difference in adherence, between the cell lines, as the 293T cells were only partially adherent and therefore some cells were lost when then cell layer was washed with PBS, prior to metabolite extraction. The PCA scores plots (not shown) of compound-feature abundances, for derivatised RP-MS and non-derivatised RP-MS/MS analysis of U87-MG and 293T cells demonstrated separation of experimental groups in principal component space and all biological replicates within 95 % confidence regions. Datasets of identified metabolites from multiple LC-MS methods were then compiled and analysed using heat maps to confirm further investigate the relationship between the IDH1 mutation and the observed metabolic changes, particularly in the non-glioblastoma-derived cell line.

5.3.1. Exploring the effect of the IDH1 mutation on glycolysis and TCA cycle metabolite abundances in multiple cell lines

As discussed in Section 3.7, although 2-HG was enriched in all 3 cell lines, the enrichment of 2-HG in 293T Mut cells was lower than the glioblastoma-derived cell lines and 2-OG was not significantly depleted, as shown in Table 5.4. Therefore, in 293T Mut cells, any metabolic effects which were also observed in the other cell lines, would suggest that

these pathways were sensitive to the enrichment of 2-HG, or another metabolic effect of the IDH1 mutation, as they could not be caused by the depletion of 2-OG.

Table 5.4: Heat map showing FC and significance for selected central carbon metabolites from LN18 (experimental replicate 1, Section 8.14), U87-MG (Section 8.15) and 293T (Section 8.16), Mut and WT cells cultured under 4.5 g / L glucose conditions.

Identified metabolite	LN18	U87-MG	293T
2-HG			
2-OG			
Cis-aconitate			
Citrate			
Fumarate		ND	
Lactate			
Malate			
Phosphoenolpyruvate			
Pyruvate			
Succinate		ND	

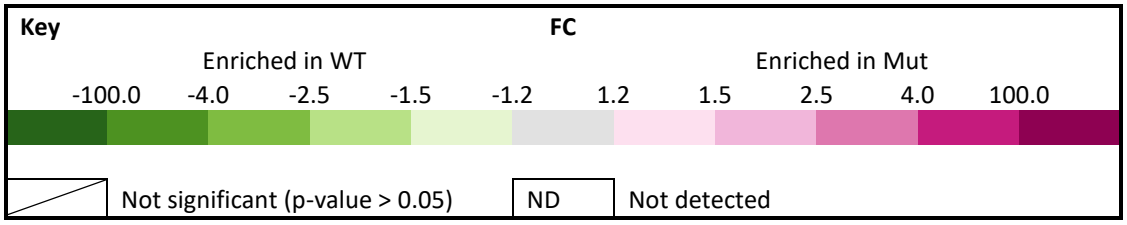

The abundance of TCA cycle metabolites, with the exception of malate (which was enriched in 293T Mut cells), were not significantly altered in all 3 cell lines, as observed for the experimental replicates of LN18 cells. This confirmed that the IDH1 mutation did not disrupt the TCA cycle, irrespective of 2-OG depletion, contrary to observations made by Reitman *et al*.[133] The depletion of phosphoenolpyruvate was only observed in the glioblastoma-derived cell lines and was indicative of increased glycolytic activity, as discussed in Section 3.7. The difference in glucose utilisation and energy metabolism based on cell type and origin was substantiated by the enrichment of fructose 6-phosphate and glucose 1-phosphate in 293T Mut cells, consistent with increased anaplerosis and reduced glycolytic activity.

5.3.2. Exploring the effect of the IDH1 mutation on the abundance of metabolites with amine functional groups in multiple cell lines

The dissimilarity between the glioblastoma-derived cell lines, for the abundance of tryptophan degradation products, is shown in Table 5.5, with an enrichment of kynurenine and tryptophan in U87-MG Mut cells, contrary to the depletion observed in LN18 Mut cells. Kynurenine and tryptophan were also significantly enriched in 293T Mut cells, suggesting that the effect on tryptophan degradation was cell line specific. The differential effect of the IDH1 mutation on kynurenine abundance, based on cellular origin, may account for the variable outcomes of immunotherapeutic treatment of IDH mutant tumours.[222]

Table 5.5: Heat map showing FC and significance for selected metabolites with amine functional groups, from LN18 (experimental replicate 1, Section 8.14), U87-MG (Section 8.15) and 293T (Section 8.16), Mut and WT cells cultured under 4.5 g / L glucose conditions.

Identified metabolite	LN18	U87-MG	293T
2-aminoadipate			
2-oxoadipate			
β-citryl glutamate			
Glucosamine 6-phosphate		ND	ND
Glutamate			
Glutamine			
Glutathione			
Kynurenine			
Lysine			
N-formyl kynurenine		ND	ND
Saccharopine		ND	ND
Tryptophan			

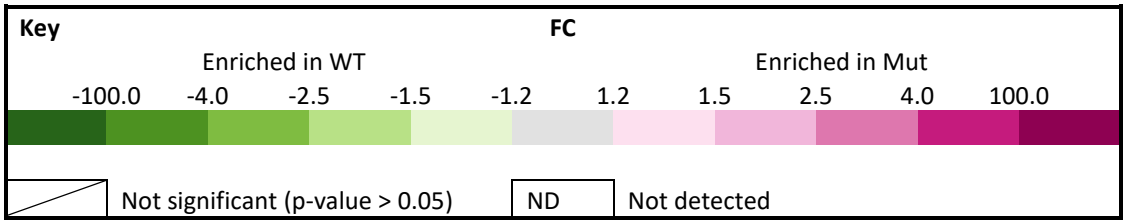

The depletion of 2-aminoadipate was observed in U87-MG Mut cells, in agreement with the depletion of lysine degradation products in LN18 cells; however, saccharopine was

not detected in either U87-MG or 293T cells. 2-oxoadipate was consistently depleted in all 3 cell lines, correlating directly with the IDH1 mutation. The variation in 2-aminoadipate abundance, across the 3 cell lines, may be related with the abundance of 2-OG, as suggested in Section 4.12; however, the 2-OG dependent lysine degradation enzyme, α-aminoadipic semialdehyde synthase may also be inhibited by 2-HG. The consistent depletion of 2-oxoadipate, in all 3 Mut cell lines, may suggest that muconate metabolites, which link tryptophan and lysine metabolism, were modified in the presence of the IDH1 mutation. For example, 2-aminomuconate is converted to 2-oxoadipate via various NADH and NADPH dependent oxidoreductases, which may be inhibited by the redox imbalance typically observed in IDH Mut cells.[42, 167]

Although glutamate was consistently observed to be significantly depleted across the 3 Mut cell lines, as shown in Table 5.5, it was not replicated in the experimental replicates of LN18 cells and was likely related with the abundance of glutamine in the media, which could have varied between different stock solutions of cell culture media. Glutathione, although not significantly depleted in LN18 cells, was depleted in U87-MG and 293T cells, consistent with the depletion of glutamate, providing further evidence for different energy pathway (or redox metabolism) activity for each of the cell lines. β-citryl glutamate was consistently depleted in IDH Mut cells in experimental replicates and different Mut cell lines, indicating a correlation with the IDH1 mutation and was therefore a prospective biomarker.

5.4. Discussion of the effect of the IDH1 mutation on metabolite abundances in multiple cell lines

RP-MS/MS was used, without sample derivatisation, to identify low and medium polarity metabolites in LN18 cells which were not characterised by IC-MS/MS or derivatised RP-MS analysis. Some highly polar metabolites such as NAAG, N-acetylglutamate and 2-oxoadipate, observed from IC-MS/MS analysis in Chapter 3, were also detected by non-derivatised RP-MS/MS and their identifications confirmed by comparison with authentic metabolite standards. Similar alterations in abundance were observed for these metabolites in both analyses, providing increased confidence that these specific metabolites were enriched and depleted in Mut cells and not an artefact of IC-MS/MS analysis.

The putative identification of N-formyl kynurenine provided further evidence for the depletion of tryptophan degradation products in LN18 Mut cells, consistent with the depletion of kynurenine, discussed in Section 4.12. As N-formyl kynurenine is the direct catabolic product of tryptophan, by the enzymes TDO and IDO, it is likely that the IDH1 mutation caused modulation of this pathway in LN18 cells.[214, 223] As a significant enrichment of kynurenine was observed in U87-MG and 293T Mut cells, the immunosuppressive effect of kynurenine in IDH WT glioma, proposed in Section 4.12, may therefore be dependent on the location of a tumour and cell type. Although immunosuppression has been studied in other diseases which exhibit an IDH mutation, such as acute myeloid leukaemia, variable results have been observed for immunotherapeutic treatment of glioma based on mutation status and neomorphic function.[224-226] Metabolic activity associated with an IDH1 mutation, may be

immunosuppressive in LN18 cells but genetic disposition for immunosuppression has previously been reported for IDH WT glioma, in accordance with the effects observed for the other cell lines.[227] Correlation analysis of kynurenine abundance in glioma (with and without an IDH mutation) and response to immunotherapeutic treatment, may be of clinical interest to further investigate the cell line specific effects and variable survival outcomes.

Variation in the abundance of lysine degradation products were also consistently observed across the different cell lines as 2-aminoadipate abundance was not significantly altered in 293T Mut and WT cells. The depletion of 2-aminoadipate correlated with the depletion of 2-OG, in LN18 and U87-MG Mut cells, and consequently the relationship between 2-OG concentration and amino acid degradation will be investigated (Chapter 6).

Glutathione, was significantly depleted in U87-MG and 293T Mut cells but not in LN18 cells. The depletion of glutathione was consistent with an intracellular limitation of NADPH (which was not measured by the LC-MS methods used here), providing further evidence that redox metabolism differs between the cell lines. Reduction of glutathione, from the disulphide state, by glutathione reductase, requires NADPH and therefore alteration of redox metabolism (as a result of the production of 2-HG) could account for the depletion of glutathione.[228] The LN18 cells may therefore be more resistant to changes in redox state, have a larger intracellular pool of NADPH, or a combination of both.

The abundance of TCA cycle and glycolytic metabolites were not consistently altered across multiple experimental replicates, or different cell lines. The changes discussed in Section 3.7, may therefore have been caused by temporal variations in metabolite

abundance, or the depletion of supplemented metabolites in the cell culture media over time.[217] The IDH1 mutation was therefore unlikely to disrupt the abundance of TCA cycle metabolites, irrespective of the depletion of 2-OG, despite the depletion of fumarate and malate in Mut cells, previously reported by Reitman *et al*.[133] Any change in TCA cycle enzyme activity, as a response to the depletion of 2-OG in LN18 and U87-MG Mut cells, was not measured and investigation would require metabolic flux measurements.

β-citryl glutamate was consistently depleted in all 3 Mut cell lines, irrespective of the abundance of glutamine, glutamate and 2-OG.The potential role of β-citryl glutamate as an activator of mitochondrial aconitase (discussed in Section 3.7) and the consistent depletion, which was negatively correlated with the abundance of 2-HG, is therefore of interest, and will be investigated further in Chapter 6.[188]

The specificity of the metabolic effects of the IDH1 mutation in different cell lines emphasises the importance of exploring the metabolic phenotype in multiple model systems. The investigation of metabolic changes in these systems also aided the identification of pathways which were consistently modified as a result of the IDH1 mutation.

5.5. Chapter summary

RP-MS/MS, without sample derivatisation, was used to provide an increased number of metabolite identifications, in the LN18, U87-MG and 293T lines, in addition to the datasets obtained in Chapters 3 and 4 from IC-MS/MS and derivatised RP-MS. Central carbon metabolites were not consistently altered as a result of the IDH1 mutation across cell lines and experimental replicates and the enrichment of pentose phosphate pathway

metabolites in 293T Mut cells was cell line specific. Heat map analysis visualised the difference in central carbon metabolism between the glioblastoma-derived cell lines and 293T cell line. This demonstrated the importance of cellular origin for a model system and the different effects observed based on the baseline metabolism of that cell line.

Amine-containing metabolite abundances were significantly altered as a result of the IDH1 mutation; however, the significant depletion of the kynurenine was only observed for experimental replicates of LN18 cells, as a significant enrichment was observed in U87-MG and 293T cells. The variation in kynurenine abundance, and consequent immunosuppressive effect, based on cellular origin was discussed and may account for the variable outcomes for immunotherapeutic treatment of tumours with an IDH mutation.[222] Lysine degradation products were also explored, across the cell lines, and although the significant depletion of 2-oxoadipate was consistently observed, variation in 2-aminoadipate abundance was associated with the abundance of 2-OG. A potential effect of the IDH1 mutation on redox metabolism was also discussed, which may account for the depletion of glutathione in U87-MG and 293T Mut cells. The depletion of β-citryl glutamate in Mut cells was consistently observed and was not associated with the abundance of glutamate or 2-OG, providing further evidence for inhibition by 2-HG (which was consistently enriched in Mut cells), or another metabolic consequence of the IDH1 mutation.

Chapter 6. Exploring the metabolic effects of altering 2-HG and 2-OG abundance in LN18 IDH1 mutant and wild-type glioblastoma cells

6.1. Introduction

Multiple metabolic pathways were modified in the presence of the IDH1 mutation, as discussed in Sections 3.7 and 5.4, and were correlated with the significant enrichment of 2-HG, which was consistent across the LN18, U87-MG and 293T cell lines studied here. For example, the depletion of β-citryl glutamate was negatively correlated with the abundance of 2-HG, suggesting that elevated intracellular 2-HG levels may directly lead to inhibition of β-citryl glutamate synthase or other non-2-OG dependent enzymes. The observed depletion of 2-OG, which is an essential metabolite for a range of metabolic processes such as transaminase, hydroxylase and oxygenase reactions, may also lead to depletion of dependent downstream metabolites, particularly in amino acid degradation pathways.[229-231]

To try and differentiate between elevated 2-HG and depleted 2-OG levels as causative factors the for metabolic differences observed between Mut and WT cells, the effect of elevated extracellular concentration of 2-HG was studied next. If the identified pathways were not 2-HG sensitive, then the depletion of 2-OG, or another effect of the IDH1 mutation, may be responsible for altering metabolite abundance. Treatment with 2-HG will also provide insight into potential tumourigenic effects that Mut cells may have, *in vivo*, on surrounding cells. The sensitivity of metabolic pathways to 2-OG concentration will also be investigated in WT cells and the potential use of 2-OG to restore metabolite abundances in Mut cells, will also be explored. The research aim of this chapter is to

establish whether observed alterations in metabolite abundance, in the presence of the ID1 mutation, are directly or indirectly associated with 2-HG and/or 2-OG abundance.

6.2. Treatment of LN18 wild-type glioblastoma cells with 2-HG

As discussed in Sections 3.7 and 5.2, various metabolites and pathways were significantly altered in LN18 Mut cells, for example β-citryl glutamate was consistently depleted in the analyses of multiple Mut cell lines. This may have been caused by competitive inhibition of 2-OG dependent enzymes, by 2-HG. To test this hypothesis, acute treatment with 2-HG was performed on LN18 WT cells.

LN18 WT cells were cultured in 4.5 g / L glucose DMEM and at 60 % confluency, the media was supplemented with 2-HG (10 mM) in DMSO (1 %) or vehicle control (1 % DMSO) for 24 hours before metabolite extraction, as described in Section 8.18. Samples were analysed by IC-MS/MS (Section 8.4), derivatised RP-MS (Section 8.7) and non-derivatised RP-MS/MS (Section 8.9), data were processed using the approach described in Section 8.12. The data associated with this experiment has been deposited in the Oxford University Research Archive (title: Metabolomics of 2-HG treated LN18 wild-type cells) and is freely accessible (https://doi.org/10.5287/bodleian:QR6NZeqO1). The abundance of 2-HG was increased 521-fold (p-value 6.59×10^{-14}) in the supplemented media, compared to control media and 2-HG was demonstrated to be cell permeable, as the intracellular abundance in treated LN18 WT cells was enriched 118-fold (p-value 5.84×10^{-12}), as shown in Fig. 6.1.

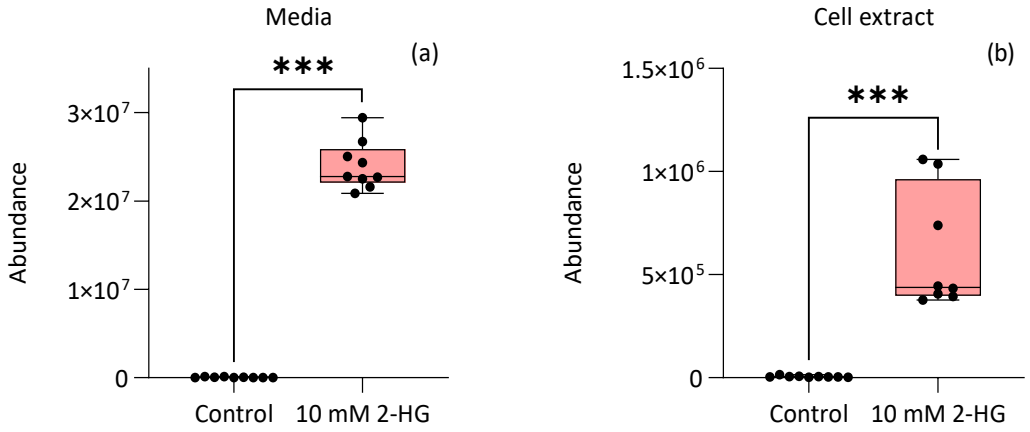

Figure 6.1: Box plots showing the abundance of 2-HG in media (a) and cell extracts (b) for LN18 WT cells cultured under 4.5 g / L glucose conditions, treated with 10 mM 2-HG or vehicle control for 24 hours (Section 8.18), analysed by IC-MS/MS (Section 8.4). The box plots show the mean, 25-75th percentiles and whiskers extend from the minimum to maximum values. The number of samples are denoted with dots and significance from t-tests are annotated (ns, p-value greater than 0.05; *, p-value less than 0.05; **, p-value less than 0.01; and ***, p-value less than 0.001).

6.2.1. Exploring the effect of 2-HG treatment on TCA cycle, glycolysis and pentose phosphate pathway metabolite abundances

Despite an over hundred-fold enrichment of 2-HG in LN18 WT cells, the abundance of metabolites in the TCA cycle, glycolysis and pentose phosphate pathway were generally not altered, as shown in Fig. 6.2. The abundance of 2-OG was also not significantly altered in 2-HG treated cells. Any alteration of metabolite abundance, in 2-OG dependent metabolic pathways, would therefore provide evidence for competitive inhibition of 2-OG dependent enzymes, by 2-HG.

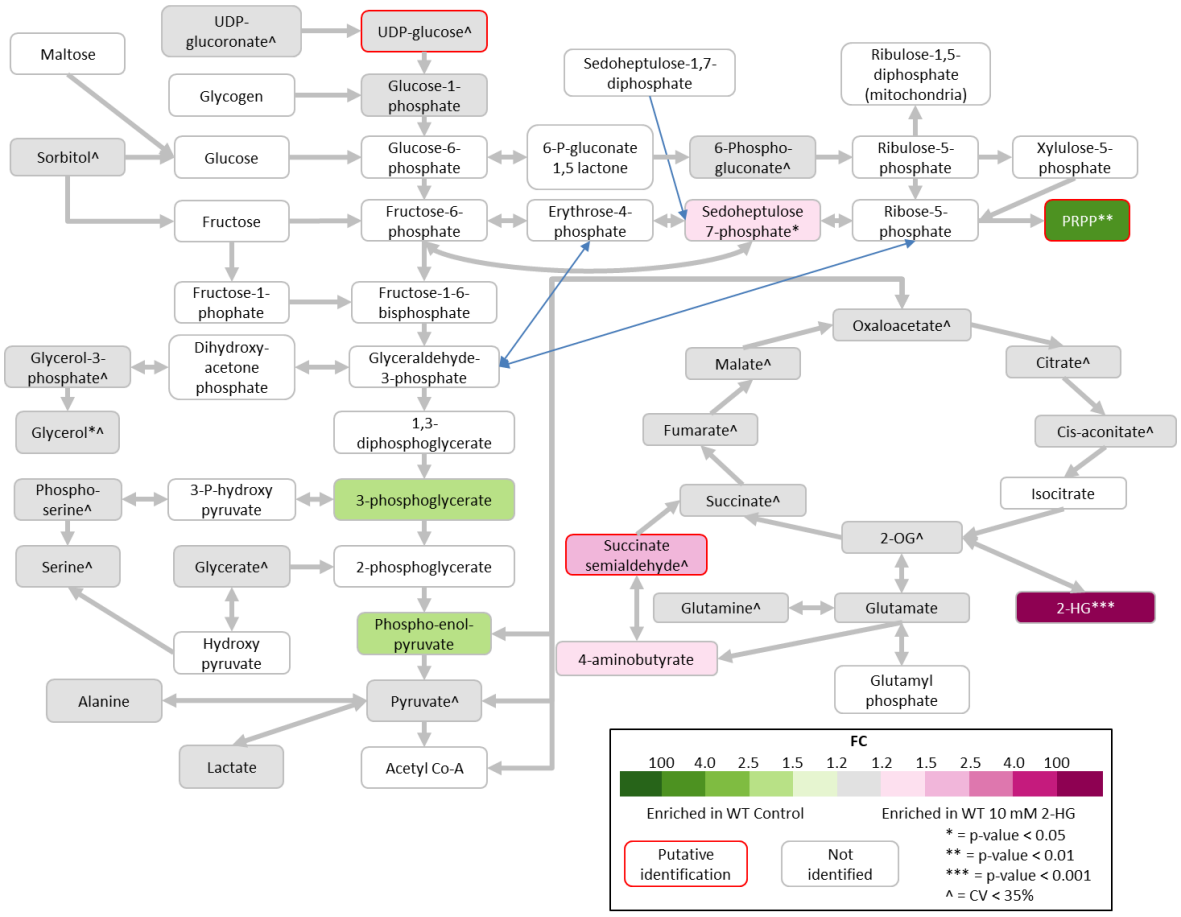

Figure 6.2: Pathway heat map of the TCA cycle, glycolysis and pentose phosphate pathway for the analysis of LN18 WT cells cultured under 4.5 g / L glucose conditions, treated with 10 mM 2-HG or vehicle control for 24 hours (Section 8.18), analysed by IC-MS/MS (Section 8.4), derivatised RP-MS (Section 8.7) and non-derivatised RP-MS/MS (Section 8.9).

Although 3-phosphophoglyerate (FC 1.65) and phosphoenolpyruvate (FC 1.80) were depleted in LN18 WT cells treated with 2-HG (and in LN18 Mut cells), neither depletion was significant, due to high CV (49.9 % and 109 %). The measurements may not have been significant due to the high CV for 2-HG (47.9 %), corresponding to variation in intracellular concentration of 2-HG in the LN18 WT cells. Consequently any inhibitory effects of 2-HG would also result in increased CV for any altered metabolites. CV was less than 35 % for the majority of identified metabolites (122 of 167, all CV data are found in the ESM). Analytical variation was therefore assumed to be low and that the any increased variation was only for the metabolites which had their abundance altered as a result of treatment with 2-HG.

Coverage of pentose phosphate pathway metabolites was poor, however, sedoheptulose 7-phosphate was significantly depleted by 1.49-fold (p-value $3.82x10^{-2}$), suggesting an inhibitory effect of 2-HG. Phosphoribosyl pyrophosphate (PRPP) was significantly depleted in 2-HG treated LN18 WT cells by 4.41-fold (p-value $3.39x10^{-3}$), possibly caused by inhibition of PRPP synthase (or transketolase A or B), which would also account for the enrichment of sedoheptulose 7-phosphate. The enrichment of sedoheptulose 7-phosphate may also be caused by the non-enzymatic reduction of 2-HG and corresponding enrichment of the redox cofactor NADH, compared to NAD^+.[232]

6.2.2. Exploring the effect of 2-HG treatment on tryptophan and lysine degradation product abundances

No significant effect on the abundance of tryptophan and lysine degradation products was observed, with the exception of the depletion of glutarate, as shown in Fig. 6.3.

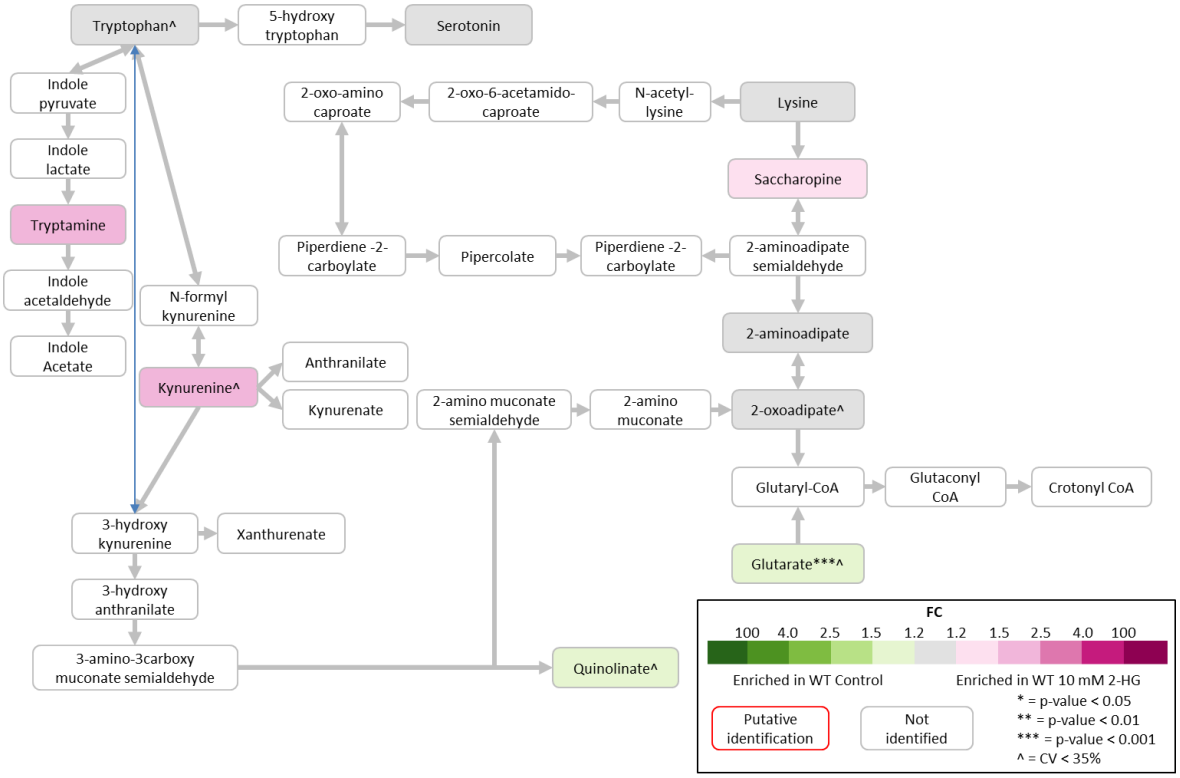

Figure 6.3: Pathway heat map of the tryptophan and lysine degradation pathways for the analysis of LN18 WT cells cultured under 4.5 g / L glucose conditions, treated with 10 mM 2-HG or vehicle control for 24 hours (Section 8.18), analysed by IC-MS/MS (Section 8.4), derivatised RP-MS (Section 8.7) and non-derivatised RP-MS/MS (Section 8.9).

Kynurenine and saccharopine were both enriched, in 2-HG treated LN18 WT cells, by 1.57-fold and 1.45-fold respectively, but neither FC was significant. The depletion of tryptophan and lysine degradation products in LN18 Mut cells, discussed in Section 4.12, seems to be more likely caused by the depletion of 2-OG (or another metabolic consequence of the IDH1 mutation), rather than the enrichment of 2-HG. Glutarate was significantly depleted in 2-HG treated LN18 WT cells by 1.37-fold (p-value 1.44×10^{-4}) contrary to the enrichment observed in Section 3.3, for LN18 Mut cells. The potential alteration of muconate metabolites, discussed in Section 5.2, was therefore also likely to be related to another metabolic effect of the IDH1 mutation, such as the imbalance of redox cofactors, instead of the enrichment of 2-HG.

6.2.3. Exploring the effect of 2-HG treatment on glutamine and glutamate -derived metabolite abundances

Glutamine and glutamate metabolite abundances were also not significantly altered, with the exception of succinate semialdehyde which was enriched 1.69-fold (p-value 1.96×10^{-5}), in 2-HG treated LN18 WT cells, as shown in Fig. 6.4.

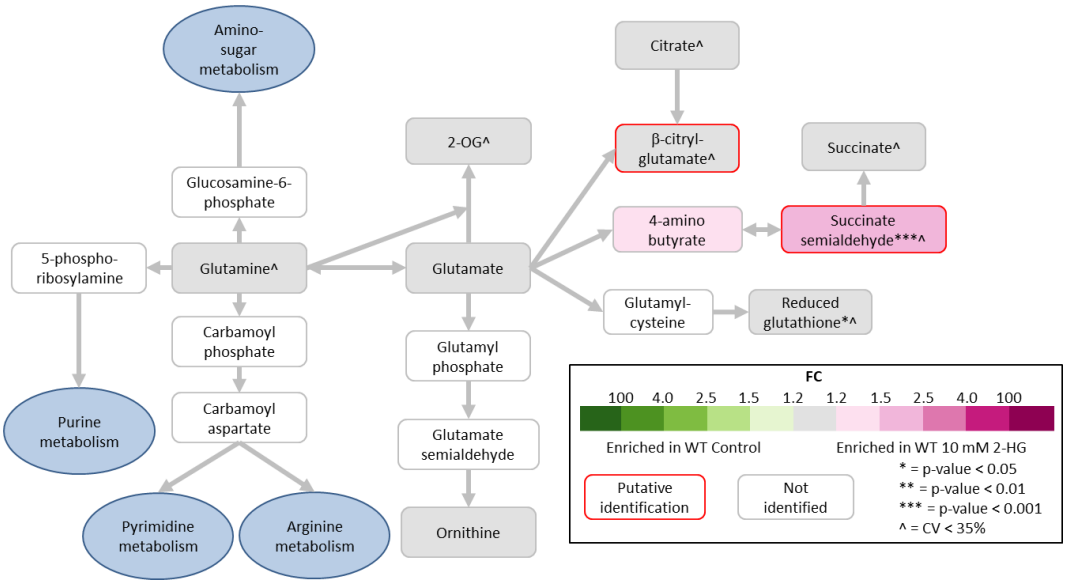

Figure 6.4: Pathway heat map of glutamine and glutamate metabolism for the analysis of LN18 WT cells cultured under 4.5 g / L glucose conditions, treated with 10 mM 2-HG or vehicle control for 24 hours (Section 8.18), analysed by IC-MS/MS (Section 8.4), derivatised RP-MS (Section 8.7) and non-derivatised RP-MS/MS (Section 8.9).

The depletion of β-citryl glutamate, observed in LN18 Mut cells (Sections 3.3 and 5.2), was therefore unlikely to be caused by a regulatory effect of 2-HG, despite the association with 2-HG concentration discussed in Section 5.3. NAAG was significantly depleted in 2-HG treated LN18 WT cells by 1.20-fold (p-value 2.90×10^{-2}), which was consistent with the observations by Reitman *et al.* in 2-HG treated oligodendroglioma-derived cells.[133] The inhibitory effect of 2-HG on specific enzymes was therefore unlikely to be the predominant metabolic influence in Mut cells.

In summary, treatment with 2-HG was not observed to have a significant effect on the abundance of metabolites in glycolysis or the TCA cycle, although some pentose phosphate pathway intermediates were significantly altered. No significant effect was observed on the abundance of metabolites with amine functional groups, with the exception of glutarate and NAAG which were significantly depleted in 2-HG treated LN18 WT cells. 2-HG therefore could have caused depletion of glutamate and glutamine-derived metabolites as a result of cooperative inhibition in Mut cells, but was not likely to be the primary factor. Despite lower significance, the conclusions drawn from those experiments was that metabolic pathways were not altered in LN18 Mut cells as a direct result of the enrichment of 2-HG, and therefore the relationship between intracellular concentrations of 2-OG and these pathways was investigated next.

6.3. Treatment of LN18 IDH1 mutant and wild-type glioblastoma cells with 2-OG

Extracellular treatment of LN18 Mut cells with 2-OG was investigated to evaluate whether the depletion of metabolite abundances, observed with the IDH1 mutation, could be recovered. Of particular interest was the consistent depletion of β-citryl glutamate which was observed in all Mut cell lines, but not depleted in LN18 WT cells with treated with 2-HG. 2-OG dependent enzymes, such as α-aminoadipic semialdehyde synthase (discussed in Section 4.12), may have reduced activity in Mut cells as a result of the depletion of 2-OG. The relationship between the abundance of 2-amioadipate (and other metabolites with amine functional groups) and 2-OG levels in LN18 Mut and WT cells, was therefore explored to assess the sensitivity of amino acid degradation pathways to 2-OG concentration.

LN18 Mut and WT cells were cultured in 4.5 g / L glucose DMEM and at 60 % confluency, the media was supplemented with 2-OG (10 mM) in DMSO (1 %) or vehicle control (1 % DMSO) for 24 hours before metabolite extraction, as described in Section 8.18. Samples were analysed by IC-MS/MS (Section 8.4), derivatised RP-MS (Section 8.7) and non-derivatised RP-MS/MS (Section 8.9), data were processed as described in Section 8.12. The data associated with this experiment has been deposited in the Oxford University Research Archive (title: Metabolomics of 2-OG treated LN18 IDH wild-type and mutant cells) and is freely accessible (https://doi.org/10.5287/bodleian:w4rd6d2D6). As observed for extracellular treatment of 2-HG (Section 6.2), 2-OG was cell permeable and was significantly enriched in LN18 Mut and WT cells by 58.2-fold (p-value 6.29×10^{-14}) and 29.4-fold (p-value 2.33×10^{-15}) respectively, as shown in Fig. 6.5.

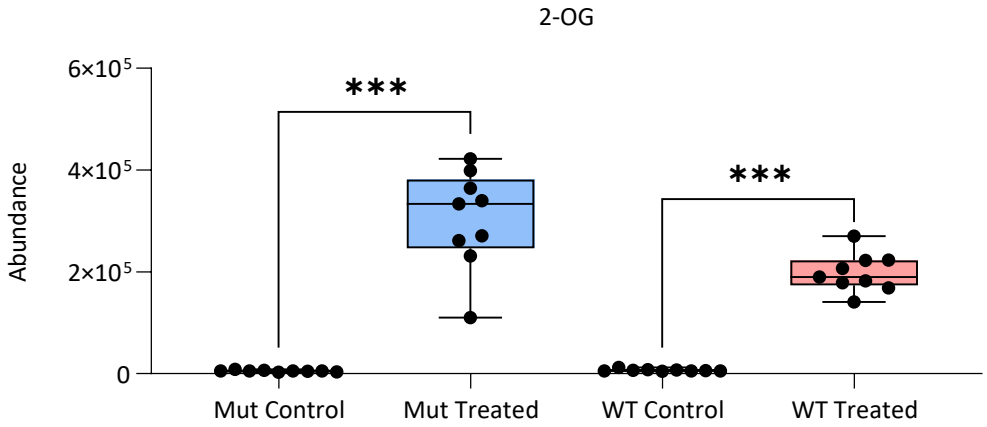

Figure 6.5: Box plots showing the abundance of 2-OG in LN18 Mut and WT cells cultured under 4.5 g / L glucose conditions, treated with 10 mM 2-OG or vehicle control for 24 hours (Section 8.18), analysed by IC-MS/MS (Section 8.4). The box plots show the mean, 25-75th percentiles and whiskers extend from the minimum to maximum values. The number of samples are denoted with dots and significance from t-tests are annotated (ns, p-value greater than 0.05; *, p-value less than 0.05; **, p-value less than 0.01; and ***, p-value less than 0.001).

The variability in ion abundance for 2-OG, was lower than observed for 2-HG in treated LN18 WT cells (Section 6.2), with a CV of 30.4 % for Mut cells and 18.9 % for WT cells. The

decrease in CV suggested that transport of 2-OG across the LN18 cell membrane was more efficient than the transport of 2-HG, possibly facilitated by active transport mechanisms for TCA cycle intermediates, which have previously been observed in neuronal cells.[233] The enrichment of 2-OG was higher in LN18 Mut cells (Fig. 6.5(a)) compared with WT cells (Fig. 6.5(b)), despite treatment with the same initial concentration, suggesting an increased transport rate of 2-OG into Mut cells or increased membrane permeability. The intracellular concentration of 2-OG in treated LN18 Mut cells was higher than the concentration observed in WT control cells (Fig. 6.5) and was therefore sufficient to counteract any metabolic effects caused by the depletion of 2-OG in Mut cells. The increased intracellular concentration of 2-OG could therefore be used to assess the sensitivity of the pathways identified to be altered in Mut cells, to 2-OG and potentially distinguish opposite alterations of metabolite abundance.

6.3.1. Exploring the effect of 2-OG treatment on TCA cycle, glycolysis and pentose phosphate pathway metabolite abundances

Although no consistent alterations of central carbon metabolite abundances were observed between Mut and WT cells across multiple cell lines (discussed in Section 5.3), treatment of LN18 Mut cells with 2-OG caused significant enrichment for the majority of metabolites in the TCA cycle, glycolysis and the pentose phosphate for the LN18 Mut cells, as shown in Fig. 6.6.

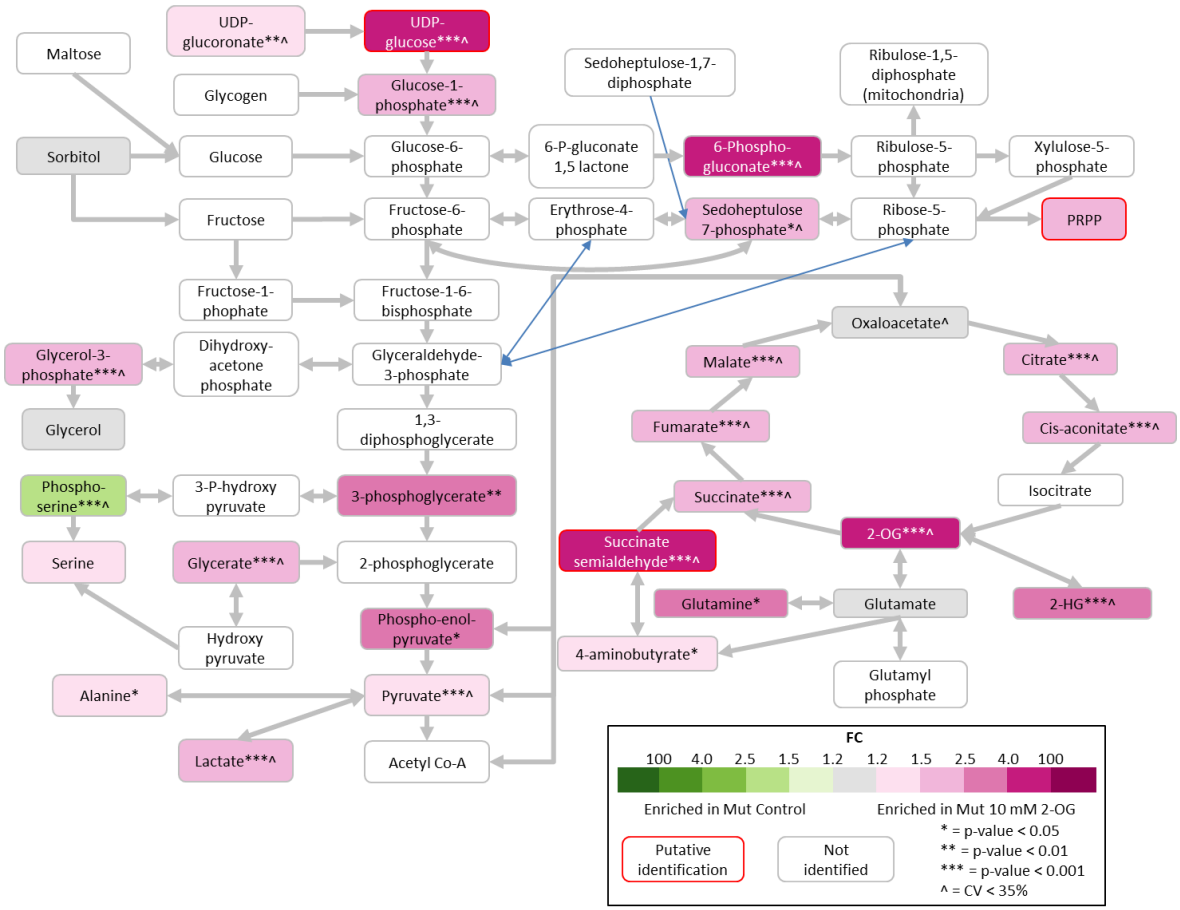

Figure 6.6: Pathway heat map of the TCA cycle, glycolysis and pentose phosphate pathway for the analysis of LN18 Mut cells cultured under 4.5 g / L glucose conditions, treated with 10 mM 2-OG or vehicle control for 24 hours (Section 8.18), analysed by IC-MS/MS (Section 8.4), derivatised RP-MS (Section 8.7) and non-derivatised RP-MS/MS (Section 8.9).

Phosphoserine was depleted 2.25-fold (p-value 5.38×10^{-9}) in LN18 Mut cells treated with 2-OG, possibly due to competitive inhibition. Phosphoserine transaminase is a 2-OG dependent enzyme, which interconverts between phosphoserine and 3-phosphohydroxypyruvate (not detected), and has previously been shown to be inhibited by 2-HG.[220] 2-HG was significantly enriched 3.58-fold (p-value 8.00×10^{-8}) in 2-OG treated LN18 Mut cells, likely due to the enrichment of isocitrate (not detected) concomitant with the significant enrichment of citrate (FC 1.56, p-value 6.05×10^{-5}) and cis-aconitate (FC 1.71, p-value 2.03×10^{-4}). Enrichment of 2-HG, as a result of treatment with 2-OG, would not be favourable if the previously reported inhibitory effects (and regulation of methylation status) were confirmed to be tumourigenic.[234] Treatment with

2-OG therefore may not be a viable clinical strategy, for the recovery of WT metabolism. Enrichment of succinate (FC 2.07, p-value $2.18x10^{-7}$), fumarate (FC 1.78, p-value $2.59x10^{-4}$) and malate (FC 1.86, p-value $6.85x10^{-6}$) in treated LN18 Mut cells suggests that 2-OG was transported into the mitochondria, and consequently supplemented cellular respiration, causing an enrichment of TCA cycle metabolites. Glutamate abundance was not significantly altered as a result of treatment and the CV for glutamate and glutamine were both greater than 35 %. The pentose phosphate pathway was also altered as a consequence of 2-OG treatment, with significant enrichment of sedoheptulose 7-phosphate (FC 1.85, p-value $2.40x10^{-2}$) and 6-phosphogluconate (FC 8.45, p-value $1.99x10^{-7}$). Pentose phosphate intermediates may have also been affected by the change in abundance for the glycolytic intermediates 3-phosphoglycerate (FC 3.58, p-value $2.33x10^{-3}$), phosphoenolpyruvate (FC 3.05, p-value $2.49x10^{-2}$) and pyruvate (FC 1.32, p-value $4.38x10^{-2}$), which were all enriched. The resulting excess of downstream metabolites in central carbon metabolism could therefore cause product inhibition and further enrichment of upstream metabolites. The enrichment of lactate (FC 2.46, p-value $7.20x10^{-6}$) was consistent with an upregulation of aerobic metabolism, as a result of 2-OG treatment.[235] The measurement of metabolic flux, would provide evidence for possible product inhibition and a change in energy utilisation, as a consequence of 2-OG treatment.

Despite the lower intracellular abundance of 2-OG in treated LN18 WT cells (Fig. 6.5), similar metabolic effects to treated LN18 Mut cells were observed; however, the abundance of 2-HG was not significantly altered, as shown in Table 6.1. 2-HG was likely not enriched as the IDH1 mutation was not present and therefore would only be produced in small quantities as a result of the normal enzymatic reduction of 2-OG by

oxidoreductases.[212] The significant enrichment of glycolysis and pentose phosphate intermediates was not observed for LN18 WT cells apart from lactate (FC 1.99, p-value 5.03×10^{-5}) and 6-phosphogluconate (FC 4.09, p-value 2.01×10^{-9}).

Table 6.1: Heat map showing FC and significance for selected central carbon metabolites from LN18 Mut and WT cells cultured under 4.5 g / L glucose conditions, treated with 10 mM 2-OG or vehicle control for 24 hours (Section 8.18), analysed by IC-MS/MS (Section 8.4), derivatised RP-MS (Section 8.7) and non-derivatised RP-MS/MS (Section 8.9).

Identified metabolite	Mut	WT
2-HG		
2-OG		
6-phosphogluconate		
Citrate		
Lactate		
O-phosphoserine		
Phosphoenolpyruvate		
Pyruvate		
UDP-glucose		

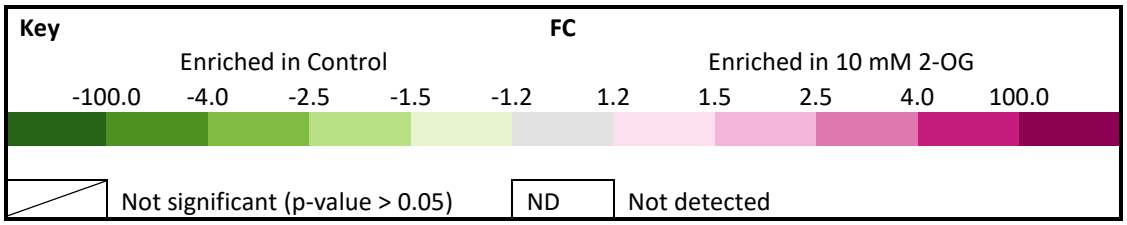

Generally, the magnitude of FC, for the abundance of central carbon metabolites in 2-OG treated LN18 WT cells, was lower compared to 2-OG treated LN18 Mut cells. This effect may have been caused by the lower intracellular 2-OG concentration observed in WT cells (Fig. 6.5), or may be due to different utilisation of glycolysis in Mut cells, as a consequence of the IDH1 mutation. A titration of 2-OG concentration could be used to investigate these hypotheses; however, the enrichment of 2-HG in LN18 Mut cells as a result of treatment, means that 2-OG supplementation is not likely to be beneficial. The absence of pyruvate enrichment in 2-OG treated LN18 WT cells resulted in a higher lactate / pyruvate ratio, than the control cells, and was indicative of an upregulation of glycolysis.[181, 182] The different enrichments of central carbon metabolites provides

evidence for different cellular energy capacities in LN18 Mut and WT cells. Investigation of cellular respiration in Mut and WT cells may reveal whether metabolic stress could be used as a selective treatment.

6.3.2. Exploring the effect of 2-OG treatment on tryptophan and lysine degradation product abundances

As discussed in Sections 4.12 and 5.2, 2-aminoadipate, 2-oxoadipate, saccharopine and kynurenine were all significantly depleted, as a consequence of the IDH1 mutation, in multiple experimental replicates of LN18 cells. As treatment of LN18 WT cells with 2-HG (Section 6.2) did not significantly alter the abundance of lysine and tryptophan degradation products, the effect of increased intracellular 2-OG concentration was also investigated to assess the sensitivity of these pathways to 2-OG. Despite the dependency of α-aminoadipic semialdehyde synthase on 2-OG (discussed in Section 4.12), lysine was only depleted 1.06-fold (p-value 3.88×10^{-2}) in 2-OG treated LN18 Mut cells and saccharopine was not significantly altered, as shown in Fig. 6.7.

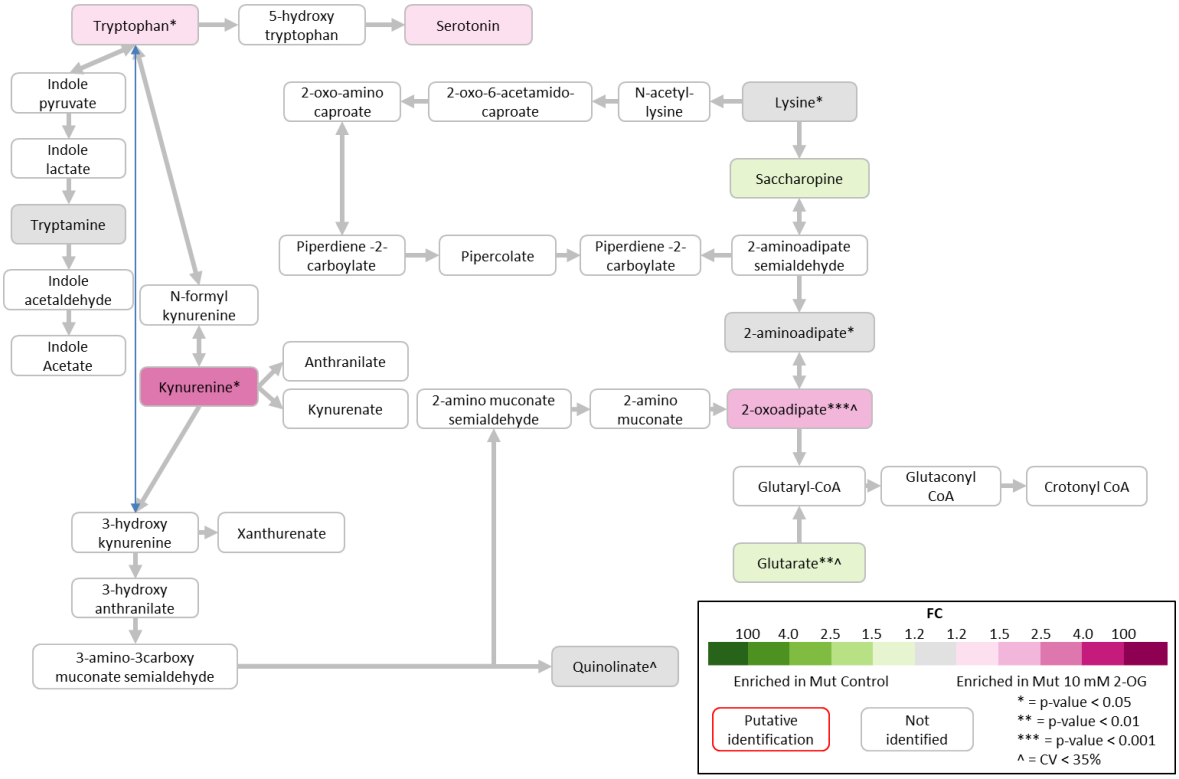

Figure 6.7: Pathway heat map of the tryptophan and lysine degradation pathways for the analysis of LN18 Mut cells cultured under 4.5 g / L glucose conditions, treated with 10 mM 2-OG or vehicle control for 24 hours (Section 8.18), analysed by IC-MS/MS (Section 8.4), derivatised RP-MS (Section 8.7) and non-derivatised RP-MS/MS (Section 8.9).

The lysine degradation product 2-oxoadipate, was significantly enriched in 2-OG treated LN18 Mut cells by 1.90-fold (p-value 1.96×10^{-7}), and was associated with a depletion of glutarate (FC 1.22, p-value 3.43×10^{-3}). The potential alteration of muconate and CoA metabolites, discussed in Section 5.2, therefore appears to be sensitive to both 2-OG and 2-HG concentration. Despite the enrichment of 2-oxoadipate, in 2-OG treated LN18 Mut cells, its abundance was not fully recovered to the baseline level in LN18 WT cells, as shown in Fig. 6.8. The depletion of 2-OG, in LN18 Mut cells, was therefore unlikely to be exclusively causing depletion of lysine degradation products. This provides further evidence for an additional inhibitory effect on amino acid metabolism in LN18 Mut cells, possibly related with redox metabolism or the depletion of glutarate, observed in LN18 WT cells, treated with 2-HG (Section 6.2).

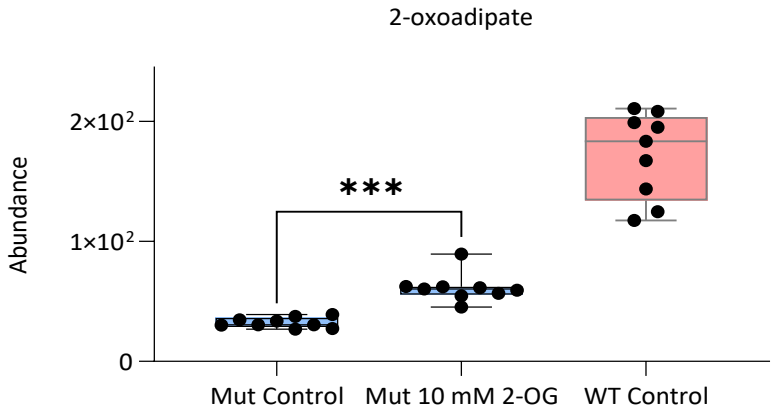

Figure 6.8: Box plot showing the abundance of 2-oxoadipate in LN18 Mut and WT cells cultured under 4.5 g / L glucose conditions, treated with 10 mM 2-OG or vehicle control for 24 hours (Section 8.18), analysed by IC-MS/MS (Section 8.4). The box plot shows the mean, 25-75th percentiles and whiskers extend from the minimum to maximum values. The number of samples are denoted with dots and significance from t-tests are annotated (ns, p-value greater than 0.05; *, p-value less than 0.05; **, p-value less than 0.01; and ***, p-value less than 0.001).

The tryptophan degradation product kynurenine was also significantly enriched in 2-OG treated LN18 Mut cells by 2.84-fold (p-value 2.01x10^{-2}), despite a CV of 77.8 % (which was likely caused by the variation in intracellular 2-HG concentration). Kynurenine was enriched to the same abundance observed in LN18 WT cells, as shown in Fig. 6.9. The reduced immunosuppressive effect in LN18 Mut cells, as discussed in Section 4.12, was therefore probably caused by the depletion of 2-OG. The enrichment of kynurenine in 293T Mut cells (Section 5.3), when 2-OG was not significantly depleted, suggesting that the pathway was also sensitive to tryptophan concentration.

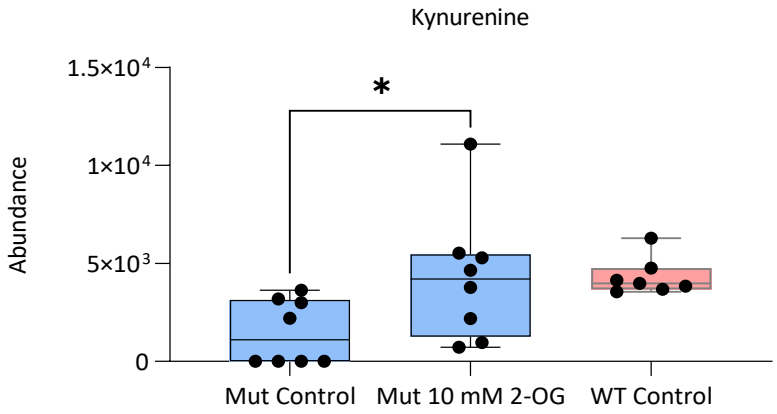

Figure 6.9: Box plot showing the abundance of kynurenine in LN18 Mut and WT cells cultured under 4.5 g / L glucose conditions, treated with 10 mM 2-OG or vehicle control for 24 hours (Section 8.18), analysed by derivatised RP-MS (Section 8.7). The box plot shows the mean, 25-75th percentiles and whiskers extend from the minimum to maximum values. The number of samples are denoted with dots and significance from t-tests are annotated (ns, p-value greater than 0.05; *, p-value less than 0.05; **, p-value less than 0.01; and ***, p-value less than 0.001).

The sensitivity of kynurenine abundance with 2-OG treatment was also observed in LN18 WT cells, with a 2.03-fold enrichment (p-value 7.85×10^{-4}), concomitant with a 1.45-fold (p-value 8.64×10^{-4}) depletion of tryptophan, as shown in Table 6.2. The enrichment of kynurenine with 2-OG treatment, as a consequence of increased substrate availability for the enzymes TDO and IDO, may cause increased immunosuppression. 2-OG may consequently hinder effective treatment, if used clinically as a supplement in IDH1 mutant tumours. The modulation of 2-OG and tryptophan concentration may, however, allow selective treatment in combination with immunotherapy.

Table 6.2: Heat map showing FC and significance for selected tryptophan and lysine degradation products from LN18 Mut and WT cells cultured under 4.5 g / L glucose conditions, treated with 10 mM 2-OG or vehicle control for 24 hours (Section 8.18), analysed by IC-MS/MS (Section 8.4), derivatised RP-MS (Section 8.7) and non-derivatised RP-MS/MS (Section 8.9).

Identified metabolite	Mut	WT
2-aminoadipate		
2-oxoadipate		
Glutarate		
Kynurenine		
Lysine		
Saccharopine		
Tryptophan		

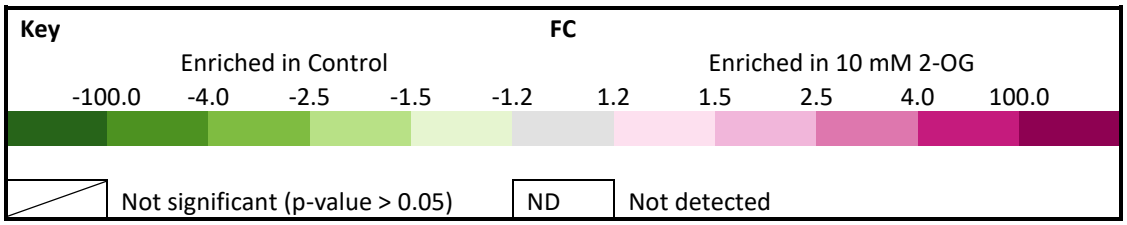

The lysine degradation products, 2-oxoadipate and 2-aminoadipate, were both enriched in 2-OG treated LN18 WT cells by 5.27-fold (p-value 2.29×10^{-10}) and 2.36-fold (p-value 1.82×10^{-2}) respectively. The depletion of lysine degradation products in LN18 Mut cells (Section 5.2), was therefore most likely to be related with the depletion of 2-OG. This was corroborated by the greater enrichment of 2-oxoadipate in LN18 WT cells, which had an increased baseline abundance of 2-OG, compared with LN18 Mut cells. 2-oxoadipate was still significantly depleted in 293T Mut cells, as observed in Section 5.3, when 2-OG abundance was not depleted and therefore, the pathway may also be regulated by another effect of the IDH1 mutation.

Glutarate abundance, was not significantly altered in LN18 WT cells and therefore sensitivity to 2-HG and 2-OG concentration was only observed in LN18 Mut cells. This provides further evidence for alteration of muconate or CoA metabolism in IDH1 mutant cells. The larger FC magnitudes observed for LN18 WT cells, demonstrated increased sensitivity to 2-OG concentration compared with LN18 Mut cells, further confirming the

possibility of an inhibitory effect on tryptophan and lysine degradation pathways in addition to the enrichment of 2-HG and depletion of 2-OG.

6.3.3. Exploring the effect of 2-OG treatment on glutamine and glutamate-derived metabolite abundances

Glutamine and glutamate metabolites were also investigated in LN18 cells treated with 2-OG, as the depletion of β-citryl glutamate was consistently observed in all Mut cell lines (Section 5.3), and was not significantly altered in LN18 WT cells treated with 2-HG (Section 6.2). The enrichment of a number of glutamate-derived metabolites was observed in 2-OG treated LN18 Mut cells, although glutamate abundance was not significantly altered, as shown in Fig. 6.10.

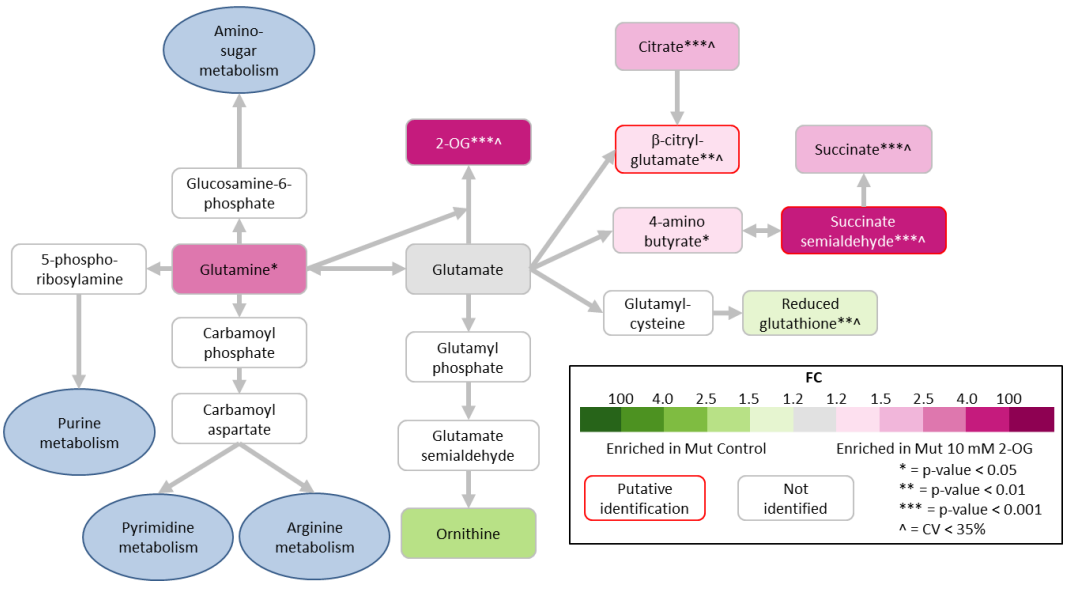

Figure 6.10: Pathway heat map of glutamine and glutamate metabolism for the analysis of LN18 Mut cells cultured under 4.5 g / L glucose conditions, treated with 10 mM 2-OG or vehicle control for 24 hours (Section 8.18), analysed by IC-MS/MS (Section 8.4), derivatised RP-MS (Section 8.7) and non-derivatised RP-MS/MS (Section 8.9).

Glutathione was significantly depleted (FC 1.25, p-value 6.89×10^{-3}) in LN18 Mut cells, likely in response to the intracellular acidification caused by 2-OG treatment, and consequent alteration of the cellular redox state. In addition to the enrichment of the TCA

cycle intermediates citrate and succinate, discussed earlier in this Section, β-citryl glutamate was enriched 1.26-fold (p-value 1.23×10^{-2}) in LN18 Mut cells treated with 2-OG, as shown in Fig. 6.11.

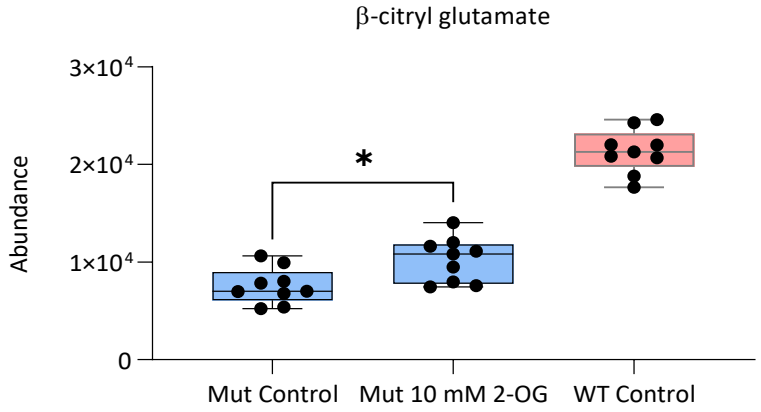

Figure 6.11: Box plot showing the abundance of β-citryl glutamate in LN18 Mut and WT cells cultured under 4.5 g / L glucose conditions, treated with 10 mM 2-OG or vehicle control for 24 hours (Section 8.18), analysed by IC-MS/MS (Section 8.4). The box plot shows the mean, 25-75th percentiles and whiskers extend from the minimum to maximum values. The number of samples are denoted with dots and significance from t-tests are annotated (ns, p-value greater than 0.05; *, p-value less than 0.05; **, p-value less than 0.01; and ***, p-value less than 0.001).

Recovery of β-citryl glutamate abundance, to the level observed in LN18 WT cells, was not achieved with 2-OG treatment of LN18 Mut cells, as was observed for the recovery of 2-oxoadipate (Fig. 6.8) abundance. Recovery of WT metabolism in Mut cells, by treatment with 2-OG is therefore not a viable therapeutic approach. Depletion of β-citryl glutamate in Mut cells was more likely to be caused another effect of the IDH1 mutation and not the depletion of 2-OG.

Similar effects on glutamine and glutamate metabolism were observed, for LN18 WT cells treated with 2-OG, as shown in Table. 6.3. Glutathione was significantly depleted (FC 1.27, p-value 1.33×10^{-3}) as a result of treatment with 2-OG, providing further evidence for different baseline redox states in Mut and WT cells, which could potentially be exploited clinically for selective treatment.

Table 6.3: Heat map showing FC and significance for selected glutamine and glutamate metabolites from LN18 Mut and WT cells cultured under 4.5 g / L glucose conditions, treated with 10 mM 2-OG or vehicle control for 24 hours (Section 8.18), analysed by IC-MS/MS (Section 8.4), derivatised RP-MS (Section 8.7) and non-derivatised RP-MS/MS (Section 8.9).

Identified metabolite	Mut	WT
4-aminobutyrate		
β-citryl glutamate		
Glutamate		
Glutamine		
Glutathione		

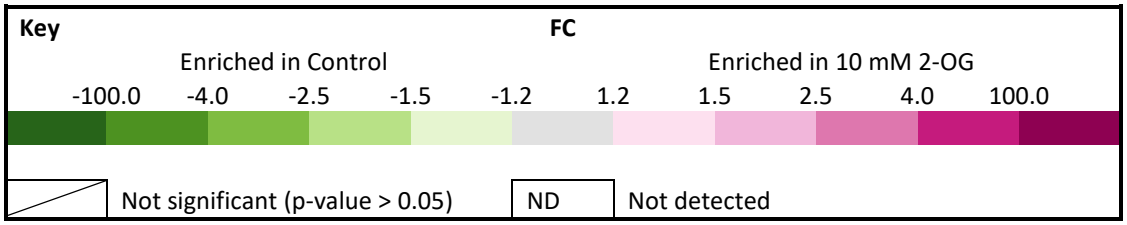

β-citryl glutamate was significantly enriched (FC 1.74, p-value 1.12×10^{-6}), to a greater extent in LN18 WT cells as a result of treatment with 2-OG, despite a lower intracellular abundance of 2-OG compared to LN18 Mut cells. This provides further evidence for an inhibitory effect on β-citryl glutamate related enzymes, which was diminishing the recovery effect in LN18 Mut cells (with 2-OG treatment), compared to LN18 WT cells. The depletion of β-citryl glutamate in the Mut cell lines was, in all probability, not exclusively caused by 2-OG depletion.

6.4. Discussion of the effects associated with extracellular treatment of LN18 IDH1 mutant and wild-type glioblastoma cells with 2-HG and 2-OG

Extracellular treatment of cells with 2-HG and 2-OG led to an intracellular enrichment of both metabolites in LN18 Mut and WT cells; however, the CV of their intracellular abundance was greater than 35 %, which suggested that extracellular treatment was not a reproducible delivery method and future investigations would benefit from using a more cell permeable form, such as dimethyl 2-OG, which could be dealkylated by cellular

mechanisms.[236] Statistically significant effects on metabolite abundance were still observed as a result of treatment with 2-HG and 2-OG and therefore some conclusions could still be drawn from the data.

Interestingly, few metabolites were significantly altered in LN18 WT cells as a result of treatment with 2-HG, although NAAG was significantly depleted, consistent with the observations by Reitman *et al*.[133] The enrichment of amino acids and depletion of malate and fumarate observed by Reitman *et al*. was not replicated in 2-HG treated LN18 cells and may therefore have been a cell line specific effect.[133] It is also possible that extracellular treatment with 10 mM 2-HG may not have been sufficient to replicate the effects observed in LN18 Mut cells, as only a hundred-fold enrichment was achieved. Although alterations in metabolite abundance were observed for 293T cells, where 2-HG was only 11.1-fold enriched, and therefore the hundred-fold enrichment of 2-HG should have replicated the metabolic effects, in LN18 cells. Treatment with 2-HG was not a model for the changes to redox metabolism associated with an IDH1 mutation, such as the depletion of NADPH, and therefore did not subject the cells to the same metabolic stress.[42] The absence of distinct inhibition of biological processes as a result of treatment with 2-HG suggests that the metabolic effects observed in Mut cells (discussed in Section 5.4) were either caused by depletion of 2-OG or were a consequence of other factors associated with the IDH1 mutation. Treatments which only reduce the enrichment of 2-HG, therefore may not be sufficient to be effective therapeutically.

Treatment of LN18 cells with 2-OG caused significant enrichment of the majority of identified central carbon metabolites, as a consequence of the increased intracellular availability of 2-OG. The enrichment of pyruvate and lactate was consistent with an

upregulation of aerobic glycolysis in Mut and WT cells, as a result of 2-OG treatment. The relationship between 2-OG abundance and the modulation of mitochondrial respiratory chain and redox processes, as reported by Vatrinet *et al*., may therefore be utilised in Mut cells as part of tumourigenesis or selective adaptation.[237] The enrichment of glutathione in 2-OG treated LN18 WT cells, combined with a higher lactate / pyruvate ratio, provided further evidence for a different baseline redox state in LN18 WT cells. The reduced capacity for glycolytic activity of Mut cells, as discussed in Section 3.7, is corroborated by *in situ* MS imaging and metabolite tracer experiments carried out in patient-derived xenograft models, by Fack *et al.*, demonstrating reduced glucose turnover and energy potential in IDH1 Mut glioma.[238] Evidence for decreased oxidative metabolism has also previously been demonstrated in IDH1 mutant cells using live cell metabolic assays.[239] IDH1 mutant cells may therefore be dependent on glutaminolysis and vulnerable to therapeutic intervention.[240] The difference in redox state could also have been related with the baseline 2-OG concentration in LN18 WT compared with Mut cells, or the variation in intracellular 2-OG concentration, as a result of distinct membrane permeabilities of Mut and WT cells. The difference in membrane permeability between LN18 Mut and WT cells, may provide evidence for the increased sensitivity of IDH mutant cells to treatments such as chemotherapy.[241]

Glutamate abundance was not significantly altered in 2-OG treated LN18 Mut and WT cells, despite a significant enrichment of both 2-OG and glutamine, which suggests that transaminase enzymes were not upregulated in response to the enrichment of 2-OG. Glutamate abundance may also have been tightly regulated in the glioma-derived cell line, due to its role as a neurotransmitter.[242]

A partial recovery of 2-oxoadipate abundance, at high intracellular 2-OG concentration, suggests that the depletion of lysine and tryptophan degradation products in LN18 Mut cells were not exclusively caused by 2-OG depletion, but that it may have had some effect. The abundance of the immunosuppressive metabolite kynurenine was, however, closely associated with 2-OG abundance and was also shown be sensitive to tryptophan abundance. As some IDH mutant tumours have been reported to have immunosuppressive characteristics, it may therefore be possible to improve immunotherapeutic treatment with modulation of amino acid availability.[222] β-citryl glutamate abundance was also partially recovered in LN18 Mut cells with 2-OG treatment; however, the FC observed for treated LN18 WT cells was greater, despite a lower intracellular concentration of 2-OG. Therefore, β-citryl glutamate may not have been depleted in Mut cells solely as a result of the depletion of 2-OG and other effects of the IDH1 mutation may have also contributed.

6.5. Chapter summary

Potential biological consequences of the IDH1 mutation, which were discussed in Section 5.2, were investigated with the treatment of LN18 Mut and WT cells with 2-HG and 2-OG. These treatments were used to explore the relationship between the alteration of metabolism in Mut cells, with the enrichment of 2-HG and the depletion of 2-OG. Extracellular supplementation of 2-HG and 2-OG, altered metabolite abundance in both LN18 WT and Mut cells and enabled the investigation of potential inhibition by 2-HG on 2-OG dependent enzymes, as well as the evaluation of 2-OG sensitivity. Differential uptake of 2-OG was also observed between LN18 Mut and WT cells.

Treatment of LN18 WT cells with 2-HG did not cause a significant alteration of central carbon metabolism, possibly as a result of an imbalance of redox cofactors and increased cellular acidification. Tryptophan and lysine metabolites were also not significantly altered as a result of treatment with 2-HG, suggesting that the depletion of degradation products in Mut cells was caused by the enrichment of 2-HG. Despite a significant depletion of both glutarate and NAAG with 2-HG treatment, the abundance of β-citryl glutamate was not significantly altered.

Treatment of LN18 Mut cells with 2-OG caused enrichment of kynurenine, 2-oxoadipate and β-citryl glutamate, with partial recovery to the abundance observed in LN18 WT cells, suggesting another regulatory effect of the IDH1 mutation, in addition to the depletion of 2-OG. Metabolic treatment of Mut and WT cells, by way of selective supplementation or depletion of metabolites, has potential for clinical treatment but requires further investigation.

Chapter 7. Conclusions and further work

7.1. Conclusions

The research described in this thesis focussed on the development and application of IC-MS/MS and RP-IMS-MS/MS (with sample derivatisation), as new techniques for metabolic profiling of biological samples. The methods were applied to untargeted analysis of cell extracts and were compared with commonly used RP-MS/MS (without sample derivatisation) and HILIC-MS/MS approaches. The metabolic effects of an IDH1 mutation were investigated in LN18, U87-MG and 293T cell lines, using these LC-MS/MS techniques and statistical analysis.

The IC-MS/MS method was shown to resolve, and allow identification of, a wide range of physiologically polar and ionic metabolites and to have significantly better reproducibility, sensitivity and linearity compared to HILIC-MS/MS. Univariate and multivariate statistical analysis of LN18 WT cells cultured under different glucose conditions revealed a greater number of significantly altered metabolites by IC-MS/MS, with comprehensive coverage of central carbon metabolism including glycolysis, pentose phosphate pathway and TCA cycle intermediates. The substantial number of metabolite identifications made using accurate mass, isotope distribution, RT and fragmentation pattern of compound-features with authentic standards, enabled the investigation of the metabolic differences between Mut and WT cells. Significant enrichment of 2-HG was observed with an IDH1 mutation in all 3 cell lines, however, different metabolite abundances were observed, that correlated with the depletion of 2-OG. Adenylate energy charge was also observed to be augmented by the IDH1 mutation, concomitant with modification of cofactors or additional redox stress from intracellular acidification by 2-HG. IC-MS/MS also revealed that 2-oxoadipate

was significantly depleted in Mut cells and therefore, to further explore alterations in metabolism, a novel hyphenation of RP-IMS-MS/MS with sample derivatisation was developed.

Derivatised RP-MS was demonstrated to be more sensitive and have increased dynamic range compared with HILIC-MS. Hyphenation to IMS provided additional and orthogonal separation based on metabolite CCS. Drift time separation was also used to demonstrate the extent of derivatisation in cell samples and provide increased specificity of metabolite identification based on fragmentation patterns. Saccharopine and 2-aminoadipate in the lysine degradation pathway were depleted in Mut cells, consistent with the depletion of 2-oxoadipiate observed by IC-MS/MS. Kynurenine, an immunosuppressive metabolite in the tryptophan degradation pathway was also observed to be depleted in Mut cells which may account for improved Mut cell survival, despite intracellular acidification by 2-HG.

RP-MS/MS, without sample derivatisation, was also used to improve coverage of the metabolome in Mut and WT cell samples with the identification of low and medium polarity metabolites. Alteration in metabolite abundance, identified using multiple chromatographic techniques hyphenated to MS were visualised using pathway heat maps and VBA macros were written to partially automate the process. Heat maps were used to illustrate the metabolic changes of an IDH1 mutation in U87-MG, 293T and multiple experimental replicates of LN18 cells.

Depletion of β-citryl glutamate, as well as tryptophan and lysine degradation products, as a result of the IDH1 mutation, were not caused by enrichment of 2-HG and may be related to the depletion of 2-OG. Partial recovery of these metabolites, in LN18 Mut cells, by treatment with 2-OG demonstrated that regulatory effects, in addition to the

depletion of 2-OG, were present in Mut cells. Combination therapies would therefore be required to selectively treat IDH mutant cells. Treatment of LN18 WT cells with 2-HG in this case, did not reveal any metabolic alterations that were also observed in LN18 Mut cells, suggesting that these metabolic effects are not directly associated with acute accumulation of 2-HG. Another study into the treatment of mammalian cancer cell lines with 2-HG has also shown that 2-HG is not readily metabolised, and therefore suggests that phenotypic alterations associated with an IDH mutation are not induced by metabolic products of 2-HG.[243] T-cell metabolism has been shown to been altered by treatment with 2-HG, causing increased oxidative phosphorylation and glucose uptake in T-cells by interfering with hypoxia-inducible factor 1-α, but treatment did not alter cell proliferation or senescence.[244] The metabolic effects of acute treatment with 2-HG therefore may be related to cell type or function and requires further study, including cell lines with different p53 and PTEN status, to assess the relationship between 2-HG and the multiple genetic alterations associated with IDH1 mutations.

The techniques developed for untargeted metabolic profiling of ionic, polar and amine-derived metabolites have subsequently been used for the analysis of a range biological sample types including: T-cells, tissue samples and blood plasma. The application of these methods, beyond the analysis of cells with and without an IDH1 mutation, is therefore of benefit for a broad range of metabolic investigations, especially for the metabolites involved in cellular energy processes.

7.2. Limitations

IC-MS/MS and derivatised RP-IMS-MS/MS provided increased coverage of identified metabolites, compared with HILIC-MS/MS. Even with additional analyses using

RP-MS/MS, without sample derivatisation, the entire metabolome was not profiled for the cell lines analysed in this research. Metabolite classes such as lipids were not suitable for analysis with the methods demonstrated here, but could be studied in Mut and WT cells to improve understanding of the metabolic impact of an IDH1 mutation, using other methods, such as supercritical fluid chromatography coupled to MS.[245] Acyl-CoA metabolism is involved in TCA cycle function and lipid metabolism and therefore linked to the changes to glutarate abundance and the lysine degradation pathway, observed in Mut and WT cells. CoA metabolites degrade quickly after extraction and are not sensitive to analysis by most types of untargeted approaches.[246] Although samples were snap frozen and prepared on ice to minimise metabolite degradation, the effect of cell lysis and metabolite extraction on the metabolome is not easily measured. It was assumed that the same effects would be observed across experimental groups and therefore not effect relative quantitation, however, concentration and pH have been shown to cause different rates of metabolite degradation during processing and storage.[247]

All of the cell lines used as model systems for this research have been manipulated to proliferate indefinitely, such as the introduction of the simian virus 40 large T antigen in the 293T cell line.[176] This manipulation allows a cell line to be studied over multiple passages and in large quantities, however, as the cell lines consist of only a single cell type, they do not exhibit the heterogeneity or diverse cooperative effects which are typically observed in tumours.[248, 249] The stability of immortalised cell lines allows the study of a range of cellular alterations, through the introduction of genetic material, such as the transduction of the IDH1 mutation studied in this thesis.[250, 251] The expression of any introduced genetic material can change over time through various cellular activities such as mitosis.[250] The expression of IDH1 may therefore have been different between

the 3 cell lines studied here, and contributed to the variation in metabolic effects that were observed. Variation in expression of the IDH1 mutation could be measured with immunofluorescence antibody staining or western blot.[252] Variation in the metabolic effects of the IDH1 mutation may also have been caused by the difference in PTEN and P53 status between the cell lines however this research provided insight into metabolic effects associated with these genetic mutations.

The cell models used here provided insight into the metabolic effects of an IDH1 mutation and enabled the investigation of treatment with 2-HG and 2-OG, but did not reflect *in vivo* conditions. Glucose concentration for example, as discussed in Sections 2.7 and 4.8, had significant effects on metabolism and therefore the 4.5 g / L glucose conditions, used for the culture of glioblastoma cell lines, reflect hyperglycaemic conditions in neurological tissue (brain glucose concentration is typically ca. 0.8 g / L).[253] Cell models also do not account for the diverse network of cells which make up tissues and therefore the metabolic changes observed here, for Mut and WT cells, require *in vivo* corroboration.[254] To date, culture of primary cells with an IDH1 mutation has not been published. Analysis of a heterogeneous cell system could provide insight into the tumour microenvironment typically observed in patients and the metabolic progression associated with and without an IDH1 mutation.[255] The heterogeneity of primary cell culture, however, means that finding appropriate experimental controls is not as trivial as for stable cell lines, and variability between samples is increased.[256]

Extracellular treatment of cells with glucose, 2-HG and 2-OG was not an efficient method of increasing intracellular concentration. High CV were observed for the abundances of 2-HG and 2-OG in treated cells and different abundances in Mut and WT cells suggested

different rates of transport across cell membranes. Treatment with methylated forms of 2-HG or 2-OG may have better cell permeability due to lower functional group polarity and therefore increase reproducibility.[236] Although treatment concentrations were not optimised in the cell lines, metabolic effects were still observed and can subsequently be confirmed with *in vitro* or *in vivo* experiments.

7.3. Future work

The results from this thesis suggested several metabolic changes linked directly to the IDH1 mutation. It would therefore be of interest to explore whether similar changes in metabolite abundance are observed in tumour tissue. The metabolites identified to be significantly altered from analysis of Mut cells (such as β-citryl glutamate) may be useful biomarkers, for clinical classification of an IDH mutation. Additional LC-MS/MS approaches could also be applied to the cell models used here, particularly for the investigation of lipids and short-chain fatty acids, which have previously been reported to be perturbed in IDH mutant tumours.[257] The hyphenation of IMS-MS/MS to other chromatographic methods, such as IC, would be of technical interest to increase confidence in metabolite identification. The relationship between drift time and *m/z*, particularly the shorter drift times for highly polar metabolites (observed in Section 4.6), compared with less polar metabolites with the same *m/z*, should also be explored further.

To elucidate whether the turnover rate of metabolic pathways was altered as a consequence of the IDH1 mutation, metabolic flux experiments would help define atom relationships and enzyme kinetics.[258] For example, metabolic flux experiments could provide further evidence for enzyme inhibition or confirm the mechanism of metabolite enrichment and depletion in Mut cells. The activity of α-aminoadipic semialdehyde

synthase, TDO and IDO would be of interest, given the Mut specific depletion of amino acid degradation products, observed in Chapters 4 and 5. Proteomic analysis would also reveal any alteration of enzyme expression in response to an IDH1 mutation, or treatment with 2-OG or 2-HG.

As the metabolic effects of treatment with 2-OG and 2-HG was only studied in LN18 Mut and WT cells, the effects, observed in Sections 6.2 and 6.3, could be cell line specific. The treatment of U87-MG and 293T Mut and WT cells would provide additional insight into the effect of 2-OG and 2-HG concentration. The treatment conditions were also not optimised and a range of concentrations and delivery methods have been published previously.[133, 243, 244] Cell viability studies could be performed to find optimal concentrations of 2-HG for the treatment of various cell lines and the duration of exposure could also be investigated. Chronic exposure to 2-HG and intracellular acidity may induce metabolic effects that were not observed for acute expose, especially as cancer cells adapt to physiological and metabolic conditions over time.[259] Proteomic analysis could also be used to investigate any alterations in protein expression with chronic exposure to 2-HG. Further *in vitro* analysis of isolated systems or enzymes could confirm the inhibition of 2-OG dependent pathways by 2-HG including investigation of enzyme kinetics and cellular energy capacity.

Since the discovery of IDH mutations in multiple cancer types, development of inhibitors has been of interest and the first mutant-specific therapeutic, AG-120 (Ivosidenib), was approved by the Food and Drug Administration, during the research for this thesis.[260, 261] Resistance to treatment has subsequently been reported, including a second-site mutation and consequently, new therapeutic approaches are still required.[58] The

sensitivity of IDH Mut cells to further changes in redox state and 2-OG concentration (discussed in Sections 5.4 and 6.4) suggests that combination therapies, which leverage the metabolic differences between Mut and WT cells, may provide more selective and effective treatments. The metabolic impact of chemotherapeutics and any differential effects in Mut and WT cells could also be investigated, with the aim of developing more selective treatments. Ribonucleic acid interference and clustered regularly interspaced short palindromic repeats screening can both be used to identify genetic vulnerabilities associated with cancer.[262] Genome-wide investigation using knockout or loss-of-function screening can be used to identify specific genes which are essential for cell proliferation and survival.[172] These genes can subsequently be targeted chemotherapeutically, however, perturbation of a gene that is identified to be associated with cancer survival or progression may also have off-target effects if the treatment isn't specific to the cancer cells. A synthetic lethal interaction occurs when two or more genes are perturbed, leading to loss of cell viability.[263] Typically, at least one genetic mutation or genetic instability is associated with cancer cells and therefore therapeutically targeting an additional gene which causes synthetic lethality may provide a targeted treatment.[264] Metabolomics can be used to screen for metabolic deficiencies or weaknesses and reveal genetic targets which can subsequently be used to exploit the differences between cancer and non-cancer cells using synthetic lethality. Exploiting cancer associated vulnerabilities requires drug discovery and design, as discussed in Chapter 1. Potential vulnerabilities can be identified from untargeted metabolomics, drug discovery can be aided with high-throughput metabolite screening and drug design can be improved by understanding the metabolic impacts of a chemotherapeutic, or its metabolised forms.[30, 77, 264]

The untargeted metabolomics methods developed in this thesis are translatable to other biological material, including blood plasma, macrophages and endothelial cells and have revealed alterations in metabolism associated with intrahepatic cholangiocarcinoma, butyrate and gene expression respectively.[265-267] The IC-MS/MS method could be of particular benefit for untargeted analysis of mitochondrial diseases including the various inborn errors of metabolism, which have been shown to cause changes in abundance of highly polar metabolites.[268-270]

It remains to be seen what impact IC-MS/MS and IMS-MS/MS will have in untargeted metabolomics, but the robustness and dynamic range of the methods and the insights into IDH1 mutant metabolism they provided in this thesis, demonstrate considerable advantages for hypothesis-driven and hypothesis-generating research.

Chapter 8. Materials and methods

8.1. Mobile phases and solvents

Solvents for LC-MS/MS analysis were obtained as HPLC grade or better from Sigma Aldrich (Gillingham, UK). Water was purified using a MilliQ Direct 8 system (Merck Millipore, Burlington, MA, USA).

8.2. Mobile phase additives

Ammonium acetate, LC-MS grade, was obtained from Sigma Aldrich (Gillingham, UK). Formic acid, 99 % for analysis, was obtained from Fisher Scientific (Loughborough, UK).

8.3. Authentic metabolite standards

Authentic metabolite standards and pharmaceuticals were obtained from Sigma Aldrich (Gillingham, UK) unless otherwise specified.

8.4. IC-MS/MS method for Q Exactive

A 5 µL partial loop injection was used for all analyses and chromatographic separation was performed using a Dionex ICS-5000+ Capillary HPIC system (Thermo Scientific, San Jose, CA, USA) coupled to a Q Exactive hybrid quadrupole-Orbitrap mass spectrometer (Thermo Scientific, San Jose, CA, USA). A Dionex IonPac AS11-HC column (2×250 mm, 4 µm; Thermo Scientific, San Jose, CA, USA) at 30 ^{o}C was used with an aqueous hydroxide ion gradient was used as follows: 0.0 min, 0.0 mM; 1.0 min, 0.0 mM; 15.0 min, 60.0 mM; 25.0 min, 100.0 mM; 30.0 min, 100.0 mM; 30.1 min, 0.0 mM; and 37.0 min, 0.0 mM. On-line conductive ion suppression was achieved using a Dionex AERS 500e 2 mm (Thermo Scientific, San Jose, CA, USA) in external water mode. The flow

rate was 0.250 mL / min and the total run time was 37.0 min. The Q Exactive mass spectrometer was equipped with a HESI II probe in negative ion mode with source parameters set as follows: sheath gas flow rate, 70; auxiliary gas flow rate, 20; sweep gas flow rate, 0; spray voltage, 3.6 kV; capillary temperature, 320 ^{o}C; S-lens RF level, 70; and heater temperature, 350 ^{o}C. MS scan parameters were set as follows: microscans, 2; resolution, 7x10^{4}; AGC target, 1x10^{6} ions; maximum IT, 120 ms; and scan range, 60-900 *m/z*. MS/MS scan parameters were set as follows: microscans, 2; resolution, 1.75x10^{4}; AGC target, 1x10^{5} ions; maximum IT, 250 ms; loop count, 10; multiplex count, 1; isolation window, 2.0 *m/z*; collision energy, 35; minimum AGC target, 5x10^{3} ions; apex trigger 1-15 s; charge exclusion, 3-8, > 8; and dynamic exclusion, 20.0 s.

8.5. HILIC-MS/MS method for Q Exactive

A 5 µL partial loop injection was used for all analyses and chromatographic separation was performed using a Dionex Ultimate 3000 UHPLC system (Thermo Scientific, San Jose, CA, USA) coupled to a Q Exactive hybrid quadrupole-Orbitrap mass spectrometer (Thermo Scientific, San Jose, CA, USA. A BEH Amide column (2.1x100 mm, 1.7 µm; Waters, Milford, MA, USA) at 40 ^{o}C, was used with mobile phase A: 95.0 % acetonitrile$_{(aq)}$ containing 10.0 mM ammonium acetate, and mobile phase B: 50.0 % acetonitrile$_{(aq)}$ containing 10.0 mM ammonium acetate. The linear gradient used was: 0.0 min, 1.0 % B; 1.0 min, 1.0 % B; 6.0 min 45.0 % B; 10.0 min, 95.0 % B; 12.0 min, 99.0 % B; 12.1 min, 1.0 % B; and 15.0 min, 1.0 % B. The flow rate was 0.40 mL / min and the total analysed time was 15.0 min. The Q Exactive mass spectrometer was equipped with a HESI II probe, operating in negative and positive ion modes, with source parameters set as follows: sheath gas flow rate, 25; auxiliary gas flow rate, 8; sweep gas flow rate, 0;

spray voltage, ± 3.5 kV; capillary temperature, 300 °C; S-lens RF level, 55; and heater temperature, 300 °C. MS scan parameters were set as follows: microscans, 2; resolution, $7x10^4$; AGC target, $5x10^6$ ions; maximum IT, 120 ms; and scan range, 60-900 *m/z*. MS/MS scan parameters were set as follows: microscans, 2; resolution, $1.75x10^4$; AGC target, $1x10^5$ ions; maximum IT, 80 ms; loop count, 10; multiplex count, 1; isolation window, 2.0 *m/z*; collision energy, 35; minimum AGC target, $5x10^3$ ions; charge exclusion, 3-8, > 8; and dynamic exclusion, 20.0 s.

8.6. HILIC-MS/MS method for Vion IMS QTof

HILIC-MS/MS as described in Section 8.5 also performed on an ACQUITY I-Class PLUS UPLC System (Waters, Milford, MA, USA) coupled to a Vion IMS QTof mass spectrometer (Waters, Milford, MA, USA) equipped with an ESI probe, in positive and negative ion modes, with source parameters set as follows: capillary voltage, +2.0 kV or -1.0 kV; source temperature, 120 °C; cone voltage, 40 V; desolvation temperature, 500 °C; cone gas flow, 50 L / h; and desolvation gas flow, 900 L / h. Scan parameters were set as follows: analyser mode, sensitivity High Definition MS^E; scan range, 50-1000 *m/z*; scan time, 0.20 s; low energy, 6.0 eV; and high energy ramp, 30.0-60.0 eV. Lockmass data were collected every 5.0 min using leucine enkephalin and used for accurate mass correction.

8.7. Derivatised RP-MS method for Q Exactive

Samples were derivatised using an AccQ-Tag Derivatisation Kit (Waters, Milford, MA, USA), following the manufacturer recommended protocol. A 5 µL partial loop injection was used for all analyses and chromatographic separation was performed using a Dionex Ultimate 3000 UHPLC system (Thermo Scientific, San Jose, CA, USA) coupled to a

Q Exactive hybrid quadrupole-Orbitrap mass spectrometer (Thermo Scientific, San Jose, CA, USA). An AccQ-Tag Ultra C18 column (2.1x100 mm, 1.7µm; Waters, Milford, MA, USA) at 50 ^{o}C was used with mobile phase A: water with 10.0 % Eluent A concentrate (Waters, Milford, MA, USA), and mobile phase B: acetonitrile with 1.3 % formic acid. The linear gradient used was: 0.00 min, 0.1 % B; 0.54 min, 9.1 % B; 5.74 min 21.2 % B; 7.74 min, 59.6 % B; 8.04 min, 90.0 % B; 8.05 min, 90.0 % B; 8.64 min, 0.1 % B; and 9.50 min, 0.1 % B. The flow rate was 0.50 mL / min and the total analysed time was 9.50 min. The Q Exactive mass spectrometer was equipped with a HESI II probe in positive ion mode with source parameters set as follows: sheath gas flow rate, 50; auxiliary gas flow rate, 20; sweep gas flow rate, 3; spray voltage, 3.7 kV; capillary temperature, 300 ^{o}C; S-lens RF level, 70; and heater temperature, 250 ^{o}C. MS scan parameters were set as follows: in-source CID, 0.0 eV; microscans, 1; resolution, 70,000; AGC target, 3x10^{6} ions; maximum IT, 200 ms; and scan range, 70-1050 *m/z*.

8.8. Derivatised RP-IMS-MS/MS method for Vion IMS QTof

Derivatised RP chromatography, as described in Section 8.7, was also performed on an ACQUITY I-Class PLUS UPLC System (Waters, Milford, MA, USA) coupled to a Vion IMS QTof mass spectrometer (Waters, Milford, MA, USA) equipped with an ESI probe in positive and negative ion modes with source parameters set as follows: capillary voltage, +2.0 kV or -1.5 kV; cone voltage, 40 V; source temperature, 130 ^{o}C; desolvation temperature, 450 ^{o}C; cone gas flow, 50 L / h; and desolvation gas flow, 900 L / h. Scan parameters were set as follows: analyser mode, sensitivity High Definition MS^{E}; scan range, 50-1000 *m/z*; scan time, 0.200 s; low energy, 6.0 eV; and high energy

ramp, 20.0-30.0 eV. Lockmass data were collected every 5.0 min using leucine enkephalin and used for accurate mass correction.

8.9. Non-derivatised RP-MS/MS method for Q Exactive

A 5 µL partial loop injection was used for all analyses and chromatographic separation was performed using a Dionex Ultimate 3000 UHPLC system (Thermo Scientific, San Jose, CA, USA) coupled to a Q Exactive hybrid quadrupole-Orbitrap mass spectrometer (Thermo Scientific, San Jose, CA, USA). A CORTECS T3 C18 column (2.1x100 mm, 1.6 µm; Waters, Milford, MA, USA) at 40 ^{o}C was used with mobile phase A: water with 0.1 % formic acid and mobile phase B: methanol with 0.1 % formic acid. The linear gradient used was: 0.0 min, 5.0 % B; 4.0 min, 50.0 % B; 12.0 min 99.9 % B; 14.0 min, 99.0 % B; and 15.1 min, 5.0 % B. The flow rate was 0.30 mL / min and the total analysed time was 18.0 min. The Q Exactive mass spectrometer was equipped with a HESI II probe in negative ion mode with source parameters set as follows: sheath gas flow rate, 25; auxiliary gas flow rate, 8; sweep gas flow rate, 0; spray voltage, 3.5 kV; capillary temperature, 300 ^{o}C; S-lens RF level, 70; and heater temperature, 300 ^{o}C. MS scan parameters were set as follows: microscans, 2; resolution, 7x10^{4}; AGC target, 5x10^{6} ions; maximum IT, 120 ms and scan range, 60-900 *m/z*. MS/MS scan parameters were set as follows: microscans, 2; resolution, 1.75x10^{4}; AGC target, 1x10^{5} ions; maximum IT, 80 ms; loop count, 10; multiplex count, 1; isolation window, 2.0 *m/z*; collision energy, 35; minimum AGC target, 5x10^{3} ions; charge exclusion, 3-8, > 8; and dynamic exclusion, 20.0 s.

8.10. Non-derivatised RP-MS/MS method for Xevo G2-XS QTof

A 10 µL full loop injection was used for all analyses and chromatographic separation was performed using an ACQUITY UPLC System (Waters, Milford, MA, USA) coupled to a Xevo G2-XS QTof mass spectrometer (Waters, Milford, MA, USA). A CORTECS T3 C18 column (2.1x100 mm, 1.6µm; Waters, Milford, MA, USA) at 40 ^{o}C was used with mobile phase A: water with 0.1 % formic acid and mobile phase B: methanol with 0.1 % formic acid. The linear gradient used was: 0.0 min, 5.0 % B; 4.0 min, 50.0 % B; 12.0 min 99.9 % B; 14.0 min, 99.0 % B; and 15.1 min, 5.0 % B. The flow rate was 0.30 mL / min and the total analysis time was 18.0 min. The Xevo G2-XS QTof mass spectrometer was equipped with an ESI probe, in positive and negative ion modes, with source parameters set as follows: capillary voltage, +2.0 kV or -1.5 kV; cone voltage, 40 V; source offset; 80 V; source temperature, 140 ^{o}C; desolvation temperature, 600 ^{o}C; cone gas flow, 50 L / h; and desolvation gas flow, 800 L / h. Scan parameters were set as follows: analyser mode, sensitivity MS^{E}; scan range, 50-900 *m/z*; scan time, 0.5 s; low energy, 6.0 eV; and high energy ramp, 20.0-40.0 eV. Lockmass data were collected every 3.0 min using leucine enkephalin and used for accurate mass correction.

8.11. Data processing for untargeted metabolomics using MetaboAnalyst

Samples were analysed by LC-MS/MS methods based on the metabolites of interest (IC, Section 8.4; HILIC, Sections 8.5 and 8.6; derivatised RP, Sections 8.7 and 8.8; and RP, Sections 8.9 and 8.10). The raw data files from LC-MS/MS analysis were processed for untargeted metabolomics using Progenesis QI (Nonlinear Dynamics, Newcastle upon Tyne, UK) to perform RT and *m/z* alignment as well as peak-picking. All runs were assessed for suitability as the alignment reference and chromatograms were

automatically aligned to correct for RT drift. Peak picking utilised run aggregation, chromatographic peak detection, isotope and adduct deconvolution was performed using automatic sensitivity adjustment and no minimum chromatographic peak width or retention time limits. The non-normalised dataset was exported as a .csv file, listing ion abundances in all samples for each compound-feature, filtered to ensure that compound-features were detected in at least 50 % of the samples, and was analysed using MetaboAnalyst.[166] Pathways analysis was performed using FC values and statistical significance for compound-features which were identified (level 5) using the Mummichog algorithm and mapped onto KEGG human metabolic pathways.[167, 196] Ions were normalised by sum and Pareto scaled before univariate and multivariate statistical analysis. Parametric and nonparametric statistical tests were both evaluated and despite the small number of samples in each experimental group only small differences were observed. The non-normal distribution and number of data points for each analyses means that parametric analyses were used to leverage their additional statistical power. Univariate statistical analysis was performed using a FC threshold of 1.5 and an FDR-adjusted t-test p-value above 0.05. Unsupervised multivariate statistical analysis consisted of PCA to validate the reproducibility of the method, to assess the differentiation between two experimental groups and to check for outliers. Supervised multivariate statistical analysis consisted of PLS-DA to model important compound-features which differentiated between experimental groups. Models were assessed on cross validation with R^2 and Q^2 values as well as a separation distance testing using 100 permutations.

8.12. Data processing for metabolite identification

Samples were processed and analysed as described in the untargeted method (Section 8.11) with normalisation to all compounds. After processing in Progenesis QI, metabolites were identified by comparison of accurate mass (within 5 ppm), RT (within 3 min), isotopic distribution (greater than 85 % similarity), fragmentation pattern matching (greater than 25 % similarity, where available) and CV (less than 35 % for QC samples) with the appropriate database for each chromatographic method (IC, Section 10.2; derivatised RP, Section 10.3 and RP, Section 10.4). Putative identifications (level 2) were made using accurate mass (within 5 ppm), isotopic distribution (greater than 85 % similarity) and fragmentation pattern matching (greater than 20 % similarity to predicted fragmentation pattern, where available), and added to the database as validated identifications (level 1) when the RT of an authentic metabolite standard was confirmed. This approach enabled the measurement of metabolite abundances and relative changes between experimental groups which were graphically represented using heat maps displaying associated metabolism and tabulated, showing FC and significance for all identified metabolites.

8.13. Lentiviral vector transduction of IDH1 mutant cells

LN18, U87-MG and 293T cell lines were genetically modified to express R132H mutant IDH1 by Dr. Chiara Bardella as described previously.[251] Human IDH1 complementary DNA was amplified by polymerase chain reaction using primers which added 1X-FLAG tag to the 3’ end of the sequence. This was cloned as ClaI-NheI fragment into the pCC.sin.36.MCS.PPTWpre.CMV.tTA-S2tet lentiviral transfer vector. Subsequently a recombinant polymerase chain reaction-based approach, using IDH1 complementary DNA

as a template was applied to construct the IDH1 R132H mutant, which was cloned into the same lentiviral transfer vector as a ClaI-BmgBI fragment, by substituting the IDH1 cassette with the IDH1 R132H mutant cassette. Vector stocks were produced by transient transfection of 293T cells. Serial dilutions of freshly harvested conditioned medium were used to infect 10^5 cells in a six-well plate, in the presence of polybrene (8 μg / ml). The viral p24 antigen concentration was measured by an HIV-1 p24 core profile enzyme-linked immunosorbent assay by enzyme-linked immunosorbent assay (Lenti-X p24 rapid titer kit, Clontech Laboratories, Mountain View, CA, USA) to determine the number of infective particles before transduction and to demonstrate that transduced cells did not produce viral particles after transduction. Cell lines were checked by Dr. Chara Bardella for expression of R132H mutant IDH1 using western blot and provided as frozen aliquots.

8.14. Metabolomics of LN18 IDH1 mutant and wild-type glioblastoma cells cultured at 2 glucose concentrations

LN18 Mut and WT cells were cultured in either 4.5 g / L or 1.0 g / L glucose DMEM (without HEPES or sodium pyruvate) supplemented with 10 % FBS and 1 % GlutaMAX. Experimental groups with 9 biological replicates were cultured in 6 cm diameter plates with a seeding density of 20 % and a total media volume of 5 mL. At 80 % cell confluency (after ca. 48 hours), media was removed and the adherent monolayer of cells were washed with ca. 10 mL phosphate buffered saline. Cells were snap frozen with ca. 3 mL liquid N_2 to arrest metabolic processes and cells mechanically lysed, with the addition of 300 μL ice-cold 80 % $methanol_{(aq)}$, to extract metabolites into solution. Prior to analysis, the DNA concentration of the samples were measured using a NanoDrop One microvolume UV-Vis Spectrophotometer (Thermo Scientific, San Jose, CA,

USA) and normalised to a concentration of ca. 100 ng / μL, ensuring that experimental groups had the same DNA concentration and therefore number of cells. Metabolite extracts were centrifuged at $2.2x10^4$ x g for 20 min to remove cell debris and filtered using 10 kDa MWCO filters (Merck Millipore, Darmstadt, Germany), following the manufacturers protocol, prior to analysis. A QC sample was prepared by the pooling of equal volumes of all individual samples and analysed before, during and at the end of each LC-MS method to assess analytical reproducibility.

Experimental replicates were performed to assess variability, with cells harvested at passage 21 (experimental replicate 1), passage 24 (experimental replicate 2) and passage 22 (experimental replicate 3). Experimental replicate 3 comprised of only 5 biological replicates as it was part of a larger study on the metabolic effect of glucose concentration. All samples were analysed by IC-MS/MS (Section 8.4), derivatised RP-MS (Section 8.7) and non-derivatised RP-MS/MS (Section 8.9). The raw data were processed using an untargeted approach (Section 8.11) with metabolite identifications made using authentic standards where possible (Section 8.12). The LN18 cells harvested at passage 21 were cultured by Dr. Joan Gannon, the samples were processed, analysed and interpreted by the author.

8.15. Metabolomics of U87-MG IDH1 mutant and wild-type glioblastoma cells

U87-MG Mut and WT cells were cultured in 4.5 g / L glucose DMEM (without HEPES or sodium pyruvate) supplemented with 10 % FBS and 1 % GlutaMAX in 6 cm diameter plates with a seeding density of 20 % and a total media volume of 5 mL. Experimental groups with 9 biological replicates were harvested at passage 15 as described in Section 8.14. Samples were analysed by IC-MS/MS (Section 8.4), derivatised

RP-IMS-MS/MS (Section 8.8) and non-derivatised RP-MS/MS (Section 8.10). The raw data were processed using an untargeted approach (Section 8.11) with metabolite identifications made using authentic standards where possible (Section 8.12).

8.16. Metabolomics of 293T IDH1 mutant and wild-type embryonic kidney cells

293T Mut and WT cells were cultured in 4.5 g / L glucose DMEM (without HEPES or sodium pyruvate) supplemented with 10 % FBS and 1 % GlutaMAX in 6 cm diameter plates with a seeding density of 20 % and a total media volume of 5 mL. Experimental groups with 5 biological replicates were harvested at passage 19 as described in Section 8.14. Samples were analysed by IC-MS/MS (Section 8.4), derivatised RP-MS (Section 8.7) and non-derivatised RP-MS/MS (Section 8.9). The raw data were processed using an untargeted approach (Section 8.11) with metabolite identifications made using authentic standards where possible (Section 8.12).

8.17. Metabolomics of 293T wild-type embryonic kidney cells cultured at 2 glucose concentrations

293T WT cells were cultured in 1.0 g / L or 4.5 g / L glucose DMEM (without HEPES or sodium pyruvate) supplemented with 10 % FBS and 1 % GlutaMAX in 6 cm diameter plates with a seeding density of 20 % and a total media volume of 5 mL. Experimental groups with 9 biological replicates were harvested at passage 17 as described in Section 8.14. Samples were analysed by derivatised RP-IMS-MS/MS (Section 8.8) and raw data were processed using an untargeted approach (Section 8.11).

8.18. Metabolomics of LN18 IDH1 mutant and wild-type glioblastoma cells treated with 2-OG or 2-HG

LN18 Mut and WT cells with 9 biological replicates in each experimental group were cultured in 4.5 g / L glucose DMEM (without HEPES or sodium pyruvate) supplemented with 10 % FBS and 1 % Glutamax in 6 cm diameter plates with a seeding density of 20 % and a total media volume of 5 mL at P23. At 60 % confluency the media was supplemented with: 2-HG (10 mM) in DMSO (1 %), 2-OG (10 mM) in DMSO (1 %), or vehicle control (1 % DMSO) for 24 hours and harvested as described in Section 8.14. Samples were analysed by IC-MS/MS (Section 8.4), derivatised RP-MS (Section 8.7) and non-derivatised RP-MS/MS (Section 8.9). The raw data were processed using an untargeted approach (Section 8.11) with metabolite identifications made using authentic standards where possible (Section 8.12).

Chapter 9. References

1. C. M. Delude, *Nature*, 2015, **527**, S14-S15.

2. J. L. Jameson and D. L. Longo, *New Engl. J. Med.*, 2015, **372**, 2229-2234.

3. P. N. Robinson, *Hum. Mutat.*, 2012, **33**, 777-780.

4. E. Holmes, I. D. Wilson and J. K. Nicholson, *Cell*, 2008, **134**, 714-717.

5. R. J. DeBerardinis and C. B. Thompson, *Cell*, 2012, **148**, 1132-1144.

6. R. D. Beger, W. Dunn, M. A. Schmidt, S. S. Gross, J. A. Kirwan, M. Cascante, L. Brennan, D. S. Wishart, M. Oresic, T. Hankemeier, D. I. Broadhurst, A. N. Lane, K. Suhre, G. Kastenmüller, S. J. Sumner, I. Thiele, O. Fiehn and R. Kaddurah-Daouk, *Metabolomics*, 2016, **12**, 149.

7. K. Hollywood, D. R. Brison and R. Goodacre, *Proteomics*, 2006, **6**, 4716-4723.

8. C. H. Johnson and F. J. Gonzalez, *J. Cell. Physiol.*, 2012, **227**, 2975-2981.

9. N. N. Pavlova and C. B. Thompson, *Cell Metab.*, 2016, **23**, 27-47.

10. O. Warburg, F. Wind and E. Negelein, *J. Gen. Physiol.*, 1927, **8**, 519-530.

11. R. J. DeBerardinis and N. S. Chandel, *Sci. Adv.*, 2016, **2**, e1600200.

12. M. V. Liberti and J. W. Locasale, *Trends Biochem. Sci*, 2016, **41**, 211-218.

13. B. Vogelstein, N. Papadopoulos, V. E. Velculescu, S. Zhou, L. A. Diaz and K. W. Kinzler, *Science*, 2013, **339**, 1546-1558.

14. T. Ozaki and A. Nakagawara, *J. Biomed. Biotechnol.*, 2011, **2011**, 603925.

15. M. Ljungman and D. P. Lane, *Nat. Rev. Cancer*, 2004, **4**, 727-737.

16. T. Riley, E. Sontag, P. Chen and A. Levine, *Nat. Rev. Mol. Cell Biol.*, 2008, **9**, 402-412.

17. H. Hermeking, *Nat. Rev. Cancer*, 2012, **12**, 613-626.

18. F. Kruiswijk, C. F. Labuschagne and K. H. Vousden, *Nat. Rev. Mol. Cell Biol.*, 2015, **16**, 393-405.

19. A. V. Follis, F. Llambi, L. Ou, K. Baran, D. R. Green and R. W. Kriwacki, *Nat. Struct. Mol. Biol.*, 2014, **21**, 535-543.

20. R. A. Cairns and T. W. Mak, *Cancer Discov.*, 2013, **3**, 730-741.

21. A. R. Grassian, S. J. Parker, S. M. Davidson, A. S. Divakaruni, C. R. Green, X. Zhang, K. L. Slocum, M. Pu, F. Lin, C. Vickers, C. Joud-Caldwell, F. Chung, H. Yin, E. D. Handly, C. Straub, J. D. Growney, M. G. Vander Heiden, A. N. Murphy, R. Pagliarini and C. M. Metallo, *Cancer Res.*, 2014, **74**, 3317-3331.

22. D. Hanahan and R. A. Weinberg, *Cell*, 2011, **144**, 646-674.

23. S. Y. Lunt and M. G. Vander Heiden, *Annu. Rev. Cell Dev. Biol.*, 2011, **27**, 441-464.

24. S. Agnihotri and G. Zadeh, *Neuro Oncol.*, 2015, **18**, 160-172.

25. C. J. Libby, A. N. Tran, S. E. Scott, C. Griguer and A. B. Hjelmeland, *Biochim. Biophys. Acta*, 2018, **1869**, 175-188.

26. C. D. Katsetos, H. Anni and P. Dráber, *Semin. Pediatr. Neurol.*, 2013, **20**, 216-227.

27. K. Y. Yeung, A. Dickinson, J. F. Donoghue, G. Polekhina, S. J. White, D. K. Grammatopoulos, M. McKenzie, T. G. Johns and J. C. S. John, *Acta Neuropathol. Commun.*, 2014, **2**, 1.

28. C. M. Labak, P. Y. Wang, R. Arora, M. R. Guda, S. Asuthkar, A. J. Tsung and K. K. Velpula, *Am. J. Cancer Res.*, 2016, **6**, 1599-1608.

29. A. Emami Riedmaier, P. Fisel, A. T. Nies, E. Schaeffeler and M. Schwab, *Trends Pharmacol. Sci.*, 2013, **34**, 126-135.

30. B. T. Hennessy, D. L. Smith, P. T. Ram, Y. Lu and G. B. Mills, *Nat. Rev. Drug Discov.*, 2005, **4**, 988-1004.

31. M. Milella, I. Falcone, F. Conciatori, U. Cesta Incani, A. Del Curatolo, N. Inzerilli, C. M. A. Nuzzo, V. Vaccaro, S. Vari, F. Cognetti and L. Ciuffreda, *Front. Oncol.*, 2015, **5**, 24.

32. C.-Y. Chen, J. Chen, L. He and B. L. Stiles, *Front. Endocrinol. (Lausanne)*, 2018, **9**, 338.

33. J. Bi, S. Chowdhry, S. Wu, W. Zhang, K. Masui and P. S. Mischel, *Nat. Rev. Cancer*, 2020, **20**, 57-70.

34. M. D. Lloye and W. M. Todd, *Curr. Drug Targets*, 2014, **15**, 65-79.

35. A. M. Mendes-Pereira, S. A. Martin, R. Brough, A. McCarthy, J. R. Taylor, J.-S. Kim, T. Waldman, C. J. Lord and A. Ashworth, *EMBO Mol. Med.*, 2009, **1**, 315-322.

36. T. R. Fenton, D. Nathanson, C. Ponte de Albuquerque, D. Kuga, A. Iwanami, J. Dang, H. Yang, K. Tanaka, S. M. Oba-Shinjo, M. Uno, M. del Mar Inda, J. Wykosky, R. M. Bachoo, C. D. James, R. A. DePinho, S. R. Vandenberg, H. Zhou, S. K. N. Marie, P. S. Mischel, W. K. Cavenee and F. B. Furnari, *Proc. Natl. Acad. Sci.*, 2012, **109**, 14164–14169.

37. D. W. Parsons, S. Jones, X. Zhang, J. C.-H. Lin, R. J. Leary, P. Angenendt, P. Mankoo, H. Carter, I.-M. Siu, G. L. Gallia, A. Olivi, R. McLendon, B. A. Rasheed, S. Keir, T. Nikolskaya, Y. Nikolsky, D. A. Busam, H. Tekleab, L. A. Diaz, J. Hartigan, D. R. Smith, R. L. Strausberg, S. K. N. Marie, S. M. O. Shinjo, H. Yan, G. J. Riggins, D. D. Bigner, R. Karchin, N. Papadopoulos, G. Parmigiani, B. Vogelstein, V. E. Velculescu and K. W. Kinzler, *Science*, 2008, **321**, 1807-1812.

38. K. Ichimura, *Brain Tumor Pathol.*, 2012, **29**, 131-139.

39. J. Balss, J. Meyer, W. Mueller, A. Korshunov, C. Hartmann and A. von Deimling, *Acta Neuropathol.*, 2008, **116**, 597-602.

40. L. Dang, D. W. White, S. Gross, B. D. Bennett, M. A. Bittinger, E. M. Driggers, V. R. Fantin, H. G. Jang, S. Jin, M. C. Keenan, K. M. Marks, R. M. Prins, P. S. Ward, K. E. Yen, L. M. Liau, J. D. Rabinowitz, L. C. Cantley, C. B. Thompson, M. G. Vander Heiden and S. M. Su, *Nature*, 2009, **462**, 739-744.

41. K. Smolková and P. Ježek, *Int. J. Cell Biol.*, 2012, **2012**, 273947.

42. L. Dang, K. Yen and E. C. Attar, *Ann. Oncol.*, 2016, **27**, 599-608.

43. E. R. Mardis, L. Ding, D. J. Dooling, D. E. Larson, M. D. McLellan, K. Chen, D. C. Koboldt, R. S. Fulton, K. D. Delehaunty, S. D. McGrath, L. A. Fulton, D. P. Locke, V. J. Magrini, R. M. Abbott, T. L. Vickery, J. S. Reed, J. S. Robinson, T. Wylie, S. M. Smith, L. Carmichael, J. M. Eldred, C. C. Harris, J. Walker, J. B. Peck, F. Du, A. F. Dukes, G. E. Sanderson, A. M. Brummett, E. Clark, J. F. McMichael, R. J. Meyer, J. K. Schindler, C. S. Pohl, J. W. Wallis, X. Shi, L. Lin, H. Schmidt, Y. Tang, C. Haipek, M. E. Wiechert, J. V. Ivy, J. Kalicki, G. Elliott, R. E. Ries, J. E. Payton, P. Westervelt, M. H. Tomasson, M. A. Watson, J. Baty, S. Heath, W. D. Shannon, R. Nagarajan, D. C. Link, M. J. Walter, T. A. Graubert, J. F. DiPersio, R. K. Wilson and T. J. Ley, *New Engl. J. Med.*, 2009, **361**, 1058-1066.

44. O. Kosmider, V. Gelsi-Boyer, L. Slama, F. Dreyfus, O. Beyne-Rauzy, B. Quesnel, M. Hunault-Berger, B. Slama, N. Vey, C. Lacombe, E. Solary, D. Birnbaum, O. A. Bernard and M. Fontenay, *Leukemia*, 2010, **24**, 1094-1096.

45. D. R. Borger, K. K. Tanabe, K. C. Fan, H. U. Lopez, V. R. Fantin, K. S. Straley, D. P. Schenkein, A. F. Hezel, M. Ancukiewicz, H. M. Liebman, E. L. Kwak, J. W. Clark, D. P. Ryan, V. Deshpande, D. Dias-Santagata, L. W. Ellisen, A. X. Zhu and A. J. Iafrate, *The Oncologist*, 2012, **17**, 72-79.

46. J.-A. Losman and W. G. Kaelin, *Genes Dev.*, 2013, **27**, 836-852.

47. J. Kalinina, A. Carroll, L. Wang, Q. Yu, D. E. Mancheno, S. Wu, F. Liu, J. Ahn, M. He, H. Mao and E. G. Van Meir, *J. Mol. Med.*, 2012, **90**, 1161-1171.

48. R. Chowdhury, K. K. Yeoh, Y. M. Tian, L. Hillringhaus, E. A. Bagg, N. R. Rose, I. K. H. Leung, X. S. Li, E. C. Y. Woon, M. Yang, M. A. McDonough, O. N. King, I. J. Clifton, R. J. Klose, T. D. W. Claridge, P. J. Ratcliffe, C. J. Schofield and A. Kawamura, *EMBO reports*, 2011, **12**, 463-469.

49. W. Xu, H. Yang, Y. Liu, Y. Yang, P. Wang, S. H. Kim, S. Ito, C. Yang, P. Wang, M. T. Xiao, L. X. Liu, W. Q. Jiang, J. Liu, J. Y. Zhang, B. Wang, S. Frye, Y. Zhang, Y. H. Xu, Q. Y. Lei, K. L. Guan, S. M. Zhao and Y. Xiong, *Cancer Cell*, 2011, **19**, 17-30.

50. W. Kim and L. M. Liau, *Neurosurg. Clin. N. Am.*, 2012, **23**, 471-480.

51. V. Patil, J. Pal and K. Somasundaram, *Oncotarget*, 2015, **6**, 43452-43471.

52. H. Yang, D. Ye, K.-L. Guan and Y. Xiong, *Clin. Cancer. Res.*, 2012, **18**, 5562-5571.

53. A. Ploumakis and M. L. Coleman, *Mol. Cell*, 2015, **58**, 729-741.

54. F. E. Bleeker, N. A. Atai, S. Lamba, A. Jonker, D. Rijkeboer, K. S. Bosch, W. Tigchelaar, D. Troost, W. P. Vandertop, A. Bardelli and C. J. F. Van Noorden, *Acta Neuropathol.*, 2010, **119**, 487-494.

55. J. Shi, B. Sun, W. Shi, H. Zuo, D. Cui, L. Ni and J. Chen, *Tumor Biol.*, 2015, **36**, 655-662.

56. T. Watanabe, S. Nobusawa, P. Kleihues and H. Ohgaki, *Am. J. Pathol.*, 2009, **174**, 1149-1153.

57. B. Philip, D. X. Yu, M. R. Silvis, C. H. Shin, J. P. Robinson, G. L. Robinson, A. E. Welker, S. N. Angel, S. R. Tripp, J. A. Sonnen, M. W. VanBrocklin, R. J. Gibbons, R. E. Looper, H. Colman and S. L. Holmen, *Cell Rep.*, 2018, **23**, 1553-1564.

58. A. M. Intlekofer, A. H. Shih, B. Wang, A. Nazir, A. S. Rustenburg, S. K. Albanese, M. Patel, C. Famulare, F. M. Correa, N. Takemoto, V. Durani, H. Liu, J. Taylor, N. Farnoud, E. Papaemmanuil, J. R. Cross, M. S. Tallman, M. E. Arcila, M. Roshal, G. A. Petsko, B. Wu, S. Choe, Z. D. Konteatis, S. A. Biller, J. D. Chodera, C. B. Thompson, R. L. Levine and E. M. Stein, *Nature*, 2018, **559**, 125-129.

59. D. Golub, N. Iyengar, S. Dogra, T. Wong, D. Bready, K. Tang, A. S. Modrek and D. G. Placantonakis, *Front. Oncol.*, 2019, **9**, 417.

60. X. Ding, Z. Wang, D. Chen, Y. Wang, Z. Zhao, C. Sun, D. Chen, C. Tang, J. Xiong, L. Chen, Z. Yao, Y. Liu, X. Wang, D. P. Cahill, J. F. de Groot, T. Jiang, Y. Yao and L. Zhou, *J. Neurooncol.*, 2018, **140**, 591-603.

61. J. Beiko, D. Suki, K. R. Hess, B. D. Fox, V. Cheung, M. Cabral, N. Shonka, M. R. Gilbert, R. Sawaya, S. S. Prabhu, J. Weinberg, F. F. Lang, K. D. Aldape, E. P. Sulman, G. Rao, I. E. McCutcheon and D. P. Cahill, *J. Neurooncol.*, 2013, **16**, 81-91.

62. M. C. Tom, D. P. Cahill, J. C. Buckner, J. Dietrich, M. W. Parsons and J. S. Yu, *American Society of Clinical Oncology Educational Book*, 2019, 133-145.

63. S. M. Lee, H.-J. Koh, D.-C. Park, B. J. Song, T.-L. Huh and J.-W. Park, *Free Radical Biol. Med.*, 2002, **32**, 1185-1196.

64. R. Goodacre, S. Vaidyanathan, W. B. Dunn, G. G. Harrigan and D. B. Kell, *Trends Biotechnol.*, 2004, **22**, 245-252.

65. A. Zhang, H. Sun, P. Wang, Y. Han and X. Wang, *Analyst*, 2012, **137**, 293-300.

66. T. Çakır and M. J. Khatibipour, *Front. Bioeng. Biotech.*, 2014, **2**, 62.

67. W. B. Dunn, N. J. C. Bailey and H. E. Johnson, *Analyst*, 2005, **130**, 606-625.

68. K. Eckel-Mahan and P. Sassone-Corsi, *Physiol. Rev.*, 2013, **93**, 107-135.

69. I. Roci, J. D. Watrous, K. A. Lagerborg, L. Lafranchi, A. Lindqvist, M. Jain and R. Nilsson, *Cell Rep.*, 2019, **26**, 1691-1700.

70. D. Saigusa, Y. Okamura, I. N. Motoike, Y. Katoh, Y. Kurosawa, R. Saijyo, S. Koshiba, J. Yasuda, H. Motohashi, J. Sugawara, O. Tanabe, K. Kinoshita and M. Yamamoto, *PLoS One*, 2016, **11**, e0160555.

71. B. Kamlage, S. Neuber, B. Bethan, S. González Maldonado, A. Wagner-Golbs, E. Peter, O. Schmitz and P. Schatz, *Metabolites*, 2018, **8**.

72. L. V. Stevens, E. Hoover, Y. Wang and A. K. Zanetti, *Metabolites*, 2019, **9**.

73. P. Masson, A. C. Alves, T. M. D. Ebbels, J. K. Nicholson and E. J. Want, *Anal. Chem.*, 2010, **82**, 7779-7786.

74. C. Junot, G. Madalinski, J. C. Tabet and E. Ezan, *Analyst*, 2010, **135**, 2203-2219.

75. A.-H. Emwas, R. Roy, T. R. McKay, L. Tenori, E. Saccenti, A. N. G. Gowda, D. Raftery, F. Alahmari, L. Jaremko, M. Jaremko and S. D. Wishart, *Metabolites*, 2019, **9**.

76. L. J. Livermore, M. Isabelle, I. M. Bell, C. Scott, J. Walsby-Tickle, J. Gannon, P. Plaha, C. Vallance and O. Ansorge, *Neuro-Oncol. Adv.*, 2019, **1**, 1-12.

77. D. S. Wishart, *Nat. Rev. Drug Discov.*, 2016, **15**, 473-484.

78. C. H. Johnson, J. Ivanisevic and G. Siuzdak, *Nat. Rev. Mol. Cell Biol.*, 2016, **17**, 451-459.

79. B. O. Keller, J. Sui, A. B. Young and R. M. Whittal, *Anal. Chim. Acta*, 2008, **627**, 71-81.

80. E. de Hoffmann and V. Stroobant, *Mass Spectrometry: Principles and Applications*, Wiley, 2013.

81. P. E. Miller and M. B. Denton, *J. Chem. Educ.*, 1986, **63**, 617-623.

82. W. E. Stephens, *Phys. Rev.*, 1946, **69**, 691.

83. B. A. Mamyrin, *Int. J. Mass spectrom.*, 2001, **206**, 251-266.

84. A. Makarov, *Anal. Chem.*, 2000, **72**, 1156-1162.

85. J. Přichystal, K. A. Schug, K. Lemr, J. Novák and V. Havlíček, *Anal. Chem.*, 2016, **88**, 10338-10346.

86. G. D. Tredwell, J. G. Bundy, M. De Iorio and T. M. D. Ebbels, *Metabolomics*, 2016, **12**, 152.

87. D. D. Marshall and R. Powers, *Prog. Nucl. Magn. Reson. Spectrosc.*, 2017, **100**, 1-16.

88. J. Kalinina, J. Ahn, N. S. Devi, L. Wang, Y. Li, J. J. Olson, M. Glantz, T. Smith, E. L. Kim, A. Giese, R. L. Jensen, C. C. Chen, B. S. Carter, H. Mao, M. He and E. G. Van Meir, *Clin. Cancer. Res.*, 2016, **22**, 6256-6265.

89. U. E. Emir, S. J. Larkin, N. de Pennington, N. Voets, P. Plaha, R. Stacey, K. Al-Qahtani, J. McCullagh, C. J. Schofield, S. Clare, P. Jezzard, T. Cadoux-Hudson and O. Ansorge, *Cancer Res.*, 2016, **76**, 43-49.

90. A. Tebani, C. Afonso and S. Bekri, *J. Inherited Metab. Dis.*, 2018, **41**, 379-391.

91. N. Kadian, K. S. R. Raju, M. Rashid, M. Y. Malik, I. Taneja and M. Wahajuddin, *J. Pharm. Biomed. Anal.*, 2016, **126**, 83-97.

92. A. C. Schrimpe-Rutledge, S. G. Codreanu, S. D. Sherrod and J. A. McLean, *J. Am. Soc. Mass. Spectrom.*, 2016, **27**, 1897-1905.

93. L. W. Sumner, A. Amberg, D. Barrett, M. H. Beale, R. Beger, C. A. Daykin, T. W. M. Fan, O. Fiehn, R. Goodacre, J. L. Griffin, T. Hankemeier, N. Hardy, J. Harnly, R. Higashi, J. Kopka, A. N. Lane, J. C. Lindon, P. Marriott, A. W. Nicholls, M. D. Reily, J. J. Thaden and M. R. Viant, *Metabolomics*, 2007, **3**, 211-221.

94. J. Zhou and Y. Yin, *Analyst*, 2016, **141**, 6362-6373.

95. C. D. Broeckling, E. Hoyes, K. Richardson, J. M. Brown and J. E. Prenni, *Anal. Chem.*, 2018, **90**, 8020-8027.

96. L. A. Gethings, K. Richardson, J. Wildgoose, S. Lennon, S. Jarvis, C. L. Bevan, J. P. C. Vissers and J. I. Langridge, *Rapid Commun. Mass Spectrom.*, 2017, **31**, 1599-1606.

97. O. Begou, H. G. Gika, I. D. Wilson and G. Theodoridis, *Analyst*, 2017, **142**, 3079-3100.

98. E. J. Want, P. Masson, F. Michopoulos, I. D. Wilson, G. Theodoridis, R. S. Plumb, J. Shockcor, N. Loftus, E. Holmes and J. K. Nicholson, *Nat. Protoc.*, 2013, **8**, 17-32.

99. M. M. W. B. Hendriks, F. A. v. Eeuwijk, R. H. Jellema, J. A. Westerhuis, T. H. Reijmers, H. C. J. Hoefsloot and A. K. Smilde, *Trends Analyt. Chem.*, 2011, **30**, 1685-1698.

100. W. Bradley and P. Robert, *Current Metabolomics*, 2013, **1**, 92-107.

101. J. Bartel, J. Krumsiek and F. J. Theis, *Comput. Struct. Biotec.*, 2013, **4**, e201301009.

102. E. Saccenti, H. C. J. Hoefsloot, A. K. Smilde, J. A. Westerhuis and M. M. W. B. Hendriks, *Metabolomics*, 2014, **10**, 361-374.

103. N. Vinayavekhin and A. Saghatelian, *Curr. Protoc. Mol. Biol.*, 2010, **90**, 30.01.01-30.01.24.

104. G. J. Patti, *J. Sep. Sci.*, 2011, **34**, 3460-3469.

105. A. Alonso, S. Marsal and A. Julià, *Front. Bioeng. Biotech.*, 2015, **3**, 23.

106. J.-L. Ren, A.-H. Zhang, L. Kong and X.-J. Wang, *RSC Adv.*, 2018, **8**, 22335-22350.

107. Z. Tong and G. W. David, *Current Metabolomics*, 2013, **1**, 58-83.

108. R. George, A. Haywood, S. Khan, M. Radovanovic, J. Simmonds and R. Norris, *Ther. Drug Monit.*, 2018, **40**.

109. J. H. Knox and G. R. Laird, *J. Chromatogr. A*, 1976, **122**, 17-34.

110. J. F. Keefer and S. M. Schuster, *J. Chromatogr., B, Biomed. Sci. Appl.*, 1986, **383**, 297-305.

111. M. Armstrong, K. Jonscher and N. A. Reisdorph, *Rapid Commun. Mass Spectrom.*, 2007, **21**, 2717-2726.

112. J. Zhang, T. Raglione, Q. Wang, B. Kleintop, F. Tomasella and X. Liang, *J. Chromatogr. Sci.*, 2011, **49**, 825-831.

113. B. Buszewski and S. Noga, *Anal. Bioanal. Chem.*, 2012, **402**, 231-247.

114. G. Greco and T. Letzel, *J. Chromatogr. Sci.*, 2013, **51**, 684-693.

115. I. Aikaterini and M. Kouskoura, *J. Chromatogr. Sep. Tech.*, 2016, **7**, 326.

116. K. Contrepois, L. Jiang and M. Snyder, *Mol. Cell. Proteomics*, 2015, **14**, 1684-1695.

117. D. Q. Tang, L. Zou, X. X. Yin and C. N. Ong, *Mass Spectrom. Rev.*, 2016, **35**, 574-600.

118. L. Sonnenschein and A. Seubert, *J. Chromatogr. Sci.*, 2011, **49**, 589-595.

119. M. Dell'mour, G. Koellensperger and S. Hann, in *Amino Acid Analysis: Methods and Protocols*, eds. M. A. Alterman and P. Hunziker, Humana Press, 2012. 39-46.

120. R. Ramautar, A. Demirci and G. J. d. Jong, *Trends Analyt. Chem.*, 2006, **25**, 455-466.

121. M. Švidrnoch, A. Přibylka, V. Bekárek, J. Ševčík, V. Smolka and V. Maier, *J. Chromatogr. A*, 2016, **1467**, 383-390.

122. F. Gritti and G. Guiochon, *J. Chromatogr. A*, 2013, **1302**, 1-13.

123. A. J. P. Martin and R. L. M. Synge, *Biochem. J*, 1941, **35**, 1358-1368.

124. K. DeLaney, S. C. Sauer, Q. N. Vu and L. Li, *Molecules*, 2018, **24**, 42.

125. C. C. Liu, J. Zhang and N. J. Dovichi, *Rapid Commun. Mass Spectrom.*, 2005, **19**, 187-192.

126. M. Schwaiger, E. Rampler, G. Hermann, W. Miklos, W. Berger and G. Koellensperger, *Anal. Chem.*, 2017, **89**, 7667-7674.

127. H. Small, T. S. Stevens and W. C. Bauman, *Anal. Chem.*, 1975, **47**, 1801-1809.

128. C. A. Lucy, *J. Chromatogr. A*, 2003, **1000**, 711-724.

129. C. Sarzanini, *J. Chromatogr. A*, 2002, **956**, 3-13.

130. B. Buszewski, M. Jaćkowska, S. Bocian, P. Kosobucki and B. Gawdzik, *J. Sep. Sci.*, 2011, **34**, 601-608.

131. J. Wang, T. T. Christison, K. Misuno, L. Lopez, A. F. Huhmer, Y. Huang and S. Hu, *Anal. Chem.*, 2014, **86**, 5116-5124.

132. H. Kaspar, K. Dettmer, W. Gronwald and P. J. Oefner, *Anal. Bioanal. Chem.*, 2009, **393**, 445-452.

133. Z. J. Reitman, G. Jin, E. D. Karoly, I. Spasojevic, J. Yang, K. W. Kinzler, Y. He, D. D. Bigner, B. Vogelstein and H. Yan, *Proc. Natl. Acad. Sci.*, 2011, **108**, 3270-3275.

134. D. J. Beale, F. R. Pinu, K. A. Kouremenos, M. M. Poojary, V. K. Narayana, B. A. Boughton, K. Kanojia, S. Dayalan, O. A. H. Jones and D. A. Dias, *Metabolomics*, 2018, **14**, 152.

135. M.-E. P. Papadimitropoulos, C. G. Vasilopoulou, C. Maga-Nteve and M. I. Klapa, in *Metabolic Profiling: Methods and Protocols*, eds. G. A. Theodoridis, H. G. Gika and I. D. Wilson, Springer New York, 2018. 133-147.

136. R. Jiang, Y. Jiao and F. Xu, *Bioanalysis*, 2016, **8**, 1881-1883.

137. C. C. W. Willacey, M. Naaktgeboren, E. Lucumi Moreno, A. B. Wegrzyn, D. van der Es, N. Karu, R. M. T. Fleming, A. C. Harms and T. Hankemeier, *J. Chromatogr. A*, 2019, 460413.

138. J. G. Bollinger, G. Rohan, M. Sadilek and M. H. Gelb, *J. Lipid Res.*, 2013, **54**, 3523-3530.

139. A. Nordström, P. Tarkowski, D. Tarkowska, K. Dolezal, C. Åstot, G. Sandberg and T. Moritz, *Anal. Chem.*, 2004, **76**, 2869-2877.

140. I. Aretz and D. Meierhofer, *Int. J. Mol. Sci.*, 2016, **17**, 632.

141. S. A. Cohen and D. P. Michaud, *Anal. Biochem.*, 1993, **211**, 279-287.

142. P. W. Moser and E. E. Rickli, *J. Chromatogr. A*, 1979, **176**, 451-455.

143. S. A. Cohen and D. J. Strydom, *Anal. Biochem.*, 1988, **174**, 1-16.

144. R. F. Ebert, *Anal. Biochem.*, 1986, **154**, 431-435.

145. B. A. Boughton, D. L. Callahan, C. Silva, J. Bowne, A. Nahid, T. Rupasinghe, D. L. Tull, M. J. McConville, A. Bacic and U. Roessner, *Anal. Chem.*, 2011, **83**, 7523-7530.

146. K. Dursun and Z.-K. Birgül, *Chem. Pap.*, 2012, **66**, 54-60.

147. M. Kijewska, A. Kuc, A. Kluczyk, M. Waliczek, A. Man-Kupisinska, J. Lukasiewicz, P. Stefanowicz and Z. Szewczuk, *J. Am. Soc. Mass. Spectrom.*, 2014, **25**, 966-976.

148. S. A. Cohen, in *Amino Acid Analysis Protocols*, eds. C. Cooper, N. Packer and K. Williams, Humana Press, Totowa, NJ, 2000, DOI: 10.1385/1-59259-047-0:039. 39-47.

149. J. M. Armenta, D. F. Cortes, J. M. Pisciotta, J. L. Shuman, K. Blakeslee, D. Rasoloson, O. Ogunbiyi, D. J. Sullivan and V. Shulaev, *Anal. Chem.*, 2010, **82**, 548-558.

150. E. A. Mason and E. W. McDaniel, *Transport Properties of Ions in Gases*, John Wiley & Sons, New York, 1988.

151. K. Giles, S. D. Pringle, K. R. Worthington, D. Little, J. L. Wildgoose and R. H. Bateman, *Rapid Commun. Mass Spectrom.*, 2004, **18**, 2401-2414.

152. J. A. Picache, B. S. Rose, A. Balinski, K. L. Leaptrot, S. D. Sherrod, J. C. May and J. A. McLean, *Chem. Sci.*, 2019, **10**, 983-993.

153. V. D'Atri, M. Porrini, F. Rosu and V. Gabelica, *J. Mass Spectrom.*, 2015, **50**, 711-726.

154. Z. Zhou, X. Shen, J. Tu and Z.-J. Zhu, *Anal. Chem.*, 2016, **88**, 11084-11091.

155. J. Walsby-Tickle, J. Gannon, I. Hvinden, C. Bardella, M. I. Abboud, A. Nazeer, D. Hauton, E. Pires, T. Cadoux-Hudson, C. J. Schofield and J. S. O. McCullagh, *Commun. Biol.*, 2020, **3**, 247.

156. S. Wernisch and S. Pennathur, *Anal. Bioanal. Chem.*, 2016, **408**, 6079-6091.

157. S. Lu, X. Sun, C. Shi and Y. Zhang, *J. Chromatogr. A*, 2003, **1012**, 161-168.

158. C. S. Tsai, *Can. J. Chem.*, 1967, **45**, 873-880.

159. Z. J. Reitman, C. G. Duncan, E. Poteet, A. Winters, L.-J. Yan, D. M. Gooden, I. Spasojevic, L. G. Boros, S.-H. Yang and H. Yan, *J. Biol. Chem.*, 2014, **289**, 23318-23328.

160. M. Fang, J. Ivanisevic, H. P. Benton, C. H. Johnson, G. J. Patti, L. T. Hoang, W. Uritboonthai, M. E. Kurczy and G. Siuzdak, *Anal. Chem.*, 2015, **87**, 10935-10941.

161. T. Ashmore, L. D. Roberts, A. J. Morash, A. O. Kotwica, J. Finnerty, J. A. West, S. A. Murfitt, B. O. Fernandez, C. Branco, A. S. Cowburn, K. Clarke, R. S. Johnson, M. Feelisch, J. L. Griffin and A. J. Murray, *BMC Biol.*, 2015, **13**, 110.

162. D. G. Sitnikov, C. S. Monnin and D. Vuckovic, *Sci. Rep.*, 2016, **6**, 38885.

163. Y.-F. Xu, W. Lu and J. D. Rabinowitz, *Anal. Chem.*, 2015, **87**, 2273-2281.

164. *ISO 11843-2:2000 Capability of Detection - Part 2: Methodology in the Linear Calibration Case*, International Organization for Standardization, 2000.

165. *ICH Harmonised Tripartite Guideline: Validation of Analytical Procedures: Text and Methodology Q2(R1)*, International Conference on Harmonisation of Technical Requirements for Registration of Pharmaceuticals for Human Use, 2005.

166. J. Chong, D. S. Wishart and J. Xia, *Curr, Protoc, Bioinformatics*, 2019, **68**, e86.

167. M. Kanehisa and S. Goto, *Nucleic Acids Res.*, 2000, **28**, 27-30.

168. D. S. Wishart, Y. D. Feunang, A. Marcu, A. C. Guo, K. Liang, R. Vázquez-Fresno, T. Sajed, D. Johnson, C. Li, N. Karu, Z. Sayeeda, E. Lo, N. Assempour, M. Berjanskii, S. Singhal, D. Arndt, Y. Liang, H. Badran, J. Grant, A. Serra-Cayuela, Y. Liu, R. Mandal, V. Neveu, A. Pon, C. Knox, M. Wilson, C. Manach and A. Scalbert, *Nucleic Acids Res.*, 2017, **46**, D608-D617.

169. M. R. Antoniewicz, *Exp. Mol. Med.*, 2018, **50**, 19.

170. J. M. Flaman, T. Frebourg, V. Moreau, F. Charbonnier, C. Martin, P. Chappuis, A. P. Sappino, I. M. Limacher, L. Bron and J. Benhattar, *Proc. Natl. Acad. Sci.*, 1995, **92**, 3963-3967.

171. A. C. Diserens, N. de Tribolet, A. Martin-Achard, A. C. Gaide, J. F. Schnegg and S. Carrel, *Acta Neuropathol.*, 1981, **53**, 21-28.

172. G. S. Cowley, B. A. Weir, F. Vazquez, P. Tamayo, J. A. Scott, S. Rusin, A. East-Seletsky, L. D. Ali, W. F. J. Gerath, S. E. Pantel, P. H. Lizotte, G. Jiang, J. Hsiao, A. Tsherniak, E. Dwinell, S. Aoyama, M. Okamoto, W. Harrington, E. Gelfand, T. M. Green, M. J. Tomko, S. Gopal, T. C. Wong, H. Li, S. Howell, N. Stransky, T. Liefeld, D. Jang, J. Bistline, B. Hill Meyers, S. A. Armstrong, K. C. Anderson, K. Stegmaier, M. Reich, D. Pellman, J. S. Boehm, J. P. Mesirov, T. R. Golub, D. E. Root and W. C. Hahn, *Sci. Data*, 2014, **1**, 140035.

173. M. Allen, M. Bjerke, H. Edlund, S. Nelander and B. Westermark, *Sci. Transl. Med.*, 2016, **8**, 354re353.

174. E. G. Van Meir, T. Kikuchi, M. Tada, H. Li, A.-C. Diserens, B. E. Wojcik, H. J. S. Huang, T. Friedmann, N. de Tribolet and W. K. Cavenee, *Cancer Res.*, 1994, **54**, 649-652.

175. C. S. Djuzenova, V. Fiedler, S. Memmel, A. Katzer, S. Hartmann, G. Krohne, H. Zimmermann, C.-J. Scholz, B. Polat, M. Flentje and V. L. Sukhorukov, *Exp. Cell Res.*, 2015, **330**, 346-357.

176. R. B. DuBridge, P. Tang, H. C. Hsia, P. M. Leong, J. H. Miller and M. P. Calos, *Mol. Cell. Biol.*, 1987, **7**, 379-387.

177. L. Sun, X. Shen, Y. Liu, G. Zhang, J. Wei, H. Zhang, E. Zhang and F. Ma, *Acta Bioch. Bioph. Sin.*, 2010, **42**, 230-235.

178. Y.-C. Lin, M. Boone, L. Meuris, I. Lemmens, N. Van Roy, A. Soete, J. Reumers, M. Moisse, S. Plaisance, R. Drmanac, J. Chen, F. Speleman, D. Lambrechts, Y. Van de Peer, J. Tavernier and N. Callewaert, *Nat. Commun.*, 2014, **5**, 4767.

179. J.-M. Yang, P. Schiapparelli, H. N. Nguyen, A. Igarashi, Q. Zhang, S. Abbadi, L. M. Amzel, H. Sesaki, A. Quiñones-Hinojosa and M. Iijima, *Oncogene*, 2017, **36**, 3673-3685.

180. D. Xiao, L. Zeng, K. Yao, X. Kong, G. Wu and Y. Yin, *Amino Acids*, 2016, **48**, 2067-2080.

181. D. H. Williamson, P. Lund and H. A. Krebs, *Biochem. J*, 1967, **103**, 514-527.

182. H. A. Krebs and T. Gascoyne, *Biochem. J*, 1968, **108**, 513-520.

183. H. Massudi, R. Grant, G. J. Guillemin and N. Braidy, *Redox Report*, 2012, **17**, 28-46.

184. K. Tateishi, H. Wakimoto, A. J. Iafrate, S. Tanaka, F. Loebel, N. Lelic, D. Wiederschain, O. Bedel, G. Deng, B. Zhang, T. He, X. Shi, R. E. Gerszten, Y. Zhang, J.-R. J. Yeh, W. T. Curry, D. Zhao, S. Sundaram, F. Nigim, M. V. A. Koerner, Q. Ho, D. E. Fisher, E. M. Roider, L. V. Kemeny, Y. Samuels, K. T. Flaherty, T. T. Batchelor, A. S. Chi and D. P. Cahill, *Cancer Cell*, 2015, **28**, 773-784.

185. M. Miyake, Y. Kakimoto and M. Sorimachi, *Biochim. Biophys. Acta*, 1978, **544**, 656-666.

186. J. H. Neale, T. Bzdega and B. Wroblewska, *J. Neurochem.*, 2000, **75**, 443-452.

187. F. Collard, V. Stroobant, P. Lamosa, C. N. Kapanda, D. M. Lambert, G. G. Muccioli, J. H. Poupaert, F. Opperdoes and E. Van Schaftingen, *J. Biol. Chem.*, 2010, **285**, 29826-29833.

188. M. Hamada-Kanazawa, M. Narahara, M. Takano, K. S. Min, K. Tanaka and M. Miyake, *Biol. Pharm. Bull.*, 2011, **34**, 1455-1464.

189. M. Hamada-Kanazawa, M. Narahara, M. Takano, K.-S. Min, K. Tanaka and M. Miyake, *Biol. Pharm. Bull.*, 2013, **36**, 1068-1079.

190. P. M. Long, J. R. Moffett, A. M. A. Namboodiri, M. S. Viapiano, S. E. Lawler and D. M. Jaworski, *J. Biol. Chem.*, 2013, **288**, 26188-26200.

191. L. C. Lee, C.-Y. Liong and A. A. Jemain, *Analyst*, 2018, **143**, 3526-3539.

192. J. A. Westerhuis, H. C. J. Hoefsloot, S. Smit, D. J. Vis, A. K. Smilde, E. J. J. van Velzen, J. P. M. van Duijnhoven and F. A. van Dorsten, *Metabolomics*, 2008, **4**, 81-89.

193. J. A. Williams, R. Lalonde, J. R. Koup, D. D. Christ and S. Ekins, *Predictive Approaches in Drug Discovery and Development: Biomarkers and In Vitro / In Vivo Correlations*, Wiley, 2012.

194. L. V. Eggleston and H. A. Krebs, *Biochem. J*, 1974, **138**, 425-435.

195. S. J. Gelman, F. Naser, N. G. Mahieu, L. D. McKenzie, G. P. Dunn, M. G. Chheda and G. J. Patti, *Cell Rep.*, 2018, **22**, 512-522.

196. S. Li, Y. Park, S. Duraisingham, F. H. Strobel, N. Khan, Q. A. Soltow, D. P. Jones and B. Pulendran, *PLoS Comp. Biol.*, 2013, **9**, e1003123.

197. D. E. Atkinson and G. M. Walton, *J. Biol. Chem.*, 1965, **240**, 757-763.

198. J. R. Aprille, *FASEB J.*, 1988, **2**, 2547-2556.

199. G. Shaw, S. Morse, M. Ararat and F. L. Graham, *FASEB J.*, 2002, **16**, 869-871.

200. M. Strickland and E. A. Stoll, *Front. Cell Dev. Biol.*, 2017, **5**, 43.

201. K. S. McCommis and B. N. Finck, *Biochem. J*, 2015, **466**, 443-454.

202. J. Bremmer, *Eur. J. Biochem.*, 1969, **8**, 535-540.

203. R. L. Tyson, J. Perron and G. R. Sutherland, *Neuroreport*, 2000, **11**, 1845-1848.

204. Z. Zhelev, D. Ivanova, R. Bakalova, I. Aoki and T. Higashi, *Anticancer Res.*, 2016, **36**, 6011-6020.

205. L. E. Huang, *Carcinogenesis*, 2019, **40**, 1299-1307.

206. T. Miyazaki, J. Miyazaki, H. Yamane and M. Nishiyama, *Microbiology*, 2004, **150**, 2327-2334.

207. K. Ortmayr, T. J. Causon, S. Hann and G. Koellensperger, *Trends Analyt. Chem.*, 2016, **82**, 358-366.

208. S. Bröer and A. Bröer, *Biochem. J*, 2017, **474**, 1935-1963.

209. P. D. Rainville, I. D. Wilson, J. K. Nicholson, G. Isaac, L. Mullin, J. I. Langridge and R. S. Plumb, *Anal. Chim. Acta*, 2017, **982**, 1-8.

210. S. Wiklund, E. Johansson, L. Sjöström, E. J. Mellerowicz, U. Edlund, J. P. Shockcor, J. Gottfries, T. Moritz and J. Trygg, *Anal. Chem.*, 2008, **80**, 115-122.

211. P. J. Markovitz, D. T. Chuang and R. P. Cox, *J. Biol. Chem.*, 1984, **259**, 11643-11646.

212. D. Ye, K.-L. Guan and Y. Xiong, *Trends in Cancer*, 2018, **4**, 151-165.

213. P. P. Sordillo, L. A. Sordillo and L. Helson, *Anticancer Res.*, 2017, **37**, 2159-2171.

214. C. Bilir and C. Sarisozen, *J. Oncol. Sci.*, 2017, **3**, 52-56.

215. S. Adams, N. Braidy, A. Bessesde, B. J. Brew, R. Grant, C. Teo and G. J. Guillemin, *Cancer Res.*, 2012, **72**, 5649-5657.

216. K. E. French, J. Harvey and J. S. O. McCullagh, *Sci. Rep.*, 2018, **8**, 1695.

217. E. Ahn, P. Kumar, D. Mukha, A. Tzur and T. Shlomi, *Mol. Syst. Biol.*, 2017, **13**, 953.

218. M. A. García-Campos, J. Espinal-Enríquez and E. Hernández-Lemus, *Front. Physiol.*, 2015, **6**, 383.

219. S. Ghosh, H. J. Blumenthal, E. Davidson and S. Roseman, *J. Biol. Chem.*, 1960, **235**, 1265-1273.

220. G. Zhao and M. E. Winkler, *J. Bacteriol.*, 1996, **178**, 232-239.

221. S. K. McBrayer, J. R. Mayers, G. J. DiNatale, D. D. Shi, J. Khanal, A. A. Chakraborty, K. A. Sarosiek, K. J. Briggs, A. K. Robbins, T. Sewastianik, S. J. Shareef, B. A. Olenchock, S. J. Parker, K. Tateishi, J. B. Spinelli, M. Islam, M. C. Haigis, R. E. Looper, K. L. Ligon, B. E. Bernstein, R. D. Carrasco, D. P. Cahill, J. M. Asara, C. M. Metallo, N. H. Yennawar, M. G. Vander Heiden and W. G. Kaelin, *Cell*, 2018, **175**, 101-116.

222. M. Friedrich, L. Bunse, W. Wick and M. Platten, *Curr. Opin. Oncol.*, 2018, **30**, 368-374.

223. G. Frumento, R. Rotondo, M. Tonetti, G. Damonte, U. Benatti and G. B. Ferrara, *J. Exp. Med.*, 2002, **196**, 459-468.

224. A. S. Berghoff, B. Kiesel, G. Widhalm, D. Wilhelm, O. Rajky, S. Kurscheid, P. Kresl, A. Wöhrer, C. Marosi, M. E. Hegi and M. Preusser, *Neuro Oncol.*, 2017, **19**, 1460-1468.

225. B. D. Choi and W. T. Curry, *Transl. Cancer Res.*, 2017, **6**, S1253-S1256.

226. Z. Li, M. Philip and P. B. Ferrell, *Oncogene*, 2020, **39**, 3611–3619.

227. T. Doucette, G. Rao, A. Rao, L. Shen, K. Aldape, J. Wei, K. Dziurzynski, M. Gilbert and A. B. Heimberger, *Cancer Immunol. Res.*, 2013, **1**, 112-122.

228. E. F. Pai and G. E. Schulz, *J. Biol. Chem.*, 1983, **258**, 1752-1757.

229. L. Tretter and V. Adam-Vizi, *Phil. Trans. R. Soc. Lon. B*, 2005, **360**, 2335-2345.

230. K. Okada, C. Angkawidjaja, Y. Koga, K. Takano and S. Kanaya, *PLoS One*, 2012, **7**, e40307.

231. M. S. Islam, T. M. Leissing, R. Chowdhury, R. J. Hopkinson and C. J. Schofield, *Annu. Rev. Biochem.*, 2018, **87**, 585-620.

232. H. Tarhonskaya, A. M. Rydzik, I. K. H. Leung, N. D. Loik, M. C. Chan, A. Kawamura, J. S. O. McCullagh, T. D. W. Claridge, E. Flashman and C. J. Schofield, *Nat. Commun.*, 2014, **5**, 3423.

233. R. P. Shank and D. J. Bennett, *Neurochem. Res.*, 1993, **18**, 401-410.

234. M. S. Waitkus, B. H. Diplas and H. Yan, *Neuro Oncol.*, 2015, **18**, 16-26.

235. M. G. Vander Heiden, L. C. Cantley and C. B. Thompson, *Science*, 2009, **324**, 1029-1033.

236. A. M. Intlekofer, R. G. Dematteo, S. Venneti, L. W. Finley, C. Lu, A. R. Judkins, A. S. Rustenburg, P. B. Grinaway, J. D. Chodera, J. R. Cross and C. B. Thompson, *Cell Metab*, 2015, **22**, 304-311.

237. R. Vatrinet, G. Leone, M. De Luise, G. Girolimetti, M. Vidone, G. Gasparre and A. M. Porcelli, *Cancer & Metabolism*, 2017, **5**, 3.

238. F. Fack, S. Tardito, G. Hochart, A. Oudin, L. Zheng, S. Fritah, A. Golebiewska, P. V. Nazarov, A. Bernard, A.-C. Hau, O. Keunen, W. Leenders, M. Lund-Johansen, J. Stauber, E. Gottlieb, R. Bjerkvig and S. P. Niclou, *EMBO Mol. Med.*, 2017, **9**, 1681-1695.

239. M. Khurshed, R. J. Molenaar, K. Lenting, W. P. Leenders and C. J. F. van Noorden, *Oncotarget*, 2017, **8**, 49165-49177.

240. R. J. Molenaar, J. P. Maciejewski, J. W. Wilmink and C. J. F. van Noorden, *Oncogene*, 2018, **37**, 1949-1960.

241. Q. SongTao, Y. Lei, G. Si, D. YanQing, H. HuiXia, Z. XueLin, W. LanXiao and Y. Fei, *Cancer Sci.*, 2012, **103**, 269-273.

242. J. L. Johnson, *Brain Res.*, 1972, **37**, 1-19.

243. S. J. Gelman, N. G. Mahieu, K. Cho, E. M. Llufrio, T. A. Wencewicz and G. J. Patti, *Cancer. Metab.*, 2015, **3**, 13.

244. M. Böttcher, K. Renner, R. Berger, K. Mentz, S. Thomas, Z. E. Cardenas-Conejo, K. Dettmer, P. J. Oefner, A. Mackensen, M. Kreutz and D. Mougiakakos, *OncoImmunology*, 2018, **7**, e1445454.

245. L. Laboureur, M. Ollero and D. Touboul, *Int. J. Mol. Sci.*, 2015, **16**, 13868-13884.

246. X. Liu, S. Sadhukhan, S. Sun, G. R. Wagner, M. D. Hirschey, L. Qi, H. Lin and J. W. Locasale, *Mol. Cell. Proteomics*, 2015, **14**, 1489-1500.

247. Z. Ser, X. Liu, N. N. Tang and J. W. Locasale, *Anal. Biochem.*, 2015, **475**, 22-28.

248. M. E. Katt, A. L. Placone, A. D. Wong, Z. S. Xu and P. C. Searson, *Front. Bioeng. Biotechnol.*, 2016, **4**, 12.

249. U. Ben-David, R. Beroukhim and T. R. Golub, *Nat. Rev. Cancer*, 2019, **19**, 97-109.

250. T. K. Kim and J. H. Eberwine, *Anal. Bioanal. Chem.*, 2010, **397**, 3173-3178.

251. C. Bardella, O. Al-Dalahmah, D. Krell, P. Brazauskas, K. Al-Qahtani, M. Tomkova, J. Adam, S. Serres, H. Lockstone, L. Freeman-Mills, I. Pfeffer, N. Sibson, R. Goldin, B. Schuster-Böeckler, P. J. Pollard, T. Soga, J. S. O. McCullagh, C. J. Schofield, P. Mulholland, O. Ansorge, S. Kriaucionis, P. J. Ratcliffe, F. G. Szele and I. Tomlinson, *Cancer Cell*, 2016, **30**, 578-594.

252. D. Capper, S. Weißert, J. Balss, A. Habel, J. Meyer, D. Jäger, U. Ackermann, C. Tessmer, A. Korshunov, H. Zentgraf, C. Hartmann and A. Von Deimling, *Brain Pathol.*, 2010, **20**, 245-254.

253. R. Gruetter, E. J. Novotny, S. D. Boulware, D. L. Rothman, G. F. Mason, G. I. Shulman, R. G. Shulman and W. V. Tamborlane, *Proc. Natl. Acad. Sci.*, 1992, **89**, 1109.

254. M. L. Shuler, *J. Biotechnol.*, 1999, **71**, 225-228.

255. D. C. Earl, P. B. Ferrell, N. Leelatian, J. T. Froese, B. J. Reisman, J. M. Irish and B. O. Bachmann, *Nat. Commun.*, 2018, **9**, 39.

256. G. Miserocchi, L. Mercatali, C. Liverani, A. De Vita, C. Spadazzi, F. Pieri, A. Bongiovanni, F. Recine, D. Amadori and T. Ibrahim, *J. Transl. Med.*, 2017, **15**, 229.

257. S. J. Parker and C. M. Metallo, *Pharmacol. Ther.*, 2015, **152**, 54-62.

258. Z. Dai and J. W. Locasale, *Metab. Eng.*, 2017, **43**, 94-102.

259. P. Kreuzaler, Y. Panina, J. Segal and M. Yuneva, *Mol. Metab.*, 2020, **33**, 83-101.

260. J. Popovici-Muller, R. M. Lemieux, E. Artin, J. O. Saunders, F. G. Salituro, J. Travins, G. Cianchetta, Z. Cai, D. Zhou, D. Cui, P. Chen, K. Straley, E. Tobin, F. Wang, M. D. David, V. Penard-Lacronique, C. Quivoron, V. Saada, S. de Botton, S. Gross, L. Dang, H. Yang, L. Utley, Y. Chen, H. Kim, S. Jin, Z. Gu, G. Yao, Z. Luo, X. Lv, C. Fang, L. Yan, A. Olaharski, L. Silverman, S. Biller, S.-S. M. Su and K. Yen, *ACS Med. Chem. Lett.*, 2018, **9**, 300-305.

261. B. Kaminska, B. Czapski, R. Guzik, K. S. Król and B. Gielniewski, *Molecules*, 2019, **24**, 968.

262. S. Lagziel, W. D. Lee and T. Shlomi, *BMC Biol.*, 2019, **17**, 37.

263. N. J. O'Neil, M. L. Bailey and P. Hieter, *Nat. Rev. Genet.*, 2017, **18**, 613-623.

264. L. H. Hartwell, P. Szankasi, C. J. Roberts, A. W. Murray and S. H. Friend, *Science*, 1997, **278**, 1064-1068.

265. H. Winter, P. J. Kaisaki, J. Harvey, E. Giacopuzzi, M. P. Ferla, M. M. Pentony, S. J. L. Knight, R. A. Sharma, J. C. Taylor and J. S. O. McCullagh, *Cancers (Basel)*, 2019, **11**, 1895.

266. J. Schulthess, S. Pandey, M. Capitani, K. C. Rue-Albrecht, I. Arnold, F. Franchini, A. Chomka, N. E. Ilott, D. G. W. Johnston, E. Pires, J. McCullagh, S. N. Sansom, C. V. Arancibia-Cárcamo, H. H. Uhlig and F. Powrie, *Immunity*, 2019, **50**, 432-445.

267. M. D. Favara, E. C. Zois, S. Haider, E. Pires, H. Sheldon, J. McCullagh, H. A. Banham and L. A. Harris, *Metabolites*, 2019, **9**, 287.

268. P. Rustin, T. Bourgeron, B. Parfait, D. Chretien, A. Munnich and A. Rötig, *Biochim. Biophys. Acta*, 1997, **1361**, 185-197.

269. C. Frezza, P. J. Pollard and E. Gottlieb, *J. Mol. Med.*, 2011, **89**, 213-220.

270. J. Buzkova, J. Nikkanen, S. Ahola, A. H. Hakonen, K. Sevastianova, T. Hovinen, H. Yki-Järvinen, K. H. Pietiläinen, T. Lönnqvist, V. Velagapudi, C. J. Carroll and A. Suomalainen, *EMBO Mol. Med.*, 2018, **10**, e9091.

Chapter 10. Appendices

10.1. List of 170 authentic metabolite standards

A mix of 170 authentic metabolite standards (listed in Table 10.1) was prepared to provide a reference sample for IC-MS/MS evaluation. Solids were dissolved and solutions were diluted in 80 % methanol$_{(aq)}$, producing stock solutions with a concentration of 1 mg / mL. The stock solutions were combined to produce a mix of all 170 standards in 80 % methanol$_{(aq)}$, with a final concentration of 5 μg / mL for each standard, which was frozen as aliquots.

Table 10.1: Table of 170 authentic metabolite standards in the mix used for IC-MS/MS evaluation.

HMDB code	Compound name	CAS Number	Manufacturer
HMDB0036093	(±)-Abscisic acid	14375-45-2	Sigma-Aldrich
HMDB0032797	(±)-Jasmonic acid	77026-92-7	Supelco
HMDB0001343	(±)-Mevalonic acid 5-phosphate lithium salt hydrate	73566-35-5	Sigma-Aldrich
HMDB0000357	(±)-Sodium 3-hydroxybutyrate	150-83-4	Sigma-Aldrich
N/A	(E)-1-Hydroxy-2-methyl-2-butenyl 4-pyrophosphate lithium salt	396726-03-7	Sigma-Aldrich
HMDB0000227	(R)-Mevalonic acid lithium salt	1255502-07-8	Sigma-Aldrich
HMDB0000725	(S)-(-)-trans-4-Hydroxyproline	51-35-4	Sigma-Aldrich
HMDB0000957	1,2-Dihydroxybenzene	120-80-9	Sigma-Aldrich
HMDB0001213	1-Deoxy-D-xylulose-5-phosphate sodium salt	190079-18-6	Sigma-Aldrich
HMDB0000232	2,3-Pyridinedicarboxylic acid	89-00-9	Sigma-Aldrich
HMDB0000152	2,5-Dihydroxybenzoic acid sodium salt	4955-90-2	Sigma-Aldrich
HMDB0000012	2'Deoxyuridine	951-78-0	Sigma-Aldrich
HMDB0000905	2'-Deoxyadenosine 5'-monophosphate	653-63-4	Sigma-Aldrich
HMDB0001532	2'-Deoxyadenosine 5'-triphosphate disodium salt	74299-50-6	Sigma-Aldrich
HMDB0000101	2'-Deoxyadenosine monohydrate	16373-93-6	Sigma-Aldrich
HMDB0000998	2'-Deoxycytidine 5'-triphosphate disodium salt	102783-51-7	Roche
HMDB0001044	2'-Deoxyguanosine 5'-monophosphate sodium salt hydrate	902-04-5	Sigma-Aldrich
HMDB0002166	2-Aminoisobutyric acid	62-57-7	Sigma-Aldrich
N/A	2-C-Methyl-D-erythritol 4-phosphate lithium salt	206440-72-4	Sigma-Aldrich
HMDB0001031	2-Deoxyribose 5-phosphate sodium salt	102916-66-5	Sigma-Aldrich
HMDB0000008	2-Hydroxybutyric acid sodium salt	5094-24-6	Sigma-Aldrich
HMDB0000752	2-Methylglutarate	18069-17-5	Sigma-Aldrich
HMDB0000225	2-Oxoadipic acid	3184-35-8	Supelco
HMDB0000208	2-Oxoglutaric acid monosodium salt	22202-68-2	Sigma-Aldrich
HMDB0000816	2-Phosphoglycolic acid lithium salt	13147-57-4	Sigma-Aldrich
HMDB0001376	3-Deoxy-2-keto-6-phosphogluconic acid lithium salt	27244-54-8	Supelco
HMDB0000355	3-Hydroxy-3-methylglutaric acid	503-49-1	Sigma-Aldrich
HMDB0013188	3-Hydroxypicolinic acid	874-24-8	Sigma-Aldrich
HMDB0000197	3-Indoleacetic acid	87-51-4	Sigma-Aldrich
HMDB0000402	3-Isopropylmalic acid	16048-89-8	Sigma-Aldrich
HMDB0000707	4-Hydroxyphenylpyruvic acid	156-39-8	Sigma-Aldrich
HMDB0000763	5-Hydroxyindole-3-acetic acid	54-16-0	Sigma-Aldrich

HMDB code	Compound name	CAS Number	Manufacturer
HMDB0000280	5-Phospho-D-ribose 1-diphosphate pentasodium salt	108321-05-7	Sigma-Aldrich
HMDB0001316	6-Phosphogluconic acid trisodium salt	53411-70-4	Sigma-Aldrich
HMDB0001484	Acetoacetyl-CoA sodium salt hydrate	1420-36-6	Sigma-Aldrich
HMDB0001890	Acetylcysteine	616-91-1	Sigma-Aldrich
HMDB0000532	Acetylglycine	543-24-8	Sigma-Aldrich
HMDB0011616	Adenosine 2′,3′-cyclic monophosphate sodium salt	37063-35-7	Sigma-Aldrich
HMDB0001341	Adenosine 5′-diphosphate sodium salt	20398-34-9	Sigma-Aldrich
HMDB0000045	Adenosine 5′-monophosphate disodium salt	4578-31-8	Sigma-Aldrich
HMDB0000538	Adenosine 5′-triphosphate disodium salt hydrate	34369-07-8	Sigma-Aldrich
HMDB0006557	Adenosine-5′-diphosphoglucose disodium salt	102129-65-7	Sigma-Aldrich
HMDB0000508	Adonitol	488-81-3	Sigma-Aldrich
HMDB0000072	cis-Aconitic acid	585-84-2	Sigma-Aldrich
HMDB0000094	Citric acid	77-92-9	Sigma-Aldrich
HMDB0001423	Coenzyme A sodium salt hydrate	55672-92-9	Sigma-Aldrich
HMDB0000095	Cytidine 5′-monophosphate disodium salt	6757-06-8	Sigma-Aldrich
HMDB0000082	Cytidine 5′-triphosphate disodium salt	36051-68-0	Sigma-Aldrich
HMDB0000807	D-(−)-3-Phosphoglyceric acid disodium salt	80731-10-8	Sigma-Aldrich
HMDB0000426	D-(−)-Citramalic acid lithium salt	6236-10-8	Sigma-Aldrich
HMDB0000660	D-(−)-Fructose	57-48-7	Sigma-Aldrich
HMDB0003072	D-(−)-Quinic acid	77-95-2	Sigma-Aldrich
HMDB0000283	D-(−)-Ribose	50-69-1	Sigma-Aldrich
HMDB0000143	D-(+)-Galactose	59-23-4	Sigma-Aldrich
HMDB0000122	D-(+)-Glucose	50-99-7	Sigma-Aldrich
HMDB0000169	D-(+)-Mannose	3458-28-4	Sigma-Aldrich
HMDB0003213	D-(+)-Raffinose pentahydrate	17629-30-0	Sigma-Aldrich
HMDB0001151	D-Allose	2595-97-3	Sigma-Aldrich
HMDB0001321	D-Erythrose 4-phosphate sodium salt	103302-15-4	Sigma-Aldrich
HMDB0001058	D-Fructose 1,6-bisphosphate trisodium salt hydrate	38099-82-0	Sigma-Aldrich
HMDB0000124	D-Fructose 6-phosphate disodium salt hydrate	26177-86-6	Sigma-Aldrich
HMDB0000625	D-Gluconic acid sodium salt	527-07-1	Sigma-Aldrich
HMDB0001254	D-Glucosamine 6-phosphate	3616-42-0	Sigma-Aldrich
HMDB0001401	D-Glucose 6-phosphate sodium salt	54010-71-8	Sigma-Aldrich
HMDB0000127	D-Glucuronic acid	6556-12-3	Sigma-Aldrich
HMDB0000139	D-Glyceric acid sodium salt	6000-40-4	Sigma-Aldrich
HMDB0001882	Dihydroxyacetone	96-26-4	Sigma-Aldrich
HMDB0001473	Dihydroxyacetone phosphate dilithium salt	102783-56-2	Sigma-Aldrich
HMDB0000650	DL-2-Aminobutyric acid	2835-81-6	Sigma-Aldrich
HMDB0000291	DL-4-Hydroxy-3-methoxymandelic acid	55-10-7	Supelco
N/A	DL-Glyceraldehyde 2-phosphate sodium salt	130998-65-1	Sigma-Aldrich
HMDB0001112	DL-Glyceraldehyde 3-phosphate solution	591-59-3	Sigma-Aldrich
HMDB0000193	DL-Isocitric acid trisodium salt hydrate	1637-73-6	Sigma-Aldrich
HMDB0000190	DL-Lactic acid	50-21-5	Sigma-Aldrich
HMDB0000744	DL-Malic acid	6915-15-7	Sigma-Aldrich
HMDB0004136	DL-Threitol	7493-90-5	Sigma-Aldrich
HMDB0059655	DL-α-Hydroxyglutaric acid disodium salt	1391194-67-4	Sigma-Aldrich
HMDB0000210	D-Pantothenic acid hemicalcium salt	137-08-6	Sigma-Aldrich
HMDB0001548	D-Ribose 5-phosphate disodium salt dihydrate	207671-46-3	Sigma-Aldrich
HMDB0000618	D-Ribulose 5-phosphate sodium salt	93-87-8	Sigma-Aldrich
HMDB0001068	D-Sedoheptulose 7-phosphate lithium salt	2646-35-7	Sigma-Aldrich
HMDB0000247	D-Sorbitol	50-70-4	Sigma-Aldrich
HMDB0000868	D-Xylulose 5-phosphate lithium salt	2080295-99-2	Sigma-Aldrich
HMDB0000622	Ethylmalonic acid	601-75-2	Sigma-Aldrich
HMDB0001248	Flavin adenine dinucleotide disodium salt hydrate	84366-81-4	Sigma-Aldrich
HMDB0000134	Fumaric acid	110-17-8	Sigma-Aldrich
HMDB0003559	Gibberelliic acid	77-06-5	Sigma-Aldrich
HMDB0000150	Gluconolactone	90-80-2	Sigma-Aldrich
HMDB0000620	Glutaconic acid	1724-02-3	Sigma-Aldrich
HMDB0000661	Glutaric acid	110-94-1	Sigma-Aldrich

HMDB code	Compound name	CAS Number	Manufacturer
HMDB0000131	Glycerol	56-81-5	Sigma-Aldrich
HMDB0000115	Glycolic acid	79-14-1	Sigma-Aldrich
HMDB0000119	Glyoxylic acid monohydrate	563-96-2	Sigma-Aldrich
HMDB0000133	Guanosine	118-00-3	Sigma-Aldrich
HMDB0001201	Guanosine 5′-diphosphate sodium salt	43139-22-6	Sigma-Aldrich
HMDB0001397	Guanosine 5′-monophosphate disodium salt hydrate	5550-12-9	Sigma-Aldrich
HMDB0001273	Guanosine 5′-triphosphate sodium salt hydrate	36051-31-7	Sigma-Aldrich
HMDB0000714	Hippuric acid	495-69-2	Sigma-Aldrich
HMDB0000118	Homovanillic acid	306-08-1	Sigma-Aldrich
HMDB0000764	Hydrocinnamic acid	501-52-0	Sigma-Aldrich
HMDB0000175	Inosine 5′-monophosphate disodium salt hydrate	352195-40-5	Sigma-Aldrich
HMDB0000189	Inosine 5′-triphosphate trisodium salt	35908-31-7	Sigma-Aldrich
HMDB0001347	Isopentenyl pyrophosphate trilithium salt	18687-43-9	Sigma-Aldrich
HMDB0032923	Kojic acid	501-30-4	Supelco
HMDB0000568	L-(−)-Arabitol	7643-75-6	Sigma-Aldrich
HMDB0001266	L-(−)-Sorbose	87-79-6	Sigma-Aldrich
HMDB0012326	L-(+)-Gulose	6027-89-0	Sigma-Aldrich
HMDB0000362	L-2-Phosphoglyceric acid disodium salt hydrate	23295-92-3	Sigma-Aldrich
HMDB0000044	L-Ascorbic acid	50-81-7	Sigma-Aldrich
HMDB0000191	L-Aspartic acid	56-84-8	Sigma-Aldrich
HMDB0000574	L-Cysteine	52-90-4	Sigma-Aldrich
HMDB0000148	L-Glutamic acid	56-86-0	Sigma-Aldrich
HMDB0000641	L-Glutamine	56-85-9	Sigma-Aldrich
HMDB0000125	L-Glutathione reduced	70-18-8	Sigma-Aldrich
HMDB0000267	L-Pyroglutamic acid	98-79-3	Sigma-Aldrich
HMDB0000621	L-Ribulose	2042-27-5	Sigma-Aldrich
HMDB0000187	L-Serine	56-45-1	Sigma-Aldrich
HMDB0000176	Maleic acid	110-16-7	Sigma-Aldrich
HMDB0000691	Malonic acid	141-82-2	Sigma-Aldrich
HMDB0002928	Maltitol	585-88-6	Sigma-Aldrich
HMDB0000749	Mesaconic acid	498-24-8	Sigma-Aldrich
HMDB0029965	Methyl β-D-glucopyranoside	709-50-2	Sigma-Aldrich
HMDB0004815	Methyl-4-hydroxybenzoate	99-76-3	Sigma-Aldrich
HMDB0000639	Mucic acid	526-99-8	Sigma-Aldrich
HMDB0000211	myo-Inositol	87-89-8	Sigma-Aldrich
HMDB0011757	N-Acety-DL-lvaline	3067-19-4	Sigma-Aldrich
HMDB0000766	N-Acetyl-L-alanine	97-69-8	Sigma-Aldrich
HMDB0000812	N-Acetyl-L-aspartic acid	997-55-7	Sigma-Aldrich
HMDB0001138	N-Acetyl-L-glutamic acid	1188-37-0	Sigma-Aldrich
HMDB0000512	N-Acetyl-L-phenylalanine	2018-61-3	Sigma-Aldrich
N/A	Nicotinate N-Oxide	2398-81-4	Sigma-Aldrich
HMDB0000678	N-Isovalerylglycine	16284-60-9	Supelco
HMDB0002393	N-Methyl-D-aspartic acid	6384-92-5	Sigma-Aldrich
N/A	N-Oxalylglycine	5262-39-5	Sigma-Aldrich
HMDB0013287	Nε,Nε-Dimethyl-L-lysine monohydrochloride	79416-87-8	Sigma-Aldrich
HMDB0000482	Octanoic acid	124-07-2	Sigma-Aldrich
HMDB0001721	O-Phospho-DL-serine	17885-08-4	Sigma-Aldrich
HMDB0002329	Oxalic acid	144-62-7	Sigma-Aldrich
HMDB0000223	Oxaloacetic acid	328-42-7	Sigma-Aldrich
HMDB0002035	p-Coumaric acid	501-98-4	Sigma-Aldrich
HMDB0000263	Phospho(enol)pyruvic acid monopotassium salt	4265-07-0	Sigma-Aldrich
HMDB0001856	Protocatechuic acid	99-50-3	Sigma-Aldrich
HMDB0001491	Pyridoxal 5'-phosphate hydrate	853645-22-4	Sigma-Aldrich
HMDB0000243	Pyruvic acid	127-17-3	Sigma-Aldrich
HMDB0006088	scyllo-Inositol	488-59-5	Sigma-Aldrich
HMDB0000792	Sebacic acid	111-20-6	Sigma-Aldrich
HMDB0003070	Shikimic acid	138-59-0	Sigma-Aldrich
HMDB0032616	Sinapic acid	530-59-6	Sigma-Aldrich

HMDB code	Compound name	CAS Number	Manufacturer
HMDB0000126	sn-Glycerol 3-phosphate lithium salt	17989-41-2	Sigma-Aldrich
HMDB0000005	Sodium 2-oxobutyrate	2013-26-5	Sigma-Aldrich
HMDB0000254	Succinic acid	110-15-6	Sigma-Aldrich
HMDB0002085	Syringic acid	530-57-4	Sigma-Aldrich
HMDB0000251	Taurine	107-35-7	Sigma-Aldrich
HMDB0001274	Thymidine 5′-diphosphate sodium salt	108322-12-9	Sigma-Aldrich
HMDB0001342	Thymidine 5′-triphosphate sodium salt	18423-43-3	Sigma-Aldrich
HMDB0000262	Thymine	65-71-4	Sigma-Aldrich
HMDB0015256	Tolbutamide	64-77-7	Sigma-Aldrich
HMDB0000954	trans-Ferulic acid	537-98-4	Sigma-Aldrich
HMDB0004284	Tyrosol	501-94-0	Supelco
HMDB0000300	Uracil	66-22-8	Sigma-Aldrich
HMDB0000289	Uric acid	69-93-2	Sigma-Aldrich
HMDB0000296	Uridine	58-96-8	Sigma-Aldrich
HMDB0000295	Uridine 5′-diphosphate disodium salt hydrate	27821-45-0	Sigma-Aldrich
HMDB0000286	Uridine 5′-diphosphoglucose disodium salt	28053-08-9	Sigma-Aldrich
HMDB0000290	Uridine 5′-diphospho-N-acetylglucosamine sodium salt	91183-98-1	Sigma-Aldrich
HMDB0000288	Uridine 5′-monophosphate disodium salt	3387-36-8	Sigma-Aldrich
HMDB0002917	Xylitol	87-99-0	Sigma-Aldrich
HMDB0001586	α-D-Glucose 1-phosphate disodium salt hydrate	56401-20-8	Sigma-Aldrich
HMDB0000056	β-Alanine	107-95-9	Sigma-Aldrich
HMDB0001487	β-NAD, reduced disodium salt hydrate	606-68-8	Sigma-Aldrich
HMDB0000221	β-NADPH, reduced tetra(cyclohexylammonium) salt	100929-71-3	Sigma-Aldrich
HMDB0001120	γ,γ-Dimethylallyl pyrophosphate ammonium salt	69382-61-2	Supelco

10.2. List of metabolites characterised by IC-MS/MS

Table 10.2: Table of metabolites characterised by IC-MS/MS (Section 8.4).

HMDB code	Compound name	Monoisotopic mass	RT / min	Formula	Fragmentation pattern
HMDB0013674	1,2,3-Trihydroxybenzene/Pyrogallol	126.03224	23.21	C6H6O3	
HMDB0000957	1,2-Dihydroxybenzene	110.03678	25.92	C6H6O2	Yes
HMDB0013593	1,4 dihydrotheritol	154.01222	14.86	C4H10O2S2	
HMDB0001213	1-Deoxy-D-xylulose 5-phosphate	214.02424	10.32	C5H11O7P	Yes
N/A	1-Hydroxy-2-methyl-2-butenyl 4-pyrophosphate	262.00074	16.68	C5H12O8P2	Yes
N/A	1-Methyl indole	131.07405	28.33	C9H9N	
N/A	1-Methyl-1H-indole-3-carboxamide	174.07986	33.86	C10H10N2O	
HMDB0000001	1-Methylhistidine	169.08513	12.89	C7H11N3O2	
HMDB0001369	1-Pyrroline hydroxycarboxylate	129.04259	4.48	C5H7NO3	
HMDB0001301	1-Pyrroline-5-carboxylate	113.04768	9.37	C5H7NO2	
HMDB0002006	2,3-Diaminopropionate	104.05913	11.75	C3H8N2O2	
HMDB0001294	2,3-Diphosphoglycerate	265.95927	22.21	C3H8O10P2	
HMDB0000152	2,5-Dihydroxybenzoate	154.02661	32.16	C7H6O4	Yes
N/A	2-amino-5-hydroxybenzoate	153.04314	33.19	C7H7NO3	
HMDB0001123	2-Aminobenzoate/Anthranilate	137.04768	25.09	C7H7NO2	Yes
HMDB0001906	2-Aminoisobutyrate	103.06333	9.92	C4H9NO2	
HMDB0032059	2-Bromophenol	171.95293	9.03	C6H5BrO	
N/A	2-butyl-3-ureido-succinate	232.10592	11.98	C9H16N2O5	
N/A	2-C-Methyl-D-erythritol-2,4-cyclopyrophosphate	277.99620	15.28	C5H12O9P2	
N/A	2-C-Methylerythritol 4-phosphate	214.02424	9.88	C5H13O7P	Yes
N/A	2-Hydroxy-4-phenylbutanoate	180.07919	14.39	C10H12O3	
HMDB0000008	2-Hydroxybutyrate	104.04734	5.41	C4H8O3	Yes
HMDB0059655	2-Hydroxyglutarate	148.03717	10.90	C5H8O5	Yes
HMDB0001624	2-Hydroxyhexanoate	132.07919	7.98	C6H12O3	

HMDB code	Compound name	Monoisotopic mass	RT / min	Formula	Fragmentation pattern
HMDB0000402	2-Isopropylmalate	176.06847	12.32	C7H12O5	Yes
HMDB0000005	2-Ketobutyrate	102.03169	7.86	C4H6O3	Yes
HMDB0000379	2-Methylcitrate	206.04320	16.09	C7H10O7	
HMDB0000208	2-Oxoglutarate	146.02152	12.85	C5H6O5	Yes
HMDB0000362	2-Phosphoglycerate	185.99294	16.34	C3H7O7P	Yes
HMDB0000397	2-Pyrocatechuate	154.02661	33.01	C7H6O4	
HMDB0002039	2-Pyrrolidinone	85.05331	13.37	C4H7NO	
HMDB0002441	3,3 Dimethyl glutarate	160.07356	11.41	C7H12O4	Yes
HMDB0012153	3,4,Dihydroxybenzylamine	139.06388	13.52	C7H9NO2	
HMDB0001336	3,4-dihydroxyphenyl acetate	168.04226	22.60	C8H8O4	
HMDB0003911	3-Aminoisobutanoate	103.06333	10.32	C4H9NO2	
HMDB0003540	3'-AMP	347.06254	13.43	C10H14N5O7P	
HMDB0012710	3-Dehydroquinate	190.04774	5.51	C7H10O6	Yes
HMDB0001376	3-deoxy-2-keto-6-phosphogluconate	258.01407	15.93	C6H11O9P	Yes
HMDB0001476	3-Hydroxyanthranilate	153.04314	26.46	C7H7NO3	
HMDB0002466	3-Hydroxybenzoate	138.03224	22.66	C7H6O3	
HMDB0000357	3-Hydroxybutyrate	104.04734	5.36	C4H8O3	Yes
HMDB0000023	3-Hydroxyisobutyrate	104.04734	5.04	C4H8O3	
HMDB0000754	3-Hydroxyisovalerate	118.06354	5.34	C5H10O3	
HMDB0000355	3-Hydroxymethylglutarate	162.05282	10.76	C6H10O5	Yes
HMDB0013188	3-Hydroxypicolinate	139.02694	18.07	C6H5NO3	Yes
HMDB0005784	3-Hydroxytyrosol	154.06299	15.76	C8H10O3	
HMDB0059969	3-methoxyphenylacetate	166.06299	10.04	C9H10O3	
HMDB0000491	3-Methyl-2-oxovalerate	130.06299	10.67	C6H10O3	
HMDB0001904	3-Nitrotyrosine	226.05897	8.77	C9H10N2O5	
HMDB0000807	3-Phosphoglycerate	185.99294	15.84	C3H7O7P	Yes
HMDB0061881	4-Acetylbutyrate	130.06354	5.09	C6H10O3	
HMDB0060466	4-Hydroxy-2-oxoglutarate	162.01644		C5H6O6	
HMDB0000291	4-Hydroxy-3-methoxymandelate	198.05282	15.77	C9H10O5	Yes
HMDB0000500	4-Hydroxybenzoate	138.03169	18.86	C7H6O3	
HMDB0000710	4-Hydroxybutyrate	104.04734	10.65	C4H8O3	
N/A	4-hydroxyphenyl glycine/Oxfenicine	167.05824	18.59	C8H9NO3	
N/A	4-Hydroxyphenylbutyrate	179.07137	17.51	C10H12O3	
HMDB0000707	4-Hydroxyphenylpyruvate	180.04226	27.88	C9H8O4	
HMDB0000725	4-Hydroxyproline	131.05824	9.68	C5H9NO3	Yes
N/A	4-Hydroxypyrrolidinone	101.04768	2.94	C4H7NO2	
N/A	4-Methyl-2-ureido-pentanoate/Carbamoyl isoleucine	174.10099	6.36	C7H14N2O3	
HMDB0000873	4-Methylcatechol	124.05298	29.91	C7H8O2	
HMDB0036619	5,7-Dihydroxyflavone	254.05846	4.33	C15H10O4	
HMDB0001149	5-Aminolevulinate	131.05879	3.89	C5H9NO3	
N/A	5-Formyl-dCTP	494.98505	20.45	C10H16N3O14P3	
HMDB0000525	5-Hydroxyhexanoate	132.07919	6.83	C6H12O3	
HMDB0000763	5-Hydroxyindoleacetate	191.05824	26.83	C10H9NO3	Yes
N/A	5-Hydroxymethyl-2'-deoxyuridine	258.08500	6.48	C10H14N2O6	
N/A	5-Hydroxy-methyl-dCTP	497.00016	19.40	C10H18N3O14P3	
HMDB0004096	5-Methoxyindoleacetate	205.07389	29.66	C11H11NO3	
N/A	5-Methyl-dCTP	481.00525	18.96	C10H18N3O13P3	
HMDB0038804	6-hydroxy-2,5,7,8-tetramethylchromane-2-carboxylate	250.12051	29.39	C14H18O4	
HMDB0001316	6-Phosphogluconate	276.02463	15.18	C6H13O10P	
HMDB0001127	6-phosphonoglucono-lactone	258.01462	11.52	C6H11O9P	
HMDB0003333	8-Hydroxy-deoxyguanosine	283.09167	19.83	C10H13N5O5	
HMDB0011615	8-Oxo-dGTP	522.99011	19.78	C10H16N5O14P3	
HMDB0036093	Abscisate	264.13616	13.64	C15H20O4	Yes
HMDB0000042	Acetate	60.02113	3.85	C2H4O2	
HMDB0000060	Acetoacetate	102.03169	5.14	C4H6O3	

HMDB code	Compound name	Monoisotopic mass	RT / min	Formula	Fragment-ation pattern
HMDB0001484	Acetoacetyl-CoA	851.13634	33.10	C25H40N7O18P3S	Yes
HMDB0001206	Acetyl-CoA	809.12577	7.59	C23H38N7O17P3S	
HMDB0001890	Acetylcysteine	163.03031	11.56	C5H9NO3S	Yes
HMDB0000532	Acetylglycine	117.04259	4.07	C4H7NO3	Yes
HMDB0001494	Acetylphosphate	139.98801	12.66	C2H5O5P	
HMDB0000034	Adenine	135.05450	15.32	C5H5N5	
HMDB0011616	Adenosine 2',3'-cyclic phosphate	329.05197	9.41	C10H12N5O6P	
HMDB0001341	Adenosine diphosphate	427.02941	19.79	C10H15N5O10P2	Yes
HMDB0000045	Adenosine monophosphate	347.06308	13.84	C10H14N5O7P	Yes
HMDB0000538	Adenosine triphosphate	506.99575	24.53	C10H16N5O13P3	Yes
HMDB0001332	Adenylsuccinate	463.07404	23.15	C14H18N5O11P	
HMDB0012882	Adipate semialdehyde	130.06299	11.34	C6H10O3	
HMDB0000508	Adonitol	152.06847	2.86	C5H12O5	Yes
HMDB0006557	ADP Glucose	589.08224	14.30	C16H25N5O15P2	Yes
HMDB0000462	Allantoin	158.04454	5.95	C4H6N4O3	
HMDB0001151	Allose	180.06339	3.04	C6H12O6	Yes
HMDB0000650	Alpha-aminobutyrate	103.06333	10.32	C4H9NO2	
HMDB0002166	Alpha-aminoisobutyrate	103.06333	10.06	C4H9NO2	
HMDB0000539	Arabinonate	166.04774	4.90	C5H10O6	Yes
HMDB0000646	Arabinose	150.05282	3.06	C5H10O5	Yes
HMDB0029942	Arabinose	150.05282	3.06	C5H10O5	Yes
HMDB0000568	Arabitol	152.06847	2.71	C5H12O5	Yes
HMDB0000044	Ascorbate	176.03209	12.36	C6H8O6	Yes
HMDB0000191	Aspartate	133.03751	11.78	C4H7NO4	Yes
N/A	Benzoyl-L-citrulline methyl ester	293.13810	11.17	C14H19N3O4	
HMDB0000056	Beta-Alanine	89.04768	4.73	C3H7NO2	Yes
HMDB0013220	Beta-Citryl-L-glutamate	321.06960	20.62	C11H15NO10	
N/A	Butyl ureidosuccinate	232.10647	10.61	C9H16N2O5	
HMDB0000039	Butyrate	88.05243	6.32	C4H8O2	Yes
HMDB0001964	Caffeate	180.04281		C9H8O4	
HMDB0001847	Caffeine	194.08092		C8H10N4O2	
HMDB0000535	Caproate/Hexanoate	116.08428	8.58	C6H12O2	
HMDB0001096	Carbamoyl phosphate	140.98271	15.06	CH4NO5P	
HMDB0000033	Carnosine	225.09931	3.93	C9H14N4O3	
HMDB0003164	Chlorogenate	354.09563		C16H18O9	
HMDB0011621	Cinnamoylglycine	205.07334	20.81	C11H11NO3	
HMDB0000072	Cis-aconitate	174.01644	18.12	C6H6O6	
HMDB0000634	Citraconate	130.02661	11.96	C5H6O4	
HMDB0000426	Citramalate	148.03717	10.75	C5H8O5	Yes
HMDB0000094	Citrate	192.02700	16.91	C6H8O7	Yes
HMDB0000904	Citrulline	175.09569	4.12	C6H13N3O3	
HMDB0015020	Clomifene	405.18594	16.22	C26H28ClNO	
HMDB0001423	Coenzyme A	767.11521	25.32	C21H36N7O16P3S	Yes
HMDB0000058	Cyclic AMP	329.05252	15.10	C10H12N5O6P	Yes
HMDB0001314	Cyclic GMP	345.04743	24.09	C10H12N5O7P	
HMDB0060150	Cysteamine	77.02992	9.87	C2H7NS	
HMDB0002757	Cysteate	169.00449	12.19	C3H7NO5S	Yes
HMDB0000574	Cysteine	121.01975	15.66	C3H7NO2S	
HMDB0000089	Cytidine	243.08607	8.48	C9H13N3O5	
HMDB0001546	Cytidine diphosphate	403.01763	16.34	C9H15N3O11P2	
HMDB0000095	Cytidine monophosphate	323.05185	11.78	C9H14N3O8P	Yes
HMDB0001176	Cytidine monophosphate N-acetylneuraminate	614.14727	9.79	C20H31N4O16P	
HMDB0000082	Cytidine triphosphate	482.98451	21.06	C9H16N3O14P3	Yes
HMDB0000630	Cytosine	111.04326	5.52	C4H5N3O	
HMDB0001508	dADP	411.03450	18.27	C10H15N5O9P2	
HMDB0000905	dAMP	331.06817	12.88	C10H14N5O6P	Yes

HMDB code	Compound name	Monoisotopic mass	RT / min	Formula	Fragment-ation pattern
HMDB0001245	dCDP	387.02327	30.12	C9H15N3O10P2	
HMDB0001202	dCMP	307.05694	10.06	C9H14N3O7P	
HMDB0000998	dCTP	466.98960	19.55	C9H16N3O13P3	Yes
N/A	Dehydrocholate	401.23335		C24H34O5	
HMDB0000101	Deoxyadenosine	251.10184	12.14	C10H13N5O3	
HMDB0001532	Deoxyadenosine triphosphate	491.00083	24.33	C10H16N5O12P3	Yes
HMDB0000014	Deoxycytidine	227.09115	4.69	C9H13N3O4	
HMDB0000085	deoxyguanosine	283.09222	4.08	C10H13N5O4	
HMDB0001031	Deoxyribose 5-phosphate	214.02424	11.06	C5H11O7P	Yes
N/A	Deoxythymidine	225.08808	7.67	C10H14N2O4	
HMDB0000012	Deoxyuridine	228.07462	7.62	C9H12N2O5	Yes
HMDB0000960	dGDP	427.02941	24.67	C10H15N5O10P2	
HMDB0001044	dGMP	347.06308	20.57	C10H14N5O7P	Yes
HMDB0001440	dGTP	506.99520	29.43	C10H16N5O13P3	
N/A	Diaminocyclohexane-N,N,N′,N′-tetraacetate	345.13034	8.92	C14H22N2O8	
HMDB0014724	Diclofenac	295.01614	1.22	C14H11Cl2NO2	
HMDB0003349	Dihydroorotate	158.03276	11.63	C5H6N2O4	Yes
HMDB0000076	Dihydrouracil	114.04238	13.43	C4H6N2O2	
HMDB0001882	Dihydroxyacetone	90.03169	4.74	C3H6O3	Yes
HMDB0001473	Dihydroxyacetone phosphate	169.99802	11.19	C3H7O6P	
HMDB0000181	Dihydroxyphenylalanine	197.06881	32.44	C9H11NO4	
HMDB0031257	Dimethyl fumarate	144.04226	13.16	C6H8O4	
HMDB0001120	Dimethylallyl pyrophosphate	246.00583	18.73	C5H12O7P2	Yes
HMDB0000092	Dimethylglycine	103.06333	10.15	C4H9NO2	
HMDB0006555	dIMP	332.05219	18.99	C10H13N4O7P	
N/A	DL-Threo-beta-Hydroxyaspartate	148.02515	10.43	C4H7NO5	
HMDB0000073	Dopamine	153.07898	19.68	C8H11NO2	
HMDB0001328	dTDP-D-glucose	564.07576	17.06	C16H26N2O16P2	
HMDB0001000	dUDP	388.00728	19.60	C9H14N2O11P2	
HMDB0001409	dUMP	308.04095	17.10	C9H13N2O8P	
HMDB0001191	dUTP	467.97361	25.45	C9H15N2O14P3	
HMDB0015109	EDTA	292.09067	10.83	C10H16N2O8	
HMDB0000900	Ergocalciferol	396.33867	4.21	C28H44O	
HMDB0000878	Ergosterol	396.33867	1.13	C28H44O	
HMDB0001321	Erythrose 4-phosphate	200.00859	12.91	C4H9O7P	
N/A	Ethionine	163.06725	33.54	C6H13NO2S	
HMDB0000622	Ethylmalonate	132.04226	11.62	C5H8O4	Yes
HMDB0001248	FAD	785.15713	28.12	C27H33N9O15P2	Yes
HMDB0000954	Ferulate	194.05791	27.02	C10H10O4	Yes
HMDB0001520	Flavin Mononucleotide	456.10461		C17H21N4O9P	
HMDB0014684	Fluorouracil	130.01786	13.57	C4H3FN2O2	
HMDB0014615	Fluoxetine	309.13460	21.52	C17H18F3NO	
HMDB0000660	Fructose	180.06339	3.06	C6H12O6	Yes
HMDB0001058	Fructose 1,6-bisphosphate	339.99605	20.44	C6H14O12P2	Yes
HMDB0001047	Fructose 2,6 diphosphate	339.99605	17.52	C6H14O12P2	
HMDB0000124	Fructose 6-phosphate	260.02972	11.88	C6H13O9P	Yes
HMDB0000134	Fumarate	116.01096	13.63	C4H4O4	Yes
HMDB0000639	Galactarate	210.03757	10.94	C6H10O8	Yes
HMDB0000143	Galactose	180.06339	3.02	C6H12O6	Yes
HMDB0000645	Galactose 1-phosphate	260.02972	9.39	C6H13O9P	Yes
N/A	Galactose-6-phosphate	260.02917	11.77	C6H13O9P	
HMDB0002545	Galacturonate	194.04265	7.52	C6H10O7	Yes
HMDB0013233	Gamma-delta-Dioxovalerate	130.02661	10.65	C5H6O4	
HMDB0003559	Gibberellin A3	346.14164	12.68	C19H22O6	Yes
HMDB0000625	Gluconate	196.05830	4.67	C6H12O7	Yes
HMDB0000150	Gluconolactone	178.04774	4.71	C6H10O6	Yes

HMDB code	Compound name	Monoisotopic mass	RT / min	Formula	Fragment-ation pattern
HMDB0001514	Glucosamine	179.07937	11.58	C6H13NO5	
HMDB0001254	Glucosamine 6-phosphate	259.04570	13.18	C6H14NO8P	Yes
HMDB0000122	Glucose	180.06339	3.43	C6H12O6	Yes
HMDB0001586	Glucose 1-phosphate	260.02972	9.66	C6H13O9P	Yes
HMDB0001401	Glucose 6-phosphate	260.02972	12.38	C6H13O9P	Yes
HMDB0000127	Glucuronate	194.04265	8.27	C6H10O7	Yes
HMDB0000620	Glutaconate	130.02661	12.69	C5H6O4	Yes
HMDB0000148	Glutamate	147.05316	14.79	C5H9NO4	Yes
HMDB0000641	Glutamine	146.06914	11.67	C5H10N2O3	
HMDB0001049	Glutamylcysteine	250.06289	16.61	C8H14N2O5S	
HMDB0000661	Glutarate	132.04226	10.87	C5H8O4	Yes
HMDB0001339	Glutaryl CoA	881.14690	19.81	C26H42N7O19P3S	
HMDB0000125	Glutathione	307.08381	15.16	C10H17N3O6S	Yes
HMDB0001112	Glyceraldehyde 3-phosphate	169.99802	11.73	C3H7O6P	Yes
HMDB0000139	Glycerate	106.02661	5.23	C3H6O4	Yes
HMDB0000131	Glycerol	92.04734	2.86	C3H8O3	Yes
HMDB0000126	Glycerol 3-phosphate	172.01367	9.79	C3H9O6P	Yes
HMDB0003344	Glycoaldehyde	60.02113	7.52	C2H4O2	
HMDB0000115	Glycolate	76.01604	5.24	C2H4O3	Yes
HMDB0000119	Glyoxylate	74.00039	8.05	C2H2O3	Yes
HMDB0000370	Glyphosate/2-Amino-3-phosphonopropionate	169.01456	14.56	C3H8NO5P	
HMDB0000133	Guanosine	283.09167	22.22	C10H13N5O5	
HMDB0001201	Guanosine diphosphate	443.02378	27.56	C10H15N5O11P2	Yes
HMDB0001397	Guanosine monophosphate	363.05800	22.22	C10H14N5O8P	Yes
HMDB0001273	Guanosine triphosphate	522.99066	30.62	C10H16N5O14P3	Yes
HMDB0012326	Gulose	180.06339	3.05	C6H12O6	Yes
HMDB0030311	Harmine	212.09551		C13H12N2O	
HMDB0005782	Hesperitin	302.07849	28.50	C16H14O6	
HMDB0000714	Hippurate	179.05824	11.63	C9H9NO3	Yes
HMDB0000870	Histamine	111.08020	7.08	C5H9N3	
N/A	Homarine	137.04768	11.66	C7H7NO2	
HMDB0000130	Homogentisate	168.04226	17.49	C8H8O4	Yes
HMDB0000118	Homovanillate	182.05791	17.21	C9H10O4	Yes
HMDB0001212	Hydantoin-5-propionate	172.04786	11.40	C6H8N2O4	
HMDB0000764	Hydrocinnamate	150.06863	15.63	C9H10O2	Yes
HMDB0000528	Hydroorotate	158.03276	10.36	C5H6N2O4	Yes
HMDB0001855	Hydroxy-indole acetate	177.07898	26.62	C10H11NO2	
HMDB0062640	Hydroxy-isobutyrate	103.04007	4.46	C4H7O3	Yes
HMDB0126088	Hydroxy-isobutyrate	104.04734	4.46	C4H8O3	Yes
HMDB0002207	Hydroxyisoheptanoate	146.09484	9.74	C7H14O3	
HMDB0000732	Hydroxykynurenine	224.08026	13.91	C10H12N2O4	
N/A	Hydroxy-methyl-dUTP	497.98418	20.48	C10H17N2O15P3	
HMDB0000711	Hydroxyoctanoate	160.11049	7.52	C8H16O3	
HMDB0000700	Hydroxypropionate	90.03224	4.88	C3H6O3	
HMDB0001352	Hydroxypyruvate	104.01096	11.64	C3H4O4	
HMDB0000965	Hypotaurine	109.01975	14.89	C2H7NO2S	Yes
HMDB0000157	Hypoxanthine	136.03851	21.34	C5H4N4O	
HMDB0011140	Hypusine	233.17449	9.42	C10H23N3O3	
HMDB0003335	IDP	428.01343	26.55	C10H14N4O11P2	Yes
HMDB0001190	Indole-3-acetaldehyde	159.06841	27.44	C10H9NO	
HMDB0000671	Indole-3-lactate	205.07389	27.23	C11H11NO3	Yes
HMDB0000197	Indoleacetate	175.06333	28.43	C10H9NO2	Yes
HMDB0000195	Inosine	268.08077	5.60	C10H12N4O5	Yes
HMDB0000175	Inosine monophosphate	348.04710	21.97	C10H13N4O8P	Yes
HMDB0000189	Inosine triphosphate	507.97976	30.13	C10H15N4O14P3	Yes
HMDB0001143	Inositol 1,3,4-trisphosphate	419.96238	25.85	C6H15O15P3	

HMDB code	Compound name	Monoisotopic mass	RT / min	Formula	Fragment-ation pattern
HMDB0000193	Isocitrate	192.02700	17.55	C6H8O7	Yes
HMDB0001347	Isopentenyl pyrophosphate	246.00583	18.45	C5H12O7P2	Yes
HMDB0000718	Isovalerate	102.06863	9.43	C5H10O2	
HMDB0000678	Isovalerylglycine	159.08954	6.07	C7H13NO3	Yes
HMDB0002092	Itaconate	130.02661	12.13	C5H6O4	Yes
HMDB0032797	Jasmonate	210.12559	12.22	C12H18O3	Yes
HMDB0032923	Kojate	142.02661	8.81	C6H6O4	Yes
HMDB0000715	Kynurenate	189.04259	27.57	C10H7NO3	
HMDB0000684	Kynurenine	208.08479	8.81	C10H12N2O3	
HMDB0000190	Lactate	90.03169	5.05	C3H6O3	Yes
HMDB0000186	Lactose	342.11676	3.04	C12H22O11	Yes
HMDB0062180	Lactoyl-isoleucine	203.11631	7.02	C9H17NO4	
N/A	Lanthionine	208.05233	33.00	C6H12N2O4S	
HMDB0004823	Lanthionine ketimine	189.01013	30.82	C6H7NO4S	
HMDB0000624	Leucate	132.07919	7.51	C6H12O3	
HMDB0000744	Malate	134.02152	11.14	C4H6O5	Yes
HMDB0000176	Maleate	116.01096	12.43	C4H4O4	Yes
HMDB0002928	Malitol	344.13186	3.08	C12H24O11	Yes
HMDB0000691	Malonate	104.01096	12.01	C3H4O4	Yes
HMDB0006112	Malondialdehyde	72.02113	8.86	C3H4O2	
HMDB0060486	Manelonitrile	133.05276	29.49	C8H7NO	
HMDB0000765	Mannitol	182.07904	2.76	C6H14O6	
HMDB0000169	Mannose	180.06339	3.14	C6H12O6	Yes
HMDB0001078	Mannose 6-phosphate	260.02972	12.73	C6H13O9P	Yes
HMDB0001892	Menadione	172.05298	11.43	C11H8O2	
HMDB0000749	Mesaconate	130.02661	12.51	C5H6O4	Yes
HMDB0002005	Methionine sulfoxide	165.04596		C5H11NO3S	
HMDB0029965	Methyl beta-D-glucopyranoside	194.07904	2.74	C7H14O6	
HMDB0001167	Methyl glyoxal/Pyruvaldehyde	72.02168	4.89	C3H4O2	
HMDB0032617	Methyl phenylacetate	150.06863	14.11	C9H10O2	
N/A	Methyl-3-hydroxybenzoate	152.04789	28.57	C8H8O3	
HMDB0004815	Methyl-4-hydroxybenzoate	152.04789	32.63	C8H8O3	
HMDB0000752	Methylglutarate	146.05791	10.73	C6H10O4	Yes
HMDB0006471	Methylisocitrate	206.04265	15.82	C7H10O7	
HMDB0032572	Methylparaben	152.04734	17.77	C8H8O3	Yes
HMDB0000227	Mevalonate	148.07356	15.14	C6H12O4	Yes
HMDB0001343	Mevalonate-5P	228.03989	14.84	C6H13O7P	Yes
N/A	Mildronate	146.10498	1.20	C6H4N2O2	
HMDB0000211	Myoinositol	180.06339	2.81	C6H12O6	Yes
HMDB0003502	Myo-inositol hexakisphosphate/Phytate	659.86192	24.31	C6H18O24P6	
HMDB0039002	Mytilin A	332.12251	3.67	C13H20N2O8	
HMDB0033442	Mytilin B	346.13816	3.50	C14H22N2O8	
HMDB0033816	Mytilitol	194.07959	2.58	C7H14O6	
N/A	N-Acetyl cytosine	153.05437	8.13	C6H7N3O2	
HMDB0003357	N-Acetyl ornithine	174.10044	8.73	C7H14N2O3	
HMDB0094701	N-Acetyl proline	157.07444	4.42	C7H11NO3	Yes
HMDB0000812	N-Acetyl-aspartate	175.04807	10.03	C6H9NO5	Yes
HMDB0001067	N-Acetylaspartylglutamate	304.09067	14.40	C11H16N2O8	
HMDB0000215	N-Acetyl-D-glucosamine	221.08994	3.02	C8H15NO6	Yes
HMDB0001062	N-Acetyl-D-Glucosamine 6-Phosphate	301.05627	12.41	C8H16NO9P	
HMDB0001121	N-Acetyl-D-mannosamine 6-phosphate	301.05627	12.11	C8H16NO9P	
HMDB0001367	N-acetyl-glucosamine-1-phosphate	301.05627	11.66	C8H16NO9P	
HMDB0001138	N-Acetylglutamate	189.06427	9.84	C7H11NO5	Yes
HMDB0000766	N-Acetyl-L-alanine	131.05824	4.23	C5H9NO3	Yes
HMDB0006488	N-Acetyl-L-glutamate 5-semialdehyde	173.06881	13.97	C7H11NO4	
HMDB0006456	N-Acetyl-L-glutamyl 5-phosphate	269.03005		C7H12NO8P	

HMDB code	Compound name	Monoisotopic mass	RT / min	Formula	Fragment-ation pattern
HMDB0011745	N-Acetyl-L-methionine	191.06161	5.91	C7H13NO3S	Yes
HMDB0000512	N-Acetyl-L-phenylalanine	207.08954	8.89	C11H13NO3	Yes
HMDB0001129	N-Acetylmannosamine	221.08994	5.39	C8H15NO6	
HMDB0000230	N-Acetylneuraminate	309.10598	4.83	C11H19NO9	Yes
HMDB0006268	N-Acetylneuraminate 9-phosphate	389.07231	13.98	C11H20NO12P	
HMDB0013713	N-Acetyltryptophan	246.10044	18.41	C13H14N2O3	Yes
HMDB0011757	N-Acetylvaline	159.08954	4.83	C7H13NO3	Yes
HMDB0000902	NAD+	664.11695	9.94	C21H28N7O14P2	
HMDB0001487	NADH	665.12477	17.00	C21H29N7O14P2	Yes
HMDB0000217	NADP+	744.08328	16.43	C21H29N7O17P3	
HMDB0000221	NADPH	745.09110	21.37	C21H30N7O17P3	Yes
HMDB0002670	Naringenin	272.06902		C15H12O5	
HMDB0013287	Ne,Ne dimethyllysine	174.13683	3.79	C8H18N2O2	
N/A	N-Formyl-DL-ethionine	191.06216	7.53	C7H13NO3S	
HMDB0001200	N-Formylkynurenine	236.08026	22.44	C11H12N2O4	
HMDB0001015	N-Formyl-methionine	177.04596	6.73	C6H11NO3S	
HMDB0001406	Nicotinamide	122.04801	24.05	C6H6N2O	
N/A	Nicotinate N-Oxide	139.02694	5.94	C6H5NO3	Yes
HMDB0002393	N-Methyl-D-aspartate	147.05316	10.06	C5H9NO4	Yes
HMDB0011717	Nonate	188.10541	13.85	C9H16O4	
HMDB0013716	Norvaline	117.07953	33.46	C5H11NO2	
N/A	N-Oxalylglycine	147.01680	12.59	C4H5NO5	Yes
HMDB0003011	O-Acetylserine	147.05316	4.36	C5H9NO4	
HMDB0000482	Octanoate	144.11503	19.95	C8H16O2	Yes
HMDB0001721	O-Phosphoserine	185.00892	14.86	C3H8NO6P	Yes
HMDB0005765	Ophthalmate	289.12793	8.51	C11H19N3O6	
HMDB0000226	Orotate	156.01711	16.58	C5H4N2O4	Yes
HMDB0000788	Orotidine	288.05882	16.11	C10H12N2O8	
HMDB0000218	Orotidylate/OMP	368.02624	9.67	C10H13N2O11P	
HMDB0000223	Oxalacetate	132.00587	10.30	C4H4O5	
HMDB0002329	Oxalate	89.99531	13.40	C2H2O4	Yes
HMDB0000225	Oxoadipate	160.03717	13.08	C6H8O5	Yes
HMDB0001865	Oxovalerate	116.04789	7.56	C5H8O3	
HMDB0014733	Oxytetracylcine	460.14818	29.58	C22H24N2O9	
HMDB0000210	Pantothenate	219.11067	5.00	C9H17NO5	Yes
HMDB0062802	Parabanate/Oxalylyurea	114.00599	8.17	C3H2N2O3	
HMDB0002035	p-Coumarate	164.04734	29.16	C9H8O3	Yes
HMDB0015050	Phenformin	241.10997	14.07	C10H16ClN5	
HMDB0040733	Phenylacetate	136.05298	13.28	C8H8O2	
HMDB0000821	Phenylacetylglycine/Phenaceturate	193.07444	9.23	C10H11NO3	
HMDB0000205	Phenylpyruvate	164.04734	30.55	C9H8O3	Yes
HMDB0001511	Phosphocreatine	211.03636	8.56	C4H10N3O5P	Yes
HMDB0000263	Phosphoenolpyruvate	167.98237	17.96	C3H5O6P	Yes
HMDB0000816	Phosphoglycolate	155.98237	16.32	C2H5O6P	Yes
HMDB0000280	Phosphoribosyl pyrophosphate	389.95181	22.27	C5H13O14P3	
HMDB0000020	p-Hydroxyphenylacetate	152.04789	16.97	C8H8O3	
HMDB0000774	Pregnenolone sulfate	396.19759	21.87	C21H32O5S	
HMDB0012283	Prephenate	226.04774	11.47	C10H10O6	
HMDB0015169	Procainamide	235.16846	21.97	C13H21N3O	
HMDB0000237	Propionate	74.03733	5.69	C3H6O2	
HMDB0001275	Propionyl-CoA	823.14197	10.52	C24H40N7O17P3S	
HMDB0001856	Protocatechuate	154.02661	25.29	C7H6O4	Yes
HMDB0001491	Pyridoxal 5'-phosphate	247.02457	21.74	C8H10NO6P	Yes
HMDB0001431	Pyridoxamine	168.08988	6.71	C8H12N2O2	
HMDB0000267	Pyroglutamate	129.04314	4.49	C5H7NO3	Yes
HMDB0000243	Pyruvate	88.01604	6.80	C3H4O3	Yes

HMDB code	Compound name	Monoisotopic mass	RT / min	Formula	Fragment-ation pattern
HMDB0005794	Quercetin	302.04210	28.65	C15H10O7	
HMDB0003072	Quinate	192.06339	4.74	C7H12O6	Yes
HMDB0000232	Quinolinate	167.02186	13.74	C7H5NO4	
N/A	Quisqualate	189.03912	14.33	C5H7N3O5	
HMDB0003213	Raffinose	504.16904	2.80	C18H32O16	Yes
HMDB0001852	Retinoate	300.20948	8.39	C20H28O2	
HMDB0000244	Riboflavin	376.13828	24.51	C17H20N4O6	
HMDB0000283	Ribose	150.05282	3.17	C5H10O5	Yes
HMDB0001548	Ribose 5-phosphate	230.01915	13.19	C5H11O8P	Yes
HMDB0000621	Ribulose	150.05282	3.51	C5H10O5	Yes
N/A	Ribulose 1,5,diphosphate	309.98603	19.79	C5H12O11P2	
HMDB0000618	Ribulose 5-phosphate	230.01915	9.67	C5H11O8P	Yes
HMDB0000663	Saccharate	210.03757	12.05	C6H10O8	Yes
HMDB0000279	Saccharopine	276.13214	13.56	C11H20N2O6	
HMDB0001185	S-adenosyl methionine	399.14506	8.71	C15H23N6O5S	
HMDB0001895	Salicylate	138.03224	32.17	C7H6O3	
HMDB0006088	Scyllitol	180.06339	2.67	C6H12O6	Yes
HMDB0000792	Sebacate	202.12051	18.30	C10H18O4	Yes
HMDB0060274	Sedoheptulose 1,7-bisphosphate	370.00661	19.08	C7H16O13P2	
HMDB0060509	Sedoheptulose 1-phosphate	290.04028	10.74	C7H15O10P	
HMDB0001068	Sedoheptulose 7-phosphate	290.04028	13.21	C7H15O10P	Yes
HMDB0000187	Serine	105.04259	14.89	C3H7NO3	Yes
HMDB0003070	Shikimate	174.05282	5.13	C7H10O5	Yes
HMDB0032616	Sinapate	224.06847	25.12	C11H12O5	Yes
HMDB0000247	Sorbitol	182.07904	2.77	C6H14O6	Yes
HMDB0005831	Sorbitol-6-phosphate	262.04537	9.23	C6H15O9P	
HMDB0001266	Sorbose	180.06339	3.06	C6H12O6	Yes
HMDB0006797	Sorbose 1-phosphate	260.02917	11.96	C6H13O9P	
HMDB0000254	Succinate	118.02661	11.11	C4H6O4	Yes
HMDB0001259	Succinate semialdehyde	102.03169	12.69	C4H6O3	
N/A	Succinyl-Homoserine	219.07400	9.41	C8H13NO6	
HMDB0002085	Syringate	198.05282	17.50	C9H10O5	Yes
HMDB0029416	Targinine	188.12787	33.55	C7H16N4O2	
HMDB0000251	Taurine	125.01466	5.14	C2H7NO3S	Yes
HMDB0001274	TDP	402.02293	21.72	C10H16N2O11P2	Yes
HMDB0000234	Testosterone	288.20948	27.34	C19H28O2	
HMDB0003193	Testosterone glucuronide	464.24047	8.06	C25H36O8	
HMDB0002833	Testosterone sulfate	368.16629	18.09	C19H28O5S	
HMDB0014897	Tetracycline	444.15272	20.98	C22H24N2O8	
HMDB0002825	Theobromine	180.06418	17.74	C7H8N4O2	
HMDB0029178	Thialysine	164.06250	33.42	C5H12N2O2S	
HMDB0002666	Thiamine monophosphate	344.07026		C12H17N4O4PS	
HMDB0001372	Thiamine pyrophosphate	425.04497	25.64	C12H19N4O7P2S	
HMDB0004136	Threitol	122.05791	2.78	C4H10O4	Yes
HMDB0001227	Thymidine 5'-phosphate	322.05660	16.77	C10H15N2O8P	Yes
HMDB0001342	Thymidine triphosphate	481.98926	25.42	C10H17N2O14P3	Yes
HMDB0000262	Thymine	126.04293	9.90	C5H6N2O2	Yes
HMDB0015256	Tolbutamide	270.10436	15.08	C12H18N2O3S	
HMDB0062562	Trans-urocanate	137.03565	18.19	C6H5N2O2	
HMDB0000303	Tryptamine	160.10060		C10H12N2	
HMDB0004284	Tyrosol	138.06808	17.77	C8H10O2	Yes
HMDB0000302	UDP-galactose	566.05502	18.00	C15H24N2O17P2	
HMDB0000935	UDP-glucoronate	580.03428	24.31	C15H22N2O18P2	
HMDB0000286	UDP-glucose	566.05502	18.40	C15H24N2O17P2	
HMDB0013112	UDP-N-acetyl-D-mannosamine	607.08157		C17H27N3O17P2	
HMDB0000300	Uracil	112.02728	8.92	C4H4N2O2	Yes

HMDB code	Compound name	Monoisotopic mass	RT / min	Formula	Fragment-ation pattern
HMDB0000289	Urate	168.02834	19.45	C5H4N4O3	Yes
HMDB0000026	Ureidopropionate	132.05404	4.46	C4H8N2O3	
HMDB0000828	Ureidosuccinate	176.04332	10.86	C5H8N2O5	
HMDB0000296	Uridine	244.06954	9.04	C9H12N2O6	Yes
HMDB0000295	Uridine 5'-diphosphate	404.00220	23.85	C9H14N2O12P2	Yes
HMDB0000288	Uridine 5'-monophosphate	324.03587	18.60	C9H13N2O9P	Yes
HMDB0000290	Uridine diphosphate-N-acetylglucosamine	607.08157	17.77	C17H27N3O17P2	Yes
HMDB0000285	Uridine triphosphate	483.96853	27.32	C9H15N2O15P3	Yes
HMDB0000892	Valerate	102.06863	9.65	C5H10O2	
HMDB0012308	Vanillin	152.04789		C8H8O3	
HMDB0001554	Xanthylate	364.04256	20.70	C10H13N4O9P	
HMDB0002917	Xylitol	152.06847	2.79	C5H12O5	Yes
HMDB0001644	Xylulose	150.05282	3.64	C5H10O5	Yes
HMDB0000868	Xylulose 5-phosphate	230.01915	13.16	C5H11O8P	Yes
HMDB0015464	Yohimbine	354.19489	26.07	C21H26N2O3	

10.3. List of derivatised metabolites characterised by RP-MS and RP-IMS-MS/MS

Table 10.3: Table of derivatised metabolites characterised by RP-MS (Section 8.7) and RP-IMS-MS/MS (Section 8.8).

HMDB code	Compound name	Monoisotopic mass	RT / min	Derivatised formula
HMDB0002166	(S)-b-aminoisobutyrate	274.11920	5.53	C14H15N3O3
HMDB0000002	1,3-Diaminopropane	244.13241	1.61	C13H16N3O
HMDB0000002	1,3-Diaminopropane (2x derivatised)	414.17988	6.31	C23H22N6O2
HMDB0029737	1H-Indole-3-carboxaldehyde	316.10860	6.79	C19H13N3O2
HMDB0000001	1-Methylhistidine	340.14100	2.80	C17H17N5O3
HMDB0000699	1-Methylnicotinamide	307.11895	8.41	C17H15N4O2
HMDB0032609	2-(Methylamino)benzoate	321.11079	6.92	C18H15N3O3
HMDB0002362	2,4-Diaminobutyrate (2x derivatised)	459.17810	5.78	C24H22N6O4
HMDB0000510	2-Aminoadipate	331.11627	5.24	C16H17N3O5
HMDB0061680	2-Aminonicotinate	309.09880	5.37	C16H12N4O3
N/A	2-Methyl-1-pyrroline	254.12930	8.17	C15H15N3O
HMDB0002039	2-Pyrrolidinone	255.10023	5.40	C14H13N3O2
N/A	3,4-Dehydro-L-proline	283.09514	5.35	C15H13N3O3
HMDB0003911	3-Amino-2-methylpropanoate	273.11189	5.88	C14H15N3O3
HMDB0031654	3-Aminobutanoate	274.11820	6.22	C14H15N3O3
HMDB0001476	3-Hydroxyanthranilate	323.09006	7.05	C17H13N3O4
HMDB0006524	3-Indoleacetonitrile	327.12460	8.41	C20H14N4O
HMDB0002096	3-Indolebutyrate	374.15050	6.88	C22H19N3O3
HMDB0060374	3-Methoxyanthranilate	338.11410	6.75	C18H15N3O4
HMDB0001904	3-Nitrotyrosine	396.10644	7.67	C19H16N4O6
HMDB0061877	4-Amino-3-hydroxybutyrate	290.11410	3.83	C14H15N3O4
HMDB0001392	4-Aminobenzoate	307.09569	7.07	C17H13N3O3
N/A	4-amino-crotonate	272.10350	4.69	C14H13N3O3
N/A	4-Guanidinobutyrate	316.14100	6.46	C15H17N5O3
HMDB0000725	4-Hydroxyproline	301.10571		C15H15N3O4
N/A	4-Methylthioamphetamine	352.14830	8.27	C20H21N3OS
N/A	5-Aminopyridine-2-carboxylate	310.10660	5.12	C16H13N4O3
N/A	5'-Deoxy-5'-methylthioadenosine	468.14540	7.58	C21H21N7O4S
HMDB0000763	5-Hydroxyindoleacetate	362.11410	7.43	C20H15N3O4

HMDB code	Compound name	Monoisotopic mass	RT / min	Derivatised formula
HMDB0000450	5-Hydroxylysine	332.14791	5.78	C16H20N4O4
HMDB0004096	5-Methoxyindoleacetate	375.12136	8.59	C21H17N3O4
HMDB0001890	Acetylcysteine	334.08620	8.57	C15H15N3O4S
HMDB0000050	Adenosine	438.15260	6.37	C20H19N7O5
HMDB0000058	Adenosine 3,5-cyclic monophosphate	499.10053	5.10	C20H18N7O7P
HMDB0000045	Adenosine monophosphate	518.11880	0.44	C20H20N7O8P
HMDB0000538	Adenosine triphosphate	678.05160	0.43	C20H22N7O14P3
HMDB0000068	Adrenaline	354.14540	5.88	C19H19N3O4
HMDB0001432	Agmatine	301.17770	4.32	C15H20N6O
HMDB0000161	Alanine	259.09569	4.86	C13H13N3O3
HMDB0000462	Allantoin	329.09980	2.90	C14H12N6O4
N/A	Amino methoxybenzoate	322.11920	6.79	C18H15N3O3
HMDB0000112	Aminobutyrate	273.11134	5.97	C14H15N3O3
HMDB0000194	Anserine	410.16970		C20H22N6O4
HMDB0001123	Anthranilate	307.09514	7.08	C17H13N3O3
HMDB0000517	Arginine	344.15969	3.10	C16H20N6O3
HMDB0000517	Arginine (2x derivatised)	514.20770	5.94	C26H26N8O4
HMDB0000052	Argininosuccinate	460.17010	3.50	C20H24N6O7
HMDB0000168	Asparagine	302.10150	7.19	C14H14N4O4
HMDB0000191	Aspartate	303.08552	7.19	C14H13N3O5
N/A	Benzoyl-L-citrulline methyl ester (underivatised)	293.13701	6.82	C14H19N3O4
HMDB0000056	beta-Alanine/aminopropionate	259.09514	4.26	C13H13N3O3
HMDB0000043	Betaine	287.12699	1.26	C15H17N3O3
HMDB0002322	Cadaverine	273.17150	7.70	C15H20N4O
HMDB0002706	Canavanine	347.14680	6.23	C15H18N6O4
HMDB0002706	Canavanine (2x derivatised)	517.19480	6.23	C25H24N8O5
HMDB0001096	Carbamoyl phosphate	311.03072	0.34	C11H10N3O6P
HMDB0000062	Carnitine	331.15321	1.98	C17H21N3O4
HMDB0000033	Carnosine	396.15460	3.10	C19H20N6O4
HMDB0000904	Citrulline	345.14371	4.08	C16H19N5O4
HMDB0000064	Creatine	302.12530	4.60	C14H15N5O3
HMDB0000562	Creatinine	283.10692	5.40	C14H13N5O2
HMDB0014405	Cycloserine	273.09880	4.01	C13H12N4O3
HMDB0002991	Cysteamine	247.07793	7.56	C12H13N3OS
HMDB0000574	Cysteine	291.06776	6.46	C13H13N3O3S
HMDB0000192	Cystine	410.07186	6.07	C16H18N4O5S2
HMDB0000089	Cytidine	414.14140	5.95	C19H19N5O6
HMDB0000095	Cytidine monophosphate	494.10770	5.45	C19H20N5O9P
HMDB0000630	Cytosine	281.09127	6.05	C14H11N5O2
HMDB0001370	Diaminopimelate	360.14392	8.58	C17H20N4O5
HMDB0000181	Dihydroxyphenylalanine	367.11627	6.13	C19H17N3O5
N/A	Dimethyl L-glutamate	345.13192	7.02	C17H19N3O5
HMDB0006045	Dityrosine	530.18070		C28H26N4O7
HMDB0006045	Dityrosine (2x derivatised)	701.23544		C38H32N6O8
HMDB0000991	DL-2-Aminooctanoate	330.18180	8.37	C18H23N3O3
HMDB0000149	Ethanolamine	231.10078	3.37	C12H13N3O2
HMDB0001049	gamma-Glutamylcysteine	420.10981		C18H20N4O6S
HMDB0001514	Glucosamine	349.12739	8.14	C16H19N3O6
HMDB0000148	Glutamate	317.10117	4.05	C15H15N3O5
HMDB0000641	Glutamine	316.11715	6.34	C15H16N4O4
HMDB0000125	Glutathione	476.12399	6.06	C20H22N5O7S
HMDB0000123	Glycine	245.08004	3.19	C12H11N3O3
N/A	Gly-Gly	302.10150	2.58	C14H14N4O4
HMDB0001397	GMP	533.10656	1.27	C20H20N7O9P
HMDB0001842	Guanidine	230.10420	3.05	C11H11N5O
HMDB0000128	Guanidineacetate	287.10184	2.79	C13H13N5O3
HMDB0000132	Guanine	322.10530	5.90	C15H11N7O2

HMDB code	Compound name	Monoisotopic mass	RT / min	Derivatised formula
HMDB0000133	Guanosine	454.14750	6.21	C20H19N7O6
HMDB0000714	Hippurate	349.10571	7.35	C19H15N3O4
HMDB0000870	Histamine	281.12711	3.08	C15H15N5O
HMDB0000177	Histidine	325.11749	1.93	C16H15N5O3
HMDB0000742	Homocysteine	305.08341	6.25	C14H15N3O3S
HMDB0000670	Homo-L-arginine (derivatised x2)	529.23120	6.44	C27H28N8O4
HMDB0000719	Homoserine	289.10626	3.31	C14H15N3O4
HMDB0034326	Hydroxyarginine	360.15460		C16H20N6O4
HMDB0034326	Hydroxyarginine (2x derivatised)	530.20262		C26H26N8O5
N/A	Hydroxyaspartate	319.08098		C14H13N3O6
HMDB0000732	Hydroxykynurenine	394.12717	6.91	C20H18N4O5
HMDB0000732	Hydroxykynurenine (2x derivatised)	564.17518		C30H24N6O6
HMDB0000472	Hydroxy-L-tryptophan	390.13226		C21H18N4O4
HMDB0000965	Hypotaurine	279.06721	2.89	C12H13N3O3S
HMDB0000157	Hypoxanthine	307.09440	5.85	C15H10N6O2
HMDB0005785	Indole-3-carbinol	318.12420	6.41	C19H15N3O2
HMDB0002302	Indole-3-propionate	360.13480	7.25	C21H17N3O3
HMDB0001190	Indoleacetaldehyde	329.11588	4.77	C20H15N3O2
HMDB0000197	Indoleacetate	361.10680	8.39	C20H15N3O4
HMDB0000671	Indolelactate	376.12970	6.86	C21H17N3O4
HMDB0034198	Isobutylamine	243.13716	7.48	C14H17N3O
N/A	Isobutylamine	244.14500	7.53	C14H17N3O
HMDB0000172	Isoleucine	301.14264	7.68	C16H19N3O3
HMDB0000715	Kynurenate	359.09006	8.41	C20H13N3O4
HMDB0000684	Kynurenine	378.13280	7.65	C20H18N4O4
HMDB0000557	L-Alloisoleucine	302.15050	7.78	C16H19N3O3
HMDB0000099	L-Cystathionine	392.11489	6.13	C17H20N4O5S
HMDB0000192	L-Cystine (2x derivatised)	580.11933		C26H24N6O6S2
HMDB0000687	Leucine	301.14264	7.78	C16H19N3O3
HMDB0034365	L-Theanine	344.14791	5.21	C17H20N4O4
HMDB0000182	Lysine	486.20155	6.55	C26H26N6O4
HMDB0060486	Mandelonitrile	303.10078	7.82	C18H13N3O2
HMDB0000696	Methionine	319.09906	4.05	C15H17N3SO3
HMDB0002005	Methionine sulfoxide	336.10180	3.65	C15H17N3O4S
N/A	Methyl picolinate	308.10350	8.29	C17H13N3O3
N/A	Methyl serine	289.10571	1.98	C14H15N3O4
HMDB0002038	Methyl-L-Lysine	330.16919	6.87	C17H22N4O3
HMDB0029416	Mono-methyl arginine/Targinine	358.17479		C17H22N6O3
N/A	N-(Phosphonomethyl)glycine	339.06147	5.68	C13H14N3O6P
N/A	N-Acetyl cytosine	292.11980	8.47	C16H13N5O
N/A	N-Acetyl-2-pyrrolidone	298.11920	8.52	C16H15N3O3
HMDB0000812	N-Acetylaspartate	345.09609	8.31	C16H15N3O6
HMDB0001138	N-Acetylglutamate	359.11119	8.39	C17H17N3O6
HMDB0000766	N-Acetyl-L-alanine	301.10626	6.24	C15H15N3O4
HMDB0011745	N-Acetyl-L-methionine	361.10908	8.39	C17H19N3O4S
HMDB0000512	N-Acetyl-L-phenylalanine	378.14540	6.34	C21H19N3O4
N/A	N-Acetylornithine	345.15630	5.03	C17H20N4O4
HMDB0003357	N-Acetyl-ornithine	344.14846	4.96	C17H20N4O4
HMDB0094701	N-Acetylproline	328.12970	6.40	C17H17N3O4
HMDB0013713	N-acetyltryptophan	416.14791	8.72	C23H20N4O4
HMDB0011757	N-Acetylvaline	329.13701	4.76	C17H19N3O4
HMDB0001015	N-Formyl-L-methionine	348.10180		C16H17N3O4S
HMDB0001488	Nicotinate	294.08790	0.59	C16H11N3O3
N/A	Nicotinate N-oxide	309.07496	8.59	C16H11N3O4
N/A	N-methyl ornithine	317.16140	8.47	C16H20N4O3
N/A	N-Methyl-L-glutamate	332.12460	6.10	C16H17N3O5
N/A	Nopaline	474.18685		C21H26N6O7

HMDB code	Compound name	Monoisotopic mass	RT / min	Derivatised formula
N/A	Nordihydroguaiaretate	474.21550	6.18	C28HH28N2O5
N/A	N-Oxalylglycine	318.07260	0.33	C14H11N3O6
N/A	N-Phenylanthranilate	384.13480	4.74	C23H17N3O3
HMDB0003011	O-Acetylserine	318.10900	4.60	C15H15N3O5
N/A	Octapine	416.18137		C19H24N6O5
HMDB0000224	O-Phosphoethanolamine	312.07490	2.31	C12H14N3O5P
HMDB0005765	Ophthalmate	460.18320	5.16	C21H25N5O7
HMDB0000214	Ornithine	302.13789	6.06	C15H18N4O3
HMDB0000226	Orotate	327.07290	8.58	C15H10N4O5
N/A	Oxfenicine	337.10571		
HMDB0003337	Oxidised Glutathione (2x derivatised)	952.24744	6.09	C40H44N10O14S2
HMDB0000210	Pantothenate	389.15869	7.04	C19H23N3O6
HMDB0000159	Phenylalanine	335.12699	7.88	C19H17N3O3
HMDB0001511	Phosphocreatine	381.08327	0.42	C14H16N5O6P
HMDB0000370	Phosphono-methylglycine	339.06147		C13H14N3O6P
HMDB0000272	Phosphoserine	355.05639	1.19	C13H14N3O7P
HMDB0002243	Picolinate	293.08059	0.39	C16H11N3O3
HMDB0000070	Pipecolate	299.12754	6.85	C16H17N3O3
HMDB0000162	Proline	285.11134	5.47	C15H15N3O3
HMDB0001856	Protocatechuate	326.09030		C17H12N2O5
HMDB0006078	Putreanine	332.18480	6.86	C17H23N4O3
HMDB0001414	Putrescine	259.15590	2.83	C14H18N4O
HMDB0001414	Putrescine (2x derivatised)	429.20390	6.68	C24H24N6O2
HMDB0001491	Pyridoxal 5-phosphate	417.07251	8.26	C18H16N3O3
HMDB0001431	Pyridoxamine	338.13844	5.50	C18H18N4O3
N/A	Pyroglutamate	299.09006	5.71	C15H13N3O4
HMDB0000805	Pyrrolidonecarboxylate	300.09840	5.61	C15H13N3O4
HMDB0001301	Pyrroline-5-carboxylate	283.09514		C15H13N3O3
HMDB0000232	Quinolinate	337.06932	0.33	C17H11N3O5
HMDB0000939	S-(5-Adenosyl)-L-homocysteine	554.16960	5.79	C24H26N8O6S
HMDB0000279	Saccharopine	446.17960	6.91	C21H26N4O7
HMDB0001185	S-Adenosylmethionine	570.20090	6.07	C25H29N8O6S
HMDB0000271	Sarcosine	259.09569	7.80	C13H13N3O3
HMDB0003966	Selenomethionine	362.05674	7.15	C15H17N3O3Se
HMDB0000187	Serine	275.09061	2.86	C13H13N3O4
HMDB0000259	Serotonin	346.14298	7.01	C20H18N4O2
HMDB0001256	Spermine	373.27160	7.56	C20H32N6O
HMDB0000848	Stearoylcarnitine	597.41417		C35H55N3O5
N/A	Strombine	317.10172		C15H15N3O5
HMDB0003334	Symmetric dimethylarginine	373.19880	4.52	C18H24N6O3
HMDB0000251	Taurine	295.06268		C12H13N3O4S
HMDB0001372	Thiamine pyrophosphate	595.09243	6.06	C22H25N6O8P2S
HMDB0000167	Threonine	289.10626	4.46	C14H15N3O4
HMDB0000262	Thymine	297.09880	6.07	C15H12N4O3
HMDB0062562	Trans-urocanate	308.09039	0.43	C16H12N4O3
HMDB0000303	Tryptamine	330.14861	8.31	C20H18N4O
HMDB0000929	Tryptophan	374.13789	8.00	C21H18N4O3
HMDB0000306	Tyramine	307.13208	7.21	C18H17N3O2
HMDB0000158	Tyrosine	351.12191	6.65	C19H17N3O4
HMDB0000300	Uracil	283.08310	8.58	C14H10N4O3
HMDB0000289	Urate	338.07635	4.89	C15H10N6O4
HMDB0000294	Urea	230.08038	3.94	C11H10N4O2
HMDB0000301	Urocanate/4-imidazole acrylate	308.09039	0.43	C16H12N4O3
HMDB0000883	Valine	287.12699	6.93	C15H17N3O3
HMDB0000292	Xanthine	322.08089	4.81	C15H10N6O3
HMDB0001554	Xanthylate/XMP	535.09780	6.52	C20H19N6O10P

10.4. List of metabolites characterised by non-derivatised RP-MS/MS

Table 10.4: Table of metabolites characterised by non-derivatised RP-MS/MS (Sections 8.9 and 8.10).

HMDB code	Compound name	Monoisotopic mass	RT / min	Formula	Fragmentation pattern
N/A	1,7-beta-estradiol	272.17818	9.39	C18H24O2	
N/A	2,2-Azino-bis-3-Ethylbenzthiazoline-6-sulfonate	514.01092	6.66	C18H18N4O6S4	
N/A	2,2-Diphenyl-1-picrylhydrazyl	394.07876	11.64	C18H12N5O6	
HMDB0001294	2,3-Diphosphoglycerate	265.95872	0.66	C3H8O10P2	
HMDB0002362	2,4-Diaminobutyrate	118.07423	0.71	C4H10N2O2	
HMDB0000152	2,5 Dihydroxybenzoate	154.02661	4.07	C7H6O4	
HMDB0060374	2-Amino-3-methoxybenzoate	167.05769	6.94	C8H9NO3	
HMDB0000370	2-Amino-3-phosphonopropionate	169.01456	0.77	C3H8NO5P	
HMDB0001123	2-Aminobenzoate	137.04823	4.80	C7H7NO2	
HMDB0000991	2-Aminocaprylate	159.12593	5.29	C8H17NO2	
N/A	2-Aminoisobutyrate	103.06388	10.95	C4H9NO2	
N/A	2-C-Methyl-D-Erythritol 4-phosphate	216.03990	0.78	C5H11O7P	
N/A	3,4-Dehydro-L-proline	113.04823	0.74	C5H7NO2	
HMDB0001336	3,4-Dihydroxyphenylacetate	168.04281	3.57	C8H8O4	
HMDB0003540	3'-AMP	347.06254	1.04	C10H14N5O7P	
HMDB0001476	3-Hydroxyanthranilate	153.04204	3.15	C7H7NO3	
HMDB0001904	3-nitrotyrosine	226.05897	3.02	C9H10N2O5	
HMDB0000707	4-Hydroxyphenylpyruvate	180.04281	5.25	C9H8O4	
HMDB0001149	5-Aminolevulinate	131.05879	1.00	C5H9NO3	
HMDB0000045	5'-AMP	347.06254	1.04	C10H14N5O7P	
HMDB0000450	5-Hydroxylysine	162.10099	0.68	C6H14N2O3	
HMDB0000472	5-Hydroxytryptophan	220.08479	1.57	C11H12N2O3	Yes
HMDB0004096	5-Methoxyindoleacetate	205.07444	6.12	C11H11NO3	
HMDB0006217	9-cis-Retinol	286.23021	11.51	C20H30O	
N/A	Acemetacin	415.08226	10.86	C21H18ClNO6	
HMDB0001206	Acetyl-CoA	809.12522	4.62	C23H38N7O17P3S	
N/A	Acetyl-cytosine	153.05437	1.15	C6H7N3O2	
HMDB0001494	Acetylphosphate	139.98746	0.99	C2H5O5P	
HMDB0000034	Adenine	135.05450	0.78	C5H5N5	Yes
HMDB0001852	all-trans-Retinoate	300.20948	13.86	C20H28O2	
HMDB0001893	alpha-Tocopherol	430.38163	16.22	C29H50O2	
N/A	Aminoheptanoate	145.11028	3.46	C7H15NO2	
HMDB0000052	Argininosuccinate	290.12263	0.77	C10H18N4O6	
HMDB0001894	Aspartame	294.12157	5.52	C14H18N2O5	
HMDB0001879	Aspirin	180.04281	5.97	C9H8O4	
N/A	Benzoyl-L-citrulline methyl ester	293.13810	5.52	C14H19N3O4	
HMDB0001252	Betaine aldehyde	102.09244	13.59	C5H12NO	
HMDB0002013	Butyrylcarnitine	231.14761	2.88	C11H21NO4	
HMDB0001964	Caffeate	180.04226	5.35	C9H8O4	
HMDB0001546	CDP	403.01763	1.07	C9H15N3O11P2	
HMDB0005032	Cetirizine	388.15482	8.65	C21H25ClN2O3	
HMDB0003164	Chlorogenate	354.09508	5.10	C16H18O9	
HMDB0011621	Cinnamoylglycine	205.07334	6.85	C11H11NO3	
HMDB0000634	Citraconate	130.02661	1.57	C5H6O4	Yes
HMDB0000426	Citramalate	148.03717	1.25	C5H8O5	
HMDB0014774	Clofibrate	242.07152	10.74	C12H15ClO3	
HMDB0001423	Coenzyme A	767.11466	0.92	C21H36N7O16P3S	
HMDB0000064	Creatine	131.06948	0.76	C4H9N3O2	
HMDB0011616	cyclic adenosine-2'-3'-monophosphate	329.05197	1.04	C10H12N5O6P	

HMDB code	Compound name	Monoisotopic mass	RT / min	Formula	Fragment-ation pattern
HMDB0000099	Cystathionine	222.06743	0.75	C7H14N2O4S	
HMDB0001508	dADP	411.03450	4.44	C10H15N5O9P2	
HMDB0001532	dATP	491.00083	7.11	C10H16N5O12P3	
HMDB0001245	dCDP	387.02272	1.06	C9H15N3O10P2	
HMDB0000998	dCTP	466.98960	5.98	C9H16N3O13P3	
HMDB0015391	Decitabine/ 5'-aza-2'-deoxycytidine	228.08531	1.02	C8H12N4O4	
HMDB0000905	Deoxyadenosine monophosphate	331.06762	1.04	C10H14N5O6P	
HMDB0000626	Deoxycholate	392.29321	12.61	C24H40O4	
HMDB0014724	Diclofenac	295.01614	11.38	C14H11Cl2NO2	
HMDB0032616	Dimethoxy-4-Hydroxycinnamate	224.06847	6.13	C11H12O5	
N/A	Dimethyl-L-Arginine di(p-hydroxyazobenzene-p-sulfonate) salt	202.14298	0.76	C8H18N4O2	
HMDB0000638	Dodecanoate	200.17763	12.83	C12H24O2	
N/A	Dopamine Hydrochloride	153.07898	0.92	C8H11NO2	
HMDB0001342	dTTP	481.98926	6.19	C10H17N2O14P3	
HMDB0000573	Elaidate	282.25533	15.47	C18H34O2	
HMDB0000068	Epinephrine	183.08954	0.76	C9H13NO3	
HMDB0001248	FAD	785.15713	4.98	C27H33N9O15P2	Yes
N/A	Fisetin	286.04719	7.67	C15H10O6	
HMDB0000121	Folate	441.14023	5.36	C19H19N7O6	
HMDB0001201	GDP	443.02378	1.13	C10H15N5O11P2	
N/A	Glyceraldehyde 2-phosphate	169.99802	0.83	C3H7O6P	
HMDB0001397	GMP	363.05800	9.52	C10H14N5O8P	Yes
HMDB0001273	GTP	522.99066	13.06	C10H16N5O14P3	
HMDB0000128	Guanidoacetate	117.05437	0.74	C3H7N3O2	
HMDB0000132	Guanine	151.04886	0.80	C5H5N5O	Yes
HMDB0005782	Hesperitin	302.07849	8.66	C16H14O6	Yes
HMDB0000870	Histamine	111.08020	0.66	C5H9N3	
HMDB0000764	Hydrocinnamate	150.06753	7.95	C9H10O2	
HMDB0000732	Hydroxykynurenine	224.08026	0.77	C10H12N2O4	
HMDB0000700	Hydroxypropionate	90.03224	0.91	C3H6O3	
HMDB0001190	Indole-3-acetaldehyde	159.06896	3.44	C10H9NO	Yes
HMDB0014473	Indomethacin	357.07624	11.53	C19H16ClNO4	
HMDB0011681	Inosine 2'-phosphate	348.04765	0.78	C10H13N4O8P	
N/A	Isovitexin	432.10565	6.50	C21H20O10	Yes
HMDB0032797	Jasmonate	210.12559	8.06	C12H18O3	Yes
HMDB0000715	Kynurenate	189.04259	1.04	C10H7NO3	Yes
HMDB0000192	L-Cystine	240.02440	0.76	C6H12N2O4S2	
HMDB0000181	L-Dopa/3,4,-dihydroxy-phenylalanine	197.06826	1.02	C9H11NO4	
HMDB0001045	Leucine Enkephalin	555.26930	6.56	C28H37N5O7	
HMDB0000673	Linoleate	280.24023	14.18	C18H32O2	
HMDB0034365	L-Theanine	174.10099	0.81	C7H14N2O3	
HMDB0014910	Malathion	330.03661	6.84	C10H19O6PS2	
HMDB0001175	Malonyl-CoA	853.11505	4.61	C24H38N7O19P3S	
HMDB0000163	Maltose	342.11621	0.73	C12H22O11	
HMDB0060486	Mandelonitrile	133.05276	4.64	C8H7NO	
HMDB0001892	Menadione	172.05298	7.91	C11H8O2	
HMDB0032572	Methyl 4-hydroxybenzoate	152.04734	6.41	C8H8O3	
HMDB0002755	Myricetin	318.03702	7.55	C15H10O8	
HMDB0000806	Myristate	228.20893	13.80	C14H28O2	
HMDB0001067	N-Acetylaspartylglutamate	304.09067	1.06	C11H16N2O8	Yes
HMDB0011757	N-Acetyl-DL-Valine	159.08954	4.27	C7H13NO3	
HMDB0001138	N-Acetylglutamate	189.06317	1.04	C7H11NO5	
HMDB0032055	N-Acetyl-histidine	197.08059	1.02	C8H11N3O3	
HMDB0000766	N-Acetyl-L-alanine	131.05879	1.04	C5H9NO3	Yes
HMDB0000812	N-Acetyl-L-aspartate	175.04752	1.03	C6H9NO5	Yes

HMDB code	Compound name	Monoisotopic mass	RT / min	Formula	Fragment-ation pattern
HMDB0011745	N-Acetyl-L-methionine	191.06107	4.28	C7H13NO3S	
HMDB0094701	N-Acetylproline	157.07444	2.96	C7H11NO3	
HMDB0013713	N-acetyltryptophan	246.10099	6.58	C13H14N2O3	
N/A	N-alpha-Benzoyl-l-arginine ethyl ester	306.16974	5.53	C15H22N4O3	
HMDB0002670	Naringenin	272.06847	8.07	C15H12O5	
HMDB0002368	Nervonate	366.34978	16.41	C24H46O2	
HMDB0001406	Nicotinamide	122.04801	4.88	C6H6N2O	
N/A	Nicotinate N-Oxide	139.02749	0.80	C6H5NO3	Yes
HMDB0012270	Nordihydroguaiaretate	302.15181	9.35	C18H22O4	
HMDB0000482	Octanoate	144.11503	9.67	C8H16O2	
HMDB0000207	Oleate	282.25588	14.62	C18H34O2	
N/A	Oxfenicine/4-hydroxyphenylglycine	167.05879	0.80	C8H9NO3	
HMDB0000220	Palmitate	256.24023	14.53	C16H32O2	
HMDB0003229	Palmitoleate	254.22458	13.91	C16H30O2	
HMDB0000222	Palmitoylcarnitine	399.33486	12.13	C23H45NO4	
HMDB0001338	Palmitoyl-CoA	1005.34433	15.50	C37H66N7O17P3S	
N/A	Phenyl acetate	136.05298	6.07	C8H8O2	
N/A	Phenyl-propionate	150.06863	6.78	C9H10O2	
HMDB0001511	Phosphocreatine	211.03636	0.76	C4H10N3O5P	
N/A	Phosphorylcholine Chloride	182.05822	5.27	C5H13NO4P	
HMDB0000272	Phosphoserine	185.01057	0.98	C3H8NO6P	
HMDB0000020	p-Hydroxyphenylacetate	152.04789	5.90	C8H8O3	
HMDB0000801	Phytanate	312.30283	15.19	C20H40O2	
HMDB0000070	Pipecolate	129.07898	0.80	C6H11NO2	
N/A	Poly-DL-Alanine	89.04768	0.76	C3H7NO2	
HMDB0000237	Propionate	74.03733	1.66	C3H6O2	
HMDB0000824	Propionylcarnitine	217.13196	0.82	C10H19NO4	
HMDB0001220	Prostaglandin E2	352.22497	9.68	C20H32O5	
HMDB0001431	Pyridoxamine	168.08988	0.90	C8H12N2O2	
HMDB0005794	Quercetin	302.04210	8.27	C15H10O7	
HMDB0004198	Reduced Vitamin K (phylloquinone)	450.35033	15.41	C31H46O2	
HMDB0000244	Riboflavin	376.13828	5.66	C17H20N4O6	Yes
HMDB0001520	Riboflavin 5-monophosphate	456.10461	5.44	C17H21N4O9P	Yes
HMDB0001895	Salicylate	138.03169	6.36	C7H6O3	
HMDB0006797	Sorbose 1-phosphate	260.02917	0.96	C6H13O9P	
HMDB0000827	Stearate	284.27153	15.16	C18H36O2	
HMDB0000848	Stearoylcarnitine	427.36616	13.22	C25H49NO4	
HMDB0000258	Sucrose	342.11621	0.79	C12H22O11	
HMDB0000036	Taurocholate	515.29222	10.14	C26H45NO7S	
HMDB0014897	Tetracycline	444.15327	5.26	C22H24N2O8	
HMDB0000027	Tetrahydrobiopterin	241.11804	0.77	C9H15N5O3	
HMDB0001846	Tetrahydrofolate	445.17153	5.01	C19H23N7O6	
HMDB0002825	Theobromine	180.06418	4.75	C7H8N4O2	
HMDB0001889	Theophylline	180.06418	4.71	C7H8N4O2	
HMDB0015256	Tolbutamide	270.10381	8.25	C12H18N2O3S	
HMDB0000954	Trans-ferulate	194.05736	6.60	C10H10O4	
HMDB0062562	Trans-urocanate	138.04348	0.77	C6H6N2O2	
N/A	Tricine	179.07937	0.76	C6H13O5N	
HMDB0000303	Tryptamine	160.10005	4.24	C10H12N2	
HMDB0015330	Tubocurarine	609.29591	8.71	C37H41N2O6	
HMDB0000301	Urocanate	138.04348	0.78	C6H6N2O2	
HMDB0012308	Vanillin	152.04734	5.66	C8H8O3	
N/A	Xanthosine 3,5 cyclic monophosphate	344.01580	0.90	C10H9N4O8P	
HMDB0000881	Xanthurenate	205.03751	4.49	C10H7NO4	

10.5. Data for LN18 IDH1 mutant and wild-type glioblastoma cells cultured at 2 glucose concentrations

Metabolite identification information for LN18 Mut and WT cells cultured under 1.0 g / L or 4.5 g / L glucose conditions (experimental replicate 1, Section 8.14), analysed by IC-MS/MS (Section 8.4), derivatised RP-MS (Section 8.7) and non-derivatised RP-MS/MS (Section 8.9), including HMDB code, fragmentation score, mass error, isotope similarity RT method and analysis method are listed in Table 10.5. Full compound-feature lists including significance, FC and CV information for LN18 Mut and WT cells cultured under 4.5 g / L glucose conditions (experimental replicate 1, Section 8.14) are found in ESM B. Compound-feature lists for LN18 Mut cells cultured under 1.0 g / L or 4.5 g / L glucose conditions (experimental replicate 1, Section 8.14) are found in ESM C.

Table 10.5: Metabolite identification information for the analysis of LN18 Mut and WT cells cultured under 1.0 g / L or 4.5 g / L glucose conditions (experimental replicate 1, Section 8.14), analysed by IC-MS/MS (Section 8.4), derivatised RP-MS (Section 8.7) and non-derivatised RP-MS/MS (Section 8.9).

HMDB code	Identification	In-house DB fragment-ation score	Mass error / ppm	Isotope similarity / %	RT error / min	Method
HMDB0033091	(Z)-3-(1-Formyl-1-propenyl)pentanedioate		1.35	91.86		IC-MS/MS
HMDB0011649	1-(sn-Glycero-3-phospho)-1D-myo-inositol	7.51	0.78	98.37		IC-MS/MS
HMDB0041500	1-Deoxy-D-glucitol	45.40	-3.79	97.25		IC-MS/MS
HMDB0001213	1-Deoxy-D-xylulose 5-phosphate	61.00	-2.62	98.97		IC-MS/MS
HMDB0000001	1-Methyl histidine		2.18	91.68	-0.09	RP-MS
HMDB0006875	1-Pyrroline-2-carboxylate	35.70	0.03	95.17		RP-MS/MS
HMDB0002234	1-Pyrroline-4-hydroxy-2-carboxylate	20.20	-3.69	93.97		IC-MS/MS
HMDB0000152	2,5 Dihydroxybenzoate		0.19	93.43	0.11	RP-MS/MS
HMDB0000510	2-Aminoadipate		3.94	96.03	0.01	RP-MS
HMDB0001241	2-Aminomuconate		-3.17	93.33		IC-MS/MS
HMDB0001280	2-Aminomuconate semialdehyde	32.20	-3.44	95.41		IC-MS/MS
HMDB0001532	2-Deoxyadenosine 5-triphosphate		2.57	94.46	-0.35	IC-MS/MS
HMDB0000008	2-Hydroxybutyrate	38.20	-0.67	98.50	-0.48	RP-MS/MS
HMDB0059655	2-Hydroxyglutarate	78.30	-3.91	99.83	-0.57	IC-MS/MS
HMDB0000005	2-Ketobutyrate	80.70	-4.19	98.11	-0.64	IC-MS/MS
HMDB0001552	2-Keto-glutaramate		-3.89	94.69		IC-MS/MS
HMDB0012152	2-O-(6-Phospho-alpha-mannosyl)-D-glycerate	1.68	0.02	99.18		IC-MS/MS
HMDB0000208	2-Oxoglutarate	23.70	-3.78			IC-MS/MS

HMDB code	Identification	In-house DB fragment-ation score	Mass error / ppm	Isotope similarity / %	RT error / min	Method
HMDB0000362	2-Phosphoglycerate	66.10	-3.81	98.23		IC-MS/MS
HMDB0002441	3,3-Dimethylglutarate		-3.66	94.85		IC-MS/MS
N/A	3,4-Dihydroxy-L-Phenylanine		-0.56	89.54	0.36	RP-MS/MS
HMDB0001336	3,4-Dihydroxyphenylacetate		0.89	93.23	0.01	RP-MS/MS
HMDB0003911	3-Amino-2-methylpropanoate		2.55	98.48		RP-MS
HMDB0000355	3-Hydroxymethylglutarate	60.50	-4.17	99.54		IC-MS/MS
HMDB0000807	3-Phosphoglceryate		-1.22		-0.03	RP-MS/MS
HMDB0001024	3-Phosphonooxypyruvate		3.07	95.19		RP-MS
HMDB0000707	4-Hydroxyphenylpyruvate	42.90	-4.17	96.66		IC-MS/MS
HMDB0000725	4-hydroxyproline		1.89	86.92	0.01	RP-MS
HMDB0001149	5-Aminolevulinate		0.11	89.83		RP-MS
HMDB0000763	5-Hydroxyindoleacetate	100.00	-3.66	98.28	-1.16	IC-MS/MS
HMDB0000472	5-hydroxytryptophan		0.70	86.42		RP-MS
HMDB0001316	6-Phosphogluconate	43.40	-1.69	98.86		IC-MS/MS
HMDB0011615	8-Oxo-dGTP		-3.11	85.12		IC-MS/MS
HMDB0036093	Abscisate	100.00	1.24	96.83	-0.83	IC-MS/MS
HMDB0001890	Acetylcysteine	100.00	-4.08	91.05	0.03	IC-MS/MS
HMDB0000532	Acetylglycine	93.70	-3.77	95.25	-0.58	IC-MS/MS
HMDB0000034	Adenine	13.10	-3.21	93.50		IC-MS/MS
HMDB0001341	Adenosine diphosphate		3.50	85.94	-3.87	IC-MS/MS
HMDB0000045	Adenosine monophosphate	75.50	0.86	96.57	-0.70	IC-MS/MS
HMDB0000538	Adenosine triphosphate	7.40	-2.19	98.02	-0.78	IC-MS/MS
HMDB0012882	Adipate semialdehyde	40.90	-3.09	99.20		IC-MS/MS
HMDB0000161	Alanine		1.69	97.06	-0.04	RP-MS
HMDB0000462	Allantoin	31.30	-3.86	97.08		IC-MS/MS
HMDB0000112	Aminobutyrate		0.69	95.87	0.01	RP-MS
HMDB0001123	Anthranilate		-3.51	81.67		RP-MS
HMDB0000539	Arabinonate	45.10	-4.46	98.18		IC-MS/MS
HMDB0000517	Arginine		2.06	94.39	0.00	RP-MS
HMDB0000168	Asparagine		2.21	95.21	-0.07	RP-MS
HMDB0000191	Aspartate		2.06	96.33	0.00	RP-MS
HMDB0028749	Aspartyl-Aspartate	55.10	-2.92	97.69		IC-MS/MS
HMDB0028755	Aspartyl-Histidine		-4.73	87.30		RP-MS/MS
HMDB0000056	Beta-Alanine	49.20	-4.54	98.17	-0.57	IC-MS/MS
HMDB0013220	Beta-Citryl-L-glutamate	9.53	0.62	98.07		IC-MS/MS
HMDB0000039	Butyrate	20.40	-4.77	99.39		IC-MS/MS
HMDB0000033	Carnosine		2.38	85.19	-0.05	RP-MS
HMDB0000072	Cis-aconitate	28.80	-4.57	98.71		IC-MS/MS
HMDB0001413	Citicoline		2.04	82.33		IC-MS/MS
HMDB0000634	Citraconate		-0.70	94.59		RP-MS/MS
HMDB0000426	Citramalate		-3.40	93.59	-2.40	IC-MS/MS
HMDB0000094	Citrate	93.90	-3.60	99.64	-0.68	IC-MS/MS
HMDB0000904	Citrulline		2.61	93.21	0.00	RP-MS
HMDB0001176	CMP N-acetylneuraminate		-2.73	98.28	-0.27	IC-MS/MS
HMDB0000064	Creatine		-0.83	94.21	0.01	RP-MS/MS
HMDB0002757	Cysteate	34.50	-4.19	91.58		IC-MS/MS
HMDB0001546	Cytidine diphosphate		2.99	98.14	0.07	IC-MS/MS
HMDB0000095	Cytidine monophosphate	100.00	0.31	95.20	-0.78	IC-MS/MS
HMDB0000082	Cytidine triphosphate		4.67	86.70	0.01	RP-MS/MS
HMDB0001016	D-4'-Phosphopantothenate		-0.40	94.01		IC-MS/MS
HMDB0001508	dADP		3.75	96.86	0.04	IC-MS/MS
HMDB0001245	dCDP		3.48	95.60		IC-MS/MS
HMDB0000998	dCTP		2.13	93.81	-0.66	IC-MS/MS
HMDB0000012	Deoxyuridine	100.00	-2.72	97.11	-0.58	IC-MS/MS
HMDB0001047	D-Fructose 2,6-bisphosphate	25.40	1.15	99.11		IC-MS/MS
HMDB0000960	dGDP		3.49	97.73	0.11	IC-MS/MS

HMDB code	Identification	In-house DB fragment-ation score	Mass error / ppm	Isotope similarity / %	RT error / min	Method
HMDB0003976	D-Glucuronate 1-phosphate	39.90	-1.59	95.31		IC-MS/MS
HMDB0001112	D-Glyceraldehyde 3-phosphate	53.80	-3.61	97.41		IC-MS/MS
HMDB0001044	dGMP	90.70	1.27	96.61	-1.15	IC-MS/MS
HMDB0001155	Diadenosine triphosphate		-1.47	90.54		IC-MS/MS
HMDB0003349	dihydroorotate		-3.75	97.03	-0.38	IC-MS/MS
HMDB0001473	Dihydroxyacetone phosphate	63.40	-3.87	98.24		IC-MS/MS
HMDB0013287	Dimethyl L-Lysine		2.49	87.41	0.01	RP-MS
HMDB0000092	Dimethylglycine	9.87	-3.79	95.24		IC-MS/MS
HMDB0000638	Dodecanoate		-1.30	87.29	-0.17	RP-MS/MS
HMDB0001548	D-Ribose 5-phosphate	58.60	-3.24	78.44		IC-MS/MS
HMDB0001068	D-Sedoheptulose 7-phosphate		-0.99	94.93		IC-MS/MS
HMDB0001328	dTDP-D-glucose		-3.10	93.95	0.00	IC-MS/MS
HMDB0001000	dUDP		4.23	93.16	0.06	IC-MS/MS
HMDB0001409	dUMP		0.40	94.26	0.02	IC-MS/MS
HMDB0001191	dUTP		1.90	94.02	-0.02	IC-MS/MS
HMDB0015109	EDTA		-0.28	95.54	-1.17	IC-MS/MS
HMDB0000613	Erythronate	23.40	-0.34	96.92		RP-MS/MS
HMDB0001321	Erythrose 4-phosphate		-2.55	97.70	1.78	IC-MS/MS
HMDB0000149	Ethanolamine		1.05	95.38	-0.06	RP-MS
HMDB0001248	FAD	0.96	-0.20	94.92	0.01	RP-MS/MS
HMDB0000660	Fructose	7.59	-3.74	98.15	1.68	IC-MS/MS
HMDB0001058	Fructose 1,6-bisphosphate	99.90	1.00		-0.66	IC-MS/MS
HMDB0000124	Fructose 6-phosphate	74.00	-3.16	99.32	0.44	IC-MS/MS
HMDB0001265	Fucose 1-phosphate	27.00	1.31	96.58		RP-MS/MS
HMDB0000134	Fumarate	52.40	-3.71	98.82	-1.63	IC-MS/MS
HMDB0003559	Giberellate		4.89	91.22	-0.06	RP-MS/MS
HMDB0000625	Gluconate	45.00	-4.09	99.01		IC-MS/MS
HMDB0000150	Gluconolactone	100.00	-4.69	99.00	-0.63	IC-MS/MS
HMDB0001254	Glucosamine 6-phosphate	92.60	-3.79	91.47	-0.45	IC-MS/MS
HMDB0001586	Glucose 1-phosphate	40.80	-2.88	99.08		IC-MS/MS
HMDB0000127	Glucuronate	100.00	-4.14	99.44	-0.58	IC-MS/MS
HMDB0000148	Glutamate		2.24	96.67	0.01	RP-MS
HMDB0002104	Glutamate-5-semialdehyde		1.50	88.86		RP-MS
HMDB0000641	Glutamine		2.47	95.80	0.00	RP-MS
HMDB0000661	Glutarate	46.50	-4.57	76.51	0.10	IC-MS/MS
HMDB0000125	Glutathione		2.20	89.16	-0.06	RP-MS
HMDB0000139	Glycerate	55.60	-4.37			IC-MS/MS
HMDB0000131	Glycerol	57.40	-4.20	99.73	-0.28	IC-MS/MS
HMDB0000126	Glycerol 3-phosphate	14.80	-3.50			IC-MS/MS
HMDB0000123	Glycine		1.16	97.73	0.00	RP-MS
HMDB0002022	Glycineamide ribonucleotide		2.98	95.17		RP-MS/MS
HMDB0000115	Glycolate	27.70	-4.66	99.04	-0.27	IC-MS/MS
HMDB0000119	Glyoxylate		-4.38	98.97	0.57	IC-MS/MS
HMDB0000133	Guanosine	18.50	-0.87	94.78		IC-MS/MS
HMDB0001163	Guanosine diphosphate mannose	0.83	-2.45	97.68		IC-MS/MS
HMDB0001397	Guanosine monophosphate	41.80	2.02	96.85	-0.27	IC-MS/MS
HMDB0001273	Guanosine triphosphate	1.96	-1.29			IC-MS/MS
HMDB0000714	Hippurate	99.70	-4.06	90.39	-0.62	IC-MS/MS
HMDB0000177	Histidine		2.44	92.97	0.07	RP-MS
HMDB0000742	Homocysteine		2.03	87.97		RP-MS
HMDB0000719	Homoserine		1.27	93.84	0.00	RP-MS
HMDB0000118	Homovanillate	78.50	-3.91	98.65	-0.70	IC-MS/MS
HMDB0000764	Hydrocinnamate	100.00	-1.20	99.34	-1.03	IC-MS/MS
HMDB0001352	Hydroxypyruvate	23.00	-4.12	99.25		IC-MS/MS
HMDB0003335	IDP	16.20	3.02	97.37	3.31	IC-MS/MS
HMDB0000671	Indole-3-lactate		-3.79	91.71	-1.38	IC-MS/MS

HMDB code	Identification	In-house DB fragment-ation score	Mass error / ppm	Isotope similarity / %	RT error / min	Method
HMDB0060484	Indole-3-pyruvate		-2.99	92.76	0.00	RP-MS
HMDB0000175	Inosine monophosphate	100.00	1.05	97.46	-0.77	IC-MS/MS
HMDB0001125	Inositol cyclic phosphate	70.80	-2.16	97.28		IC-MS/MS
HMDB0034198	Isobutylamine		1.79	95.93	-0.14	RP-MS
HMDB0000172	Isoleucine		2.11	96.86	0.00	RP-MS
HMDB0001347	Isopentenyl pyrophosphate	44.70	-3.52	99.70		IC-MS/MS
HMDB0000678	Isovalerylglycine	61.70	-4.42	99.32	-0.22	IC-MS/MS
HMDB0000715	Kynurenate	0.56	-0.42	92.92		RP-MS/MS
HMDB0000684	Kynurenine		2.62	89.79	0.01	RP-MS
HMDB0000201	L-Acetylcarnitine		-3.05	97.69		IC-MS/MS
HMDB0000190	Lactate	34.20	-4.12	99.87	-0.49	IC-MS/MS
HMDB0000687	Leucine		2.10	96.89	0.00	RP-MS
HMDB0001228	L-Glutamate 5-phosphate	24.40	0.19	92.70		RP-MS/MS
HMDB0000673	Linoleate		2.79	94.70	-0.04	RP-MS/MS
HMDB0030393	L-N-Carboxymethylserine		-2.70	93.24		IC-MS/MS
HMDB0000182	Lysine		1.67	96.54	0.02	RP-MS
HMDB0000744	Malate	85.30	-4.08	99.83	-0.56	IC-MS/MS
HMDB0000176	Maleate	80.90	-3.75	99.68	0.63	IC-MS/MS
HMDB0002928	Malitol	100.00	0.18	95.15	-0.33	IC-MS/MS
HMDB0000691	Malonate		-0.73	95.87	0.03	RP-MS/MS
HMDB0000749	Mesaconate	78.40	-3.06	99.68	-2.18	IC-MS/MS
HMDB0000696	Methionine		2.32	95.61	0.01	RP-MS
HMDB0000752	Methylglutarate	99.50	-3.72	99.47	-0.53	IC-MS/MS
HMDB0006471	Methylisocitrate		-3.70	95.95	-0.03	IC-MS/MS
HMDB0001343	Mevalonate-5P	100.00	-4.13	99.44	-0.67	IC-MS/MS
HMDB0001325	N,N,N-Trimethyllysine		2.02	91.39	-0.06	RP-MS
HMDB0001067	N-Acetylaspartylglutamate		-0.01	96.54	-0.56	IC-MS/MS
HMDB0001121	N-Acetyl-D-mannosamine 6-phosphate	7.83	-0.05	98.00		IC-MS/MS
HMDB0001367	N-acetyl-glucosamine-1-phosphate		-0.01	97.39	0.25	IC-MS/MS
HMDB0001138	N-Acetylglutamate	99.70	-3.84	91.42	-0.46	IC-MS/MS
HMDB0000766	N-Acetyl-L-alanine	83.80	-4.81	93.91	-0.07	IC-MS/MS
HMDB0000812	N-Acetyl-L-aspartate	42.70	-4.17	94.38		IC-MS/MS
HMDB0006488	N-Acetyl-L-glutamate 5-semialdehyde	1.43	-3.22	98.49		IC-MS/MS
HMDB0011745	N-Acetyl-L-methionine		-3.09	87.01	0.04	IC-MS/MS
HMDB0000512	N-Acetyl-L-phenylalanine	99.70	-4.63	98.24	-0.60	IC-MS/MS
HMDB0000230	N-Acetylneuraminate (sialate)	31.00	0.02	96.80		IC-MS/MS
HMDB0006268	N-Acetylneuraminate 9-phosphate		3.01	85.81	0.00	IC-MS/MS
HMDB0003357	N-Acetyl-ornithine		2.38	94.21	-0.10	RP-MS
HMDB0001487	NADH	0.71	-1.93	97.81		IC-MS/MS
HMDB0014304	NADH	1.97	-0.50	88.44		RP-MS/MS
HMDB0001200	N'-Formylkynurenine		-0.02	95.54		RP-MS/MS
HMDB0000833	N-Glycolylneuraminate		1.14	93.57		IC-MS/MS
HMDB0002393	N-Methyl-D-aspartate	63.10	-3.74	93.74	4.03	IC-MS/MS
HMDB0013716	Norvaline		-0.63	94.50	0.04	RP-MS/MS
N/A	N-Oxalylglycine	100.00	-4.29	98.79	0.44	IC-MS/MS
HMDB0000482	Octanoate	91.20	-4.06	98.31	-1.41	IC-MS/MS
HMDB0000207	Oleate		2.83	94.32	-0.06	RP-MS/MS
HMDB0001721	O-Phosphoserine	99.40	-4.09	95.30	-0.53	IC-MS/MS
HMDB0005765	Ophthalmate		-0.62	93.82		IC-MS/MS
HMDB0000214	Ornithine		1.93	89.25	0.00	RP-MS
HMDB0000226	Orotate	16.80	-3.69	93.23		IC-MS/MS
HMDB0002329	Oxalate		-4.31	99.38	-0.59	IC-MS/MS
HMDB0003337	Oxidized glutathione	6.66	-0.55	92.39		RP-MS/MS
HMDB0000225	Oxoadipate	97.00	-4.27	98.99	-0.56	IC-MS/MS
HMDB0000220	Palmitate		0.31	93.02	-0.13	RP-MS/MS
HMDB0000210	Pantothenate	97.60	-3.64	98.40	-0.46	IC-MS/MS

HMDB code	Identification	In-house DB fragment-ation score	Mass error / ppm	Isotope similarity / %	RT error / min	Method
HMDB0002035	p-coumarate	52.80	-3.50	97.80	1.22	IC-MS/MS
HMDB0000228	Phenol		-4.59	98.66		IC-MS/MS
HMDB0000159	Phenylalanine		2.05	96.27	0.01	RP-MS
HMDB0001511	Phosphocreatine	7.93	-3.08	95.22		IC-MS/MS
HMDB0041624	Phosphocreatinine	20.50	-3.04	95.46		IC-MS/MS
HMDB0000263	Phosphoenolpyruvate	38.00	-4.22	99.68		IC-MS/MS
HMDB0000816	Phosphoglycolate	95.00	-4.63	99.81	-0.60	IC-MS/MS
HMDB0000801	Phytanate		4.30	94.87	0.42	RP-MS/MS
N/A	Poly-DL-Alanine		0.32	95.94	0.04	RP-MS/MS
HMDB0012282	PPPi		-1.90	97.57		IC-MS/MS
HMDB0000162	Proline		1.64	95.65	0.01	RP-MS
HMDB0001491	Pyridoxal 5'-phosphate	100.00	-3.16	98.81	-0.78	IC-MS/MS
HMDB0001555	Pyridoxamine 5-phosphate		-4.70	91.56		RP-MS
HMDB0000267	Pyroglutamate	39.40	-0.07	93.84		RP-MS/MS
HMDB0000243	Pyruvate	43.10	-4.08	99.15		IC-MS/MS
HMDB0003072	Quinate	100.00	-3.96	99.23	-0.58	IC-MS/MS
HMDB0003213	Raffinose	100.00	1.89	95.03	-0.31	IC-MS/MS
HMDB0000283	Ribose	42.60	-4.37	97.55		IC-MS/MS
HMDB0011688	Ribose 1,5-bisphosphate	2.50	0.60	97.03		IC-MS/MS
N/A	Ribulose 1,5,diphosphate		-0.94	95.58	-1.81	IC-MS/MS
HMDB0000618	Ribulose 5-phosphate	48.30	-2.16	98.50	-0.02	IC-MS/MS
HMDB0000663	Saccharate		-3.58	91.85	-0.48	IC-MS/MS
HMDB0000279	Saccharopine		3.62	91.04	-0.01	RP-MS
HMDB0001895	Salicylate		-0.08	95.17	0.06	RP-MS/MS
HMDB0000271	Sarcosine		1.52	97.44	0.02	RP-MS
HMDB0000792	Sebacate	100.00	-3.90	98.49	-0.79	IC-MS/MS
HMDB0060274	Sedoheptulose 1,7-bisphosphate		2.58	95.80	0.08	IC-MS/MS
HMDB0060509	Sedoheptulose 1-phosphate		-0.42	95.44	-0.03	IC-MS/MS
HMDB0000187	Serine		1.78	96.38	0.00	RP-MS
HMDB0000259	Serotonin		2.03	85.74	-0.13	RP-MS
HMDB0003070	Shikimate	21.30	-0.56	93.78		RP-MS/MS
HMDB0031436	Silicate	18.70	-1.59	92.22		IC-MS/MS
HMDB0059660	sn-glycero-3-phosphoethanolamine	24.90	-2.79	93.01		IC-MS/MS
HMDB0000247	Sorbitol	98.40	-3.24	99.05	-0.21	IC-MS/MS
HMDB0005831	Sorbitol-6-phosphate		-3.07	97.28	0.03	IC-MS/MS
HMDB0000827	Stearate		3.19	96.32	-0.16	RP-MS/MS
HMDB0000254	Succinate	92.70	-3.56	99.09	-0.56	IC-MS/MS
HMDB0001259	Succinate semialdehyde		-4.25	98.48	-0.04	IC-MS/MS
HMDB0032523	Succinic anhydride	18.10	-3.63	97.42		IC-MS/MS
HMDB0000251	Taurine		2.17	95.47	-0.04	RP-MS
HMDB0001274	TDP	3.72	3.19	98.07	4.22	IC-MS/MS
HMDB0004136	Threitol	100.00	-3.52	97.86	-0.31	IC-MS/MS
HMDB0000167	Threonine		1.57	96.94	0.01	RP-MS
HMDB0001227	Thymidine 5'-phosphate (TMP)		0.06	95.49	0.05	IC-MS/MS
HMDB0001342	Thymidine triphosphate	44.70	1.92	98.02	0.52	IC-MS/MS
HMDB0000929	Tryptophan		2.10	95.04	0.02	RP-MS
HMDB0000158	Tyrosine		2.14	95.87	0.01	RP-MS
HMDB0041785	Tyrosol 4-sulfate		-2.95	88.23		IC-MS/MS
HMDB0000935	UDP-glucoronate		-3.29	92.83	0.00	IC-MS/MS
HMDB0000286	UDP-glucose		-2.81	96.72	0.10	IC-MS/MS
HMDB0000290	UDP-N-acetylglucosamine	38.90	-3.03	98.63	-0.70	IC-MS/MS
HMDB0000300	Uracil	100.00	-3.77	98.08	-0.62	IC-MS/MS
HMDB0000289	Urate	93.10	-3.78	93.50	-0.91	IC-MS/MS
HMDB0000296	Uridine		-0.03	94.18	-0.04	RP-MS/MS
HMDB0000295	Uridine 5'-diphosphate	71.50	2.92	98.51	2.76	IC-MS/MS
HMDB0000288	Uridine 5'-monophosphate	98.70	0.40	98.26	-0.79	IC-MS/MS

HMDB code	Identification	In-house DB fragment-ation score	Mass error / ppm	Isotope similarity / %	RT error / min	Method
HMDB0000285	Uridine triphosphate	15.40	1.52	98.31	-0.79	IC-MS/MS
HMDB0000883	Valine		1.63	97.06	0.00	RP-MS
HMDB0001554	Xanthosine-5-phosphate		2.83	95.89	0.03	IC-MS/MS
HMDB0002917	Xylitol	84.00	-4.24	98.29	-0.21	IC-MS/MS
HMDB0001644	Xylulose	26.30	-4.41	95.33	0.75	IC-MS/MS
HMDB0000868	Xylulose 5-phosphate	96.60	-3.51	98.34	-0.45	IC-MS/MS

Metabolite identification information for LN18 Mut and WT cells cultured under 4.5 g / L glucose conditions (experimental replicate 2, Section 8.14), analysed by IC-MS/MS (Section 8.4), derivatised RP-MS (Section 8.7) and non-derivatised RP-MS/MS (Section 8.9), including HMDB code, fragmentation score, mass error, isotope similarity RT method and analysis method are found in Table 10.6. Full compound-feature lists including significance, FC and CV information for LN18 Mut and WT cells cultured under 4.5 g / L glucose conditions (experimental replicate 2, Section 8.14) are found in ESM D.

Table 10.6: Metabolite identification information for the analysis of LN18 Mut and WT cells cultured under 4.5 g / L glucose conditions (experimental replicate 2, Section 8.14), analysed by IC-MS/MS (Section 8.4), derivatised RP-MS (Section 8.7) and non-derivatised RP-MS/MS (Section 8.9).

HMDB code	Identification	In-house DB fragment-ation score	Mass error / ppm	Isotope similarity / %	RT error / min	Method
HMDB0000957	1,2 Dihydroxybenzene		-0.87	97.02	0.89	RP-MS/MS
HMDB0001213	1-Deoxy-D-xylulose 5-phosphate		-0.16	93.60	0.03	IC-MS/MS
N/A	1-Hydroxy-2-methyl-2-butenyl 4-pyrophosphate		-0.62		-0.04	RP-MS/MS
HMDB0000001	1-Methyl histidine		0.65	89.44	-0.05	RP-MS
HMDB0000152	2,5 Dihydroxybenzoate		-0.25	99.58	0.10	RP-MS/MS
HMDB0000510	2-Aminoadipate		2.55	95.56	0.01	RP-MS
N/A	2-C-Methyl-D-Erythritol 4-phosphate		0.48		-0.02	RP-MS/MS
HMDB0001044	2'-Deoxyguanosine 5'-monophosphate	25.50	3.26	96.67	-0.38	IC-MS/MS
HMDB0000008	2-Hydroxybutyrate		-0.82	98.77	-0.05	RP-MS/MS
HMDB0059655	2-Hydroxyglutarate		-2.08	99.88	0.01	IC-MS/MS
HMDB0000402	2-Isopropylmalate		-2.25	95.34	0.06	IC-MS/MS
HMDB0000005	2-Ketobutyrate	10.90	-2.30	97.45		IC-MS/MS
HMDB0001865	2-Oxovalerate	19.40	-1.63	97.45		IC-MS/MS
HMDB0000181	3,4-Dihydroxy-L-Phenylanine		-1.51	89.54	0.16	RP-MS/MS
HMDB0001336	3,4-Dihydroxyphenylacetate		0.40	94.46	0.00	RP-MS/MS
HMDB0000355	3-Hydroxymethylglutarate	51.60	-1.77	98.75		IC-MS/MS
HMDB0000197	3-Indolylacetate		-0.69	98.72	-0.01	RP-MS/MS
HMDB0000807	3-Phosphoglceryate		-2.07		-0.01	RP-MS/MS
HMDB0000725	4-Hydroxyproline	93.50	-1.97	98.62	-0.12	IC-MS/MS
N/A	4-Hydroxypyridine		-1.47	99.06	-0.04	RP-MS/MS

HMDB code	Identification	In-house DB fragment-ation score	Mass error / ppm	Isotope similarity / %	RT error / min	Method
HMDB0000472	5-Hydroxy L-Tryptophan		-0.65	97.65	-0.05	RP-MS/MS
HMDB0001316	6-Phosphogluconate		0.03	99.03	0.01	IC-MS/MS
HMDB0001890	Acetylcysteine	36.30	-1.97	91.57	0.00	IC-MS/MS
HMDB0000532	Acetylglycine	82.00	-1.55	72.55	-0.08	IC-MS/MS
HMDB0000034	Adenine	27.60	-1.47	94.71		IC-MS/MS
HMDB0000058	Adenosine 3',5'-cyclic monophosphate		2.71	95.70	-0.14	RP-MS/MS
HMDB0006557	Adenosine 5'-diphosphoglucose		-0.76	93.15	0.01	RP-MS/MS
HMDB0000045	Adenosine monophosphate	31.00	2.98	96.39	-0.32	IC-MS/MS
HMDB0000538	Adenosine triphosphate	5.25	-0.46	97.87	-0.06	IC-MS/MS
HMDB0000161	Alanine		0.42	97.29	-0.04	RP-MS
HMDB0000112	Aminobutyrate		-0.54	95.91	0.01	RP-MS
HMDB0001123	Anthranilate		-4.53	81.67		RP-MS
HMDB0000517	Arginine		0.91	94.42	0.00	RP-MS
HMDB0000044	Ascorbate	5.74	-2.38	96.25	-0.04	IC-MS/MS
HMDB0000168	Asparagine		0.93	94.32	-0.06	RP-MS
HMDB0000191	Aspartate		0.87	96.40	0.00	RP-MS
HMDB0013220	Beta-Citryl-L-glutamate	1.47	2.38	98.04		IC-MS/MS
HMDB0000043	Betaine		-0.73	94.45	-0.10	RP-MS/MS
HMDB0001546	CDP	3.15	4.94	97.94		IC-MS/MS
HMDB0000072	Cis-aconitate		-2.82	97.84	0.04	IC-MS/MS
HMDB0000634	Citraconate		-0.29	99.68	-0.05	RP-MS/MS
HMDB0000094	Citrate	91.50	-1.64	99.52	-0.01	IC-MS/MS
HMDB0000904	Citrulline		1.18	93.44	0.00	RP-MS
HMDB0000095	Cytidine monophosphate	33.90	2.25	94.70	0.08	IC-MS/MS
HMDB0000082	Cytidine triphosphate	7.21	3.33	98.09	-0.07	IC-MS/MS
HMDB0000998	dCTP		3.24	93.41	-0.04	IC-MS/MS
HMDB0000085	Deoxyguanosine		-0.13	96.32	-0.01	RP-MS/MS
HMDB0013287	Dimethyl L-Lysine		1.63	91.53	0.00	RP-MS
HMDB0000638	Dodecanoate		-1.48	92.39	-0.15	RP-MS/MS
HMDB0001068	D-Sedoheptulose 7-phosphate	6.64	1.19	94.84		IC-MS/MS
HMDB0001321	Erythrose 4-phosphate		-1.13	94.14	0.05	RP-MS/MS
HMDB0000149	Ethanolamine		0.00	95.56	-0.06	RP-MS
HMDB0000622	Ethylmalonate		-1.18	99.59	0.05	RP-MS/MS
HMDB0001248	FAD		-0.36	92.69	0.03	RP-MS/MS
HMDB0000660	Fructose		-1.28	93.44	0.04	RP-MS/MS
HMDB0001058	Fructose 1,6-bisphosphate	73.70	2.90		-0.07	IC-MS/MS
HMDB0001265	Fucose 1-phosphate	7.38	-1.34	97.95		IC-MS/MS
HMDB0000134	Fumarate	62.10	-1.75	99.65	-0.02	IC-MS/MS
HMDB0000639	Galactarate	35.10	-1.74	97.08	-0.07	IC-MS/MS
HMDB0003559	Giberellate		4.01	96.98	-0.07	RP-MS/MS
HMDB0000625	Gluconate	52.60	-2.19			IC-MS/MS
HMDB0000150	Gluconolactone		-1.72	97.32	0.08	RP-MS/MS
HMDB0001254	Glucosamine 6-phosphate		-0.43	91.47	-0.01	RP-MS/MS
HMDB0001586	Glucose 1-phosphate	33.30	-1.04	99.05		IC-MS/MS
HMDB0001401	Glucose-6-phosphate		-0.51	98.57	0.02	RP-MS/MS
HMDB0000127	Glucuronate	83.10	-2.19	97.48	0.04	IC-MS/MS
HMDB0000148	Glutamate		0.99	96.81	0.01	RP-MS
HMDB0000641	Glutamine		1.12	96.20	0.00	RP-MS
HMDB0000661	Glutarate	58.00	-1.80	98.00	-0.04	IC-MS/MS
HMDB0000125	Glutathione		0.88	87.88	-0.06	RP-MS
N/A	Glyceraldehyde 2-phosphate		-1.67	95.39	-0.04	RP-MS/MS
HMDB0000139	Glycerate	63.50	-2.68			IC-MS/MS
HMDB0000131	Glycerol	55.10	-2.46	99.48	0.02	IC-MS/MS
HMDB0000126	Glycerol 3-phosphate	12.10	-1.44			IC-MS/MS
HMDB0000114	Glycerylphosphorylethanolamine	13.30	-1.15	97.37		IC-MS/MS

HMDB code	Identification	In-house DB fragment-ation score	Mass error / ppm	Isotope similarity / %	RT error / min	Method
HMDB0000123	Glycine		0.07	97.85	0.00	RP-MS
N/A	Gly-Gly		1.04	90.39	-0.08	RP-MS
HMDB0000119	Glyoxylate		-1.90	98.69	-0.01	RP-MS/MS
HMDB0000132	Guanine		2.00	92.79	0.06	RP-MS/MS
HMDB0000133	Guanosine		2.28	93.20	1.18	RP-MS/MS
HMDB0001397	Guanosine monophosphate	22.40	4.19	96.35	-0.05	IC-MS/MS
HMDB0001273	Guanosine triphosphate	3.60	0.69			IC-MS/MS
N/A	Heptadecanoate		2.83	80.69	0.07	RP-MS
HMDB0000714	Hippurate		-1.03	99.03	-0.09	RP-MS/MS
HMDB0000177	Histidine		1.21	92.80	0.05	RP-MS
HMDB0003518	Homocitrate		-2.23	95.63		IC-MS/MS
HMDB0000742	Homocysteine		0.70	84.81		RP-MS
HMDB0000719	Homoserine		0.38	94.67	0.00	RP-MS
N/A	Hydroxyproline		1.12	90.21	-0.06	RP-MS
HMDB0000157	Hypoxanthine		-4.72	96.04	-0.25	RP-MS/MS
HMDB0000671	Indole-3-lactate		-0.19	97.35	0.11	RP-MS/MS
HMDB0060484	Indole-3-pyruvate		-4.04	92.88	0.00	RP-MS
HMDB0000175	Inosinate	48.60	3.29	94.99	0.04	IC-MS/MS
HMDB0034198	Isobutylamine		0.60	92.41	0.15	RP-MS
HMDB0000172	Isoleucine		0.68	96.74	0.00	RP-MS
HMDB0032797	Jasmonate		-0.96	98.63	-0.09	RP-MS/MS
HMDB0000695	Ketoleucine	1.69	-1.38	99.39		IC-MS/MS
HMDB0000715	Kynurenate		-1.12	98.93	-0.02	RP-MS/MS
HMDB0000684	Kynurenine		1.44	90.96	0.00	RP-MS
HMDB0000190	Lactate		-2.50	99.87	-0.05	IC-MS/MS
HMDB0000687	Leucine		0.72	96.74	0.00	RP-MS
HMDB0000673	Linoleate		2.33	92.91	-0.05	RP-MS/MS
HMDB0000182	Lysine		0.58	96.50	0.01	RP-MS
HMDB0000744	Malate		-2.18	99.84	0.03	IC-MS/MS
HMDB0000176	Maleate		-0.54	96.89	2.74	RP-MS/MS
HMDB0000691	Malonate		-2.18	97.09	-0.08	IC-MS/MS
HMDB0060486	Mandelonitrile		-0.96	93.81	-0.09	RP-MS/MS
HMDB0000696	Methionine		1.01	95.71	0.01	RP-MS
HMDB0032572	Methyl 4-hydroxybenzoate		-0.46	95.05	-1.04	RP-MS/MS
HMDB0000752	Methylglutarate	34.70	-1.29	95.64	0.09	IC-MS/MS
HMDB0001343	Mevalonate 5-phosphate		-0.60	98.82	-0.07	RP-MS/MS
HMDB0000806	Myristate		-0.86	95.63	-0.13	RP-MS/MS
HMDB0001325	N,N,N-Trimethyllysine		0.61	89.53	-0.06	RP-MS
HMDB0001067	N-Acetylaspartylglutamate		1.90	97.49	-0.06	IC-MS/MS
HMDB0011757	N-Acetyl-DL-Valine		-1.60	99.17	-0.10	RP-MS/MS
HMDB0000512	N-Acetyl-D-Phenylalanine		-0.80	98.74	-0.07	RP-MS/MS
HMDB0001367	N-acetyl-glucosamine-1-phosphate	16.30	1.83	96.26		IC-MS/MS
HMDB0001138	N-Acetylglutamate	82.40	-1.81	91.51	0.01	IC-MS/MS
HMDB0000766	N-Acetyl-L-alanine	69.60	-2.64	97.84		IC-MS/MS
HMDB0000812	N-Acetyl-L-aspartate		-2.29	94.30	-0.03	IC-MS/MS
HMDB0006488	N-Acetyl-L-glutamate 5-semialdehyde		-1.45	98.33		IC-MS/MS
HMDB0000230	N-Acetylneuraminate	33.50	1.59	95.25		IC-MS/MS
HMDB0003357	N-Acetyl-ornithine		2.40	88.40	0.29	RP-MS
HMDB0001487	NADH	9.94	-0.39	97.21		IC-MS/MS
N/A	Nicotinate N-Oxide		-1.24	92.90	0.14	RP-MS/MS
HMDB0001645	Norleucine		1.79	89.93	0.26	RP-MS
HMDB0013716	Norvaline		-1.10	93.87	0.04	RP-MS/MS
HMDB0000207	Oleate		2.40	95.28	-0.07	RP-MS/MS
HMDB0001721	O-Phosphoserine	87.50	-2.04	97.02	0.00	IC-MS/MS
HMDB0000214	Ornithine		-0.99	93.51	0.02	RP-MS/MS

HMDB code	Identification	In-house DB fragment-ation score	Mass error / ppm	Isotope similarity / %	RT error / min	Method
HMDB0002329	Oxalate		-2.01	98.09	0.03	IC-MS/MS
HMDB0000225	Oxoadipate	42.10	-2.16	97.28	-0.06	IC-MS/MS
HMDB0000208	Oxoglutarate	17.60	-1.50			IC-MS/MS
HMDB0000220	Palmitate		-0.06	92.79	-0.14	RP-MS/MS
HMDB0000210	Pantothenate	86.50	-1.84	98.31	-0.04	IC-MS/MS
HMDB0000159	Phenylalanine		0.96	96.15	0.01	RP-MS
HMDB0000263	Phosphoenolpyruvate		-1.75	99.25	0.02	IC-MS/MS
N/A	Phosphorylcholine Chloride		-2.09	93.41	-0.72	RP-MS/MS
HMDB0000801	Phytanate		3.75	94.88	0.46	RP-MS/MS
HMDB0000162	Proline		0.33	95.59	0.01	RP-MS
HMDB0001491	Pyridoxal 5'-phosphate	68.00	-1.08	95.52	-0.11	IC-MS/MS
HMDB0000267	Pyroglutamate	31.90	-1.84	93.94	0.00	IC-MS/MS
HMDB0000243	Pyruvate		-2.32	99.43	-0.07	IC-MS/MS
HMDB0000232	Quinolinate		-1.83	95.61	-0.06	IC-MS/MS
HMDB0000621	Ribulose		-2.64	95.60	-0.15	IC-MS/MS
HMDB0000618	Ribulose 5-phosphate	78.40	-0.77	96.95	-0.01	IC-MS/MS
HMDB0000279	Saccharopine		2.10	91.65	0.00	RP-MS
HMDB0001895	Salicylate		-0.98	99.61	0.04	RP-MS/MS
HMDB0000271	Sarcosine		0.25	97.70	0.02	RP-MS
HMDB0000792	Sebacate		-0.15	99.09	-0.14	RP-MS/MS
HMDB0000187	Serine		0.56	96.82	-0.01	RP-MS
HMDB0000259	Serotonin		0.69	89.23	-0.14	RP-MS
HMDB0003070	Shikimate		-1.45	95.52	0.03	RP-MS/MS
HMDB0000247	Sorbitol	92.80	-1.57	99.10	0.03	IC-MS/MS
HMDB0000827	Stearate		2.79	96.37	-0.12	RP-MS/MS
HMDB0000254	Succinate	84.50	-1.56	98.58	-0.02	IC-MS/MS
HMDB0000251	Taurine		0.84	95.25	-0.02	RP-MS
HMDB0000943	Threonate	60.20	-1.94	97.91		IC-MS/MS
HMDB0000167	Threonine		0.59	96.86	0.01	RP-MS
HMDB0001342	Thymidine 5'-triphosphate	1.62	3.88	96.23	-0.01	IC-MS/MS
HMDB0000929	Tryptophan		0.80	94.89	0.02	RP-MS
HMDB0000158	Tyrosine		0.79	96.08	0.01	RP-MS
HMDB0000300	Uracil		-0.43	94.99	0.07	RP-MS/MS
HMDB0000289	Urate	59.60	-1.98	93.46	-0.11	IC-MS/MS
HMDB0000296	Uridine		-1.46	94.39	0.19	IC-MS/MS
HMDB0000295	Uridine 5'-diphosphate	4.63	4.65	98.67		IC-MS/MS
HMDB0000288	Uridine 5'-monophosphate	81.20	2.46	97.96	0.02	IC-MS/MS
HMDB0000286	Uridine diphosphate glucose		-1.08	97.10	0.46	IC-MS/MS
HMDB0000290	Uridine diphosphate-N-acetylglucosamine	8.70	-1.07	98.50	-0.05	IC-MS/MS
HMDB0000285	Uridine triphosphate	12.70	3.32	98.46	-0.12	IC-MS/MS
HMDB0000883	Valine		0.30	96.94	0.00	RP-MS
HMDB0000881	Xanthurenate		-0.69	98.36	0.92	RP-MS/MS
HMDB0002917	Xylitol		-1.65	98.82	0.06	RP-MS/MS
HMDB0000868	Xylulose 5-phosphate	57.00	-0.15	96.47	-0.33	IC-MS/MS

Metabolite identification information for LN18 Mut and WT cells cultured under 4.5 g / L glucose conditions (experimental replicate 3, Section 8.14), analysed by IC-MS/MS (Section 8.4), derivatised RP-MS (Section 8.7) and non-derivatised RP-MS/MS (Section 8.9), including HMDB code, fragmentation score, mass error, isotope

similarity RT method and analysis method are listed in Table 10.7.Full compound-feature lists including significance, FC and CV information for LN18 Mut and WT cells cultured under 4.5 g / L glucose conditions (experimental replicate 3, Section 8.14) are found in ESM E.

Table 10.7: Metabolite identification information for the analysis of LN18 Mut and WT cells cultured under 4.5 g / L glucose conditions (experimental replicate 3, Section 8.14), analysed by IC-MS/MS (Section 8.4), derivatised RP-MS (Section 8.7) and non-derivatised RP-MS/MS (Section 8.9).

HMDB code	Identification	In-house DB fragment-ation score	Mass error / ppm	Isotope similarity / %	RT error / min	Method
HMDB0001213	1-Deoxy-D-xylulose 5-phosphate		0.21	95.02	1.07	IC-MS/MS
HMDB0000001	1-Methyl histidine		-1.07	90.71	-0.02	RP-MS
HMDB0001294	2,3-Diphosphoglycerate		0.29	98.91	0.59	IC-MS/MS
HMDB0000510	2-Aminoadipate		0.20	95.33	0.04	RP-MS
N/A	2-Aminobut-2-enoate		0.58	95.26		RP-MS
HMDB0001280	2-Aminomuconate semialdehyde	35.5	-0.80	97.12		IC-MS/MS
N/A	2-C-Methylerythritol 4-phosphate		0.53	85.50	0.12	IC-MS/MS
HMDB0001532	2-Deoxyadenosine 5-triphosphate		4.76	95.39	0.11	IC-MS/MS
HMDB0001044	2'-Deoxyguanosine 5'-monophosphate	70.7	3.66	96.42	-0.65	IC-MS/MS
HMDB0000008	2-Hydroxybutyrate	63.4	-1.34	97.94	-0.25	IC-MS/MS
HMDB0059655	2-Hydroxyglutarate	56.2	-1.64	99.87	-0.18	IC-MS/MS
N/A	2-Iminobutanoate		0.70	95.14		RP-MS
HMDB0000005	2-Ketobutyrate	7.3	-4.37	97.31		RP-MS/MS
HMDB0000208	2-Oxoglutarate	61.1	-1.40		-0.17	IC-MS/MS
HMDB0000362	2-Phosphoglycerate		-1.12	99.19	-0.26	IC-MS/MS
HMDB0003911	3-Amino-2-methylpropanoate		-3.81	95.68		RP-MS
HMDB0000355	3-Hydroxymethylglutarate		-1.17	98.67	-0.14	IC-MS/MS
HMDB0000019	3-Methyl-2-oxobutanoate	17.9	-1.16	99.75		IC-MS/MS
HMDB0000807	3-Phosphoglceryate		-4.13			RP-MS/MS
HMDB0000500	4-Hydroxybenzoate		-0.64	94.15	1.25	IC-MS/MS
HMDB0000710	4-Hydroxybutyrate		-1.40	99.25	0.45	IC-MS/MS
HMDB0000725	4-Hydroxyproline	37.5	-2.50	96.99	-0.16	IC-MS/MS
HMDB0001149	5-Aminolevulinate		-1.19	93.61		RP-MS
N/A	5-Hydroxytryptamine creatinine		-1.62	86.23	-0.82	RP-MS
HMDB0001316	6-Phosphogluconate		0.83	99.02	-0.13	IC-MS/MS
HMDB0006557	Adenosine 5'-diphosphoglucose		-3.01	90.04	0.24	RP-MS/MS
HMDB0000045	Adenosine monophosphate	69.2	3.81	95.32	-0.49	IC-MS/MS
HMDB0000538	Adenosine triphosphate	17.2	0.19	97.89	-0.29	IC-MS/MS
HMDB0012882	Adipate semialdehyde		-0.82	99.81	-0.39	IC-MS/MS
HMDB0000508	Adonitol	77.0	-1.48	97.89	-0.10	IC-MS/MS
HMDB0000161	Alanine		-0.83	97.12	-0.01	RP-MS
HMDB0000112	Aminobutyrate		-1.94	95.39	0.04	RP-MS
HMDB0000539	Arabinonate		-1.69	94.34	0.10	IC-MS/MS
HMDB0000517	Arginine		-1.39	94.65	0.02	RP-MS
HMDB0000044	Ascorbate	10.5	-1.66	99.65	-0.24	IC-MS/MS
HMDB0000168	Asparagine		-0.89	92.93	-0.06	RP-MS
HMDB0000191	Aspartate		-1.36	96.31	0.03	RP-MS
HMDB0013220	Beta-Citryl-L-glutamate		2.99	98.06	1.58	IC-MS/MS
HMDB0000033	Carnosine		-1.20	92.04	-1.69	RP-MS
HMDB0000072	Cis-aconitate		-1.67	98.70	-0.36	IC-MS/MS

HMDB code	Identification	In-house DB fragment-ation score	Mass error / ppm	Isotope similarity / %	RT error / min	Method
HMDB0000094	Citrate	95.3	-1.06	99.63	-0.25	IC-MS/MS
HMDB0000904	Citrulline		-1.13	93.96	0.03	RP-MS
HMDB0001176	CMP N-acetylneuraminate		-0.11	98.34	0.21	IC-MS/MS
HMDB0000064	Creatine		-3.75	94.21	0.06	RP-MS/MS
HMDB0000574	Cysteine		-2.16	82.96	-0.33	RP-MS
HMDB0000095	Cytidine monophosphate	53.3	3.10	93.42	-0.31	IC-MS/MS
HMDB0000082	Cytidine triphosphate	20.1	4.06	98.05	-0.25	IC-MS/MS
HMDB0000998	dCTP		3.96	95.47	-0.16	IC-MS/MS
HMDB0001264	Dehydroascorbate	5.0	-1.71	97.52		IC-MS/MS
HMDB0001321	D-Erythrose 4-phosphate	43.2	-0.73	96.81		IC-MS/MS
HMDB0001112	D-Glyceraldehyde 3-phosphate	38.4	-1.60	97.27		IC-MS/MS
HMDB0001473	Dihydroxyacetone phosphate	47.1	-4.26	95.39	0.14	RP-MS/MS
HMDB0001328	dTDP-D-glucose		-0.58	94.70	0.53	IC-MS/MS
HMDB0001409	dUMP		2.19	94.49	0.62	IC-MS/MS
HMDB0001191	dUTP		4.27	94.91	0.64	IC-MS/MS
HMDB0000149	Ethanolamine		-1.23	93.48	-0.03	RP-MS
HMDB0000622	Ethylmalonate	47.7	-3.59	97.92		RP-MS/MS
HMDB0001248	FAD	1.1	-2.30	94.68	0.10	RP-MS/MS
HMDB0000660	Fructose		-1.41	98.14	1.83	IC-MS/MS
HMDB0001058	Fructose 1,6-bisphosphate	83.5	3.64		-0.13	IC-MS/MS
HMDB0000134	Fumarate	75.0	-1.51	99.59	1.35	IC-MS/MS
HMDB0000639	Galactarate	75.7	-1.09	96.59	-0.11	IC-MS/MS
N/A	Galactose-6-phosphate		1.80	92.64	0.16	IC-MS/MS
HMDB0000625	Gluconate	93.7	-1.68		-0.19	IC-MS/MS
HMDB0000150	Gluconolactone	74.3	-4.10	94.02		RP-MS/MS
HMDB0000122	Glucose		-1.12	98.51	-0.28	IC-MS/MS
HMDB0001586	Glucose 1-phosphate		-0.22	98.85	-0.11	IC-MS/MS
HMDB0000127	Glucuronate	96.4	-1.36	98.48	-0.06	IC-MS/MS
HMDB0000620	Glutaconate	49.5	-0.45	97.62	-0.25	IC-MS/MS
HMDB0000148	Glutamate		-1.26	96.71	0.03	RP-MS
HMDB0000641	Glutamine		-1.32	96.13	0.02	RP-MS
HMDB0000661	Glutarate	84.9	-2.37	93.93	-0.21	IC-MS/MS
HMDB0000125	Glutathione	76.6	2.48	94.83	0.68	IC-MS/MS
HMDB0000139	Glycerate		-2.26		-0.10	IC-MS/MS
HMDB0000131	Glycerol	63.4	-1.79	99.43	-0.13	IC-MS/MS
HMDB0000126	Glycerol 3-phosphate	77.7	-0.89		-0.07	IC-MS/MS
HMDB0000123	Glycine		-1.47	97.79	0.03	RP-MS
HMDB0000115	Glycolate		-2.33	97.99	0.79	IC-MS/MS
HMDB0000133	Guanosine	26.3	-0.47	93.01		RP-MS/MS
HMDB0001397	Guanosine monophosphate	35.8	4.86	95.05	-0.36	IC-MS/MS
HMDB0001273	Guanosine triphosphate	9.0	0.98		-0.49	IC-MS/MS
HMDB0000714	Hippurate	68.5	-1.14	90.46	-0.22	IC-MS/MS
HMDB0000177	Histidine		-1.19	93.09	0.07	RP-MS
HMDB0000742	Homocysteine		-1.14	88.52		RP-MS
HMDB0000719	Homoserine		-1.83	93.85	0.03	RP-MS
HMDB0000118	Homovanillate	1.1	-0.66	98.54	-0.88	IC-MS/MS
HMDB0000528	Hydroorotate		-1.06	96.43	1.45	IC-MS/MS
HMDB0000472	Hydroxytryptophan		-1.03	87.23	0.88	RP-MS
HMDB0000671	Indole-3-lactate		-1.38	96.78	-0.54	IC-MS/MS
HMDB0000175	Inosine monophosphate		4.02	93.38	-0.14	IC-MS/MS
HMDB0034198	Isobutylamine		-1.19	94.15	-0.71	RP-MS
HMDB0000172	Isoleucine		-1.28	97.01	0.04	RP-MS
HMDB0001347	Isopentenyl pyrophosphate		-0.19	95.91	0.01	IC-MS/MS
HMDB0000678	Isovalerylglycine		-1.65	97.14	-0.34	IC-MS/MS
HMDB0000715	Kynurenate	25.8	-3.43	96.42	-0.09	RP-MS/MS
HMDB0000684	Kynurenine		-0.98	90.19	0.04	RP-MS

HMDB code	Identification	In-house DB fragment-ation score	Mass error / ppm	Isotope similarity / %	RT error / min	Method
HMDB0000190	Lactate	33.9	-2.18	99.95	0.03	IC-MS/MS
HMDB0000186	Lactose		2.27	94.87	-0.27	IC-MS/MS
HMDB0011163	L-beta-aspartyl-L-aspartate	62.6	-0.45	96.97		IC-MS/MS
HMDB0000687	Leucine		-1.46	97.00	0.04	RP-MS
N/A	L-threo-3-methylaspartate		2.57	93.66		IC-MS/MS
HMDB0000182	Lysine		-0.82	97.80	0.04	RP-MS
HMDB0000744	Malate	76.0	-1.69	99.80	-0.09	IC-MS/MS
HMDB0000176	Maleate	74.8	-0.60	98.68	-1.27	IC-MS/MS
HMDB0060486	Mandelonitrile		-3.84	91.15	-0.22	RP-MS/MS
HMDB0000749	Mesaconate	80.8	-0.46	99.72	-1.79	IC-MS/MS
HMDB0000696	Methionine		-1.41	95.80	0.04	RP-MS
HMDB0000752	Methylglutarate	44.8	-0.90	96.77	-0.17	IC-MS/MS
HMDB0006471	Methylisocitrate		-1.14	97.83	0.79	IC-MS/MS
HMDB0002038	Methyl-L-Lysine		-1.65	89.14	-0.13	RP-MS
HMDB0001325	N,N,N-Trimethyllysine		-1.39	92.18	-0.04	RP-MS
HMDB0001067	N-Acetylaspartylglutamate		2.65	96.35	-0.17	IC-MS/MS
HMDB0000215	N-Acetyl-D-glucosamine		0.10	92.69	0.72	IC-MS/MS
HMDB0001062	N-Acetyl-D-Glucosamine 6-Phosphate		2.01	96.65	0.09	IC-MS/MS
HMDB0000512	N-Acetyl-D-Phenylalanine	22.7	-3.25	95.10		RP-MS/MS
HMDB0001138	N-Acetylglutamate	74.4	-0.96	98.12	0.30	IC-MS/MS
HMDB0000766	N-Acetyl-L-Alanine	25.2	-4.19	96.04	-0.09	RP-MS/MS
HMDB0000812	N-Acetyl-L-aspartate		-1.50	97.32	-0.07	IC-MS/MS
HMDB0011745	N-Acetyl-L-methionine		-1.10	95.92	0.40	IC-MS/MS
HMDB0000230	N-Acetylneuraminate (sialate)		2.52	96.15	0.08	IC-MS/MS
HMDB0003357	N-Acetyl-ornithine		-1.05	94.29	-0.07	RP-MS
HMDB0000221	NADPH		1.15	90.42	1.10	IC-MS/MS
HMDB0001200	N'-Formylkynurenine		-2.63	92.49		RP-MS/MS
HMDB0002393	N-Methyl-D-Aspartate	61.5	-3.13	93.56		RP-MS/MS
HMDB0012270	Nordihydroguaiaretate		0.29	93.71	-0.17	RP-MS/MS
HMDB0001721	O-Phosphoserine	88.4	-1.57	97.74	-0.05	IC-MS/MS
HMDB0000214	Ornithine		-1.08	94.00	0.01	RP-MS
HMDB0000226	Orotate		-1.09	94.63	-0.26	IC-MS/MS
HMDB0002329	Oxalate		-1.42	99.45	-0.13	IC-MS/MS
HMDB0000225	Oxoadipate	87.0	-1.74	96.44	-0.04	IC-MS/MS
HMDB0000210	Pantothenate	81.0	-1.18	98.08	-0.07	IC-MS/MS
HMDB0000159	Phenylalanine		-1.48	96.49	0.04	RP-MS
HMDB0000205	Phenylpyruvate		-0.96	92.22	1.17	IC-MS/MS
HMDB0001511	Phosphocreatine	12.9	-0.86	95.15		IC-MS/MS
HMDB0000263	Phosphoenolpyruvate		-1.33	99.28	-0.12	IC-MS/MS
N/A	Poly-DL-Alanine		-3.15	95.94	0.10	RP-MS/MS
HMDB0000162	Proline		-1.57	95.20	0.04	RP-MS
HMDB0001856	Protocatechuate		-1.90	91.85	1.77	IC-MS/MS
HMDB0001491	Pyridoxal 5'-phosphate	77.3	-0.60	95.46	-0.15	IC-MS/MS
HMDB0000267	Pyroglutamate	21.5	-1.26	93.95	-0.07	IC-MS/MS
HMDB0000243	Pyruvate		-2.15	99.96	-0.01	IC-MS/MS
HMDB0000232	Quinolinate		-1.53	97.50	0.02	IC-MS/MS
HMDB0000244	Riboflavin	4.4	2.63	92.84	-0.10	RP-MS/MS
HMDB0000283	Ribose		-4.28	93.63	0.02	RP-MS/MS
HMDB0011688	Ribose 1,5-bisphosphate	16.8	2.65	98.32		IC-MS/MS
HMDB0001548	Ribose 5-phosphate		-0.39	81.12	-0.05	IC-MS/MS
HMDB0000618	Ribulose 5-phosphate	69.5	-0.08	98.47	0.47	IC-MS/MS
HMDB0000279	Saccharopine		0.21	90.01	0.02	RP-MS
HMDB0000271	Sarcosine		-1.39	97.42	0.05	RP-MS
HMDB0000792	Sebacate		-0.83	93.28	-0.29	IC-MS/MS
HMDB0060509	Sedoheptulose 1-phosphate		1.38	95.25	0.50	IC-MS/MS

HMDB code	Identification	In-house DB fragment-ation score	Mass error / ppm	Isotope similarity / %	RT error / min	Method
HMDB0001068	Sedoheptulose 7-phosphate	45.4	1.89		0.07	IC-MS/MS
HMDB0000187	Serine		-1.44	96.57	0.02	RP-MS
HMDB0000259	Serotonin		-0.87	88.73	-0.10	RP-MS
HMDB0000247	Sorbitol	94.2	-1.09	99.19	-0.08	IC-MS/MS
HMDB0005831	Sorbitol-6-phosphate		-0.35	97.31	0.49	IC-MS/MS
HMDB0001257	Spermidine		-1.50	89.91	-0.06	RP-MS
HMDB0000254	Succinate	79.4	-0.90	99.76	-0.09	IC-MS/MS
HMDB0001259	Succinate semialdehyde		-1.80	98.70	-1.60	IC-MS/MS
HMDB0002085	Syringate		-2.38	94.19	-0.61	IC-MS/MS
HMDB0000251	Taurine		-1.16	94.65	-0.02	RP-MS
HMDB0004136	Threitol	85.6	-0.92	98.76	-0.03	IC-MS/MS
HMDB0000167	Threonine		-1.76	96.94	0.04	RP-MS
HMDB0001227	Thymidine 5'-phosphate		3.12	97.66	0.51	IC-MS/MS
HMDB0001342	Thymidine 5'-triphosphate	5.6	4.47	96.98	-0.22	IC-MS/MS
HMDB0000929	Tryptophan		-1.04	95.15	0.05	RP-MS
HMDB0000158	Tyrosine		-1.51	95.96	0.05	RP-MS
HMDB0000935	UDP-glucoronate		-0.72	94.45	0.66	IC-MS/MS
HMDB0000286	UDP-glucose		-0.40	96.67	0.63	IC-MS/MS
HMDB0000290	UDP-N-acetylglucosamine	29.9	-0.05	98.64	-0.18	IC-MS/MS
HMDB0000300	Uracil		-3.73	76.14	0.07	RP-MS/MS
HMDB0000289	Urate	88.1	-1.89	94.38	-0.32	IC-MS/MS
HMDB0000294	Urea		-0.95	92.78	0.03	RP-MS
HMDB0000296	Uridine		-0.59	98.27	-1.91	IC-MS/MS
HMDB0000288	Uridine 5'-monophosphate	86.4	3.16	97.77	-0.14	IC-MS/MS
HMDB0000285	Uridine triphosphate	23.8	3.81	98.24	-0.27	IC-MS/MS
HMDB0000883	Valine		-1.61	97.03	0.03	RP-MS
HMDB0001644	Xylulose		-1.66	95.53	1.08	IC-MS/MS

10.6. Data for U87-MG IDH1 mutant and wild-type glioblastoma cells

Metabolite identification information for the analysis of U87-MG Mut and WT cells cultured under 4.5 g / L glucose conditions (Section 8.15), analysed by IC-MS/MS (Section 8.4), derivatised RP-IMS-MS/MS (Section 8.8) and non-derivatised RP-MS/MS (Section 8.10), including HMDB code, fragmentation score, mass error, isotope similarity RT method and analysis method are listed in Table 10.8. Full compound-feature lists including significance, FC and CV information for U87-MG Mut and WT cells cultured under 4.5 g / L glucose conditions (Section 8.15) are found in ESM F.

Table 10.8: Metabolite identification information for the analysis of U87-MG Mut and WT cells cultured under 4.5 g / L glucose conditions (Section 8.15), analysed by IC-MS/MS (Section 8.4), derivatised RP-IMS-MS/MS (Section 8.8) and non-derivatised RP-MS/MS (Section 8.10).

HMDB code	Identification	In-house DB fragment-ation score	Mass error / ppm	Isotope similarity / %	RT error / min	Method
HMDB0000002	1,3-Diaminopropane		-2.23	89.16	0.04	RP-IMS-MS/MS
HMDB0001213	1-Deoxy-D-xylulose 5-phosphate	3.98	-1.81	94.75	0.28	IC-MS/MS
N/A	1-Hydroxy-2-methyl-2-butenyl 4-pyrophosphate		4.81		-0.05	RP-MS/MS
HMDB0001369	1-Pyrroline hydroxycarboxylate		-2.98	93.94	-0.37	IC-MS/MS
HMDB0001294	2,3-Diphosphoglycerate		-2.48	99.27	-0.62	IC-MS/MS
HMDB0000510	2-Aminoadipate		0.18	95.52	0.05	RP-IMS-MS/MS
HMDB0000991	2-Aminocaprylate		3.30	92.32	-0.99	RP-MS/MS
N/A	2-C-Methylerythritol 4-phosphate		-1.18	94.80	-0.51	IC-MS/MS
HMDB0059655	2-Hydroxyglutarate	42.5	-2.85	99.81	-0.52	IC-MS/MS
HMDB0000402	2-Isopropylmalate		-3.64	91.58	-1.34	IC-MS/MS
HMDB0000208	2-Oxoglutarate	47.2	-3.09		-0.65	IC-MS/MS
HMDB0000362	2-Phosphoglycerate	76.3	-2.63	98.26	-1.18	IC-MS/MS
N/A	3-(2,5-Dioxoimidazolidin-4-yl)propanoate		-3.70	93.70		IC-MS/MS
HMDB0002441	3,3 Dimethyl glutarate	78.1	-3.13	97.21	-0.71	IC-MS/MS
HMDB0003911	3-Amino-2-methylpropanoate		-4.26	95.84	0.26	RP-IMS-MS/MS
HMDB0012710	3-Dehydroquinate	16.7	-3.68	98.40	0.03	IC-MS/MS
HMDB0000197	3-Indolylacetate		1.29	98.92	-2.38	RP-MS/MS
HMDB0059969	3-methoxyphenylacetate		-3.33	96.84	1.81	IC-MS/MS
HMDB0000491	3-Methyl-2-oxovalerate		-2.48	99.77	-0.07	IC-MS/MS
HMDB0000291	4-Hydroxy-3-methoxymandelate		-4.60	95.87	-0.01	IC-MS/MS
HMDB0000707	4-Hydroxyphenylpyruvate		-3.05	93.57	-1.58	IC-MS/MS
HMDB0000725	4-Hydroxyproline		-0.80	93.80		RP-IMS-MS/MS
HMDB0004517	5-hydroxydopamine		-3.43	99.53	0.68	RP-MS/MS
HMDB0000763	5-Hydroxyindoleacetate	19.6	-3.54	88.81	-1.32	IC-MS/MS
HMDB0001316	6-Phosphogluconate		-1.73	98.73	-1.06	IC-MS/MS
N/A	8-oxo-dGTP		-0.84	91.85		RP-MS/MS
HMDB0001890	Acetylcysteine	5.03	-2.84	96.07	1.52	IC-MS/MS
HMDB0000532	Acetylglycine	79.9	-4.99	97.94	-0.23	IC-MS/MS
HMDB0000045	Adenosine monophosphate	54.5	-2.91	95.65	-0.65	IC-MS/MS
HMDB0000538	Adenosine triphosphate	5.86	-2.27	97.74	-1.03	IC-MS/MS
HMDB0001332	Adenylsuccinate		-0.93	94.88	-0.66	IC-MS/MS
HMDB0000161	Alanine		-0.39	96.66	0.09	RP-IMS-MS/MS
HMDB0001852	all-trans-Retinoate		-2.71	97.22	-2.70	RP-MS/MS
HMDB0000112	Aminobutyrate-GABA		-1.98	95.25	0.00	RP-IMS-MS/MS
HMDB0000539	Arabinonate	86.9	-3.80	94.80	-0.67	IC-MS/MS
HMDB0000568	Arabitol		-3.18	97.34	0.01	IC-MS/MS
HMDB0000517	Arginine		-1.01	95.26	0.04	RP-IMS-MS/MS
HMDB0000044	Ascorbate	8.56	-3.61	99.67	-0.75	IC-MS/MS
HMDB0001894	Aspartame		0.19	97.70	-2.70	RP-MS/MS
HMDB0000191	Aspartate	83.1	-2.78	94.75	-0.57	IC-MS/MS
HMDB0000056	beta-Alanine/aminopropionate		0.81	96.42	0.08	RP-IMS-MS/MS
HMDB0013220	Beta-Citryl-L-glutamate		-3.12	97.87	0.47	IC-MS/MS
HMDB0000039	Butyrate	94.3	-3.83	90.98	-0.64	IC-MS/MS
HMDB0000033	Carnosine		-4.05	88.36	0.04	RP-IMS-MS/MS
HMDB0000072	Cis-aconitate		-3.67	97.71	-2.00	IC-MS/MS
HMDB0000094	Citrate	87.3	-2.72	99.56	-0.79	IC-MS/MS
HMDB0000904	Citrulline		-1.68	93.64	0.05	RP-IMS-MS/MS
HMDB0001423	Coenzyme A		0.04	90.58	-1.23	IC-MS/MS
HMDB0002757	Cysteate	69.6	-3.31	91.09	-0.70	IC-MS/MS
HMDB0000574	Cysteine		-2.02	94.01	-1.00	RP-IMS-MS/MS
HMDB0001546	Cytidine diphosphate		-1.18	97.65	-0.44	IC-MS/MS

HMDB code	Identification	In-house DB fragment-ation score	Mass error / ppm	Isotope similarity / %	RT error / min	Method
HMDB0000095	Cytidine monophosphate	45.9	-3.24	93.63	-1.27	IC-MS/MS
HMDB0001176	Cytidine monophosphate N-acetylneuraminate		-0.31	98.54	-0.68	IC-MS/MS
HMDB0000082	Cytidine triphosphate	6.93	-1.57	98.03	-0.70	IC-MS/MS
HMDB0001508	dADP		-2.60	95.19	0.04	IC-MS/MS
HMDB0001245	dCDP		3.80	93.40	-0.17	RP-MS/MS
HMDB0000998	dCTP	86.9	-1.48	96.93	-0.11	IC-MS/MS
HMDB0001532	Deoxyadenosine triphosphate	88.8	-0.56	96.26	-1.19	IC-MS/MS
HMDB0000626	Deoxycholate		3.92	94.85	-0.14	RP-MS/MS
HMDB0000012	Deoxyuridine		-1.71	93.66	1.11	IC-MS/MS
HMDB0000960	dGDP		-2.39	97.90	-1.17	IC-MS/MS
HMDB0001044	dGMP	46.3	-3.00	96.25	-1.37	IC-MS/MS
HMDB0001440	dGTP		-0.60	90.81	0.63	IC-MS/MS
HMDB0003349	Dihydroorotate	15.1	-3.39	86.17	-0.65	IC-MS/MS
HMDB0001473	Dihydroxyacetone phosphate		-1.94	92.81	-0.08	IC-MS/MS
HMDB0000181	Dihydroxyphenylalanine		-3.67	94.47	1.27	IC-MS/MS
HMDB0031257	Dimethyl fumarate		-3.02	95.30	-1.45	IC-MS/MS
HMDB0000638	Dodecanoate		-1.26	87.29	-2.26	RP-MS/MS
HMDB0001229	Dopaquinone		-2.38	89.56	-2.20	RP-MS/MS
HMDB0001328	dTDP-D-glucose		-0.71	97.76	-0.60	IC-MS/MS
HMDB0001409	dUMP		-2.75	95.56	-0.87	IC-MS/MS
HMDB0001191	dUTP		-1.22	95.70	-0.18	IC-MS/MS
HMDB0001321	Erythrose 4-phosphate		-2.63	97.62	1.21	IC-MS/MS
HMDB0000149	Ethanolamine		-4.18	92.55	0.04	RP-IMS-MS/MS
HMDB0001248	FAD		1.83	96.86	-1.86	RP-MS/MS
HMDB0000121	Folate		-1.21	99.12	-2.19	RP-MS/MS
HMDB0001058	Fructose 1,6-bisphosphate	45	-3.19		-0.75	IC-MS/MS
HMDB0001047	Fructose 2,6 diphosphate		-3.19	98.85	0.66	IC-MS/MS
HMDB0000124	Fructose 6-phosphate	78.5	-2.78	98.00	-0.77	IC-MS/MS
HMDB0000639	Galactarate	29.8	-3.16	94.22	-0.56	IC-MS/MS
HMDB0002545	Galacturonate	38.6	-4.49	95.05	-1.22	IC-MS/MS
HMDB0000625	Gluconate	59.9	-3.51		-0.56	IC-MS/MS
HMDB0000150	Gluconolactone	33.8	-3.92	93.75	-0.36	IC-MS/MS
HMDB0001586	Glucose 1-phosphate	46.5	-2.58	99.12	-0.69	IC-MS/MS
HMDB0000127	Glucuronate	75.9	-3.93	97.94	-0.51	IC-MS/MS
HMDB0000148	Glutamate		-0.19	95.35	0.07	RP-IMS-MS/MS
HMDB0000641	Glutamine		-0.91	94.86	-0.01	RP-IMS-MS/MS
HMDB0000661	Glutarate	54.1	-3.41	98.33	-0.59	IC-MS/MS
HMDB0000125	Glutathione	43.4	-2.90	94.62	-0.55	IC-MS/MS
HMDB0000131	Glycerol	57.4	-4.56	99.50	-0.14	IC-MS/MS
HMDB0000126	Glycerol 3-phosphate	77.2	-2.44		-0.68	IC-MS/MS
HMDB0000123	Glycine		-1.02	96.69	0.10	RP-IMS-MS/MS
HMDB0000115	Glycolate	47.9	-2.61	98.31	0.54	IC-MS/MS
N/A	Gly-Gly		-1.86	95.44	-0.35	RP-IMS-MS/MS
HMDB0001201	Guanosine diphosphate	98.6	-0.58	96.14	-1.26	IC-MS/MS
HMDB0001397	Guanosine monophosphate	31	-2.10	96.28	-0.87	IC-MS/MS
HMDB0001273	Guanosine triphosphate	0.987	-1.30		-1.23	IC-MS/MS
HMDB0000714	Hippurate	64.6	-3.07	99.26	-0.80	IC-MS/MS
HMDB0000177	Histidine		-1.64	94.92	0.00	RP-IMS-MS/MS
HMDB0000742	Homocysteine		-2.03	92.33	-0.14	RP-IMS-MS/MS
HMDB0000130	Homogentisate		-4.15	96.92	-1.73	IC-MS/MS
HMDB0000719	Homoserine		-3.08	91.95	0.09	RP-IMS-MS/MS
HMDB0000118	Homovanillate	1.06	-2.67	98.61	-1.31	IC-MS/MS
HMDB0001212	Hydantoin-5-propionate		0.17	96.57	0.09	IC-MS/MS
HMDB0000472	Hydroxy-L-tryptophan		-0.86	91.91		RP-IMS-MS/MS
HMDB0000965	Hypotaurine		1.12	93.04	0.15	RP-IMS-MS/MS

HMDB code	Identification	In-house DB fragment-ation score	Mass error / ppm	Isotope similarity / %	RT error / min	Method
HMDB0001190	Indole-3-acetaldehyde		2.60	91.93	0.62	RP-MS/MS
HMDB0000671	Indole-3-lactate	80.3	-2.22	93.37	-1.58	IC-MS/MS
HMDB0000175	Inosine monophosphate	37.3	-2.85	94.39	-1.10	IC-MS/MS
HMDB0001143	Inositol 1,3,4-trisphosphate		-2.00	97.81	-0.06	IC-MS/MS
HMDB0034198	Isobutylamine		-4.51	91.53	0.18	RP-IMS-MS/MS
HMDB0000172	Isoleucine		0.13	95.62	0.08	RP-IMS-MS/MS
HMDB0001347	Isopentenyl pyrophosphate		-2.21	95.64	0.28	RP-MS/MS
HMDB0000678	Isovalerylglycine	17.4	-4.22	95.78	-0.53	IC-MS/MS
HMDB0002092	Itaconate	67.2	-1.96	99.80	-1.75	IC-MS/MS
HMDB0000684	Kynurenine		-1.99	92.15	0.07	RP-IMS-MS/MS
HMDB0000190	Lactate	25	-4.30	99.86	-0.29	IC-MS/MS
HMDB0000099	L-Cystathionine		0.54	86.75	0.04	RP-IMS-MS/MS
HMDB0000192	L-Cystine		4.94	89.46	-0.04	RP-MS/MS
HMDB0000687	Leucine		0.08	95.41	0.08	RP-IMS-MS/MS
HMDB0000673	Linoleate		-1.56	97.57	-2.27	RP-MS/MS
HMDB0000182	Lysine		0.12	95.58	0.06	RP-IMS-MS/MS
HMDB0000744	Malate	67.3	-3.26	99.92	-0.54	IC-MS/MS
HMDB0000752	Methylglutarate	22.9	-3.32	95.37	-0.70	IC-MS/MS
HMDB0006471	Methylisocitrate		-2.76	98.32	-0.42	IC-MS/MS
HMDB0002038	Methyl-L-Lysine		-2.83	92.13	0.07	RP-IMS-MS/MS
HMDB0029416	Mono-methyl arginine/Targinine		-0.14	95.73		RP-IMS-MS/MS
HMDB0000211	Myoinositol	93.2	-3.00	98.49	1.64	IC-MS/MS
HMDB0000806	Myristate		-1.55	97.41	-2.33	RP-MS/MS
HMDB0000812	N-Acetyl-aspartate	92.5	-3.20	94.44	-0.54	IC-MS/MS
HMDB0001067	N-Acetylaspartylglutamate		-2.45	97.22	-0.69	IC-MS/MS
HMDB0001062	N-Acetyl-D-Glucosamine 6-Phosphate		-3.81	94.45	1.19	IC-MS/MS
HMDB0011757	N-Acetyl-DL-Valine		3.26	91.65	-1.54	RP-MS/MS
HMDB0001367	N-acetyl-glucosamine-1-phosphate		-3.02	97.85	-0.17	IC-MS/MS
HMDB0000766	N-Acetyl-L-alanine	70.6	-3.60	96.28	-0.39	IC-MS/MS
HMDB0006488	N-Acetyl-L-glutamate 5-semialdehyde		-2.27	91.46	-0.65	IC-MS/MS
HMDB0011745	N-Acetyl-L-methionine	52.7	-2.60	96.64	-0.37	IC-MS/MS
HMDB0000512	N-Acetyl-L-phenylalanine		-3.17	93.17	-0.16	IC-MS/MS
HMDB0000230	N-Acetylneuraminate	76.5	-3.11	96.68	-0.48	IC-MS/MS
HMDB0006268	N-Acetylneuraminate 9-phosphate		-2.57	93.89	-0.38	IC-MS/MS
HMDB0003357	N-Acetyl-ornithine		1.91	89.64	0.81	RP-IMS-MS/MS
HMDB0013713	N-acetyltryptophan		-1.88	98.44	-1.67	RP-MS/MS
HMDB0001487	NADH	78.8	-0.08	96.24	-0.04	IC-MS/MS
HMDB0000221	NADPH		-0.16	91.00	1.91	IC-MS/MS
HMDB0002670	Naringenin		-3.41	92.38		IC-MS/MS
HMDB0002368	Nervonate		-1.13	89.43	-2.80	RP-MS/MS
HMDB0006044	Norsalsolinol		-0.94	98.96	-0.02	RP-MS/MS
HMDB0000482	Octanoate		-3.04	95.08	-0.38	IC-MS/MS
HMDB0000207	Oleate		-1.30	97.19	-2.34	RP-MS/MS
HMDB0001721	O-Phosphoserine	40.3	-2.22	97.40	-0.64	IC-MS/MS
HMDB0005765	Ophthalmate		-3.83	91.49	-0.24	IC-MS/MS
HMDB0000214	Ornithine		-3.05	93.28	0.16	RP-IMS-MS/MS
HMDB0000226	Orotate	22.9	-2.95	93.17	-0.94	IC-MS/MS
HMDB0002329	Oxalate	48.4	-3.84	99.48	-0.71	IC-MS/MS
N/A	Oxfenicine/4-hydroxyphenylglycine		-1.85	96.88	0.42	RP-MS/MS
HMDB0003337	Oxidised Glutathione		-0.36	86.01	0.01	RP-IMS-MS/MS
HMDB0000225	Oxoadipate	40	-2.84	97.19	-0.99	IC-MS/MS
HMDB0000220	Palmitate		-1.50	97.85	-2.38	RP-MS/MS
HMDB0003229	Palmitoleate		-1.68	97.33	-2.19	RP-MS/MS
HMDB0000210	Pantothenate	59.1	-3.19	98.06	-0.55	IC-MS/MS
HMDB0002035	p-Coumarate	8.55	-1.88	91.13	-0.54	IC-MS/MS
HMDB0000159	Phenylalanine		0.21	93.72	0.08	RP-IMS-MS/MS

HMDB code	Identification	In-house DB fragment-ation score	Mass error / ppm	Isotope similarity / %	RT error / min	Method
HMDB0001511	Phosphocreatine	65.1	-4.79	95.28	-0.29	IC-MS/MS
HMDB0000263	Phosphoenolpyruvate	7.25	-2.96	99.19	-0.62	IC-MS/MS
HMDB0000280	Phosphoribosyl pyrophosphate		-2.01	99.01	-0.54	IC-MS/MS
N/A	Phosphorylcholine Chloride		-0.72	96.14	-2.54	RP-MS/MS
HMDB0000801	Phytanate		-0.32	98.67	-2.05	RP-MS/MS
HMDB0000162	Proline		-1.10	94.57	0.08	RP-IMS-MS/MS
HMDB0001220	Prostaglandin E2		-0.46	98.93	-1.06	RP-MS/MS
HMDB0001856	Protocatechuate		-2.67	98.58	-0.82	IC-MS/MS
HMDB0001491	Pyridoxal 5'-phosphate	78.6	-2.74	97.04	-0.77	IC-MS/MS
N/A	Pyroglutamate		-1.01	93.13	-1.02	RP-IMS-MS/MS
HMDB0000243	Pyruvate	52.4	-4.33	99.67	-0.50	IC-MS/MS
HMDB0000232	Quinolinate		-3.74	91.53	-1.05	IC-MS/MS
HMDB0003213	Raffinose		3.00	95.11	1.03	RP-MS/MS
HMDB0000244	Riboflavin		-0.02	95.70	-1.85	RP-MS/MS
HMDB0001520	Riboflavin 5-monophosphate		0.55	90.33	-2.01	RP-MS/MS
HMDB0001548	Ribose 5-phosphate	73.7	-2.17	96.40	0.93	IC-MS/MS
HMDB0000618	Ribulose 5-phosphate	43.3	-2.28	98.99	-0.43	IC-MS/MS
HMDB0000271	Sarcosine		-4.58	93.07	-0.69	RP-IMS-MS/MS
HMDB0000792	Sebacate		-1.96	93.60	-0.85	IC-MS/MS
HMDB0060274	Sedoheptulose 1,7-bisphosphate		-2.78	96.45	-0.40	IC-MS/MS
HMDB0060509	Sedoheptulose 1-phosphate		-2.69	96.97	-0.36	IC-MS/MS
HMDB0001068	Sedoheptulose 7-phosphate	29.5	-2.46		-0.63	IC-MS/MS
HMDB0000187	Serine		-1.67	95.94	0.08	RP-IMS-MS/MS
HMDB0000259	Serotonin		-4.21	88.90	-0.06	RP-IMS-MS/MS
HMDB0000247	Sorbitol	69.5	-2.54	98.51	-0.05	IC-MS/MS
HMDB0000827	Stearate		-1.46	98.59	-2.46	RP-MS/MS
HMDB0000893	Suberate		-2.20	96.02	-1.67	RP-MS/MS
HMDB0000251	Taurine		-1.67	94.51		RP-IMS-MS/MS
HMDB0000036	Taurocholate		-1.22	98.16	-1.88	RP-MS/MS
HMDB0001274	TDP	32.5	-2.49	94.51	-0.13	IC-MS/MS
HMDB0004136	Threitol	87.2	-4.56	98.81	-0.06	IC-MS/MS
HMDB0000167	Threonine		-0.27	96.03	0.08	RP-IMS-MS/MS
HMDB0001227	Thymidine 5'-phosphate		-3.66	95.38	-0.43	IC-MS/MS
HMDB0001342	Thymidine triphosphate	5.88	-0.87	97.78	-0.15	IC-MS/MS
HMDB0000303	Tryptamine		0.27	98.36	-1.10	RP-MS/MS
HMDB0000929	Tryptophan		-0.74	93.49	0.06	RP-IMS-MS/MS
HMDB0000158	Tyrosine		-0.10	94.86	0.06	RP-IMS-MS/MS
HMDB0000302	UDP-galactose		-0.57	97.61	-0.18	IC-MS/MS
HMDB0000935	UDP-glucoronate		-0.14	93.12	-0.59	IC-MS/MS
HMDB0000289	Urate	66	-3.69	93.79	-1.01	IC-MS/MS
HMDB0000296	Uridine	67.6	-2.58	97.89	-0.54	IC-MS/MS
HMDB0000295	Uridine 5'-diphosphate	11.3	-3.14	94.47	-0.13	IC-MS/MS
HMDB0000288	Uridine 5'-monophosphate	44.6	-3.03	97.93	-0.91	IC-MS/MS
HMDB0000290	Uridine diphosphate-N-acetylglucosamine	3.55	-0.27	98.72	-1.31	IC-MS/MS
HMDB0000285	Uridine triphosphate	6.83	-1.46	98.24	-1.02	IC-MS/MS
HMDB0000883	Valine		-0.20	95.83	0.09	RP-IMS-MS/MS
HMDB0001554	Xanthylate		-4.01	94.15	0.17	IC-MS/MS
HMDB0001644	Xylulose	53.1	-3.80	94.20	0.34	IC-MS/MS
HMDB0000868	Xylulose 5-phosphate	37.8	-2.59	68.24	-0.69	IC-MS/MS

10.7. Data for 293T IDH1 mutant and wild-type embryonic kidney cells

Metabolite identification information for the analysis of 293T Mut and WT cells cultured under 4.5 g / L glucose conditions (Section 8.16), analysed by IC-MS/MS (Section 8.4), derivatised RP-MS (Section 8.7) and non-derivatised RP-MS/MS (Section 8.9), including HMDB code, fragmentation score, mass error, isotope similarity RT method and analysis method are listed in Table 10.9. Full compound-feature lists including significance, FC and CV information for 293T Mut and WT cells cultured under 4.5 g / L glucose conditions (Section 8.16) are found in ESM G.

Table 10.9: Metabolite identification information for the analysis of 293T Mut and WT cells cultured under 4.5 g / L glucose conditions (Section 8.16), analysed by IC-MS/MS (Section 8.4), derivatised RP-MS (Section 8.7) and non-derivatised RP-MS/MS (Section 8.9).

HMDB code	Identification	In-house DB fragment-ation score	Mass error / ppm	Isotope similarity / %	RT error / min	Method
HMDB0000957	1,2-dihydroxybenzene		-1.45	85.70	-1.31	IC-MS/MS
HMDB0001213	1-Deoxy-D-xylulose 5-phosphate	59	3.87	97.22	-0.18	IC-MS/MS
HMDB0001294	2,3-Diphosphoglycerate	49.7	3.06	99.42		IC-MS/MS
HMDB0000510	2-Aminoadipate		0.94	96.37	0.03	RP-MS
N/A	2-C-Methyl-D-Erythritol 4-phosphate		-1.22		0.00	RP-MS/MS
HMDB0000008	2-Hydroxybutyrate	66	-0.70	99.00	-1.23	IC-MS/MS
HMDB0059655	2-Hydroxyglutarate	74.9	2.15	99.75		IC-MS/MS
HMDB0000005	2-Ketobutyrate	68.6	-0.63	98.31	-1.39	IC-MS/MS
HMDB0000208	2-Oxoglutarate	40.2	2.09			IC-MS/MS
HMDB0002039	2-Pyrrolidinone		4.14	97.56	0.52	RP-MS
HMDB0002441	3,3-Dimethylglutarate	83.8	2.19	97.91	-0.06	IC-MS/MS
HMDB0001336	3,4-dihydroxyphenyl acetate		-1.08	95.17	-0.58	IC-MS/MS
HMDB0003911	3-Amino-2-methylpropanoate		-2.08	85.38	-0.38	RP-MS
HMDB0003540	3'-AMP		-1.20	95.19	-0.19	RP-MS/MS
HMDB0000355	3-Hydroxymethylglutarate	82.5	2.07	99.09	-0.60	IC-MS/MS
HMDB0000807	3-Phosphoglycerate	67.9	2.43	99.43		IC-MS/MS
HMDB0004096	5-Methoxyindoleacetate		2.19	97.35	1.63	IC-MS/MS
N/A	6-Hydroxy-2,5,7,8-tetramethylchromane-2-carboxylate		-1.53		0.21	RP-MS/MS
HMDB0001316	6-Phosphogluconate	68.5	3.98	98.69		IC-MS/MS
HMDB0003333	8-Oxo-deoxyguanosine	28.8	3.07	94.59		IC-MS/MS
HMDB0001890	Acetylcysteine	40.8	2.32	98.19		IC-MS/MS
HMDB0000532	Acetylglycine	83.9	0.17	96.80	-0.25	IC-MS/MS
HMDB0001341	Adenosine diphosphate	84.8	3.65	97.31		IC-MS/MS
HMDB0000045	Adenosine monophosphate	75.1	2.33	96.78		IC-MS/MS
HMDB0000538	Adenosine triphosphate	78.5	3.43	97.67		IC-MS/MS
HMDB0001332	Adenylsuccinate		4.53	96.22	-1.59	IC-MS/MS
HMDB0012882	Adipate semialdehyde	21.3	2.74	99.74		IC-MS/MS
HMDB0000508	Adonitol	21.2	1.92	97.29	-0.67	IC-MS/MS
HMDB0000161	Alanine		0.16	95.78	0.05	RP-MS
HMDB0001852	all-trans-Retinoate		-4.24	85.44	-0.63	RP-MS/MS
HMDB0000112	Aminobutyrate		-1.19	99.23	0.13	RP-MS
N/A	Aminoheptanoate		-2.22	84.78	0.87	RP-MS/MS
HMDB0000194	Anserine		-2.64	93.33		RP-MS
HMDB0000539	Arabinonate	72.1	1.45	97.24	-0.87	IC-MS/MS
HMDB0000517	Arginine		-0.39	96.25	0.05	RP-MS
HMDB0000044	Ascorbate	41.3	1.84	99.72		IC-MS/MS
HMDB0001894	Aspartame		-1.60	95.34	-0.84	RP-MS/MS
HMDB0000191	Aspartate	89.1	2.46	94.72	0.48	IC-MS/MS
HMDB0000056	beta-Alanine		1.05	99.25	0.05	RP-MS
HMDB0013220	Beta-Citryl-L-glutamate	21.5	2.02	98.47		IC-MS/MS
HMDB0000039	Butyrate	90.5	1.22	96.35	0.88	IC-MS/MS
HMDB0001964	Caffeate		-2.63	89.89	0.54	RP-MS/MS
HMDB0000033	Carnosine		0.81	93.29	0.02	RP-MS
HMDB0000072	Cis-aconitate		1.91	96.78	1.50	IC-MS/MS
HMDB0000634	Citraconate		-2.54	96.01	-0.61	RP-MS/MS
HMDB0000426	Citramalate		-2.78	98.73	-0.29	RP-MS/MS
HMDB0000094	Citrate	85.2	2.44	99.56	-1.84	IC-MS/MS
HMDB0000904	Citrulline		-0.05	95.03	0.02	RP-MS
HMDB0000064	Creatine		-2.06	96.64	0.02	RP-MS/MS
HMDB0002757	Cysteate	80	2.30	91.10	-1.20	IC-MS/MS
HMDB0001546	Cytidine diphosphate	62.7	2.72	97.33		IC-MS/MS

HMDB code	Identification	In-house DB fragment-ation score	Mass error / ppm	Isotope similarity / %	RT error / min	Method
HMDB0000095	Cytidine monophosphate	69.7	2.34	96.58		IC-MS/MS
HMDB0001176	Cytidine monophosphate N-acetylneuraminate	70.7	4.99	98.81		IC-MS/MS
HMDB0000082	Cytidine triphosphate	75.9	4.02	97.95		IC-MS/MS
HMDB0001508	dADP	56.7	3.24	94.91		IC-MS/MS
HMDB0001245	dCDP		2.89	87.50	-0.13	RP-MS/MS
HMDB0001202	dCMP		2.50	92.83	-0.02	IC-MS/MS
HMDB0000998	dCTP	95.7	4.06	98.04	-0.42	IC-MS/MS
HMDB0015391	Decitabine/ 5'-aza-2'-deoxycytidine		-4.98	95.50	-0.27	RP-MS/MS
HMDB0000905	Deoxyadenosine monophosphate		3.17	93.37	-0.44	IC-MS/MS
HMDB0000012	Deoxyuridine	53.4	3.14	90.22		IC-MS/MS
HMDB0001044	dGMP	45.6	2.40	96.74	-0.86	IC-MS/MS
HMDB0031257	Dimethyl fumarate		1.94	94.53	-1.90	IC-MS/MS
HMDB0000638	Dodecanoate		-2.87	91.58	-0.27	RP-MS/MS
HMDB0001274	dTDP	96.4	3.07	97.89	1.30	IC-MS/MS
HMDB0001000	dUDP		3.60	93.81	-0.57	IC-MS/MS
HMDB0001409	dUMP	19.4	2.68	96.67		IC-MS/MS
HMDB0001191	dUTP		4.07	94.67	-1.27	IC-MS/MS
HMDB0001321	Erythrose 4-phosphate		3.91	97.51	-1.43	IC-MS/MS
HMDB0000149	Ethanolamine		2.35	97.22	0.00	RP-MS
HMDB0001248	FAD		-2.10	84.56	0.27	RP-MS/MS
HMDB0001520	Flavin Mononucleotide	42.6	4.44	94.85		IC-MS/MS
HMDB0000121	Folate		-3.62	94.95	-0.42	RP-MS/MS
HMDB0001058	Fructose 1,6-bisphosphate	55.6	2.33			IC-MS/MS
HMDB0001047	Fructose 2,6 diphosphate	78.9	2.08	99.00		IC-MS/MS
HMDB0000124	Fructose 6-phosphate	75.6	2.21	92.32	-0.62	IC-MS/MS
HMDB0000134	Fumarate	54.3	-0.16	99.54	-0.34	IC-MS/MS
HMDB0000639	Galactarate	54.4	2.23	98.11		IC-MS/MS
HMDB0002545	Galacturonate	30	1.95	93.61	-1.87	IC-MS/MS
HMDB0000625	Gluconate	52.4	1.67			IC-MS/MS
HMDB0000122	Glucose	58	1.99	98.99		IC-MS/MS
HMDB0001586	Glucose 1-phosphate	70.9	2.65	98.94		IC-MS/MS
HMDB0000127	Glucuronate	78.4	1.99	98.75	-1.28	IC-MS/MS
HMDB0000148	Glutamate		-0.04	98.74	0.05	RP-MS
HMDB0000641	Glutamine		2.40	96.22	-0.31	IC-MS/MS
HMDB0000661	Glutarate	80.1	1.98	96.25	-1.54	IC-MS/MS
HMDB0000125	Glutathione		1.71	92.47	0.00	RP-MS
N/A	Glyceraldehyde 2-phosphate		-2.39	96.19	-0.01	RP-MS/MS
HMDB0000139	Glycerate	49.7	-1.51			IC-MS/MS
HMDB0000131	Glycerol	58.1	0.85	99.37	-0.56	IC-MS/MS
HMDB0000126	Glycerol 3-phosphate	48.8	2.52			IC-MS/MS
HMDB0000123	Glycine		0.17	99.14	0.05	RP-MS
HMDB0001201	Guanosine diphosphate	98.2	4.64	97.28	-0.90	IC-MS/MS
HMDB0001397	Guanosine monophosphate	79.9	3.00	96.79		IC-MS/MS
HMDB0001273	Guanosine triphosphate	79.6	4.04			IC-MS/MS
HMDB0000714	Hippurate	63	2.54	90.14	-1.72	IC-MS/MS
HMDB0000177	Histidine		3.71	97.62	0.06	RP-MS
HMDB0000742	Homocysteine		0.35	94.35	-0.18	RP-MS
HMDB0000719	Homoserine		0.38	95.47	0.54	RP-MS
HMDB0000528	Hydroorotate		2.12	97.04	0.07	IC-MS/MS
HMDB0000763	Hydroxyindoleacetate		2.71	92.53	-1.91	IC-MS/MS
HMDB0000732	Hydroxykynurenine		1.89	94.66	-0.76	IC-MS/MS
HMDB0000472	Hydroxy-L-tryptophan		2.93	94.17		RP-MS
N/A	Hydroxy-methyl-dUTP		4.34		0.63	IC-MS/MS
HMDB0000157	Hypoxanthine		-4.20	95.68	-0.34	RP-MS
HMDB0000671	Indolelactate		-4.88	89.98	0.09	RP-MS

HMDB code	Identification	In-house DB fragment-ation score	Mass error / ppm	Isotope similarity / %	RT error / min	Method
HMDB0000195	Inosine	9.65	-1.96	95.07		IC-MS/MS
HMDB0000175	Inosine monophosphate	46.1	0.98	96.77	-0.31	IC-MS/MS
HMDB0001143	Inositol 1,3,4-trisphosphate	55.3	3.73	96.33		IC-MS/MS
HMDB0034198	Isobutylamine		-2.35	98.36	0.13	RP-MS
HMDB0000172	Isoleucine		0.11	96.03	0.03	RP-MS
HMDB0002092	Itaconate	31.8	3.72	99.46		IC-MS/MS
HMDB0032923	Kojate		2.20	92.83	-0.08	IC-MS/MS
HMDB0000684	Kynurenine		0.86	97.85	0.03	RP-MS
HMDB0000201	L-Acetylcarnitine	22.8	-2.21	97.31		RP-MS/MS
HMDB0000190	Lactate	33.5	1.21	99.82	-0.98	IC-MS/MS
HMDB0000186	Lactose		0.42	93.12	-0.70	IC-MS/MS
HMDB0000099	L-Cystathionine		2.53	92.04	0.00	RP-MS
HMDB0000192	L-Cystine		2.70	93.35		RP-MS
HMDB0000687	Leucine		-0.07	96.81	0.02	RP-MS
HMDB0011170	L-gamma-glutamyl-L-isoleucine	51.6	-2.27	95.75		RP-MS/MS
HMDB0000673	Linoleate		-2.07	91.63	-0.13	RP-MS/MS
HMDB0000696	L-Methionine	6.78	-2.12	89.12		RP-MS/MS
HMDB0000182	Lysine		0.81	97.32	0.01	RP-MS
HMDB0000744	Malate	68.2	1.90	99.84	-1.34	IC-MS/MS
HMDB0000176	Maleate		-0.02	96.94	0.91	IC-MS/MS
HMDB0000691	Malonate	72.6	-0.09	98.55	-1.37	IC-MS/MS
HMDB0006112	Malondialdehyde		1.55	97.69	1.66	IC-MS/MS
HMDB0029965	Methyl beta-D-glucopyranoside	7.24	1.66	95.31		IC-MS/MS
HMDB0006471	Methylisocitrate	25.8	2.29	99.06		IC-MS/MS
HMDB0002038	Methyl-L-Lysine		0.13	96.76	0.02	RP-MS
HMDB0032572	Methylparaben		2.05	93.90	1.53	IC-MS/MS
HMDB0029416	Mono-methyl arginine/Targinine		2.63	94.39		RP-MS
HMDB0000806	Myristate		-1.70	90.39	-0.23	RP-MS/MS
HMDB0001067	N-Acetylaspartylglutamate	60.2	2.49	98.13		IC-MS/MS
HMDB0001367	N-acetyl-glucosamine-1-phosphate	70.9	1.94	95.95		IC-MS/MS
HMDB0001138	N-Acetylglutamate		0.42	96.29	0.00	RP-MS/MS
HMDB0000766	N-Acetyl-L-alanine	74.4	0.98	97.55	-0.09	IC-MS/MS
HMDB0000812	N-Acetyl-L-aspartate	91.4	4.79	92.84	-0.45	IC-MS/MS
HMDB0011745	N-Acetyl-L-methionine		0.11	94.53	-0.38	RP-MS/MS
HMDB0000512	N-Acetyl-L-phenylalanine		2.03	95.18	-1.04	IC-MS/MS
HMDB0001129	N-Acetylmannosamine		2.04	92.32	-0.72	IC-MS/MS
HMDB0000230	N-Acetylneuraminate	82.7	2.21	96.63	-0.89	IC-MS/MS
HMDB0006268	N-Acetylneuraminate 9-phosphate		3.69	95.60	-1.77	IC-MS/MS
HMDB0003357	N-Acetyl-ornithine		-0.02	94.98	-0.08	RP-MS
HMDB0013713	N-acetyltryptophan		-4.89	95.28	-0.67	RP-MS/MS
HMDB0011757	N-Acetylvaline	7.26	1.52	97.62	-0.12	IC-MS/MS
HMDB0000207	Oleate		-2.02	92.97	-0.17	RP-MS/MS
HMDB0000214	Ornithine		-0.63	89.95	0.12	RP-MS
HMDB0000226	Orotate		2.69	93.17	0.61	IC-MS/MS
HMDB0002329	Oxalate	77.8	1.84	99.37	-0.84	IC-MS/MS
HMDB0003337	Oxidised Glutathione		-0.91	94.95	-0.03	RP-MS
HMDB0000225	Oxoadipate	31.5	2.15	96.70		IC-MS/MS
HMDB0000220	Palmitate		-1.53	93.42	-0.20	RP-MS/MS
HMDB0000210	Pantothenate		0.80	91.44	0.02	RP-MS
HMDB0000159	Phenylalanine		-0.15	96.74	0.03	RP-MS
HMDB0000205	Phenylpyruvate	34.4	2.63	96.48		IC-MS/MS
HMDB0001511	Phosphocreatine		-0.05	96.02	-0.03	IC-MS/MS
HMDB0000263	Phosphoenolpyruvate	9.6	2.11	99.41		IC-MS/MS
HMDB0000280	Phosphoribosyl pyrophosphate	76.1	3.38	99.03		IC-MS/MS
HMDB0000020	p-Hydroxyphenylacetate		-1.82	91.45	-0.46	IC-MS/MS
HMDB0000801	Phytanate		-1.84	85.03	0.33	RP-MS/MS

HMDB code	Identification	In-house DB fragment-ation score	Mass error / ppm	Isotope similarity / %	RT error / min	Method
HMDB0000070	Pipecolate		0.63	94.93	-0.18	RP-MS
N/A	Poly-DL-Alanine		-3.04	96.29	0.02	RP-MS/MS
HMDB0000162	Proline		0.70	95.68	0.04	RP-MS
HMDB0001220	Prostaglandin E2		-2.09	94.54	0.90	RP-MS/MS
HMDB0001856	Protocatechuate	16	2.49	93.95	1.03	IC-MS/MS
HMDB0000267	Pyroglutamate	10.2	-2.01	94.00	-0.16	IC-MS/MS
HMDB0000243	Pyruvate	53.8	1.19	99.85	-1.15	IC-MS/MS
HMDB0003072	Quinate		2.83	91.28	-0.92	IC-MS/MS
HMDB0001548	Ribose 5-phosphate		3.67	88.94	0.05	IC-MS/MS
HMDB0000618	Ribulose 5-phosphate	73.3	3.17	98.73		IC-MS/MS
HMDB0001895	Salicylate		-1.63	93.84	0.12	IC-MS/MS
HMDB0060274	Sedoheptulose 1,7-bisphosphate	30.2	2.59	98.46		IC-MS/MS
HMDB0060509	Sedoheptulose 1-phosphate	74.3	3.38	97.98		IC-MS/MS
HMDB0001068	Sedoheptulose 7-phosphate	76.6	3.40			IC-MS/MS
HMDB0000187	Serine		4.06	97.47	0.06	RP-MS
HMDB0000259	Serotonin		-0.16	91.69	-0.10	RP-MS
HMDB0000247	Sorbitol	67.7	2.87	98.84	-0.50	IC-MS/MS
HMDB0006797	Sorbose 1-phosphate		-0.21	91.60	-0.14	RP-MS/MS
HMDB0000827	Stearate		-1.87	94.88	-0.20	RP-MS/MS
HMDB0000254	Succinate	90.4	0.09	99.74	-1.45	IC-MS/MS
HMDB0001259	Succinate semialdehyde	38.9	-0.96	99.35		IC-MS/MS
N/A	Succinyl-Homoserine		3.57	97.91	0.51	IC-MS/MS
HMDB0000251	Taurine		2.63	97.63		RP-MS
HMDB0004136	Threitol	84.2	1.04	97.93	-0.60	IC-MS/MS
HMDB0000167	Threonine		-0.45	98.57	0.05	RP-MS
HMDB0001342	Thymidine 5'-triphosphate	70.4	4.46	98.40		IC-MS/MS
HMDB0000954	trans-Ferulate		-0.22	91.35	-0.37	RP-MS/MS
HMDB0000929	Tryptophan		-0.68	96.92	0.02	RP-MS
HMDB0000158	Tyrosine		0.12	98.35	0.03	RP-MS
HMDB0000300	Uracil	10.7	-1.08	95.01	-1.26	IC-MS/MS
HMDB0000294	Urea		0.84	96.28	0.03	RP-MS
HMDB0000295	Uridine 5-diphosphate	78.6	2.82	98.09		IC-MS/MS
HMDB0000288	Uridine 5'-monophosphate	80.6	3.22	98.10		IC-MS/MS
HMDB0000285	Uridine triphosphate	74.3	3.85	98.26		IC-MS/MS
HMDB0000883	Valine		0.11	95.79	0.03	RP-MS
HMDB0000292	Xanthine	38.8	-3.01	93.75		RP-MS/MS
HMDB0001554	Xanthylate	66.1	3.08	95.90		IC-MS/MS
HMDB0001644	Xylulose	45	1.29	95.61		IC-MS/MS

10.8. Data for LN18 IDH1 mutant and wild-type glioblastoma cells treated with 2-HG or 2-OG

Metabolite identification information for the analysis of LN18 Mut and WT cells cultured under 4.5 g / L glucose conditions, treated with 10 mM 2-HG, 10 mM 2-OG or vehicle control for 24 hours (Section 8.18), analysed by IC-MS/MS (Section 8.4), derivatised RP-MS (Section 8.7) and non-derivatised RP-MS/MS (Section 8.9), including HMDB code, fragmentation score, mass error, isotope similarity RT method and analysis method are

listed in Table 10.10. Full compound-feature lists including significance, FC and CV information for LN18 WT cells cultured under 4.5 g / L conditions, treated with 10 mM 2-HG (Section 8.18) are found in ESM H. Compound-feature lists for LN18 Mut and WT cells cultured under 4.5 g / L conditions, treated with 10 mM 2-OG (Section 8.18) are found in ESM I and J respectively.

Table 10.10: Metabolite identification information for the analysis of LN18 Mut and WT cells cultured under 4.5 g / L glucose conditions, treated with 10 mM 2-HG, 10 mM 2-OG or vehicle control for 24 hours (Section 8.18), analysed by IC-MS/MS (Section 8.4), derivatised RP-MS (Section 8.7) and non-derivatised RP-MS/MS (Section 8.9).

HMDB code	Identification	In-house DB fragment-ation score	Mass error / ppm	Isotope similarity / %	RT error / min	Method
HMDB0000001	1-Methyl histidine		-2.08	94.35	0.02	RP-MS
HMDB0000152	2,5-dihydroxybenzoate		-1.05	96.14	-0.68	IC-MS/MS
HMDB0000510	2-Aminoadipate		-0.39	95.35	0.10	RP-MS
N/A	2-Aminobut-2-enoate		-0.30	96.39		RP-MS
HMDB0000991	2-Aminocaprylate		-1.84	90.84	1.07	RP-MS/MS
N/A	2-C-Methyl-D-Erythritol 4-phosphate		0.09		0.12	RP-MS/MS
HMDB0001044	2'-Deoxyguanosine 5'-monophosphate	28.50	2.77	96.10	-0.35	IC-MS/MS
HMDB0059655	2-Hydroxyglutarate	81.10	-3.37	99.90	-0.92	IC-MS/MS
N/A	2-Iminobutanoate		-0.18	96.66		RP-MS
HMDB0000402	2-Isopropylmalate		-2.89	98.67	-0.12	IC-MS/MS
HMDB0000208	2-Oxoglutarate	57.40	-3.88		0.05	IC-MS/MS
HMDB0002441	3,3-Dimethylglutarate		-3.16	96.85	0.40	IC-MS/MS
HMDB0003911	3-Amino-2-methylpropanoate		-4.44	96.20		RP-MS
HMDB0000355	3-Hydroxymethylglutarate		-3.04	98.96	-0.05	IC-MS/MS
HMDB0000807	3-Phosphoglycerate		-1.55	97.46	-0.01	IC-MS/MS
HMDB0000707	4-Hydroxyphenylpyruvate		-2.70	93.91	-0.16	IC-MS/MS
HMDB0000725	4-Hydroxyproline	85.30	-3.51	97.52	-0.84	IC-MS/MS
HMDB0001149	5-Aminolevulinate		2.05	91.53		RP-MS
HMDB0004096	5-Methoxyindoleacetate		-3.88	96.96	0.04	RP-MS/MS
N/A	6-Hydroxy-2,5,7,8-tetramethylchromane-2-carboxylate		-0.25		0.69	RP-MS/MS
HMDB0001316	6-Phosphogluconate		-0.28	97.89	0.00	IC-MS/MS
HMDB0000532	Acetylglycine	82.50	-2.06	85.66	-0.15	IC-MS/MS
HMDB0000045	Adenosine monophosphate		2.62	94.96	0.10	IC-MS/MS
HMDB0000538	Adenosine triphosphate		-0.78	98.13	0.10	IC-MS/MS
HMDB0000508	Adonitol		-1.95	96.02	-0.01	IC-MS/MS
HMDB0000161	Alanine		-1.05	97.16	0.06	RP-MS
HMDB0000112	Aminobutyrate		-2.72	94.37	0.11	RP-MS
HMDB0000539	Arabinonate		-3.48	94.76	-0.59	IC-MS/MS
HMDB0000517	Arginine		-2.39	95.58	0.07	RP-MS
HMDB0000044	Ascorbate	41.70	-3.45	99.73		IC-MS/MS
HMDB0000168	Asparagine		-2.07	95.40	0.05	RP-MS
HMDB0001894	Aspartame		0.92	95.20	0.26	RP-MS/MS
HMDB0000191	Aspartate		-2.17	96.37	0.09	RP-MS
N/A	Benzoyl-L-citrulline methyl ester		-0.25	94.12	-1.42	RP-MS/MS
HMDB0013220	Beta-Citryl-L-glutamate		1.42	98.30	0.73	IC-MS/MS
HMDB0001964	Caffeate		-2.26	95.92	1.01	RP-MS/MS
HMDB0000033	Carnosine		-1.82	92.93	0.03	RP-MS

HMDB code	Identification	In-house DB fragment-ation score	Mass error / ppm	Isotope similarity / %	RT error / min	Method
HMDB0000072	Cis-aconitate		-3.69	97.52	-0.01	IC-MS/MS
HMDB0000094	Citrate	83.40	-2.75	99.59	0.00	IC-MS/MS
HMDB0000904	Citrulline		-1.82	94.91	0.09	RP-MS
HMDB0001423	Coenzyme A		0.36	84.54	-1.00	IC-MS/MS
HMDB0002757	Cysteate		-3.32	90.58	-0.69	IC-MS/MS
HMDB0001546	Cytidine diphosphate		4.66	97.80	-0.31	IC-MS/MS
HMDB0000095	Cytidine monophosphate		2.70	91.78	0.02	IC-MS/MS
HMDB0001176	Cytidine monophosphate N-acetylneuraminate		-1.32	98.72	-0.61	IC-MS/MS
HMDB0000082	Cytidine triphosphate	34.40	2.83	98.10		IC-MS/MS
HMDB0001245	dCDP		4.97	94.02		IC-MS/MS
HMDB0000998	dCTP	0.92	3.31	95.57		IC-MS/MS
HMDB0001532	Deoxyadenosine triphosphate		3.48	95.03	0.28	IC-MS/MS
HMDB0001031	Deoxyribose 5-phosphate		-0.83		-0.01	IC-MS/MS
HMDB0013287	Dimethyl L-Lysine		-1.76	94.63	0.09	RP-MS
HMDB0001328	dTDP-D-glucose		-1.03	92.23	-0.40	IC-MS/MS
HMDB0001191	dUTP		3.24	94.81	0.11	IC-MS/MS
HMDB0000149	Ethanolamine		-2.02	96.69	0.03	RP-MS
HMDB0012228	Ethylphosphate	0.77	-1.93	96.70		IC-MS/MS
HMDB0001248	FAD	0.35	-1.42	92.03	0.32	RP-MS/MS
HMDB0000121	Folate		4.40	95.84	-0.14	RP-MS/MS
HMDB0001047	Fructose 2,6 diphosphate		2.08	98.71	-0.34	IC-MS/MS
HMDB0000134	Fumarate	67.00	-2.64	99.14	0.45	IC-MS/MS
HMDB0000639	Galactarate	39.90	-2.87	92.58	-0.97	IC-MS/MS
HMDB0003351	GDP-glucose		-0.93	95.79		IC-MS/MS
HMDB0000625	Gluconate	81.40	-3.36		-0.11	IC-MS/MS
HMDB0000150	Gluconolactone	12.60	-3.33	98.01	-0.26	IC-MS/MS
HMDB0001109	Glucosamine-1P	4.28	-1.76	97.88		IC-MS/MS
HMDB0001586	Glucose 1-phosphate		-1.51	99.01	-0.12	IC-MS/MS
HMDB0000127	Glucuronate	75.20	-3.34	98.27	-0.04	IC-MS/MS
HMDB0000148	Glutamate		-2.09	96.79	0.09	RP-MS
HMDB0000641	Glutamine		-2.06	96.49	0.08	RP-MS
HMDB0000661	Glutarate	67.30	-3.28	85.91	-0.13	IC-MS/MS
HMDB0000125	Glutathione	47.90	0.96	95.04		IC-MS/MS
HMDB0000139	Glycerate		-3.71		0.08	IC-MS/MS
HMDB0000131	Glycerol	54.00	-3.20	99.05	0.10	IC-MS/MS
HMDB0000126	Glycerol 3-phosphate	60.20	-2.50		-0.17	IC-MS/MS
HMDB0000123	Glycine		-2.03	97.59	0.09	RP-MS
HMDB0000119	Glyoxylate		-3.97	98.41	0.16	IC-MS/MS
HMDB0001273	Guanosine triphosphate	10.10	-0.23	97.66		IC-MS/MS
HMDB0000177	Histidine		-2.12	94.88	0.04	RP-MS
HMDB0000742	Homocysteine		-2.04	92.46		RP-MS
HMDB0006462	Homocysteinesulfinate	10.60	-3.27	89.46		IC-MS/MS
HMDB0000719	Homoserine		-1.83	95.70	0.22	RP-MS
HMDB0000528	Hydroorotate		-1.22	95.39	0.03	IC-MS/MS
HMDB0000175	Inosine monophosphate		3.09	78.03	0.01	IC-MS/MS
HMDB0034198	Isobutylamine		-1.91	97.57	0.00	RP-MS
HMDB0000172	Isoleucine		-1.69	97.30	0.12	RP-MS
HMDB0000678	Isovalerylglycine		-3.50	96.33	-0.20	IC-MS/MS
HMDB0000684	Kynurenine		-1.94	93.47	0.12	RP-MS
HMDB0000190	Lactate	19.60	-3.91	99.91	-0.01	IC-MS/MS
HMDB0000186	Lactose		2.72	93.23	-0.65	IC-MS/MS
HMDB0000687	Leucine		-1.85	97.32	0.12	RP-MS
HMDB0034365	L-Theanine		-4.37	98.65	1.31	RP-MS/MS
HMDB0000182	Lysine		-1.47	98.15	0.09	RP-MS
HMDB0000744	Malate	92.00	-3.14	99.73	0.01	IC-MS/MS

HMDB code	Identification	In-house DB fragment-ation score	Mass error / ppm	Isotope similarity / %	RT error / min	Method
HMDB0000691	Malonate	67.90	-2.64	98.19	-0.04	IC-MS/MS
HMDB0000696	Methionine		-2.13	96.44	0.12	RP-MS
HMDB0032572	Methyl 4-hydroxybenzoate		-1.52	92.82	-2.55	RP-MS/MS
HMDB0006471	Methylisocitrate		-3.14	98.37	-0.25	IC-MS/MS
HMDB0002038	Methyl-L-Lysine		-2.34	90.84	-0.06	RP-MS
HMDB0000806	Myristate		-0.89	89.45	0.28	RP-MS/MS
HMDB0001325	N,N,N-Trimethyllysine		-2.47	94.82	0.02	RP-MS
HMDB0001067	N-Acetylaspartylglutamate		1.27	97.64	0.00	IC-MS/MS
HMDB0001121	N-Acetyl-D-mannosamine 9-phosphate		3.58	85.81	0.05	IC-MS/MS
HMDB0001367	N-acetyl-glucosamine-1-phosphate		1.37	94.20	-0.06	IC-MS/MS
HMDB0001138	N-Acetylglutamate	57.30	-2.68	97.57	-0.83	IC-MS/MS
HMDB0032055	N-Acetyl-histidine		-4.33	96.32	0.13	RP-MS/MS
HMDB0000812	N-Acetyl-L-aspartate		-3.05	93.57	-0.79	IC-MS/MS
HMDB0011745	N-Acetyl-L-methionine		-2.58	96.90	-0.05	IC-MS/MS
HMDB0000512	N-Acetyl-L-phenylalanine	56.80	-2.52	96.77	0.45	IC-MS/MS
HMDB0000230	N-Acetylneuraminate		1.01	95.59	-0.74	IC-MS/MS
HMDB0003357	N-Acetyl-ornithine		-1.91	94.67	-0.01	RP-MS
HMDB0094701	N-Acetylproline		-4.20	95.87	1.02	RP-MS/MS
HMDB0013713	N-acetyltryptophan		-2.96	96.06	-0.30	RP-MS/MS
HMDB0011757	N-Acetylvaline		-2.44	97.99	-0.03	IC-MS/MS
HMDB0001487	NADH		-0.01	83.83	-0.16	IC-MS/MS
HMDB0000833	N-Glycolylneuraminate	5.93	1.56	97.32		IC-MS/MS
HMDB0013716	Norvaline		-1.89	97.21	-0.07	RP-MS
HMDB0000207	Oleate		3.00	93.63	0.37	RP-MS/MS
HMDB0001721	O-Phosphoserine	47.30	-2.36	98.11	-0.03	IC-MS/MS
HMDB0000214	Ornithine		-2.00	95.04	0.08	RP-MS
HMDB0000223	Oxalacetate		-2.55	94.63		IC-MS/MS
HMDB0002329	Oxalate		-3.11	99.39	-0.03	IC-MS/MS
HMDB0000225	Oxoadipate	35.70	-2.69	97.32	0.04	IC-MS/MS
HMDB0000220	Palmitate		-1.11	96.00	0.34	RP-MS/MS
HMDB0000210	Pantothenate	89.20	-2.81	97.84	-0.08	IC-MS/MS
HMDB0000159	Phenylalanine		-2.13	96.90	0.14	RP-MS
HMDB0000205	Phenylpyruvate		-2.96	92.86	0.17	IC-MS/MS
HMDB0029438	Phosphoarginine		2.15	96.59		RP-MS
HMDB0001511	Phosphocreatine	12.40	-1.82	95.11		IC-MS/MS
HMDB0000263	Phosphoenolpyruvate		-2.06	98.04	-0.08	IC-MS/MS
HMDB0000280	Phosphoribosyl pyrophosphate		4.78	97.66	-0.31	IC-MS/MS
N/A	Phosphorylcholine Chloride		-2.91	96.58	-1.05	RP-MS/MS
HMDB0000162	Proline		-2.33	96.51	0.11	RP-MS
HMDB0001220	Prostaglandin E2		2.73	95.42	1.36	RP-MS/MS
HMDB0001491	Pyridoxal 5'-phosphate	8.95	-1.33	95.65	0.01	IC-MS/MS
HMDB0000267	Pyroglutamate	11.10	-3.07	94.01	0.05	IC-MS/MS
HMDB0000243	Pyruvate		-3.59	99.57	-0.15	IC-MS/MS
HMDB0000232	Quinolinate		-3.54	91.53	-0.11	IC-MS/MS
HMDB0000244	Riboflavin	39.10	4.63	93.22	0.25	RP-MS/MS
HMDB0011688	Ribose 1,5-bisphosphate		2.18	95.50		IC-MS/MS
HMDB0000279	Saccharopine		-1.94	88.62	0.08	RP-MS
HMDB0000271	Sarcosine		-1.98	97.28	0.11	RP-MS
HMDB0006088	Scyllitol		-3.00	99.34	1.00	IC-MS/MS
HMDB0000792	Sebacate		-2.23	92.48	0.08	IC-MS/MS
HMDB0001068	Sedoheptulose 7-phosphate		1.45		0.01	IC-MS/MS
HMDB0000187	Serine		-2.24	97.08	0.09	RP-MS
HMDB0000259	Serotonin		-1.63	89.89	-0.03	RP-MS
HMDB0000247	Sorbitol	80.70	-2.49	98.14	0.00	IC-MS/MS
HMDB0000827	Stearate		3.34	90.63	0.29	RP-MS/MS
HMDB0000254	Succinate	69.60	-2.90	99.42	0.08	IC-MS/MS

HMDB code	Identification	In-house DB fragment-ation score	Mass error / ppm	Isotope similarity / %	RT error / min	Method
HMDB0001259	Succinate semialdehyde		-3.86	99.63	-0.49	IC-MS/MS
HMDB0002085	Syringate		-3.27	95.85	-0.51	IC-MS/MS
HMDB0000251	Taurine		-2.07	95.55	0.06	RP-MS
HMDB0004136	Threitol		-3.26	91.04	-0.03	RP-MS
HMDB0000167	Threonine		-2.24	97.04	0.10	RP-MS
HMDB0001227	Thymidine 5'-phosphate		2.51	94.35	-0.25	IC-MS/MS
HMDB0001342	Thymidine 5'-triphosphate	1.27	3.51	98.21	-0.08	IC-MS/MS
HMDB0000303	Tryptamine		-1.97	89.04	-0.14	RP-MS/MS
HMDB0000929	Tryptophan		-1.93	95.58	0.14	RP-MS
HMDB0000158	Tyrosine		-2.38	96.23	0.12	RP-MS
HMDB0000935	UDP-glucoronate		-1.67	95.42	-0.21	IC-MS/MS
HMDB0000286	UDP-glucose		-1.36	95.50	-0.30	IC-MS/MS
HMDB0013112	UDP-N-acetyl-D-mannosamine		-1.32	98.79		IC-MS/MS
HMDB0000289	Urate	33.50	-3.38	94.30	-0.03	IC-MS/MS
HMDB0000294	Urea		-1.44	96.59	0.09	RP-MS
HMDB0000296	Uridine		-2.25	95.18	0.76	IC-MS/MS
HMDB0000295	Uridine 5'-diphosphate	17.00	4.68	98.28	-0.04	IC-MS/MS
HMDB0000285	Uridine triphosphate	7.70	2.85	98.42		IC-MS/MS
HMDB0001644	Xylulose		-3.58	96.32	0.39	IC-MS/MS